

UNIVERSITY OF ALBERTA

**In-Situ Ground Freezing to Obtain Undisturbed Samples of
Loose Sand for Liquefaction Assessment**

by

Barbara A. Hofmann



A thesis submitted to the Faculty of Graduate Studies and Research in partial fulfillment
of the requirements for the degree of **Doctor of Philosophy**

in

Geotechnical Engineering

Department of Civil and Environmental Engineering

Edmonton, Alberta
Spring, 1997



**National Library
of Canada**

**Acquisitions and
Bibliographic Services**

**385 Wellington Street
Ottawa ON K1A 0N4
Canada**

**Bibliothèque nationale
du Canada**

**Acquisitions et
services bibliographiques**

**385, rue Wellington
Ottawa ON K1A 0N4
Canada**

Your file *Votre référence*

Our file *Notre référence*

The author has granted a non-exclusive licence allowing the National Library of Canada to reproduce, loan, distribute or sell copies of his/her thesis by any means and in any form or format, making this thesis available to interested persons.

The author retains ownership of the copyright in his/her thesis. Neither the thesis nor substantial extracts from it may be printed or otherwise reproduced with the author's permission.

L'auteur a accordé une licence non exclusive permettant à la Bibliothèque nationale du Canada de reproduire, prêter, distribuer ou vendre des copies de sa thèse de quelque manière et sous quelque forme que ce soit pour mettre des exemplaires de cette thèse à la disposition des personnes intéressées.

L'auteur conserve la propriété du droit d'auteur qui protège sa thèse. Ni la thèse ni des extraits substantiels de celle-ci ne doivent être imprimés ou autrement reproduits sans son autorisation.

0-612-21578-4

to

***Mom and Dad
for teaching me to enjoy learning
and to see commitments through***

and to

***Daniel
for your love, support and encouragement***

Abstract

Evaluating whether or not a sand deposit has the potential to undergo a liquefaction failure in the event of adverse loading conditions, is an important engineering task, often related to public safety, that requires detailed characterization of the in-situ state of the deposit. Liquefaction assessment requires that the in-situ values of void ratio, shear stress, and mean normal effective stress be determined and compared with the ultimate or steady state conditions that develop after significant deformation. Therefore, to completely characterize a sand deposit, it is necessary to obtain undisturbed samples from the ground for carrying out laboratory assessment of the in-situ strength and deformation properties.

Ideally, if samples are to be considered as truly undisturbed, the void ratio, fabric, structure, stress history and degree of saturation should be preserved during the sampling and handling process. To meet this requirement, in the last approximately fifteen years the technique of utilizing in-situ ground freezing for obtaining undisturbed samples of loose, saturated sand has been investigated. This thesis was undertaken to evaluate the extent to which characteristics such as void ratio, fabric, structure and degree of saturation can be preserved during in-situ ground freezing, sampling and handling in the laboratory for a variety of granular subsoil conditions.

High quality undisturbed samples of sand are an instrumental part of carrying out a liquefaction assessment. This research demonstrated that in-situ ground freezing is an excellent technique for obtaining undisturbed samples of loose sand from below the groundwater table. The technique of undisturbed sampling can be used to assess the stability of many existing structures, such as dams, embankments, tailings impoundments, etc., that have been constructed on or with sand and may be at risk of liquefaction. The liquefaction potential of natural, often highly structured, sand deposits existing along many coastal regions near major cities, can also be more accurately assessed, utilizing high quality undisturbed samples obtained by in-situ ground freezing.

Acknowledgments

I would like to express my sincere gratitude to Dr. D. C. Seago and Dr. P. K. Robertson for their wisdom and guidance during my research program. They both contributed immensely to my technical development, while allowing for personal growth, and provided much appreciated financial support. Brain storming with Dr. Seago regarding various aspects of ground freezing was indeed inspirational. The challenges put forward by Dr. Robertson to continually expand my knowledge across a wide range of liquefaction associated phenomena contributed significantly to my development as an engineer.

I would also like to thank Dr. N. R. Morgenstern, whose technical expertise, teaching skills and professional conduct have deeply inspired me throughout my career.

Special thanks are extended to Dr. K. Tokimastu, who took time out of his busy schedule at the Tokyo Institute of Technology to come to Edmonton and review this work. Discussions with Dr. J.-M. Konrad, Dr. J. Sobkowicz and Dr. B. Ladanyi regarding various aspects of this research were also greatly appreciated.

Sincere thanks are forwarded to Gerry Cyre for his extensive assistance and the many long hours of work associated with the ground freezing activities undertaken as part of this research. The support provided by Christine Hereygers and Steve gamble in the laboratory were also greatly appreciated.

Special gratitude is extended to my husband, Daniel St-Gelais, without whom completion of this research would not have been possible. Daniel's love and continual support of my evolving goals were the pillars that supported me through the tough times. I would also

like to thank my parents for their love and encouragement, as well as for showing me that learning is truly one of life's rewards.

This research would not have been possible without the generous financial support provided by the Canadian Liquefaction Experiment (CANLEX) project. The CANLEX project was supported through a collaborative Research and Development Grant from NSERC, BC Hydro, Quebec Hydro, Syncrude Canada Ltd. and Suncor. Collaborative technical and financial support was also provided by the geotechnical consultants: EBA Engineering Consultants Ltd., HBT AGRA Ltd., Klohn-Crippen Ltd., Golder Associates and Thurber Engineering Ltd., as well as faculty and students from the University of Alberta, University of British Columbia, Université de Laval, Carleton University and Sherbrooke University. This project has been a highlight in my career and I have appreciated the opportunity to participate in a collaborative approach to research. Sincere gratitude is extended to CANLEX for this exciting research opportunity and for the extensive financial contributions.

Sincere gratitude is also extended to the University of Alberta for providing financial assistance through the Alberta Ph.D. Scholarship and Alberta Ph.D. Fellowship during each year of this research.

Table of contents

Chapter 1

Introduction

1.0	INTRODUCTION	1
1.1	FRAMEWORK FOR DESCRIBING SOIL BEHAVIOUR	2
1.2	DISTURBANCE CAUSED BY CONVENTIONAL SAMPLING	6
1.3	UNDISTURBED SAMPLING BY IN-SITU GROUND FREEZING	11
1.4	RESEARCH BACKGROUND AND THESIS OBJECTIVES	12
1.5	ORGANIZATION OF THE THESIS	14
1.6	REFERENCES	16

Chapter 2

Feasibility of Obtaining Undisturbed Samples of Loose Sand by In-Situ Ground Freezing

2.0	INTRODUCTION	22
2.1	FREEZING OF FINE GRAIN SOILS	23
2.2	FREEZING OF GRANULAR SOILS	25
2.3	GENERAL DESCRIPTION OF THE GROUND FREEZING PROCESS	25
2.4	EVALUATION OF SOIL FROST HEAVE SUSCEPTIBILITY	28
	2.4.1 Characteristics of the Sand Deposit	28
	2.4.1.1 <i>Grain Size Distribution and Fines Mineralogy</i>	28
	2.4.1.2 <i>Unfrozen Water Content</i>	31
	2.4.2 Characteristics of the Site	32
	2.4.2.1 <i>Stratigraphy and Drainage Conditions</i>	32
	2.4.2.2 <i>Overburden Stress and Rate of Cooling</i>	33
	2.4.2.3 <i>Groundwater Temperature, Salinity and Flow Conditions</i>	35
2.5	LABORATORY DETERMINATION OF FROST HEAVE POTENTIAL	38
2.6	THEORETICAL PREDICTION OF GROUND FREEZING PROCESS TO EVALUATE TIME AND COSTS REQUIREMENTS	39
	2.6.1 Growth of the Frozen Radius	41
	2.6.2 Volume of Liquid Nitrogen Required	42
2.7	CONCLUSIONS	42
2.8	REFERENCES	43

Chapter 3

Design of In-Situ Ground Freezing System Utilizing Liquid Nitrogen

3.0	INTRODUCTION	50
3.1	DESIGN OF EXPERIMENTAL FREEZING SYSTEM	51
3.1.1	Freezing Chamber	51
3.1.2	Freezing System	51
3.1.3	Monitoring of the Freezing Process	51
3.1.4	Theoretical Prediction of the Freezing Process	52
3.2	PROCEDURES AND TEST RESULTS FOR FREEZING EXPERIMENTS CONDUCTED IN WATER	53
3.2.1	Experiment 1	55
3.2.2	Experiment 2	59
3.2.3	Experiment 3	62
3.2.4	Experiment 4	64
3.3	PROCEDURES AND TEST RESULTS FOR EXPERIMENTS CONDUCTED IN SAND	66
3.3.1	Experiment 5	66
3.3.2	Experiment 6	68
3.4	CONCLUSIONS	70
3.5	REFERENCES	72

Chapter 4

Case History of Undisturbed Sampling of a Man-Made Sand Deposit by In-Situ Ground Freezing

4.0	INTRODUCTION	91
4.1	BACKGROUND	92
4.2	GROUND FREEZING FEASIBILITY STUDY	93
4.2.1	Frost Heave Susceptibility of Subsoil	93
4.2.1.1	<i>Grain Size Distribution</i>	94
4.2.1.2	<i>Sand Mineralogy</i>	94
4.2.1.3	<i>Laboratory Frost Heave Testing</i>	96
4.2.1.4	<i>Unfrozen Water Content</i>	96
4.2.1.5	<i>Density Condition</i>	97
4.2.2	Groundwater Conditions	97
4.2.2.1	<i>Initial Groundwater Temperature</i>	98
4.2.2.2	<i>Groundwater Flow</i>	98
4.2.3	Prediction of the Freezing Process at the Phase I Test Site	99
4.2.3.1	<i>Estimated Time Required for Freezing</i>	100
4.2.3.2	<i>Effect of Groundwater Flow on the Growth of the Frozen Radius</i>	100

	4.2.3.3	<i>Estimated Volume of Liquid Nitrogen Required</i>	101
4.3		GROUND FREEZING SYSTEM DESIGN	102
4.4		PHASE I FIELDWORK	103
	4.4.1	Borehole Layout	103
	4.4.2	Installation of Casing to the Top of The Target Zone	104
	4.4.3	Installation of Freeze Pipe	105
	4.4.4	Mapping Borehole Alignment	106
	4.4.5	Initiation of Ground Freezing	107
	4.4.6	Monitoring of Ground Temperatures During Freezing	109
	4.4.7	Actual Liquid Nitrogen Consumption	110
4.5		COMPARISON OF THE RATE OF GROUND FREEZING WITH THEORETICAL PREDICTIONS	111
	4.5.1	Growth of the Frozen Radius	111
	4.5.2	Consumption of Liquid Nitrogen	112
4.6		CORING OF IN-SITU FROZEN SAND	113
4.7		CATALOG OF IN-SITU FROZEN SAND CORE SAMPLES	114
4.8		IN-SITU VOID RATIOS	116
4.9		CONCLUSIONS	117
4.10		REFERENCES	118

Chapter 5.0

Case History of Undisturbed Sampling at a Natural Deposit By In-Situ Ground Freezing

5.1		INTRODUCTION	139
5.2		BACKGROUND	140
5.3		SCOPE OF WORK FOR IN-SITU GROUND FREEZING AND SAMPLING	141
5.4		DESCRIPTION OF THE PHASE II TEST SITES	141
	5.4.1	Location	141
	5.4.2	Target Zones	141
5.5		GROUND FREEZING FEASIBILITY STUDIES	142
	5.5.1	KIDD 2 Site	143
	5.5.1.1	<i>Frost Heave Susceptibility</i>	143
	5.5.1.2	<i>Site Conditions</i>	145
	5.5.2	Massey Tunnel Site	146
	5.5.2.1	<i>Frost Heave Susceptibility</i>	147
	5.5.2.2	<i>Site Conditions</i>	148
5.6		PREDICTION OF THE GROUND FREEZING PROCESS	149
	5.6.1	Growth of the Frozen Radius	149
	5.6.2	Consumption of Liquid Nitrogen	149
5.7		GROUND FREEZING AND SAMPLING SYSTEM	150
5.8		PHASE II FIELDWORK	150
	5.8.1	Borehole Layout	151

5.8.2	Boreholes Advanced for Installation of the Freeze Pipe and Later Sampling.	151
5.8.3	Installation of Freeze Pipes	152
5.8.4	Mapping of Borehole Alignment	154
5.9	GROUND FREEZING AT THE MASSEY TUNNEL SITE	156
5.9.1	Initiation of Ground Freezing	156
5.9.2	Monitoring of Ground Temperatures During Freezing	156
5.9.3	Consumption of Liquid Nitrogen	157
5.9.4	Growth of the Frozen Radius	158
5.10	GROUND FREEZING AT THE KIDD 2 SITE	159
5.10.1	Initiation of Ground Freezing	159
5.10.2	Monitoring of Ground Temperatures During Freezing	160
5.10.3	Consumption of Liquid Nitrogen	160
5.10.4	Growth of the Frozen Radius	162
5.11	CORING OF IN-SITU FROZEN SAND	162
5.12	IN-SITU FROZEN CORE QUALITY	164
5.13	VOID RATIO MEASUREMENTS	171
5.14	VOID RATIOS DETERMINED FROM GEOPHYSICAL LOGGING	172
5.15	CONCLUSIONS	172
5.16	REFERENCES	174

Chapter 6.0

In-situ Ground Freezing and Sampling at the Phase III Event Site

6.1	INTRODUCTION	207
6.2	LOCATION OF UNDISTURBED SAMPLING	208
6.3	GROUND FREEZING FEASIBILITY STUDIES	209
6.3.1	Frost Heave Susceptibility	209
6.3.2	Site Conditions	211
6.4	PREDICTION OF GROUND FREEZING PROCESS	212
6.4.1	Growth of Frozen Radius	212
6.4.2	Consumption of Liquid Nitrogen	212
6.5	PHASE III GROUND FREEZING AND SAMPLING SYSTEM	213
6.5.1	Installation of Freeze Pipe	213
6.5.2	Borehole Layout	214
6.6	GROUND FREEZING AT THE PHASE III EVENT SITE	215
6.6.1	Initiation of Ground Freezing	215
6.6.2	Consumption of Liquid Nitrogen	215
6.6.3	Monitoring of Ground Temperatures During Freezing	216
6.7	COMPARISON OF THEORETICAL PREDICTIONS WITH FIELD CONDITIONS	216
6.7.1	Growth of Frozen Radius	216

6.7.2	Consumption of Liquid Nitrogen	217
6.8	CORING OF IN-SITU FROZEN SAND	218
6.9	IN-SITU FROZEN CORE QUALITY	219
6.10	COMPARISON OF IN-SITU FROZEN CORE AND GEOPHYSICAL LOGGING VOID RATIOS	225
6.11	CONCLUSIONS	225
6.12	REFERENCES	226

Chapter 7.0

Thawing Protocol for Undisturbed In-Situ Frozen Specimens

7.1	INTRODUCTION	247
7.2	FREEZING PROCESS	249
7.3	DISTURBANCE DURING THAWING	250
	7.3.1 Thawing Methodology	250
	7.3.2 Degree of Saturation	251
7.4	IN-SITU STRESS CONDITIONS DURING FREEZING AND SAMPLING	254
7.5	STRESS CONDITIONS DURING THAWING	257
	7.5.1 Stresses Induced in the Triaxial Cell	257
	7.5.2 Finite Element Analysis of Thawing in the Triaxial Cell	260
7.6	LABORATORY THAWING PROTOCOL STUDY	264
	7.6.1 Reconstituted Specimens	265
	7.6.2 Undisturbed Specimens	274
7.7	CALCULATION OF VOID RATIO CHANGES DURING THAWING	276
	7.7.1 Saturated Specimens	277
	7.7.2 Unsaturated Specimens	281
	7.7.3 Source of Errors Involved in Void Ratio Determination	281
7.8	TEST RESULTS	283
	7.8.1 Reconstituted Specimens	283
	7.8.2 Undisturbed Specimens	285
7.9	CONCLUSIONS	288
7.10	REFERENCES	291

Chapter 8.0

Conclusions and Recommendations

8.1	CONCLUSIONS	315
8.2	RECOMMENDATIONS FOR FURTHER RESEARCH	323

Appendices:

Appendix A	
<i>Data Obtained From Freezing Experiments</i>	327
Appendix B	
<i>Phase I Test Site Ground Freezing Data.</i>	370
Sample calculations regarding void ratio changes due to unfrozen water freezing in place at colder temperatures	401
Appendix C	
<i>Phase II Test Site Ground Freezing Data.</i>	405
Appendix D	
<i>Phase III Test Site Ground Freezing Data.</i>	433
Appendix E	
<i>Thaw Protocol and Laboratory Testing Data.</i>	447
Sample calculations are provided in Appendix E as follows:	
CSS8 Specimen Data Sheet with Void Ratio Calculations.	464
CSS9 Specimen Data Sheet with Void Ratio Calculations.	465
CSS11 Specimen Data Sheet with Void Ratio Calculations.	466
CSS14 Specimen Data Sheet with Void Ratio Calculations.	467
CSS15 Specimen Data Sheet with Void Ratio Calculations.	468
CSS17 Specimen Data Sheet with Void Ratio Calculations.	469
SS1 Specimen Data Sheet with Void Ratio Calculations.	470
SS2 Specimen Data Sheet with Void Ratio Calculations.	471
SS3 Specimen Data Sheet with Void Ratio Calculations.	472
SS4 Specimen Data Sheet with Void Ratio Calculations.	473
SS7 Specimen Data Sheet with Void Ratio Calculations.	474
SS8 Specimen Data Sheet with Void Ratio Calculations.	475
Undisturbed Specimen FS4C14A Data Sheet with Void Ratio Calculations.	476
Undisturbed Specimen FS3C17B Data Sheet with Void Ratio Calculations.	477
Undisturbed Specimen FS5C14 Data Sheet with Void Ratio Calculations.	478
Reconstituted Specimen FS5C14R Data Sheet with Void Ratio Calculations.	479
Undisturbed Specimen FS5C10A Data Sheet with Void Ratio Calculations.	480
Undisturbed Specimen FS4C16-2 Data Sheet with Void Ratio Calculations.	481
Appendix F	
<i>Costs Associated with In-Situ Ground Freezing at Each Test Site.</i>	482

List of Tables

Table 4-1:	Summary of Fines Content Determined for Split Spoon Samples Taken at the Phase I Test Site	120
Table 4-2:	Summary of Fines Content Determined for Split Spoon Samples Taken at the Phase I Test Site.	121
Table 4-3:	Estimated Mineral Content for Split Spoon Samples Taken at the Phase I Test Site	121
Table 4-4:	Summary of Sample Borehole Deflections	122
<hr/>		
Table 5-1:	Mineralogy of the Fine Fraction at the KIDD 2 Test Site (based on area of the major x-ray reflections in percentage).	176
Table 5-2:	Mineralogy of the Fine Fraction at the Massey Tunnel Test Site (based on area of the major x-ray reflections in percentage).	177
Table 5-3:	Input Parameters used for Prediction of the Freezing Process at the Phase II Test Sites	177
<hr/>		
Table 6-1:	Mineralogy of Fines Fraction	229
Table 6-2:	Input Parameters for Prediction of Freezing Process	229
<hr/>		
Table 7-1:	Summary of Void Ratio Changes During Thawing of Undisturbed Specimens, Recovered from the CANLEX Test Sites, under an Effective Stress of 20 kPa.	294
<hr/>		
Table A1:	Ice Bulb Radii Measured During Field Experiments.	328
Table A2:	Liquid Nitrogen Consumption During Field Experiments	329
Table A3:	Spread Sheet used for Freezing Predictions during Experiment #1.	330
Table A4:	Actual Freezing Data gathered during Experiment #1.	331
Table A5:	Spread Sheet used for Revised Freezing Predictions during Experiment #1, assuming 2/3 Liquid and 1/3 gas nitrogen.	332
Table A6:	Spread Sheet used for Freezing Predictions during Experiment #2.	333
Table A7:	Actual Freezing Data gathered during Experiment #2.	334
Table A8:	Spread Sheet used for Freezing Predictions during Experiment #3.	335
Table A9:	Actual Freezing Data gathered during Experiment #3.	336
Table A10:	Spread Sheet used for Freezing Predictions during Experiment #4.	337
Table A11:	Actual Freezing Data gathered during Experiment #4.	338
Table A12:	Spread Sheet used for Revised Freezing Predictions during Experiment #4, assuming 1/3 Liquid and 2/3 gas nitrogen.	339
Table A13:	Spread Sheet used for Freezing Predictions during Experiment #5.	340
Table A14:	Actual Freezing Data gathered during Experiment #5.	341
Table A15:	Spread Sheet used for Freezing Predictions during Experiment #6.	342

Table A16:	Actual Freezing Data gathered during Experiment #6.	343
Table A17:	Spread Sheet used for Revised Freezing Predictions during Experiment #6, assuming (2/4.4)m Liquid and (2.4/4.4)m gas nitrogen.	344
Table A18:	Temperature Data gathered during Experiment #1.	346
Table A19:	Temperature Data gathered during Experiment #2.	349
Table A20:	Temperature Data gathered during Experiment #3.	353
Table A21:	Temperature Data gathered during Experiment #4.	357
Table A22:	Temperature Data gathered during Experiment #5.	361
Table A23:	Temperature Data gathered during Experiment #6.	365

Table B1:	Summary of Normalized In-Situ Testing Data.	371
Table B2:	Summary of Sample Borehole Deflections.	371
Table B3:	Temperature Data Recorded at 27 m in Each Sample Borehole.	372
Table B4:	Temperature Data Recorded in RTD Boreholes.	373
Table B5:	Liquid Nitrogen Consumption during Ground Freezing.	374
Table B6:	Phase I Test Site - Frozen Core Catalogue.	375

Table C1:	RTD Ground Temperature Data at the KIDD 2 Site.	406
Table C2:	RTD Ground Temperature Data at the Massey Tunnel Site.	407
Table C3:	KIDD 2 Site core catalogue.	408
Table C4:	KIDD 2 Site Trimmed Frozen Core Samples.	412
Table C5:	Massey Tunnel Site core catalogue.	413

Table D1:	Spread Sheet used for Ground Freezing Predictions at the Phase III Test Site.	434
Table D2:	RTD Ground Temperature Data obtained at the Phase III Test Site.	435
Table D3:	Catalogue of 100 mm diameter Frozen Core.	439
Table D4:	Catalogue of 200 mm diameter Frozen Core.	440

Table E1:	Reconstituted CSS Specimen Summary Sheet.	448
Table E2:	Reconstituted SS Specimen Summary Sheet.	449
Table E3:	Summary of Reconstituted Specimen Void Ratio Changes.	450
Table E4:	Comparison of Void Ratio Changes for Reconstituted Specimens Thawed Under the In-Situ Stress or a Small Effective Stress.	451
Table E5:	Undisturbed Phase I Specimen Summary Sheet.	452
Table E6:	Specimen Summary Data Sheet from UBC.	453
Table E7:	Void Ratio Changes from Initial to Steady State Conditions.	454

Table F1:	Costs Associated with Carrying out In-Situ Ground Freezing at the Phase I test site.	483
Table F2:	Costs Associated with Sample Collection and Handling at the Phase I Test Site.	483
Table F3:	Costs Associated with Carrying out In-Situ Ground Freezing at the Phase II KIDD 2 and Massey Tunnel test sites.	484
Table F4:	Costs Associated with Sample Collection and Handling at the Phase II KIDD 2 and Massey Tunnel Test Sites.	484
Table F5:	Costs Associated with Carrying out In-Situ Ground Freezing at the Phase III test site.	485
Table F6:	Costs Associated with Sample Collection and Handling at the Phase III Test Site.	485

List of Figures

Figure 1.1:	Typical Steady State Line in $e - \ln p'$ Space	20
Figure 1.2:	Behaviour of Sand Subject to Monotonic Undrained Triaxial Compression (modified from Robertson and Fear, 1995)	20
Figure 1.3:	Schematic Diagram of the Ultimate States of Sand in 3-Dimensional Space	21
Figure 2-1:	Schematic of Freeze Pipe System	46
Figure 2-2:	Surface Area Criteria Plot for Evaluation of Frost Heave Susceptibility (modified from Davila, et al. 1992)	47
Figure 2-3:	Schematic Illustration of Impeded Drainage of Unfrozen Water Surrounding Clay Minerals in a Sand Sample.	47
Figure 2-4:	Effect of Overburden Stress on Volumetric Expansion during Freezing (modified from Konrad, 1990)	48
Figure 2-5:	Typical Temperature Profile through Frozen and Unfrozen Soil Surrounding a Freeze Pipe (modified from Sanger and Sayles, 1979).	48
Figure 2-6:	Theoretical Prediction of the Growth of a Frozen Column around a Freeze Pipe for Different Initial Ground Temperatures.	49
Figure 2-7:	Theoretical Prediction of Liquid Nitrogen Consumption during Freezing of a Column of Sand around a Freeze Pipe.	49
Figure 3-1:	Schematic of the Cased Borehole showing Typical Freeze Pipe Configuration.	75
Figure 3-2:	Dimensions of the Frozen Zone Recorded for Experiment 1.	76
Figure 3-3:	Comparison of Predicted Frozen Radius with Actual Maximum and Minimum Frozen Radii attained in Experiment 1.	77
Figure 3-4:	Comparison Between Predicted and Actual Liquid Nitrogen Consumption during Experiment 1.	77
Figure 3-5:	Frozen Radius Prediction for both Liquid and Gas Nitrogen in Freeze Pipe during Experiment 1.	78
Figure 3-6:	Liquid Nitrogen Consumption Prediction for both Liquid and Gas Nitrogen in Freeze Pipe during Experiment 1.	78
Figure 3-7:	Dimensions of the Frozen Zone Recorded for Experiment 2.	79
Figure 3-8:	Comparison of Predicted Frozen Radius with Actual Maximum and Minimum Frozen Radii attained in Experiment 2.	80
Figure 3-9:	Comparison Between Predicted and Actual Liquid Nitrogen Consumption during Experiment 2.	80
Figure 3-10:	Dimensions of the Frozen Zone Recorded for Experiment 3.	81
Figure 3-11:	Comparison of Predicted Frozen Radius with Actual Maximum and Minimum Frozen Radii attained in Experiment 3.	82

Figure 3-12:	Comparison Between Predicted and Actual Liquid Nitrogen Consumption during Experiment 3.	82
Figure 3-13:	Dimensions of the Frozen Zone Recorded for Experiment 4.	83
Figure 3-14:	Comparison of Predicted Frozen Radius with Actual Maximum and Minimum Frozen Radii attained in Experiment 4.	84
Figure 3-15:	Comparison Between Predicted and Actual Liquid Nitrogen Consumption during Experiment 4.	84
Figure 3-16:	Frozen Radius Prediction for both Liquid and Gas Nitrogen in Freeze Pipe during Experiment 4.	85
Figure 3-17:	Liquid Nitrogen Consumption Prediction for both Liquid and Gas Nitrogen in Freeze Pipe during Experiment 4.	85
Figure 3-18:	Dimensions of the Frozen Zone Recorded for Experiment 5.	86
Figure 3-19:	Comparison of Predicted Frozen Radius with Actual Maximum and Minimum Frozen Radii attained in Experiment 5.	87
Figure 3-20:	Comparison Between Predicted and Actual Liquid Nitrogen Consumption during Experiment 5.	87
Figure 3-21:	Dimensions of the Frozen Zone Recorded for Experiment 6.	88
Figure 3-22:	Comparison of Predicted Frozen Radius with Actual Maximum and Minimum Frozen Radii attained in Experiment 6.	89
Figure 3-23:	Comparison Between Predicted and Actual Liquid Nitrogen Consumption during Experiment 6.	89
Figure 3-24:	Frozen Radius Prediction for both Liquid and Gas Nitrogen in Freeze Pipe during Experiment 6.	90
Figure 3-25:	Liquid Nitrogen Consumption Prediction for both Liquid and Gas Nitrogen in Freeze Pipe during Experiment 6.	90

Figure 4-1:	Plan View of Phase I Test Site.	123
Figure 4-2:	Grain Size Curve for Split Spoon Sample Obtained at 25.91 m.	124
Figure 4-3:	Surface Area Criteria Plot for Evaluating Frost Heave Susceptibility (modified from Davila et al., 1992).	124
Figure 4-4:	Frost Heave Test Results for Sample with 15.2 % Fines.	125
Figure 4-5:	Frost Heave Test Results for Sample with 6.2 % Fines.	125
Figure 4-6:	Phase I Test Site Considering Different Initial Groundwater Temperatures	126
Figure 4-7:	Effect of Seepage Flow on Frozen Zone (modified from Hashemi and Sliepcevich, 1973)	126
Figure 4-8:	Predicted Volume of Liquid Nitrogen Required to Freeze a 1 m Radius Column of Sand at the Phase I Test Site Considering Different Initial Groundwater Temperatures.	127
Figure 4-9:	Schematic of Borehole Layout for Freezing and Sampling,	128
Figure 4-10:	Plan View Showing Proposed Freeze Pipe Layout and Sample Borehole Layout at the Phase I Test Site.	129
Figure 4-11:	As Built Cross, Section of Freeze Pipe and Sample Boreholes.	130

Figure 4-12:	Schematic Diagram of Freeze Pipe System used at the Phase I Test Site.	131
Figure 4-13:	Site Plan Showing Final Borehole Locations.	132
Figure 4-14:	Disturbance Caused by Installation of Freeze Pipe (modified from Yoshimi et al., 1978)	132
Figure 4-15:	Ground Temperatures Measured During Ground Freezing at Sample Borehole and RTD Borehole Locations at a depth of 27 m.	133
Figure 4-16:	Ground Temperatures Measured During Ground Freezing at Borehole RTD1 through Target Zone.	133
Figure 4-17:	Actual Liquid Nitrogen Consumption during Ground Freezing at Phase I Test Site.	134
Figure 4-18:	Comparison of Actual and Predicted Growth of the Frozen Radius assuming Freeze Pipe Reservoir Contained Liquid Nitrogen at all times.	135
Figure 4-19:	Comparison of Actual and Predicted Consumption of Liquid Nitrogen assuming Freeze Pipe Reservoir Contained Liquid Nitrogen at all times.	135
Figure 4-20:	Comparison of Actual and Predicted Consumption of Liquid Nitrogen assuming Freeze Pipe Reservoir Contained 2/3 Liquid Nitrogen and 1/3 Gaseous Nitrogen.	136
Figure 4-21:	Comparison of Actual and Predicted Growth of Frozen Radius assuming Freeze Pipe Reservoir Contained 2/3 Liquid Nitrogen and 1/3 Gaseous Nitrogen.	136
Figure 4-22:	Comparison of Actual and Predicted Consumption of Liquid Nitrogen assuming Freeze Pipe Reservoir Contained 2/3 Liquid Nitrogen and 1/3 Gaseous Nitrogen followed by only Liquid Nitrogen after 192 hrs.	137
Figure 4-23:	Comparison of Actual and Predicted Growth of Frozen Radius assuming Freeze Pipe Reservoir Contained 2/3 Liquid Nitrogen and 1/3 Gaseous Nitrogen followed by only Liquid Nitrogen after 192 hrs.	137
Figure 4-24:	Comparison of In, Situ Void Ratios determined from Frozen Core Samples and from Geophysical Logging.	138
<hr/>		
Figure 5-1:	Phase II Site Location Plan	178
Figure 5-2:	KIDD 2 Site Location Plan	179
Figure 5-3:	Massey Tunnel Site Location Plan	180
Figure 5-4:	Target Zones for Characterization and Sampling.	181
Figure 5-5:	Sand Grain Size Distributions at the Phase II Test Sites.	182
Figure 5-6:	Surface Area Critical Plot for Evaluation of Frost Heave Susceptibility (modified from Davila et al., 1992).	183
Figure 5-7:	Predicted Growth of Frozen Radius at the Phase II Test Sites.	184

Figure 5-8:	Predicted Liquid Nitrogen Consumption at the Phase II Test Sites.	184
Figure 5-9:	Detailed Characterization Zone at the KIDD 2 Site.	185
Figure 5-10:	Detailed Characterization Zone at the Massey Tunnel Site.	185
Figure 5-11:	Alignment of Sampling Boreholes at the Massey Tunnel Site.	186
Figure 5-12:	Alignment of Sampling Boreholes at the KIDD 2 Site.	186
Figure 5-13:	RTD Temperature Measurements Recorded at the Massey Tunnel Site at a 0.6 m Radius.	187
Figure 5-14:	RTD Temperature Measurements Recorded at the Massey Tunnel Site at a 1.0 m Radius.	187
Figure 5-15:	Comparison of Actual and Predicted Liquid Nitrogen Consumption at the Massey Tunnel Site (initial groundwater temperature of 11.2 °C).	188
Figure 5-16:	Comparison of Actual and Predicted Predicted Freezing Time at the Massey Tunnel Site (initial groundwater temperature of 11.2 °C).	188
Figure 5-17:	RTD Temperature Measurements Recorded at the KIDD 2 Site at a 0.6 m Radius.	189
Figure 5-18:	RTD Temperature Measurements Recorded at the KIDD 2 Site at a 1.0 m Radius.	189
Figure 5-19:	Comparison of Actual and Predicted Liquid Nitrogen Consumption at the KIDD 2 Site (initial groundwater temperature of 9.6 °C).	190
Figure 5-20:	Comparison of Actual and Predicted Predicted Freezing Time at the KIDD 2 Site (initial groundwater temperature of 9.6 °C).	190
Figure 5-21:	In-Situ Frozen Core Sample obtained from Boreholes K94F3 and K94F2 at the KIDD 2 Site Exhibiting Fine Grain Vein Features.	191
Figure 5-22:	In-Situ Frozen Core Sample obtained from Borehole M94F5 at the Massey Tunnel Site Exhibiting Fine Grain Vein Features.	191
Figure 5-23:	In-Situ Frozen Core Sample obtained from Borehole M94F2 at the Massey Tunnel Site Exhibiting Fine Grain Vein Features.	192
Figure 5-24:	In-Situ Frozen Core Sample obtained from Borehole M94F6 at the Massey Tunnel Site Exhibiting Fine Grain Vein Features.	192
Figure 5-25:	Elemental Analysis of Clean Sand obtained from Frozen Core Samples at the KIDD 2 Site.	193
Figure 5-26:	Elemental Analysis of Native Fines Extracted from Frozen Core Samples at the KIDD 2 Site.	193
Figure 5-27a:	Elemental Analysis of Vein Material Extracted from Frozen Core Samples at the KIDD 2 Site.	194
Figure 5-27b:	Elemental Analysis of Vein Material Extracted from Frozen Core Samples at the KIDD 2 Site.	194
Figure 5-28:	Elemental Analysis of Clean Sand obtained from Frozen Core Samples at the Massey Tunnel Site.	195
Figure 5-29:	Elemental Analysis of Native Fines Extracted from Frozen Core Samples at the Massey Tunnel Site.	195

Figure 5-30a:	Elemental Analysis of Vein Material Extracted from Frozen Core Samples at the Massey Tunnel Site.	196
Figure 5-30b:	Elemental Analysis of Vein Material Extracted from Frozen Core Samples at the Massey Tunnel Site.	196
Figure 5-31:	Elemental Analysis of KIM Drilling Mud used at the KIDD 2 Site.	197
Figure 5-32:	Elemental Analysis of the Bentonite Drilling Mud used at the Massey Tunnel Site.	197
Figure 5-33:	Sites in the Fraser River Delta where Sand Dykes were Encountered (modified from Clague et al., 1992).	198
Figure 5-34:	Geological Profile of the KIDD 2 Site Based on PiezoCone Resistivity Logs (prepared by the Univerisity of British Columbia for CANLEX).	198
Figure 5-35:	Comparison of Void Ratios Determined from In-Situ Frozen Core and Geophysical Logging at the Phase II Test Sites.	199

Figure 6-1:	Phase III Test SiteSite	230
Figure 6-2:	Cone Penetration Test Profiles in Detailed Characterization Zone	231
Figure 6-3:	Fines Content Determined from SPT Samples in Detailed Characterization Zone	232
Figure 6-4:	Surface Area Criteria Plot for Evaluation of Frost Heave Susceptibility (modified from Davila et al., 1992)	233
Figure 6-5:	Frost Heave Test Results for Phase III Sand with 22 % Fines	234
Figure 6-6:	Ground Temperature Prior to Conducting In-Situ Ground Freezing.	235
Figure 6-7:	Prediction of Growth of Frozen Zone	236
Figure 6-8:	Prediction of Volume of Liquid Nitrogen	236
Figure 6-9:	Schematic of Freeze Pipe Installation	237
Figure 6-10:	Layout of Freeze Pipe and Sample Boreholes.	238
Figure 6-11:	Actual Liquid Nitrogen Consumption at Phase III Test Site	238
Figure 6-12:	RTD 1 Temperature Measurements at 1.0 m during Ground Freezing	239
Figure 6-13:	RTD 2 Temperature Measurements at 0.56 m during Ground Freezing	239
Figure 6-14:	Comparison of Actual Growth of the Frozen Radius with Predictions for Gaseous Nitrogen and Liquid Nitrogen in Freeze Pipe Reservoir	240
Figure 6-15:	Comparison of Actual Growth of the Frozen Radius with Prediction for 1/3 Gaseous Nitrogen and 2/3 Liquid Nitrogen in Freeze Pipe Reservoir	240
Figure 6-16:	Comparison of Actual Liquid Nitrogen Consumption with Predictions for Liquid Nitrogen in Freeze Pipe Reservoir	241

Figure 6-17:	Comparison of Actual Liquid Nitrogen Consumption with Prediction for 1/3 Gaseous Nitrogen and 2/3 Liquid Nitrogen in Freeze Pipe Reservoir	241
Figure 6-18:	Estimated Progression of the Freezing Front at the Phase III Test Site	242
Figure 6-19:	Porewater Attraction and Expulsion During Freezing as a Function of Effective Stress and Applied Step Temperature	242
Figure 6-20:	Comparison of Estimated Actual Progression of the Freezing Front at the Phase III Test Site with the Theoretical Prediction.	243
Figure 6-21:	Frost Heave Test Results for Sand from Specimen FS26C3-1 with Fines Added (modified from Arvidson, 1973).	244
Figure 6-22:	Comparison of In-Situ Void Ratios Determined from Frozen Core and Geophysical Logging at the Phase III Test Site	244
<hr/>		
Figure 7-1:	Estimated In-Situ Degree of Saturation for Phase I Undisturbed Specimens	294
Figure 7-2:	Estimated In-Situ Degree of Saturation for Phase II Undisturbed Specimens	295
Figure 7-3:	Estimated In-Situ Degree of Saturation for Phase III Undisturbed Specimens	295
Figure 7-4a:	Unfrozen Soil Element in Ground Under Anisotropic Stress Condition	296
Figure 7-4b:	Soil Element after In-Situ Ground Freezing	296
Figure 7-4c:	Frozen Soil Element Removed from the Ground	296
Figure 7-4d:	Apply In-Situ Stresses to Frozen Soil in Triaxial Cell	296
Figure 7-5a:	Unfrozen Soil Element in Ground Under Isotropic In-Situ Stress Condition	297
Figure 7-5b:	Soil Element after In-Situ Ground Freezing	297
Figure 7-5c:	Frozen Soil Element Removed from the Ground	297
Figure 7-5d:	Apply In-Situ Stresses to Frozen Soil in Triaxial Cell	298
Figure 7-5e:	Commence Thawing at Bottom of Specimen where Soil has Access to Pore Water at 50 kPa.	298
Figure 7-5f:	Apply Isotropic Stresses of 20 kPa to Frozen Soil in Triaxial Cell	298
Figure 7-5g:	Commence Thawing at Bottom of Specimen where Soil has Access to Pore Water at 0 kPa.	298
Figure 7-6a:	Stress Path Taken by Specimen Thawed under the In-Situ Effective Stress	299
Figure 7-6b:	Stress Path Taken by Specimen Thawed under a Small Effective Stress	299
Figure 7-7:	SIGMA/W Results, assuming Ice Acts Like a Viscous Pore Fluid, for Specimen Thawed Under a Small Effective Stress	300
Figure 7-8:	SIGMA/W Results, assuming Modulus of Frozen and Unfrozen Sand are Different, for Specimen Thawed Under the In-Situ Effective Stress	301

Figure 7-9:	SIGMA/W Results, assuming Modulus of Frozen and Unfrozen Sand are Different, for Specimen Thawed Under a Small Effective Stress	302
Figure 7-10:	SIGMA/W Results, Comparing Maximum Shear Strains for Specimens with High In-Situ Stresses, Thawed Under a Small Effective Stress or Under the In-Situ Effective Stress.	303
Figure 7-11:	Triaxial Cell Cooling Coil used to Prevent Premature Uncontrolled Thawing of Reconstituted Specimens	304
Figure 7-12:	Comparison of Void Ratio Changes for Different Thawing Methodologies used on Reconstituted Syncrude Sand Specimens and the Effect of Degree of Saturation.	304
Figure 7-13:	Comparison of Void Ratio Changes during Thawing and Consolidation of Reconstituted Syncrude Sand Specimens Thawed under the In-Situ Effective Stress or under a Small Effective Stress.	305
Figure 7-14:	Comparison of Change in Void Ratio During Thawing and Consolidation of Undisturbed Phase I Specimens subject to the In-Situ Effective Stress or a Small Effective Stress during Thawing.	305
Figure 7-15:	Undrained Triaxial Compression Test Results for Undisturbed Specimen FS4C14A	306
Figure 7-16:	Undrained Triaxial Compression Test Results for Undisturbed Specimen FS3C17B	307
Figure 7-17:	Undrained Triaxial Compression Test Results for Undisturbed Specimen FS5C14	308
Figure 7-18:	Undrained Triaxial Compression Test Results for Undisturbed Specimen FS5C14R	309
Figure 7-19:	Undrained Triaxial Extension Test Results for Undisturbed Specimen FS5C10A	310
Figure 7-20:	Undrained Triaxial Compression Test Results for Undisturbed Specimen FS4C16-2	311
Figure 7-21a:	Stress Strain Curves Obtained for Specimens FS5C14, FS5C14R and FS3C17B, Illustrating Effect of Degree of Saturation.	312
Figure 7-21b:	Pore Pressure Response Curves Obtained for Specimens FS5C14, FS5C14R and FS3C17B, Illustrating Effect of Degree of Saturation.	312
Figure 7-22:	Summary of Stress Paths followed by Undisturbed Phase I Specimens during Undrained Triaxial Compression and Triaxial Extension Tests	313
Figure 7-23:	Steady State Diagram for Undisturbed Phase I Specimens	313
Figure 7-24:	Effective of Void Ratio Disturbance Caused by Thawing Undisturbed Phase I Specimens under a Small Effective Stress with Respect to the Steady State Line.	314

Figure A1:	Grain Size Curve for Sand Used in Experiments 5 at 1.7 m.	368
Figure A2:	Grain Size Curve for Sand Used in Experiments 5 at 1.9 m.	369
Figure B1:	CPT Profiles obtained at Phase I Test Site.	380
Figure B2:	Grain Size Curve obtained for Sample recovered at 18.29 m.	381
Figure B3:	Grain Size Curve obtained for Sample recovered at 19.81 m.	382
Figure B4:	Grain Size Curve obtained for Sample recovered at 21.34 m.	383
Figure B5:	Grain Size Curve obtained for Sample recovered at 22.86 m.	384
Figure B6:	Grain Size Curve obtained for Sample recovered at 25.91 m.	385
Figure B7:	Grain Size Curve obtained for Sample recovered at 27.43 m.	386
Figure B8:	Grain Size Curve obtained for Sample recovered at 30.48 m.	387
Figure B9:	Grain Size Curve obtained for Sample recovered at 36.58 m.	388
Figure B10:	Grain Size Curve obtained for Sample recovered at 24.38 m.	389
Figure B11:	Grain Size Curve obtained for Sample recovered at 28.96 m.	390
Figure B12:	Grain Size Curve obtained for Sample recovered at 32.00 m.	391
Figure B13:	Deflection Profile of Sample Borehole FS1.	392
Figure B14:	Deflection Profile of Sample Borehole FS2.	393
Figure B15:	Deflection Profile of Sample Borehole FS3.	394
Figure B16:	Deflection Profile of Sample Borehole FS4.	395
Figure B17:	Deflection Profile of Sample Borehole FS5.	396
Figure B18:	Deflection Profile of Sample Borehole RTD1.	397
Figure B19:	Deflection Profile of Sample Borehole RTD2.	398
Figure B20:	Deflection Profile of Sample Borehole RTD3.	399
Figure B21:	Frozen Cores Recovered from Sample Borehole FS1.	400
Figure B22:	Frozen Cores Recovered from Sample Borehole FS3.	401
Figure B23:	Frozen Cores Recovered from Sample Borehole FS4.	402
Figure B24:	Frozen Cores Recovered from Sample Borehole FS5.	403
Figure C1:	Alignment of Frozen Sample Boreholes at KIDD 2 Site.	417
Figure C2:	Deflection of Sample Borehole K94F1.	418
Figure C3:	Deflection of Sample Borehole K94F2.	419
Figure C4:	Deflection of Sample Borehole K94F3.	420
Figure C5:	Deflection of Sample Borehole K94F4.	421
Figure C6:	Deflection of Sample Borehole K94F5.	422
Figure C7:	Deflection of Sample Borehole K94F7.	423
Figure C8:	Alignment of Frozen Sample Boreholes at Massey Tunnel Site.	424
Figure C9:	Deflection of Freeze Pipe Borehole at Massey Tunnel Site.	425
Figure C10:	Deflection of Sample Borehole M94F1.	426
Figure C11:	Deflection of Sample Borehole M94F2.	427
Figure C12:	Deflection of Sample Borehole M94F4.	428
Figure C13:	Deflection of Sample Borehole M94F5.	429
Figure C14:	Deflection of Sample Borehole M94F6.	430

Figure C15:	Deflection of Sample Borehole M94S1.	431
Figure C16:	Deflection of Sample Borehole M94S2.	432
<hr/>		
Figure D1:	Grain Size Curves Obtained from Split Spoon Samples recovered from Borehole SPT1.	442
Figure D2:	Grain Size Curves Obtained from Split Spoon Samples recovered from Borehole SPT2.	443
Figure D3:	Grain Size Curves Obtained from Split Spoon Samples recovered from Borehole SPT3.	444
Figure D4:	Grain Size Curves Obtained from FS26 C3-1.	445
Figure D5:	Grain Size Curves Obtained from FS4 C1-3.	446
<hr/>		
Figure E1:	Grain Size Curve for CSS Sand.	455
Figure E2:	Triaxial Cell Thawing Base.	456
Figure E3:	CSS8 Specimen Void Ratio Change Plot.	457
Figure E4:	CSS9 Specimen Void Ratio Change Plot.	457
Figure E5:	CSS11 Specimen Void Ratio Change Plot.	458
Figure E6:	CSS14 Specimen Void Ratio Change Plot.	458
Figure E7:	CSS15 Specimen Void Ratio Change Plot.	459
Figure E8:	CSS17 Specimen Void Ratio Change Plot.	459
Figure E9:	CSS18 Specimen Void Ratio Change Plot.	460
Figure E10:	SS1 Specimen Void Ratio Change Plot.	460
Figure E11:	SS2 Specimen Void Ratio Change Plot.	461
Figure E12:	SS3 Specimen Void Ratio Change Plot.	461
Figure E13:	SS4 Specimen Void Ratio Change Plot.	462
Figure E14:	SS7 Specimen Void Ratio Change Plot.	462
Figure E15:	SS8 Specimen Void Ratio Change Plot.	463
<hr/>		

List of Photographs

Photo 3-1:	Frozen Zone Obtained From Experiment 2.	73
Photo 3-2:	Frozen Zone Obtained From Experiment 4.	73
Photo 3-3:	Frozen Zone Obtained From Experiment 6.	74
<hr/>		
Photo 5-1:	150 mm Diameter CRREL Core Barrel Used to Recover Samples of In-Situ frozen Sand from the Phase II Test Sites.	200
Photo 5-2:	Hydraulic Extruder used to Remove In-Situ Frozen Core from the CRREL Core Barral.	200
Photo 5-3:	In-Situ frozen Core Sample Obtained from the Massey Tunnel Site - shown after Extrusion into an Insulated Box Containing Dry Ice.	201
Photo 5-4:	In-Situ Frozen Core Stored in a Freezer for Transportation from the Site to the University of Alberta.	201
Photo 5-5:	Fine Grain Vein Feature Encountered in In-Situ frozen Core Sample M94F6-C7A Obtained from the Massey Tunnel Site.	202
Photo 5-6:	Fine Grain Vein Feature Encountered in In-Situ frozen Core Sample M94F5-C2C Obtained from the Massey Tunnel Site.	202
Photo 5-7:	SEM Image of Fine Grain Vein Feature Encountered in In-Situ frozen Core Sample from the KIDD 2 Site.	203
Photo 5-8:	SEM Image of Fine Grain Vein Feature Encountered in In-Situ frozen Core Sample from the Massey Tunnel Site.	203
Photo 5-9:	SEM Image of Platey Clay Minerals Comprising Fine Grain Vein Feature at the KIDD 2 Site.	204
Photo 5-10:	SEM Image of Platey Clay Minerals Comprising Fine Grain Vein Feature at the Massey Tunnel Site.	204
Photo 5-11:	SEM Image of Reconstituted Sand Sample Subject to Freezing Cycles showing Alignment of the Thin Clay Mineral Edge Perpendicular to the Freeze Front.	205
Photo 5-12:	SEM Image of Reconstituted Sand Sample Subject to Freezing Cycles showing a Clay Mineral Particle Aligned with an Ice Grain Boundary.	205
Photo 5-13:	SEM Image of Reconstituted Sand Sample Subject to Freezing Cycles showing Clay Mineral Particles Aligned both Perpendicular and Parallel to the Freezing Front.	206
<hr/>		
Photo 6-1:	SEM Image of In-Situ Frozen Specimen FS26C3-1	245
Photo 6-2:	SEM Image of In-Situ Frozen Specimen FS4C1-3	245
Photo 6-3:	SEM Image of Clay Particle Alignment Found in MFT (after Alberta Department of Energy, Oil Sands and Research Division, 1995).	246
<hr/>		

List of Symbols:

A	cross-sectional area (m^2)
A_s	frozen area after setup (m^2)
A_t	area of specimen after thawing (m^2)
A_u , A	pore pressure coefficient
A_o	initial cross-sectional area (m^2)
a_r	factor, which when multiplied by R, defines the zone of influence of freeze pipe outside frozen column (generally, $a_r=3.0$)
B	pore pressure coefficient
C_f	volumetric heat capacity of the frozen soil ($J/m^3 \text{ } ^\circ K$)
C_{GN2}	volumetric heat capacity of gaseous nitrogen ($kJ/m^3 \text{ } ^\circ K$)
CM	clay content of the soil expressed as a percentage of the total weight of the soil (%)
CM_f	clay mineral content as a percentage by weight of the clay particles in the clay fraction (%)
C_u	volumetric heat capacity of the unfrozen soil ($J/m^3 \text{ } ^\circ K$)
e	void ratio
e_c	void ratio after consolidation of frozen specimen
e_f	final void ratio
e_o	initial void ratio
e_s	void ratio after setup of frozen specimen
e_t	void ratio after thawing of frozen specimen
ϵ_{ax}	axial thermal strain
ϵ_r	radial thermal strain
E_{ufz}	unfrozen elastic modulus (MPa)
G_{ice}	specific gravity of ice (0.917)
G_s	specific gravity of solids
h	height (m)
Δh	change in height (m)
Δh_c	change in specimen height due to consolidation (m)
Δh_m	change in specimen height due to multidirectional thawing (m)
Δh_u	change in specimen height due to unidirectional thawing (m)
γ_d	dry density of the soil (kg/m^3)
γ_{max}	maximum shear strain
γ_w	unit weight of water (kg/m^3)
k_f	thermal conductivity of the frozen soil ($J/sm \text{ } ^\circ K$)
k_o	coefficient of earth pressure at rest
k_u	thermal conductivity of the unfrozen soil ($J/sm \text{ } ^\circ K$)
I_{SSA}	$= S_c/S_f$
L	volumetric latent heat of fusion (J/m^3)
L	latent heat of fusion (334 kJ/kg)
L	thickness of zone of groundwater flow (m)

L_l	the total latent heat and volumetric heat capacity expressed as a specific energy, which when multiplied by the frozen volume gives the same total as the two calculated separately (J/m^3)
L_{LN2}	latent heat of liquid nitrogen (199 kJ/Mg)
M_f	frozen mass (g)
Ω_z	surface area index
p_i	pore ice pressure (kPa)
P_o	stress defining the boundary between pore water expulsion and pore water attraction (kPa)
p_w	pore water pressure (kPa)
Q	total heat extracted from the ground (J/m length of freeze pipe)
Q_{GN2}	total heat extracted by the volumetric heat capacity of the gaseous nitrogen (J/m length of freeze pipe)
Q_{LN2}	total heat extracted by the latent heat of liquid nitrogen (J/m length of freeze pipe)
$Q(R)$	total groundwater flow (m^2/s m thickness)
r_c	size of the largest continuous pore openings through the soil and the maximum radius which an ice-water interface can have if the interface is to advance through the pore system (m)
r_{iw}	radius of the ice-water interfaces in the pore spaces (m)
r_o	radius of the freeze pipe (m)
ρ_d	dry density of soil (g/m^3)
$(\rho_d)_f$	total frozen density (g/m^3)
ρ_w	density of water (g/m^3)
R	frozen radius (m)
S_c	specific surface area of the fraction of the soil with a mean particle diameter smaller than $2 \mu m$ (m^2/g)
S_f	specific surface area of the fraction of the soil with a mean particle diameter smaller than $74 \mu m$ (m^2/g)
S_r	degree of saturation
σ'	effective stress (kPa)
$\Delta\sigma_1$	change in maximum principal stress (kPa)
$\Delta\sigma_3$	change in minimum principal stress (kPa)
σ_{ice}	pressure in the pore ice (kPa)
σ_{iw}	ice-water surface tension (0.03 N/m)
σ_{vo}'	in-situ vertical effective stress (kPa)
t	time required to freeze a given radius of soil (s)
T	T is the absolute temperature ($^{\circ}K$)
T_f	freezing temperature of water ($^{\circ}K$)
T_{fp}	skin temperature of freeze pipe ($^{\circ}K$)
T_o	initial temperature of ground ($^{\circ}K$)
T_o	normal freezing point of water ($^{\circ}K$), which is equal to $273.15 - 0.0074P_i$ (MPa)
τ_{max}	maximum shear stress (kPa)

v_o	difference between the initial temperature of the ground and the freezing point of water ($^{\circ}\text{K}$)
$(v_o)_{\text{GN}_2}$	initial temperature of the gaseous nitrogen ($^{\circ}\text{K}$)
$(v_o)_{\text{LN}_2}$	initial temperature of the liquid nitrogen ($^{\circ}\text{K}$)
v_s	difference between the skin temperature of the freeze pipe and freezing point of water ($^{\circ}\text{K}$)
Δv_g	increase in temperature of the gas nitrogen due to absorption of heat from the surrounding ground ($^{\circ}\text{K}$)
V	critical groundwater flow velocity (m/s)
V_{LN_2}	volume of liquid nitrogen required to freeze a given radius of soil (m^3 equivalent gaseous volume)
V_s	volume of solids (cm^3)
V_t	total volume of soil sample (cm^3)
V_v	volume of voids (cm^3)
V_w	molar volume of water (1000 cm^3/kg)
ΔV	change in pore water volume of a freezing soil (cm^3)
ΔV_c	volume change due to consolidation of thawed specimen (cm^3)
v	poisons ratio
W	total weight of soil
W_s	weight of solids
ω	water content (%)
ω_{ice}	ice content (%)
Z_v	finer mineralogy ratio

CHAPTER 1: Introduction

1.0 Introduction

In many areas in Canada and around the world, large structures such as dams, embankments, tailings impoundments, etc., are constructed on or with sand. Extensive natural sand deposits are also found along many coastal regions near major cities. Saturated loose sands can experience a large loss in shear strength (strain softening behaviour) when subject to rapid loading from events such as earthquakes, placement of fill or changes in groundwater conditions. This rapid collapse of the soil structure results in the development of high pore pressures under undrained conditions. In relatively loose sand deposits, this liquefaction phenomenon may result in catastrophic flow slides or large ground deformations causing loss of life and significant costs.

Sladen et al. (1985) define liquefaction as a phenomenon wherein a mass of soil loses a large percentage of shear resistance when subject to monotonic, cyclic or shock loading, and flows in a manner resembling liquid until the shear stresses acting on the mass of soil become less than the reduced shear resistance. Robertson (1994) distinguishes two main categories of liquefaction. The first type, flow liquefaction, may occur when loose granular soil is subject to either monotonic or cyclic undrained loading and experiences strain softening with an associated sudden increase in pore pressure resulting in collapse of the soil to its ultimate, or steady state, undrained shear strength. Flow failure may occur if the driving shear stresses are greater than the steady state undrained shear strength within a significant proportion of the deposit. The second type, cyclic liquefaction or cyclic softening, may occur as a result of undrained cyclic loading where shear stress reversal occurs resulting in a condition of zero effective stress. Deformations

during cyclic liquefaction may be very large, however, they usually stabilize once cyclic loading stops.

Evaluating whether or not a sand deposit has the potential to undergo a liquefaction failure in the event of adverse loading conditions, is an extremely important engineering task. Liquefaction assessment requires that the in-situ state of the deposit, including the in-situ values of void ratio, shear stress, and mean normal effective stress, be determined and compared with the ultimate or steady state condition that develops after significant deformation.

It will be shown that information regarding the in-situ state and the steady state conditions serves to indicate how the soil will behave under various loading conditions. In the next section, the framework for describing soil behaviour in terms of the potential for liquefaction will be reviewed, followed by a discussion of the information necessary to carry out a liquefaction assessment.

1.1 Framework for Describing Soil Behaviour

Laboratory testing has shown that the theoretical framework established for clay by Roscoe et al. (1958) can be adopted for sands. According to McRoberts and Sladen (1990), the steady state approach to evaluating the behaviour of sand is essentially the same as the critical state approach applied to clay. Based on laboratory testing of clay, glass beads and steel balls, Roscoe et al. (1958) noted that at the critical state, defined as the state of unlimited deformation at a constant effective normal stress, shear stress and void ratio, can be applied to the yielding of both clays and granular media. Sladen et al. (1985) present an excellent summary of the historical development of steady state concepts for granular soils and show that, for all practical purposes, the critical state and steady state can be considered as the same.

As demonstrated by numerous researchers (Castro, 1975, Sladen et al., 1985, Ishihara, 1993, Verdugo and Ishihara, 1996, among others), the effective stresses corresponding to the steady state condition are a function only of the initial void ratio. For a given sand, the steady state is attained after significant deformation has occurred that destroys the initial fabric, therefore, the steady state forms a reasonably unique line in void ratio (e) versus mean normal effective stress (p') space. As shown in Figure 1-1, the steady state line (SSL) is linear in e - $\ln(p')$ space over a limited stress range. Verdugo and Ishihara, 1996, also state that the SSL is independent of initial state conditions and stress history for a given sand. Therefore, since the SSL is independent of initial conditions, it can be established by conducting a series of triaxial tests on either specimens recovered from a site, that need not be undisturbed, or on reconstituted specimens of the same sand.

Evaluation of the flow liquefaction potential of a granular deposit requires not only determination of the SSL but also determination of the in-situ state of the soil with respect to the steady state conditions (Sladen et al., 1985 ; Verdugo and Ishihara, 1996). Loose sands, whose state in e - $\ln(p')$ space falls above the SSL, are contractant or strain softening (SS) at large strains when sheared undrained and are therefore prone to flow liquefaction. Dense sands, defined by a state which falls below the SSL, tend to be dilative or strain hardening (SH) at large strains and are not at risk of flow liquefaction, however, some deformation may occur during severe cyclic loading (Robertson, 1994). Laboratory testing of various sands by Ishihara (1993), and Tavenas and Leroueil (1987), has shown that medium dense sand specimens, with an initial state that falls just above the SSL, often exhibit a quasi-steady state behaviour, or limited strain softening (LSS), prior to reaching steady state at large strains. In this case, sand specimens subject to undrained triaxial compression tests initially behave in a contractive manner, up to moderate levels of strain, and then go through a phase transformation whereupon the behaviour becomes dilative. Figure 1-2, modified from Robertson and Fear (1995),

shows the various behavioural patterns of sands subject to undrained loading with different initial states.

Verdugo and Ishihara (1996), state that for a given sand it is useful to compare the SSL with the isotropic consolidation lines (ICL) defined for the loosest and densest states possible. As shown in Figure 1-1, the zone between the SSL and the loosest ICL represents the soil states where flow liquefaction can be triggered while the zone between the SSL and the densest ICL represents states where the soil is dilatent and cannot be triggered to undergo flow liquefaction by monotonic undrained loading. The factors which affect the actual flow liquefaction susceptibility of a soil deposit include material properties which govern the relative positions of these reference lines, hence the range of in-situ states where flow liquefaction could be triggered (Verdugo and Ishihara, 1996). These properties include grain size distribution, particle shape, particle hardness, fines content and fines plasticity. Similarly, according to Singh, et al. (1982), the cyclic liquefaction characteristics of sand deposits are a function of both material properties and site conditions, including void ratio, the structural arrangement of sand grains (fabric, mineralogy, and degree of cementation), seismic history, the in-situ lateral stress condition and the age of the deposit. Directly assessing the net effect of all of the above factors on the response of a sand to certain loading conditions requires appropriate laboratory testing of undisturbed samples.

Expanding on the concept of steady state, Sladen et al. (1985) presented a collapse surface approach to analyze the loss of limiting equilibrium that results from flow liquefaction. The collapse surface is defined in 3-dimensional e - p' - q space, where e is the void ratio, p' is the mean principal effective stress and q is the shear stress, and represents the soil state required for liquefaction to be triggered by an undrained load increment. The stress path up to the collapse surface may be either drained or undrained (Sasitharan et al., 1993; Sladen et al., 1985). The collapse surface, defined by a straight line passing through the peak undrained shear strength mobilized and the steady state shear strength

determined for soil samples with the same void ratio, represents the limit of stability if drainage is impeded under load controlled conditions. However, the post peak stress path can pass slightly above the collapse surface and therefore, it does not represent a state boundary (Sladen et al., 1985; Sasitharan et al., 1993, 1994). Both the collapse surface and state boundary surface with respect to the SSL are shown in 3-dimensional e - p' - q space in Figure 1-3.

According to Sladen et al. (1985), laboratory testing indicates that the collapse surface appears to be affected slightly by prior stress history, where the collapse surface is steeper for anisotropically consolidated specimens than for those that are isotropically consolidated. Therefore, if the collapse behaviour is a function of stress history, accurate assessment of flow liquefaction potential requires that undisturbed samples be obtained with the in-situ conditions preserved, both to determine the slope of the collapse surface and to compare the in-situ state with the steady state. Ultimately, the laboratory response of undisturbed specimens can also be linked with the results of field tests, such as Cone Penetration Testing (CPT) and Standard Penetration Testing (SPT), that can be carried out over a much greater area across a given site or within many sites containing sands with similar characteristics and geological history.

Unfortunately, obtaining high quality undisturbed samples of loose, saturated sand is often difficult, especially if conventional sampling techniques are utilized. In 1985, Sladen et al. noted that utilizing the collapse surface concept as a design tool is hampered by the lack of techniques available for confidently established the in-situ void ratio. Disturbance associated with conventional sampling may result in misleading laboratory test results, as will be discussed in the following sections. However, in the last approximately fifteen years, the technique of utilizing in-situ ground freezing for obtaining undisturbed samples of sand has been demonstrated to be effective by both Japanese and North American researchers.

This thesis has been undertaken to determine the subsoil and site conditions under which in-situ ground freezing is an appropriate methodology to obtain undisturbed samples. for the assessment of liquefaction potential. To avoid disturbance of the frozen samples once they have been recovered, the most appropriate method for thawing frozen specimens without causing disturbance of the in-situ void ratio or fabric was also evaluated. It will be shown that in-situ ground freezing is an excellent technique for obtaining high quality undisturbed samples from a wide range of granular deposits.

1.2 Disturbance Caused by Conventional Sampling

Conventional sampling of soils has generally been carried out utilizing thin walled tube samples or, in the case of stiff clays and dense cemented sands, by carefully trimming block samples. There are numerous sources of potential disturbance of the subsoil void ratio, fabric, structure, moisture content and stress history during sampling. These include:

- disturbance during drilling of the borehole,
- disturbance due to soil displacement during tube insertion.
- disturbance due to stress relief,
- disturbance when the soil sample is brought to the surface,
- disturbance during transportation of samples from the field to the laboratory.
- disturbance during storage of samples, and
- disturbance during preparation and laboratory testing of samples.

Broms (1980) provides a detailed discussion of the causes of sample disturbance due to tube sampling; Milovic (1970) and Iwasaki et al. (1977) describe some of the sources of tube sampling disturbance associated with block sampling. Hight (1993) and Hight and Georgiannou (1995), present detailed discussions regarding the effects of sample disturbance on the behaviour of clayey sands. Based on the work presented by these

authors, the various sources of sample disturbance due to conventional sampling and the ensuing effects on soil behaviour are summarized below.

Disturbance during drilling of the borehole.

The bottom of the borehole, where tube samples are normally recovered, may be severely disturbed by the drilling process in soft clays or loose sands. If the base of the borehole has not been cleaned thoroughly prior to sampling, the sample tube may contain material that has sloughed off the borehole sidewalls. Disturbance due to heaving at the bottom of the borehole may also occur if drilling fluid has not been used that is maintained at the same level as the groundwater surrounding the borehole. The various forms of disturbance associated with advancing boreholes tend to loosen or weaken the soil, resulting in reduced shear strength and stiffness.

Disturbance due to soil displacement as the sampling tube is inserted into the soil.

When a tube is pushed into soft clayey soils, the soil close to the wall of the sample tube is remolded, and therefore significantly disturbed. In soft clays pore water migration away from the center of the tube to the ends of the sample and away from disturbed zones usually occurs. It may be possible to trim away the disturbed zones if larger diameter tube samples can be recovered. In general, disturbance due to tube sampling can be reduced by following the recommendations provided by Hvorslev (1949) regarding outside and inside tube clearance ratios, however, it can not be completely eliminated.

Hight (1993) reviewed the strains that develop during sampler penetration into both clays and sands. Based on the strain path method of evaluating strains during undrained tube sampling (Baligh, 1985), the soil at the center line of a typical thin walled Shelby tube sampler, with a diameter to wall thickness ratio of 40, was subject to compressive strains in advance of the tube of 0.5 to 1.0 %, followed by extension strains of 0.5 to 1.0 % as the

soil entered the tube. The magnitude of these strains increased as the tube sidewall was approached. Laboratory testing conducted by Hight and Georgiannou (1995) on sand samples containing 5 to 15 % clay, indicated that compression strains of only 0.5 % during undrained tube sampling caused the clayey sand to undergo undrained yielding. Hight (1995) also showed that typical strains induced during sampling generally exceed yield strains in both sands and lightly overconsolidated clays of low plasticity.

According to Hight (1993), the initial fabric is disrupted due to both shear and volumetric strains that occur during drained tube sampling. In loose cemented sands, if sampling causes disruption of bonds, the small strain stiffness is reduced, while compaction of the sand grains may tend to increase stiffness and strength. Conversely, in dense cemented sands, disruption of bonds results in reduced stiffness and strength. In addition, according to Tokimatsu and Hosaka (1986), the shear stress history occurring during sampling may significantly reduce the undrained cyclic shear strength and modulus of sand samples. Yoshimi et al. (1994) showed that conventional sampling of dense sand causes loosening of the soil, thereby resulting in considerable underestimation of the liquefaction resistance (defined as the undrained cyclic shear strength). Antithetically, the liquefaction resistance of loose sand may be overestimated based on conventional tube samples since tube sampling tends to cause densification.

It follows from the above discussions, that it is not possible to recover completely undisturbed samples utilizing conventional sampling techniques.

Disturbance due to stress relief

Both tube sampling and cutting of block samples results in relief of the in-situ stresses. Pore pressure reduction accompanying stress relief can result in the release of previously dissolved pore gases which, in turn, may cause expansion of the soil. According to Broms (1980), the release of gas tends to reduce the undrained shear strength and the

stiffness of normally consolidated clays. In block samples of stiff clay, stress release may result in widening of fissures and therefore, increased compressibility and permeability as well as reduced shear resistance compared to the properties which exist in-situ.

It is commonly assumed that if samples are reconsolidated to the in-situ stress condition, the disturbance caused by stress relief may be reduced. However, laboratory tests conducted by Hight and Georgiannou (1995) showed that after undrained tube sampling reconsolidation of clayey sand results in significant reductions in void ratio which consequently increase the ultimate strength beyond that which exists in-situ.

Disturbance when the soil sample is brought to the surface.

As the sample is brought to the ground surface, pore pressures decrease. This may cause the release of previously dissolved gas that can loosen the soil fabric and therefore affect the stress strain behaviour.

Disturbance during transportation of the samples from the field to the laboratory.

Vibrations during transportation may cause pore water migration or the development of elevated pore pressures in a manner similar to the excess pore pressure caused by cyclic loading. In very loose sand samples, vibrations due to transportation may cause cyclic liquefaction. Laboratory tests have shown that vibrations and shock loading resulted in a reduction of shear strength compared to undisturbed specimens (Broms, 1980), thereby indicating disturbance of the soil structure. In relatively free draining soils, disturbance due to transportation can be avoided by freezing the samples unidirectionally prior to removing them from the site.

Disturbance during storage of samples.

Storage of samples that are not adequately sealed will result in changes in moisture content. In clays, reduction of the residual pore pressure during storage results in a reduction of the shear strength, probably due to relaxation of the soil structure as negative pore pressures dissipate. In clayey sands reduction of the residual pore water suction due to drying and/or stress relaxation may result in loss of sample integrity upon extrusion (Hight and Georgiannou, 1995).

Disturbance during preparation and testing of samples.

In relatively soft clay soils, the force required to extrude the sample may exceed the unconfined compressive strength, thereby causing yielding of the soil prior to laboratory testing. Extrusion of loose sand samples may also result in excessive disturbance and, if the sand has undergone drying, a complete loss of sample integrity may occur. Trimming of silty soils may result in "tearing" along the sample perimeter. Stress relief that occurs during trimming of block samples obtained from stiff clay, may result in further opening of fissures thereby affecting the compressibility, permeability and shear strength of the soil.

The above discussion regarding the various sources of sample disturbance highlight how difficult it can be to determine the in-situ shear strength and deformation characteristics utilizing conventional sampling methods. However, it has been shown that evaluation of the liquefaction potential of a particular granular deposit not only requires determination of the SSL or the collapse line, but also requires that undisturbed samples be obtained from the deposit for both void ratio determination and carrying out laboratory tests to determine the actual strength and deformation characteristics associated with the in-situ state. The technique of utilizing in-situ ground freezing to obtain highly undisturbed samples of granular soil will be presented in the following section as an alternative to conventional sampling.

1.3 Undisturbed Sampling by In-Situ Ground Freezing

In the past, in-situ ground freezing was undertaken primarily for control of loose granular soils and groundwater flow during construction of tunnels, access shafts and excavations. In these cases local ground disturbance was not usually a concern and ground freezing was undertaken by circulation of a coolant through a number of closely spaced freeze pipes. This configuration of closely spaced freeze pipes resulted in impeded drainage of pore water in advance of the freezing front, causing frost heave disturbance. However, in the appropriate subsoils, disturbance due to frost heave can be avoided by carrying out radial ground freezing from a single freeze pipe, whereby pore water drainage is unimpeded.

Several authors, including Yoshimi et al. (1977 and 1978), Yoshimi et al. (1984, 1994), Tokimatsu and Hosaka (1986), Hatanaka et al. (1985 and 1995), and Singh et al. (1982) have shown that in-situ ground freezing, under conditions of unimpeded drainage, followed by coring of the frozen sand, is a much more effective way of obtaining undisturbed samples of sand compared to conventional tube sampling. Yoshimi (1978), Singh et al. (1982) and Seed et al. (1982) have shown that the undrained static or cyclic shear strength of a sand was not affected by one freeze-thaw cycle, provided that disturbance did not occur during the freezing process due to impeded drainage. Konrad and St-Laurent (1995) showed that the stiffness characteristics, measured by the small strain modulus, are not affected by one freeze-thaw cycle. Yoshimi et al. (1977 and 1978) conducted a series of laboratory tests to study the conditions under which in-situ ground freezing is appropriate for obtaining undisturbed samples of cohesionless soils, including: soil type, surcharge, fines content and rate of cooling. The authors also showed that the mean stress and shear stress are not altered by the freezing process, provided that the overburden stress exceeds 15 kPa.

The subsoil and site conditions under which in-situ ground freezing can be used as a method of obtaining undisturbed samples of granular soil will be addressed in further detail in the following chapters of the thesis. The next section will describe the thesis objectives and the work undertaken.

1.4 Research Background and Thesis Objectives

The research conducted for this thesis was undertaken as part of the Canadian Liquefaction Experiment (CANLEX). The CANLEX project (List and Robertson, 1995) was established to evaluate various methods of characterizing sand deposits with respect to the potential for liquefaction. As part of this project, in-situ ground freezing was evaluated as a means of obtaining undisturbed samples of loose sand.

This thesis was undertaken to examine whether or not in-situ ground freezing, utilizing liquid nitrogen as the coolant, is generally an effective method of obtaining undisturbed samples of loose sand below the groundwater table. Ideally, if samples are to be considered as truly undisturbed, the void ratio, fabric, structure, stress history and degree of saturation should be preserved during the sampling and handling process. To evaluate whether or not disturbance of these parameters has occurred, the void ratio and degree of saturation of frozen core specimens can be measured and compared with the in-situ values. However, changes in fabric, structure and/or stress history must be assessed based on whether or not the stress-strain behaviour changes due to subjecting the soil to a freeze-thaw cycle. As stated previously, numerous researchers have shown that the stress-strain behaviour of sand does not change as a result of subjecting the soil to a freeze-thaw cycle, provided that disturbance does not occur during freezing. Therefore, the research for this thesis, concentrated on evaluating how changes in void ratio and degree of saturation can be avoided during ground freezing, sampling and handling in the laboratory.

Although laboratory studies carried out previously on reconstituted sands, have shown that, under appropriate conditions, volumetric strain during freezing can be avoided, there has been no comparison between void ratios measured from in-situ frozen core specimens with independent field measurements of void ratio, which could be obtained from geophysical measurements. This comparison was undertaken as part of the research. Previously documented cases of in-situ ground freezing for undisturbed sampling have also not provided information regarding void ratio changes during thawing of frozen specimens. If significant disturbance occurs during thawing, the value of undisturbed samples obtained by in-situ ground freezing would be significantly reduced. Therefore, a study was conducted to determine the most appropriate protocol for thawing of frozen specimens to minimize disturbance of the void ratio and fabric.

The research objectives include the following:

- Conduct in-situ ground freezing experiments to confirm that the theoretical equations available, adequately predict the freezing process in terms of heat extraction requirements and the rate of growth of the frozen radius.
- Conduct ground freezing feasibility studies to confirm that ground freezing can be undertaken in a specific sand deposit, given the existing site conditions. This includes evaluation of the characteristics of the sand deposit (grain size, mineralogy of fines, permeability) and the characteristics of the site (groundwater temperature, groundwater flow, salinity, drainage boundaries and overburden stresses).
- Conduct in-situ ground freezing at several test sites, including both man-made and native sand deposits, and obtain undisturbed frozen core samples.
- Compare void ratios measured from the in-situ frozen core with void ratios determined based on independent, high quality geophysical logging measurements.
- Evaluate the most appropriate method of thawing the undisturbed specimens in the laboratory to preserve the in-situ void ratio and degree of saturation.

- Conduct a limited number of laboratory tests to evaluate the response of the sand to undrained loading for evaluation of the liquefaction potential.

1.5 Organization of the Thesis

This thesis is organized into a series of 9 chapters. After the introduction of **Chapter 1**, **Chapter 2** describes the factors which must be considered as part of a feasibility study undertaken to confirm that in-situ ground freezing can be utilized to obtain undisturbed samples at a specific test site. Both the characteristics of the sand deposit and that of the site are reviewed in terms of what conditions are generally appropriate for conducting insitu ground freezing. The theoretical prediction of the ground freezing process, to allow for estimating the time and liquid nitrogen volume requirements to freeze a given radius, are also reviewed.

The design of a typical in-situ ground freezing system, utilizing liquid nitrogen as the coolant, is described in **Chapter 3**. This chapter highlights the features of the system required to avoid disturbance of the subsoils during freezing. The results of several large scale freezing experiments conducted in water and sand under various boundary conditions are presented. The actual growth of the frozen radius and the consumption of liquid nitrogen during the experiments are compared with theoretical predictions.

Chapter 4 describes a case history where in-situ ground freezing and coring was undertaken in a man-made, hydraulically placed sand deposit located a Syncrude Canada Ltd. in Fort McMurray, Alberta. The feasibility study undertaken prior to carrying out in-situ ground freezing is described in detail. Temperature and liquid nitrogen consumption data, gathered as freezing progressed at the test site, are also presented. The quality of the in-situ frozen core specimens is discussed, based on visual inspection and

comparison of the void ratios determined from the frozen core with void ratio measurements made independently at the site by high quality geophysical logging.

Chapter 5 describes a case history where in-situ ground freezing and coring was carried out in two native sand deposits located in the Fraser River Delta, near Vancouver, British Columbia. The feasibility study carried out prior to commencing in-situ ground freezing is described and the data gathered during the freezing process is presented. Void ratios determined from the in-situ frozen core are compared with void ratio measurements from geophysical logging undertaken within a 5 m radius of the zone where the undisturbed frozen core samples were recovered.

A third case history is presented in **Chapter 6**, which describes the in-situ ground freezing and frozen core sampling undertaken at the Phase III CANLEX event site, at Syncrude Canada Ltd. The feasibility studies conducted to determine whether or not ground freezing could be carried out at this site, where the sand had a high fines content and high initial groundwater temperature, without causing disturbance of the in-situ conditions, are described. Theoretical predictions of the ground freezing process are compared with the actual field data and the quality of the frozen core is discussed.

Chapter 7 describes the thawing protocol study undertaken to evaluate the most appropriate method of thawing frozen undisturbed specimens without causing significant disturbance of the in-situ void ratio, fabric, stress history or degree of saturation. Two methods of thawing frozen specimens that have been used by researchers in the past are investigated. The first method considered is multidirectional thawing, under a small effective stress of about 20 kPa, followed by consolidation to the in-situ stresses. The second method investigated involves unidirectional thawing under the in-situ effective stress and pore water pressure.

Laboratory tests results obtained from anisotropic, undrained triaxial compression and extension tests conducted on undisturbed frozen samples obtained from one of the test sites are also presented in **Chapter 7**. The conclusions drawn from the work carried out for this thesis are presented in **Chapter 8**.

Appendix A includes detailed information gathered during the ground freezing experiments. **Appendices B, C and D** contain additional detailed information obtained during in-situ ground freezing activities carried out at three test sites. **Appendix E** contains detailed information regarding the thawing protocol study and laboratory tests carried out on undisturbed and reconstituted samples of sand obtained from the Phase I test site. **Appendix F** contains typical cost estimate calculations for carrying out in-situ ground freezing at three CANLEX test sites.

1.6 References

- Baligh, M. M., 1985. Strain Path Method. *Journal of Geotechnical Engineering Division, ASCE GT2*, Vol. 111, pp. 65-98.
- Broms, B. B., 1980. Soil Sampling in Europe: State-of-the-Art. *Journal of Geotechnical Engineering Division, ASCE GT1*, Vol. 106, Paper 15149, pp. 1108-1136.
- Castro, G., 1975. Liquefaction and Cyclic Mobility of Saturated Sands. *Journal of Geotechnical Engineering Division, ASCE GT6*, Vol. 101, Paper 11388, pp. 551-569.
- Castro, G., 1977. Factors affecting Liquefaction and Cyclic Mobility. *Journal of Geotechnical Engineering Division, ASCE GT6*, Vol. 103, pp. 501-516,
- Hatanaka, M., Sugimoto, M., and Yoshio, S., 1985. Liquefaction Resistance of Two Alluvial Volcanic Soils Sampled by In-Situ Freezing. *Soils and Foundations*. Vol., 25, No. 3, pp. 49-63.

- Hatanaka, M., Uchida, A., Oh-oka, H., 1995. Correlation between the Liquefaction Strengths of Saturated Sands Obtained by In-situ Freezing Method and Rotary-Type Triple Tube Method, *Soils and Foundations*, Vol. 35, No. 2, pp. 67-75.
- Hight, D. W., 1993. A Review of Sampling Effects in Clays and Sands. *Offshore Site Investigations and Foundation Behaviour*, Vol. 28, pp. 115-146.
- Hight, D. W. and Georgiannou, V. N., 1995. Effects of Sampling on the Undrained Behaviour of Clayey Sands. *Géotechnique*, Vol. 45, No. 2, pp. 237-247.
- Hvorslev, M. J., 1949, *Subsurface Exploration and Sampling of Soils for Civil Engineering Purposes*. U. S. Army Engineer Waterways Experiment Station. Vicksburg, Mississippi.
- Ishihara, K., 1993. Liquefaction and Flow Failure during Earthquakes. The 33rd Rankine Lecture, *Géotechnique*, Vol. 43, No. 3, pp. 351-415.
- Iwasaki, Y. T., Hashimoto, T., Hongo, T., Hirayama, H., and Murakami, S., 1977. On the Undisturbed Sampling for Stiff Clay. Specialty Session, 9th International Conference on Soil Mechanics and Foundation Engineering, Tokyo, pp. 57-62.
- Konrad, J-M. and St-Laurent, S., 1995. Controlled Freezing and Thawing as a way to Test Intact Sand: A Laboratory Investigation. 48th Canadian Geotechnical Conference, Vancouver, B.C., September, 1995, pp. 213-222.
- List, B. R. and Robertson. P. K., 1995. Canadian Liquefaction Experiment Update - Characterization of Sand for Static and Dynamic Liquefaction. 48th Canadian Geotechnical Conference. Vancouver, B.C., September. 1995. pp. 49-58.
- Marcuson, W. F. and Franklin, A. G., 1979. State of the Art of Undisturbed Sampling of Cohesive Soils. *Proceedings of the International Symposium of Soil Sampling, State of the Art on Current Practice of Soil Sampling*, Singapore, pp. 57-71.
- McRoberts, E. D. and Sladen, J. A., 1990. Observations on Static and Cyclic Sand Liquefaction Methodologies. 43rd Canadian Geotechnical Conference Proceedings, Quebec, pp. 215-226.

- Milovic, D. M., 1970. Effect of Sampling on Some Soil Characteristics. American Society for Testing and Materials, Symposium on Sampling of Soils and Rock. STP 483, pp. 164-179.
- Plewes, H. D., Pillai, V. S., Morgan, M. R., and Kilpatrick, B. L., 1993. In-situ sampling, density measurements and testing of foundation soils at Duncan Dam. Proceedings of the 46th Canadian Geotechnical Conference Saskatoon. Saskatchewan, pp. 223-235.
- Robertson P. K., 1994. Suggested Terminology for Liquefaction. 47th Canadian Geotechnical Conference, September 21-23, 1994, Halifax Nova Scotia. pp. 277-286.
- Robertson, P. K. and Fear, C. E., 1995. Liquefaction of Sands and its Evaluation. IS Tokyo '95, First International Conference on Earthquake Geotechnical Engineering, Keynote Lecture.
- Roscoe, K. H., Schofield, A. N. and Wroth, C. P., 1958. On the Yielding of Soils. Géotechnique. Vol. 8, No. 1, pp. 22-52.
- Sasitharan, S., Robertson, P. K., Sego, D. C. and Morgenstern, N. R., 1993. Collapse Behaviour of Sand. Canadian Geotechnical Journal, Vol. 30, No. 4, pp. 569-577.
- Sasitharan, S., Robertson, P. K., Sego, D. C. and Morgenstern, N. R., 1994. State Boundary Surface for Very Loose Sand and its Practical Implications. Canadian Geotechnical Journal, Vol. 31, No. 3, pp. 321-334.
- Seed, H. B., Singh, M., Chan, C. K., and Vilela, T. F., 1982. Considerations in Undisturbed Sampling of Sands. Journal of Geotechnical Engineering Division. ASCE GT2 Vol. 108, pp. 265-283.
- Sego, D. C., Robertson, P. K., Sasitharan, S., Kilpatrick, B. L., and Pillai, V. S., 1994. Ground Freezing and Sampling of Foundation Soils at Duncan Dam. Canadian Geotechnical Journal, Vol. 31, No. 6, pp. 939-950.
- Shibuya, S. and Hight, D. W., 1987. Patterns of Cyclic and Principal Stress Rotation and Liquefaction. 8th Regional Conference on Soil Mechanics and Foundation Engineering, Kyoto, Japan, 20 to 24th July, 1987, pp. 265-268.

- Singh, S., Seed, H. B. and Chan, C. K., 1982, Undisturbed Sampling of Saturated Sands by Freezing. *Journal of Geotechnical Engineering Division, ASCE GT2* Vol. 108. pp. 247-263.
- Sladen, J. A., D'Hollander, R. D., and Krahn, J., 1985. The Liquefaction of Sands, a Collapse Surface Approach. *Canadian Geotechnical Journal*, Vol. 22. No. 4. pp. 564-578.
- Tavenas, F. and Leroueil, S., 1987. Laboratory and In-Situ Stress-Strain-Time Behaviour of Soft Clays: State-of-the-Art. *Proceedings of the International Symposium on Geotechnical Engineering in Soft Soils, Mexico City*, Vol. 2, pp. 1-46.
- Tokimatsu, K. and Hosaka, Y., 1986. Effects of Sample Disturbance on Dynamic Properties of Sand. *Soils and Foundations*, Vol. 26, No. 1, pp. 53-64.
- Verdugo, R. and Ishihara K. (1996). The Steady State of Sandy Soils. *Soils and Foundations*, Vol. 36, No. 2, pp. 81-91.
- Yoshimi, Y., Hatanaka, M., and Oh-Oka, H., 1977. A Simple Method of Undisturbed Sand Sampling by Freezing. *Proceedings of Specialty Session 2 on Soil Sampling, 9th International Conference on Soil Mechanics and Foundation Engineering*, pp. 23-28.
- Yoshimi, Y., Hatanaka, M., and Oh-Oka. H., 1978. Undisturbed Sampling of Saturated Sands by Freezing. *Soils and Foundations*. Vol. 18, pp. 59-73.
- Yoshimi, Y., Tokimatsu K., Kaneko, O. and Makihara. Y., 1984. Undrained Cyclic Shear Strength of a Dense Niigata Sand. *Soils and Foundations*. Vol. 24, No. 4. pp. 131-145.
- Yoshimi, Y., Tokimatsu, K. and Ohara, J. 1994. In-Situ Liquefaction Resistance of Clean Sands over a wide Density Range. *Géotechnique*, Vol. 44, No. 3, pp. 479-494.

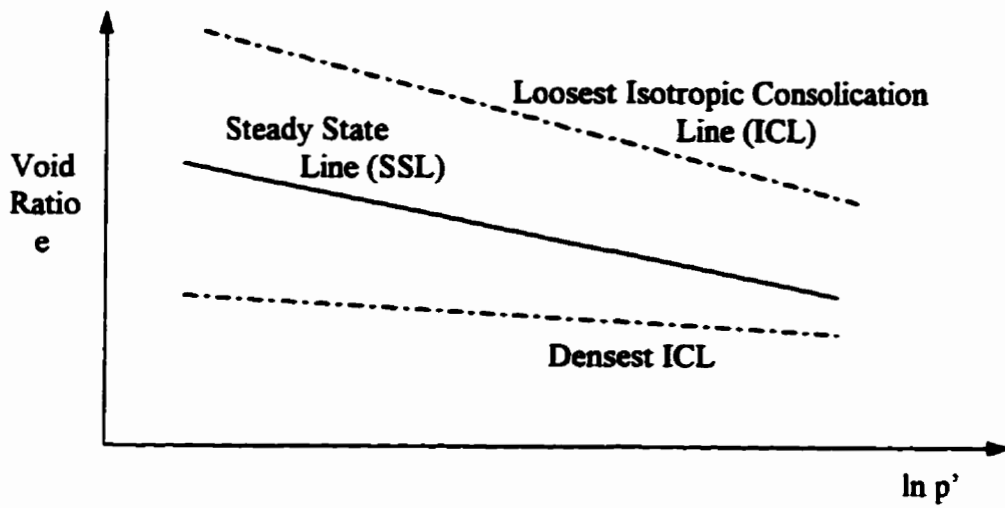


Figure 1-1: Typical Steady State Line in $e - \ln p'$ Space.

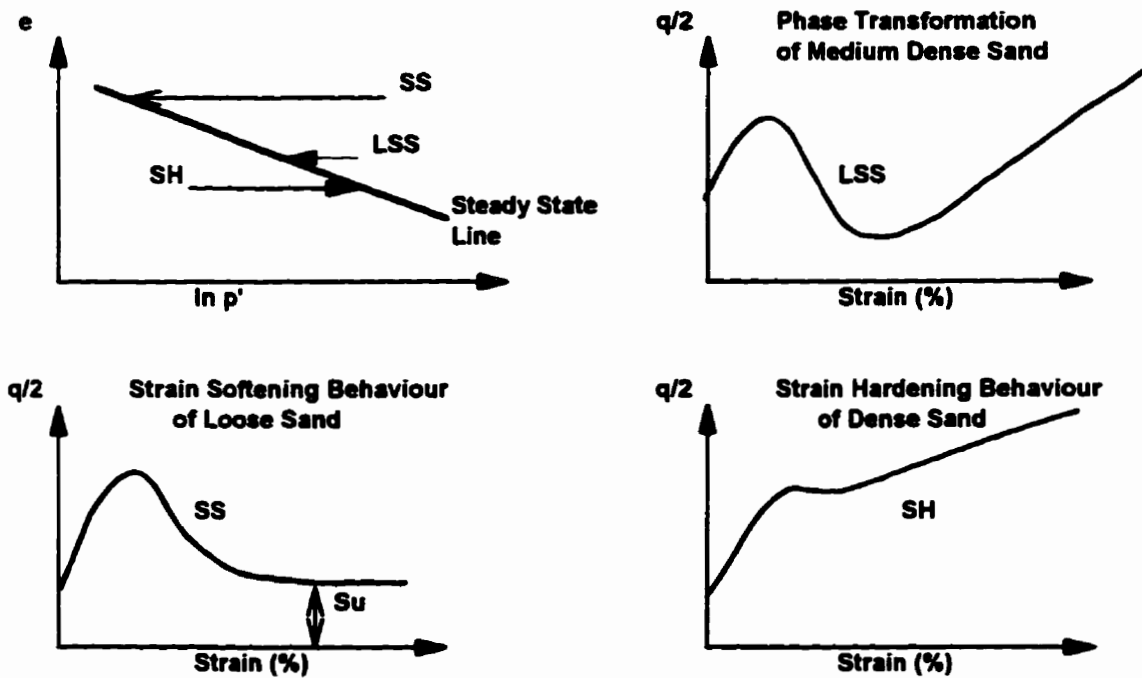


Figure 1-2: Behaviour of Sand Subject to Monotonic Undrained Triaxial Compression (modified from Robertson and Fear, 1995).

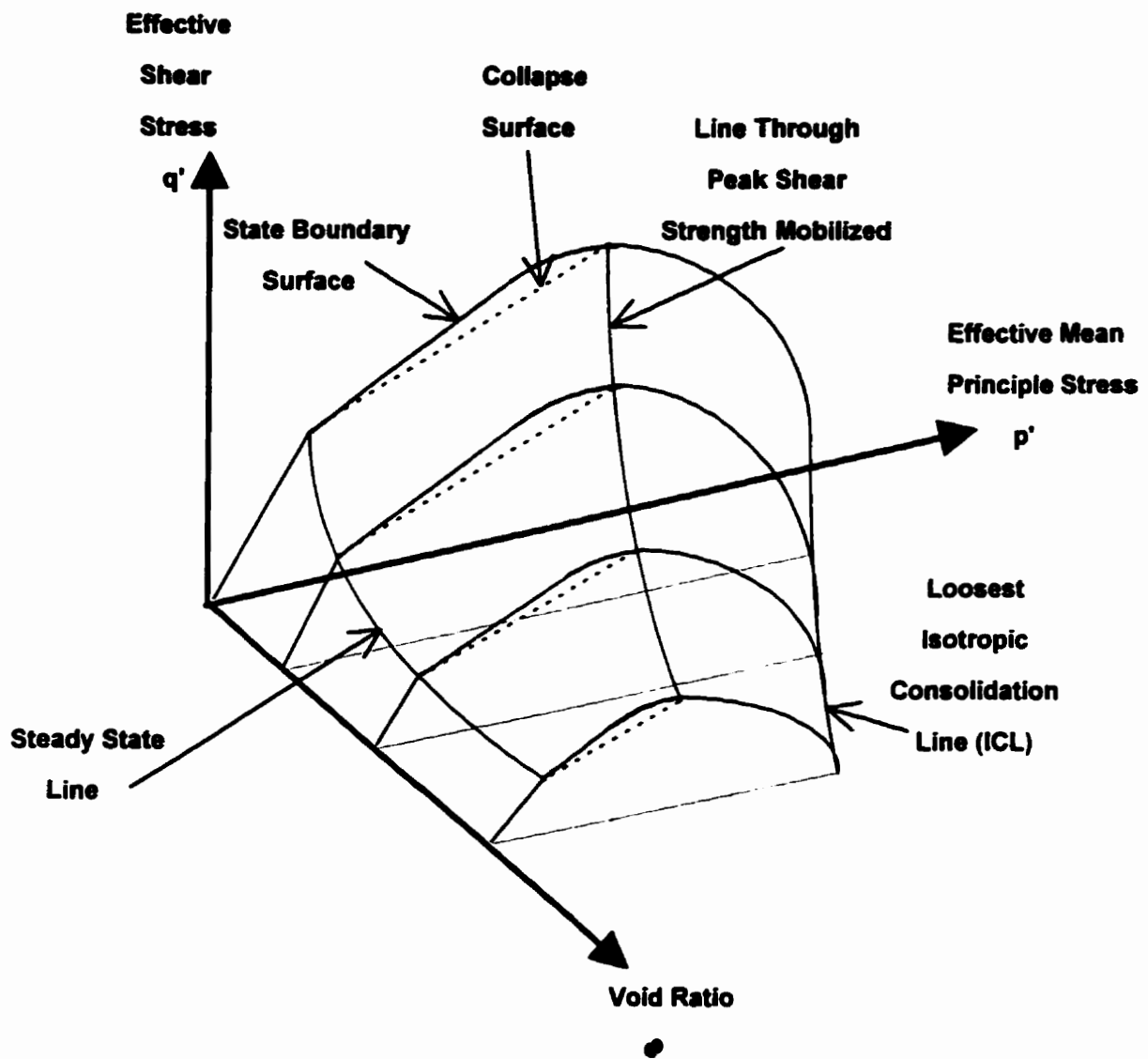


Figure 1-3: Schematic Diagram of the Ultimate States of Sand in 3-Dimensional e - p' - q Space.

CHAPTER 2 : Feasibility of Obtaining Undisturbed Samples of Loose Sand by In-Situ Ground Freezing

2.0 Introduction

Prior to utilizing in-situ ground freezing to obtain undisturbed samples of a granular deposit, feasibility studies must be carried out to determine whether or not the sand deposit can be frozen in-situ without causing frost heave disturbance that would alter the in-situ void ratio and fabric. Previous research has shown that when saturated soils freeze, disturbance may result either when ice lenses form in frost heave susceptible soils or when freezing is undertaken too rapidly and pore water freezes in place, undergoing a 9 % volume expansion in the void spaces.

As the freezing front progresses through saturated soil, the conditions which develop near the freezing front are influenced by the soil type, stress level, and rate of freezing. Depending upon these conditions, water may be either expelled from or attracted to the freezing front (McRoberts and Morgenstern, 1975). In fine grain soils, such as clay or silt, water tends to be attracted to the freezing front, thereby causing disturbance due to frost heave, while in coarse grain soils, such as sand or gravel, water tends to be expelled in advance of the freezing front.

Since many native sand deposits where liquefaction is a concern contain some fines, it is important to understand the potential frost heave mechanisms associated with freezing of fine grain soils. Hence, freezing of fine soils will first be reviewed, followed by discussion of freezing in granular soils. Once the soil freezing mechanisms have been reviewed, the important factors to consider when carrying out a feasibility study, to

confirm that in-situ freezing can be used in a particular deposit for obtaining undisturbed samples will be discussed.

After confirming that the characteristics of a sand deposit and the site conditions are appropriate for conducting in-situ ground freezing, it is necessary to assess the heat extraction requirements to estimate the time and costs associated with this method of undisturbed sampling. For this purpose, the theoretical prediction of the ground freezing process will be reviewed at the end of the chapter.

2.1 Freezing of Fine Grain Soils

According to Anderson and Morgenstern (1973), during freezing most saturated fine grain soils, under low stresses, exhibit an affinity for water and ice lensing can occur. Konrad and Morgenstern (1983) present a summary of the physical processes associated with freezing of fine grain soils. As the frost front progresses through a soil, ice nucleates in the pore water. In fine grain soils, some water remains unfrozen as the temperature falls below 0 °C due to a freezing point depression. The magnitude of the freezing point depression depends upon the mineralogy, chemistry and specific surface area of the clay particle surfaces, the pressure and temperature of the soil/water matrix, the presence of undissolved ions, the void ratio and fabric of the soil (Anderson and Morgenstern, 1973, Mitchel, 1976, Nersesova and Tsytoveck, 1963, and Tyutyunov, 1963).

More specifically, the pore water in the soil matrix may be divided into three zones. Water molecules immediately adjacent to negatively charged clay particle surfaces become oriented. Internal bonds between water molecules are broken and external bonds between individual water molecules and clay mineral ions are formed. This water is usually called strongly bonded water (Tyutyunov, 1963). Water that is strongly bonded to particle surfaces does not freeze even if temperatures drop well below 0 °C. The attraction between water molecules and clay mineral surfaces decreases as the distance of

the water molecules from the solid surfaces increases. Adjacent to the strongly bonded water, the next zone contains adsorbed water which is weakly bonded to soil particle surfaces. Weakly bonded water freezes when the temperature drops below the freezing point depression required to overcome the bonding. Free water, which fills the void spaces between soil particles, freezes at 0 °C under 1 atmosphere, if no dissolved salts are present.

In fine grain soils, free water is attracted to the freezing front as a result of a suction gradient that develops due to the temperature gradient set up by the freezing point depression (Konrad and Morgenstern, 1980). According to Mitchell (1976), less energy is required to transport water from adjacent pores to the freezing front via the unfrozen water film, than to freeze the adsorbed water surrounding the particles at the freezing front. When enough water accumulates near the freezing front in fine grain soils, ice lenses tend to grow just behind the front (Konrad and Morgenstern, 1980). Unless very high overburden stresses are present (Konrad and Morgenstern, 1982), these soils often cannot be frozen without disturbing the in-situ void ratio.

For fine grain soils, Konrad and Morgenstern (1983) presented a method of evaluating the frost heave susceptibility based on the segregation potential, which is equal to the water intake flux divided by the temperature gradient across the frozen fringe. The segregation potential varies with suction at the frost front, the rate of cooling at the fringe, and the permeability of the zone between the frost front and the segregation front, where an ice lens forms if the conditions are appropriate. These parameters are strongly dependent upon the applied stress level, since stress affects the average unfrozen water content, the permeability of the frozen fringe, and the segregation freezing temperature. To estimate the frost heave potential of a fine grain soil, the segregation potential can be measured readily in the laboratory by conducting frost heave tests in which the water intake rate and temperature profile are measured with time (Konrad and Morgenstern, 1983).

2.2 Freezing of Granular Soils

Conversely, in sands the mineralogy and chemistry are such that attractive forces between soil particles and water molecules are extremely weak. There is no strongly bound water around clean sand grains. Less energy is required to expel the excess 9 % pore water volume than to move apart soil grains to accommodate the increase in volume associated with water changing to ice. Therefore, as the freezing front progresses through sandy soil, 9 % of the free pore water volume is expelled away from the freezing front. The theoretical 9 % volume of expelled pore water is given by McRoberts and Morgenstern (1975) as:

$$\Delta V = 0.09 V_v S_r \quad [2-1]$$

where: V_v is the volume of voids (cc) and S_r is the degree of saturation.

Provided that drainage around the zone in which in-situ ground freezing is being undertaken is unimpeded by physical constraints, and that the soil is frozen at a rate which is slow enough compared to the permeability of the soil to allow for expulsion of pore water, there is little or no disturbance of the in-situ void ratio or fabric.

2.3 General Description of the Ground Freezing Process

Since many sands can be frozen without causing disturbance of the in-situ void ratio or fabric, in-situ ground freezing can often be used for obtaining undisturbed samples of sand. The most effective method of undertaking in-situ ground freezing, without causing disturbance of the void ratio or fabric, involves unidirectional freezing from a central freeze pipe. A column of sand can be frozen by circulating a coolant through the freeze pipe. Figure 2-1 shows a schematic freeze pipe arrangement. This method, allows for unimpeded drainage of pore water in advance of the freezing front, as the column of sand

is frozen around the freeze pipe, and therefore reduces the risk of causing disturbance due to the excess 9 % pore water volume freezing in place.

Historically, ground freezing has been carried out utilizing various brine solutions as the coolant, with the heat transfer mechanism to freeze the soil being conduction. Brine coolants, such as magnesium chloride or calcium chloride, typically can be maintained at temperatures of -34°C to -55°C (Stoss and Valk, 1979). Where ground freezing is undertaken for construction purposes to seal off loose granular soils or groundwater flow, frost heave is not usually a concern and freeze pipes can be closely spaced, thereby reducing the time for joining of the frozen columns. However, in the case of conducting in-situ ground freezing for undisturbed sampling, where only one freeze pipe is utilized, the use of brine coolants result in a slow freezing process. It may be necessary to maintain a brine cooling system for as long as two months to freeze a column of sand, with a 1 m radius around the freeze pipe.

Alternatively, liquid nitrogen, with a phase change temperature of -196°C , may be used as the coolant. In this case, heat extraction is accomplished through two heat transfer mechanisms. Firstly, liquid nitrogen in the freeze pipe, at a temperature of approximately -196°C , absorbs heat from the surrounding ground through conduction. Secondly, a significant amount of heat is absorbed by the liquid nitrogen when it undergoes a phase change to gas. Phase change occurs spontaneously such that mass is transferred from the phase with a higher partial molar free energy to the phase with a lower partial molar free energy (Colbeck, 1981). After the phase change, nitrogen gas is then vented back to the atmosphere as more liquid nitrogen is injected into the freeze pipe reservoir. Therefore, cooling of the ground occurs due to both the use of the volumetric latent heat and specific heat, since both the liquid and gas nitrogen are substantially colder than the surrounding soil. Therefore, when liquid nitrogen is used as the coolant, the rate of heat extraction is significantly greater than when a brine coolant is used to extract heat solely by absorbing heat from the surrounding freezing soil which causes the brine temperature to increase.

To increase efficiency, a reservoir for the liquid nitrogen can be created within a given length of the freeze pipe, corresponding to a target zone of interest where undisturbed samples are required. As illustrated in Figure 2-1, a copper pipe can be used to feed liquid nitrogen into the reservoir and a second copper pipe can be used to vent gaseous nitrogen back into the atmosphere, the two copper pipes being separated at the top of the reservoir by a large rubber seal. The length and location of the freezing target zone can be altered in the field, depending upon the actual ground conditions encountered, by simply moving the location of the rubber seals within the freeze pipe. Hatanaka et al. (1985) also recognized the value of freezing along discrete target zones of interest. They advanced a large diameter borehole to the top of the target zone, which was subsequently filled with circulating warm water, to prevent freezing above the zone of interest. A freeze pipe was then extended through the casing, down the center of the large diameter borehole to the bottom of the target zone.

Once a column of sand is frozen around the freeze pipe, a large number of undisturbed samples can be obtained by continuously coring through the target zone in cased boreholes advanced to the top of the frozen column. As will be described in the case histories presented in Chapters 4, 5 and 6, a core barrel can be used to extract continuous samples of frozen sand, utilizing a dry coring method. Frozen samples, retrieved to the surface, can then be placed in freezers with dry ice and transported directly to the laboratory without risk of disturbing the specimens during transportation. Yoshimi et al. (1978 and 1984), have used an overcoring technique and crane to recover the entire column of frozen sand around the freeze pipe. This procedure works well if the deposit is frozen from the ground surface down. However, since the frozen sand closest to the freeze pipe is disturbed by insertion of the freeze pipe, the entire column of sand cannot be considered as undisturbed. Yoshimi, et al. (1978) showed that a zone of approximately 2 times the freeze pipe diameter was disturbed around a 73 mm freeze pipe, installed with a self-boring technique in sands of various densities.

2.4 Evaluation of Soil Frost Heave Susceptibility

Prior to undertaking in-situ ground freezing, feasibility studies should be carried out to confirm that ground freezing can be utilized at a given site without causing disturbance of the in-situ ground conditions. To undertake feasibility studies, detailed information regarding the subsoil and groundwater conditions are required. Factors which control whether or not frost heave may develop in a sandy soil include:

- amount of fines in the sand deposit (grain size distribution)
- mineralogy of fines
- unfrozen water content
- drainage boundary conditions
- overburden stress and rate of cooling compared to the permeability of the soil

In addition, the characteristics of the site, including the groundwater temperature and flow conditions, are relevant with respect to the feasibility of conducting in-situ ground freezing for undisturbed sampling. In the following sections of Chapter 2, each of the above factors will be discussed in terms of the frost heave susceptibility of a granular soil deposit.

2.4.1 Characteristics of the Sand Deposit

2.4.1.1 Grain Size Distribution and Fines Mineralogy

One of the first steps in conducting a ground freezing feasibility study includes determining the grain size distribution of the sand deposit within which undisturbed samples are required. In general, the higher the percentage of clay and silt sized particles within a sand deposit, the more constraints will be placed on in-situ ground freezing to avoid disturbance of the void ratio and fabric.

Most natural and many man-made sand deposits contain a certain amount of silt sized (between 2 μm and 74 μm) and clay sized ($<2 \mu\text{m}$) particles, or fines. Davila, et al. (1992) conducted a study to examine the amount and type of fines which could be contained within sand without causing disturbance during freezing. The study included open system, unidirectional freezing of sand samples containing varying amounts of kaolin, bentonite, illite and Devon silt fines. The temperature gradient used during the freezing tests was approximately the same as that which exists at the sampling locations around a freeze pipe, approximately 0.4 $^{\circ}\text{C}/\text{cm}$. The pore water flux, pressure and sample height were monitored to evaluate whether or not measurable disturbance of the soil occurred during freezing.

Based on this study, Davila, et al. (1992) developed a chart which relates the specific surface area of the fines to the frost heave susceptibility of the soil. The axes of the chart, shown in Figure 2-2, include: the fines mineralogy ratio, Z_v , on the horizontal axis, and the surface area index, Ω_z , on the vertical axis. The fines mineralogy ratio is defined by:

$$Z_v = CM_f / I_{SSA} \quad [2-2]$$

where, CM_f is the clay mineral content, as a percentage by weight of the clay particles in the fines fraction, and

$$I_{SSA} = S_c / S_f \quad [2-3]$$

where S_c is the specific surface area of the fraction of the soil with a mean particle diameter smaller than 2 μm , and S_f is the specific surface area with mean particle diameter smaller than 74 μm .

The surface area index is defined by:

$$\Omega_z = \sqrt{CM \times S_f} \quad [2-4]$$

where CM is the clay content of the soil expressed as a percentage of the total weight of the soil and S_f is the specific surface area of the fraction of soil with a mean particle diameter smaller than 74 μm .

The study indicated that sands with fines contents of up to 18.7 %, containing 4.2 % clay sizes and 14.5 % silt sizes, could be frozen without disturbance due to frost heave, provided that the clay minerals within the fines were relatively inactive such as Devon silt. The Activity, or plasticity index divided by the clay fraction as a percent by weight, of the Devon silt used in the study was 0.80. According to Holtz and Kovacs (1981), soils with an Activity of less than about 0.75 are considered to be inactive, while soils with an Activity of between 0.75 and 1.25 are classified as normal and those with an Activity of greater than 1.25 are classified as active. Based on determination of the fines mineralogy, Davila et al.'s (1992) chart can be used to provide a preliminary evaluation of the frost heave susceptibility of a sand deposit where in-situ ground freezing may be undertaken. The preliminary evaluation of frost heave susceptibility, conducted for each of the test sites evaluated as part of this research utilizing Davila et al.'s (1992) chart, are presented in more detail in Chapters 4 and 5.

If the sand deposit in question has a relatively high fines content and if a preliminary evaluation of the frost heave susceptibility, using the chart provided by Davila et al. (1992), suggests that disturbance of the sand during freezing may be a concern, frost heave tests should be conducted. Bulk samples of sand should be recovered from the site, and frozen unidirectionally in the laboratory under the same overburden stress and thermal gradient that will be induced in the sampling region during in-situ ground freezing.

The sample should be placed in a rigid insulated cell with a floating top cap and frozen, preferably from the bottom upwards to avoid frictional resistance, under constant temperature boundary conditions at either end and free drainage. Changes in sample height and pore water volume should be recorded during the test to determine whether or not freezing will cause disturbance. If the conditions are favorable for expulsion of the excess 9 % pore water volume, the volume of pore water expelled should be approximately equal to the theoretical volume given by Equation [2-1].

Several frost heave tests could be conducted under various thermal gradients to determine the limits of freezing rates under which measurable disturbance of the soil will not occur. Typically, for a 1 m radius column of frozen sand, core samples are recovered around the freeze pipe at a radius of about 0.6 m where the freezing gradient can either be specified in terms of 0.15 °C/hr to 0.30 °C/hr, or 0.4 °C/cm to 0.6 °C/cm. The actual gradient depends upon the ground conditions. However, there may be some flexibility regarding the radius of the column of sand that can be frozen. In this case the location of the boreholes advanced for sampling could be varied to correspond with the thermal gradient under which frost heave tests determined that disturbance would be negligible.

2.4.1.2 Unfrozen Water Content

Konrad (1995) noted that during rapid freezing of sandy soils containing clay fines, loosely bonded water that is unfrozen at temperatures slightly below 0 °C, could freeze in place under conditions of impeded drainage as temperatures drop quickly to well below 0 °C. A schematic diagram of a clayey sand matrix, assumed to be at a temperature of about -0.5 °C, is shown in Figure 2-3. Since the quartz sand grains have a very high thermal conductivity (5 W/mK) compared to that of water (0.6 W/mK), freezing of the water-soil matrix will commence around the perimeter of the clean sand grains (Hivon and Segó, 1994) in the largest pore voids first. In zones where clay minerals have been deposited within the soil matrix, a layer of unfrozen water surrounds the clay mineral surfaces. If the amount of clay mineral fines and the corresponding unfrozen water content is sufficient, rapid freezing of sand containing clayey fines could result in impeded drainage conditions that would result in some pore water freezing in place, thereby causing disturbance of the in-situ fabric and possible alteration of the void ratio. The magnitude of possible disturbance due to loosely bound water around clay minerals freezing in place should be estimated as part of a ground freezing feasibility study. Example calculations of void ratio changes occurring due to trapped unfrozen water freezing in place under very cold temperatures will be given in Chapter 4.

2.4.2 Characteristics of the Site

The characteristics of the site play an important role in the feasibility of carrying out in-situ ground freezing for obtaining undisturbed samples of sand. The factors related to a particular sand deposit, which may influence frost heave susceptibility, including the drainage conditions, the overburden stress, the rate of cooling compared to the permeability of the deposit, the groundwater temperature, salinity and flow conditions, are discussed in the following sections.

2.4.2.1 Stratigraphy and Drainage Conditions

As stated previously, it is imperative that in-situ ground freezing be carried out under conditions of free drainage, to allow for expulsion of the excess 9 % pore water volume in advance of the freezing front. For example, if a native sand deposit from which undisturbed samples are required contains numerous or extensive silt lenses that may impede drainage, it may be difficult to avoid disturbance due to excess 9 % pore water freezing in place. It is therefore necessary to advance several boreholes or soundings across the site to delineate, without disturbance, a zone where the sand deposit is relatively uniform and in-situ ground freezing could be undertaken. Normally, carrying out a study to identify the liquefaction potential of a site includes identification of the region(s) where the soil under investigation is loosest. At this time, potential zone(s) for undisturbed sampling should be identified and measures taken to prevent any premature disturbance of the area where sampling would be carried out.

The permeability of a sand deposit also affects pore water expulsion. Yoshimi, et al. (1978) conducted laboratory freezing tests on Tonegawa sand which indicated that as the relative density of the sand increased, corresponding to a decrease in permeability, the percent expansion due to freezing increased. Yoshimi et al. (1978) concluded that expansion during freezing is more strongly related to the ease at which pore water can be

expelled, as governed by the hydraulic conductivity of the unfrozen sand, than by the quantity of pore water, or void ratio. The results also showed that the effect of decreased permeability on frost heave potential could be reduced if the overburden stress is increased. The effects of overburden stress will be discussed further in the following section.

2.4.2.2 Overburden Stress and Rate of Cooling

Yoshimi et al. (1978; 1994), Konrad (1990) and Williams (1967) have shown that volumetric expansion during freezing of various sands is dependent upon the overburden stress, or externally applied load. Using the capillary model, Williams (1967) provided an excellent summary of how overburden stress affects the frost heave susceptibility of soil. According to Williams (1967), ice lenses develop when the following condition is satisfied:

$$p_i - p_w = 2 \sigma_{iw} / r_{iw} < 2 \sigma_{iw} / r_c \quad [2-5]$$

where p_i is the ice pressure; p_w is the pressure in the pore water; σ_{iw} is the ice-water surface tension; r_{iw} is the radius of the ice-water interfaces in the pore spaces and r_c is the size of the largest continuous pore openings through the soil and the maximum radius which an ice-water interface can have if the interface is to advance through the pore system. The pressure in the ice is generally equal to the total overburden or confining pressure and the pore water pressure is related to the hydrostatic groundwater pressure. Therefore, since the density of soil is greater than that of the groundwater, as the overburden stress increases with depth, p_i increases more quickly than p_w and there is a limiting depth for which Equation [2-5] is no longer true. Beyond the limiting depth, growth of an ice lens cannot occur.

The laboratory freezing tests conducted by Yoshimi et al. (1978) indicated that the expansive strains during one-dimensional freezing under laterally confined conditions

decreased with increasing surcharge. Data obtained by Yoshimi, et al. (1978) for three different sands subject to increasing surcharge loads is shown in Figure 2-4 (modified from Konrad, 1990). The test results indicated that surcharge and soil type had the most significant effect on volumetric expansion. For Tonegawa sand, the expansive strains during freezing became less than 0.1 percent once the surcharge exceeded about 33 kPa, for a cooling rate of about 16 cm/hr; while no volume change was noted during freezing of Niigata and Toyoura sand under a surcharge of only 9 kPa at the same rate of cooling. As shown in Figure 2-4, although the Toyoura sand had a lower permeability than the Niigata sand, it exhibited a lower tendency towards heaving. As pointed out by Yoshimi, et al. (1978), the difference in behaviour may therefore be a function of not only the permeability and gradation but also of the fines mineralogy of the soil. Since clay mineralogy plays an important role in the development of the freezing point depression, associated suctions and the unfrozen water content, the type of clay mineral would affect the forces that must be overcome to allow for pore water expulsion. If less than 9 % of the pore water volume is expelled prior to advance of the freeze front, some volumetric expansion will occur due to freezing.

Konrad and Morgenstern (1982) showed that, depending on the applied pressure and soil type, water is expelled when saturated silts are frozen under rates of cooling that are larger than a critical rate. Tests conducted by Konrad (1990) on fine Ottawa sand indicated that for a given stress, the vertical strain due to pore water freezing in place increased with increasing rates of cooling above approximately 20 °C/hr. Here the rate of cooling is defined as the change in temperature at the frost front per unit time. As shown by the test results in Figure 2-4, the volumetric expansion during freezing decreased with increasing applied stress and the stress under which volume expansion became negligible depended upon the cooling rate. According to Konrad (1990) specimens subject to a cooling rate of 20 °C/hr, or less, under an applied stress of about 3.5 kPa, did not exhibit frost heave. This stress level corresponds to approximately 0.2 m of dry soil. Konrad (1990) points out that analysis of the data presented by Yoshimi et al. (1978), indicated

that for specimens subject to stresses ranging from 0.3 to 14 kPa, no frost heave occurred in specimens frozen under rates of cooling of less than 15 °C/hr.

The above information illustrates the importance of including overburden stresses when evaluating the feasibility of obtaining undisturbed samples of sand by in-situ ground freezing. The effect of overburden stress can be taken into account directly by conducting one-dimensional frost heave tests in the laboratory under the same stress level and temperature gradients that would exist at the site where undisturbed samples are required.

2.4.2.3 Groundwater Temperature, Salinity and Flow Conditions

Temperature and groundwater flow conditions can have a significant effect on the freezing process and must be considered when estimating the energy and length of time required to carry out ground freezing, even when liquid nitrogen is used as the coolant. As will be discussed in a later section, the initial groundwater temperature is needed as an input parameter for the theoretical determination of the heat extraction requirements to freeze a given radius of soil.

Salts present in groundwater cause a freezing point depression, which becomes more pronounced as the salt concentration increases (Hivon and Segó, 1994). If liquid nitrogen is used as the coolant for in-situ ground freezing in saline soil, the freezing point depression is very small compared to the capacity for heat extraction by the liquid nitrogen. Therefore, the rate of freezing is not affected significantly by saline groundwater. However, in sands containing clay fines, the amount of unfrozen water will increase as salinity increases. This may in turn result in more significant volumes of trapped unfrozen water freezing in place as the temperature drops below the freezing point depression. If the volumes of unfrozen water are significant, disturbance of the soil fabric and void ratio may occur.

Where in-situ ground freezing may be used to recover undisturbed samples of saline soil, freezing tests should be undertaken in the laboratory on samples with the same pore water chemistry that exists at the site to determine whether or not the soil can be frozen without causing disturbance. It may be possible to avoid disturbance caused by trapped unfrozen water freezing in place by decreasing the rate of cooling to allow for the unfrozen water to be expelled in advance of the freeze front. As discussed, disturbance may also be avoided by increasing the overburden stress.

Evaluation of the effect of groundwater flow on the growth of the frozen zone around the freeze pipe requires numerical analysis, since an exact solution does not exist that simultaneously solves the groundwater flow velocity and temperature distributions in two dimensions (Hashemi and Sliepcevich, 1973; Sanger and Sayles, 1979; Takashi, 1969). Numerical solutions to this problem have been published by Hashemi and Sliepcevich (1973), utilizing finite difference, and by Comini and Frivik (1980), utilizing a finite element program.

In general, as shown by Hashemi and Sliepcevich (1973), groundwater flow across a site where in-situ ground freezing is being undertaken causes elongation of the frozen column in the down stream direction and foreshortening in the upstream direction. If the groundwater flow velocity is significantly high, pore water that is cooled as liquid nitrogen is circulated through the freeze pipe may be transported away from the freezing zone where sampling is required before it can change to ice in place. In this extreme case, it may not be possible to carry out in-situ ground freezing for undisturbed sampling unless the groundwater flow can be slowed.

Hashemi and Sliepcevich (1973) show that for closure of a frozen soil curtain between two adjacent freeze pipes, the steady state rate of cooling attained by the freeze pipe must be greater than the volumetric heat capacity (amount of sensible heat) that can be removed by groundwater flow. The steady state rate of cooling attained by the freeze

pipe surrounded by a frozen column of soil, of radius R can be determined by calculating the increment of total heat extracted per increment of time, or dQ/dt (Sanger and Sayles, 1979). This steady state heat flow to the freeze pipes is therefore given by:

$$2\pi k_f (T_f - T_{fp}) / \ln (R/r_o) = 2\pi k_f v_s / \ln (R/r_o) \quad [2-6]$$

where: $v_s = (T_f - T_{fp})$ is the difference between the surface of the freeze pipe and the freezing temperature of water ($^{\circ}\text{K}$); k_f is the mean thermal conductivity of the frozen soil ($\text{J}/\text{sm}^{\circ}\text{K}$); T_f is the freezing temperature of water ($^{\circ}\text{K}$); T_{fp} is the skin temperature of the freeze pipe ($^{\circ}\text{K}$); and r_o is the radius of the freeze pipe (m).

To reach a given frozen radius, R , the rate of heat removal by the groundwater flow must be less than the rate of heat extraction required to freeze the pore water in place. This relation is expressed by Hashemi and Sliepcevich (1973) as:

$$k_f v_s / \ln (R/r_o) > Q(R) C_u v_o ; \text{ for } r_o < R < L \quad [2-7]$$

where: $v_o = (T_o - T_f)$ is the difference between the initial temperature of the ground and the freezing point of water ($^{\circ}\text{K}$); $Q(R)$ is the total flow through the region ($\text{m}^3/\text{s m}$ of thickness); and C_u is the unfrozen volumetric heat capacity of the seepage stream ($\text{J}/\text{m}^3\text{K}$).

When brine is used as the coolant, several authors, including Sanger and Sayles (1979) and Takashi (1969), have shown that the limiting seepage velocity for closure of a frozen soil curtain is approximately 1 m per day. As noted previously, the temperature of brine coolants is typically -40°C . However, if liquid nitrogen is used as the coolant, closure can be achieved in the presence of significantly higher groundwater flow. By replacing the total flow through the region with the critical groundwater flow velocity and cross-sectional area in Equation [2-7] and rearranging the terms, it can be seen that the critical groundwater flow velocity is proportional to the freezing pipe temperature, where:

$$V = \{ k_f / C_u \} \times \{ (T_f - T_{fp}) / (T_o - T_f) \} \times \{ L / A \} \times \{ 1 / \ln (R/r_o) \} \quad [2-8]$$

In Equation [2-8], L is the thickness of the zone of groundwater flow (m) and A is the cross-sectional area (m^2). Hence, given the same initial ground conditions, the critical flow velocity when freezing with liquid nitrogen would be approximately 5 times the allowable velocity when a brine coolant is used. An evaluation of the effect of groundwater flow on the shape of the frozen column will be discussed in further detail with respect to a specific site in Chapter 4.

2.5 Laboratory Determination of Frost Heave Potential

Many of the factors related to frost heave susceptibility of a sand deposit are interrelated. As described in the preceding sections, Konrad and Morgenstern (1982) showed that small changes in the overburden pressure or externally applied load, result in dramatic changes to the critical rate of cooling, below which frost heave disturbance can be avoided. Due to the interrelated nature of these factors, in-situ ground freezing feasibility studies should include conducting frost heave tests in the laboratory which simulate field freezing conditions.

Ideally, laboratory frost heave tests should be conducted on sand obtained from the site where in-situ ground freezing may be used. Test specimens may be reconstituted from bulk samples obtained from the site, however, the grain size distribution and fines mineralogy of the reconstituted specimen should have characteristics that are similar to those existing in-situ. One-dimensional frost heave tests should be conducted allowing free drainage, under the in-situ stress and pore water pressure conditions. The thermal gradient applied to the sample should be equal to the temperature gradient that would exist in the field, at the radial distance from the freeze pipe where samples would be recovered. Based on temperature measurements at either end of the specimen, the test should be carried out until all of the soil freezes.

If frost heave tests, conducted under conditions which model the in-situ conditions, do not show any significant expansion (< 0.5 mm) due to freezing, in-situ ground freezing can be carried out to obtain undisturbed samples, provided that the time and cost associated with this method are not preclusive. Theoretical modeling of the in-situ ground freezing process will be discussed in the following section, to show how predictions of the heat extraction requirements and the associated costs can be evaluated.

2.6 Theoretical Prediction of Ground Freezing Process to Evaluate Time and Costs Requirements

Feasibility studies should also include an estimation of costs and freezing time required to conduct in-situ ground freezing. Typical cost estimates associated with carrying out in-situ ground freezing at three test sites are provided in Appendix F. The heat extraction requirements to freeze a given soil depends on the subsoil and groundwater conditions. The parameters which effect the amount of liquid nitrogen required to freeze a given soil include: soil moisture content, soil density, frozen and unfrozen thermal conductivity and heat capacity, latent heat, and initial groundwater temperature. The moisture content has a greater impact on the heat extraction requirements than the soil density, since less heat must be extracted to cool mineral grains than to cool and transform pore water into ice. Therefore, soils with a high moisture content require the removal of larger amounts of heat to initiate phase change in the pore water. The heat extraction requirements govern the volumes of liquid nitrogen required to freeze a column of soil at a specific site and therefore, directly affect the costs associated with undertaking in-situ ground freezing.

As shown in Figure 2-5, after Sanger and Sayles (1979), at the boundary between the frozen and unfrozen soil a discontinuity exists due to the change in thermal conductivity and specific heat capacity that occurs with a change in phase. The equations derived by Sanger and Sayles (1979), expressing the temperature distributions through the frozen (v_f) and unfrozen (v_u) soils are also shown in the Figure 2-5. As a result of the discontinuity,

simplifying assumptions must be used, along with heat conduction theory, to determine the heat extraction requirement and length of time to freeze a given radius of soil. In the development of the equation describing heat extraction, Sanger and Sayles (1979) assumed that the isotherms move slowly enough to resemble steady state conditions. According to the authors, although this is not strictly correct, experience has shown this assumption to be adequate for engineering design purposes.

To predict the volume of liquid nitrogen required to freeze a given radius of soil, the equation given by Sanger and Sayles (1979) for the total energy extracted from the ground to freeze a cylinder of soil can be utilized by dividing the expression for the energy extracted by the latent heat of phase change of liquid nitrogen. The equation for the total energy extracted includes four terms: (1) the volumetric latent heat of the frozen soil liberated when the unfrozen soil changes phase; (2) the unfrozen volumetric heat capacity, governing the amount of heat that was extracted to cool the soil, that constitutes the frozen column at the time under consideration, from its original temperature to the freezing point of the pore water; (3) the frozen volumetric heat capacity, governing the amount of heat that must be extracted to cool the frozen soil from 0° C to its temperature at the time under consideration; and (4) the unfrozen volumetric heat capacity for cooling the unfrozen soil outside the frozen cylinder, but within the radius of influence of the freeze pipe.

The equation for the total heat energy extracted given by Sanger and Sayles (1979) is:

$$Q = \pi R^2 \{ L + ((a_r^2 - 1)/2 \ln(a_r)) C_u v_o + C_f v_s / (2 \ln(R/r_o)) \} \quad [2-9]$$

where: Q is the total heat extracted from the ground (J/m length of freeze pipe); L is the volumetric latent heat of fusion (J/m³); a_r is the factor which when multiplied by the frozen radius, R (m), defines the radius of temperature influence of the freeze pipe outside the frozen cylinder (a_r is generally assumed to be 3); C_u is the volumetric latent heat of the unfrozen soil (J/m³°K); v_o is the difference between the original ground temperature and the freezing point of water (°K); C_f is the volumetric heat capacity of the

frozen soil (J/m^3K); v_s is the difference between the skin temperature of the freeze pipe and the freezing point of water ($^{\circ}K$); and r_o is the radius of the freeze pipe (m).

Sanger and Sayles (1979) also give an equation for the time required to freeze a column of soil with radius R . The expression is based on the fact that the rate of heat flow through the wall of the freeze pipe must be sufficient to sustain the growth of the freezing soil column. Applying the Fourier Equation for steady state heat flow to a cylinder, the authors give the following expression:

$$t = (R^2 L_1 / 4k_f v_s) \{ 2 \ln(R/r_o) - 1 + C_f v_s / L_1 \} \quad [2-10]$$

where:

$$L_1 = \{ L + ((a_r^2 - 1) / 2 \ln(a_r)) C_u v_o \} \quad [2-11]$$

where k_1 is the thermal conductivity of the frozen soil ($J/sm^{\circ}K$).

2.6.1 Growth of the Frozen Radius

The growth of a frozen column of soil around a freeze pipe can be predicted by solving Equation [2-10], repeatedly, for specified radial increments up to the final design radius. Utilizing a spread sheet and specifying the soil moisture content, density, both the frozen and unfrozen soil thermal properties, and the temperatures of the groundwater and freeze pipe, the frozen radius versus time can be obtained. A typical plot of the growth of the frozen radius with time is shown in Figure 2-6. Initially, the frozen radius increases quickly since the unfrozen soil is in close proximity to the freeze pipe containing liquid nitrogen at $-196^{\circ}C$. As the frozen radius increases, the unfrozen soil is in contact with the frozen column of sand which is considerably warmer than the freeze pipe. Hence, the rate of growth of the frozen zone decreases with time. The selection of thermal properties will be discussed further as part of the case histories presented in Chapters 4 and 5. Comparisons between the actual growth of the frozen zone and the theoretical predictions will also be presented.

2.6.2 Volume of Liquid Nitrogen Required

The volume of liquid nitrogen required to freeze a given radius, R , can be determined by dividing Equation [2-9] by the volumetric latent heat of liquid nitrogen, since this represents the capacity of the liquid nitrogen to extract heat from the ground. The liquid nitrogen consumption can then be plotted against time, utilizing Equations [2-10] and [2-11] for increments of frozen radius up to the final radius. Figure 2-7 shows a typical plot of liquid nitrogen consumption with time. Corresponding to the growth of the frozen radius with time, the rate of liquid nitrogen consumption decreases with time, however, the decrease is less pronounced. This is due to the fact that although the rate of growth of the frozen radius is decreasing with time, the volume of soil being frozen as the radius progresses is increasing dramatically.

2.7 Conclusions

In summary, the following conclusions can be made:

- Disturbance by frost heave is due to either ice lenses forming in frost heave susceptible soils or when the excess 9 % of pore water volume freezes in place.
- The frost heave susceptibility of a soil depends on the soil grain size distribution, including the percentage of fines and their mineralogy, the unfrozen water content, the drainage boundary conditions, the overburden stress and rate of cooling compared to the permeability of the deposit.
- The risk of disturbance due to frost heave can be reduced by conducting radial ground freezing, such that pore water expulsion can take place in advance of the freezing front.
- The chart presented by Davila et al. (1992), which takes into account the effect of the fines mineralogy on frost heave potential, can be utilized, in conjunction with bulk

samples obtained from a specific site, as a preliminary estimate of the frost heave susceptibility of the deposit.

- Prior to conducting in-situ ground freezing, it is prudent to carry out frost heave tests in the laboratory, under the conditions that exist in-situ, to confirm that this method is appropriate for obtaining undisturbed samples.
- Theoretical equations are available for predicting the rate of growth of the frozen zone and the consumption of liquid nitrogen during ground freezing. This will help identify the costs associated with undertaking in-situ ground freezing for undisturbed sampling.

2.8 References

- Anderson, D. and Morgenstern, N. R., 1973, Physics, Chemistry and Mechanics of Frozen Ground: A Review. Proceedings of 2nd International Permafrost Conference. Yakutsk, U.S.S.R.
- Anderson, D. M. and Tice, A. R., 1972. Prediction of Unfrozen Water Contents in Frozen Soils from Surface Area Measurements. . Highway Research Record. No. 393. p.12-18.
- Colbeck, S. C.. 1981, Introduction to the Basic Thermodynamics of Cold Capillary Systems, U.S. Army CRREL Special Report 81-6, Hanover New Hampshire, USA. 9p.
- Davila, R. S., Segó, D. C. and Robertson, P. K., 1992. Undisturbed Sampling of Sandy Soil by freezing, Canadian Geotechnical Conference Proceedings, Toronto, pp. 13A-1 to 13A-10.
- Hashemi, H. T. and Sliepcevich, C. M., 1973, Effect of Seepage Stream on Artificial Soil Freezing, Proceedings, Ground Freezing Conference, Developments in Geotechnical Engineering, V 28,189-201.

- Hatanaka, M., Sugimoto, M., and Yoshio, S., 1985, Liquefaction Resistance of Two Alluvial Volcanic Soils Sampled by In Situ Freezing., *Soils and Foundations*. Vol. 25, No. 3, pp. 49-63.
- Hivon, E. and Segoo, D. C., 1994, Strength of Frozen Saline Soils. *Canadian Geotechnical Journal*, Vol. 32, No. 2, pp. 336-354.
- Holtz, R. D. and Kovacs, W. D., 1981, *An Introduction to Geotechnical Engineering*. Prentice-Hall, Inc., Englewood Cliffs, New Jersey, 07632, p.41.
- Konrad, J.-M., 1995, personal communication.
- Konrad, J.-M., 1990, Sampling of Saturated and Unsaturated Sands by Freezing. *Geotechnical Testing Journal*, ASCE, V 13, No. 2, pp. 88-96.
- Konrad, J.-M. and Morgenstern, N. R., 1980, A Mechanistic Theory of Ice Lens Formation in Fine Grained Soils, *Canadian Geotechnical Journal*. V 17. 473-486.
- Konrad, J.-M. and Morgenstern, N. R., 1982. Effects of Applied Pressure on Freezing Soils, *Canadian Geotechnical Journal*, V. 19, pp. 494-505.
- Konrad, J.-M. and Morgenstern, N. R., 1983. Frost Susceptibility of Soils in Terms of their Segregation Potential, 4th International Conference on Permafrost. Fairbanks National Academy of Science, Washington, D. C., pp. 660-665.
- Konrad, J.-M. and St-Laurent, S., 1995, Controlled Freezing and Thawing as a way to Test Intact Sand: A Laboratory Investigation.. 48th Canadian Geotechnical Conference Proceedings, Vancouver, September, 1995, pp. 213-222.
- McRoberts, E. C. and Morgenstern, N. R., 1975, Pore Water Expulsion during Freezing. *Canadian Geotechnical Journal*, V 12, No. 1, pp. 130-141.
- Mitchel, J. K., 1976, *Fundamentals of Soil Behaviour: Chapter 15 - Heat Flow Through Soil*, John Wiley and Sons Inc., New York, pp. 340-383.
- Nerseova, Z. A. and Tsytoovich, V. A., 1963, Unfrozen Water in Frozen Soils, 1st International Conference on Permafrost, Proceedings, Lafayette, Indiana, USA.
- Sanger, F. J. and Sayles, F. H., 1979, Thermal and Rheological Computations for Artificially Frozen Ground Construction, *Engineering Geology*, 13, pp. 311-337.
- Stoss, K. and Valk, J., 1979, Uses and Limitations of Ground Freezing with Liquid Nitrogen., *Engineering Geology*, V 13, pp. 485-494.

- Takashi, Tsutomou, 1969, Influence of Seepage Stream on the Joining of Frozen Soil Zones in Artificial Soil Freezing, National Research Council, Proceedings of Int. Conference. on Effects of Temperature and Heat on Engineering Behaviour of Soils, Special Report, No. 103, pp. 273-286.
- Tyutyunov, V. A., 1963, Phase Transformations of Water in Soils and the Nature of Migration and Heaving., 1st International Conference on Permafrost, Proceedings, Lafayette, Indiana, USA.
- Williams, P. S., 1967, The Nature of Freezing Soil and its Field Behaviour. Properties and Behaviour of Freezing Soils. Norwegian Geotechnical Institute. Publication No. 72, Oslo, pp. 91-119.
- Yoshimi, Y., Hatanaka, M., and Oh-Oka, H., 1977, A Simple Method for Undisturbed Sand Sampling by Freezing, Proceedings. Spec. Session 2, 9th Int. Conference. on Soil Mech. and Foundation Engineering. Eng., pp. 23-28.
- Yoshimi, Y., Hatanaka, M., and Oh-Oka, H., 1978. Undisturbed Sampling of Saturated Sands by Freezing, Soils and Foundations. Vol. 18. Sept., pp. 59-73.
- Yoshimi, Y., Tokimatsu, K., Kaneko, O. and Makihara, Y., 1984. Undrained Cyclic Shear Strength of a Dense Niigata Sand, Soils and Foundations. Vol. 24, No. 4, pp. 131-145.
- Yoshimi, Y. Tokimatsu, K. and Ohara, J. 1994. In Situ Liquefaction Resistance of Clean Sands over a wide Density Range. Géotechnique, Vol. 44, No. 3, pp. 479-494.

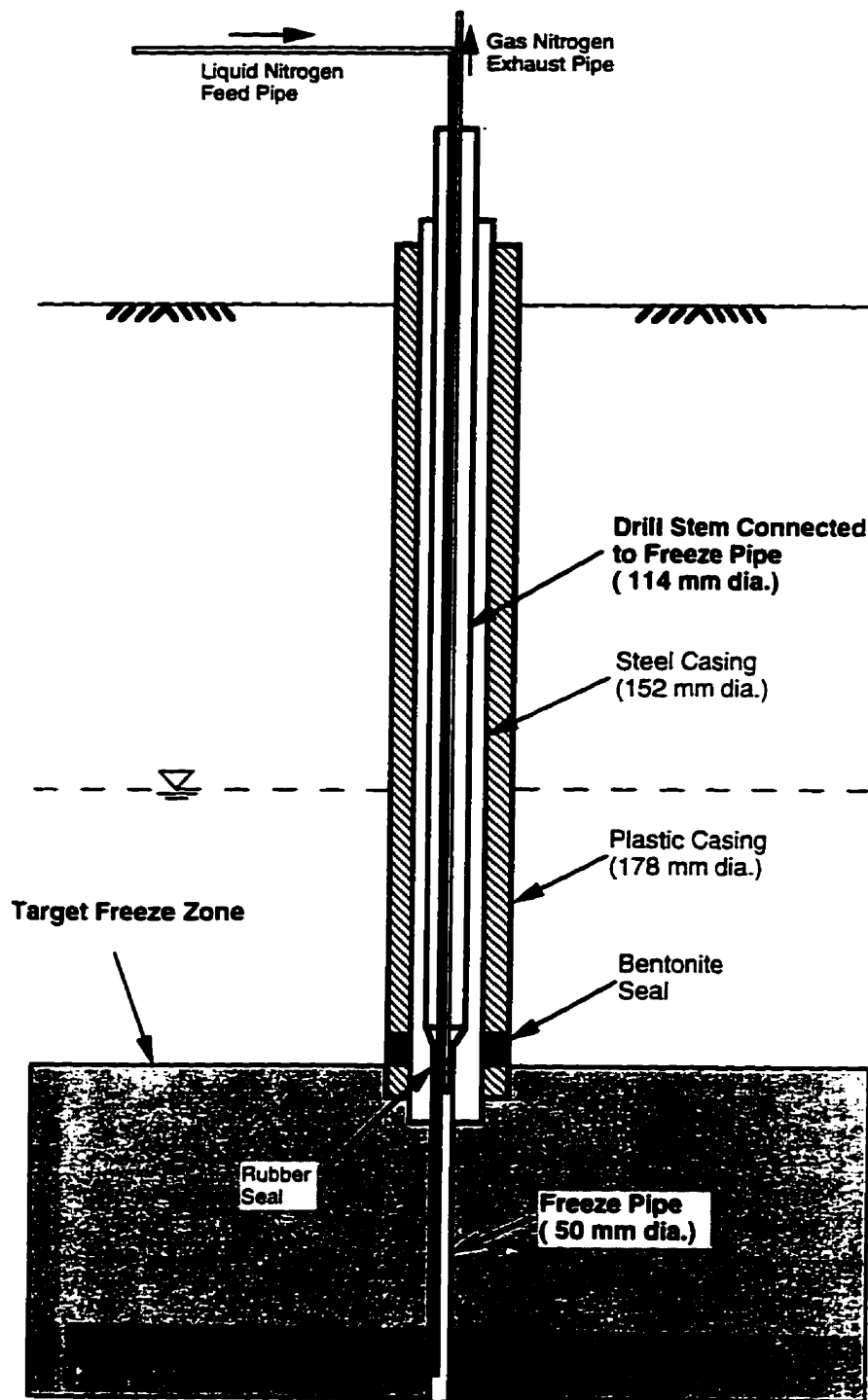


Figure 2-1: Schematic of Freeze Pipe System

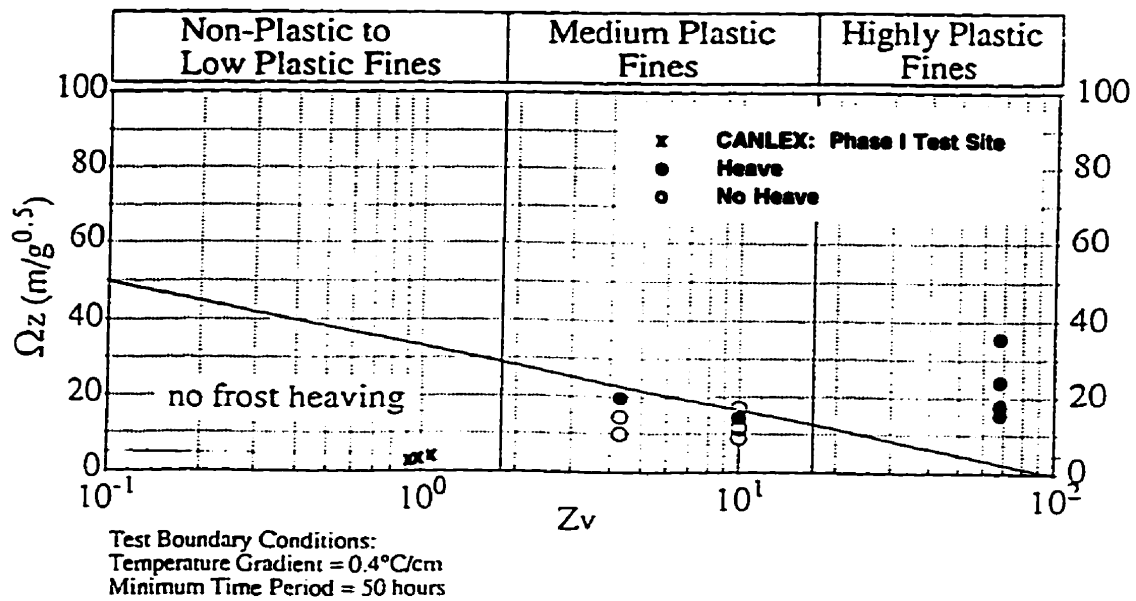


Figure 2-2: Surface Area Criteria Plot for Evaluation of Frost Heave Susceptibility (modified from Davila, et al. 1992)

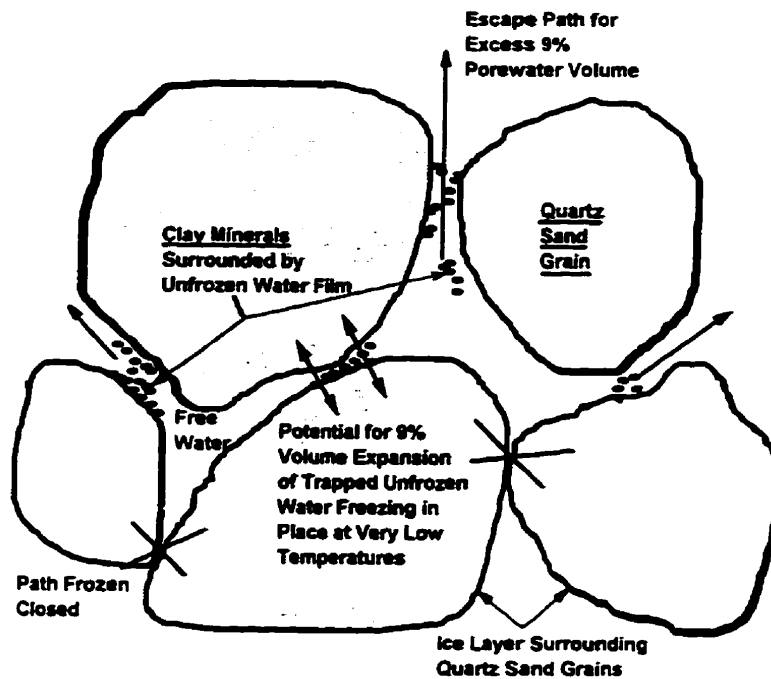


Figure 2-3: Schematic Illustration of Impeded Drainage of Unfrozen Water Surrounding Clay Minerals in a Sand Sample.

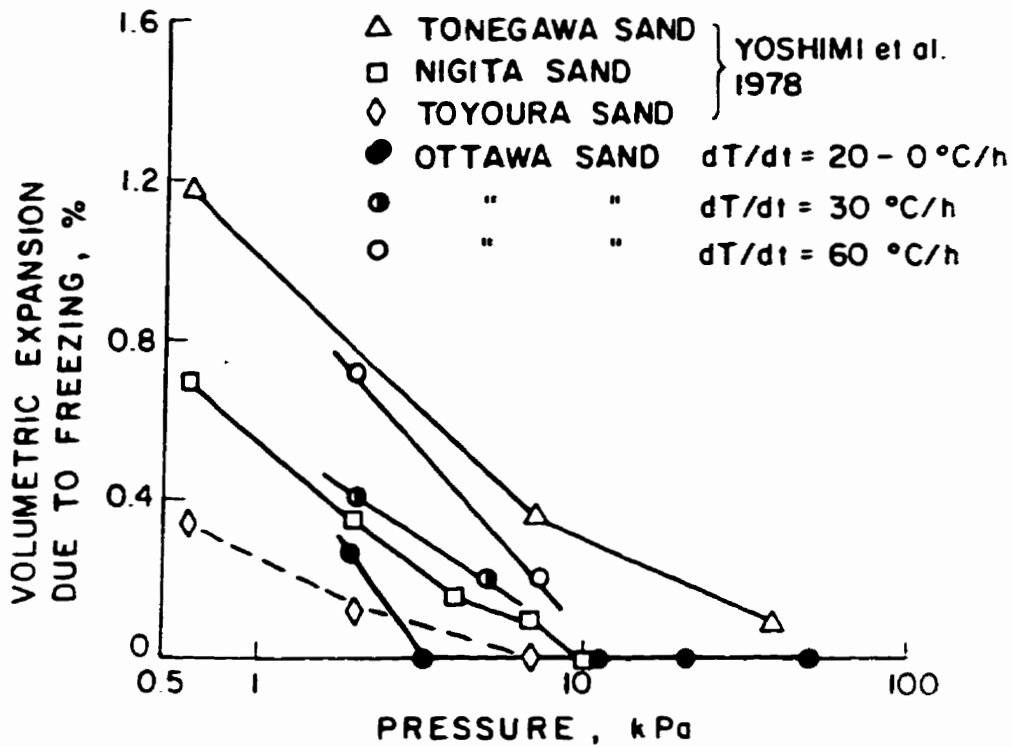


Figure 2-4: Effect of Overburden Stress on Volumetric Expansion during Freezing (modified from Konrad, 1990)

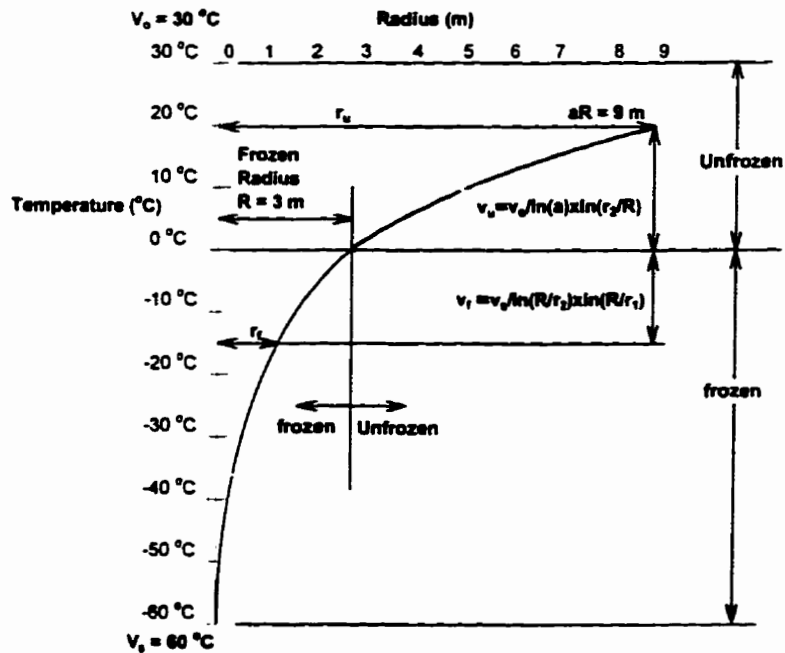


Figure 2-5: Typical Temperature Profile through Frozen and Unfrozen Soil Surrounding a Freeze Pipe (modified from Sanger and Sayles, 1979).

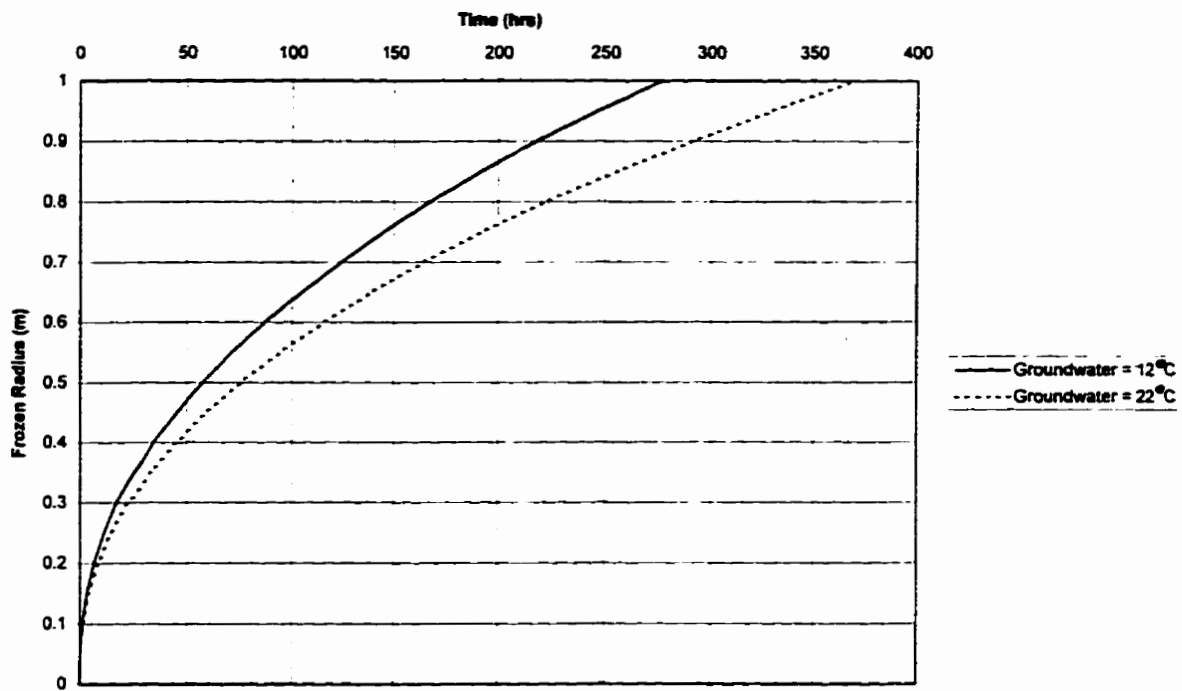


Figure 2-6: Theoretical Prediction of the Growth of a Frozen Column around a Freeze Pipe for Different Initial Ground Temperatures.

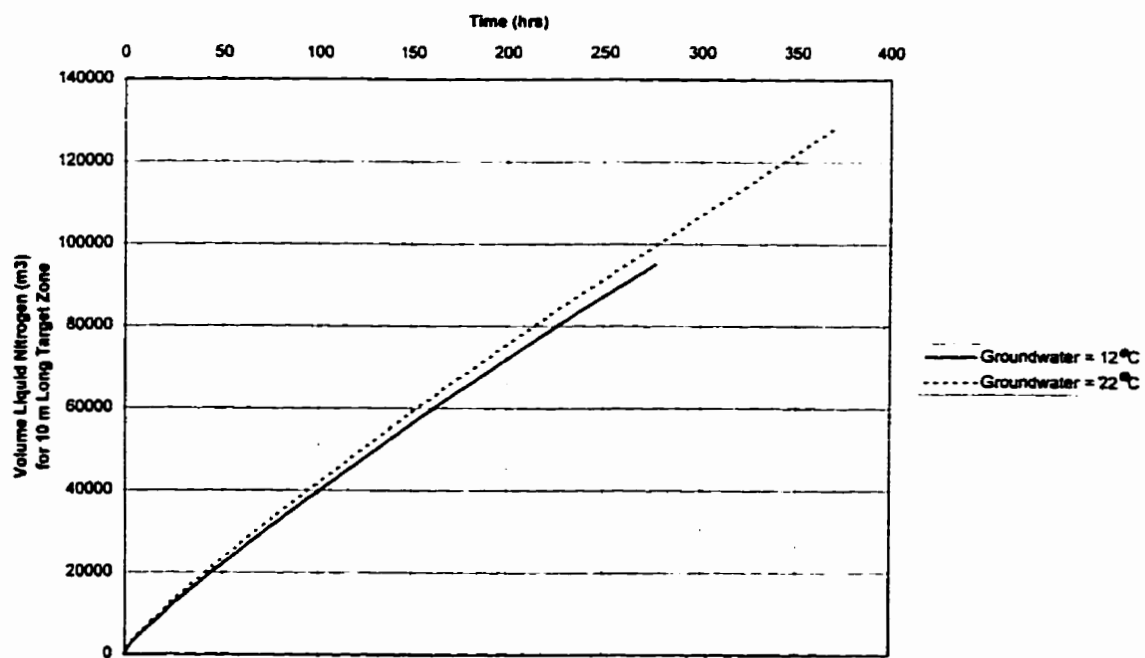


Figure 2-7: Theoretical Prediction of Liquid Nitrogen Consumption during Freezing of a Column of Sand around a Freeze Pipe.

CHAPTER 3: Design of In-Situ Ground Freezing System Utilizing Liquid Nitrogen

3.0 Introduction

At the beginning of this research project, a ground freezing study was undertaken to develop an efficient freezing system that could be utilized at various test sites to recover undisturbed samples of relatively loose granular soils for the CANLEX project. The study included conducting large scale, in-situ ground freezing experiments in a large diameter cased borehole, extending 10 m below the ground surface, that would serve as a freezing chamber. Four experiments were conducted in a 10 m deep column of water and two were conducted in a 5 m deep column of wet sand, to monitor the growth of the frozen zone around a prototype freezing pipe under different boundary conditions.

The primary objectives of the ground freezing experiments conducted for the study included:

- comparison of the actual and predicted growth of the frozen zone around a freeze pipe system to check how well the available heat flow equations model the actual freezing process;
- design of a freezing system to promote the efficient use of liquid nitrogen and reduce the rate of liquid nitrogen consumption; and
- development of a system for freezing of target zones, along specified lengths of the freeze pipe, to reduce the volume of soil to be frozen and thus the liquid nitrogen consumption.

3.1 Design of Experimental Freezing System

3.1.1 Freezing Chamber

To form a large, below ground chamber to conduct the experiments, a 0.9 m diameter borehole was excavated at the University of Alberta Farm test site to a depth of approximately 12 m below the ground surface. The borehole was advanced through clayey subsoils utilizing a large diameter auger drilling rig. A steel casing was lowered down the borehole to the full depth. Concrete was then placed at the bottom of the casing to prevent groundwater from entering the cased hole. The completed inside depth of the cased hole was approximately 10 m below the ground surface, with the casing protruded approximately 0.75 m above the ground surface. Upon completion, the cased hole was filled with clean water to the ground surface. The final configuration of the cased hole, prepared for the ground freezing experiments, is shown in Figure 3-1.

3.1.2 Freezing System

The freezing system was comprised of a 51 mm diameter steel freeze pipe that contained two, 13 mm diameter copper pipes. One of the copper pipes was used for injecting liquid nitrogen into the freeze pipe, and the other to eliminate gas nitrogen after the liquid nitrogen had undergone phase change. Rubber seals were placed at selected depths to create reservoirs within the freeze pipe where liquid nitrogen would be allowed to completely fill that section of the freeze pipe. A schematic diagram, showing a typical freezing system configuration utilized during the experiments is shown in Figure 3-1.

3.1.3 Monitoring of the Freezing Process

Resistance Temperature Devices (RTDs) were hung at regular intervals from a bracket attached near the top of the freeze pipe and fastened to a similar bracket located at the

base of the freeze pipe. Four strings of RTDs were installed such that the temperature distribution during freezing could be determined in a radial direction and along the length of the freezing zone. The RTD strings were installed at radial distances of 0.06 m, 0.16 m, 0.26 m and 0.36 m along the full length of the freeze pipe, as shown in Figure 3-1.

3.1.4 Theoretical Prediction of the Freezing Process

In Chapter 2 of this thesis, a detailed discussion of the theoretical prediction of the ground freezing process was presented. However, it is necessary to highlight some of the key features regarding the theoretical equations presented by Sanger and Sayles (1979) that describe the heat energy extraction requirements. This will facilitate an understanding of the discrepancies between experimental measurements and the theoretical predictions.

Given the discontinuity that exists in the temperature curve at the frozen/unfrozen boundary, Sanger and Sayles (1979) made some simplifying assumptions to allow for development of a mathematical expression describing heat extraction during ground freezing. Included in these, was the assumption that the isotherms move slowly enough that the conditions at any given frozen radius can be assumed to be steady state. Thus, the equation, which describes the total energy that must be extracted from the ground at any given radius, includes the following four terms:

1. the volumetric latent heat of the frozen soil liberated when the unfrozen soil changes phase;
2. the unfrozen volumetric heat capacity, governing the amount of heat that must be extracted to cool the soil, that constitutes the frozen column at the time under consideration, from its initial temperature to the freezing point of the pore water;

3. the frozen volumetric heat capacity, governing the amount of heat that must be extracted to cool the frozen soil from the freezing point of the pore water to its temperature at the time under consideration, and
4. the unfrozen volumetric heat capacity for cooling the unfrozen soil outside the frozen cylinder, but within the radius of influence of the freeze pipe.

The volume of liquid nitrogen required to freeze a given radius of soil can then be estimated by dividing the summation of these terms by the latent heat of liquid nitrogen. since this represents the capacity of the liquid nitrogen to extract heat from the ground. The effect of assuming that steady state conditions prevail at a given frozen radius. for theoretical prediction of the ground freezing process, will be discussed along with the experimental results later in this chapter. Copies of the spread sheets used for predicting the volumes of liquid nitrogen used during each experiment are provided in Appendix A.

3.2 Procedures and Test Results for Freezing Experiments Conducted in Water

Four experiments were conducted with the freezing chamber full of water and two experiments were conducted in clean wet sand. Water was frozen for the first set of experiments since the thermal properties of water are known, thereby facilitating evaluation of how well the theoretical equations for heat extraction requirements presented by Sanger and Sayles (1979) model the actual freezing process.

The thermal properties used for the calculations in which water was frozen included:

Thermal conductivity of water =	0.61 J/sm°K
Thermal conductivity of ice =	2.20 J/sm°K
Volumetric Heat Capacity of water =	4.187 MJ/m ³ °K
Volumetric Heat Capacity of ice =	1.88 MJ/m ³ °K
Latent Heat of Fusion =	334 kJ/kg

After the completion of the water freezing experiments, two experiments were conducted where saturated, clean sand was frozen. Modeling of the freezing process during these experiments required estimation of the thermal properties of the sand. The volumetric heat capacity of the unfrozen (C_u) and frozen (C_f) sand were estimated using the following relations provided by Farouki (1986):

$$C_u = \gamma_d / \gamma_w \{0.18 + 1.0\omega/100\} C_w \quad (\text{J/m}^3\text{°K}) \quad [3-1]$$

$$C_f = \gamma_d / \gamma_w \{0.18 + 0.5\omega/100\} C_w \quad (\text{J/m}^3\text{°K}) \quad [3-2]$$

where γ_d is the dry density of the soil in kg/m^3 , γ_w is the unit weight of water in kg/m^3 , ω is the water content in percent, and C_w is the volumetric heat capacity of water in $\text{J/m}^3\text{°K}$.

Initially, the dry density and water content of the sand were estimated based on experience with similar soils. However, once a sample of the frozen sand could be recovered, two block samples were cut from the frozen bulb obtained during Experiment 6 for grain size and moisture content analysis. After the moisture contents had been corrected for 9 % expulsion of pore water during freezing, the information obtained from the laboratory tests conducted on the block samples was used to re-calculate the in-pur parameters required for analytical predictions. The grain size curves obtained from the two block samples are shown in Appendix A. Figure A1. The moisture contents determined for the two block samples were 23.8 % and 27.5 %, giving the average moisture content of 25.7 % that was used for theoretical predictions.

Initial predictions of the frozen and unfrozen thermal conductivity of the sand were made based on charts provided by Kersten (1949), where thermal conductivity is presented as a function of dry density and moisture content. The charts given by Kersten predicted an unfrozen thermal conductivity of about $1.75 \text{ J/sm}^{\circ}\text{K}$ and a frozen thermal conductivity of about $3.1 \text{ J/sm}^{\circ}\text{K}$. However, after data was available from the freezing experiments, it was evident that these unfrozen and frozen thermal conductivities were not correct, since

the actual growth of the frozen radius was significantly faster than the initial theoretical prediction.

According to Farouki (1981), although Kersten's method does not consider the quartz content of a soil, the thermal conductivity of a granular soils is strongly related to the thermal conductivity of the soil grains, which is a function of quartz content. By comparing measured and predicted values, Farouki concluded that the best method for estimating the thermal conductivity of granular soil, which takes into account quartz content, is given by Johansen (1975). Therefore, the unfrozen and frozen thermal conductivities of the sand were revised based on the charts presented by Farouki (1981). The revised thermal properties used to predict the growth of the frozen radius and liquid nitrogen consumption in the experiments where sand was frozen, were as follows:

$$k_u = 2.3 \text{ J/sm}^\circ\text{K}$$

$$k_f = 4.3 \text{ J/sm}^\circ\text{K}$$

The specific freeze pipe configurations and procedures followed during each experiment are presented in the following sections along with a brief description of the test results. This is followed by a more detailed discussion and comparison of the experimental results with the theoretical predictions.

3.2.1 Experiment 1

Procedure

Experiment 1 involved freezing a column of water of approximately 1 m in length, between a depth of 4 and 5 m below the ground surface. Rubber seals were placed at depths of 4 m and 5 m below the ground surface to allow for the accumulation of liquid nitrogen in the freeze pipe between these depths during the experiment. The exhaust, or riser, pipe was cut off just above the upper rubber seal and gaseous nitrogen was allowed

to escape through the riser pipe, into the freeze pipe above the target zone and then into the atmosphere.

The initial set of temperature readings taken from the RTDs prior to freezing indicated that the temperature of the water in the steel casing (freezing chamber) was approximately 6.2 °C near the bottom of the freezing chamber and 8.7 °C near the ground surface. Prior to connecting the freezing system to the liquid nitrogen, the column of water in the freezing chamber was cooled to reduce the volume of liquid nitrogen needed for the experiment and the length of time required to freeze the target zone. This was achieved by feeding small volumes of liquid nitrogen directly into the column of water through an open-ended, 0.05 m diameter copper pipe with a length of about 4.6 m. After 8 hours of cooling, the water temperature in the casing was reduced to approximately 0.35 °C, in the upper 4.5 m zone, and approximately 4.0 °C, below this depth. In the target zone, the initial water temperature was approximately 3.3 °C. Liquid nitrogen was then connected to the freezing system and radial freezing commenced.

Test Results

Freezing during Experiment 1 was carried out for a total of 11.8 hours. During freezing, the temperatures were monitored at the RTD locations. Temperature data collected during the experiments are provided in Appendix A. Once freezing was complete, the freeze pipe with the frozen bulb attached was lifted out of the casing utilizing a crane. The dimensions of the frozen zone were then recorded. A schematic of the frozen bulb is shown in Figure 3-2, with the dimensions recorded at 1 m intervals.

The frozen zone extended from just below the ground surface to a depth of approximately 6.0 m. Since the copper exhaust pipe had been cut off just above the rubber seal at the top of the target zone, gaseous nitrogen, and probably some excess liquid nitrogen, was allowed to fill the freeze pipe above the upper target zone, thereby also causing freezing in this region. The frozen column had an average radius of approximately 0.14 m between depths of 1 m and 3 m. In the target zone, the minimum frozen radius, measured

at the top of the target zone, was 0.18 m, and the maximum frozen radius, measured at the bottom of the target zone, was 0.22 m. Once the measurements of the frozen zone had been taken, the ice was removed from the freeze pipe and the RTD strings. The freezing system was then repositioned in the borehole for the next experiment.

A comparison of the frozen radius predicted for an initial groundwater temperature of 3.3 °C, assuming that the freeze pipe was full of liquid nitrogen in the target zone, was made with the actual measured maximum and minimum frozen radii attained. Figure 3-3 shows that the measured minimum frozen radius, at the top of the target zone, fell below the growth of the frozen radius predicted for liquid nitrogen, while the maximum radius of the frozen zone, near the bottom of the target zone, agreed with the theoretical prediction. Figure 3-4 also shows that the predicted liquid nitrogen consumption was significantly greater than the actual consumption.

The discrepancy with respect to liquid nitrogen consumption was likely due to the fact that during the first experiment some difficulty was encountered in maintaining the freeze pipe reservoir completely full of liquid nitrogen at all times within the target zone. Hence, in the upper portion of the target zone, heat loss to gaseous nitrogen in the freeze pipe by conduction would have been substantially less than heat loss due to the phase change of liquid nitrogen. Since, the theoretical predictions considered thus far assume that heat extraction is due solely to the latent heat of liquid nitrogen, the growth of the frozen zone near the bottom of the target zone, where liquid nitrogen filled the freeze pipe throughout the duration of the experiment, would be expected to agree with theoretical predictions. However, Figure 3-3 also shows that when it was assumed that only gaseous nitrogen existed in the freeze pipe at a temperature of about -120 °C, the minimum frozen radius near the top of the target zone agreed with the theoretical prediction.

To confirm the hypothesis that the freeze pipe in the target zone was partially filled with liquid nitrogen and partially filled with gas nitrogen, the thermal predictions were revised. Since the actual proportions of liquid and gaseous nitrogen were unknown, it

was assumed that the upper 1/3 of the freeze pipe in the target zone was filled with gaseous nitrogen and the lower 2/3 was filled with liquid nitrogen. To predict the growth of the frozen zone under these conditions, a weighted average of the liquid nitrogen temperature and the gaseous nitrogen temperature was used to calculate the time required to reach a given frozen radius. The weighted average temperature was calculated as:

$$(1/2) \times \{ [(1/3) \times 120^\circ\text{C}] + [(2/3) \times 196^\circ\text{C}] \} = 170^\circ\text{C}$$

The equation for calculating the time to freeze a given radius of soil is given by Sanger and Sayles (1979) and was discussed in Chapter 2. For reference here, the equation is:

$$t = (R^2 L_1 / 4 k_f v_s) \{ 2 \ln(R/r_o) - 1 + C_f v_s / L_1 \} \quad [3-3]$$

where:

$$L_1 = \{ L + ((a_r^2 - 1) / 2 \ln(a_r)) C_u v_o \} \quad [3-4]$$

and L is the volumetric latent heat of fusion of the pore water (J/m^3); a_r is the factor which when multiplied by the frozen radius, R (m), defines the radius of temperature influence of the freeze pipe outside the frozen cylinder (a_r is generally assumed to be 3); C_u is the volumetric latent heat of the unfrozen soil ($\text{J}/\text{m}^3\text{K}$); v_o is the difference between the original ground temperature and the freezing point of water ($^\circ\text{K}$); k_f is the thermal conductivity of the frozen soil ($\text{J}/\text{sm}^\circ\text{K}$); C_f is the volumetric heat capacity of the frozen soil ($\text{J}/\text{m}^3\text{K}$); v_s is the difference between the skin temperature of the freeze pipe and the freezing point of water ($^\circ\text{K}$); and r_o is the radius of the freeze pipe (m). Figure 3-5 shows that the revised prediction agrees with the average of the maximum and minimum frozen radii measured along the target zone.

In Chapter 2 it was stated that, when liquid nitrogen is used as the coolant in a freeze pipe, the volume of liquid nitrogen required to freeze a given radius of soil can be estimated by dividing the total heat energy that must be extracted, by the latent heat of liquid nitrogen. Calculation of the volume of liquid nitrogen that would be required to freeze a given radius, when the freeze pipe contains both liquid and gaseous nitrogen, requires evaluation of the contribution to heat extraction by the latent heat of liquid

nitrogen and by the volumetric heat capacity of the gaseous nitrogen times the temperature change of the gas.

Hence for Experiment 1, where it was assumed that the freeze pipe reservoir contained 1/3 gas nitrogen and 2/3 liquid nitrogen, the equation used to calculate the volume of liquid nitrogen included the heat extraction, Q_{LN2} , related to the latent heat of liquid nitrogen and the heat extraction, Q_{GN2} , related to the volumetric heat capacity of the gaseous nitrogen. Therefore, the total volume of liquid nitrogen required to freeze a given radius was determined based on the following equation:

$$V_{LN2} = (Q_{LN2} / L_{LN2}) + (Q_{GN2} / C_{GN2} \Delta v_g)$$

$$V_{LN2} = \frac{\pi R^2 \{ L + ((a_r^2 - 1) / 2 \ln(a_r)) C_u (v_o)_{LN2} + C_f v_s / (2 \ln(R/r_o)) \}}{L_{LN2}} + \frac{\pi R^2 \{ L + ((a_r^2 - 1) / 2 \ln(a_r)) C_u (v_o)_{GN2} + C_f v_s / (2 \ln(R/r_o)) \}}{C_{GN2} \Delta v_g} \quad [3-5]$$

where: L_{LN2} is the latent heat of liquid nitrogen (kJ/m^3); C_{GN2} is the volumetric heat capacity of gaseous nitrogen ($\text{kJ/m}^3\text{K}$), Δv_g is the increase in temperature of the gas nitrogen due to absorption of heat from the surrounding ground ($^{\circ}\text{K}$), $(v_o)_{LN2}$ is the initial temperature of the liquid nitrogen ($^{\circ}\text{K}$) and $(v_o)_{GN2}$ is the initial temperature of the gaseous nitrogen ($^{\circ}\text{K}$). Figure 3-6 shows that the revised theoretical prediction of volume of liquid nitrogen utilized during Experiment 1 agrees with the actual consumption of liquid nitrogen.

3.2.2 Experiment 2

Procedure

Experiment 2 involved freezing two target zones in water, between depths of 4 to 5 m and 7 to 8 m. Rubber seals were placed at depths of 4, 5, 7 and 8 m below the ground surface

to create reservoirs for the liquid nitrogen along specific target zones. The copper exhaust pipe was cut off just above the rubber seal at 4 m, such that after the liquid nitrogen underwent a phase change in the upper reservoir, the gas nitrogen could flow into the freeze pipe where it could then be exhausted into the atmosphere at the ground surface.

The RTDs indicated that the initial temperature of the water in the freezing chamber was between 3.3 and 3.9 °C throughout the full depth. The entire column of water was cooled to approximately 0.6 °C by circulating liquid nitrogen directly into the water through an open-ended copper pipe that extended to the bottom of the cased hole. Once the water had been cooled, the freezing system was connected to the liquid nitrogen supply.

Test Results

Freezing during Experiment 2 was carried out for a total of 19.8 hours. The dimensions of the frozen zones were measured after 7.5 hours and 19.8 hours of freezing. Two sets of measurements were taken in order to compare the growth of the ice with the theoretical predictions. Two distinct bulbs of ice were formed at the target zone locations, as shown in Photograph 3-1. The measured dimensions of the frozen zones are shown in Figure 3-7. The radius of the frozen zone decreased significantly between the two target zones, indicating that the liquid nitrogen was isolated from the freeze pipe in this region in accordance with the placement of the rubber seals at 5 and 7 m. Again, freezing occurred above the upper target zone since the copper exhaust pipe had been cut off just above the rubber seal at 4 m, thereby allowing gas and excess liquid nitrogen to fill the freeze pipe above the target zone and cause freezing in that region. Once the measurements of the frozen zone had been taken, the ice was removed from the freeze pipe and RTD strings. The freeze pipe was then placed back into the water in the freezing chamber utilizing a crane.

In Figure 3-8, the maximum and minimum frozen radii measured in the target zones for Experiment 2 are shown in comparison to the predicted frozen radius for an initial

groundwater temperature of 0.6°C, assuming that the freeze pipe reservoirs in the target zones were completely full of liquid nitrogen. The maximum frozen radius, measured at the lower target zone, exceeded the predicted value, while the minimum frozen radius measured at the base of the upper target zone agreed with the theoretical prediction. As shown in Figure 3-9, for this experiment the consumption of liquid nitrogen agreed well with the theoretical prediction, based on assuming liquid nitrogen was contained within the freeze pipe reservoirs.

The theoretical predictions assumed a constant initial groundwater temperature. Hence, the maximum frozen radius measured at the bottom of the lower target zone, may have exceeded the theoretical predictions due to colder water accumulating at the bottom of the freezing chamber by convection as the experiment progressed. However, lower groundwater temperatures, of between 0.6 °C and 0 °C, would not fully account for the frozen radius exceeding the predicted value by 0.06 m.

It therefore appears that the theoretical equations under-predict the growth of the frozen radius at the base of the freeze pipe, where liquid nitrogen first accumulates. As noted in Chapter 2, the theoretical prediction of freezing time is based on assuming that steady state conditions have been attained. However, the actual time recorded during progression of the freezing front, corresponds to the instant at which a temperature of 0 °C is recorded at an RTD location, which may not represent the steady state condition. Hence, the experimental data indicates that when liquid nitrogen is used as the refrigerant for in-situ ground freezing, the assumption that the isotherms move slowly enough to resemble steady state conditions is conservative.

3.2.3 Experiment 3

Procedure

Experiment 3 also involved freezing two target zones between 4 to 5 m and 7 to 8 m. however, some modifications to the copper riser pipe (vent pipe) were made. The growth of ice above the target zone in Experiments 1 and 2 occurred due to the fact that cold gaseous nitrogen, and probably some excess liquid nitrogen, was allowed to fill the freeze pipe above the upper seal. The growth of the frozen zone in this region indicated that the freezing system may be more efficient if the copper vent pipe were extended above the seal to the ground surface. In this way, the air surrounding the riser pipe would act as an insulator and reduce the amount of radial freezing that would take place above the target zone. In response to the test results obtained from the first two experiments. for Experiment 3 the copper exhaust pipe was extended above the ground surface into the atmosphere.

RTD measurements indicated that the initial water temperature varied from about 0.5 °C to 0.9 °C. Initial temperature differences of this magnitude make very little difference to the predicted growth of the frozen radius. It is not until the initial temperature is varied by about 10 °C that the theoretical curve shifts significantly (see Figure 2-6 in Chapter 2). For calculation purposes, the initial water temperature was assumed to be 0.9 °C. Since the initial water temperatures in the chamber were only slightly above freezing. Experiment 3 was started immediately.

Test Results

Freezing during Experiment 3 was carried out for a total of 18 hours. Due to a delay in the arrival of the crane, it was not possible to remove the ice column from the casing for measurement of the frozen zones until 2 hours after the liquid nitrogen supply had expired. Two isolated frozen bulbs located at 4 to 5 m and 7 to 8 m were evident when the freeze pipe was lifted from the casing, as shown in Figure 3-10. These results show

that the freezing system designed to freeze discrete target zones was successful when the copper exhaust pipe was extended to the ground surface.

It is possible that some melting of the ice occurred between the time that the supply of liquid nitrogen expired and the time that the ice was removed from the casing. Therefore, the dimensions of the frozen section, immediately after the freezing system was shut down, may have been slightly larger. However, since the water surrounding the ice was at a temperature of less than 1 °C, the amount of melting was likely limited. Once the measurements of the frozen zone had been taken, the ice was removed from the freeze pipe and the RTD strings, and the freezing system was placed back into the water.

In Figure 3-11, the maximum and minimum measured frozen radii measured in the target zones are compared with the theoretical predictions, assuming that the target zones were completely full of liquid nitrogen at all times during the experiment. The actual maximum frozen radius measured at the lower target zone, 2 hours after freezing was complete, was greater than the predicted value. However, the frozen radius measured at the upper target zone agreed with the theoretical prediction. Similarly to Experiment 2, the actual rate of liquid nitrogen consumption agreed well with the theoretical prediction, based on assuming that the freeze pipe contained only liquid nitrogen in the target zones, as shown in Figure 3-12.

These results also indicate that at the bottom of the freeze pipe, where liquid nitrogen accumulates first, the theoretical equations are somewhat conservative with respect to prediction of the length of time required to freeze a given radius. As noted previously, the conservatism inherent in the theoretical prediction of time to freeze a given radius stems from the fact that the theory is based on assuming steady state conditions have been attained; however, when liquid nitrogen is used to freeze the ground, the rate of growth of the frozen zone likely exceeds the rate that can be approximated by steady state conditions. This conservatism may also be caused by assuming that the unfrozen and frozen thermal conductivities are constant, whereas the very cold temperature of the

liquid nitrogen (-196 °C) may result in significantly higher values for the soil in the immediate vicinity of the freeze pipe. In addition, the discrepancy may also result from additional heat loss from poorly insulated regions of the freeze pipe adjacent to the target zones that is not taken into account by the theoretical equations, which assume one-dimensional freezing. Although the liquid nitrogen in the copper pipes outside the target zones were insulated from the freeze pipe by the air space between the copper pipes and the wall of the freeze pipe, the steel freeze pipe most likely conducted cold temperatures along its entire length, thereby causing cooling of the water surrounding the freeze pipe outside the target zones. Convection of the colder water to the lower portions of the freezing chamber, such that the initial temperature used in thermal calculations was not constant, may have thus resulted in an increase in the rate of growth of the frozen zone in this region.

3.2.4 Experiment 4

Procedure

Experiment 4 involved freezing a continuous 8 m long column of water. The rubber seals were positioned such that freezing would take place between depths of 1.25 m and 9.25 m below the ground surface. The location of one of the RTD strings was modified slightly for the remaining experiments. The RTD string initially located at a radial distance of 0.36 m from the freeze pipe was removed and installed directly along the outside of the freeze pipe. The remaining RTD strings were left in their original positions at radial distances of 0.6 m, 0.16 m, and 0.26 m from the freeze pipe.

The water in the casing was warmed slightly prior to commencing freezing to include the energy extraction required to cool the water to the freezing point. This was accomplished by mixing hot water into the freezing chamber. The initial temperatures just prior to connecting the freezing system varied from approximately 1.5 °C to 2.2 °C. An initial groundwater temperature of 1.9 °C was used for theoretical predictions.

Test Results

Freezing during Experiment 4 was carried out for a total of approximately 19 hours. The frozen column was removed from the water immediately after the supply of liquid nitrogen was turned off and measurements of the frozen zone were taken. The frozen column was slightly tapered, as shown in Photograph 3-2 and Figure 3-13, with a radius of approximately 0.21 m near the top of the column and a maximum radius of approximately 0.28 m at the base. Once the measurements were taken, the ice was removed from the freezing system, which was then modified for Experiment 5.

The maximum and minimum frozen radii measured in Experiment 4 are shown in Figure 3-14. The maximum frozen radius measured near the bottom of the frozen column slightly exceeded the theoretical prediction, assuming that the freeze pipe was completely full of liquid nitrogen in the target zone at all times. However, the minimum frozen radius measured was less than predicted. Figure 3-15 also shows that the actual consumption of liquid nitrogen during freezing of a continuous 8 m column of water in Experiment 4 was considerably less than the predicted, assuming the freeze pipe within the target zone contained liquid nitrogen.

The slower rate of cooling at the top of the target zone was likely due to the fact that since the target zone reservoir was 8 m long, it was difficult to maintain a sufficient flow rate of liquid nitrogen to keep the reservoir full of liquid nitrogen at all times during the experiment. Figure 3-13 shows that the frozen radius increased at a depth of approximately 6 m. It therefore appears that during most of the experiment, the bottom 1/3 of the freeze pipe most likely contained liquid nitrogen while the top 2/3 contained gaseous nitrogen. The revised thermal predictions based this assumption are shown in Figures 3-16 and 3-17. Once again, the revised predicted growth of the frozen radius marks the approximate average of the measured maximum and minimum frozen radius, while the predicted and actual liquid nitrogen consumption show good agreement.

To increase the efficiency of ground freezing, higher liquid nitrogen flow rates would have to be maintained to prevent the level of liquid nitrogen in the freeze pipe from falling below the top of the target freeze zone. To aid in keeping the freeze pipe reservoir consistently full of liquid nitrogen, installation of a valve on the exhaust pipe, to apply a slight back pressure, would likely be beneficial.

3.3 Procedures and Test Results for Experiments Conducted in Sand

3.3.1 Experiment 5

Procedure

As the ice was being removed from the freezing system at the end of Experiment 4, most of the ice was placed on the ground, outside the casing. However, some pieces of ice fell back into the freezing chamber. This ice froze to the walls of the steel casing, forming an ice cap at the water surface with a thickness of approximately 0.5 m. In order to place the freeze pipe back in the borehole, the ice cap had to be broken up. This was accomplished by the addition of hot water and circulation of the water in the casing with warm gaseous nitrogen at a temperature of approximately +5° C. This process resulted in a slight temperature gradient in the water.

Experiment 5 involved freezing a 5 m column of wet sand. The target freeze zone was located between 1 m and 5.4 m below the ground surface. To facilitate removal of the frozen zone at the end of the experiment, the freeze pipe was shortened such that freezing would take place only within the upper section of the freezing chamber. Once the ice had been broken up, the freezing chamber was filled with sand by hand. The sand was allowed to settle through the water contained in the cased hole, to a depth of 5.25 m below the ground surface. The freeze pipe was then hung in the water above the sand with a crane such that it extended from 1.2 m above the ground surface to 5.8 m below the ground surface. Sand was then placed around the freeze pipe up to the ground surface. RTD measurements indicated that the initial temperature of the saturated sand.

prior to freezing, was approximately 3.5 to 4.1 °C. An initial temperature of 3.5 °C was used for the theoretical predictions.

Test Results

Based on theoretical predictions using the thermal properties estimated from Kersten's charts (Kersten, 1949), freezing during Experiment 5 was carried out for a total of approximately 20.4 hours. After freezing was complete, a vacuum truck was utilized to remove the saturated, unfrozen sand from between the frozen soil and the casing to allow for removal of the frozen column of sand. However, during removal of the unfrozen saturated sand, it was discovered that the frozen radius extended to within 14 cm of the casing at the ground surface and the frozen column of sand could not be removed with a crane. Hence, it was assumed that the frozen sand likely extended all the way to the wall of the casing at depth. Figure 3-18, shows the estimated extent of the frozen column sand developed during Experiment 5.

To thaw the sand frozen to the casing, hot water was circulated through the freeze pipe for several days. Once the RTDs indicated that the temperature of the sand was above 0° C at all locations, circulation of the hot water was stopped. The same freeze pipe configuration was then used for Experiment 6, where the sand was frozen for a shorter period of time.

The estimated maximum and minimum frozen radii attained in Experiment 5 are shown in comparison with the predicted values in Figure 3-19. Prediction 1, which was based on the thermal conductivities estimated from Kersten's method, does not agree with either the maximum or minimum growth of the frozen radius. Therefore, it was assumed that the thermal properties may not be correct and new parameters were selected based on Johansen's charts (Johansen, 1975), as presented by Farouki (1981). The growth of the frozen radius given by Prediction 2 agrees with the maximum frozen radius estimated at the bottom of the frozen column. The minimum frozen radius at the top of the target zone likely does not match with the theoretical predictions due to the presence of only gas

nitrogen in the upper portion of the target zone, as indicated in Experiments 1 and 4. In support of this assumption, the actual consumption of liquid nitrogen during Experiment 5 also does not agree with the theoretical predictions, as shown in Figure 3-20. Since the actual frozen radii were not measured for Experiment 5, modification of the thermal predictions to account for gaseous nitrogen in the freeze pipe was not undertaken.

3.3.2 Experiment 6

Procedure

Experiment 6 involved repeating Experiment 5, but freezing was undertaken for a shorter period of time. A 5 m column of wet sand was frozen between 1 m and 5.4 m below the ground surface. RTD measurements indicated that the initial temperature of the saturated sand prior to commencing freezing was 9.5 °C to 10.3 °C. The thermal predictions were carried out assuming an initial temperature of 9.9 °C.

In order to improve the efficiency of the freezing system, a piezometer was installed to measure the liquid nitrogen level in the copper feeder pipe such that it could be kept constant during freezing. Prior to conducting Experiment 6, a 3 mm diameter copper standpipe was installed through the exhaust pipe, down to the bottom of the liquid nitrogen reservoir in the target zone.

Continued fluctuations in the piezometer level indicated that the reservoir was filled with liquid nitrogen until a critical level of fluid had accumulated and then the liquid nitrogen rapidly underwent a phase change to the gaseous state. By monitoring the piezometer levels, it was possible to maintain a more constant flow of liquid nitrogen during freezing. However, with the equipment being utilized on the liquid nitrogen tanker at the time, it was not possible to completely eliminate surging of the coolant.

Test Results

By exercising more careful control over the flow of liquid nitrogen, the rate of usage of the liquid nitrogen was kept more constant during Experiment 6. The RTD measurements taken during Experiment 6 indicated that, provided the supply of liquid nitrogen was kept constant, the groundwater temperatures did not fluctuate significantly, but continued to decrease smoothly throughout the freezing process.

Freezing during Experiment 6 was carried out for a total of approximately 10 hours. A vacuum truck was used to remove the saturated, unfrozen sand from inside the cased hole. The frozen column was then raised from the casing utilizing a crane, as shown in Photograph 3-3. The dimensions of the frozen column are shown in Figure 3-21. The frozen bulb was slightly tapered, with a radius of 0.26 m at the top of the column and 0.24 m near the midpoint, with a maximum radius of about 0.38 m near the bottom.

The maximum and minimum frozen radii attained within the target zone during Experiment 6 are shown in Figure 3-22. The average of the maximum and minimum measured frozen radii corresponded with the predicted frozen radius, assuming that the freeze pipe within the target zones contained liquid nitrogen at all times during the experiment. This suggested that freezing during Experiment 6 progressed due to both liquid and gaseous nitrogen in the reservoir. Moreover, as shown in Photograph 3-3, the shape of the frozen column was not uniform and it appears that liquid nitrogen was probably contained within only the lowermost 2 m of the target zone for the duration of the experiment. As shown in Figure 3-23, the actual consumption of liquid nitrogen for freezing during Experiment 6 was also significantly less than predicted.

Figures 3-24 and 3-25 show revised predictions assuming that liquid nitrogen existed in the lowermost 2 m of the reservoir and gas nitrogen filled the rest of the freeze pipe. As shown by the figures, the predicted frozen radius is acceptable, since it falls in between the maximum and minimum measured frozen radii, and the actual consumption of liquid nitrogen agrees very well with the predicted volumes of liquid nitrogen consumed.

3.4 Conclusions

The experimental results indicated that the theoretical predictions, undertaken assuming that liquid nitrogen was contained within the freeze pipe reservoir(s) in the target zone(s) at all times during freezing, generally showed good agreement with the average of the minimum and maximum frozen radii measured in the target zone. However, in cases where the level of liquid nitrogen in the freeze pipe fell below the top of the target zone during most of the experiment, these theoretical predictions showed poor agreement with the actual consumption of liquid nitrogen. The actual minimum frozen radius, found to occur near the top of the target zone, agreed well with the theoretical prediction, based on assuming that the freeze pipe contained gaseous nitrogen. This result indicated that the phase change interface, where the liquid nitrogen changed to gas, was located below the top of the target zone. Revised predictions, that considered the heat extraction contributions from both the latent heat of liquid nitrogen, in the lower portion of the target zone, and the volumetric heat capacity of the gaseous nitrogen, in the upper portion of the target zone, predicted the average of the measured frozen radii well and showed very good agreement with the actual consumption of liquid nitrogen.

The actual maximum frozen radius, found to occur near the bottom of the target zone, slightly exceed the theoretical prediction, based on assuming that liquid nitrogen was contained within the freeze pipe reservoir in the target zone at all times. This discrepancy likely arose from the fact that the theoretical prediction of freezing time was based on assuming that steady state conditions existed, while the actual time recorded during progression of the freezing front corresponded to the instant at which a temperature of 0 °C was recorded at the RTD locations, which may not correspond to steady state conditions. Hence, the experimental data indicates that when liquid nitrogen is used as the refrigerant for in-situ ground freezing, assuming that the isotherms move slowly enough to resemble steady state conditions is conservative during initial ground freezing. This conservatism may also be caused by assuming that the unfrozen and frozen thermal conductivities are constant, whereas the very cold temperature of the liquid nitrogen

(-196 °C) may result in significantly higher values for the soil in the immediate vicinity of the freeze pipe. During the experiments where water was frozen, convection of colder groundwater to the bottom of the freezing chamber may have also resulted in more rapid freezing near the bottom of the target zone, compared to the theoretical predictions.

In spite of the above inaccuracies, prior to undertaking in-situ ground freezing, the theoretical equations presented by Sanger and Sayles (1979) can be used to predict the time required to freeze a specified average radius reasonably well. However, if the level of liquid nitrogen in the freeze pipe falls below the top of the target zone during much of the freezing process, the predicted volume of liquid nitrogen will likely be significantly higher than the actual requirement. This results since significant cooling of the ground is achieved by conduction of heat from the ground to the gaseous nitrogen in the freeze pipe which is at a temperature of about -120 °C.

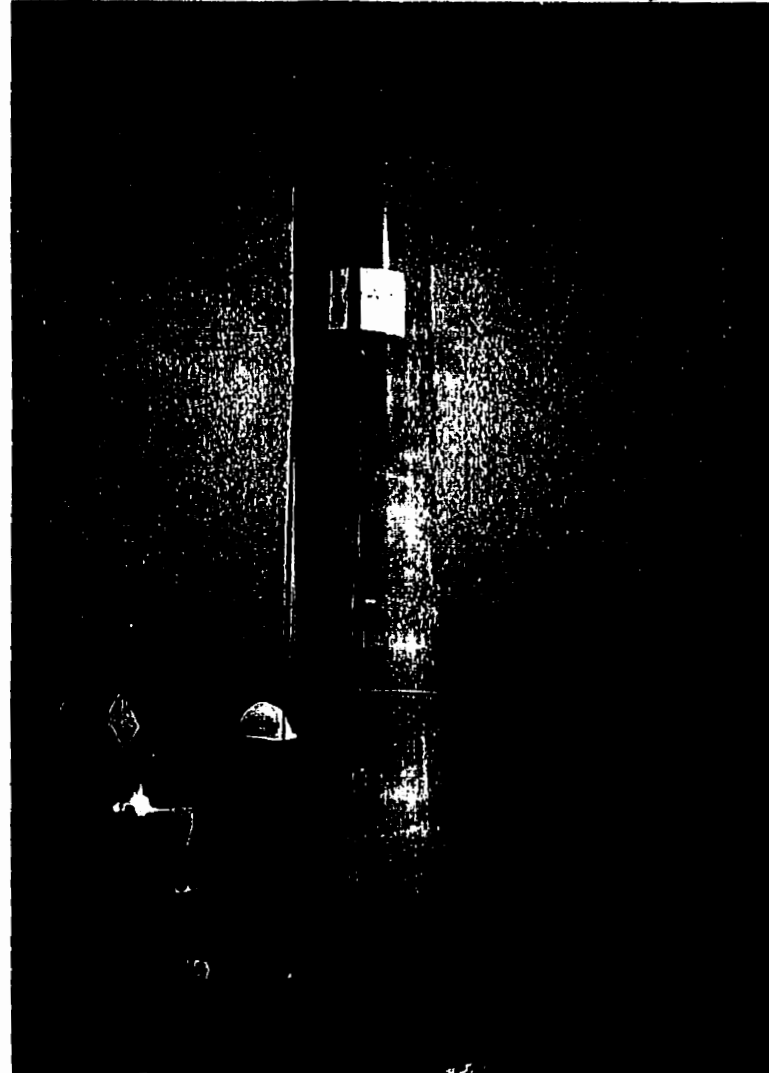
Although it may be possible to determine the relative proportions of gas and liquid nitrogen by installing temperature measurement devices that can withstand the temperatures and turbulence in the freeze pipe, it is preferable to freeze the soil in the form of a right cylinder by maintaining only liquid nitrogen in the freeze pipe. Freezing a uniform column of soil will both reduce the risk of disturbance of the soils, due to sub-vertical freezing fronts, and facilitate coring of the frozen sand upon completion of in-situ ground freezing. To avoid difficulties associated with coring of the frozen sand and inaccurate prediction of the liquid nitrogen requirements, modifications to the freezing system could be undertaken to ensure that the freeze pipe reservoir is full of liquid nitrogen at all times. Utilizing higher liquid nitrogen flow rates and installation of a valve on the exhaust pipe, to apply a slight back pressure, should aid in keeping the freeze pipe reservoir consistently full of liquid nitrogen.

3.5 References

- Farouki, O. T., 1981, Thermal Properties of Soils Relevant to Ground Freezing. Design Techniques for their Estimation. 3rd International Symposium on Ground Freezing, Hanover, New Hampshire, USA , pp. 139-146.
- Farouki, O. T., 1986. Thermal Properties of Soils. Trans Tech Publications. Series on Rock and Soil Mechanics, Vol. 11, D-3392 Clausthal-Zellerfeld, Germany, 135 p.
- Johansen, C., 1975. Thermal Conductivity of Soils, Ph.D. thesis. University of Trondheim, Norway. (Available as USA CRREL Draft Translation 637, 1977).
- Kersten, M. S., 1949. Thermal Properties of Soils. University of Minnesota Engineering Experiment Station Bulletin No. 28.
- Sanger, F. J., and Sayles, F. H., 1979. Thermal and Rheological Computations for Artificially Frozen Ground Construction. Engineering Geology, 13: 311-337.



Photograph 3-1: Frozen Zone Obtained from
Experiment 2



Photograph 3-2: Frozen Zone Obtained from
Experiment 4



Photograph 3-3: Frozen Zone Obtained From Experiment 6.

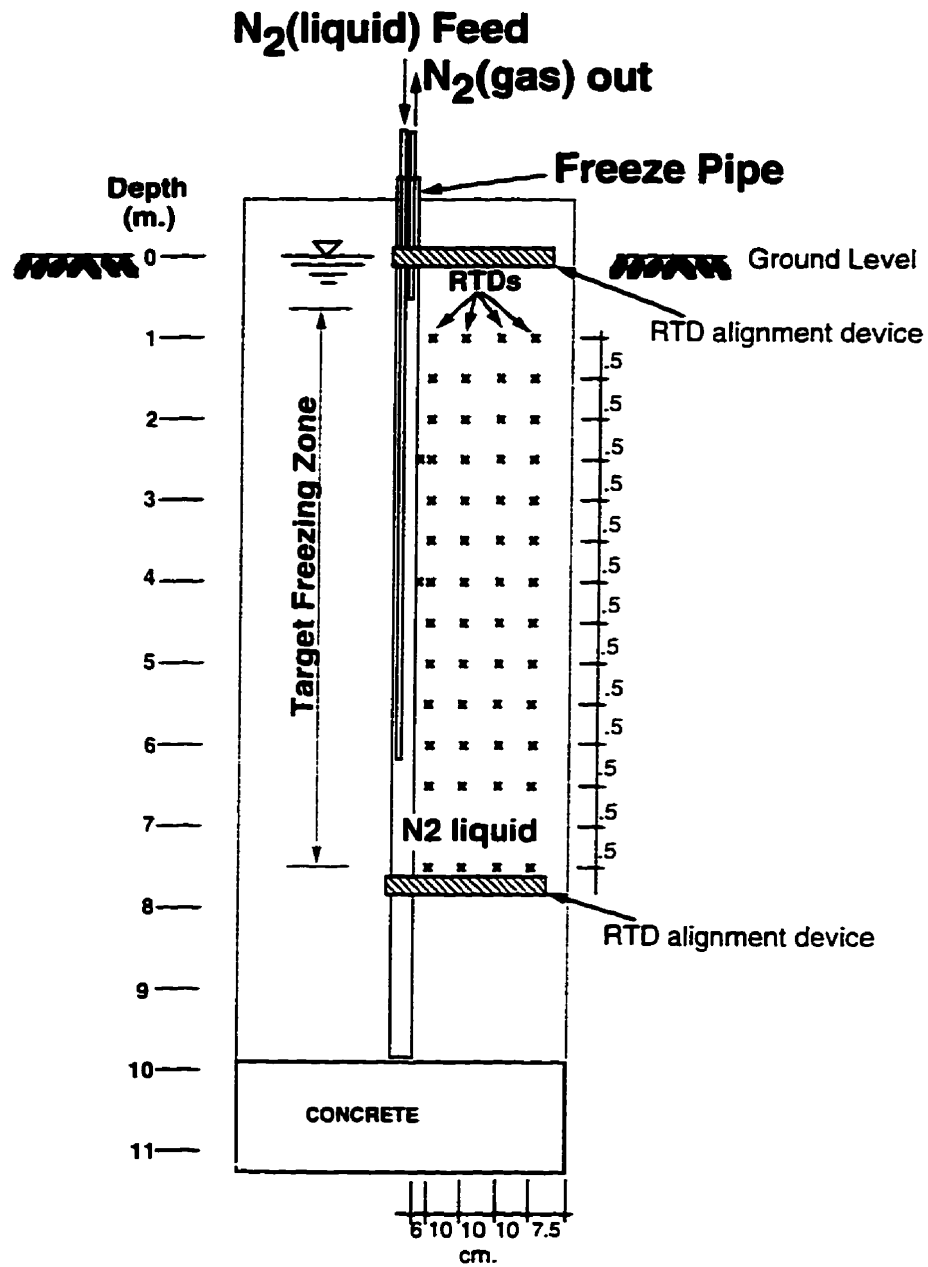


Figure 3-1: Schematic of the Cased Borehole showing Typical Freeze Pipe Configuration.

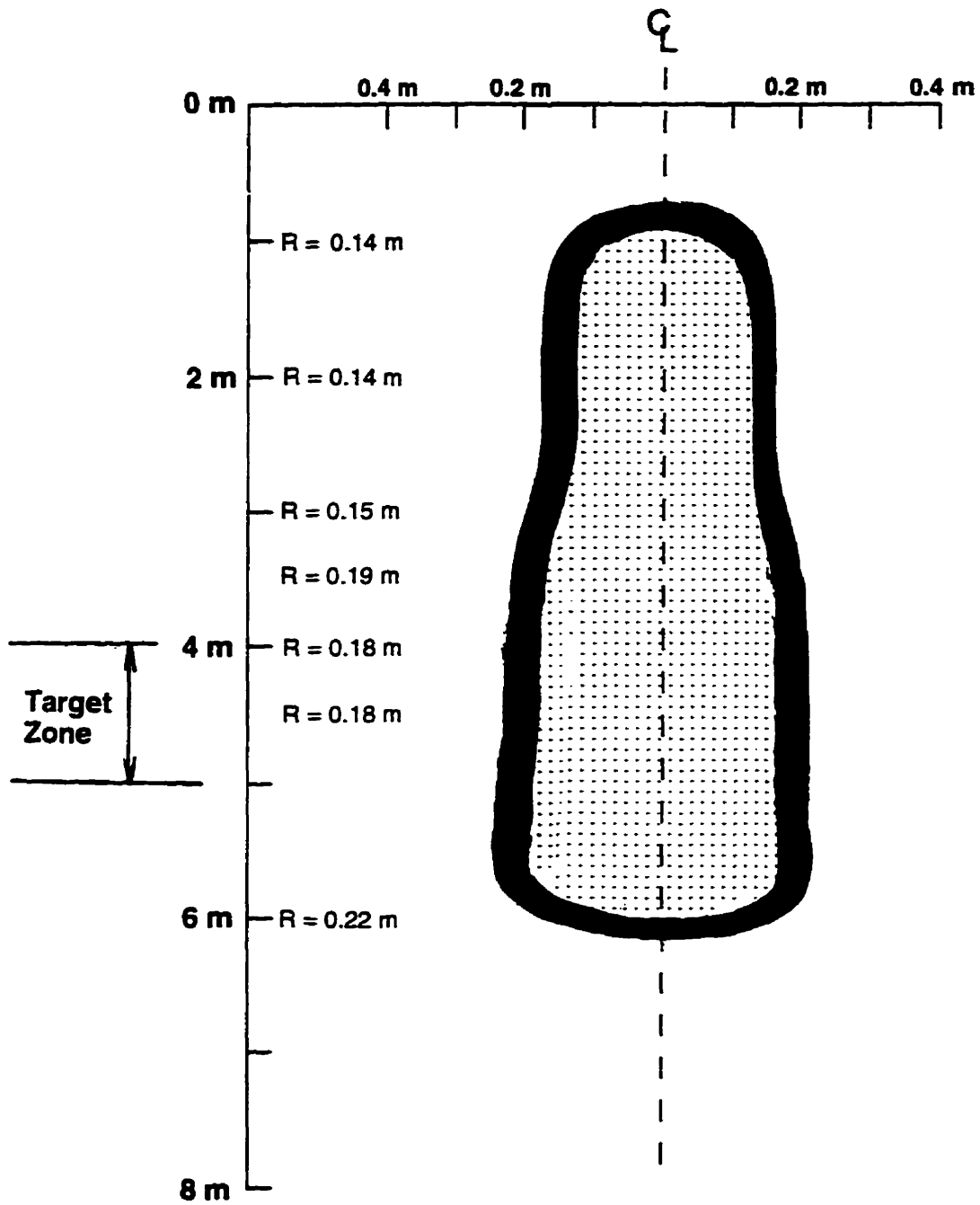


Figure 3-2: Dimensions of the Frozen Zone Recorded for Experiment 1.

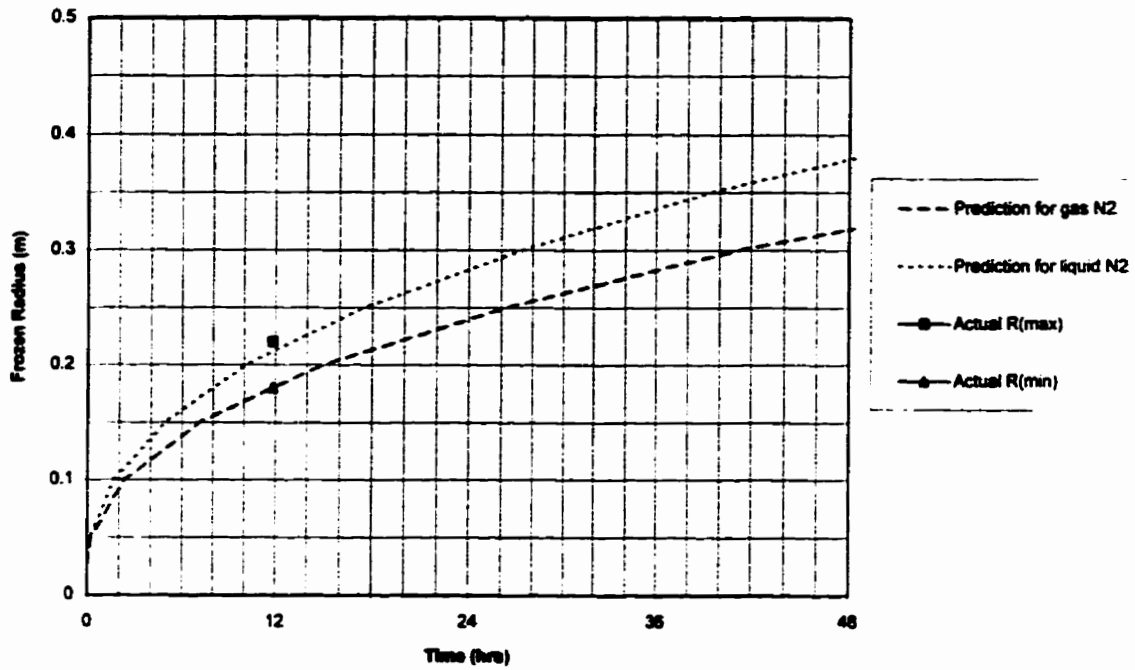


Figure 3-3: Comparison of Predicted Frozen Radius with Actual Maximum and Minimum Frozen Radii attained in Experiment 1.

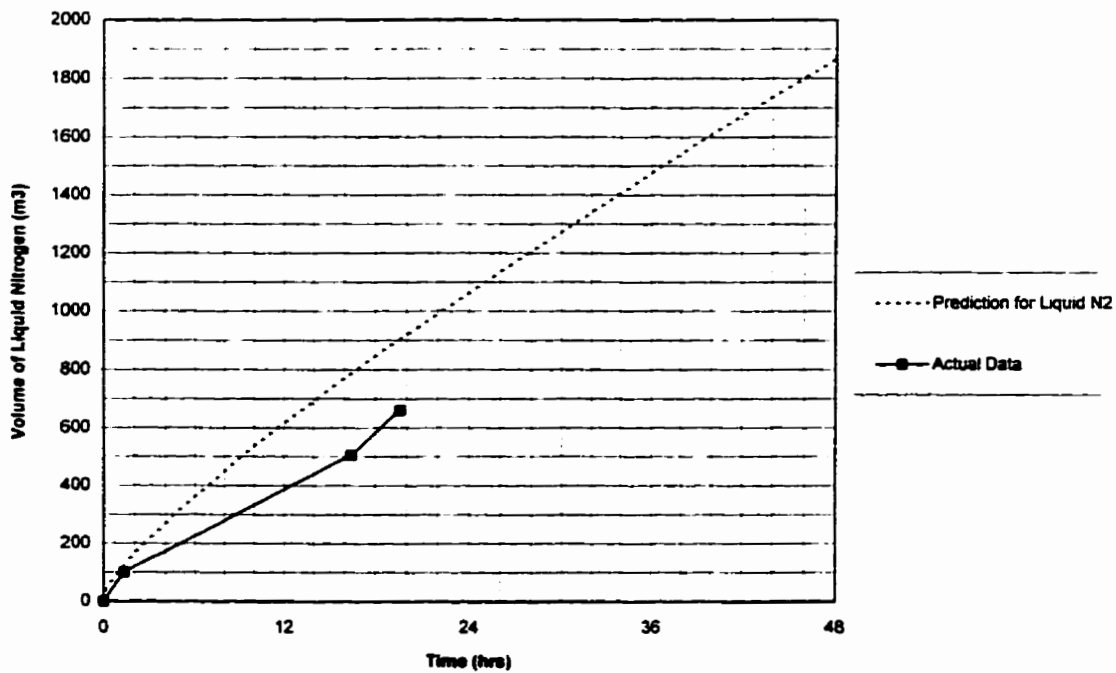


Figure 3-4: Comparison Between Predicted and Actual Liquid Nitrogen Consumption during Experiment 1.

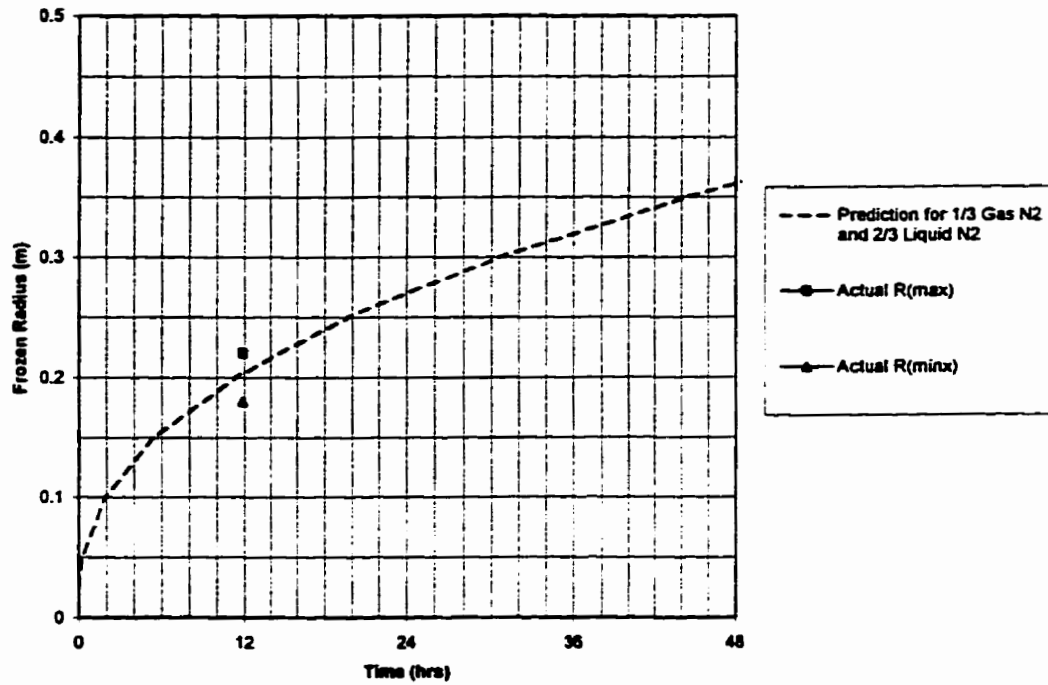


Figure 3-5: Frozen Radius Prediction for both Liquid and Gas Nitrogen in Freeze Pipe during Experiment 1.

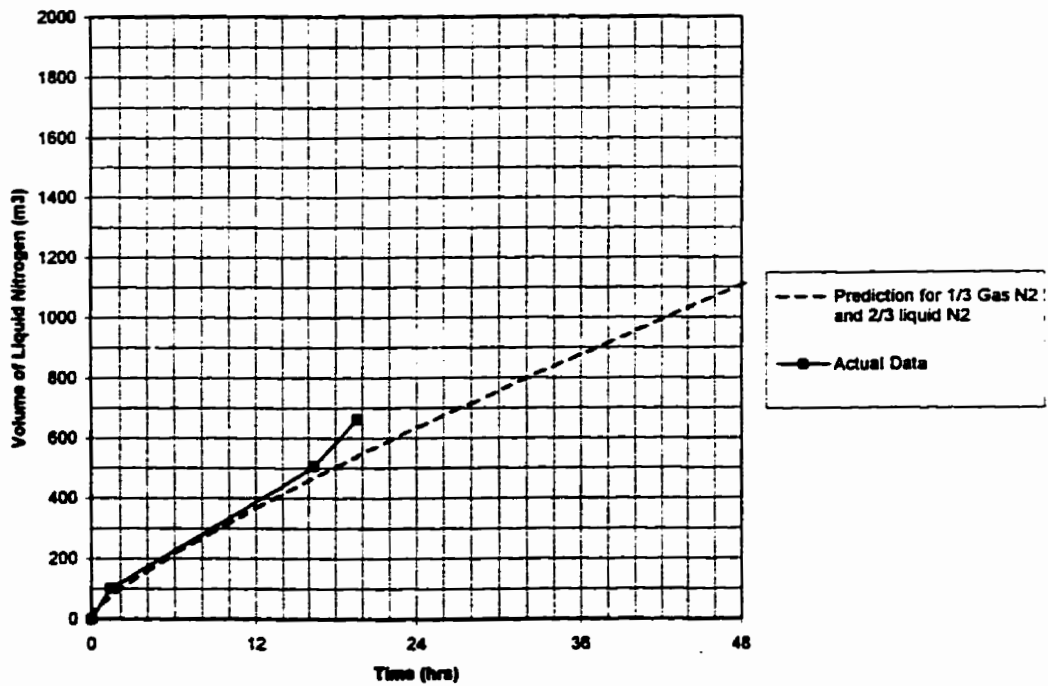


Figure 3-6: Liquid Nitrogen Consumption Prediction for both Liquid and Gas Nitrogen in Freeze Pipe during Experiment 1.

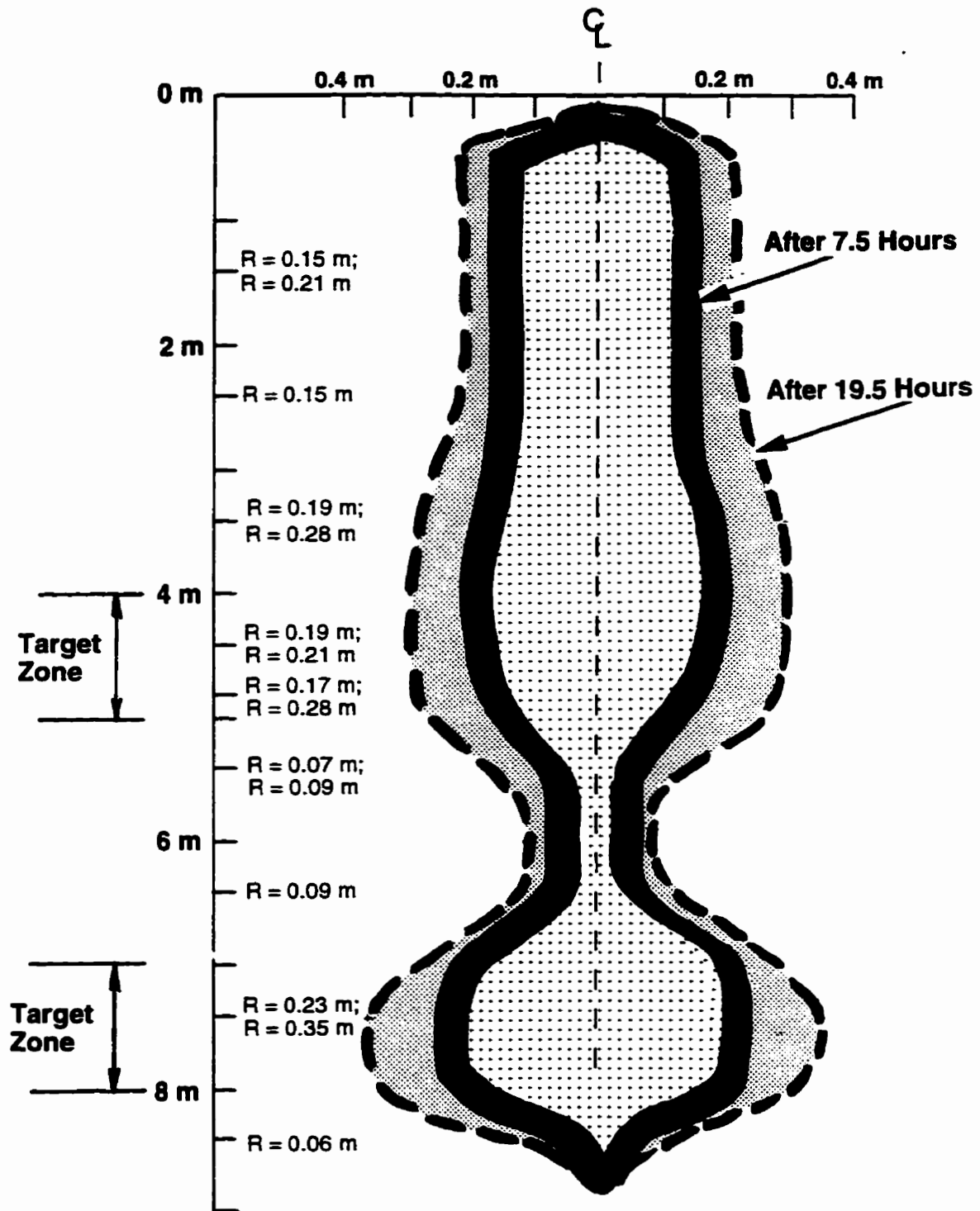


Figure 3-7: Dimensions of the Frozen Zone Recorded for Experiment 2.

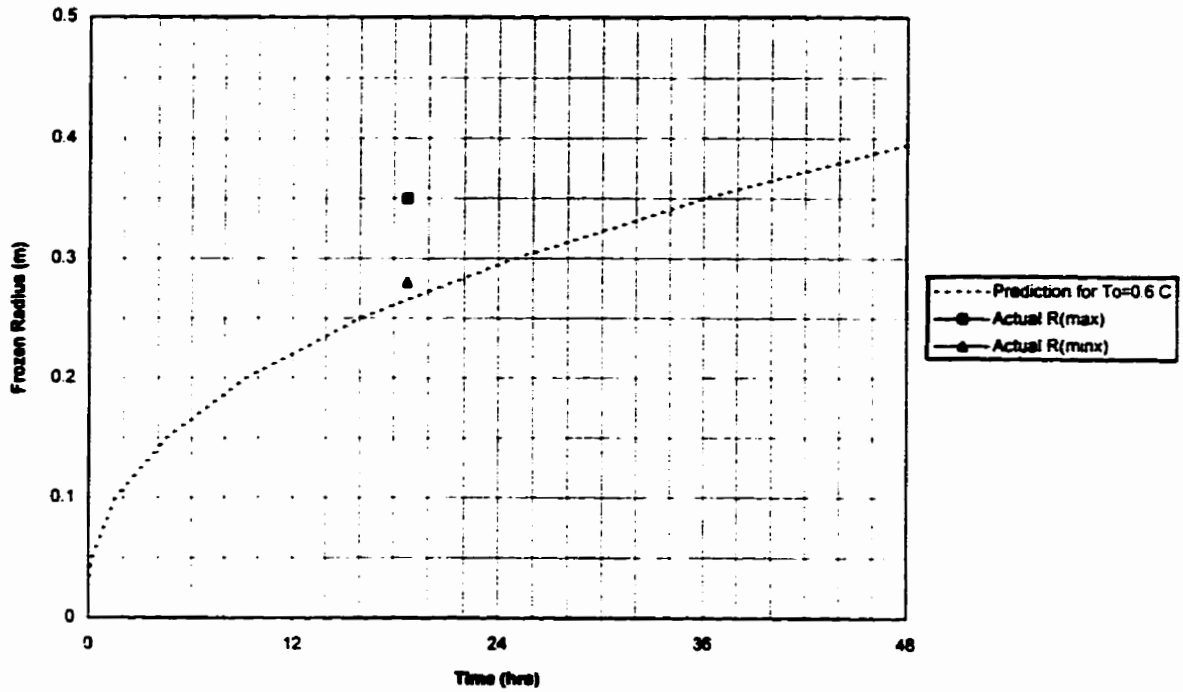


Figure 3-8: Comparison of Predicted Frozen Radius with Actual Maximum and Minimum Frozen Radii attained in Experiment 2.

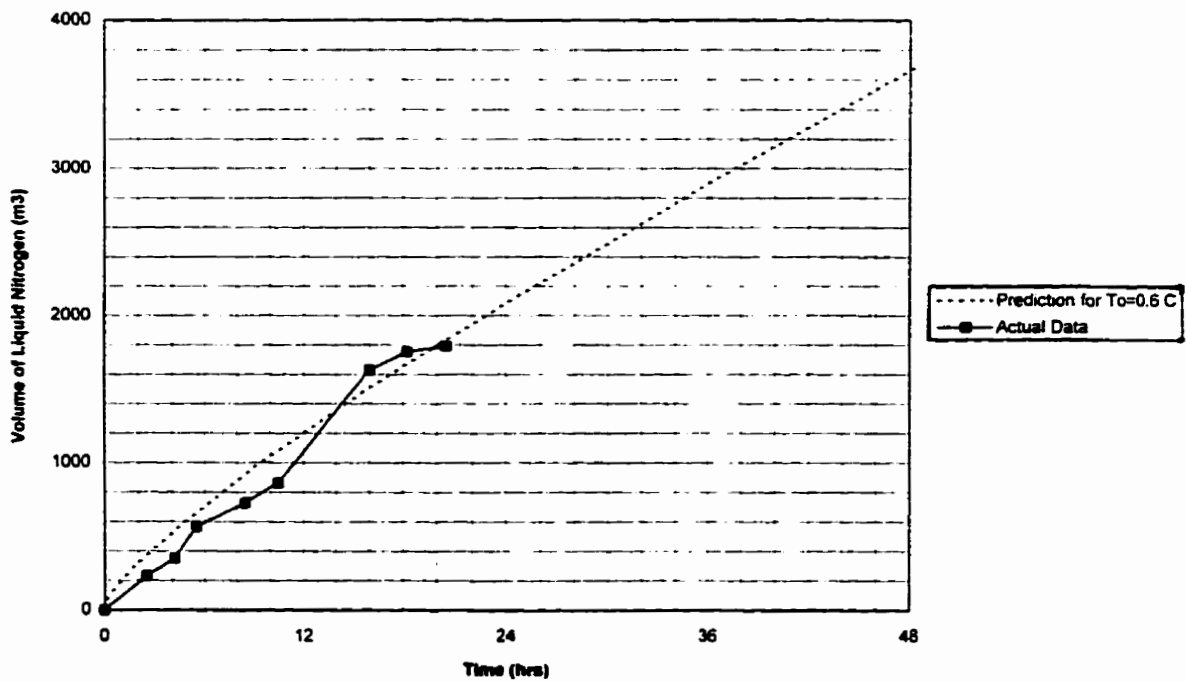


Figure 3-9: Comparison Between Predicted and Actual Liquid Nitrogen Consumption during Experiment 2.

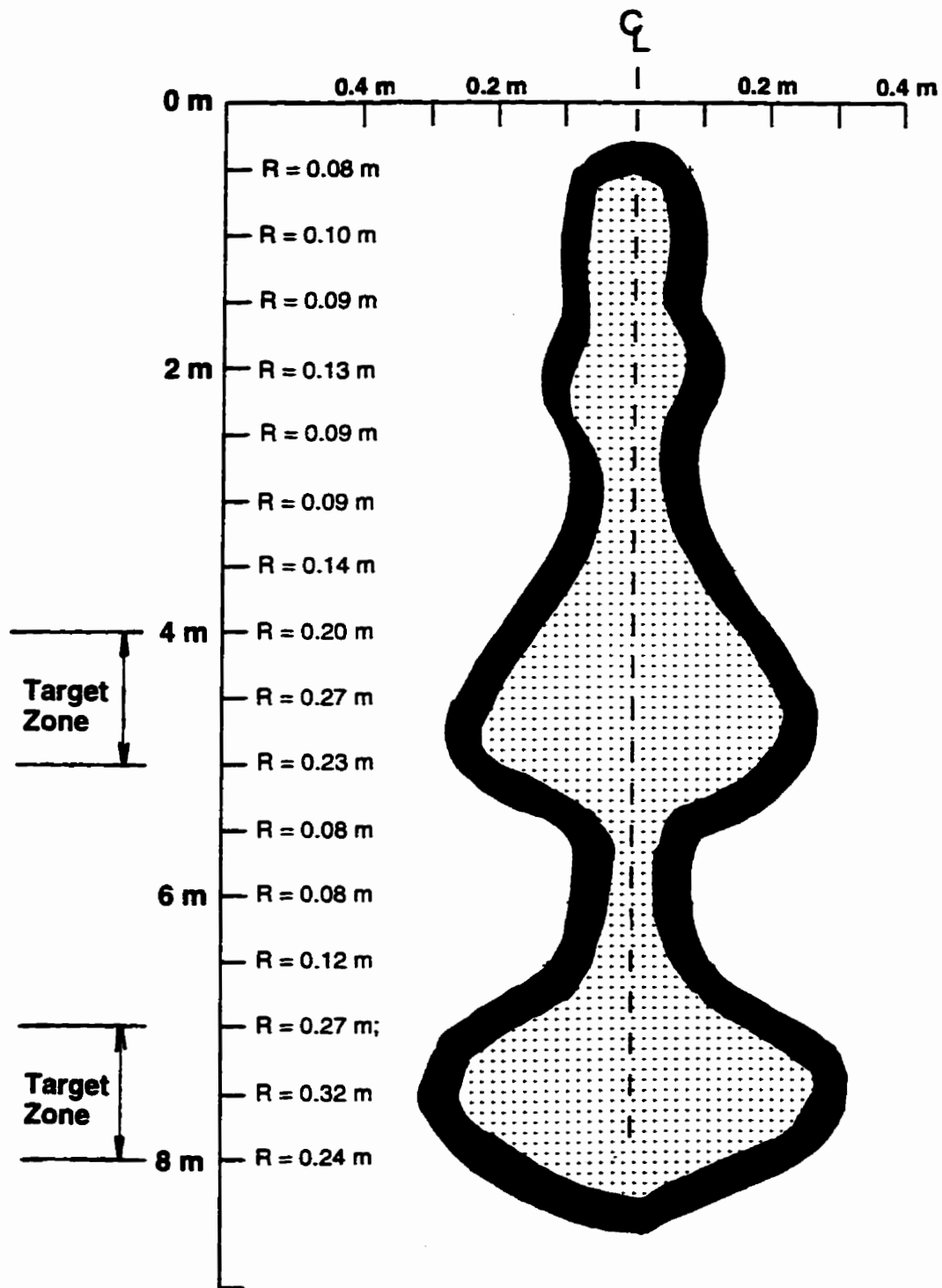


Figure 3-10: Dimensions of the Frozen Zone Recorded for Experiment 3.

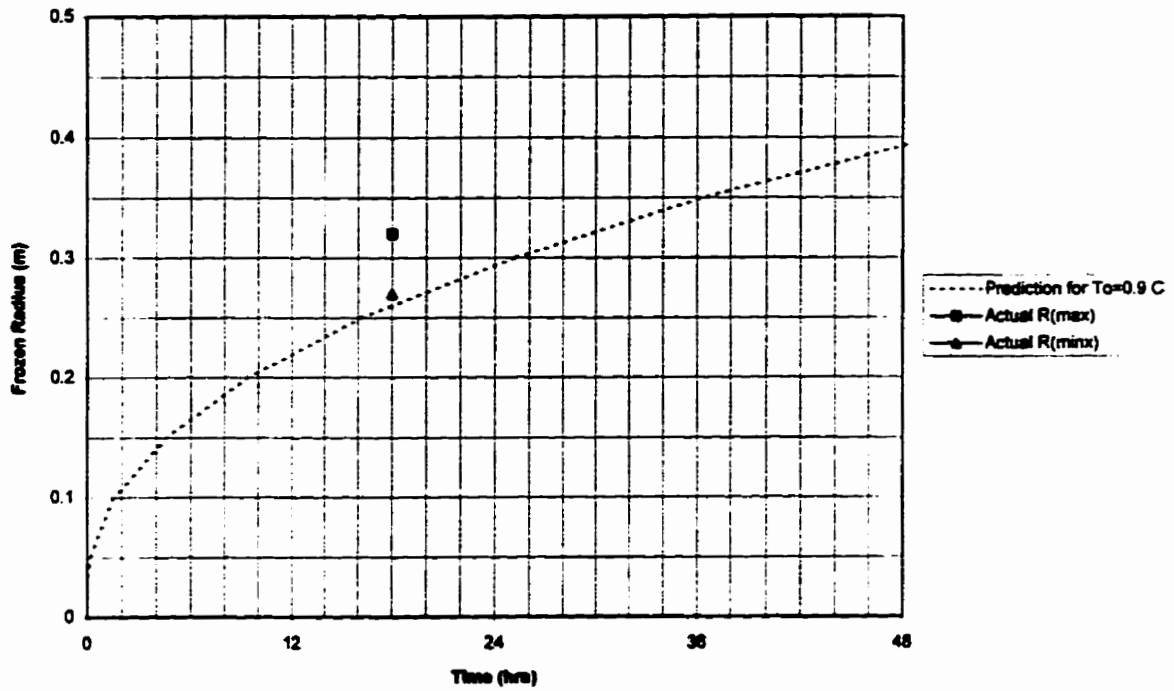


Figure 3-11: Comparison of Predicted Frozen Radius with Actual Maximum and Minimum Frozen Radii attained in Experiment 3.

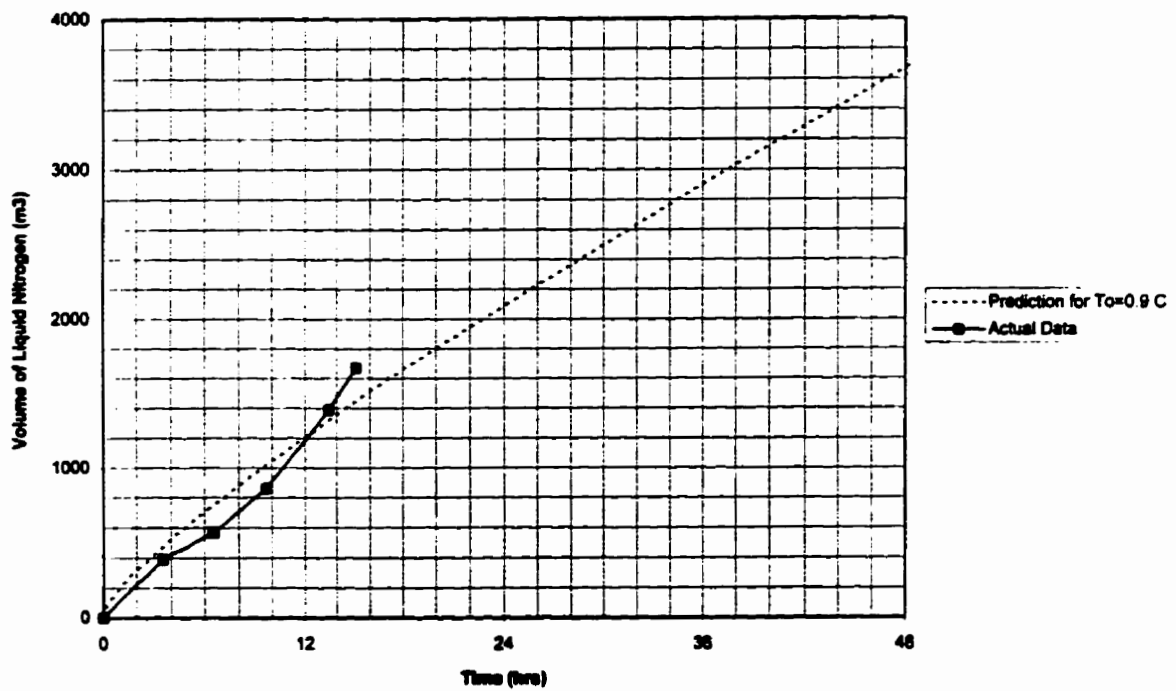


Figure 3-12: Comparison Between Predicted and Actual Liquid Nitrogen Consumption during Experiment 3.

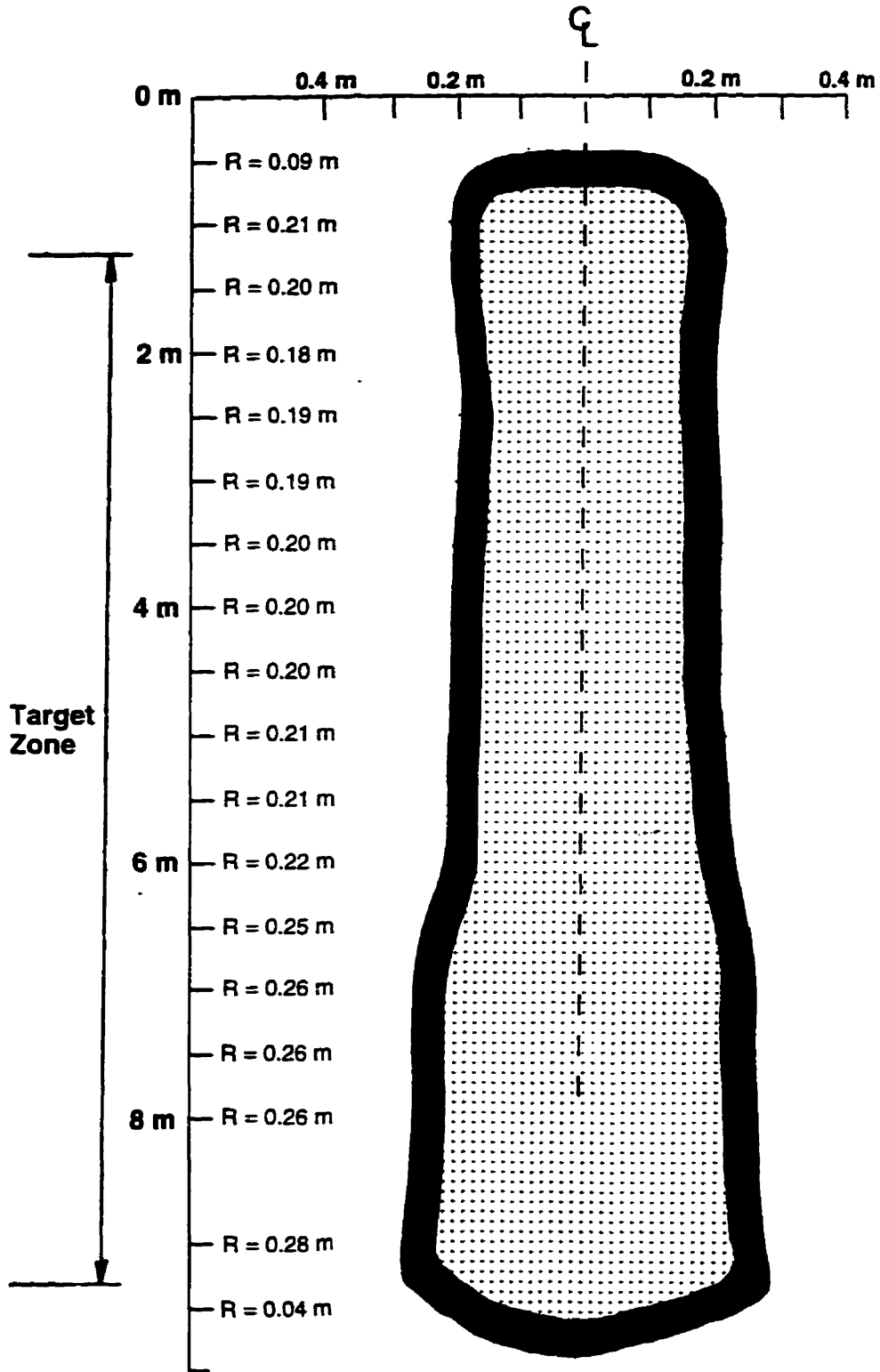


Figure 3-13: Dimensions of the Frozen Zone Recorded for Experiment 4.

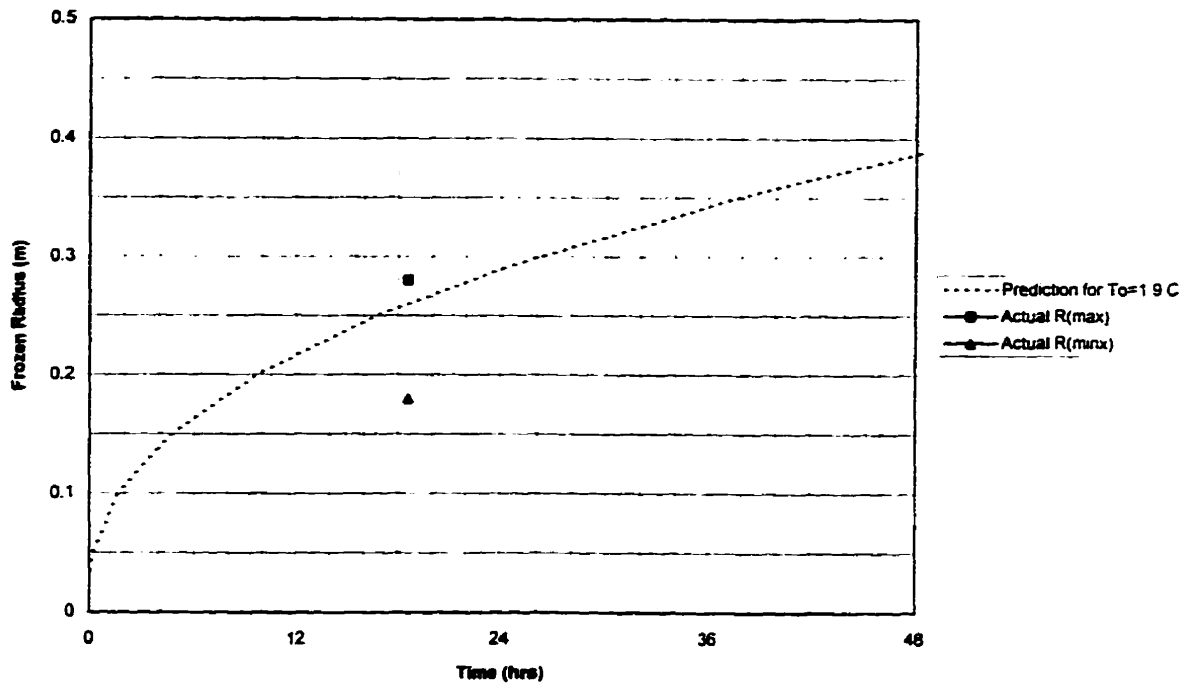


Figure 3-14: Comparison of Predicted Frozen Radius with Actual Maximum and Minimum Frozen Radii attained in Experiment 4.

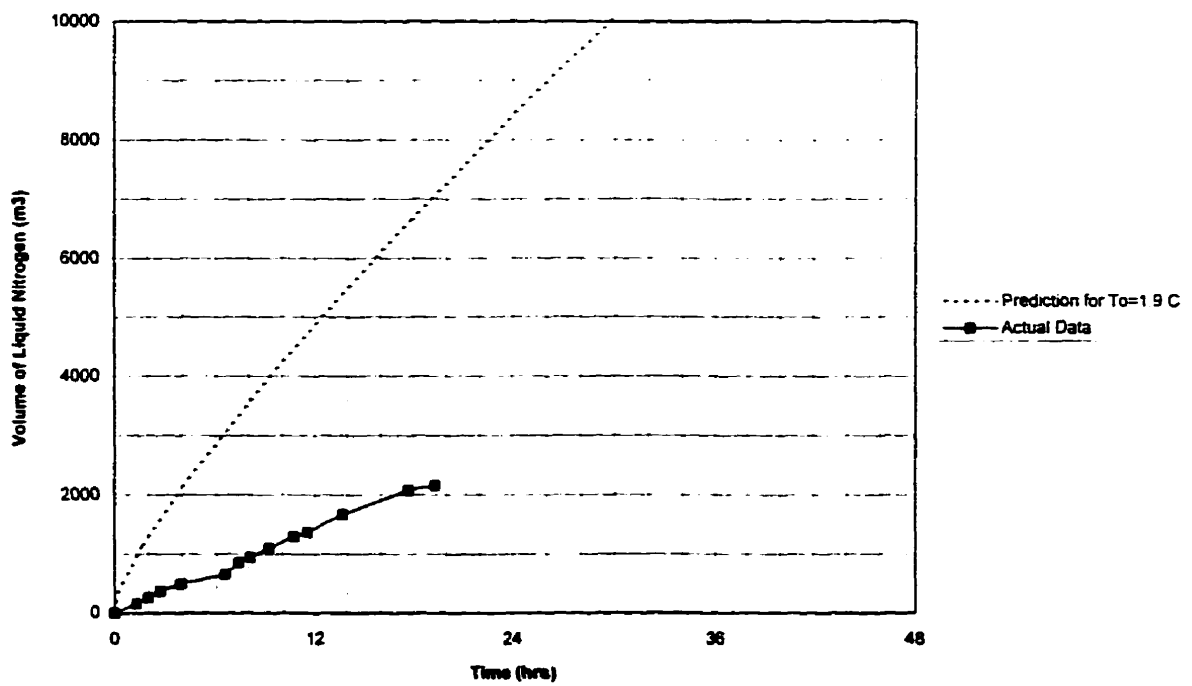


Figure 3-15: Comparison Between Predicted and Actual Liquid Nitrogen Consumption during Experiment 4.

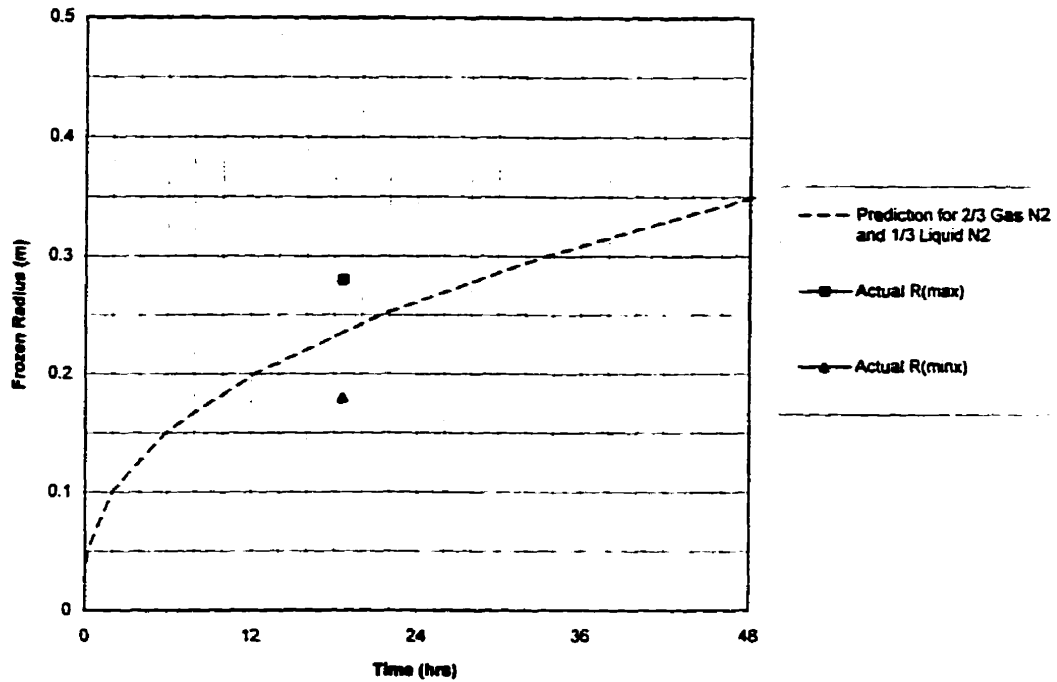


Figure 3-16: Frozen Radius Prediction for both Liquid and Gas Nitrogen in Freeze Pipe during Experiment 4.

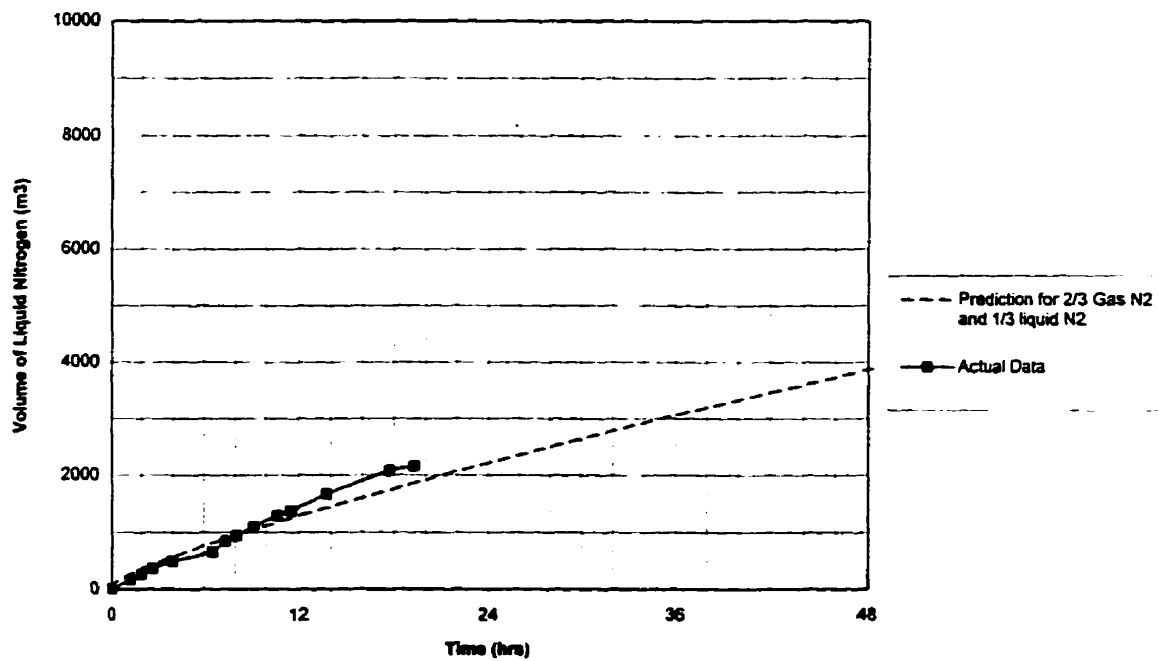


Figure 3-17: Liquid Nitrogen Consumption Prediction for both Liquid and Gas Nitrogen in Freeze Pipe during Experiment 4.

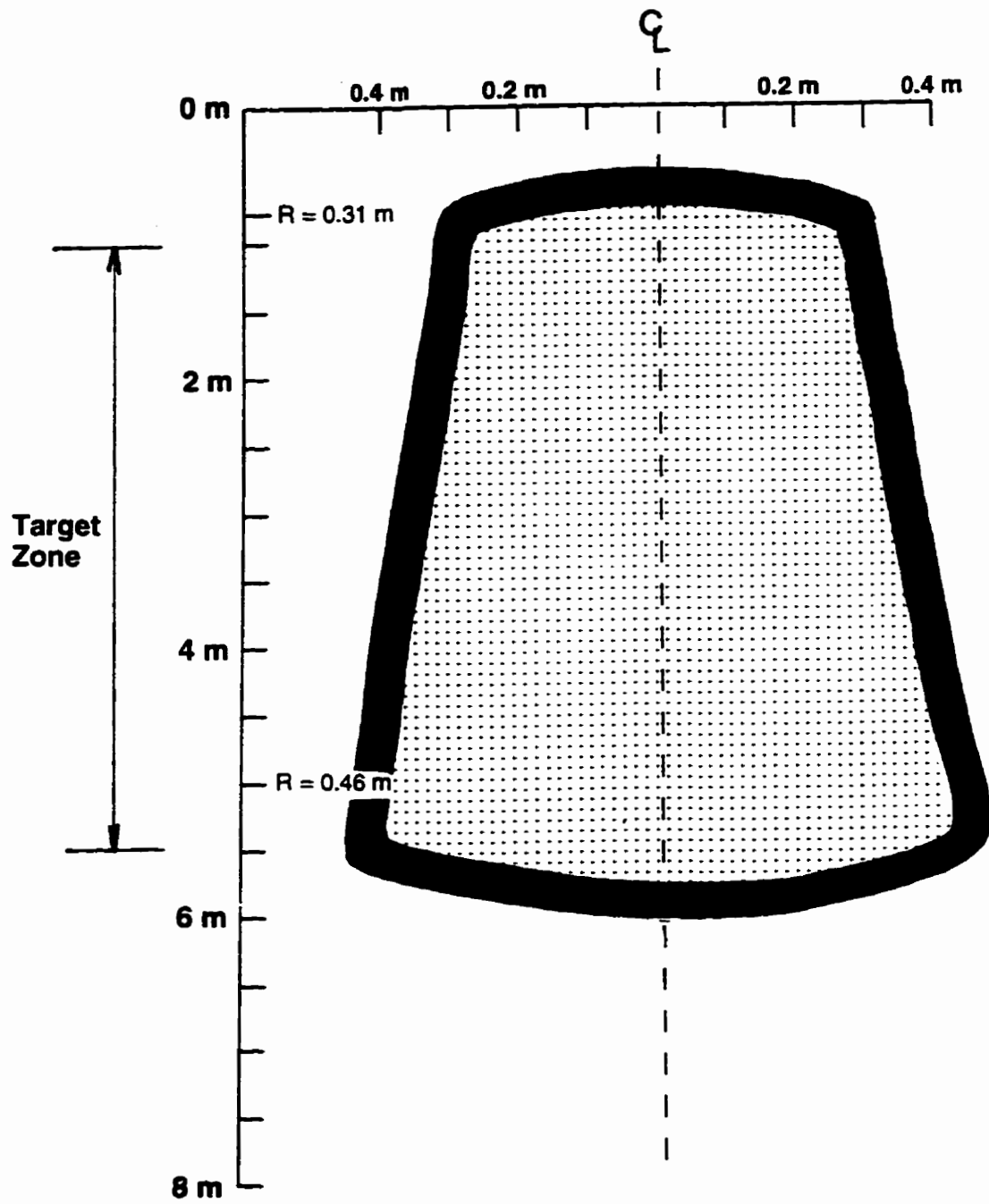


Figure 3-18: Dimensions of the Frozen Zone Recorded for Experiment 5.

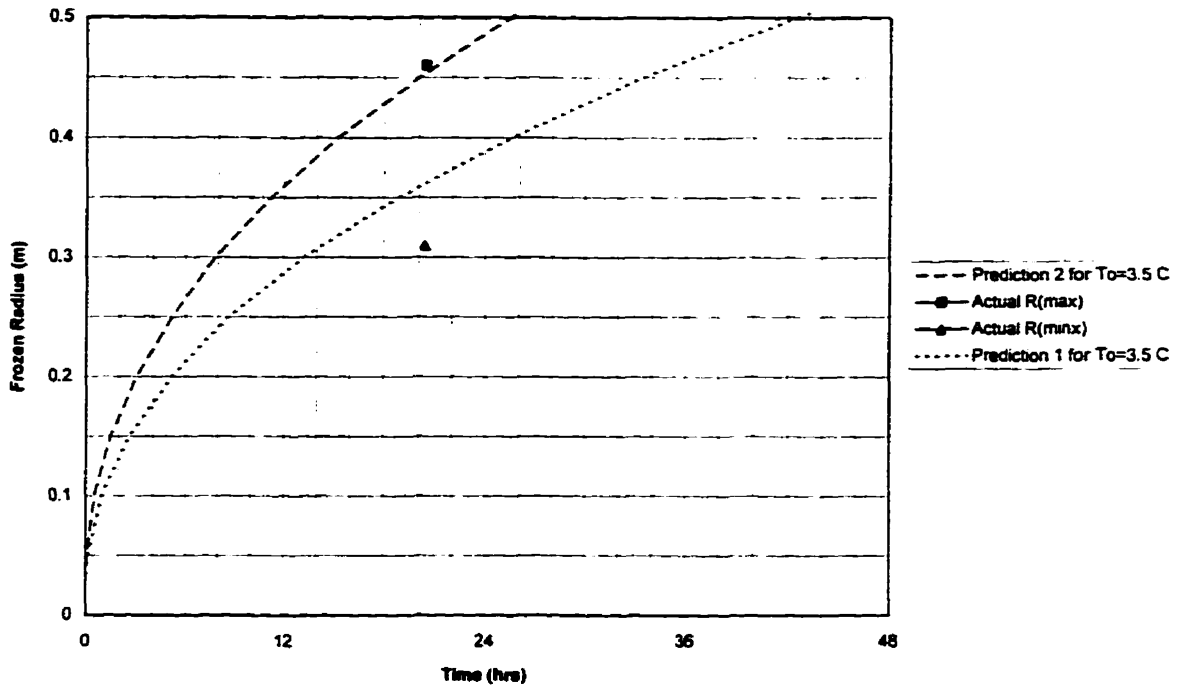


Figure 3-19: Comparison of Predicted Frozen Radius with Actual Maximum and Minimum Frozen Radii attained in Experiment 5.

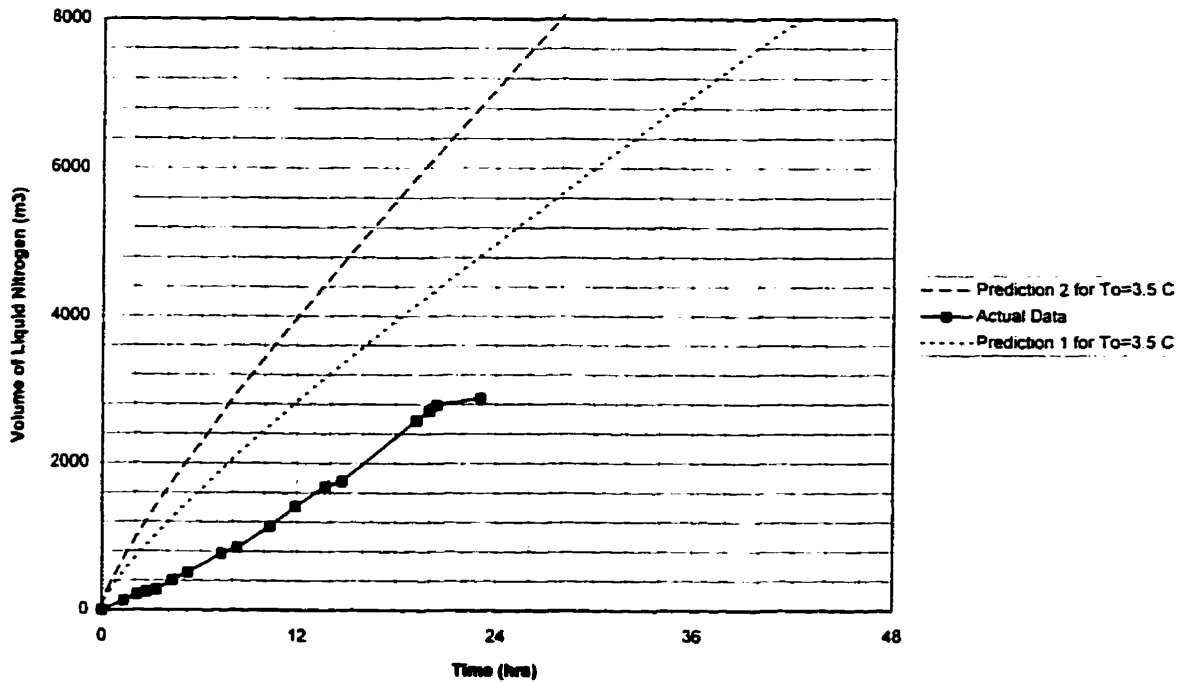


Figure 3-20: Comparison Between Predicted and Actual Liquid Nitrogen Consumption during Experiment 5.

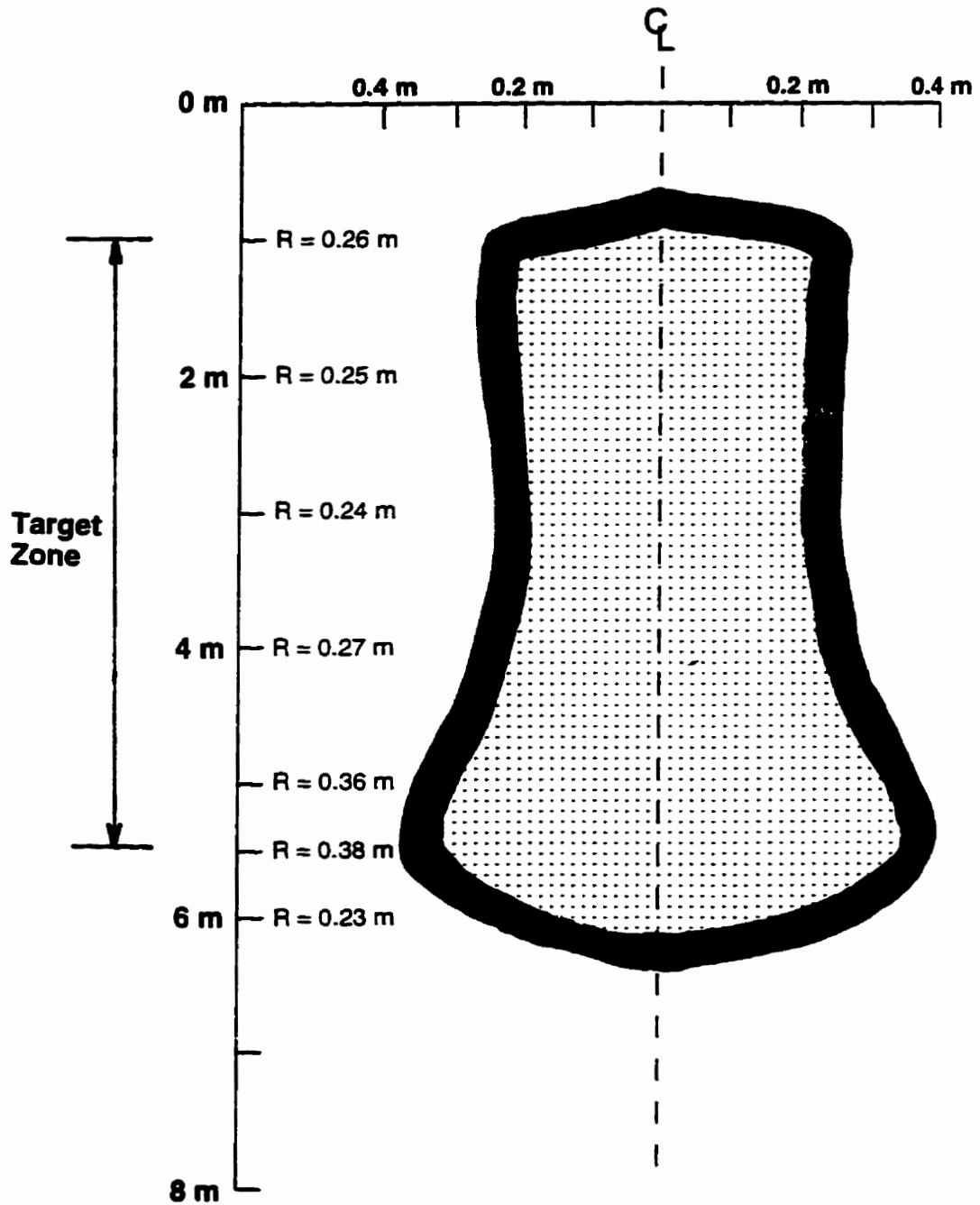


Figure 3-21: Dimensions of the Frozen Zone Recorded for Experiment 6.

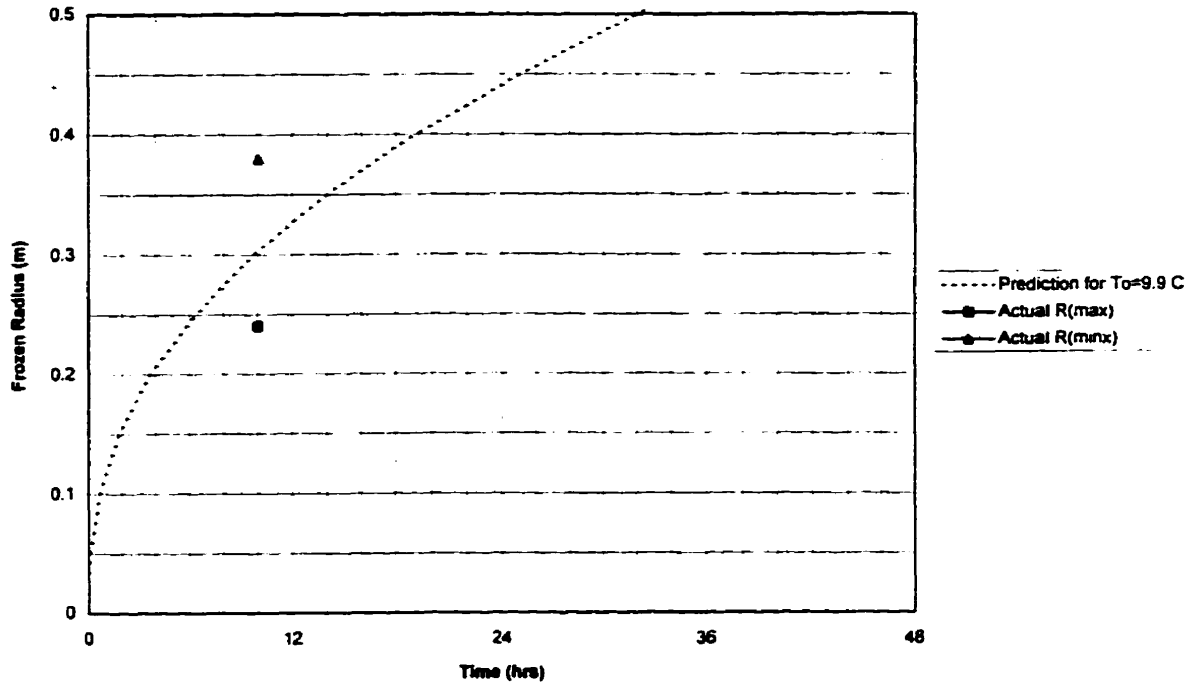


Figure 3-22: Comparison of Predicted Frozen Radius with Actual Maximum and Minimum Frozen Radii attained in Experiment 6.

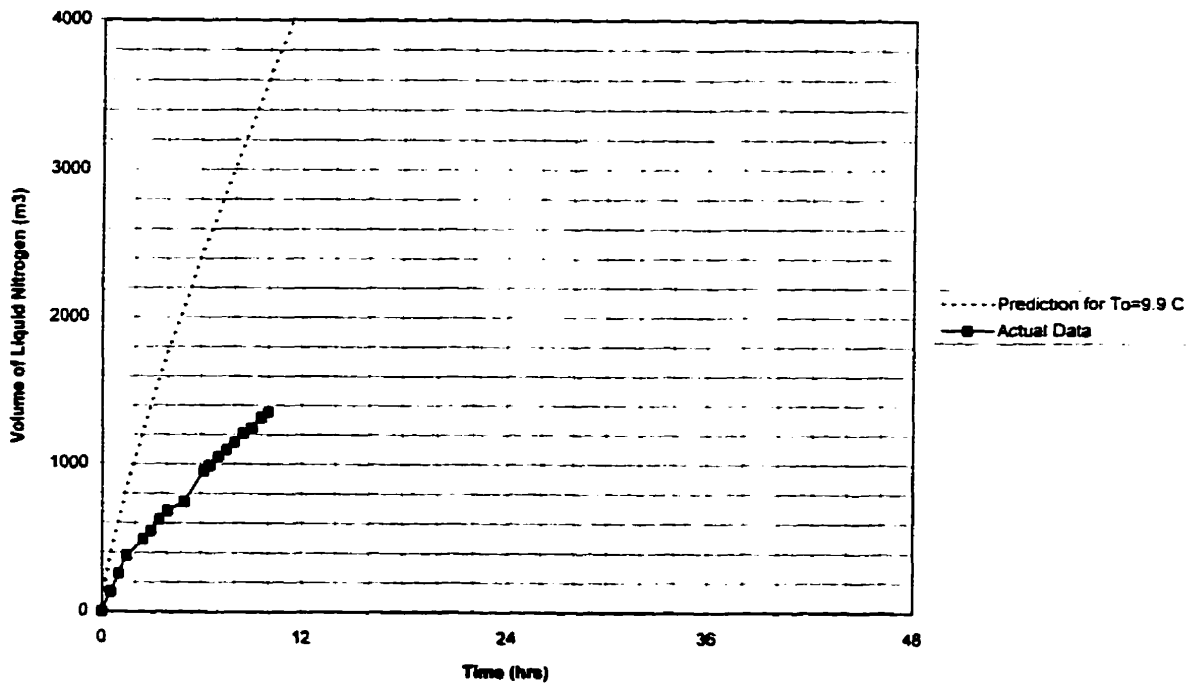


Figure 3-23: Comparison Between Predicted and Actual Liquid Nitrogen Consumption during Experiment 6.

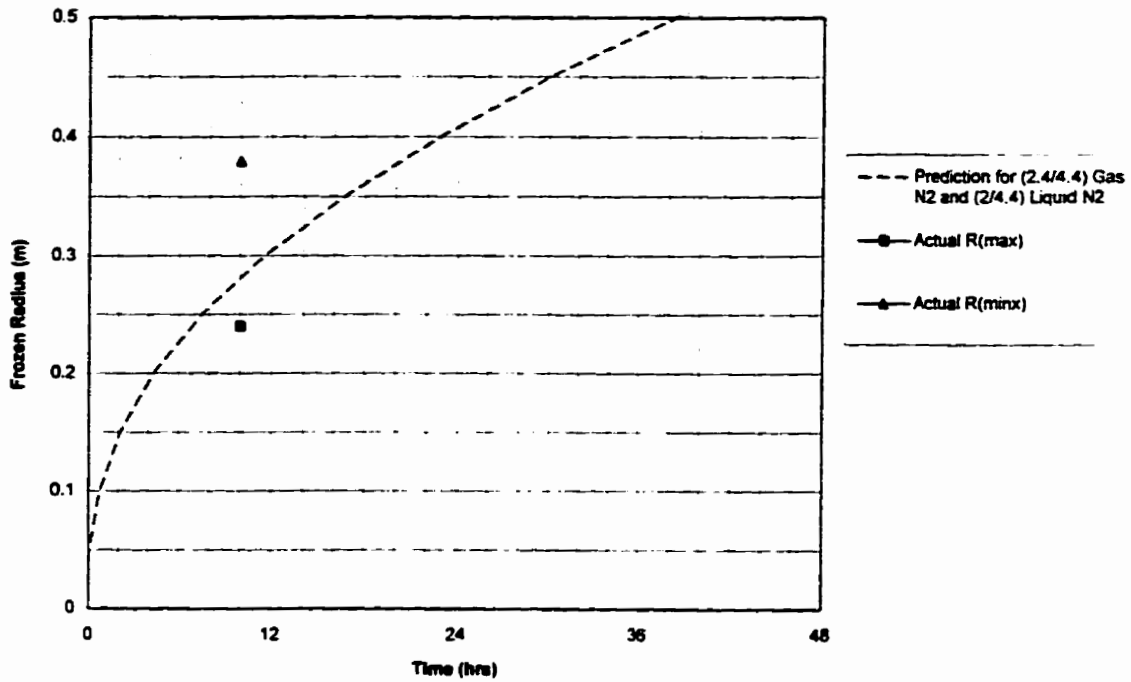


Figure 3-24: Frozen Radius Prediction for both Liquid and Gas Nitrogen in Freeze Pipe during Experiment 6.

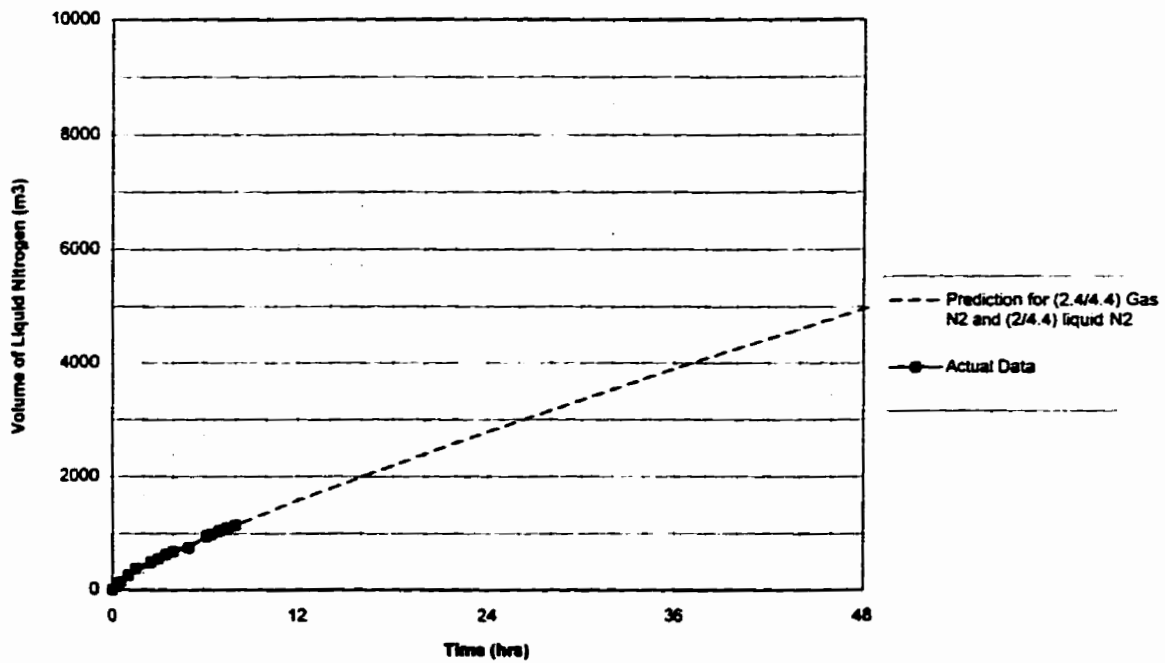


Figure 3-25: Liquid Nitrogen Consumption Prediction for both Liquid and Gas Nitrogen in Freeze Pipe during Experiment 6.

Chapter 4: Case History of Undisturbed Sampling of a Man-Made Sand Deposit by In-Situ Ground Freezing

4.0 Introduction

The Canadian Liquefaction Experiment (CANLEX) was undertaken to determine the most effective methods of characterizing sand to evaluate the potential for dynamic and static liquefaction. The main objectives of the project included: development of test sites to study sand characterization, development of economical undisturbed sampling techniques, and establishing a greater understanding of soil liquefaction (Robertson, et al. 1994). As part of the CANLEX project, in-situ ground freezing was undertaken at the centre of the Phase I test site to obtain undisturbed samples of loose sand. Within a 5 m radius of the zone where in-situ ground freezing and sampling was undertaken, conventional Fixed Piston sampling and various in-situ testing techniques, such as Cone Penetration Tests, Standard Penetration Tests, Geophysical Logging, Self Boring Pressuremeter Tests were undertaken for comparison of different sand characterization methods.

The scope of work for the ground freezing and sampling activity included the following:

- Conduct a site specific feasibility study to confirm that in-situ ground freezing of a sand deposit at the Phase I test site to obtain undisturbed samples of sand without disturbing the existing void ratio or fabric.
- Design an efficient freezing system, utilizing liquid nitrogen, to freeze the ground without causing disturbance in the most cost-effective manner.
- Obtain undisturbed core samples of the in-situ frozen sand for evaluation of the in-situ void ratio and for subsequent laboratory testing by CANLEX participants to evaluate the liquefaction potential of the sand deposit.

The following chapter describes in-situ ground freezing and coring of the frozen sand deposit undertaken at the Phase I test site. The feasibility studies conducted prior to executing the fieldwork are reviewed. The ground freezing system utilized at the test site is described, the data measured during the freezing process are presented and the actual progress of ground freezing at the test site is compared with theoretical predictions. The procedure utilized for coring of the in-situ frozen sand is described. Measurements of the in-situ void ratios determined from the frozen cores are compared with the void ratios determined by the geophysical logging conducted within a 5 m radius of the freeze pipe.

4.1 Background

The location and target depths for undertaking ground freezing and sampling at the Phase I test site was selected as part of a separate activity for the CANLEX Project. The criteria for site selection included identifying the loosest available deep deposit of sand in the southeast end of the Mildred Lake Settling Basin (MLSB) dike at Syncrude Canada Ltd. (SCL). Seismic Cone Penetration Tests (SCPT), with shear wave velocity measurements, and Standard Penetration Tests (SPT) were carried out in Cells 22 to 28 of the MLSB to identify the best location for the Phase I test site. The zone selected that satisfied these criteria was located in Cell 24, between depths of 27 m and 37 m below the ground surface, corresponding to elevations of approximately 324 m and 314 m, respectively. The test site location is shown in Figure 4-1. The CPT profiles obtained during the initial site screening are provided in Appendix B, Figure B1, and the normalized values of q_{c1} , v_{s1} and N_1 obtained from the SCPTs and SPTs are shown in Table B1.

Once the site location had been selected, SPT split spoon samples were recovered from the target zone to evaluate the sand with respect to the feasibility of conducting in-situ ground freezing for undisturbed sampling. Information obtained from Cell 24 which was relevant to the ground freezing study, including the characteristics of the sand, the density

of the sand deposit and the groundwater conditions are discussed in the following sections.

4.2 Ground Freezing Feasibility Study

Feasibility studies were conducted prior to undertaking in-situ ground freezing at the Phase I test site to confirm that the sand deposit could be frozen without altering the in-situ void ratio or fabric of the deposit. To meet this objective, the following studies were completed between May, 1993 and October, 1993:

- Evaluation of the frost heave susceptibility of the sand deposit at the Phase I test site.
- Evaluation of the groundwater conditions at the site, including expected groundwater temperatures and in-situ flow gradients.
- Evaluation of the cooling system and freeze pipe configuration that would result in the most efficient system for ground freezing.
- Evaluation of the dimensions of the frozen column of sand required in order to recover the desired amount of frozen core for subsequent in-situ void ratio determination and laboratory testing.
- Evaluation of the time and volume of liquid nitrogen required to freeze a column of sand with given dimensions.

4.2.1 Frost Heave Susceptibility of Subsoil

Laboratory testing was carried out to determine the grain size distribution and the mineralogy of the sand at the test site. Frost heave tests were also conducted on two samples of sand to evaluate the frost heave susceptibility of the MLSB sand.

4.2.1.1 Grain Size Distribution

Grain size curves established for the Split Spoon samples recovered from depths of 27.4 m and 36.6 m during the site selection study indicated fines contents of 9.5 and 14.7 percent, respectively. To supplement the grain size information obtained from these samples, additional SPT Split Spoon samples were retrieved from Cell 24 from a borehole advanced to install a groundwater observation well near the test site. The samples were taken from depths of between 18.3 m and 32.0 m. Grain size analyses undertaken by both the University of Alberta (U of A) and SCL indicated that the target zone contained fine uniform, angular to subangular sand with traces of silt and clay. The average D_{50} of the samples tested was approximately 0.20 mm. The fines content varied from 7.9 to 13.9 percent between depths of approximately 21 m and 35 m, and the average fines content in the target zone was about 12 %. A typical grain size curve obtained from a sample recovered from just above the target zone is shown in Figure 4-2. A summary of the fines content determined for each of the samples taken is provided in Table 4-1 and the grain size curves established for all of the samples are presented in Appendix B.

4.2.1.2 Sand Mineralogy

The fines mineralogy was evaluated for the split spoon samples obtained from depths of 28.7, 31.7 and 34.8 m in the borehole advanced for the groundwater observation well. The percent clay, by weight of the total fines content, was determined as part of the mineralogical evaluation of the samples. As shown in Table 4-2, the percent of clay sized particles in the fines fraction of the samples was found to be 10, 8 and 9, for the samples obtained from depths of 28.7, 31.7 and 34.8 m, respectively. These percentages correspond to approximate clay contents, expressed as percent by weight of the total sample, of 1.2, 1.0 and 1.1%, respectively. Therefore, the percentage of clay size particles in the sand encountered at depth in Cell 24 was minimal.

The surface area of the clay fraction and the estimated mineral content determined for each sample, are summarized in Tables 4-2 and 4-3. The mineralogical evaluation indicated that the clay size particle fraction (<2 mm) was comprised of between 60 and 64 percent kaolinite, with approximately 26 percent mica and 10 to 14 percent quartz. The silt size particle fraction (2-74 μm) was comprised of approximately 90 percent quartz, 5 percent kaolinite and 5 percent feldspar, with a trace of mica. These results show that the silt sized particles were comprised of predominantly non-clay quartz minerals and the clay size fraction was comprised of mainly kaolinite clay minerals, which exhibit relatively low frost heave susceptibility since kaolinite is an inactive clay mineral (see Chapter 2). Therefore, the sand deposit likely has a very low potential for disturbance due to frost heave.

Based on the mineralogical information, a preliminary evaluation of the potential for frost heave during freezing was undertaken using the parameters proposed by Davila (1992). Based on determination of the specific surface areas of the fines soil fraction (< 74 μm) and the clay size soil fraction (< 2 μm), the Fines Mineralogy Ratio, Z_v , and the Surface Area Index, Ω_z , were calculated. These parameters were then plotted on the chart provided by Davila (1992) for evaluating whether or not a soil will heave during freezing, as shown in Figure 4-3.

Figure 4-3 indicates that, according to Davila's work, heave will not occur during freezing of the sand encountered between approximately 21 m and 35 m in Cell 24. It should be noted that Davila's chart was developed for soil frozen under a confining stress of 24 kPa. The confining stress at the test site would be considerably higher than 24 kPa and, as discussed in Chapter 3, this further reduces the potential for heave during freezing (Konrad and Morgenstern, 1982).

4.2.1.3 Laboratory Frost Heave Testing

To confirm the conclusion based on Davila et al. (1992), that the sand at the Phase I test site could be frozen without disturbance due to frost heave, two frost heave tests were conducted on bulk samples of tailings sand recovered near the Phase I test site. The fines contents of the samples tested were 6.2 % and 15.2 % and, therefore, in the same range as that determined from SPT Split Spoon samples obtained at the Phase I test site in the target zone.

The frost heave tests were conducted over a period of approximately 150 hours, under the same temperature gradient of 0.6 to 1.1 °C/cm as that expected in the sampling zone during in-situ ground freezing. Both samples indicated that pore water was expelled in advance of the freezing front and negligible heaves of approximately 0.1 mm were recorded at the end of the tests. Plots of the test results are shown in Figures 4-4 and 4-5. The frost heave tests therefore agreed with the results from Davila's chart, confirming that disturbance due to frost heave would not occur during ground freezing at the Phase I test site.

4.2.1.4 Unfrozen Water Content

The magnitude of possible disturbance at the Phase I test site, caused by unfrozen water surrounding clay minerals freezing under conditions of impeded drainage, was evaluated. The Syncrude sand deposits at the Phase I, where in-situ ground freezing was undertaken, had a silt and clay size fraction (fines content) of about 12 % by dry weight, with only approximately 1.2 % of the fines comprising clay sizes. Grain size analysis and mineralogical evaluation of the fines indicated that the Syncrude sand could contain up to 0.28 % Mica minerals, as a percent by weight of the sand fraction, and up to 0.70 % Kaolin minerals, as a percent by weight. Both of these clay minerals have a specific

surface area of approximately $5 \text{ m}^2/\text{g}$ to $50 \text{ m}^2/\text{g}$, which is directly related to the amount of unfrozen water content (Anderson and Tice, 1972).

For calculation purposes, a sample of Syncrude sand with a total weight of 780 g and a high moisture content of 30 % was considered. Based on assuming an unfrozen water content at $-1 \text{ }^\circ\text{C}$ of approximately 0.30 g water/g dry soil, from measurements undertaken for Kaolin by Tice, et. al. (1976), the 9 % volume expansion that could occur due to the all of unfrozen water freezing in place at lower temperatures is 0.15 ml. See Appendix B for calculation details. This volume expansion represents an increase in the void ratio of approximately 0.0007. Disturbance of this small magnitude is below the limits of accurate weight measurement and can be neglected.

4.2.1.5 Density Condition

Information obtained from a Fixed Piston sampling program undertaken in April, 1987 at the MLSB prior to the CANLEX project, indicated that the sand had an average dry density of 1.8 Mg/m^3 and an average moisture content of about 22 %. This information was used for predicting the rate of ground freezing that could be achieved at the site and the volumes of liquid nitrogen that would be required to freeze a 1 m radius column of sand. Theoretical prediction of the freezing rate at the Phase I test site will be discussed latter in this chapter.

4.2.2 Groundwater Conditions

The groundwater conditions at the test site which would have an effect on the freezing process, including the groundwater temperature and flow gradients, are discussed in the following sections.

4.2.2.1 Initial Groundwater Temperature

Groundwater temperatures measured in standpipes in Cells 27 and 28, in March 1993, indicated groundwater temperatures in the order of +10 °C. However, a review of data obtained for Cell 24 during the Fixed Piston Sampling program undertaken in 1987, indicated groundwater temperatures in the order of 20 °C to depths of 23 m below the ground surface. Temperature measurements taken in the MLSB pond during May, 1987, indicated temperatures varying from 19 °C at the pond surface to 14 °C at a depth of approximately 23 m. To incorporate a range of temperatures, theoretical predictions for in-situ ground freezing were carried out considering temperatures of 12 °C and 22 °C.

4.2.2.2 Groundwater Flow

Information regarding the groundwater flow gradients was obtained from groundwater well and pond level measurements taken in the vicinity of the Phase I test site and from a report prepared by Klohn Leonoff Ltd. (1991), for SCL. Based on the groundwater level measurements taken in existing standpipes near the test site and on the elevation of the tailings pond, it was estimated that a groundwater flow gradient of 4.3 percent existed across the site. The report prepared by Klohn Leonoff provided information regarding groundwater seepage expected through the MLSB dike. Based on a review of the report, it was estimated that the seepage flow in the vicinity of the test site would likely be in the order of 0.25 m³/day m². The effect of the groundwater flow on the shape of the frozen zone will be discussed in the next section.

4.2.3 Prediction of the Freezing Process at the Phase I Test Site

Thermal computations were carried out to evaluate the amount of energy that would have to be extracted and the length of time that would be required to freeze a 10 m long column of sand with a 1 m radius. The computations were based on available information regarding the site conditions and estimated thermal properties for the sand encountered at the site. The input parameters used for the theoretical predictions included:

$$\begin{array}{ll} k_u = 1.45 \text{ J/sm}^\circ\text{K} & C_u = 3.17 \text{ MJ/m}^3\text{K} \\ k_f = 2.8 \text{ J/sm}^\circ\text{K} & C_f = 2.34 \text{ MJ/m}^3\text{K} \\ \rho_d = 1.80 \text{ Mg/ m}^3 & \omega = 22 \%, \end{array}$$

where k_u and k_f are the unfrozen and frozen thermal conductivities, respectively. C_u and C_f are the unfrozen and frozen volumetric heat capacities, respectively. ρ_d is the dry density and ω is the moisture content. k_u and k_f were estimated based on the charts of thermal conductivity for granular soils, with different moisture contents and densities, published by Farouki (1981, 1986) and C_u and C_f were calculated using Equations [3-1] and [3-2], given in Chapter 3.

The steady state heat flow equations provided by Sanger and Sayles (1978) were used as a basis for the thermal computations, as described in Chapter 2 (see Equations [2-9] and [2-10]). The energy and time requirements for undertaking ground freezing at the Phase I site were first evaluated neglecting groundwater flow. The effect of groundwater flow was then estimated, based on a review of the transient heat conduction modeling carried out by Hashemi and Sliepcevich (1973) for seepage velocities in the order of those expected at the Phase I site.

4.2.3.1 Estimated Time Required for Freezing

The growth of the frozen column was predicted by solving Equation [2-10] repeatedly for 0.25 m frozen radius increments up to a final radius of 1.0 m. Calculations indicated that the estimated time required to freeze a 1 m radius column of sand in the target zone would be in the order of 12 to 16 days, depending on the groundwater temperature and assuming negligible groundwater flow. Figure 4-6, shows the predicted growth of the frozen radius with time for initial groundwater temperatures of 12 °C and 22 °C, assuming no groundwater flow. The ordinate in Figure 4-6 could be considered as an approximate average frozen radius, since groundwater flow velocities, in the order of those expected at the test site, would have the effect of causing the frozen column to grow more quickly in the down stream direction and somewhat more slowly in the upstream direction, as will be discussed in the next section.

4.2.3.2 Effect of Groundwater Flow on the Growth of the Frozen Radius

As noted in Chapter 2, evaluation of the effect of groundwater flow on the growth of the frozen zone around the freeze pipe requires numerical analysis, since an exact solution does not exist that simultaneously solves the groundwater flow velocity distribution and the temperature distribution (Hashemi and Sliepcevich, 1973; Sanger and Sayles, 1979). Since a numerical model that incorporates transient heat and groundwater flow conditions was not available at the U of A, at the time that this study was undertaken, in order to estimate the effects of seepage at the Phase I test site, data presented by Hashemi and Sliepcevich (1973) regarding the effect of groundwater flow on the shape of the frozen zone was reviewed. Using a finite difference technique, Hashemi and Sliepcevich estimated the deformed shape of a frozen column around a freeze pipe for different groundwater flow velocities, assuming a freeze pipe coolant temperature of -35 °C. The flow velocities considered by Hashemi and Sliepcevich were in the order of the groundwater flow expected at the Phase I test site.

A comparison of the shape of the frozen zone predicted for no groundwater flow and for a groundwater flow of $0.4 \text{ m}^3/\text{day m}^2$ is shown in Figure 4-7, assuming a coolant temperature of $-35 \text{ }^\circ\text{C}$. The figure confirms that when groundwater flow exists, the frozen zone tends to be elongated in the downstream direction and foreshortened in the upstream direction. However, for a groundwater flow of $0.4 \text{ m}^3/\text{day m}^2$, which is slightly greater than that expected at the Phase I test site, the total volume frozen is not reduced significantly nor is its shape distorted such that it could not be cored easily. Furthermore, it was shown in Chapter 2, Equation [2-8], that the critical groundwater flow velocity is 5 times greater when liquid nitrogen is used as the coolant, at a temperature of $-196 \text{ }^\circ\text{C}$, than when brine is used as the coolant, at a temperature of $-35 \text{ }^\circ\text{C}$. This indicates that higher groundwater flow velocities can be tolerated when liquid nitrogen is used as the coolant before the effects on the shape of the frozen zone become significant.

However, to account for some elongation of the frozen column in the downstream direction, it was planned to advance boreholes for sampling slightly downstream of the freeze pipe. It was also decided that temperature measuring devices, or RTDs, would be installed at the base of each of the cased sample boreholes to confirm that the sand was frozen prior to commencing sampling.

4.2.3.3 Estimated Volume of Liquid Nitrogen Required

The volume of liquid nitrogen required to freeze a 1 m radius column of sand was determined by dividing Equation [2-9], in Chapter 2, by the latent heat of liquid nitrogen. This volume was then multiplied by 10 to determine the total volume of liquid nitrogen required to freeze a 10 m long column of soil between depths of 27 and 37 m below the ground surface. Figure 4-8 shows the total predicted volumes of liquid nitrogen required for initial groundwater temperatures of $12 \text{ }^\circ\text{C}$ and $22 \text{ }^\circ\text{C}$; the total predicted volume of liquid nitrogen was 96,000 to 128,000 m^3 (equivalent gaseous volume), respectively. It

was recognized that the volume of liquid nitrogen required to freeze a 1 m radius may be greater if groundwater flow velocities would be significantly higher than anticipated.

4.3 Ground Freezing System Design

As discussed in Chapter 2, radial freezing can be accomplished by circulating coolant through a freeze pipe located in the center of the material being frozen. When liquid nitrogen is used as the coolant, ground freezing is accomplished as heat is withdrawn from the ground surrounding the freeze pipe, when the liquid nitrogen changes phase at a temperature of -196°C .

The CPTs undertaken during the site screening phase of the project indicated that the loosest sand available for the Phase I test site was located in Cell 24, between an elevation of approximately 314 m and 324 m. As indicated by the freezing experiments described in Chapter 3, creating a reservoir for the liquid nitrogen in the target zone results in the most efficient use of liquid nitrogen for freezing. Therefore, the freeze pipe was designed with a 10 m long liquid nitrogen reservoir to be installed between 27 and 37 m below the ground surface.

The diameter of the freeze pipe was kept as small as possible to minimize the zone of disturbance around the freeze pipe due to installation, yet allowing sufficient internal space for a liquid nitrogen feed pipe and a gaseous nitrogen exhaust pipe. A steel freeze pipe was selected with a diameter of 51 mm. A rubber seal was placed at the top of the 10 m long reservoir to maintain liquid nitrogen below the seal. A copper feed pipe was installed to extend from the liquid nitrogen supply tank, through the rubber seal, to the bottom of the reservoir. A copper exhaust pipe was provided to extend from just below the rubber seal to the ground surface, to allow for the nitrogen that had undergone a phase change to escape into the atmosphere. The feed pipe had a diameter of 13 mm in the

target zone and a diameter of 19 mm above the target zone to increase the flow of liquid nitrogen.

4.4 Phase I Fieldwork

The in-situ ground freezing and coring of the frozen sand undertaken at the Phase I test site are described in the following sections. Details regarding drilling and installation of the freezing and sampling system are provided, followed by a discussion of the actual freezing process.

4.4.1 Borehole Layout

Since the target freeze zone was located at a significant depth, it was decided that the material overlying the target zone would be predrilled to a depth of 27 m and casing would be installed to facilitate installation and operation of the ground freezing system as well as sampling in the target zone. To allow for installation of the freeze pipe and to provide sufficient clearance for the core barrel during sampling, large diameter boreholes (approximately 180 mm) were advanced to 27 m below the ground surface and PVC casing was installed.

The borehole layout included a central freeze pipe with four boreholes for sampling of the frozen core located within a 1 m radius of the freeze pipe. Figure 4-9 shows a schematic cross-section illustrating the cased boreholes extending from the surface down to the top of the target ground freezing zone around the central freeze pipe. In the event that groundwater flow velocities would cause significant downstream elongation of the frozen zone, three of the four sample boreholes were proposed to be located downstream of the freeze pipe with one located in the upstream direction. Figure 4-10 shows a plan view of the proposed freeze pipe and sampling borehole locations.

4.4.2 Installation of Casing to the Top of The Target Zone

Large diameter (260 mm) boreholes were advanced to the top of the target zone utilizing a truck-mounted Failing 1500, wet rotary drill rig supplied by Elgin Exploration Ltd. Biodegradable, Kim mud was used as the drilling fluid. One borehole was advanced and cased to the top of the target zone for later installation of the freeze pipe. Four Boreholes were then advanced and cased at radial distances of approximately 0.5 m, measured from the centreline of the freeze pipe, for later coring of the frozen sand. To advance a vertical borehole to the top of the target zone at 27 m, care was taken to ensure that the drilling rig was level and that the kelly was centered on the drill table prior to commencing drilling.

The boreholes were first advanced utilizing a 159 mm (6¹/₄") tricone drill bit on the end of 114 mm (4¹/₂") drill rods. The borehole was then reamed out with a 260 mm (10¹/₄") tricone bit attached to a 4.5 m long, 178 mm (7") diameter stabilizer on the end of the drill stem. Once the reamed boreholes had been advanced to the desired depth, 200 mm diameter PVC casing was installed. The drilling mud was then replaced with clean water and a 600 mm thick bentonite seal was placed at the bottom of each borehole. The water was then blown out of the cased boreholes to avoid problems during later sampling associated with melting of the outer layer of the frozen sand by relatively warm water in the casing, as the frozen core was brought to the ground surface.

The boreholes advanced for later sampling of the frozen sand were designated as FS1, FS3, FS4 and FS5. The borehole advanced for installation of the freeze pipe was designated as FS2. Temperature measurement devices (RTDs) were installed at the bottom of each of the cased sampling boreholes to ensure that the ground at the base of the sample boreholes was frozen prior to commencing coring.

Two additional small diameter boreholes, were also advanced around the outside perimeter of the target freezing zone for installation of additional RTDs to confirm that the target radius had been frozen before commencing coring of the frozen sand. These

boreholes were advanced with a Longyear 38 drilling rig provided by Elgin Exploration Ltd. A 67 mm ($2\frac{5}{8}$ ") tricone drill bit was utilized to advance the borehole and Kim mud was used as the drilling fluid. One of these boreholes, RTD 3, extended to a depth of 27 m, at a radial distance of 0.8 m downstream of the freeze pipe centreline, and the other borehole, RTD 1, extended for the full depth of the target freezing zone, from 27 to 37 m, at a radial distance of 0.9 m from the freeze pipe centreline. Figure 4-11 shows the as-built cross-section of the freeze pipe, sample boreholes and RTD boreholes.

4.4.3 Installation of Freeze Pipe

Steel casing, with a diameter of approximately 150 mm (6") was installed through the bentonite plug at the bottom of Borehole FS2, located in the center of the test site. This was done to prevent squeezing of the bentonite during installation of the freeze pipe through the target zone. A Longyear 38 drill rig was centered over the borehole and a smaller diameter borehole was advanced through the target zone for installation of the freeze pipe. The borehole for the freeze pipe was drilled utilizing a 67 mm ($2\frac{5}{8}$ ") tricone drilling bit and Kim mud as the drilling fluid. The 51 mm diameter steel freeze pipe was then connected to the end of a 114 mm ($4\frac{1}{2}$ ") drill stem and lowered down the borehole, where it was positioned between 27 and 37 m below the ground surface. Figure 4-12 shows a schematic illustration of the freeze pipe configuration as installed at the Phase I site.

Once the steel freeze pipe was in place, the drill stem was uncoupled at the ground surface and a rubber seal, with the copper feed and exhaust pipes, were installed down to the target zone. This is also illustrated in Figure 4-12. RTDs, attached to the copper piping, were installed inside the freeze pipe at approximately 2.5 m and 7.8 below the rubber seal for monitoring whether or not the freeze pipe reservoir in the target zone was completely filled with liquid nitrogen.

4.4.4 Mapping Borehole Alignment

To confirm that the bottom of each of the cased boreholes advanced for sampling fell within a 1 m radius of the freeze pipe, the deflection of each of the borehole casings was mapped with a Digitilt Inclinator. Grooved ABS inclinometer casing was installed in the large diameter PVC casing from the surface down to the top of the target zone. Plastic centralizers were used to keep the inclinometer casing in the center of each borehole. A Digitilt Inclinator was then lowered down each borehole and the exact alignment and location of each of the borehole casings were mapped.

Figure 4-13 shows the top of each borehole in plan and the bottom of each borehole at a depth of approximately 27 m. Table 4-4 shows the deflections from the ground surface to the top of the target zone measured for each borehole casing. Plots of the borehole deflection measured between the ground surface and a depth of 27 m are presented in Appendix B. The maximum deviation from vertical, measured over a distance of 27 m in either the casing installed for the freeze pipe (FS2) or the sample boreholes was only 375 mm. The boreholes advanced for later sampling of the frozen sand column fell well within a 0.76 m radius, upstream of the freeze pipe centerline at a depth of 27 m, and a 0.6 m radius, downstream of the freeze pipe.

Yoshimi et al. (1978), undertook studies to determine the extent of the zone of disturbance around a freeze pipe installed in large samples of sand in the laboratory. The results from this work, shown in Figure 4-14, indicated that the zone of disturbance around a 73 mm freeze pipe installed with a cup auger extended approximately 15 cm in loose sand, 8 cm in medium dense sand and 6 cm in dense sand. The maximum zone of disturbance in the loose sand was therefore about two times the diameter of the freeze pipe.

The borehole for the freeze pipe installed at the Phase I test site had a diameter of 67 mm. Based on the studies undertaken by Yoshimi et al. (1978), the zone of disturbance may

extend a distance of approximately 134 mm from the wall of the borehole advanced for the freeze pipe. Figure 4-13 shows that the minimum distance from the bottom of any of the sample holes to the freeze pipe Borehole, FS2, was approximately 475 mm. Therefore, the minimum distance between Borehole FS2 and any of the sampling boreholes was well in excess of two times the diameter of the freeze pipe borehole. Thus, no frozen samples would be obtained from within the zone of possible disturbance due to installation of the freeze pipe.

4.4.5 Initiation of Ground Freezing

Installation of the freeze pipe and the cased boreholes for sampling of the frozen sand was complete, by November 4, 1993. A 15,000 cubic meter capacity liquid nitrogen truck, supplied by Praxair Canada Inc., was transported to the test site and the liquid nitrogen was connected to the copper feed pipe. Freezing commenced at 15:30 hours on November 4, 1993.

The RTDs installed inside the freeze pipe indicated that the liquid nitrogen was undergoing a phase change prior to reaching the bottom of the reservoir for several hours after commencing freezing as the freeze pipe system was being cooled. The RTDs located at the base of the sample boreholes indicated that the initial ground temperature was approximately 18.5°C at a depth of 27 m.

After approximately 4 hours of freezing, the lower RTD in the freeze pipe was not measuring temperatures in the range that would indicate that liquid nitrogen was accumulating in the lower region of the reservoir. The upper RTD was recording a temperature of approximately -20 °C and the lower RTD was recording a temperature of -7 °C. It was not clear whether the freezing system was still cooling down or whether there was something wrong with the liquid nitrogen flow path.

After some time it became evident that the rubber seal was leaking since significant volumes of nitrogen vapors were seen escaping from the drill stem attached to the freeze pipe. Small volumes of water were poured down the freeze pipe in an attempt to seal the leak with ice. Bentonite chips were also dropped down the freeze pipe to ensure a proper seal. After this procedure, gas nitrogen vapors no longer emanated from the drill stem at the ground surface, indicating that a complete seal had been formed.

Although the leak in the seal near the top of the target zone had been repaired, the RTDs in the freeze pipe continued to indicate that liquid nitrogen was not accumulating in the reservoir along the target freezing zone. On November 8, 1993, it was decided that the copper tubing and rubber seal should be removed from the freeze pipe to determine where the additional leak was and to install a new seal. A steam truck and air compressor were used to melt the ice/bentonite seal and the copper tubing with the rubber seal were removed from the freeze pipe. Examination of the copper feed pipe indicated that a leak had developed at one of the joints just above the rubber seal. The leak had allowed most of the liquid nitrogen to circumvent the reservoir and escape back to the ground surface.

The defective copper tubing was replaced and new tubing was installed in the freeze pipe. A new rubber seal was installed in the freeze pipe just above the top of the target freezing zone. After the repairs were complete, liquid nitrogen was again hooked up to the copper feed pipe and freezing commenced at 18:00 hours on November 11, 1993. No leaks were detected in the newly repaired freezing system. The RTDs installed in Boreholes RTD 1 and RTD 3, indicated that the ground temperatures just prior to recommencing freezing were 16.5 °C at a depth of 27 m and 14.4 °C at a depth of 37 m.

The flow of liquid nitrogen in the freeze pipe was controlled on a regular basis to fill the freeze pipe with as much liquid nitrogen as possible without expelling the liquid before it had a chance to change phase. During the first few days of freezing, it was difficult to completely fill the freeze pipe reservoir with liquid nitrogen. However, as the freezing system and the ground immediately surrounding the freeze pipe cooled to near 0 °C, it

was possible to increase the flow of liquid nitrogen and gradually bring the level of liquid nitrogen up to the top of the reservoir.

4.4.6 Monitoring of Ground Temperatures During Freezing

Ground freezing was carried out from November 11 to November 23, 1993. During this time the RTDs installed at the top of the target freeze zone in each borehole were monitored every six hours. The temperatures measured during ground freezing are provided in Appendix B. Figure 4-15 shows the changes in temperature recorded in each of the sample boreholes and in Boreholes RTD 1 and RTD 3 at a depth of 27 m. The figure shows that a temperature of 0 °C was attained in Sample Boreholes FS3, FS4 and FS5 after approximately 140 hours of freezing. These boreholes were located approximately 0.5 m downstream of the freeze pipe. Figure 4-15 also indicates that even after 250 hours of freezing, a temperature of 0 °C had not been reached in either Borehole FS1 or RTD 1, located upstream of the freeze pipe, or Borehole RTD 3, located downstream of the freeze pipe, at a depth of 27 m.

The temperature distribution in Borehole RTD 1 between 27 and 37 m is shown in Figure 4-16. The figure indicates that the rate of decrease in ground temperature was greater with increasing depth. This likely occurred since liquid nitrogen accumulated in the freeze pipe at the bottom of the target zone first and the level of liquid nitrogen then increased as the ground cooled and freezing progressed. This phenomenon resulted in part, due to the fact that the flow of liquid nitrogen could not be increased sufficiently during the initial stages of ground freezing to allow for liquid nitrogen to completely fill the reservoir.

Based on the temperature measurements from all of the RTDs, a cross-section of the frozen zone was established. The extent of the frozen zone, after approximately 258 hours of freezing, is shown in Figure 4-11. The cross-section indicates that the upper

portion of the target zone below Borehole FS1, located upstream of the freeze pipe, was not frozen after 258 hours.

To avoid problems with groundwater flow during coring of the in-situ frozen sand, it was desirable to freeze the upper portion of the target zone prior to coring Borehole FS1. However, since FS1 was located approximately 0.9 m upstream of the freeze pipe, the time required to freeze this portion of the target zone from the freeze pipe would have been unacceptably long. It was therefore decided to expose the top of the target zone in Sample Borehole FS1 directly to liquid nitrogen.

The liquid nitrogen supply was connected to a flexible 15 mm grout hose that extended to the top of the bentonite seal in FS1. Liquid nitrogen was then allowed to flow directly into the cased borehole. A PVC cap was placed over the borehole with 50 mm exhaust pipe and gas nitrogen was directed away from the working area via the exhaust pipe. Freezing was carried out in this manner until the RTDs indicated that the upper portion of the target zone beneath FS1 was likely frozen.

4.4.7 Actual Liquid Nitrogen Consumption

The consumption of liquid nitrogen was monitored every six hours during ground freezing. The rate of usage of liquid nitrogen was reviewed to check for any indication that problems may be developing. Figure 4-17 shows the volume of liquid nitrogen used during freezing. The figure indicates that the rate of consumption of liquid nitrogen was fairly consistent during the entire field program. Figure 4-17 also shows that approximately 6 tanks, containing 15,000 m³ (equivalent gaseous volume) of liquid nitrogen, were required to complete ground freezing and coring at the site.

4.5 Comparison of the Rate of Ground Freezing with Theoretical Predictions

4.5.1 Growth of the Frozen Radius

The actual growth of the frozen radius, based on RTD measurements, was compared with the initial theoretical predictions, assuming an initial ground temperature of 15.5 °C and that the freeze pipe reservoir in the target zone was completely full of liquid nitrogen at all times during freezing. Figure 4-18, showing the comparison between the actual data and the theoretical predictions, indicates that the actual frozen radius at a depth of 27 m was less than the predicted frozen radius and the actual frozen radius at a depth of 37 m exceeded the predicted value.

The results shown in Figure 4-18 agree with the results obtained from the large scale freezing experiment presented in Chapter 3, where a continuous 8 m long column of water was frozen (Experiment 4). In both cases, liquid nitrogen accumulated in the lower portion of the freeze pipe reservoir much sooner than in the upper portion due to insufficient flow of the liquid nitrogen into the reservoir. This resulted in slower growth of the frozen zone near the top of the target zone, where cooling occurred by conduction as heat was lost from the ground to the gaseous nitrogen, and more rapid growth at the bottom of the target zone where freezing progressed as heat was absorbed from the ground due to the phase change of liquid nitrogen.

In the lower portion of the target zone, where heat extraction occurred due the latent heat of liquid nitrogen, the theoretical equations are slightly conservative compared to the actual growth of the frozen radius, as noted in Chapter 3. This is due to the assumption inherent in the equation for calculating freezing time, that steady state conditions have been attained at the radius where ground temperature measurements are recorded. However, the times shown for the actual frozen radii shown in Figure 4-18 are the first times at which a temperature of 0 °C is recorded at the RTD locations, and does not account for any additional time required to reach steady state conditions.

Although the theoretical equations used here are somewhat of an approximation to the actual field measurements and have not yet been modified to account for the various coolant phases that existed during in-situ ground freezing, Figure 4-18 shows that the prediction of frozen radius with time represents a reasonable average of the actual conditions.

4.5.2 Consumption of Liquid Nitrogen

A comparison of the volume of liquid nitrogen used during ground freezing with the initial theoretical predictions is shown in Figure 4-19. The figure indicates that the total volume of liquid nitrogen used, of about 90,000 m³ (equivalent gaseous volume), was slightly less than the total predicted volume of 108,000 m³(equivalent gaseous volume). This was mainly due to the fact that freezing was terminated before the frozen radius extended to 1.0 m. The final frozen radius, just prior to commencing coring, was approximately 0.91 m. Figure 4-18 also shows that the actual rate of liquid nitrogen consumption was considerably less than the predicted rate. This was likely due to the fact that the flow rate of liquid nitrogen into the freeze pipe was not high enough to maintain a full liquid nitrogen level in the reservoir at all times during freezing.

To confirm this hypothesis, a revised prediction was made. Based on temperature measurements from RTD's that had been installed near the top and bottom of the freeze pipe reservoir, it was assumed that, on average during the freezing process, the phase change of liquid nitrogen resulted in 2/3 of the contribution to the total heat extraction and conductive heat loss to gaseous nitrogen resulted in 1/3 of the contribution to the total heat extraction. The revised predictions are shown in comparison with the actual data in Figures 4-20 and 4-21. Figure 4-20 shows good agreement between the actual and revised prediction of liquid nitrogen consumption during the first approximately 168 hours of freezing. The predicted frozen radius also agrees well with the actual frozen

radii measured at the top of the target zone where the freeze pipe was likely filled with gaseous nitrogen during at least the initial stages of the freezing process.

Since the flow of liquid nitrogen was increased during the later stages of in-situ ground freezing, the predictions were further modified to consider two stages in the freezing process. During the initial stages of ground freezing, it was assumed that the phase change of liquid nitrogen resulted in 2/3 of the contribution to the total heat extraction and gaseous nitrogen resulted in 1/3 of the contribution to the total heat extraction. Then, after approximately 192 hours of freezing, it was assumed that the entire freeze pipe reservoir in the target zone was completely full of liquid nitrogen. Figure 4-22 shows that the average revised prediction of liquid nitrogen consumption now agrees very well with the actual liquid nitrogen consumption, both in terms of the rate of consumption and the total volume of liquid nitrogen used. In Figure 4-23, the revised prediction of frozen radius also shows reasonable agreement with the average measured frozen radii.

4.6 Coring of In-Situ Frozen Sand

Coring of the in-situ frozen sand column was undertaken utilizing a 150 mm, outer diameter, Cold Regions Research Engineering Laboratory (CRREL) core barrel with a dry coring technique. After each run of the CRREL core barrel the borehole was reamed out utilizing a 260 mm (10¹/₄") tricone bit to avoid problems associated with slough accumulating in the borehole. Coring was undertaken during the daytime. Overnight, liquid nitrogen was hooked up to the freeze pipe and freezing was continued to maintain temperatures in the frozen zone at well below 0 °C. The ambient air temperature at the time of coring ranged from -5 °C to -25 °C.

The frozen core was extruded at the ground surface utilizing a hydraulic ram. The extruded frozen core was sprayed with water which was allowed to freeze on the surface

of the core. The length and depth of the core was recorded. The samples were then wrapped in plastic bags and stored in a freezer between layers of insulation for padding. Dry ice and generators were on hand in the event that the ambient air temperature rose above 0 °C and artificial cooling was required. The frozen core samples were transported by vehicle to the U of A in freezers containing dry ice. At the U of A, the samples were carefully placed in a cold room for long term storage. A total of 20 m of 100 mm diameter frozen core samples were recovered from the Phase I test site.

4.7 Catalog of In-Situ Frozen Sand Core Samples

During the weeks following the ground freezing and coring field program, each of the in-situ frozen core samples were logged and photographed in the U of A cold room. The sides of each core were scrapped with a sharp knife to check for any ice lens formations, bitumen or silt layers. No signs of disturbance due to pore water freezing and expanding in place or due to ice lens formation were observed. Occasional bitumen layers of up to 2 mm in thickness were noted. Discrete silt lenses were not encountered in any of the core samples examined.

As each of the core samples were logged, a catalogue of the samples was developed. The core catalogue is provided in Appendix B. Four categories of core samples were established. The categories were defined based on the quality of the core in terms of whether or not they could be used for laboratory testing. The categories were as follows:

1. Excellent Core :

- Homogeneous sand with no signs of disturbance due to freezing;
- Insignificant zone of melting around perimeter of sample during coring or extrusion;
- No significant layering of bitumen evident
- Core is of laboratory testing quality.

2. Good Core :

- Homogeneous sand with no signs of disturbance due to freezing;
- Minor zone of melting around perimeter of sample during coring or extrusion;
- No significant layering of bitumen evident
- Core is of laboratory testing quality.

3. Fair Core :

- Significant zone of melting around perimeter of sample during coring or extrusion;
- Sample may contain refrozen slough;
- Significant layering of bitumen is evident.

4. Poor Core :

- Core contains disturbed material due to either the presence of refrozen slough, excessive melting and/or fracturing during coring or extrusion.

The length of each piece of core was recorded and the number of samples that could be trimmed from each piece of core was estimated and recorded on the core catalogue. Due to the large amount of frozen core samples recovered from the test site, it was possible to trim a total of approximately 215 specimens for laboratory testing by CANLEX participants. The number of triaxial and direct simple shear specimens trimmed from either excellent or good quality core was estimated as follows:

74 Triaxial Specimens - with maximum dimensions of 125 mm (± 3.0 mm) in length by 60 mm (+ 1.0 mm; - 0.0 mm) in diameter.

144 Direct Simple Shear Specimens - with maximum dimensions of 22 mm (+ 1.0 mm; - 1.0 mm) in length by 71.1 mm (+0.0 mm, - 0.3 mm) in diameter.

The ends of several of the core samples were trimmed for moisture content and void ratio determination. The void ratios were determined based on 3 cm by 3 cm by 2 cm frozen cubes of sand, trimmed from the ends of the core samples. Void ratio calculations were

carried out based on the dry density of these cubes, without assuming full saturation. using the following relation:

$$e = (G_s \rho_w / \rho_d) - 1 \quad [4-1]$$

These void ratio measurements are discussed in the following section and are included on the core catalogue, in Appendix B. A summary of the frozen core recovered in the target zone from each borehole is also provided in Appendix B.

4.8 In-Situ Void Ratios

The void ratios measured from the frozen core trimmings were compared with the in-situ void ratios determined independently from geophysical logging undertaken within a 5 m radius of the freeze pipe at the test site. The geophysical logging was carried out using a downhole nuclear density technique with a tool that measures gamma ray scattering as a function of bulk density. Details of the Geophysical Logging are given by Küpper et al. (1995). Figure 4-24 shows that the void ratios established from the frozen core samples agree very well with the void ratios determined from 4 boreholes where geophysical logging was undertaken.

It should be noted that the precision of the void ratios measured with these two techniques differs slightly. Due to errors associated with physical measurements, it is estimated that the accuracy of void ratio measurements from frozen cubes is approximately ± 0.007 , as will be shown in Chapter 7, whereas the potential error in void ratio measurements based on geophysical logging is slightly higher at approximately ± 0.03 (Plewes et al., 1988). However, the general agreement between the independently measured void ratios shown in Figure 4-24, and the fact that there was no visual evidence of disturbance due to frost heave or due to freezing and expansion of pore water, indicates that the in-situ frozen core samples were of high quality.

4.9 Conclusions

The feasibility studies conducted prior to undertaking ground freezing at the Phase I test site, indicated that in-situ ground freezing could be used to recover undisturbed samples. Both the evaluation of frost heave potential based on mineralogical analysis of the fines contained within the sand and the laboratory frost heave tests showed that disturbance of the soil due to frost heave or to the excess 9 % pore water volume freezing in place would not occur.

A freezing system was designed to freeze a 10 m long target zone between depths of 27 m and 37 m below the ground surface. The actual growth of the frozen radius was reasonably well predicted using the theoretical equations for heat extraction provided by Sanger and Sayles (1979) as a basis. As a first approximation of the rate of freezing and the rate of liquid nitrogen consumption, predictions can be made based on assuming that the freeze pipe reservoir will be full of liquid nitrogen at all times. If the level of liquid nitrogen falls below the top of the target zone during freezing, the predicted first approximation will likely show good agreement with the average frozen radius along the length of the target zone, while the actual rate of liquid nitrogen consumption will likely be less than predicted.

A technique was described for recovering frozen core samples from significant depth by utilizing precased boreholes to the top of the target zone, careful drilling procedures and measurement of the borehole alignment to confirm that the core barrel would intersect the frozen column of sand. Once alignment of the sampling boreholes with the frozen sand column has been achieved, dry coring of the in-situ frozen sand with a CRREL core barrel is an effective means of obtaining the undisturbed samples. A total of 20 m of undisturbed frozen core samples were recovered from the Phase I test site.

The void ratios measured from the in-situ frozen core showed very good agreement with the void ratios measured independently by geophysical logging, conducted in boreholes

located at a radial distance of 5 m from the freeze pipe. Therefore, the work undertaken at the Phase I test site showed that in-situ ground freezing can be used to recover undisturbed samples from significant depth.

4.10 References:

- Anderson, D. M. and Tice, A. R., 1972, Prediction of Unfrozen Water Contents in Frozen Soils from Surface Area Measurements. , Highway Research Record, No. 393, p.12-18.
- Davila, R. S., Segó, D. C. and Robertson, P. K., 1992. Undisturbed Sampling of Sandy Soil by freezing. Canadian Geotechnical Conference Proceedings, Toronto. pp. 13A-1 to 13A-10.
- Farouki, O. T., 1981, Thermal Properties of Soils Relevant to Ground Freezing. Design Techniques for their Estimation. 3rd International Symposium on Ground Freezing. Hanover, New Hampshire, USA , pp. 139-146.
- Farouki, O. T., 1986. Thermal Properties of Soils. Trans Tech Publications, Series on Rock and Soil Mechanics, Vol. 11, D-3392 Clausthal-Zellerfeld, Germany. 135 p.
- Hashemi, H. T. and Sliepcevich, C. M., 1973, Effect of Seepage Stream on Artificial Soil Freezing, Proceedings, Ground Freezing Conference, Developments in Geotechnical Engineering, V 28,189-201.
- Klohn Leonoff Ltd., 1991. Mildred Lake Tailings Pond, Seepage Collection Optimization Study - Cell 11 through 18. Report prepared for Syncrude Canada Ltd., June, 1991, 35 pp.
- Konrad, J.-M. and Morgenstern, N. R., 1982, Effects of Applied Pressure on Freezing Soils, Canadian Geotechnical Journal, V. 19, pp. 494-505.
- Küpper, A., Lawrence, M., Howie, J., and Plewes, H., 1995. The use of Geophysical Logging Techniques at the CANLEX Project. 48th Canadian Geotechnical Conference, Vancouver, B.C. pp. 81-88.

- Plewes H. D., McRoberts, E. C. and Chan, W. K., 1988. Downhole nuclear Density Logging in Sand Tailings. ASCE Specialty Conference on Hydraulic Fill Structures, pp. 290-309.
- Robertson, P. K. R., List, B. R. and Hofmann, B. A., 1994. CANLEX (Canadian Liquefaction Experiment): A One Year Update. 3rd International Conference on Recent Advances in Geotechnical Earthquake Engineering and Soil Dynamics, October, 1994.
- Sanger, F. J. and Sayles, F. H., 1978. Thermal and rheological computations for artificially frozen ground construction. International Symposium on Ground Freezing. 8-10 March. Bochum. pp. 311-337 or Engineering Geology, Vol. 13. pp. 311-337.
- Tice, A. R., Anderson, D. M. and Banin, A., 1976. The Prediction of Unfrozen Water Contents in Frozen Soils from Liquid Limit Determinations. Corps of Engineers. U.S. Army. Cold Regions Research and Engineering Laboratory, CRREL Report 76-8, Hanover, New Hampshire.
- Yoshimi, Y., Hatanaka M. and Oh-oka, H., 1978. Undisturbed Sampling of Saturated Sands by Freezing. Soils and Foundations, Japanese Society of Engineering, vol. 8, No. 3, pp. 59-73.

Table 4-1: Summary of Fines Content Determined for Split Spoon Samples Taken at the Phase I Test Site

Borehole Number	Sample Depth (m)	Sample Elevation (m)	Sand Content (%)	Fines Content (%)	Size Passing D_{10}
SPA24S9307	18.29	332.634	91.0	9.0	0.15
SPA24S9307	19.81	331.114	91.0	35.2	0.10
SPA24S9307	21.34	329.584	86.4	13.6	0.20
SPA24S9307	22.86	328.064	86.1	13.9	0.20
SPA24S9307	24.38	326.544	85.6	14.4	0.15
SPA24S9307	25.91	325.014	88.0	12.0	0.24
SPA24S9307	27.43	323.710	85.9	9.5	0.20
SPA24S9307	28.96	321.964	87.8	12.2	0.28
SPA24S9307	30.48	320.444	92.1	7.9	0.20
SPA24S9307	32.00	318.924	88.6	11.4	0.20
BHA24S9306	36.58	314.560	85.3	14.7	0.15

Table 4-2: Summary of Fines Content Determined for Split Spoon Samples Taken at the Phase I Test Site.

Sample Number	Surface Area of Silt Fraction 2 μm - 74 μm (m^2/g)	Surface Area of Clay Fraction < 2 μm (m^2/g) (m^2/g)	Clay Content (% of fines)	Silt Content (% of fines)
BA 28.7m	11	108	10	14.4
BA 31.7m	17	159	8	12.2
BA 34.8m	14	138	9	11.4

Table 4-3: Estimated Mineral Content for Split Spoon Samples Taken at the Phase I Test Site

Sample Number	Silt Mineralogy 2 μm - 74 μm (m^2/g)	Clay Mineralogy < 2 μm (m^2/g) (m^2/g)
BA 28.7m	Kt(5), Mi(tr), Fd(5), Qtz(90)	Kt(60), Mi(26), Qtz(14)
BA 31.7m	Kt(5), Mi(tr), Fd(5), Qtz(90)	Kt(64), Mi(26), Qtz(10)
BA 34.8m	Kt(5), Mi(tr), Fd(10), Qtz(85)	Kt(63), Mi(25), Qtz(12)

Kt: kaolinite;

Mi: mica;

Fd: feldspar

Qtz: quartz

Table 4-4: Summary of Sample Borehole Deflections

Borehole Number	Direction	Deflection (mm)	Direction	Deflection (mm)
FS1 Casing	North	90	East	40
FS1 Borehole	East	35	South	12
FS2	North	70	East	235
FS3	North	40	East	375
FS4	South	30	East	310
FS5	North	150	East	280
Freeze Pipe	South	20	East	155
RTD1	South	62	West	50
RTD2	North	430	East	320
RTD3	North	0	East	80

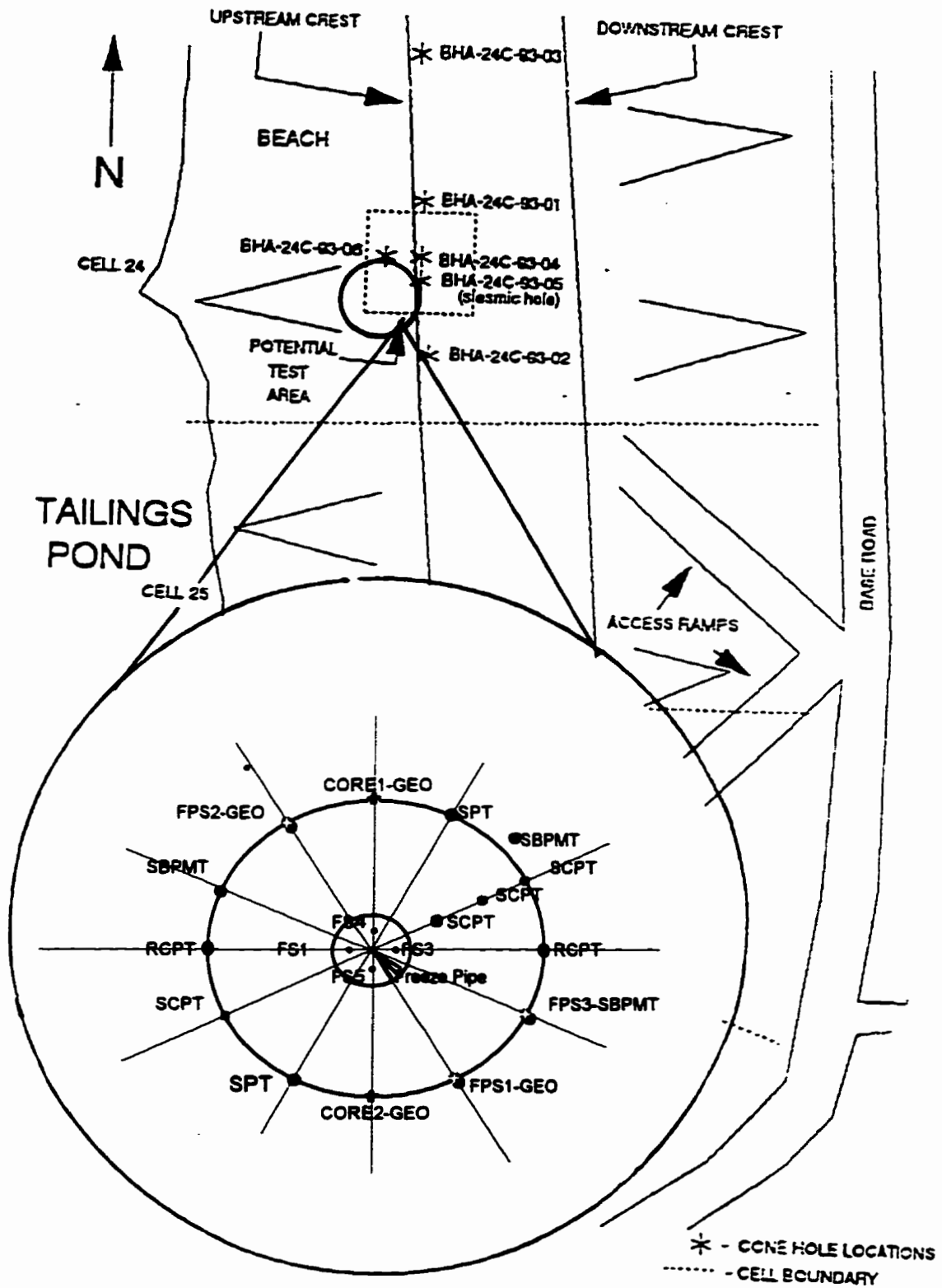


Figure 4-1: Plan View of Phase I Test Site

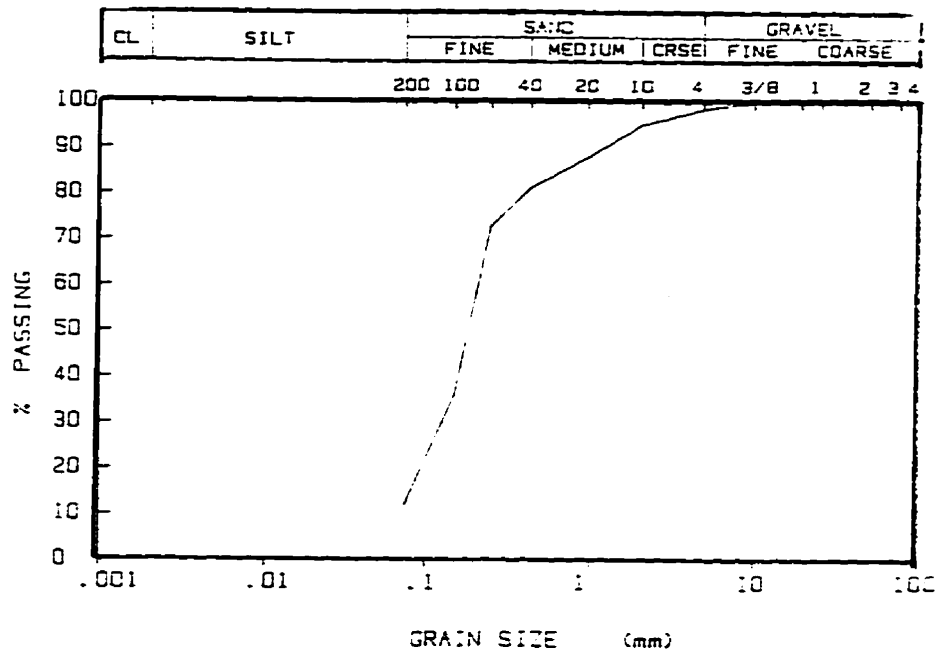


Figure 4-2: Grain Size Curve for Split Spoon Sample Obtained at 25.91 m.

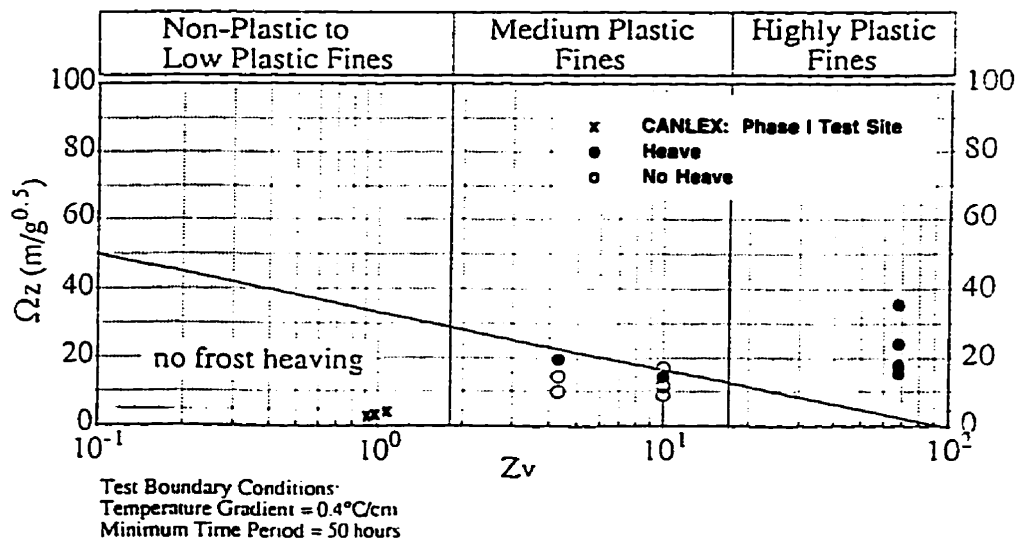


Figure 4-3: Surface Area Criteria Plot for Evaluating Frost Heave Susceptibility (modified from Davila et al., 1992)

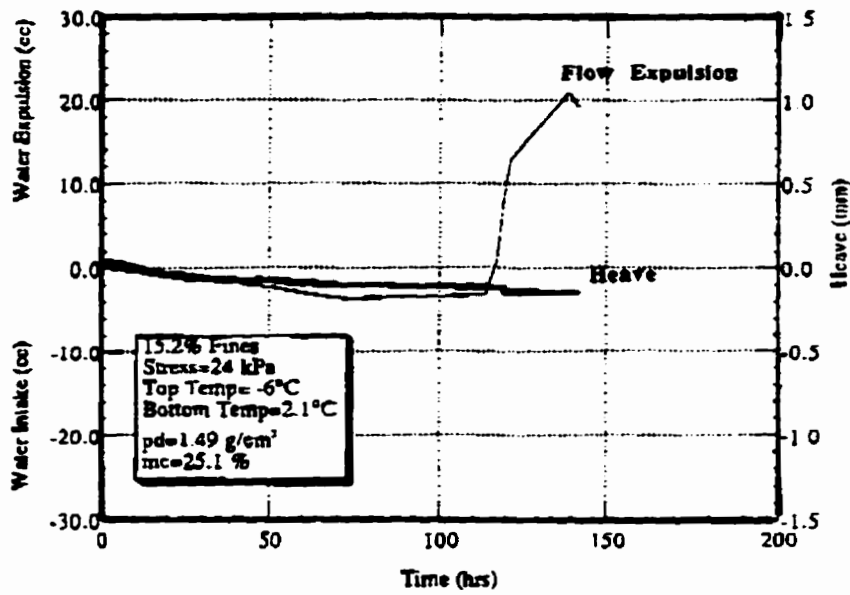


Figure 4-4: Frost Heave Test Results for Sample with 15.2 % Fines.

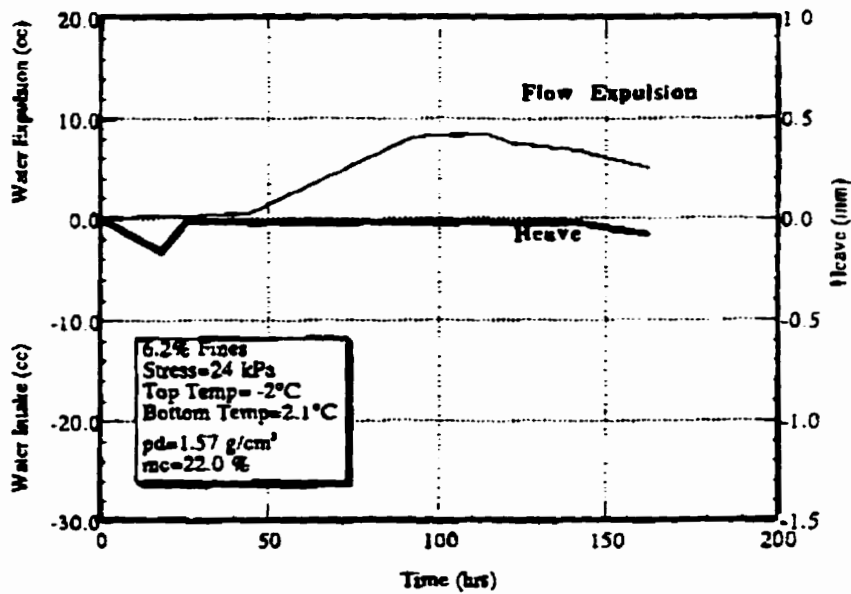


Figure 4-5: Frost Heave Test Results for Sample with 6.2 % Fines.

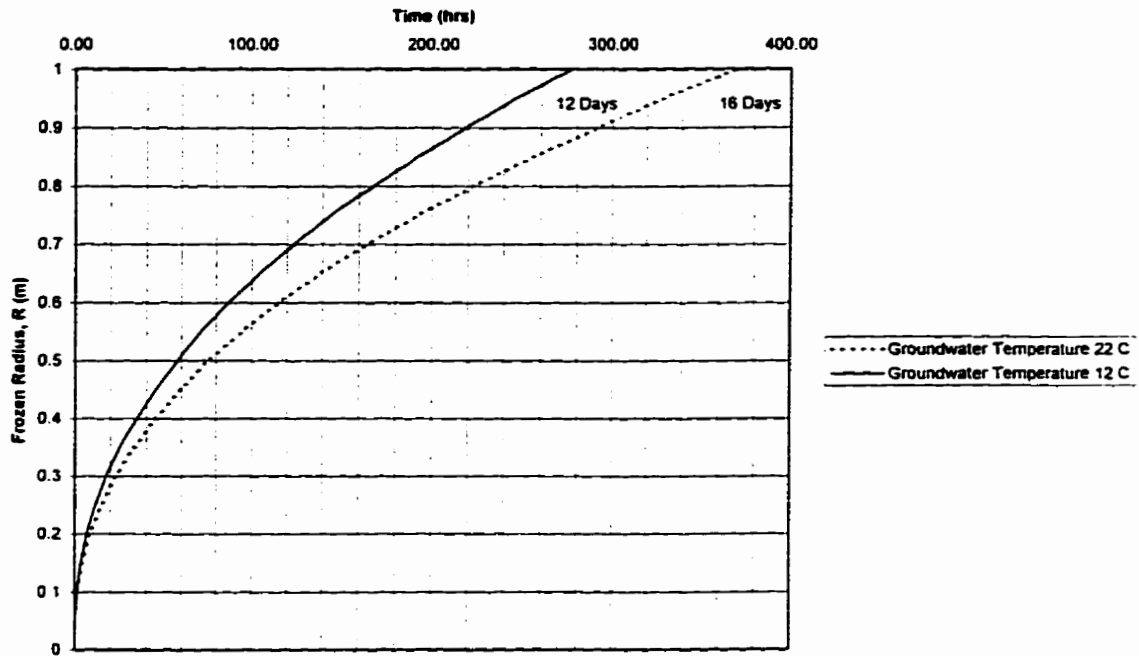


Figure 4-6: Predicted Time Required to Freeze a 1 m Radius Column of Sand at the Phase I Test Site Considering Different Initial Groundwater Temperatures.

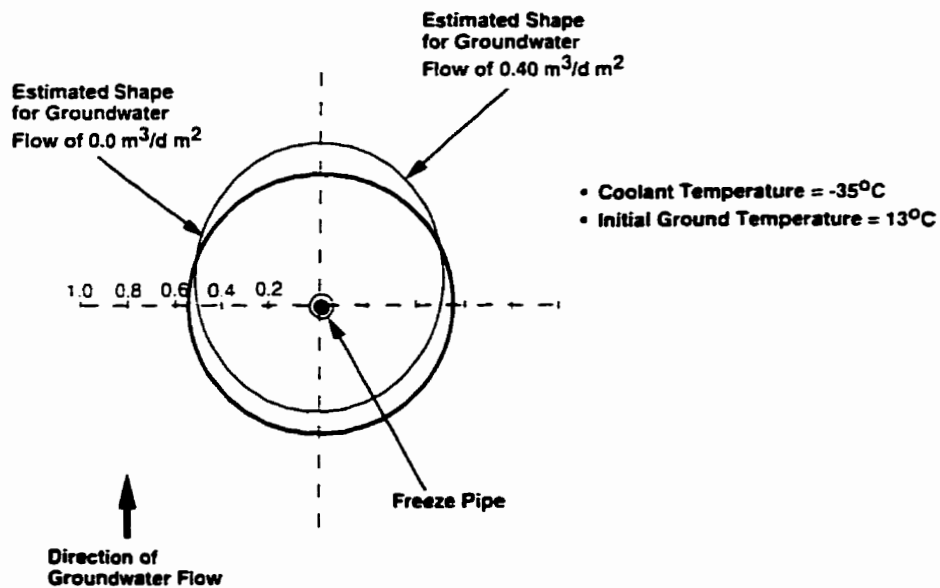


Figure 4-7: Effect of Seepage Flow on Frozen Zone (after Hashemi and Sliepcevic, 1973)

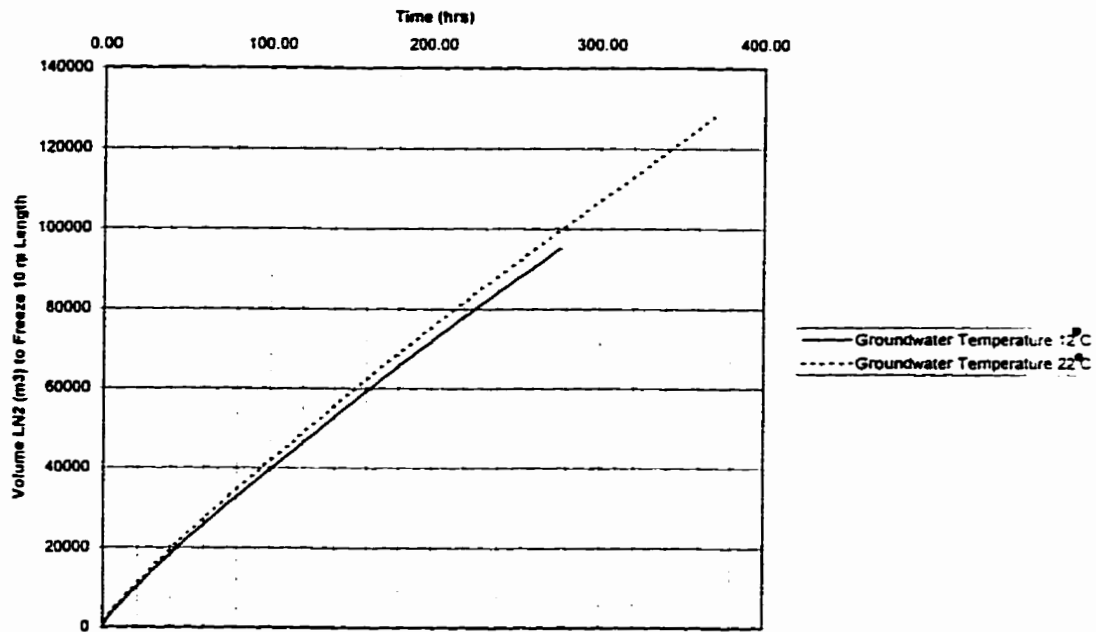


Figure 4-8: Predicted Volume of Liquid Nitrogen Required to Freeze a 1 m Radius Column of Sand at the Phase I Test Site Considering Different Initial Groundwater Temperatures.

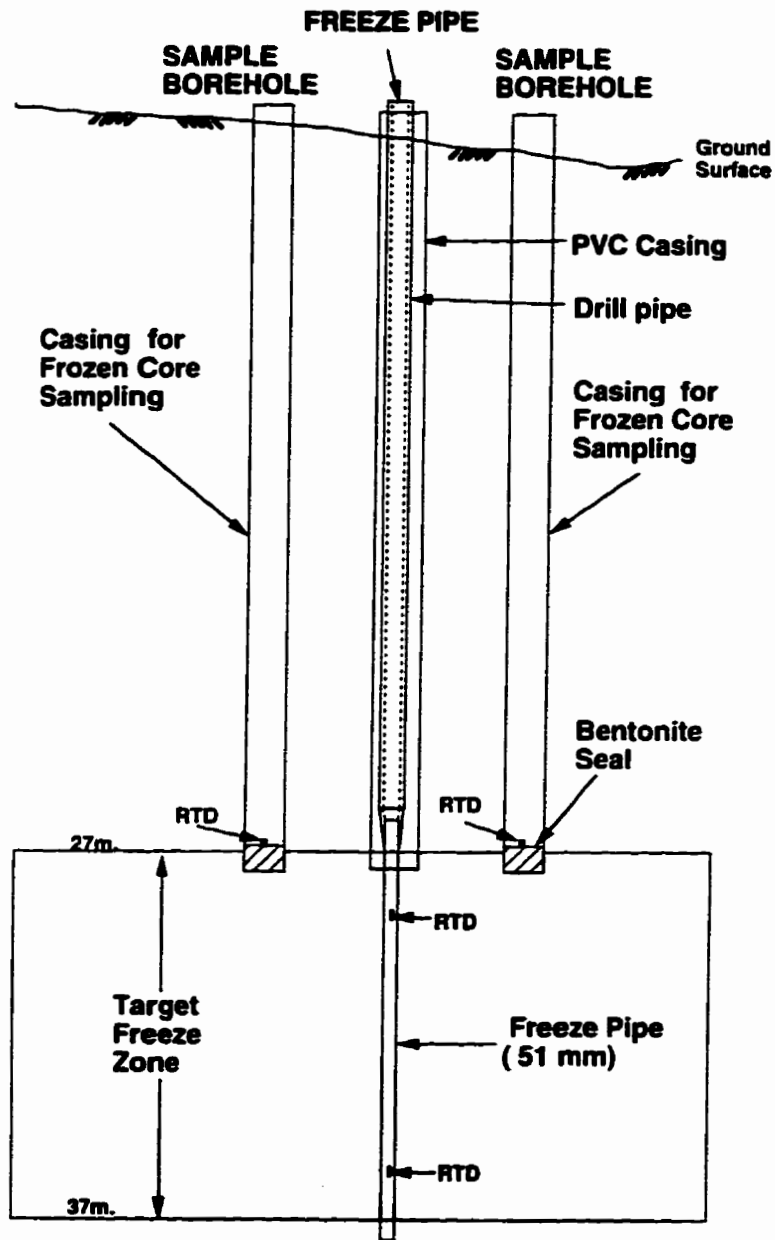


Figure 4-9: Schematic of Borehole Layout for Freezing and Sampling

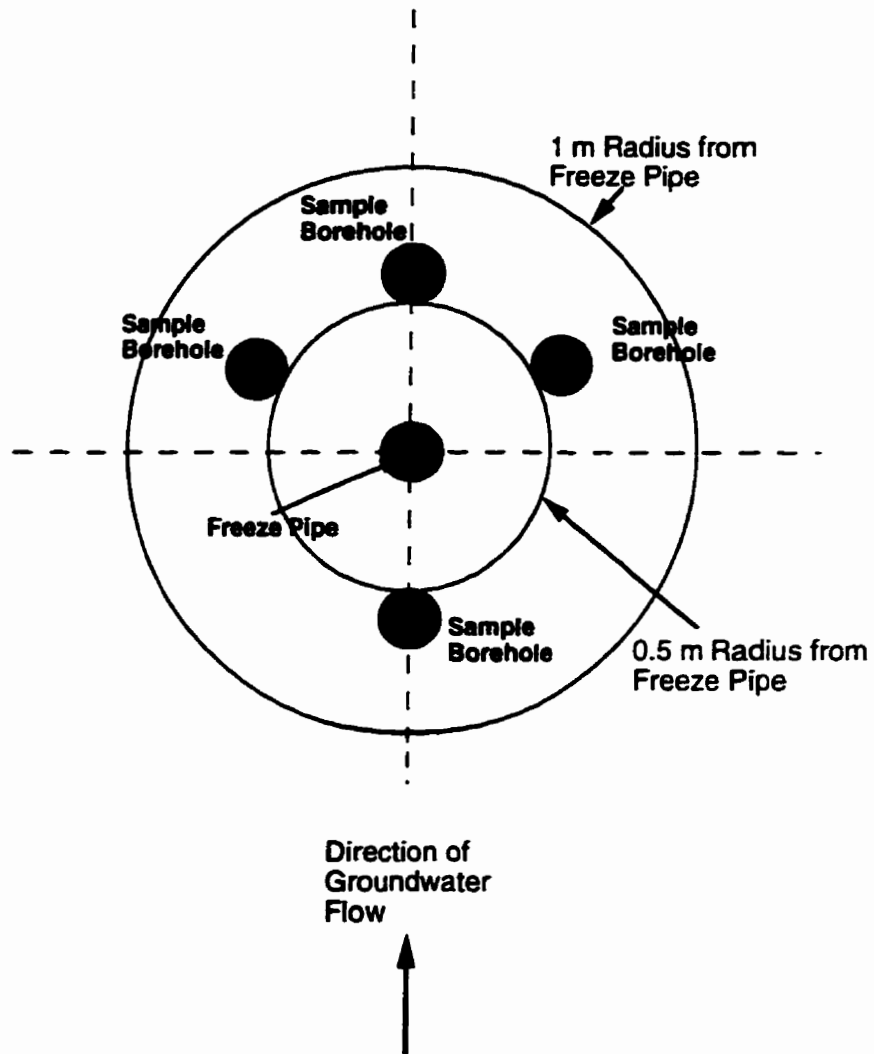
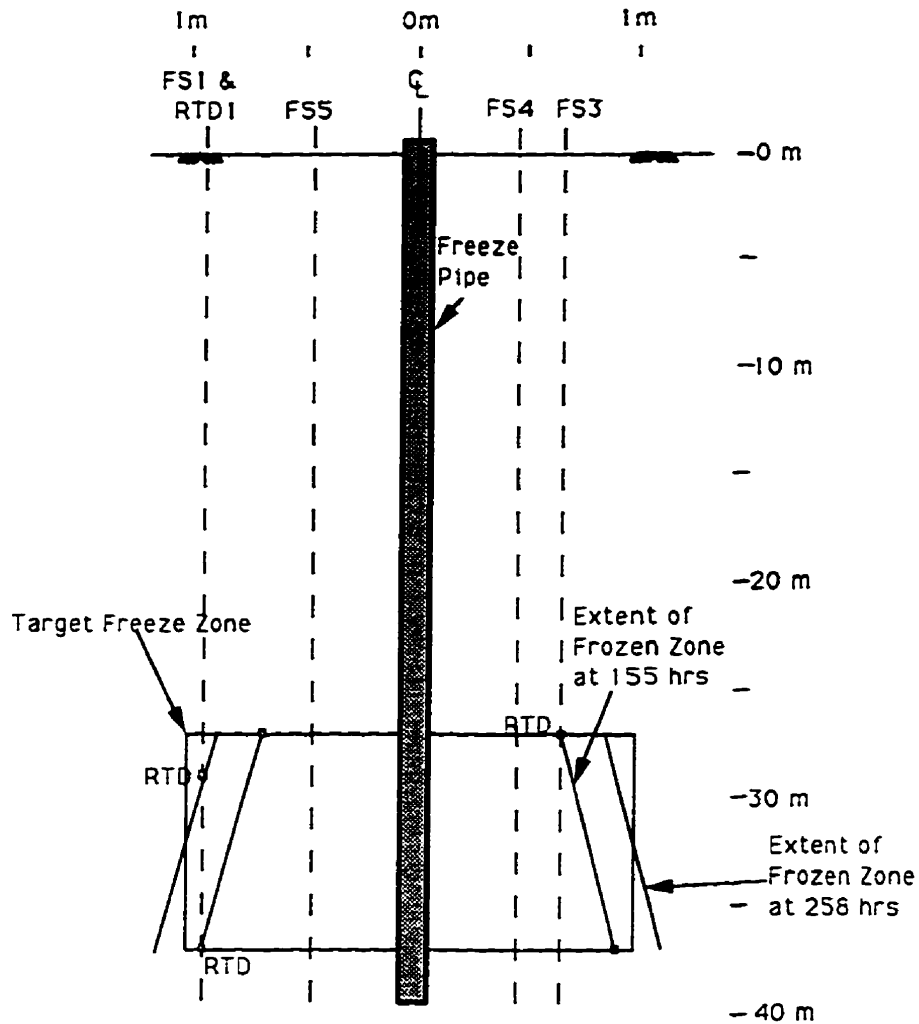


Figure 4-10: Plan View Showing Proposed Freeze Pipe Layout and Sample Borehole Layout at the Phase I Test Site.

MONITORING OF FROZEN ZONE AROUND FREEZE PIPE



Borehole No:	Distance From Freeze Pipe @ 27m
FS1	0.91m
FS3	0.64m
FS4	0.45m
FS5	0.46m
RTD1	0.91m
RTD3	0.79m

Figure 4-11: As Built Cross-Section of Freeze Pipe and Sample Boreholes.

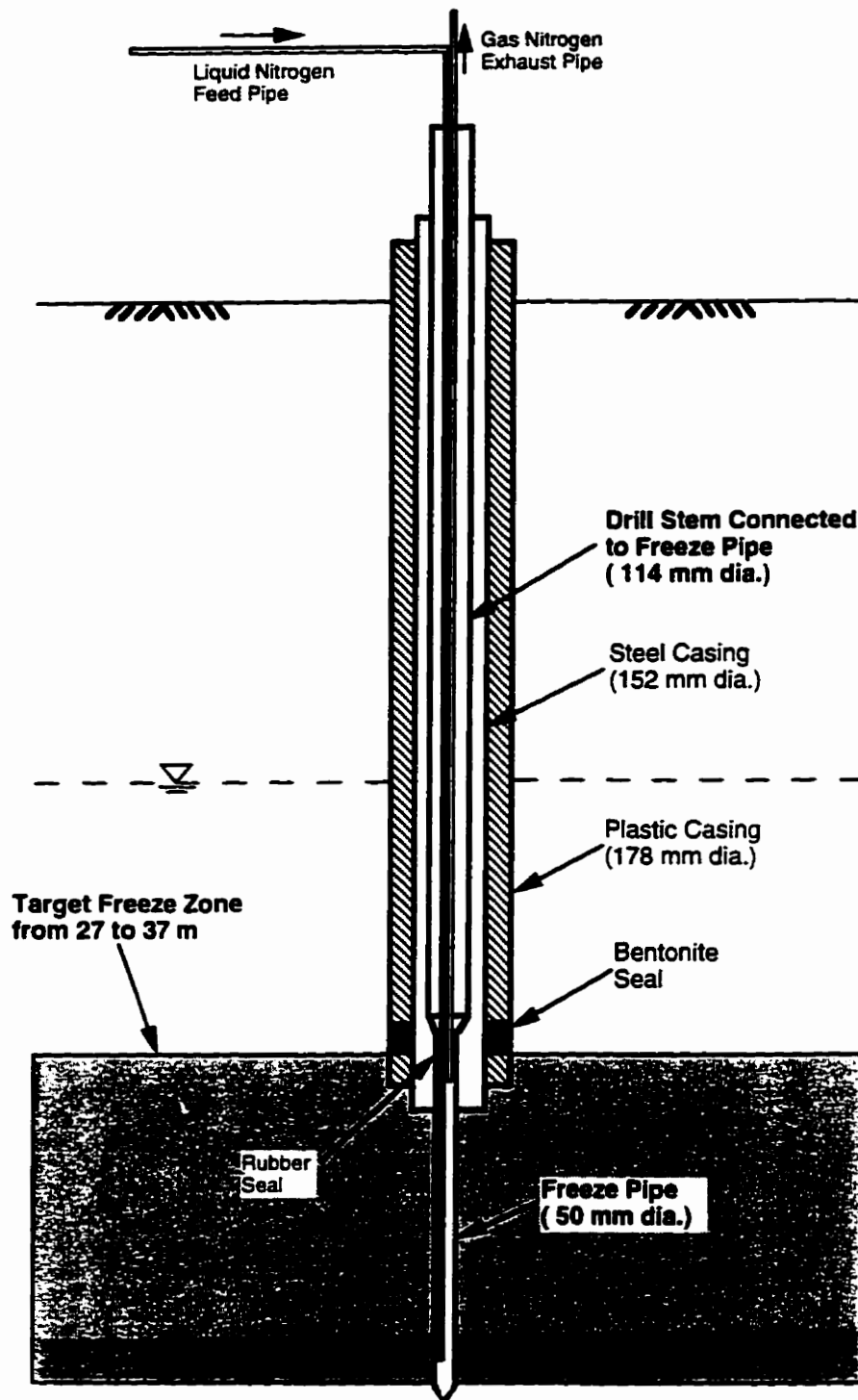


Figure 4-12: Schematic Diagram of Freeze Pipe System used at the Phase I Test Site.

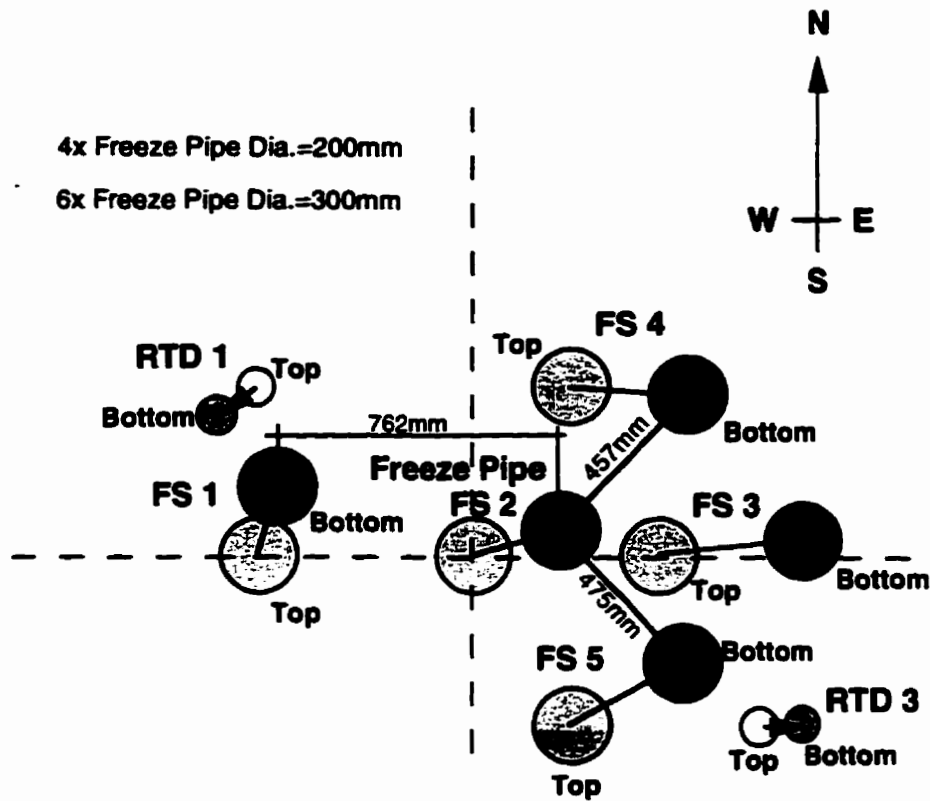


Figure 4-13: Site Plan Showing Final Borehole Locations.

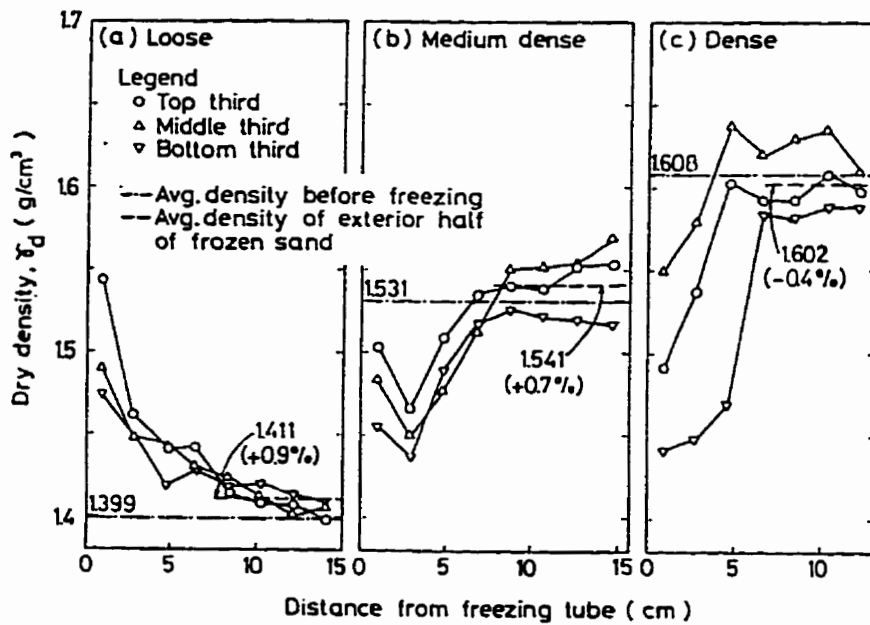


Figure 4-14: Disturbance Caused by Installation of Freeze Pipe (after Yoshimi et al., 1978)

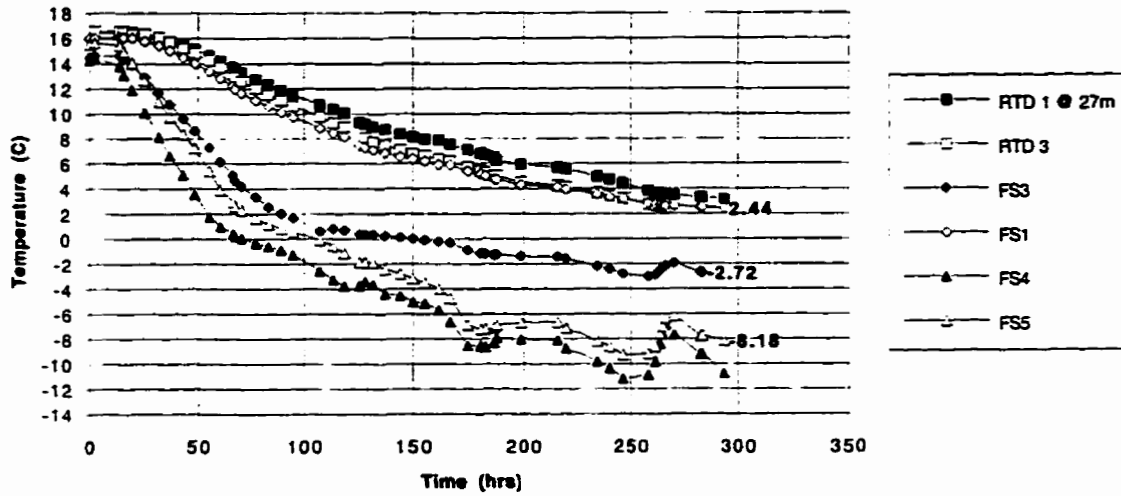


Figure 4-15: Ground Temperatures Measured During Ground Freezing at Sample Borehole and RTD Borehole Locations at a depth of 27 m.

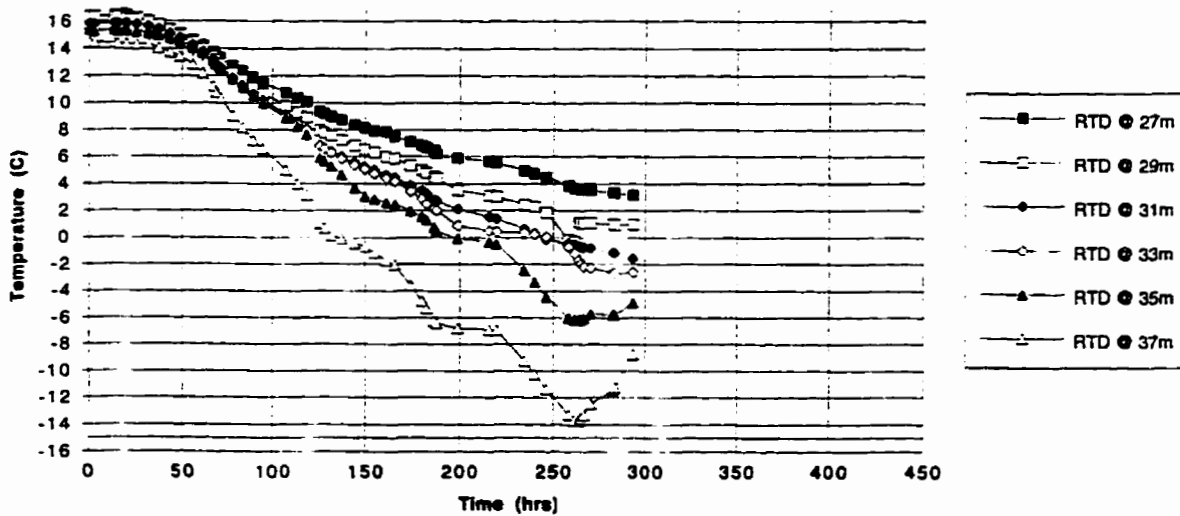


Figure 4-16: Ground Temperatures Measured During Ground Freezing at Borehole RTD1 through Target Zone.

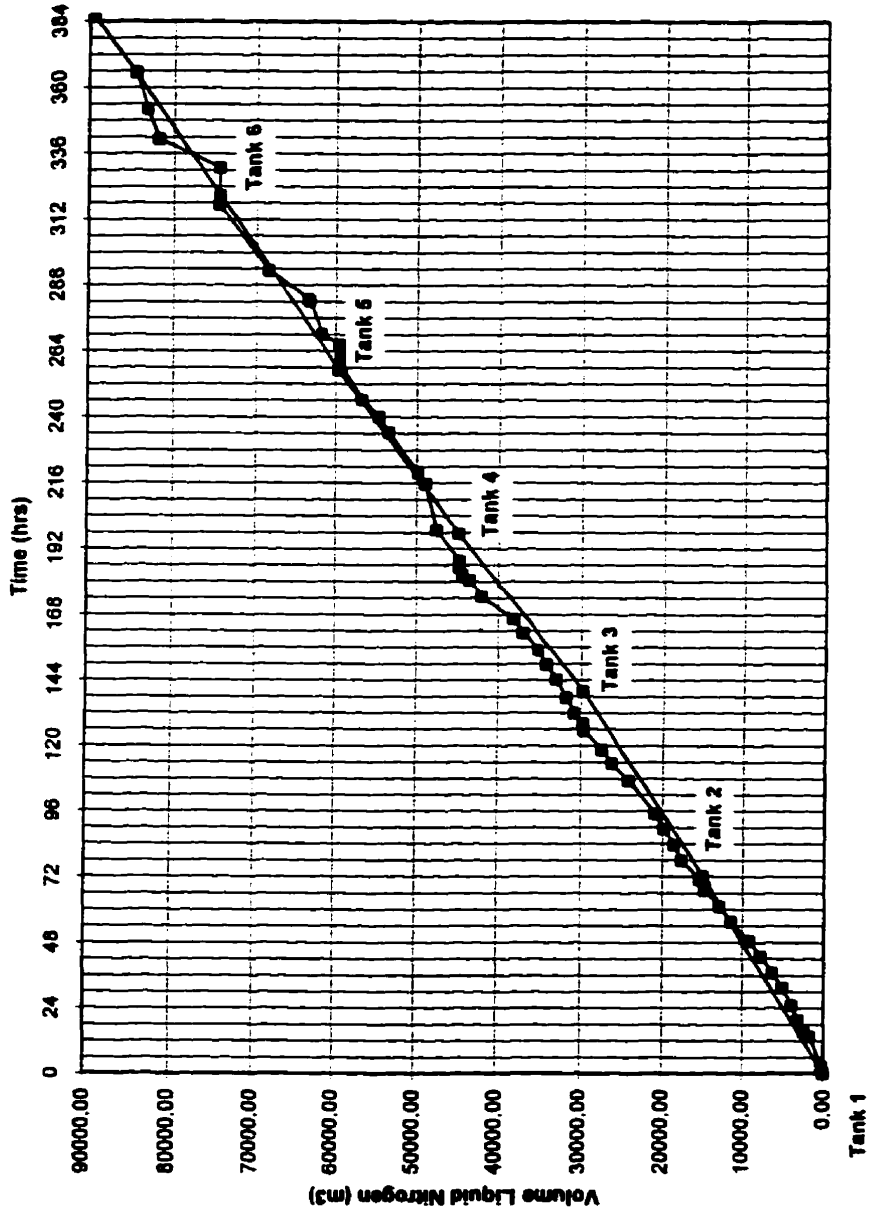


Figure 4-17: Actual Liquid Nitrogen Consumption during Ground Freezing at Phase I Test Site.

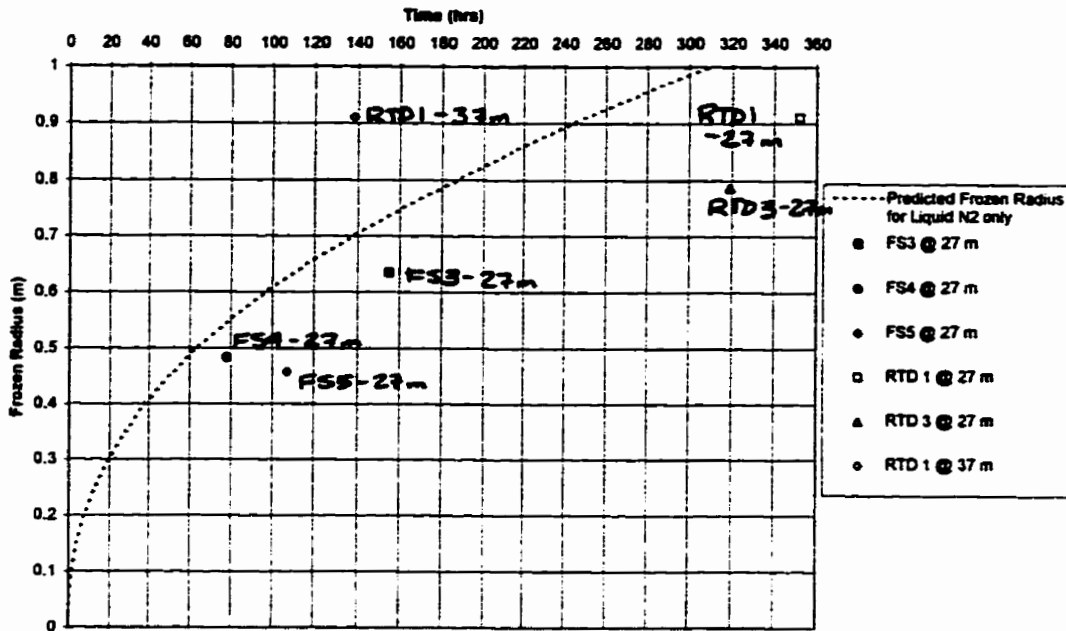


Figure 4-18: Comparison of Actual and Predicted Growth of the Frozen Radius assuming Freeze Pipe Reservoir Contained Liquid Nitrogen at all times.

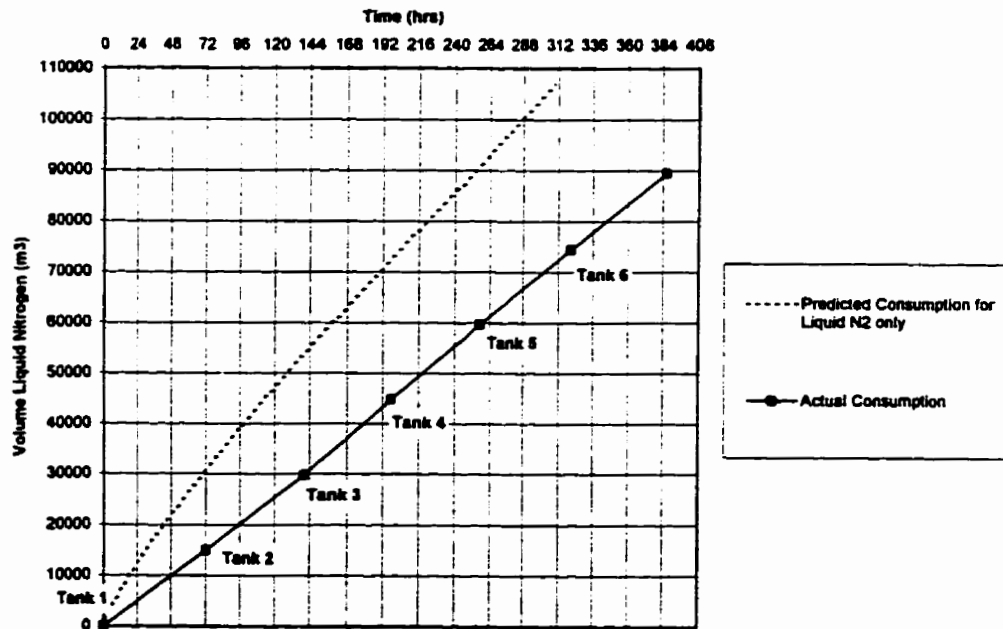


Figure 4-19: Comparison of Actual and Predicted Consumption of Liquid Nitrogen assuming Freeze Pipe Reservoir Contained Liquid Nitrogen at all times.

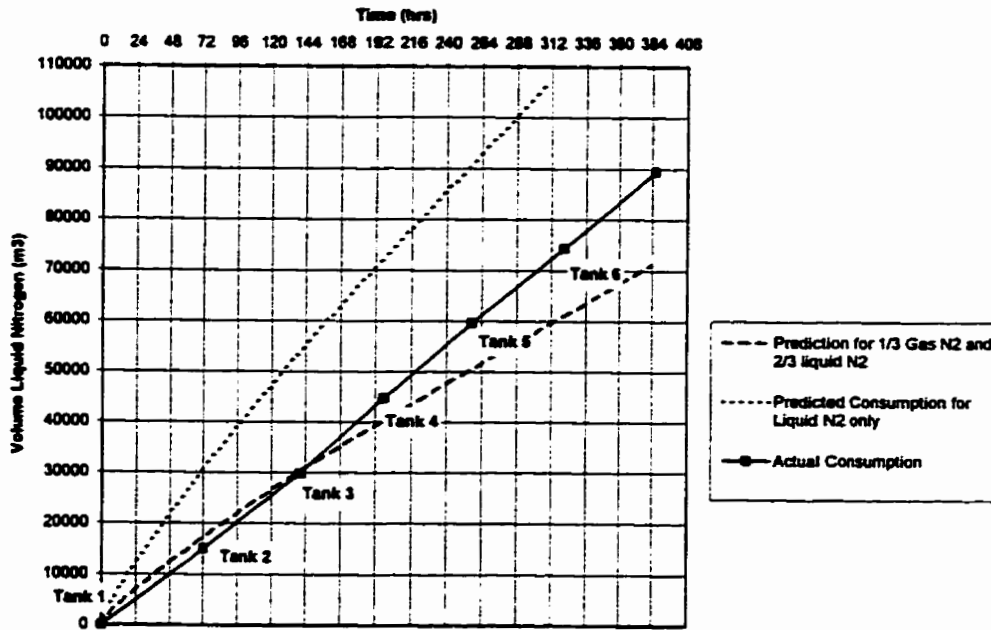


Figure 4-20: Comparison of Actual and Predicted Consumption of Liquid Nitrogen assuming Freeze Pipe Reservoir Contained 2/3 Liquid Nitrogen and 1/3 Gaseous Nitrogen.

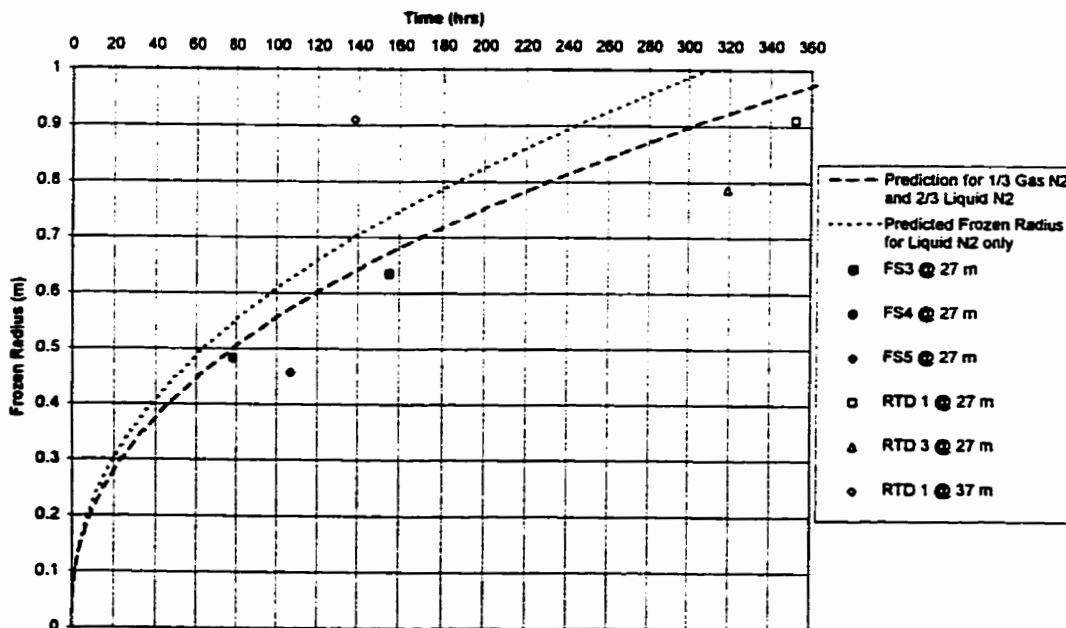


Figure 4-21: Comparison of Actual and Predicted Growth of Frozen Radius assuming Freeze Pipe Reservoir Contained 2/3 Liquid Nitrogen and 1/3 Gaseous Nitrogen.

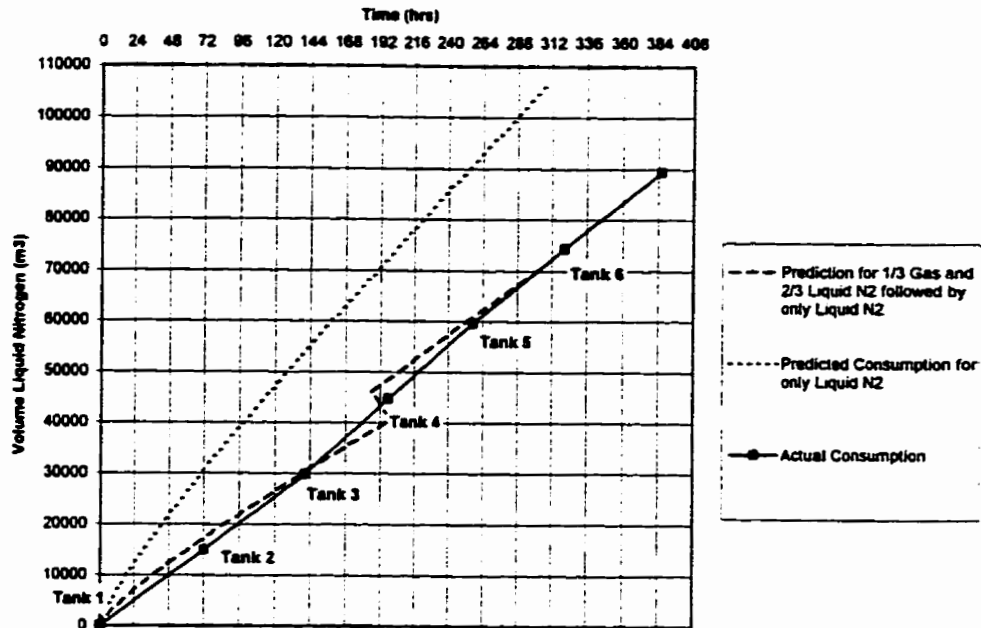


Figure 4-22: Comparison of Actual and Predicted Consumption of Liquid Nitrogen assuming Freeze Pipe Reservoir Contained 2/3 Liquid Nitrogen and 1/3 Gaseous Nitrogen followed by only Liquid Nitrogen after 192 hrs.

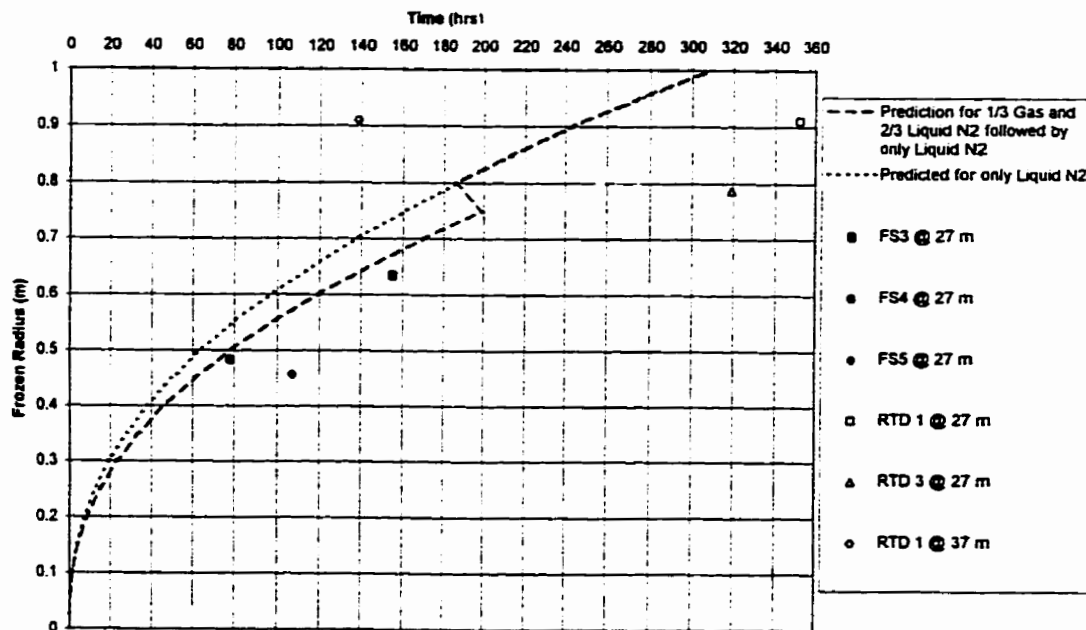


Figure 4-23: Comparison of Actual and Predicted Growth of Frozen Radius assuming Freeze Pipe Reservoir Contained 2/3 Liquid Nitrogen and 1/3 Gaseous Nitrogen followed by only Liquid Nitrogen after 192 hrs.

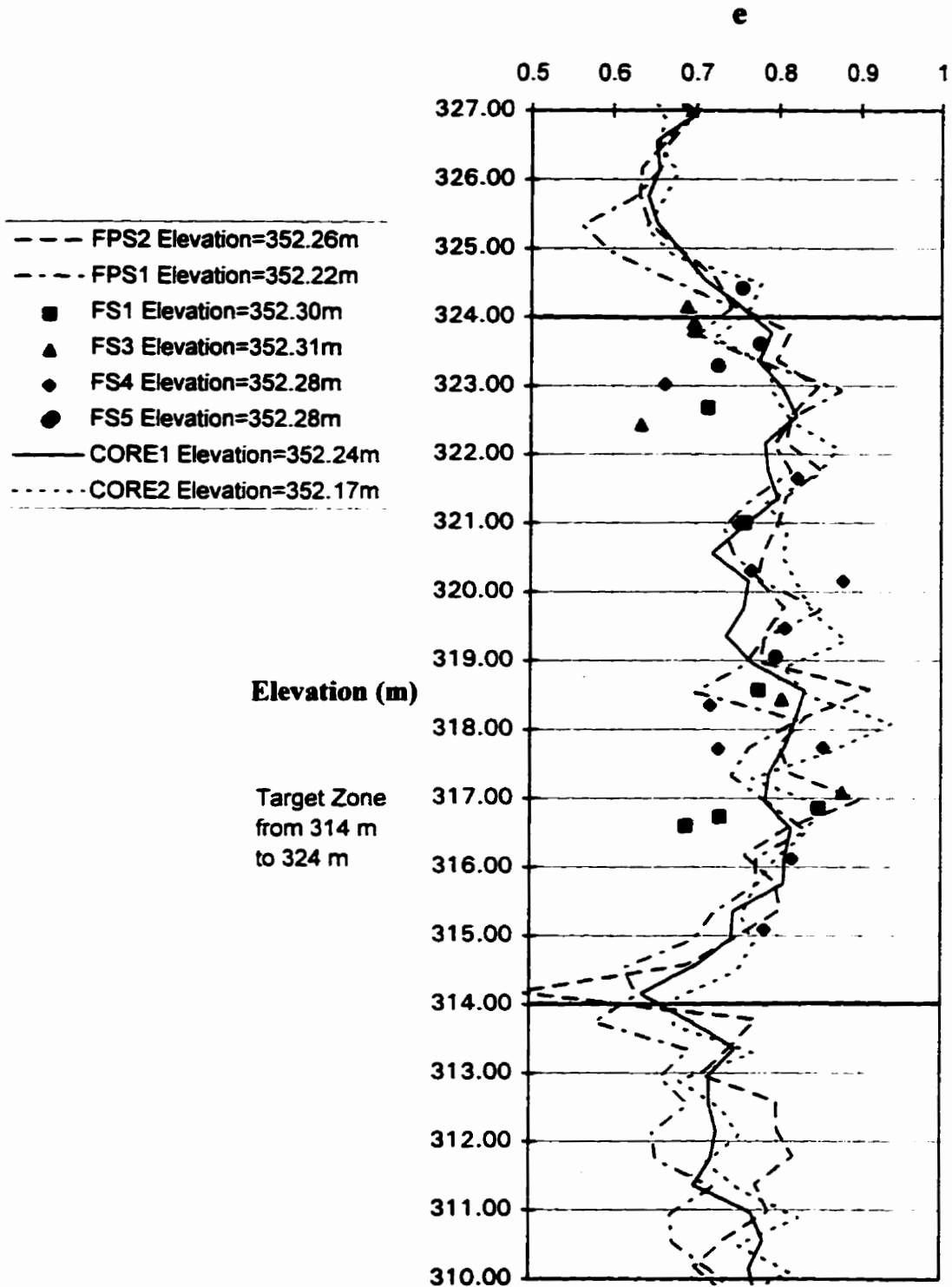


Figure 4-24: Comparison of In-Situ Void Ratios determined from Frozen Core Samples and from Geophysical Logging.

Chapter 5.0 Case History of Undisturbed Sampling at a Natural Deposit By In-Situ Ground Freezing

5.1 Introduction

Phase II of the Canadian Liquefaction Experiment (CANLEX) involved characterization of two loose natural sand deposits, in lower mainland British Columbia, with respect to the potential for static or dynamic liquefaction of the sand. During Phase II, in-situ ground freezing was conducted at each site to obtain high quality undisturbed samples of the sand deposits for determination of their in-situ void ratios and for laboratory testing to evaluate the steady state characteristics. The following Chapter describes the in-situ ground freezing and subsequent coring of the frozen sand undertaken at the Phase II test sites.

The ground freezing feasibility studies undertaken at each site to confirm that the sand deposits could be frozen without causing disturbance of the in-situ conditions are described. The methodology utilized to carry out ground freezing at each of the test sites is described. Data obtained during monitoring of the freezing process is presented and a comparison of the actual field data is made with the theoretical predictions for both the advance of the frozen zone and the consumption of liquid nitrogen. The equipment and procedures utilized for coring of the in-situ frozen sand deposits are described. The quality of the frozen core is discussed and the void ratios determined for the core are compared with the void ratios determined independently from geophysical logging.

5.2 Background

During Phase I of the CANLEX project, in-situ ground freezing was undertaken in a deep, relatively loose, hydraulically placed sand deposit, at the Mildred Lake Settling Basin in Fort McMurray, Alberta. Liquid nitrogen was used to freeze a 1 m radius column of sand between depths of 27 and 37 m below the ground surface. Upon completion of ground freezing, 20 m of high quality frozen core was recovered from the site. Visual examination of the core revealed no signs of disturbance due to frost heave during ground freezing. Moreover, the preliminary estimates of in-situ void ratios, determined from density measurements of frozen cubes removed from the ends of the core, showed good agreement with the void ratios measured from high quality geophysical logging undertaken within a 5 m radius of the frozen sand column.

Natural sand deposits tend to be less homogeneous than hydraulically placed sand and, as a result, characterization of natural deposits can be more challenging. Phase II, of the CANLEX project therefore carried out a detailed study of characterization techniques with respect to loose, native sand deposits. Due to the success of utilizing in-situ ground freezing for undisturbed sampling at the Phase I test site, this methodology was also used to obtain undisturbed samples from the Phase II test sites.

Selection of the most appropriate sites for the characterization of relatively loose sand deposits during Phase II of the CANLEX project was based on a site selection study carried out in lower mainland British Columbia under a separate activity (Stewart, 1993). This study indicated that the KIDD 2 Substation site, owned by BC Hydro, and the Massey Tunnel site (south portal), owned by the B.C. Ministry of Transportation and Highways, would be the most appropriate sites with respect to the characteristics of the sand deposits and the ability to undertake extensive field work. In-situ ground freezing and undisturbed sampling were carried out at the two test sites.

5.3 Scope of Work for In-Situ Ground Freezing and Sampling

The scope of work for the in-situ ground freezing and sampling included the following:

- Conduct feasibility studies to confirm that in-situ ground freezing could be carried out at each of the Phase II test sites without causing disturbance of the in-situ void ratio or the sand fabric.
- Evaluation of the dimensions of the column of sand that could be frozen within the budget and time constraints and confirm that sufficient frozen core could be obtained to meet the laboratory testing requirements.
- Design an efficient freezing system to freeze only the target zones at each of the test sites.
- Obtain undisturbed core samples of the in-situ frozen sand deposits at each of the test sites for determination of their in-situ void ratios and for laboratory testing.

5.4 Description of the Phase II Test Sites

5.4.1 Location

Figure 5-1 shows the location of the KIDD 2 and Massey Tunnel (South) test sites studied during Phase II. The KIDD 2 Substation is located in the northwest corner of the intersection of River Road and No. 4 Road, in Richmond, British Columbia. The south portal of the Massey Tunnel is located on Highway 99, just south of the Fraser River, in Delta, British Columbia. Figures 5-2 and 5-3 show more detailed site location plans for KIDD 2 and Massey Tunnel sites, respectively.

5.4.2 Target Zones

Delineation of the zones of interest within each sand deposit for characterization and sampling during Phase II of the CANLEX project was based on existing CPT data

available at each test site. Figure 5-4 shows typical CPT profiles available from the KIDD 2 and Massey Tunnel sites and the target zone selected at each test site. The 5 m target zones selected for characterization and sampling included the relatively loose zones between 12 and 17 m, at the KIDD 2 site, and between 8 and 13 m, at the Massey Tunnel site.

The geology of the Phase II test sites is described in detail by Monahan et al. (1995). According to Monahan et al. (1995), the target zones at both sites were located within a 20 to 30 m thick complex of distributary channel sands of the modern Fraser River delta. The sands located in the target zone at the KIDD 2 site, were deposited in channels that crossed the delta floodplain approximately 4430 ¹⁴C years ago and the sands at the Massey Tunnel site, were deposited by downstream migration of the Deas Island in historical times, about 10,000 years ago. At both sites, the distributary channel sands are underlain by silt and sand that appears to have been deposited on the delta slope.

5.5 Ground Freezing Feasibility Studies

Prior to undertaking in-situ ground freezing to obtain undisturbed samples of loose sand, it was necessary to confirm that this method of undisturbed sampling was appropriate, with respect to the subsoil and groundwater conditions that existed at the Phase II test sites. Several factors were considered. These included: the frost heave susceptibility of the soil related to the grain size distribution, fines mineralogy, and overburden stresses, as well as the groundwater temperature, salinity and flow conditions.

The feasibility study also included determining the heat extraction requirements to freeze a 1 m radius, by 5 m long, column of sand at each test site. This required that detailed information regarding the subsoil and groundwater be obtained. The parameters taken into consideration which affected the amount of liquid nitrogen required to freeze the soils included the moisture content and density, the frozen and unfrozen thermal

conductivities, the frozen and unfrozen heat capacities, the latent heat of the soil matrix, and the groundwater temperature, salinity and flow conditions. The pertinent aspects of the subsoil and groundwater conditions that existed at the Phase II test sites are described in further detail in the following sections.

5.5.1 KIDD 2 Site

The ground freezing feasibility study carried out for the KIDD 2 site was based on analysis of Split Spoon samples of sand obtained during Standard Penetration Testing from within the target zone and on available information regarding the groundwater conditions.

5.5.1.1 Frost Heave Susceptibility

To evaluate the frost heave susceptibility of the sand deposit within the target zone at the KIDD 2 site, grain size analyses and a mineralogical evaluation of the fines fraction were carried out on disturbed samples. Figure 5-5 shows the grain size distribution of five Split Spoon samples obtained between 7.8 m and 18.5 m below the ground surface. The average fines content of the sand samples obtained from the target zone at the KIDD 2 site was approximately 6.8 %.

A mineralogical analysis of the fines was also conducted. The mineralogy of the silt sized particles (2 to 74 μm) and clay sized particles (< 2 μm) is shown in Table 5-1. The clay sized particles comprised approximately 20% Smectite, 15% Chlorite, 25% Mica, 10% kaolinite and 30% Quartz and the silt sized particles comprised approximately 70% quartz, 15% feldspar, 5% chlorite and Smectite, 5% Mica and 5% kaolinite. The mineralogical results, in conjunction with the criteria for frost heave susceptibility

established by Davila et al. (1992), were used to evaluate the potential for disturbance of the sand deposit due to frost heave. Figure 5-6 shows that the criteria proposed by Davila et al. (1992) predicted a negligible risk of frost heave at the KIDD 2 test site

The criteria established by Davila et al. (1992) were based on freezing tests carried out on sand samples with various amounts and types of fines added to the sand. The freezing tests conducted by Davila et al. evaluated the potential for disturbance of the soil due to either ice lens formation, where pore water is attracted to the freezing front in the presence of clay minerals (see Chapter 2), or due to pore water freezing in place, without expulsion of 9 % of the pore water volume prior to freezing.

Provided that the conditions that exist in the field are similar to the laboratory test conditions used by Davila et al. (1992), the test results can be used to evaluate whether or not disturbance due to frost heave will occur during in-situ freezing. The samples tested by Davila et al. (1992) were frozen under an overburden stress of 24 kPa, which is approximately equal to effective stress acting on a soil element at 1.4 m below the ground surface, with the groundwater table located at 1.0 m. The minimum overburden stresses at the tops of the target zones at the KIDD 2 and Massey Tunnel sites were approximately 130 kPa and 91 kPa, respectively, and as stated in Chapter 2, the tendency to undergo disturbance due to frost heave reduces as the overburden stress increases. The temperature gradient of 0.4 °C/cm used during the tests was equivalent to that which exists in the ground (0.4 to 0.6 °C/cm), at the distance of approximately 0.4 to 0.6 m from the freeze pipe where sampling of the in-situ frozen sand would be undertaken. Therefore, since the conditions under which Davila et al.'s criteria was established are similar to those induced during ground freezing, the evaluation of frost heave susceptibility utilizing this method was considered reasonable for the Phase II test sites.

5.5.1.2 Site Conditions

The subsurface stratigraphy at the KIDD 2 site comprised a surficial cover of organic silt and clayey silt to a depth of approximately 4 m, overlying a loose to medium dense, clean sand which extended to a depth of about 22 m. Under the regional design earthquake loading, the loose to medium dense sand is generally considered to be susceptible to cyclic liquefaction.

As shown in Figure 5-1, the KIDD 2 site was located approximately 200 m south of the north arm of the Fraser River. The average groundwater level measured at the KIDD 2 site was approximately 1.5 m below the ground surface. However, due to the close proximity of the Fraser River, immediately upstream of the Strait of Georgia, it was assumed that the groundwater table at the KIDD 2 site would be subject to the influence of tidal fluctuations within the river. According to locally available information, tidal fluctuations at the mouth of the Fraser River, during the months of May to July, average approximately 0.6 m/hr. This results in a change in the river level of 4.8 m per 8-hour tidal period.

To evaluate the effect of fluctuations in the groundwater table at the site with respect to ground freezing, it was necessary to estimate the associated groundwater flow velocities. Since the sand was relatively clean in the target zone at the KIDD 2 site, the Hazen formula (1911) was used to calculate an upper estimate of the permeability. Using a permeability of 1×10^{-2} cm/s, the groundwater flow velocity, resulting from the rise and fall of the river level during each tidal period, was estimated to be in the order of 0.2 to 0.4 m/day.

In Chapter 4, the results obtained by Hashemi and Sliepcevich (1973) from numerical modeling of the effect of groundwater flows on the shape of the frozen column was reviewed. Their analysis, based on assuming a freeze pipe coolant temperature of -35 °C, indicated that in the presence of a groundwater flow velocity of $0.4 \text{ m}^3/\text{d m}^2$, the frozen

zone tended to become elongated in the downstream direction and foreshortened in the upstream direction; however, the total volume of frozen soil around the freeze pipe was not reduced significantly from the total volume frozen under static groundwater conditions. Since the direction of groundwater flow between the river and the test site would be reversed every 8 hours, it was not expected that the frozen column would be elongated in any one direction. Moreover, it was shown in Chapter 2 that if liquid nitrogen, at a temperature of $-196\text{ }^{\circ}\text{C}$, is used as the coolant rather than brine, at a temperature of $-35\text{ }^{\circ}\text{C}$, the effects of groundwater flow on the growth of the frozen column are significantly reduced. Therefore, it was concluded that the groundwater flows expected at the KIDD 2 site would not inhibit the ground freezing process significantly.

It was expected that the groundwater at the KIDD 2 test site would be saline due to the close proximity of the Pacific Ocean. Sea water freezes at a temperature of approximately $-1.8\text{ }^{\circ}\text{C}$ (Andersland, et al., 1991). However, as noted in Chapter 2, the freezing point depression caused by saline pore water is negligible with respect to the heat extraction capability of liquid nitrogen as it changes phase.

Based on information available from previous drilling investigations carried out at the KIDD 2 site for BC Hydro, the average groundwater temperature was assumed to be $8.5\text{ }^{\circ}\text{C}$. This value was used for preliminary thermal calculations prior to carrying out ground freezing, to estimate the freezing time and liquid nitrogen volume that would be required at the KIDD 2 site.

5.5.2 Massey Tunnel Site

The ground freezing feasibility study carried out for the Massey Tunnel site was based on analysis of sand samples obtained by vibratory coring within the target zone and on available information from previous drilling investigations regarding the groundwater conditions.

5.5.2.1 Frost Heave Susceptibility

To evaluate the frost heave susceptibility of the sand deposit within the target zone at the Massey Tunnel site, grain size analyses and a mineralogical evaluation of the fines fraction were carried out on disturbed samples. Figure 5-5 shows the grain size distribution of five Split Spoon samples obtained between 3.7 m and 14.4 m below the ground surface. The average fines content of the sand samples obtained from the target zone was approximately 3.0 %.

A mineralogical analysis of the fines fraction within the sand samples was also conducted. The mineralogy of the silt sized and clay sized particles is shown in Table 5-2. The clay sized particles comprised approximately 15% Smectite, 15% Chlorite, 30% Mica, 15% kaolinite, 20% Quartz, and 5% Feldspar and the silt sized particles comprised approximately 65% Quartz, 20% Feldspar, 5% Chlorite and Smectite, 5% Mica and 5% Kaolinite.

Of the clay minerals which comprised the clay size fraction of the sand, Smectite and Mica have a relatively high specific surface area. Although these minerals account for 45% of the clay size fraction, they represent about only 0.2% of the sand deposit. Only 10% of the silt size fraction was comprised of clay minerals, such as Smectite and Mica, with a relatively high specific surface area. The percentage of silt sized clay minerals represents only about 0.03 % of the sand deposit.

The mineralogical information was used in conjunction with Davila et al.'s (1992) criteria to estimate the frost heave susceptibility of the sand deposit. Figure 5-6 (after Davila et al., 1992) indicates a negligible risk of frost heave during freezing at the Massey Tunnel site.

5.5.2.2 Site Conditions

Preliminary information, obtained from Cone Penetration Testing, regarding the subsurface stratigraphy at the Massey Tunnel site, indicated a clean sand deposit between approximately 6 and 22 m below the ground surface. The sand deposit was relatively loose between 6 and 15 m, then became compact to dense with increasing depth. The sand between 6 and 15 m, at the Massey Tunnel site, was considered to be susceptible to liquefaction under dynamic loading.

The average groundwater level measured at the Massey Tunnel site was approximately 1.5 m below the ground surface. The site was located approximately 200 m south of the main channel of the Fraser River, and therefore, the groundwater table was also affected by tidal fluctuations. The groundwater flow velocity resulting from tidal fluctuations adjacent to the Massey Tunnel site was expected to be similar to that calculated at the KIDD 2 site to be approximately 0.2 to 0.4 m/day. Therefore, since liquid nitrogen would be used as the coolant for in-situ ground freezing, the effect of groundwater flow on the growth of the frozen radius was not expected to be significant.

Information regarding the average groundwater temperature was not available for the Massey Tunnel site. Hence, it was assumed that the initial groundwater temperature would be similar to that measured previously at the KIDD 2 site and an average groundwater temperature of 8.5 °C was used for the initial theoretical predictions. As stated for the KIDD 2 site, it was assumed that the groundwater salinity could be ignored, since the associated small freezing point depression, compared to the heat extraction capability of the liquid nitrogen, would have a negligible influence on the growth of the frozen zone.

5.6 Prediction of the Ground Freezing Process

5.6.1 Growth of the Frozen Radius

A 1 m radial column of sand was seen as the smallest practical frozen radius that would allow for sufficient room to sample the in-situ frozen sand deposits. Based on the thermal heat flow equations developed by Sanger and Sayles (1979), a prediction was made regarding the amount of energy that would have to be extracted from the ground and the time required to freeze a 1 m radius, by 5 m long, column of sand. Preliminary information regarding the moisture content and dry density of the sand deposits and the groundwater temperature were obtained from previous investigations and utilized as input parameters for the predictions. Table 5-3 lists these input parameters.

One prediction was carried out for both sites since the ground conditions were similar, assuming an average groundwater temperature of 8.5 °C and an average moisture content of 27.5 %. It was assumed that liquid nitrogen would be contained within the freeze pipe reservoir in the target zone at all times during freezing and groundwater flow was neglected. Figure 5-7 shows the predicted growth of the frozen radius versus time for the KIDD 2 and Massey Tunnel sites. Based on the prediction, it was estimated that approximately 10 to 12 days would be required to freeze a 1 m radius column of sand at each of the sites.

5.6.2 Consumption of Liquid Nitrogen

The equations developed by Sanger and Sayles (1979) were also used to predict the volume of liquid nitrogen that would be required to freeze a 1 m radius column at each of the test sites. Figure 5-8 shows that the predicted total volume of liquid nitrogen required to freeze a 5 m long target zone at each of the test sites was approximately 42,000 m³ (equivalent gaseous volume).

5.7 Ground Freezing and Sampling System

Two options were available for sampling of the in-situ frozen sand in the target zone. One option included freezing from the ground surface to the base of the target zone and then coring through the frozen overburden to the top of the target zone, below which samples could be taken. The second option involved freezing in the target zone only and installing cased boreholes from the ground surface to the top of the target zone. The bottom end of the casing could then be sealed by bentonite and frozen into the top of the target zone such that sampling could be carried out through dry, cased boreholes, as was done at the Phase I test site. At both the KIDD 2 and Massey Tunnel test sites, cost analyses carried out during the feasibility study indicated that it would be more economical to advance cased boreholes to the top of the target zone for sampling of the in-situ frozen core.

Based on the feasibility studies, the ground freezing system was designed to allow for radial freezing, utilizing liquid nitrogen as the refrigerant, in the target zones only. The freeze pipes were assembled to create reservoirs for the liquid nitrogen, of 5 m in length, in the target zones at each of the test sites. Steel freeze pipes were utilized with a diameter of 50 mm, as was used during Phase I of the CANLEX ground freezing program. Copper pipe, with a diameter of 13 mm, was used to feed the liquid nitrogen to the bottom of the reservoir, within the freeze pipe, and to exhaust the gaseous nitrogen from the top of the reservoir.

5.8 Phase II Fieldwork

The Phase II ground freezing and sampling work was carried out between July 4 and July 26, 1994. The work was scheduled such that coring of the in-situ frozen sand could be carried out at one site while ground freezing was being undertaken at the other site. This reduced the costs associated with drill rig support.

5.8.1 Borehole Layout

At both the KIDD 2 and Massey Tunnel sites, freeze pipes were installed in the centre of the test sites and boreholes for later sampling of the in-situ frozen sand were advanced within a 1 m radius around the freeze pipe. Other in-situ testing and sampling activities were carried out at a 5 m radius around the central freeze pipes at each site, as shown in Figures 5-9 and 5-10. The other testing included: Seismic Cone Penetration Testing (SCPT), Standard Penetration Testing with energy measurements (SPT/E), Geophysical Logging (GEO), Self-Boring Pressuremeter Testing (SBPMT), Large Diameter sampling (LDS), Vibrocore sampling (VIBRO) and Fixed Piston Sampling (FPS), carried out by others. This allowed for comparison of various characterization techniques, as described by Fear and Robertson, (1996). In the following sections of this report, the installation of the freezing and sampling systems are described.

5.8.2 Boreholes Advanced for Installation of the Freeze Pipe and Later Sampling

The freezing system and sample boreholes were installed at the Massey Tunnel site first, between July 4 and 6, 1994. A Longyear 38, wet rotary drill rig, supplied by the BC Ministry of Transportation and Highways, was utilized with a tricone drilling bit and bentonite drilling fluid. One 228 mm diameter borehole was advanced in the centre of the test site, to the top of the target zone, for later installation of the freeze pipe and four 228 mm diameter boreholes were advanced to the top of the target zone at a radial distance of about 0.6 m from the central borehole for later sampling of the in-situ frozen sand. As each borehole was advanced to the desired depth, 219 mm diameter PVC casing was installed. The cased boreholes extended to an average depth of 7.6 m below the ground surface. When all of the boreholes at the Massey Tunnel site had been advanced and cased to just above the top of the target zone, the bentonite drilling fluid was replaced with water and the bottom of the boreholes were sealed with bentonite. The water was later blown out of the cased boreholes.

At the KIDD 2 site, the freezing system and sample boreholes were advanced between July 7 and 9, 1994. A truck mounted Failing C.F. 1500 Special, wet rotary drill rig, supplied by Elgin Exploration Ltd., was utilized with biodegradable Kim mud as the drilling fluid. One borehole was advanced in the centre of the test site for later installation of the freeze pipe and five boreholes were advanced at a radial distance of about 0.6 m from the central borehole for sampling. The boreholes were advanced by first drilling a 130 mm pilot hole with a tricone bit and then using a 241 mm tricone bit to enlarge the borehole diameter. After each borehole was advanced to just above the target zone, 219 mm diameter PVC casing was installed to an average depth of 11.6 m. Once all of the sampling boreholes had been advanced, the drilling fluid in the cased holes was replaced with water. The bottom of each borehole was then sealed with bentonite and the water was blown out.

At each test site, two 75 mm diameter boreholes were advanced at radial distances of approximately 0.6 and 1.0 m from the freeze pipes for installation of Temperature Resistance Devices (RTDs). These small diameter boreholes were extended just below the bottom of the target zones and RTDs were installed at regular intervals to monitor the temperature profile with depth during ground freezing. RTDs were also installed at the bottom of each of the sampling boreholes to confirm that the sand deposit was frozen prior to commencing coring.

5.8.3 Installation of Freeze Pipes

At the Duncan Dam, Segó et al. (1994) successfully installed two freeze pipes for conducting in-situ ground freezing utilizing a self-jetting technique. The freeze pipes were jetted into place in a relatively loose sand deposit located between 12 and 21 m below the ground surface. Due to the similarity between the ground conditions

encountered at the Duncan Dam site and the Phase II test sites, this freeze pipe installation technique was also used at the KIDD 2 and Massey Tunnel sites.

At the centre of each of the Phase II test sites a 230 to 240 mm diameter borehole was advanced and cased to the top of the target zone. A 50 mm steel freeze pipe was then lowered down the cased borehole and jetted into the target zone by flushing water through a 25 mm diameter internal jetting pipe, with a perforated tip, set just inside the end of the 50 mm freeze pipe. As the freeze pipe was jetted into place, the sand cuttings were washed up the annulus between the jetting tool and the inside wall of the freeze pipe.

At the Massey Tunnel site the freeze pipe was jetted into place with little difficulty to a depth of about 13.5 m. To ensure that freezing of the ground would be complete at the bottom of the target zone, the freeze pipe was then pushed an additional 400 mm without the use of water. Once the freeze pipe was in place, the jetting tool was removed and a 0.45 m long bentonite seal was placed at the bottom end of the freeze pipe. The water inside the freeze pipe was then blown out and the copper feed and exhaust pipes were installed inside the freeze pipe with a rubber seal at approximately 7.5 m. This configuration created a reservoir for the liquid nitrogen along the full length of the target zone, between 7.5 m and 13.45 m. A back pressure valve was installed on the copper exhaust pipe to aid in regulation of the liquid nitrogen level in the reservoir during freezing.

At the KIDD 2 site the freeze pipe was installed in the same manner as described for the Massey Tunnel site. However, perhaps due to the higher overburden stresses and the slightly more dense subsoil conditions at the KIDD 2 site, some difficulty was encountered during installation of the freeze pipe. During the first attempt, it was not possible to jet the freeze pipe down to the bottom of the target zone at 17 m. A second attempt was made immediately beside the first freeze pipe and, by applying water pressures of up to approximately 200 kPa, it was possible to jet the freeze pipe down to a

depth of 17.85 m. Once the freeze pipe was in place, the jetting tool was removed. a 0.35 m long bentonite seal was placed at the bottom of the freeze pipe and the water inside the pipe was blown out. The rubber seal and copper tubing were installed inside the freeze pipe, forming a reservoir for the liquid nitrogen between 11 m and 17.5 m. A back pressure valve was installed on the copper exhaust pipe to aid in control of the liquid nitrogen levels within the freeze pipe.

After completion of the freeze pipe installations, RTDs were installed near the top and bottom of the liquid nitrogen reservoirs in each freeze pipe. This allowed for monitoring of liquid nitrogen levels inside the reservoirs at each test site during freezing.

5.8.4 Mapping of Borehole Alignment

To confirm that the bottom of each of the cased boreholes advanced for sampling fell inside a 1 m radius from the freeze pipes, the deflection of each of the borehole casings was mapped at the KIDD 2 and Massey Tunnel sites. The borehole casing alignment was checked by installing grooved ABS inclinometer casing in the centre of each 219 mm PVC casing, with plastic centralizers, and then utilizing a Digitilt Inclinometer to map the borehole deflections. Figures 5-11 and 5-12 show the layout of the freeze pipe, sampling boreholes and RTD boreholes at the test sites. The figures indicate the location of the sample borehole casings at the ground surface and at approximately the top of the target zones; the location of the freeze pipe at the ground surface and at the bottom of the target zone is also shown. The locations of the RTD boreholes at the ground surface and at the bottom of the target zones are also shown. The slope indicator data and plots of the measured borehole casing deflections are given in Appendix C.

At the Massey Tunnel site, all of the boreholes advanced were nearly vertical. The maximum deflection measured for the sampling borehole casings was that in borehole M94F2, where the casing deflected 32 mm south and 46 mm east. Figure 5-11 shows

that the freeze pipe deflected 130 mm west and 60 mm north between the ground surface and the bottom of the target zone. The boreholes advanced for the RTDs showed very little deflection.

At the KIDD 2 site greater borehole deflections were measured. Figure 5-12 shows that Borehole K94F7 deflected significantly, 415 mm in a northerly direction, and the freeze pipe deflected approximately 500 mm in a westerly direction. Figure 5-12 indicates that the horizontal distance between the edge of the freeze pipe Borehole K94F4 and the edge of the casing for Borehole K94F7, at the top of the target zone, was only approximately 150 mm. Yoshimi et al., 1978, showed that the disturbance caused by installation of a freeze pipe in loose sand, caused a zone of disturbance that extended a distance of about 2 times the freeze pipe diameter. Therefore, the zone of disturbance between Borehole K94F7 and the two 50 mm freeze pipes, installed adjacent to one another at the KIDD 2 site, likely extended 100 to 200 mm, depending upon the exact location of the two freeze pipes with respect to the sampling borehole. Since the location of the first freeze pipe at depth was unknown, it was not certain whether or not the frozen core samples recovered later from Borehole K94F7 would intersect the disturbed zone. Hence, it was noted that the frozen core obtained later from Borehole K94F7 may be disturbed.

Although the freeze pipe deflected significantly, all of the sampling boreholes fell within a 1 m radius of the freeze pipe, at the bottom of the target zone, except Borehole K94F3. The centre to centre, radial distance measured horizontally between Borehole K94F3, at the top of the target zone and the bottom of the freeze pipe was 1.0 m. This information reinforced the need to confirm that casing for Borehole K94F3 was frozen into the top of the target zone, based on RTD measurements, prior to commencing coring.

5.9 Ground Freezing at the Massey Tunnel Site

5.9.1 Initiation of Ground Freezing

Installation of the freeze pipe and the cased boreholes for sampling of the in-situ frozen sand at the Massey Tunnel site was completed on July 8, 1994. The copper liquid nitrogen feed pipe was then connected to a 15,000 m³ capacity (equivalent gaseous volume) liquid nitrogen truck, supplied by Canadian Liquid Air Ltd. and ground freezing at the Massey Tunnel site commenced on July 9, 1994.

5.9.2 Monitoring of Ground Temperatures During Freezing

Ground freezing at the Massey Tunnel Site was carried out on a 24 hour basis from 10:30 on July 9 to 8:20 on July 18, 1994, for a total of approximately 214 hours. During this time, the RTDs installed at the top of the target freeze zone in each of the sample boreholes and the those installed in the two small diameter boreholes at a radius of approximately 0.6 and 1.0 m from the freeze pipe, RTD1 and RTD2, respectively, were monitored. The temperature measurements taken during ground freezing at the Massey Tunnel site are summarized in Figures 5-13 and 5-14; the data is given in Appendix C. The RTDs indicated that the average initial groundwater temperature, prior to commencing ground freezing, was approximately 11.2 °C.

Figures 5-13 and 5-14 show that the rate of decrease in ground temperatures increased with depth and was greatest near the bottom of the target zone. This phenomenon likely resulted because, initially, the flow of liquid nitrogen was not sufficient to completely fill the reservoir in the target zone. When ground freezing commenced, the liquid nitrogen accumulated at the bottom of the reservoir, where it absorbed heat from the warm freeze pipe and surrounding subsoils, thereby immediately undergoing a phase change. Then, as the freezing system cooled, the level of the liquid nitrogen rose gradually to the top of the target zone.

Observations made during large scale ground freezing experiments conducted prior to Phase I of the CANLEX project (see Chapter 3), indicated that surging of the liquid nitrogen phase change interface occurs within the freeze pipe. This fact, along with insensitive flow regulators on the liquid nitrogen tankers used at the Phase II test sites, made it difficult to maintain the level of liquid nitrogen at the top of the target zone without wasting liquid nitrogen at the ground surface, although the back pressure valve on the copper exhaust pipe allowed for some control. As a result, regular monitoring and adjustment of the flow of liquid nitrogen was required during the freezing process. Since it was impractical to manually control the flow of liquid nitrogen on a 24 hour basis, the phase change interface occasionally dropped below the top of the reservoir in the freeze pipe. Therefore, gas nitrogen in the upper part of the reservoir, with a warmer temperature than that of liquid nitrogen, resulted in a slower rate of freezing at the top of the target zone.

Figure 5-14 shows that after approximately 214 hours of ground freezing, the frozen zone extended a radial distance of 1.0 m from the freeze pipe, between depths of approximately 8 m to 12.8 m.

5.9.3 Consumption of Liquid Nitrogen

The consumption of liquid nitrogen was monitored on a regular basis during ground freezing. This was necessary to determine the time at which another tank of liquid nitrogen would be required and to check for any indication that problems were developing. Figure 5-15 shows the volume of liquid nitrogen used during ground freezing at the Massey Tunnel site. The figure indicates that the rate of consumption of liquid nitrogen was approximately constant for the duration of the freezing program. A total of approximately 45,000 m³ (equivalent gaseous volume) of liquid nitrogen was used during freezing and sampling at the Massey Tunnel site.

The actual volume of liquid nitrogen used during ground freezing at the Massey Tunnel site was compared with the theoretical prediction, as shown in Figure 5-15. The prediction was based on assuming an initial groundwater temperature of 11.2 °C and that liquid nitrogen was contained within the freeze pipe reservoir in the target zone at all times during freezing. The figure indicates that the actual consumption rate was slightly higher than predicted. This was likely due to inefficiencies associated with controlling the flow rate of liquid nitrogen at two test sites simultaneously. On some occasions, when personnel were not on site to make adjustments, the flow of liquid nitrogen became too high, whereby some of the refrigerant was wasted at the ground surface.

5.9.4 Growth of the Frozen Radius

Based on the RTD measurements taken at the bottom of each of the sampling boreholes and in Boreholes RTD1 and RTD2, a comparison of the actual growth of the frozen radius was made with a theoretical prediction, assuming an initial groundwater temperature of 11.2 °C and that the freeze pipe reservoir in the target zone contained liquid nitrogen at all times during freezing. The time at which each RTD indicated a temperature of 0 °C was recorded and compared with the theoretical growth of the frozen zone. The comparison, shown in Figure 5-16, indicates that the average radius of the frozen sand, measured along the length of the target zone at the RTD locations, agreed reasonably well with the theoretical prediction.

As noted previously, the rate of growth of the frozen zone tends to be greater at the bottom of the target zone than at the top, due to the time required for liquid nitrogen to accumulate along the full height of the reservoir in the freeze pipe and due to persistent difficulties in maintaining the level of liquid nitrogen at the top of the target zone throughout the freezing process. This results in slower growth of the frozen radius near

the top of the target zone, as indicated by some of the RTDs installed at the bottom of the sample boreholes (top of the target zone) in Figure 5-16.

At the bottom of the target zone, the RTDs installed near the bottom of Boreholes RTD1 and RTD2 indicated that the growth of the frozen zone was greater than predicted. As noted previously (in Chapters 3 and 4), the theoretical predictions tend to be conservative in the region where liquid nitrogen is contained within the freeze pipe at all times. This discrepancy is likely due to the fact that the theoretical prediction of freezing time is based on assuming steady state conditions, while the actual time recorded corresponds to the first instance when a temperature of 0 °C is recorded at an RTD location. The predictions are also based on assuming that the thermal properties of the soil matrix do not vary with temperature.

As noted by Farouki (1986), the thermal conductivity of the frozen soil actually decreases as the temperature drops down to approximately -30 °C to -40 °C. However, at lower temperatures, the thermal conductivity of frozen sand starts to increase. It is also known that the thermal conductivity of both mineral grains and ice increase as the temperature drops. Therefore, perhaps at the very cold temperatures associated with liquid nitrogen, a marked increase in the thermal conductivity results in faster growth of the frozen radius that is not taken into account by the theoretical predictions. To confirm this, it would be necessary to measure the thermal conductivity of frozen sand samples at temperatures of -180 °C to -196 °C, however, special laboratory facilities and equipment would be needed to accommodate this temperature range.

5.10 Ground Freezing at the KIDD 2 Site

5.10.1 Initiation of Ground Freezing

Installation of the freeze pipe and the cased boreholes for sampling of the in-situ frozen sand was completed on July 11, 1994. The copper, liquid nitrogen feed pipe was then

connected to a 15,000 m³ capacity (equivalent gaseous volume) liquid nitrogen truck, supplied by Canadian Liquid Air Ltd. Ground freezing at the KIDD 2 site commenced on July 12, 1994.

5.10.2 Monitoring of Ground Temperatures During Freezing

Ground freezing at the KIDD 2 Site was carried out on a 24 hour basis from 18:00 hours on July 12 to 17:10 hours on July 21, 1994, for a total of approximately 220 hours. During this time, the RTDs installed at the top of the target freeze zone in each of the sample boreholes and the RTDs installed in the two small diameter boreholes at a radius of approximately 0.6 and 1.0 m from the freeze pipe, RTD1 and RTD2, respectively, were monitored. The temperature measurements taken during ground freezing at the KIDD 2 site are summarized in Figures 5-17 and 5-18; the data is given in Appendix C. The RTDs indicated that the average initial temperature at the KIDD 2 site, prior to commencing ground freezing, was approximately 9.6 °C.

As was the case at the Massey Tunnel site, Figures 5-17 and 5-18 show that the rate of decrease in ground temperatures increased with depth and was greatest near the bottom of the target zone. Figure 5-18 shows that after approximately 220 hours of ground freezing, the top of the frozen zone extended a radial distance of 1.0 m from the freeze pipe, between depths of approximately 12.19 m and 16.7 m.

5.10.3 Consumption of Liquid Nitrogen

The consumption of liquid nitrogen at the KIDD 2 site was monitored on a regular basis during ground freezing. Figure 5-19 shows the volume of liquid nitrogen used during ground freezing at the KIDD 2 site. The figure indicates that the rate of consumption of liquid nitrogen varied slightly for the duration of the freezing program. A total of

approximately 37,000 m³ (equivalent gaseous volume) of liquid nitrogen was used during freezing and sampling at the KIDD 2 site. The total volume of liquid nitrogen utilized at the KIDD 2 site was likely less than that used at the Massey Tunnel site due to the cooler initial groundwater temperature at the KIDD 2 site.

A comparison of the volume of liquid nitrogen used during ground freezing at the KIDD 2 site with the theoretical predictions is shown in Figure 5-19. The predictions were carried out assuming an initial groundwater temperature of 9.6 °C and that liquid nitrogen was contained within the freeze pipe reservoir in the target zone at all times during freezing. The figure indicates that the actual consumption rate agreed well with the predicted rate, since the average slopes of the two lines are nearly parallel. The total liquid nitrogen used was slightly less than the total predicted volume, based on assuming an average moisture content of 25 %. This discrepancy may have either been due to the fact that the freeze pipe was not full of liquid nitrogen during the initial stages of freezing, since heat absorption by the freezing system resulted in immediate phase change of the liquid nitrogen, or due to a lower moisture content existing in the ground than that assumed for the theoretical prediction.

The moisture content has a greater impact on the heat extraction requirements than the soil density, since less heat must be extracted to cool mineral grains than to cool pore water. Therefore, soils with high moisture contents require the removal of larger amounts of heat to initiate phase change in the pore water. The heat extraction requirements govern the total volume of liquid nitrogen required to freeze a column of soil at a specific site. Figure 5-19 shows that if an average moisture content of 20 % is assumed, the actual and predicted total volume of liquid nitrogen required to freeze a 1 m radius, by 5 m long, column of sand at the KIDD 2 site agree very well.

5.10.4 Growth of the Frozen Radius

Based on the RTD measurements taken at the bottom of each of the sampling boreholes and in Boreholes RTD1 and RTD2, a comparison of the actual growth of the frozen radius was made with the theoretical prediction, assuming that the reservoir in the target zone was full of liquid nitrogen at all times during freezing. The comparison is shown in Figure 5-20. The figure indicates that the average radius of the frozen sand in the target zone agreed reasonably well with the theoretical prediction. The RTDs installed at the bottom of the sample boreholes, on average, indicated slower growth of the frozen radius at the top of the target zone than the predicted growth. At the bottom of the target zone, the RTDs installed in Boreholes RTD1 and RTD2 indicated that the growth of the frozen zone was greater than predicted.

As noted previously, the discrepancy between the actual and predicted growth of the frozen radii is due to two factors. At the top of the freeze pipe reservoir, the level of liquid nitrogen is variable; therefore, the freezing process is slower than the ideal case where the freeze pipe is completely full of liquid nitrogen at all times. Near the bottom of the reservoir, the growth of the frozen radius is greater than the predicted rate due to the fact that the theoretical predictions are based on assuming that steady state conditions have been attained, while the actual time to freeze a given radius is taken at the instant an RTD indicates a temperature of 0 °C. As noted for the Massey Tunnel site, the use of a constant frozen thermal conductivity for the sand, rather than one that increases with decreasing temperature, may also result in under prediction of the rate of growth of the frozen zone.

5.11 Coring of In-situ Frozen Sand

Coring of the in-situ frozen sand was undertaken at the Massey Tunnel site first, commencing on July 18, 1994. Sampling at the Massey Tunnel site was completed by

July 20, 1994. Immediately following this, coring of the in-situ frozen sand was undertaken at the KIDD 2 site. Coring at the KIDD 2 site commenced on July 21 and was complete by July 24, 1994.

A 150 mm, outer diameter CRREL core barrel, shown in Photo 5-1, was utilized to core the frozen sand continuously in the target zones at the sample borehole locations. The core barrel easily advanced through the frozen sand using a dry coring technique with a tungsten carbide tipped cutting shoe. Core catchers were installed at the bottom of the CRREL barrel to prevent loss of the frozen core as the barrel was brought to the ground surface. To avoid problems associated with melted slough accumulating at the base of the boreholes, they were periodically cleaned out with a 260 mm tricone drill bit. Coring was undertaken during the daytime. During this time and overnight, a low volume flow of liquid nitrogen was maintained in the freeze pipe to preserve the cold ground temperatures.

Core runs of approximately 0.6 m in length were recovered and the frozen core was extruded directly into plastic bags at the ground surface utilizing a hydraulic ram, as shown in Photo 5-2. At the time of coring, the ambient air temperature was approximately 20 to 25 °C. Therefore, immediately after extrusion, the frozen core was placed in an insulated box filled with dry ice, as shown in Photo 5-3. The lengths and depths of the core samples were recorded; the samples were then stored in freezers between layers of insulation and dry ice, as shown in Photo 5-4. A total of 40 m of in-situ frozen core were recovered from 6 sample boreholes at the KIDD 2 site and from 4 sample boreholes at the Massey Tunnel site.

At the end of the fieldwork, the frozen core samples were transported to the University of Alberta (U of A) in freezers filled with dry ice. At the U of A the samples were carefully placed in a cold room for detailed logging and long-term storage.

5.12 In-situ Frozen Core Quality

The in-situ frozen core samples obtained from the Phase II test sites were relogged in the U of A cold room to prepare an inventory of the number and quality of the samples available for laboratory testing. To establish the core catalogues, the in-situ frozen core samples obtained from the KIDD 2 and Massey Tunnel site were examined as follows:

- the core samples were checked for signs of frost heave or other disturbance;
- the ends of each segment of core were trimmed for moisture content and void ratio determination;
- several core samples were photographed;
- the depths of all fractures within each core run were recorded and an estimate was made of the number of specimens that could be trimmed for either triaxial or direct simple shear testing.

No sign of frost heave was noted in any of the in-situ frozen core samples. The core catalogues established for the Massey Tunnel and KIDD 2 sites are provided in Appendix C.

Although no sign of frost heave disturbance was encountered, some of the samples contained thin veins of fine grained material. The veins appeared with highly random orientations across small distances of one core diameter. Photos 5-5 and 5-6 show a cross-section through Core Samples M94F6-C7A and M94F5-C2C recovered from the Massey Tunnel site, that exhibited these randomly orientated veins. These features were encountered in a total of five boreholes at various depths at the test sites, including Boreholes K94F3 and K94F2, at the KIDD 2 site, and Boreholes M94F5, M94F6 and M94F2, at the Massey Tunnel Site. The depths where core samples were encountered that exhibited distinct fine grained vein features are shown with respect to the freeze pipe location at each of the test sites in Figures 5-21 to 5-24.

An investigation was undertaken to determine whether or not these features were caused by the in-situ ground freezing activities. To confirm whether or not hydraulic fracturing could have occurred during installation of the freeze pipes, calculations of the pressure required to hydraulically fracture the ground were undertaken. Hydraulic fracturing requires that a condition of zero effective stress be induced, where the water pressure is equal to or greater than the minimum total stress. The initial fracture(s) then develop with an orientation that is perpendicular to the minimum principal stress (Guo et al., 1993). The minimum principal stress at the top of the target zone, equal to the total horizontal stress, was approximately 166 kPa, at the KIDD 2 site, and 65 kPa, at the Massey Tunnel site, assuming that the groundwater table was located at 1.5 m. Therefore, to develop a condition of zero effective stress, it would have been necessary to induce a minimum water pressure equal to the total horizontal stress as the freeze pipe was jetted into place.

At the KIDD 2 site, where some difficulty was encountered during installation of the freeze pipe, the maximum applied water pressure recorded was 200 kPa, which would have been sufficient to hydraulically fracture the ground. Unfortunately the water pressures applied during installation of the freeze pipe at the Massey Tunnel site were not recorded, although less resistance to jetting the freeze pipe into place was encountered at this site, thereby requiring less hydraulic pressure. Yet, given the lower overburden stress at the top of the target zone at the Massey tunnel site, it is possible that the ground was hydraulically fractured at this site as well.

To confirm whether or not the vein features were remnant of hydraulic fracturing, it was necessary to identify the nature of the vein material. If the ground had been hydraulically fractured during installation of the freeze pipes utilizing only water, drilling mud used to advance the cased boreholes above the target zone could have accumulated in the open fractures. To aid in identifying the nature of the vein material, elemental analyses were carried out, in conjunction with Scanning Electron Microscope (SEM) imaging, on frozen core samples obtained from both the KIDD 2 and Massey Tunnel sites. Analyses were

carried out on pieces of frozen core samples with a section cut through the core that intersected both the vein material and the frozen sand. Elemental analyses were also carried out on dry samples of the vein material extracted from the frozen core, as well as on the sand fraction, the fines fraction separated from the native sand and on samples of the drilling mud utilized at each of the test sites.

Photos 5-7 and 5-8 show SEM images of the vein features encountered in the frozen core samples from the KIDD 2 and Massey Tunnel sites, respectively. Photo 5-7 shows that the vein material encountered in one of the frozen cores at the KIDD 2 site was not in direct contact with the sand grains bounding the vein on either side. This suggests that the fines within the vein had undergone consolidation during freezing and therefore, that this feature must have existed at the time that the freezing front progressed across this location. Photo 5-8, showing one of the vein features encountered at the Massey Tunnel site, indicates that, in some cases, the boundary between the vein material and the frozen sand was less distinct than that shown in Photo 5-7.

SEM Photos 5-9 and 5-10 show that the vein material, extracted from core samples at each test site, comprised similar platy clay minerals. Comparison of the elemental analyses shown in Figures 5-26 and 5-27a to 5-27b, at the KIDD 2 site, and shown in Figures 5-29 and 5-30a to 5-30b, at the Massey Tunnel site, indicates that the elemental composition of the vein material and that of the native fines fraction extracted from the sand at each test sites were very similar. The analyses also indicated that the composition of KIM mud shown in Figure 5-31, used at the KIDD 2 site, and that of bentonite mud shown in Figure 5-32, used at the Massey Tunnel site, were significantly different from the constituent elements found in the native fines.

Given that the veins were comprised of native fines, rather than drilling mud, it remained to be determined whether or not ground freezing could have moved the native fines, originally interspersed within the sand matrix, to form discrete, randomly oriented veins. The SEM was used to study the migration of clay mineral particles within a sand sample

that had been subject to a freeze-thaw cycle. A reconstituted sand sample, containing 10 % fines, was formed using the slurry deposition method (Kuerbis and Vaid, 1988). This method of sample preparation causes less preferential particle alignment perpendicular to the long axis of a triaxial specimen, than the water pluviation method. In addition, slurry deposition also results in a reasonably saturated specimen, thereby avoiding further preferential alignment and clay particle migration that would be caused by back saturation of the soil.

Under drained conditions, a reconstituted sample was unidirectionally frozen from the bottom, upwards, thawed from the top, downwards and then refrozen from the bottom upwards. Freezing was accomplished by circulating liquid nitrogen through the base plate of the triaxial cell. After the second freezing cycle, small specimens were trimmed from the reconstituted sample with an exposed plane parallel or perpendicular to the freezing front. The specimens were then viewed under the SEM while frozen.

Photo 5-11 shows that the specimen trimmed with the exposed face parallel to the freezing front, exhibited only the edges of kaolinite particles. This photo indicates that the clay minerals were aligned with the thin edges perpendicular to the freezing front, but at various orientations across the plane. Photo 5-12 taken of a sample which had not undergone complete sublimation of the ice to allow for unobstructed viewing of the frozen soil structure, shows that the clay minerals were found with an alignment that coincided with ice grain boundaries. As shown in Photo 5-13, taken of a specimen trimmed with the exposed face perpendicular to the freezing front, most of the clay particles are aligned with the thin edge perpendicular to the freezing front (parallel to the face of the paper). However, as shown in the lower left corner of the photo, one clay particle was found with an alignment parallel to the freezing front, perhaps coinciding with an ice grain boundary.

Studies conducted by Corte (1962) on the migration of soil particles during freezing indicated the following conclusions:

- finer particles exhibit greater migration than coarse ones;
- fine particles migrate over a wide range of freezing rates;
- coarse particles migrate only under slow freezing rates;
- the greatest migration is exhibited by particles with the smallest weight per unit surface area;
- for a particle to migrate, a layer of water must be continuously present between the particle and the ice front;
- some particles do not change orientation during migration and some rotate.

Based on the information provided by Corte (1962), preferential migration of particles occurs in advance of a moving freezing plane and therefore, particles of various shapes and sizes would not likely be transported *en masse* to form discrete veins such as those encountered in some of the frozen core samples at the Phase II test sites. This suggests that the orientation of clay minerals evident in the SEM photographs of the reconstituted frozen samples may have been largely established during sample preparation and not an artifact of the freeze-thaw process.

The SEM test results presented here also suggest that movement or reorientation of clay minerals, due to freezing, takes place over relatively short distances, with alignment occurring both perpendicular and parallel to the freezing front, and some minor alignment coinciding with the ice grain boundaries. Therefore, given that in-situ ground freezing progresses unidirectionally, in a manner similar to the unidirectional freezing that the reconstituted specimens were subject to, it is unlikely that ground freezing could have caused mass movement of clay minerals, originally dispersed within the sand, to form discrete, randomly oriented veins.

An alternate source of the vein features found in the in-situ frozen core specimens was investigated. According to Naesgaard et al. (1992), Clague et al. (1992) and Luternauer et al. (1994), there is evidence of liquefaction features in the Fraser River delta that may have originated from prehistoric earthquakes. It may be that veins encountered in some of the frozen core recovered from the test sites in the Fraser River delta were features associated with prehistoric liquefaction events.

Clague et al. (1992) documented cases of intrusive sand dykes found at five test sites in the Fraser River delta and assert that these features were associated with liquefaction of relatively loose sands underlying the surface crust, that occurred during one or more earthquakes. The sites investigated by Clague et al. with evidence of sand dykes were located close to the Phase II test sites, as shown in Figure 5-33.

A typical cross-section through one of the sites, shown in Figure 5-33, is similar to the stratigraphy defined at the KIDD 2 test site as part of the CANLEX project, as shown in Figure 5-34. According to Clague et al. (1992), the sand dykes that intruded into the clayey silt of Unit 1, consisted of mainly sand that was similar in texture to Unit 2 (see Figure 5-33). However, in areas where the dykes feathered out, they consisted of silt and mud rather than sand. The contacts between the injected materials and Unit 1 were also found to be sharp everywhere.

Although some of the features described by Clague et al. (1992) appear to be similar to the fine grain veins encountered in the frozen core at the Phase II test sites, the depths at which these features were found differs. The sand dykes documented by Clague et al. (1992) intruded from loose sand deposits located between 5 and 15 m, into the surface crust layer between 2 and 5 m. This agrees with laboratory testing that has shown that sand dykes are most commonly produced by liquefaction of sandy deposits that are capped with a relatively impermeable layer, that hinders pore pressure dissipation. However, Figures 5-21 to 5-24 show that the fine grain vein features found in the frozen core samples were encountered between 8 and 17 m below the ground surface in

relatively loose sands. Therefore, unless the silty clay layer, shown between 20 and 23 m at the KIDD 2 site in Figure 5-34, could have been the source material for these veins, it cannot be concluded that the features encountered in the frozen core were artifacts of a prehistoric liquefaction event. Unfortunately, a sample of the silty clay layer was not recovered during the site work since this material was located several meters below the target zone.

To aid in determining if the vein features existed at the Phase II test sites prior to carrying out in-situ ground freezing, an additional Vibrocore sample was recovered from a borehole advanced adjacent to the zone where ground freezing had been undertaken. Unfortunately, similar vein features were not detected in the Vibrocore sample. However, given the limited thickness of these features, even if present, vibration associated with this method of sampling may have disturbed the ground sufficiently to render the features undetectable.

Although the source of the vein features encountered in the frozen core at the Phase II test sites remains to be unequivocally confirmed, some conclusions can be drawn. It is possible that hydraulic fracturing during installation of the freeze pipe occurred at the Massey Tunnel site and could possibly have occurred at the KIDD 2 site. Regardless of whether or not hydraulic fracturing was directly or indirectly responsible for the vein features, hydraulic fracturing causes disturbance of the subsoils. Therefore, installation of freeze pipes utilizing a self-jetting technique should be avoided unless it can be demonstrated that the overburden stresses are high enough to preclude hydraulic fracturing. Based on the SEM study, it can also be concluded that ground freezing was likely not responsible for mass movement of the native fines, resulting in the formation of discrete fine grain veins within the sand matrix.

5.13 Void Ratio Measurements

The frozen core samples were trimmed in the cold room at the University of Alberta for evaluation of the in-situ void ratio and to prepare specimens for laboratory testing. Estimates of the void ratios were made based on frozen cubes trimmed from one end of each frozen core, with dimensions of about 3 cm by 3 cm by 2 cm. To avoid assuming in advance that the frozen core specimens were fully saturated, the frozen total density and moisture content of the cubes were used to estimate the void ratios of the remaining core from which the chunks were trimmed. using the following equations:

$$(\rho_t)_f = M_f / V_t \quad [5-1]$$

$$\rho_d = (\rho_t)_f / (1 + \omega_{ice}) \quad [5-2]$$

$$e = G_s (\rho_w / \rho_d) - 1 \quad [5-3]$$

where: ρ_t is the total frozen density (g/cm^3); M_f is the frozen mass of the chunk (g); V_t is the frozen volume of the chunk determined by measurement of the physical dimensions (cm^3); ρ_d is the dry density (g/cm^3); ω_{ice} is the ice content; ρ_w is the density of water (g/cm^3), and G_s is the specific gravity of sand.

This method of estimating the in-situ void ratio of what would later become triaxial and direct simple shear specimens, was an approximation, due to the fact that the calculated densities depended on the measured physical volume of the frozen trimmed cubes, which was subject to some error, and the ice content of the cubes rather than that of the triaxial or direct simple shear specimens themselves. Initially, the frozen volumes of the cubes were also measured by submersion in kerosene at a temperature of less than 0°C . Comparison of these measurements with the physically measured volume showed good agreement, however, residual kerosene on the dried specimens gave incorrect values of the dry mass of the cubes. Therefore, physical volume measurements were used as a basis for future void ratio calculations. This information served as a guideline to determine which of the frozen core specimens trimmed for laboratory testing had the

highest void ratios. At the completion of laboratory testing, the total dry weight of the failed specimens and the volume change measurements taken during thawing and shearing could be used to back calculate the actual initial void ratios of the specimens.

5.14 Void Ratios Determined from Geophysical Logging

As an independent evaluation of the void ratio measured from the in-situ frozen core samples, trimmed for triaxial testing, these void ratios were compared with the void ratios estimated based on geophysical logging conducted in boreholes advanced within a 5 m radius of the in-situ frozen core samples. Figure 5-35 shows that the void ratios estimated from these two independent techniques agree to within a void ratio of approximately 0.03. The geophysical logging techniques utilized during the CANLEX project are described by Küpper et al. (1995).

5.15 Conclusions

Prior to undertaking in-situ ground freezing, it is important to conduct detailed feasibility studies to confirm that freezing with liquid nitrogen will not result in disturbance of the subsoils in the sampling zone. In appropriate subsoil conditions, in-situ ground freezing can be used successfully to obtain highly undisturbed samples of loose sand.

Examination of the in-situ frozen core obtained from the Phase II test sites, and from the Phase I test site (see Chapter 4), indicated that frost heave disturbance did not occur, as was predicted using Davila et al.'s (1992) criteria. Therefore, for the types of sands investigated by CANLEX, mineralogical evaluation of the fines content within a subsoil deposit can be utilized in conjunction with the criteria developed by Davila et al. (1992), to evaluate the potential for disturbance due to frost heave.

The theoretical equations presented by Sanger and Sayles (1978), can be used to predict the growth of the frozen radius and the volume of liquid nitrogen required to freeze a given volume of sand. Theoretical predictions undertaken for the Phase II test sites agreed well with the actual ground freezing process.

A CRREL core barrel is an effective means of obtaining undisturbed samples from in-situ frozen sand. A total of 40 m of undisturbed frozen sand core was recovered from the Phase II test sites utilizing a dry coring technique with a 150 mm, outer diameter CRREL core barrel.

Self-jetting techniques for installation of the freeze pipe should be avoided unless it can be demonstrated that hydraulic fracturing of the ground will not occur. At sites where undisturbed samples are required from relatively shallow depths, it is preferable to install the freeze pipe in a predrilled, small diameter borehole, as was carried out successfully at the Phase I test site.

The study conducted with a scanning electron microscope on reconstituted sand specimens subject to a freeze-thaw-freeze cycle, indicated that clay minerals may align either with the thin edge perpendicular or parallel to the freezing front. The study also suggested that clay minerals were not moved *en masse* to form discrete, fine grain veins within the sand matrix.

The void ratios estimated for the in-situ frozen core, based on the density of trimmed triaxial specimens, agreed well with the void ratios determined from geophysical logging. This indicates that in-situ ground freezing worked well as a means of obtaining undisturbed core samples of relatively loose sand at the Phase II test sites.

5.16 References

- Andersland, O., Berggren, A. L., Fish, A., Frémond, M., Gallavresi, F., Gonze, P., Harris, J., Jessberger, H. L., Jordon, P., Klein, J., Ladanui, B., Maisham, D., Ohrai, T., Rebhan, D., Ryokai, K., Segó, D. C., Shuster, J. A., Thimus, J. F., Changsheng, W., and Williams, P., 1991. Mechanical and Thermal Design of Frozen Soil Structures. Proceedings of the International Symposium on Ground Freezing, ISGF - Working Group 2, Beijing China, 11 p.
- Clague, J. J., Naesgaard, E. and Sy, A., 1992. Liquefaction Features of the Fraser River Delta: Evidence for Prehistoric Earthquakes? Canadian Journal of Earth Sciences, Vol. 29, p. 1734-1745.
- Corte, A. E., 1962. Vertical Migration of Particles in Front of a Moving Freezing Plane, Journal of Geophysical Research, Vol. 67, No. 3, pp. 1085-1090.
- Davila, R. S., Segó, D. C., and Robertson, P. K., 1992. Undisturbed Sampling of Sandy Soils by Freezing, 45th Canadian Geotechnical Conference, Toronto, October 26-28, 10 p.
- Farouki, O. T., 1986. Thermal Properties of Soils. Trans Tech Publications, Series on Rock and Soil Mechanics, Vol. 11, D-3392 Clausthal-Zellerfeld, Germany, 135 p.
- Fear, C. E. and Robertson, P. K., 1996. CANLEX: Phase II Data Review Report, University of Alberta, 550 pp.
- Guo, F., Morgenstern, N. R. and Scott, J. D., 1993. An Experimental Investigation into Hydraulic Fracture Propagation, Part 1. Experimental Facilities and Part 2. Single Well Tests, International Journal of Rock Mechanics and Mining Science, Vol. 30, pp. 177-188 and 189-202.
- Hashemi, H. T. and Sliepcevich, C. M., 1973. Effect of Seepage Stream on Artificial Soil Freezing, Proceedings, Ground Freezing Conference, Developments in Geotechnical Engineering, Vol. 28, pp. 189-201.
- Hazen, A., 1911. Discussion of "Dams on Sand Foundations" by A. C. Koenig. Transactions, ASCE Vol. 73, pp. 199-203.

- Konrad, J.-M. and Morgenstern, N. R., 1981. The Segregation Potential of a Freezing Soil, *Canadian Geotechnical Journal*, Vol. 18, pp. 482-491.
- Kuerbis, R. and Vaid, Y. P., 1988. Sand Sample Preparation - The Slurry Deposition Method. *Soils and Foundations*, Vol. 28, No. 4, p. 107-118.
- Küpper, A., Lawrence, M., Howie, J., and Plewes, H., 1995. The use of Geophysical Logging Techniques at the CANLEX Project. 48th Canadian Geotechnical Conference, Vancouver, B.C. pp. 81-88.
- Luternhauer, J. L., Barrie, J. V., Christian, J. J., Evoy, R. W., Hart, B. S., Hunter, J. A., Killeen, P. G., Kostaschuk, R. A., Mathewes, R. W., Monahan, P. A., Pullan, S. E., Roberts, M. C., Robertson, P. K., Tarbotton, M. R., and Woeller, D. J., 1994. Fraser River Delta: Geology, Geohazards and Human Impact. *Geological Hazards of the Vancouver Region, Southwestern British Columbia*, Geological Survey of Canada, Bulletin 481, p. 197-220.
- Monahan, P. A., Luternauer, J. L. and Barrie, J. V., 1995. The Geology of the CANLEX Phase II Sites in Delta and Richmond, British Columbia. 48th Canadian Geotechnical Conference, Vancouver, B.C., pp. 59-68.
- Naesgaard, E., Sy, A., and Clague, J. J., 1992. Liquefaction Sand Dykes at Kwantlen College, Richmond, B. C. *Geotechnique and Natural Hazards*, BiTech Publishers. Vancouver, B. C., p. 159-166.
- Sanger, F. J. and Sayles, F. H., 1978. Thermal and Rheological Computations for Artificially Frozen Ground Construction. *International Symposium on Ground Freezing*. March 8-10, Bochum. pp. 311-337 or *Engineering Geology*, 13: 311-337.
- Sego, D. C., Robertson, P. K., Sasitharan, S., Kilpatrick, B. L., and Pillai, V. S., 1994. Ground Freezing and Sampling of Foundations Soils at Duncan Dam, *Canadian Geotechnical Journal*, Vol. 31, pp. 939-950.
- Stewart, R. A., 1994. CANLEX Phase II - Site Selection Study, CANLEX Report, September, 1993.
- Yoshimi, Y., Hatanaka, M., and Oh-Oka, H., 1978, Undisturbed Sampling of Saturated Sands by Freezing, *Soils and Foundations*, Vol. 18, Sept., 59-73.

Table 5-1: Mineralogy of the Fine Fraction at the KIDD 2 Test Site (based on area of the major x-ray reflections in percentage).

Sample Number	Mineralogy < 2 μm
Sample #7	Sm(15), Ch(15), Mi(35), Kt(15), Qtz(20)
Sample #9	Sm(25), Ch(15), Mi(25), Kt(10), Qtz(25)
Sample #11	Sm(15), Ch(15), Mi(20), Kt(5), Qtz(45)
Sample #12	Sm(30), Ch(15), Mi(25), Kt(15), Qtz(15)
Sample #14	Sm(20), Ch(15), Mi(30), Kt(10), Qtz(25)
2 to 74 μm	
Sample #7	Qtz(75), Fd(10), Ch(+Sm)(5), Mi(5), Kt(5)
Sample #9	Qtz(70), Fd(15), Ch(+Sm)(5), Mi(5), Kt(5)
Sample #11	Qtz(70), Fd(15), Ch(+Sm)(5), Mi(5), Kt(5)
Sample #12	Qtz(70), Fd(15), Ch(+Sm)(5), Mi(5), Kt(5)
Sample #14	Qtz(70), Fd(15), Ch(+Sm)(5), Mi(5), Kt(5)

Sm: smectite
 Ch: chlorite
 Mi: mica
 Kt: kaolinite
 Qtz: quartz
 Fd: feldspar
 Ch(+Sm): chlorite-smectite intergrade

Table 5-2: Mineralogy of the Fine Fraction at the Massey Tunnel Test Site (based on area of the major x-ray reflections in percentage).

Sample Number	Mineralogy
	< 2 μm
Sample #4	Sm(10), Ch(15), Mi(30), Kt(15), Qtz(20), Fd(10)
Sample #5	Sm(15), Ch(20), Mi(30), Kt(15), Qtz(20), Fd(5)
Sample #6	Sm(15), Ch(10), Mi(30), Kt(15), Qtz(20), Fd(10)
	2 to 74 μm
Sample #4	Qtz(70), Fd(15), Ch(+Sm)(5), Mi(5), Kt(5)
Sample #5	Qtz(70), Fd(15), Ch(+Sm)(5), Mi(5), Kt(5)
Sample #6	Qtz(60), Fd(25), Ch(+Sm)(5), Mi(5), Kt(5)

Table 5-3: Input Parameters used for Prediction of the Freezing Process at the Phase II Test Sites

Test	Moisture	Dry	Ground	Heat Capacity		Conductivity	
Site	Content	Density	Temp.	C_u	C_f	K_u	K_f
	%	g/cm^3	$^{\circ}\text{C}$	$\text{MJ/m}^3\text{K}$	$\text{MJ/m}^3\text{K}$	W/MK	W/MK
KIDD 2	25	1.50	8.5	3.25	2.16	1.45	2.80
Massey	30	1.50	8.5	3.25	2.16	1.45	2.80

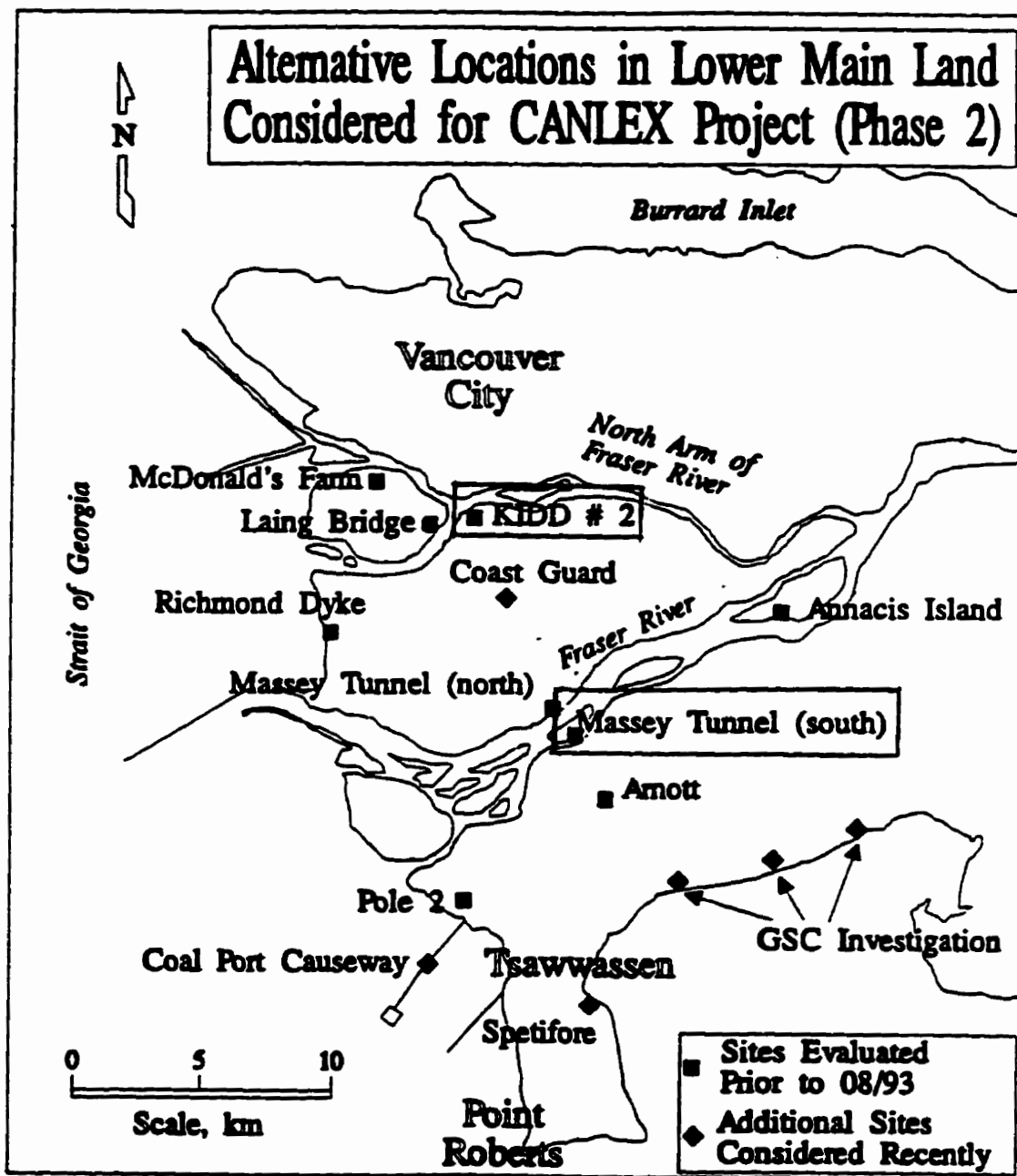


Figure 5-1: Phase II Site Location Plan

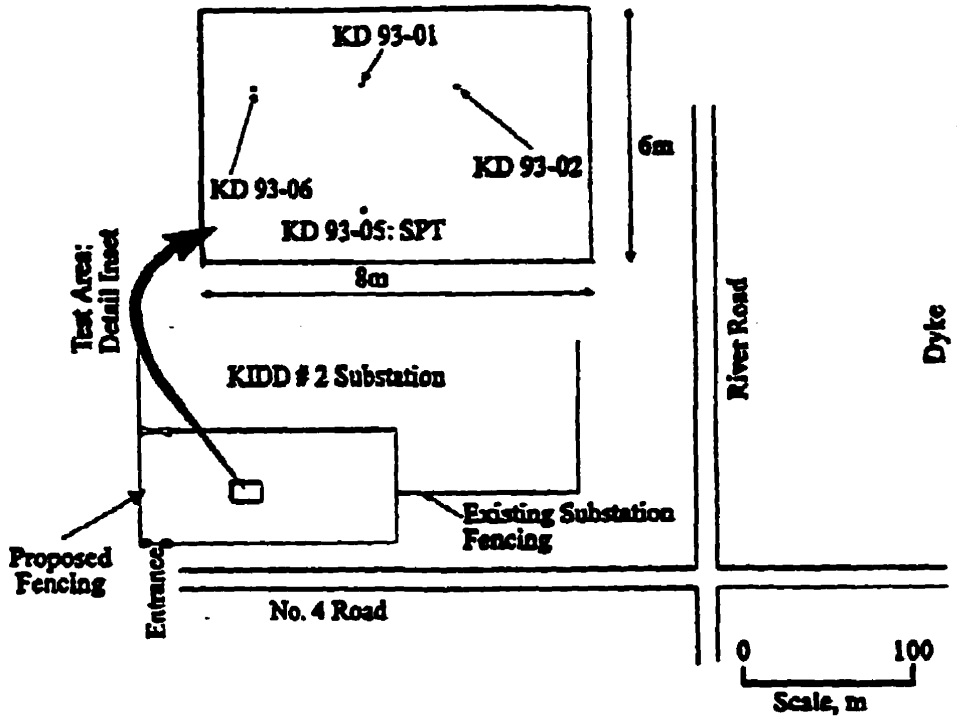


Figure 5-2: KIDD 2 Site Location Plan

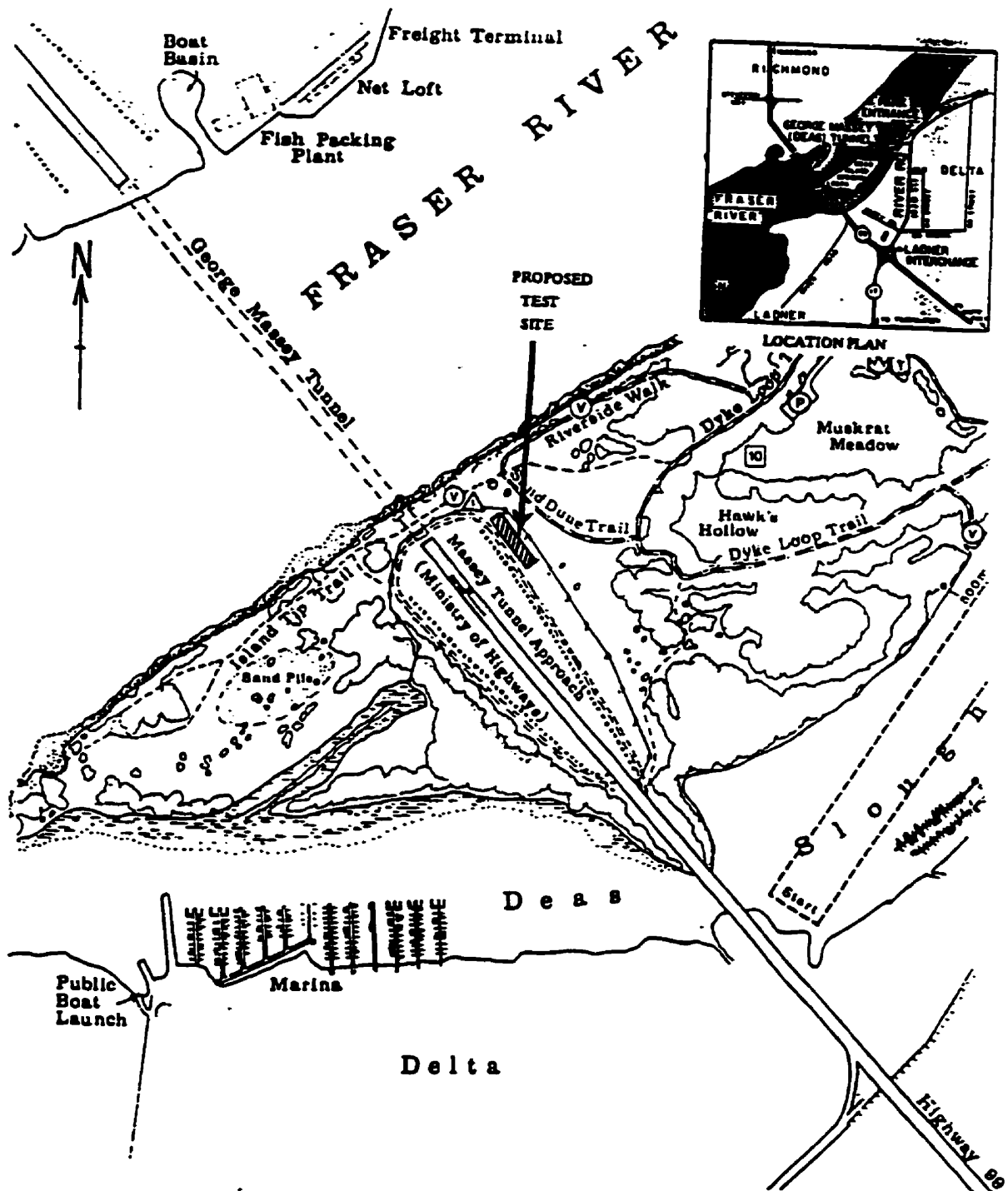


Figure 5-3: Massey Tunnel Site Location Plan

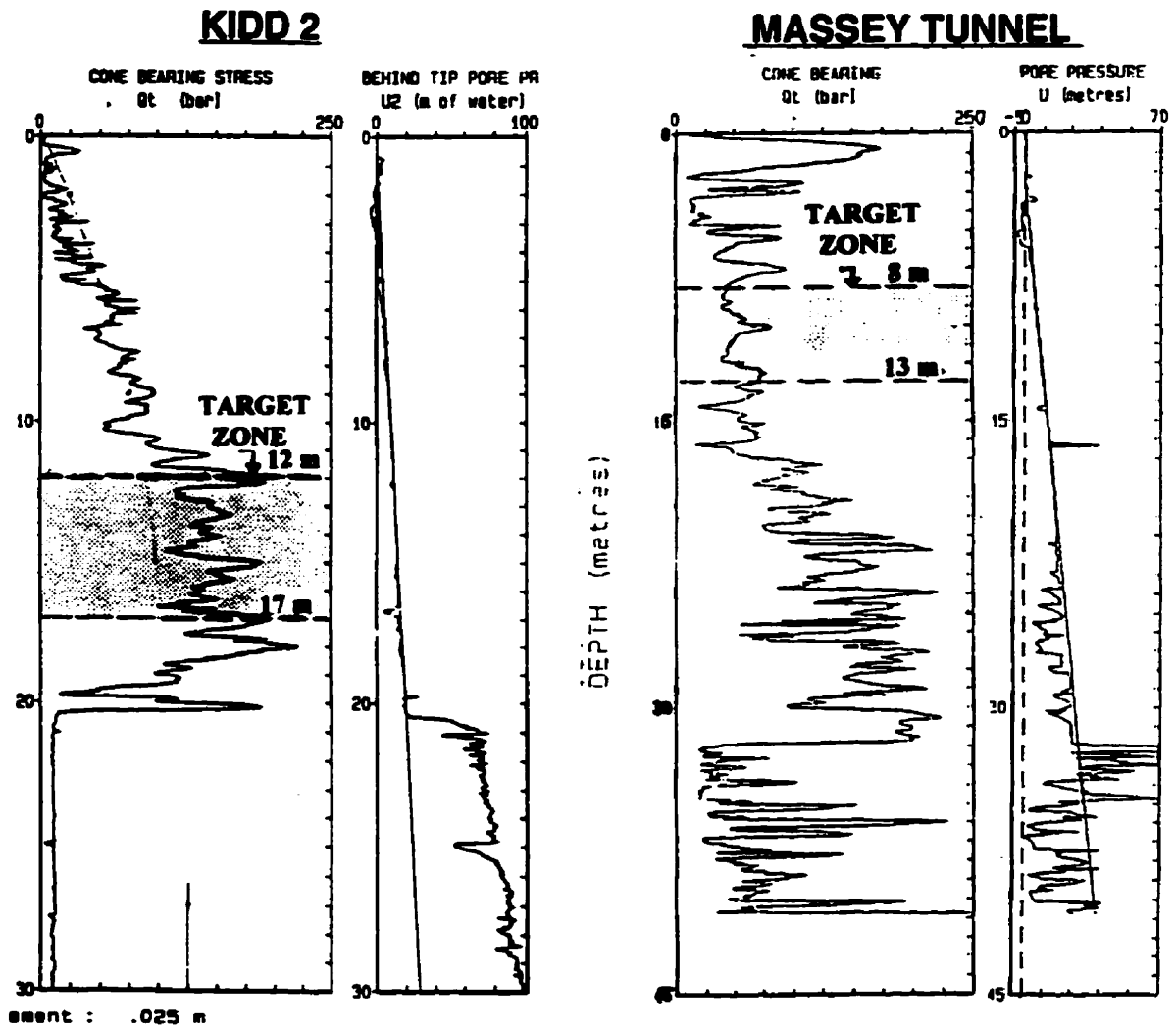
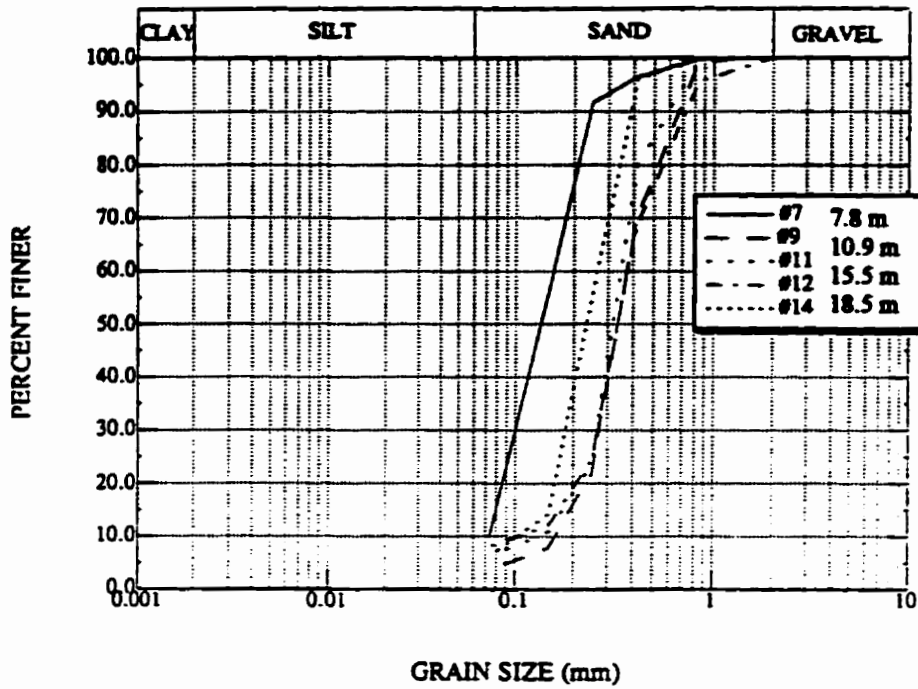


Figure 5-4: Target Zones for Characterization and Sampling.

KIDD #2



MASSEY TUNNEL SOUTH

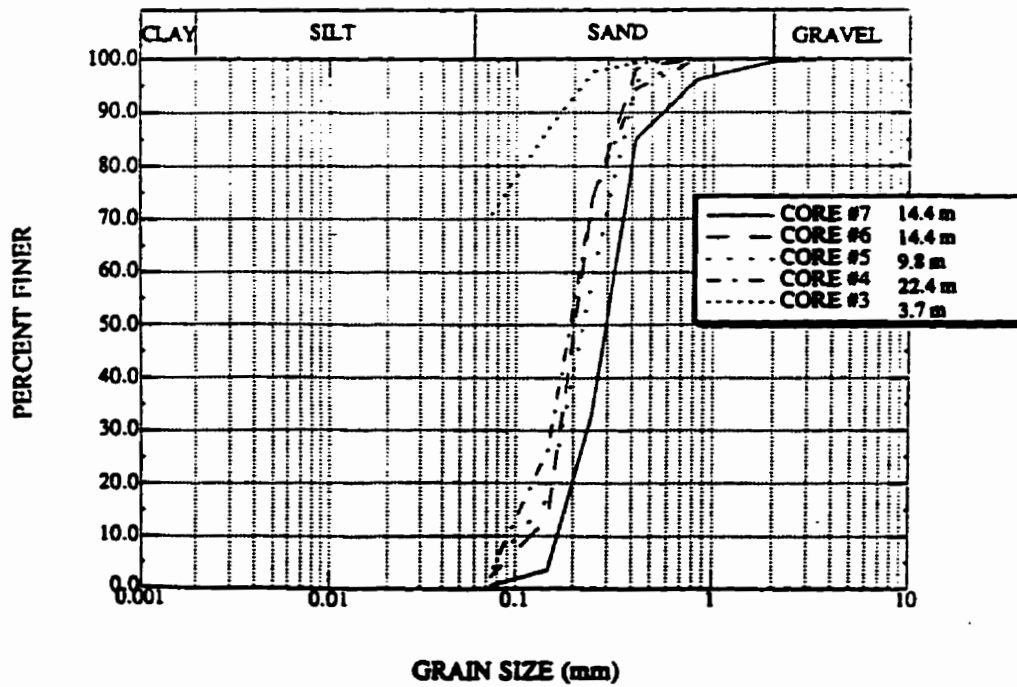


Figure 5-5: Sand Grain Size Distributions at the Phase II Test Sites.

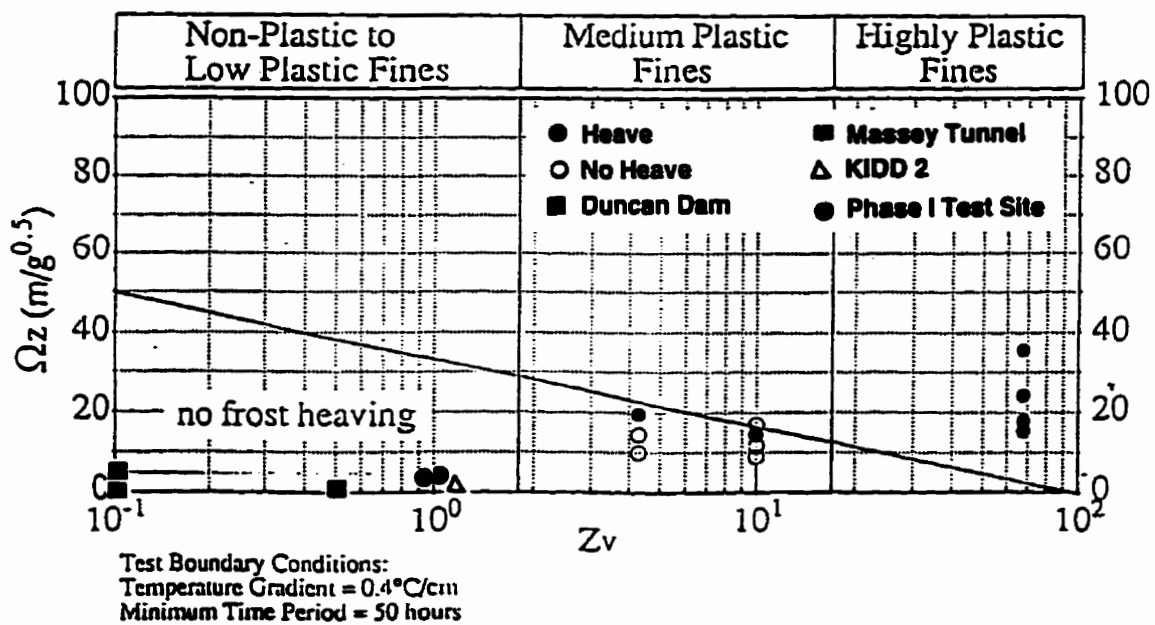


Figure 5-6: Surface Area Critical Plot for Evaluation of Frost Heave Susceptibility (after Davila et al., 1992).

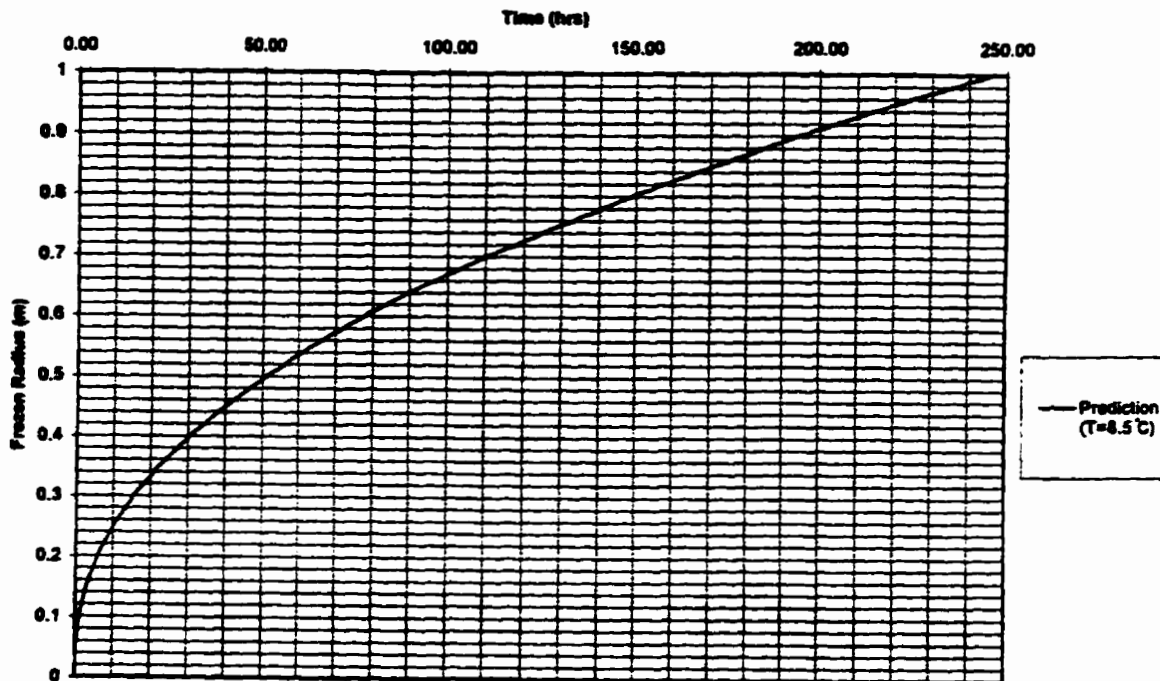


Figure 5-7: Predicted Growth of Frozen Radius at the Phase II Test Sites.

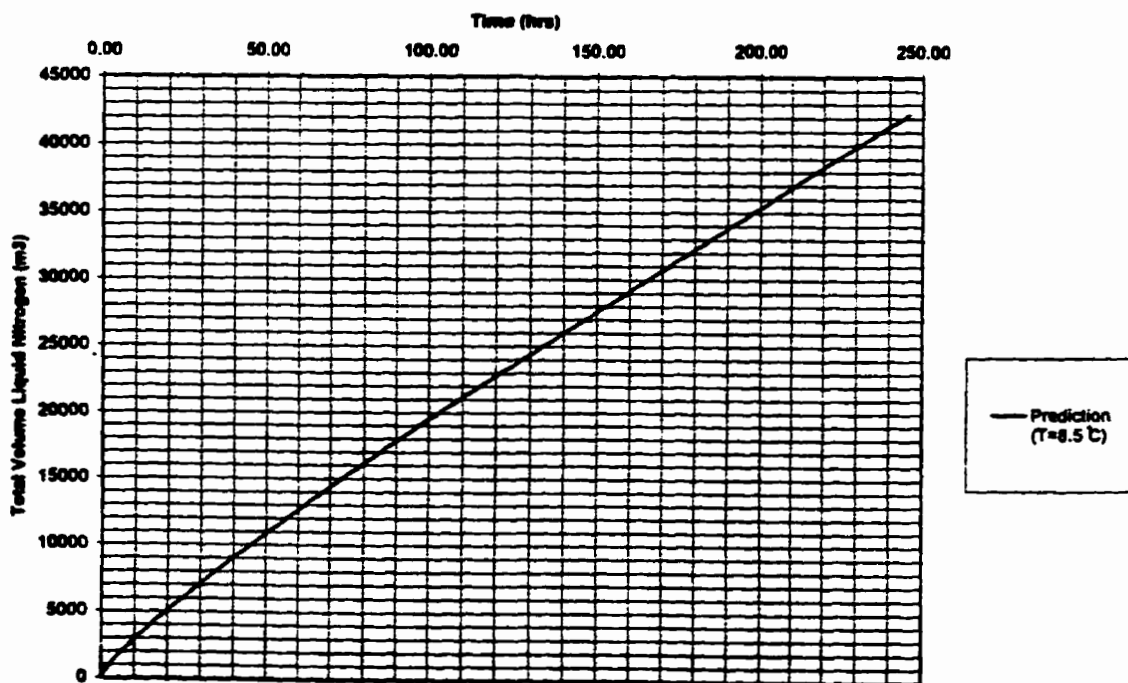


Figure 5-8: Predicted Liquid Nitrogen Consumption at the Phase II Test Sites.

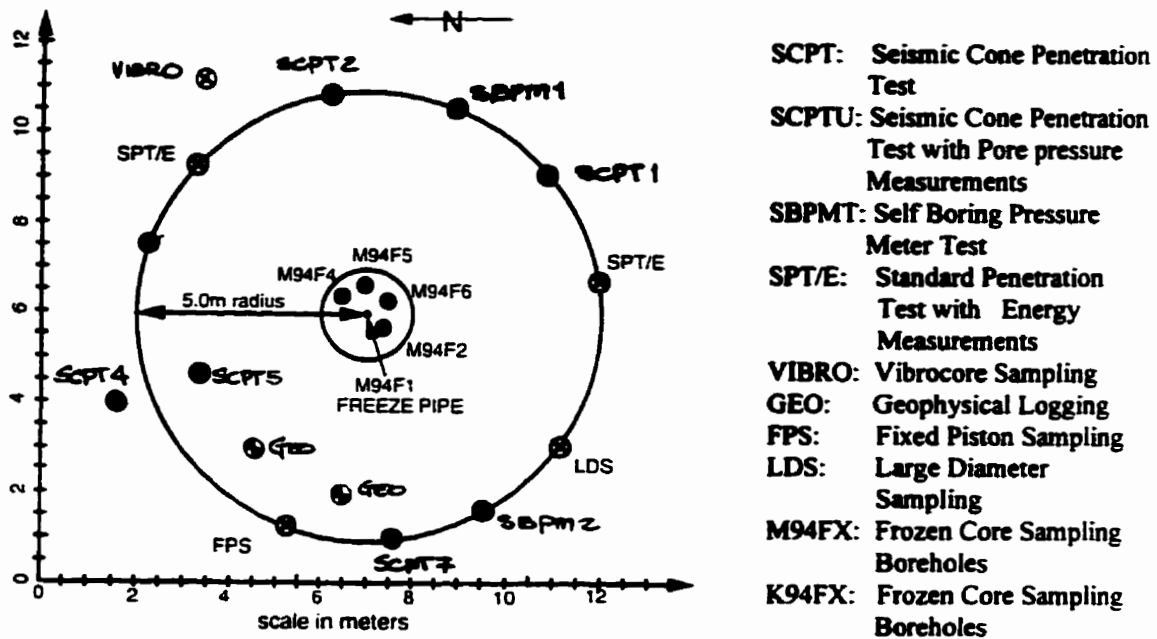


Figure 5-9: Detailed Characterization Zone at the KIDD 2 Site.

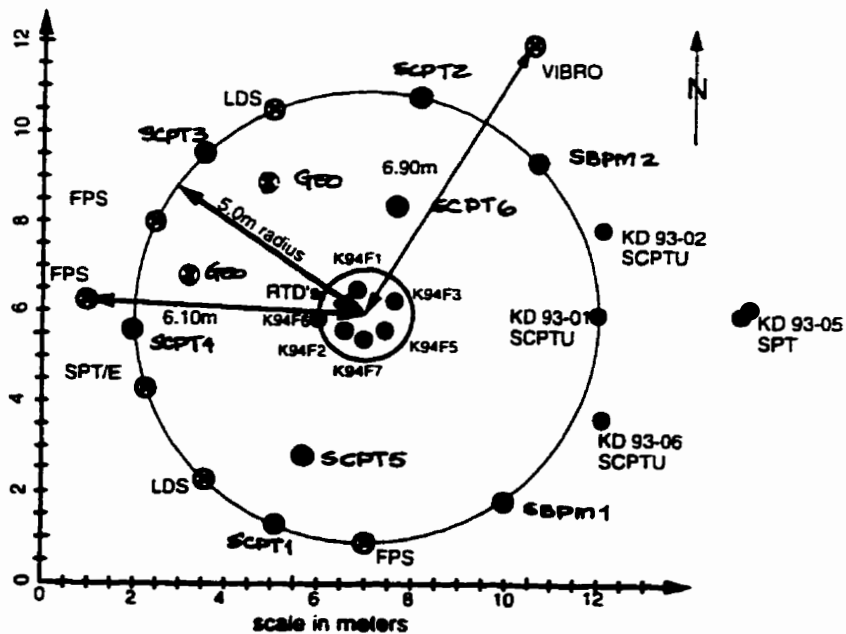


Figure 5-10: Detailed Characterization Zone at the Massey Tunnel Site.

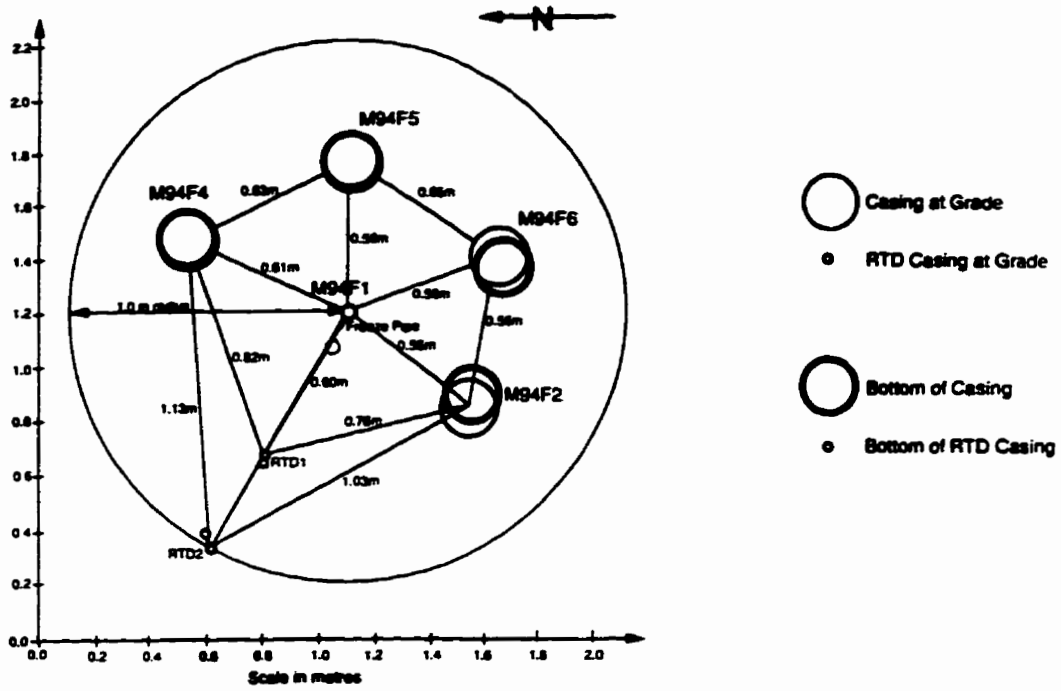


Figure 5-11: Alignment of Sampling Boreholes at the Massey Tunnel Site.

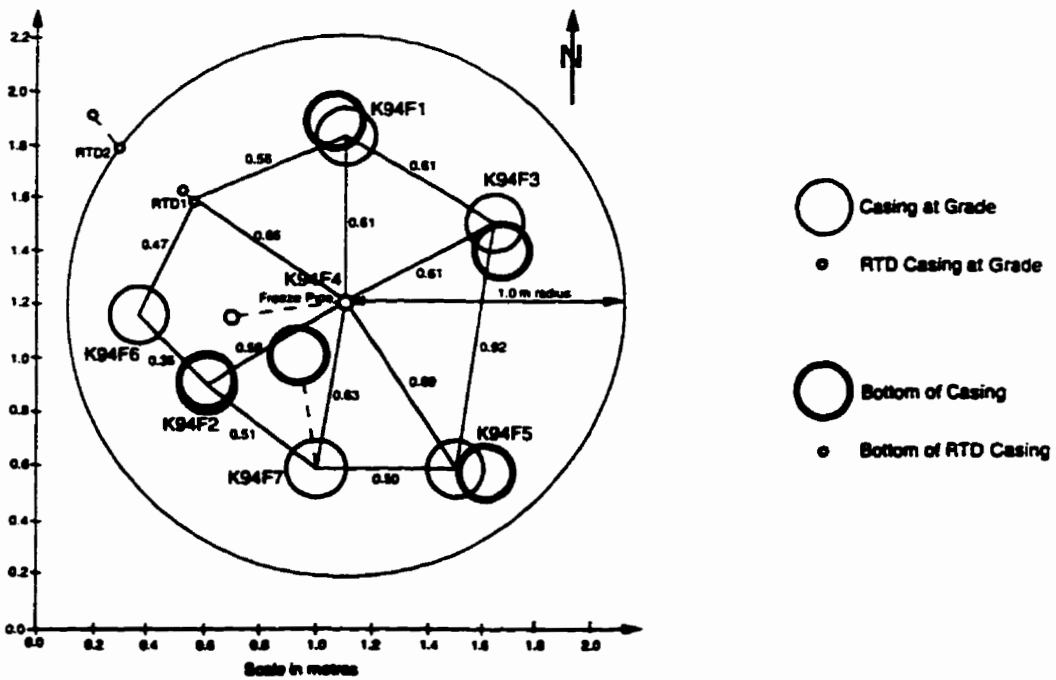


Figure 5-12: Alignment of Sampling Boreholes at the KIDD 2 Site.

TEMPERATURES @ 0.6 M FROM FREEZE PIPE :

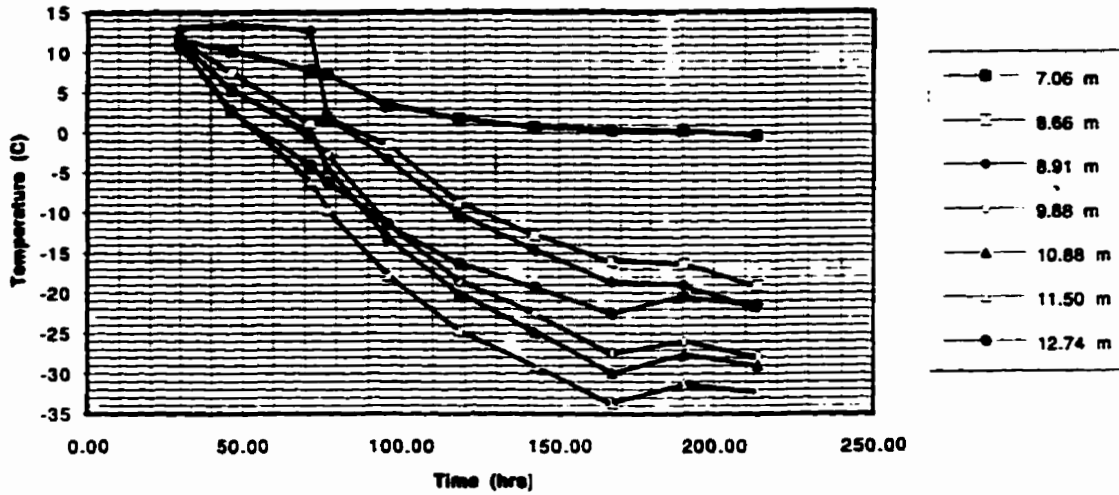


Figure 5-13: RTD Temperature Measurements Recorded at the Massey Tunnel Site at a 0.6 m Radius.

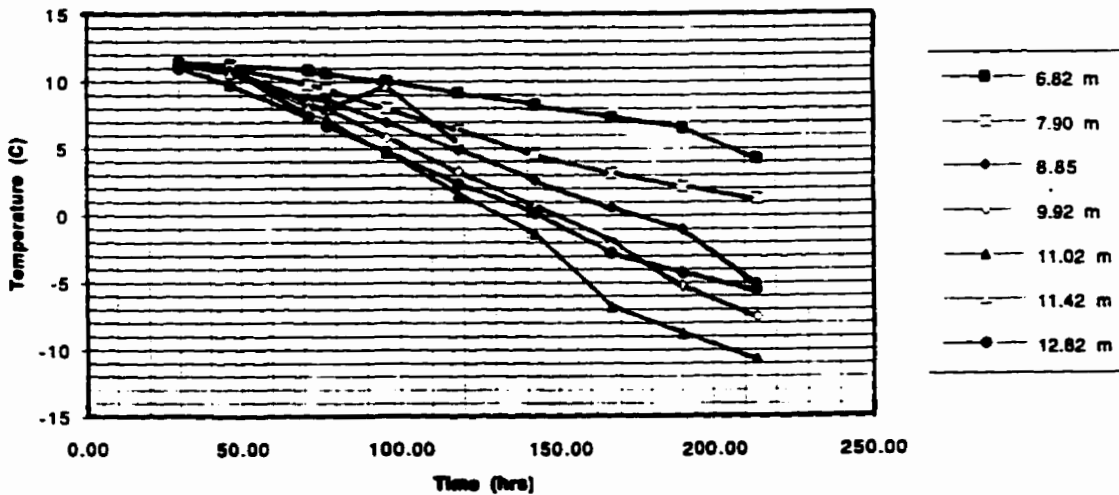


Figure 5-14: RTD Temperature Measurements Recorded at the Massey Tunnel Site at a 1.0 m Radius.

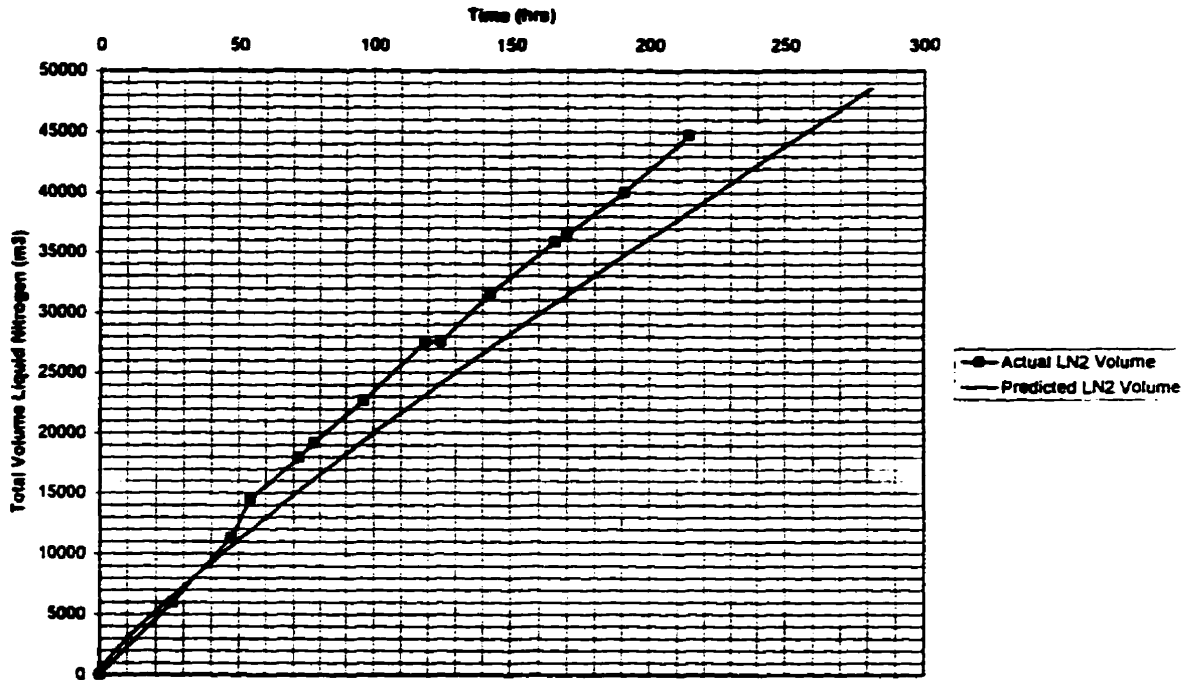


Figure 5-15: Comparison of Actual and Predicted Liquid Nitrogen Consumption at the Massey Tunnel Site (initial groundwater temperature of 11.2 °C).

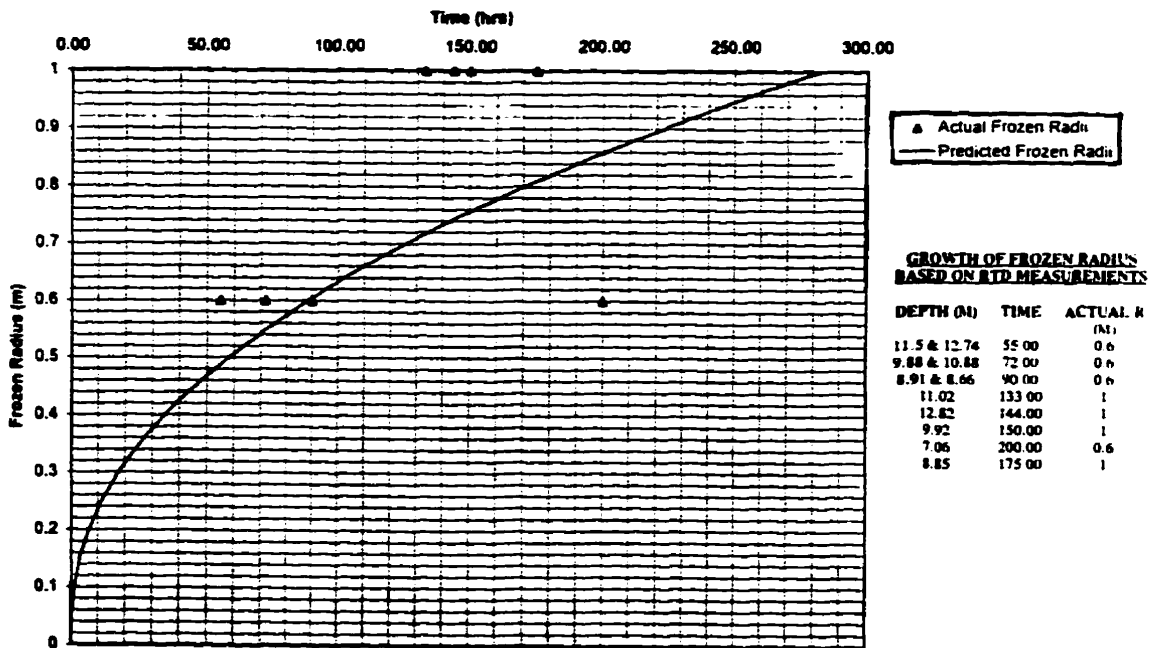


Figure 5-16: Comparison of Actual and Predicted Freezing Time at the Massey Tunnel Site (initial groundwater temperature of 11.2 °C).

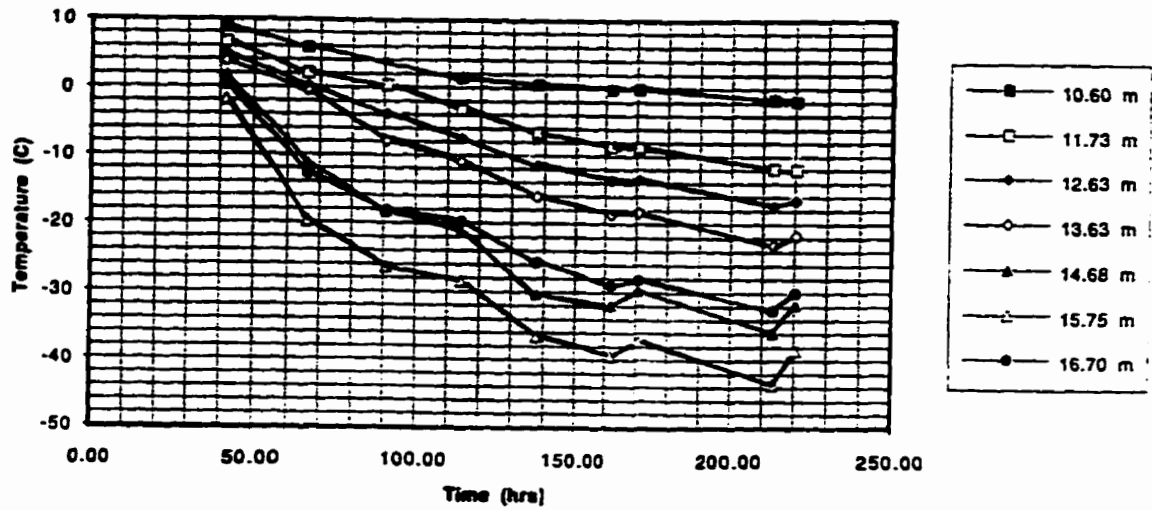


Figure 5-17: RTD Temperature Measurements Recorded at the KIDD 2 Site at a 0.6 m Radius.

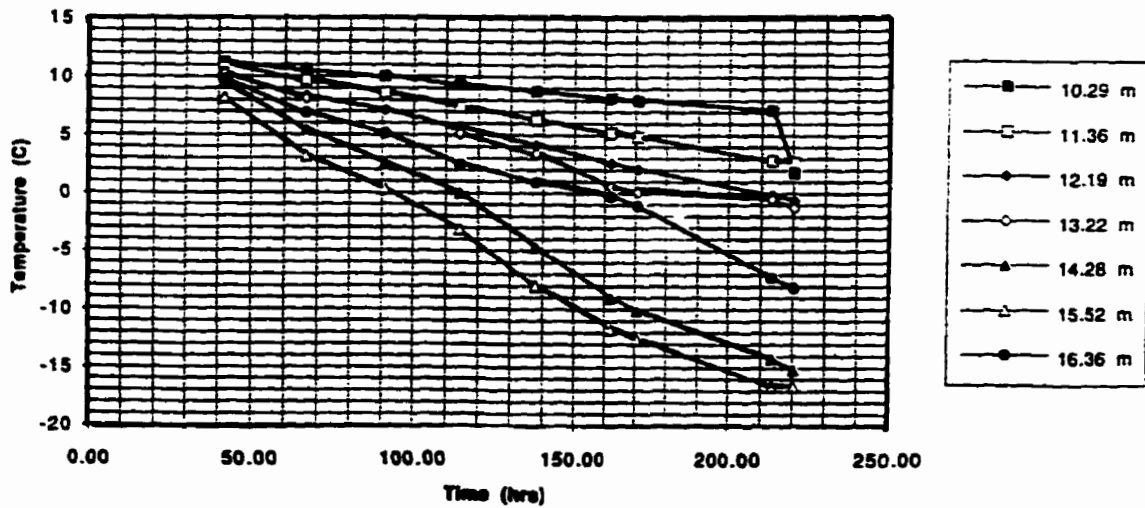


Figure 5-18: RTD Temperature Measurements Recorded at the KIDD 2 Site at a 1.0 m Radius.

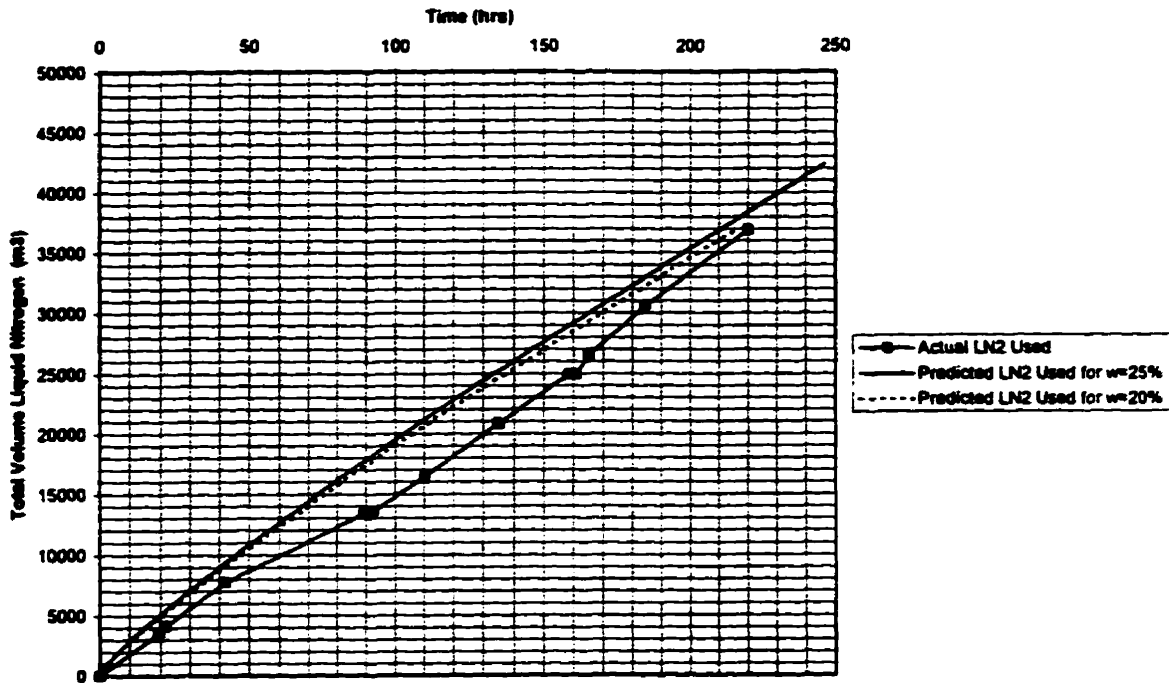


Figure 5-19: Comparison of Actual and Predicted Liquid Nitrogen Consumption at the KIDD 2 Site (initial groundwater temperature of 9.6 °C).

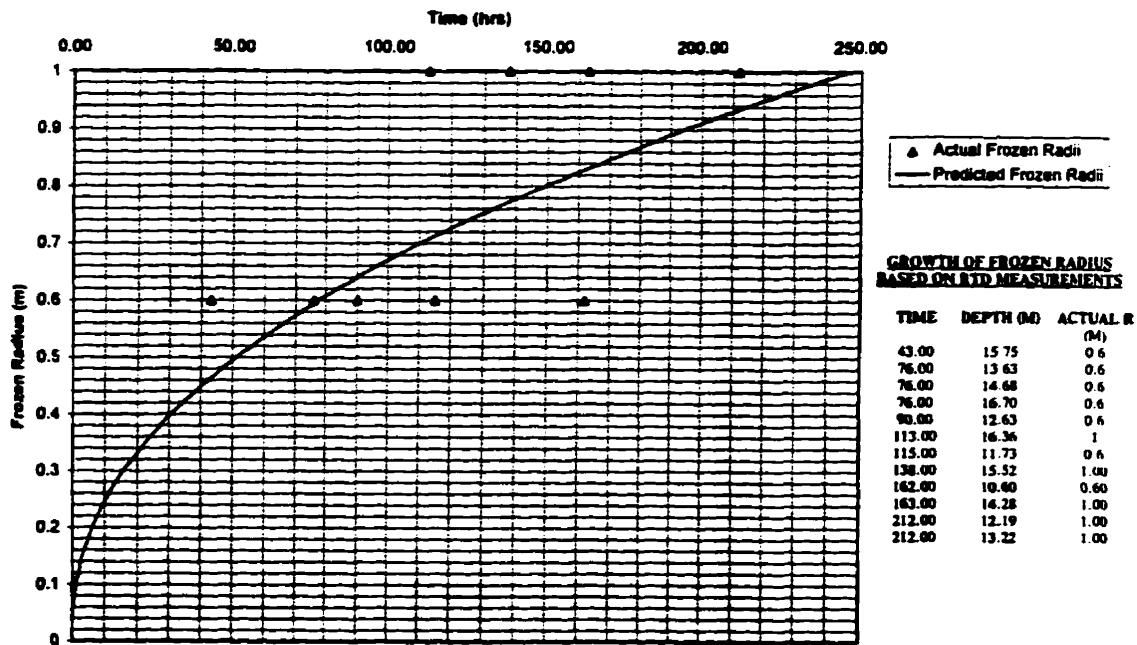


Figure 5-20: Comparison of Actual and Predicted Predicted Freezing Time at the KIDD 2 Site (initial groundwater temperature of 9.6 °C).

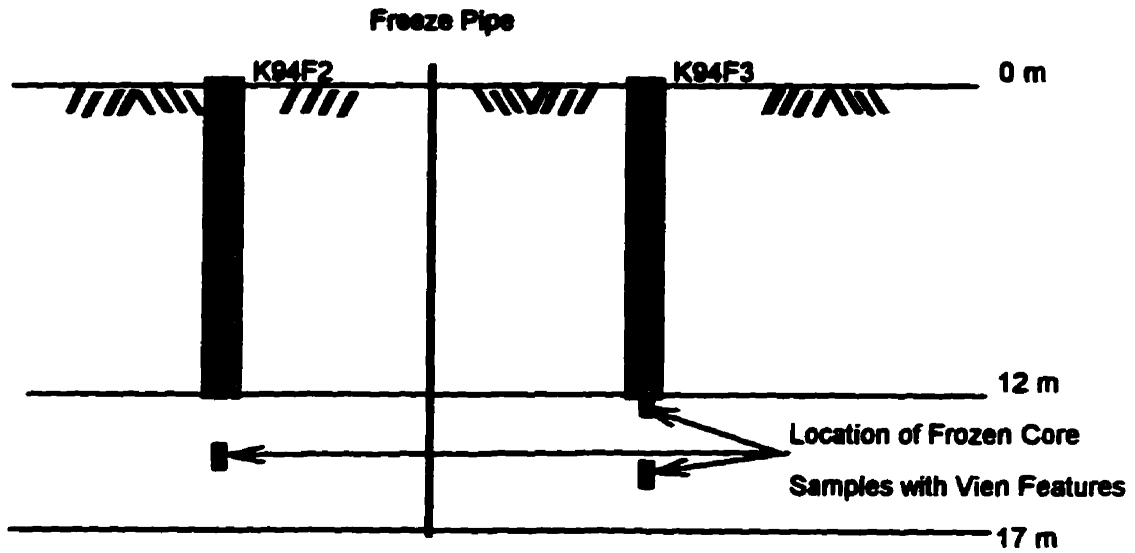


Figure 5-21: In-Situ Frozen Core Sample obtained from Boreholes K94F3 and K94F2 at the KIDD 2 Site Exhibiting Fine Grain Vein Features.

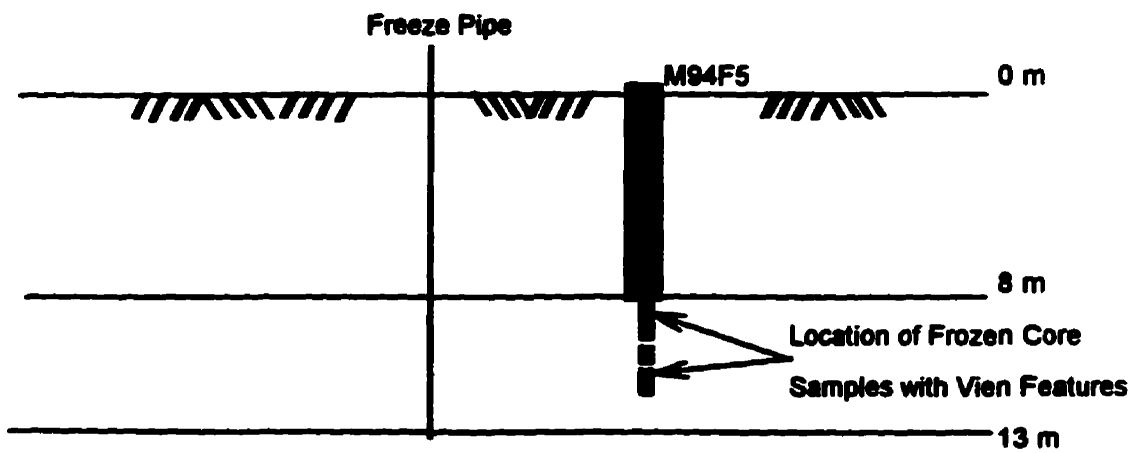


Figure 5-22: In-Situ Frozen Core Sample obtained from Borehole M94F5 at the Massey Tunnel Site Exhibiting Fine Grain Vein Features.

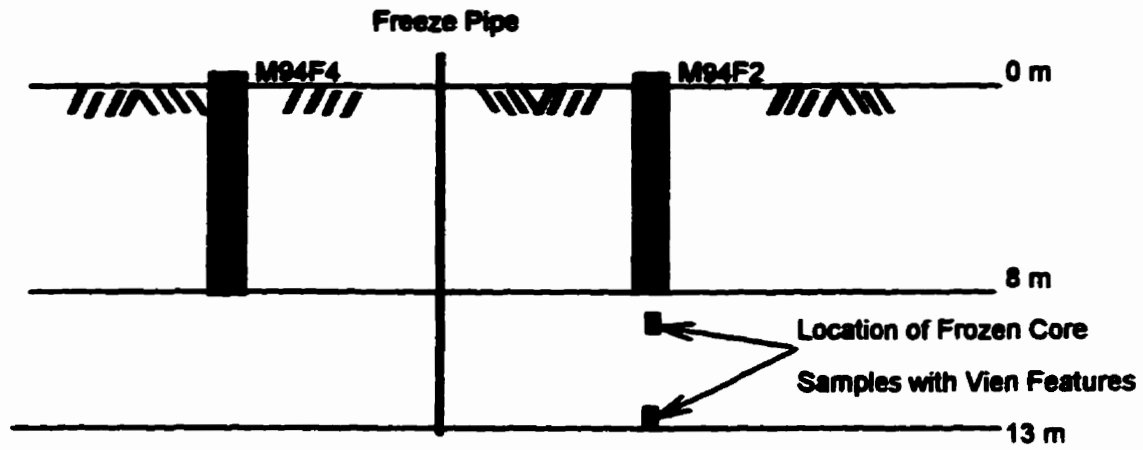


Figure 5-23: In-Situ Frozen Core Sample obtained from Borehole M94F2 at the Massey Tunnel Site Exhibiting Fine Grain Vein Features.

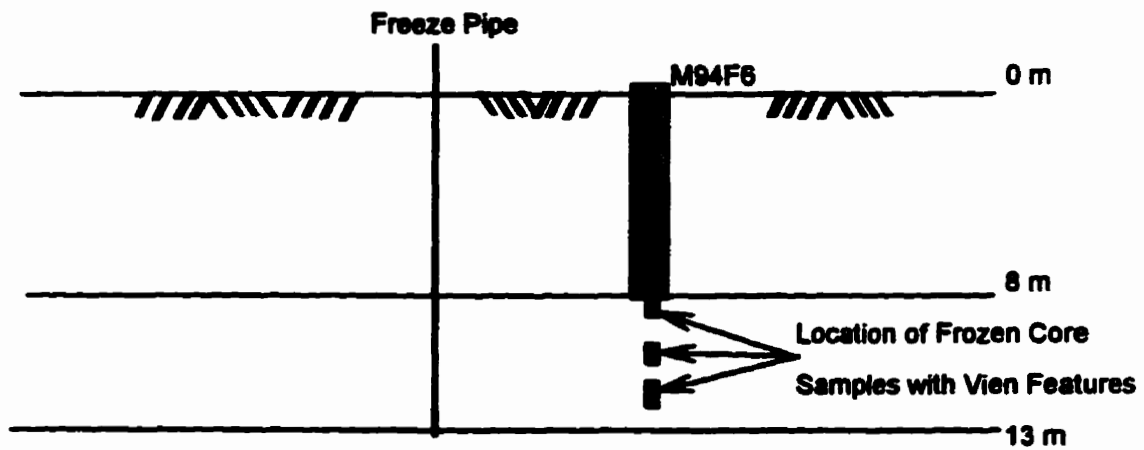


Figure 5-24: In-Situ Frozen Core Sample obtained from Borehole M94F6 at the Massey Tunnel Site Exhibiting Fine Grain Vein Features.

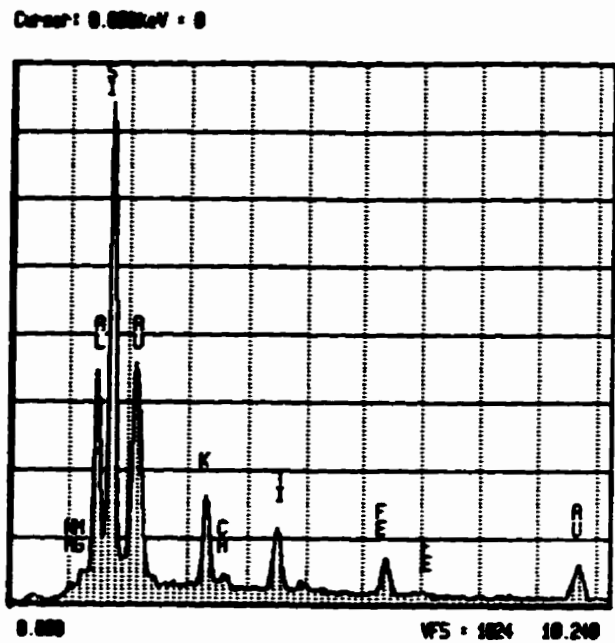


Figure 5-25: Elemental Analysis of Clean Sand obtained from Frozen Core Samples at the KIDD 2 Site.

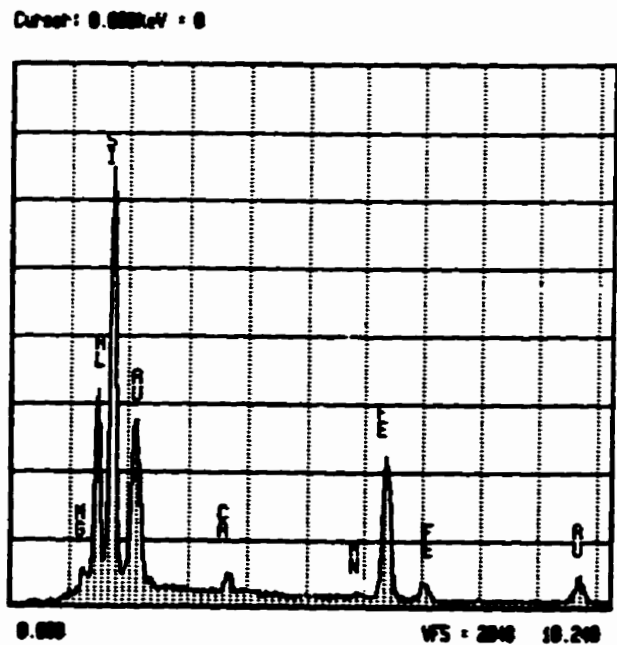


Figure 5-26: Elemental Analysis of Native Fines Extracted from Frozen Core Samples at the KIDD 2 Site.

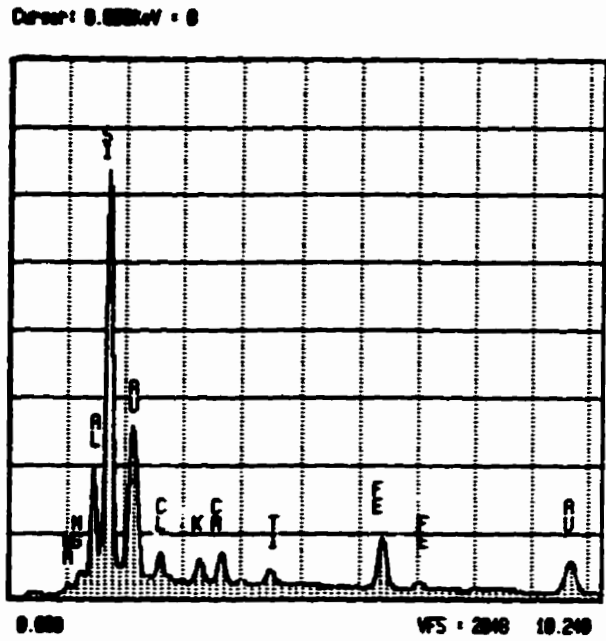


Figure 5-27a: Elemental Analysis of Vein Material Extracted from Frozen Core Samples at the KIDD 2 Site.

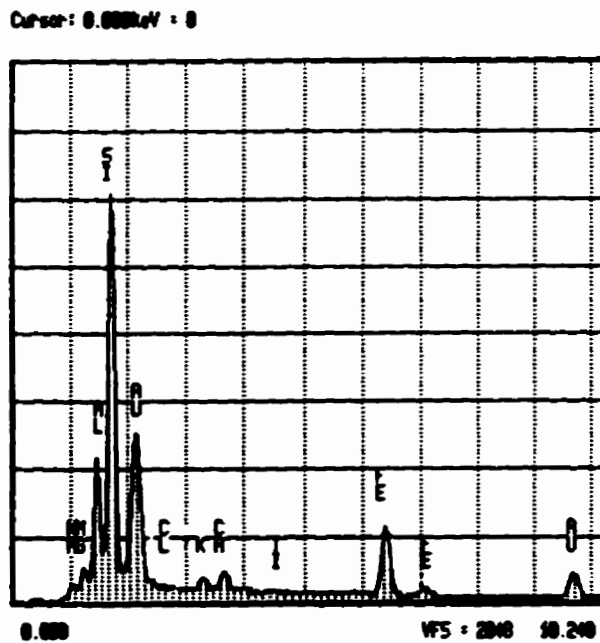


Figure 5-27b: Elemental Analysis of Vein Material Extracted from Frozen Core Samples at the KIDD 2 Site.

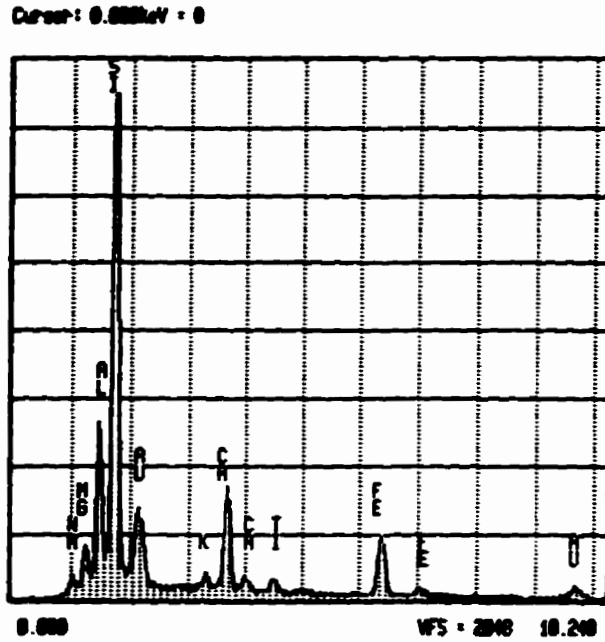


Figure 5-28: Elemental Analysis of Clean Sand obtained from Frozen Core Samples at the Massey Tunnel Site.

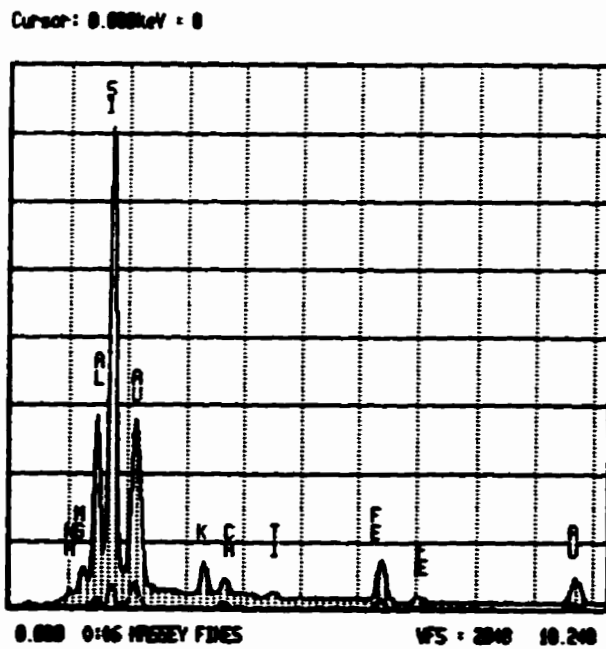


Figure 5-29: Elemental Analysis of Native Fines Extracted from Frozen Core Samples at the Massey Tunnel Site.

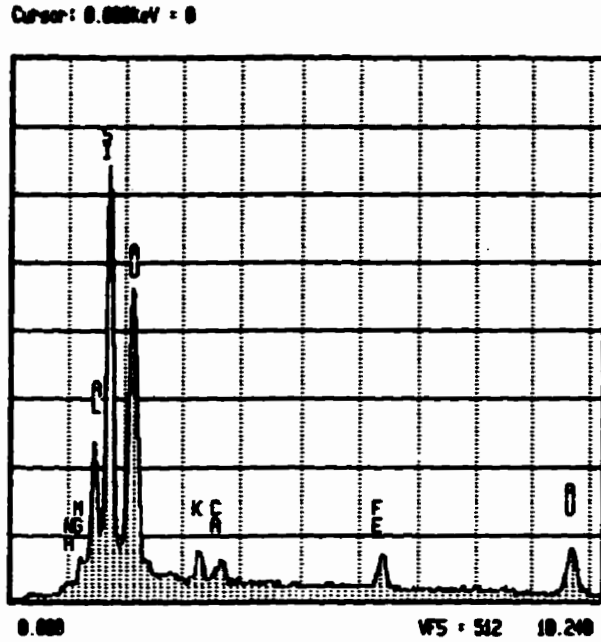


Figure 5-30a: Elemental Analysis of Vein Material Extracted from Frozen Core Samples at the Massey Tunnel Site.

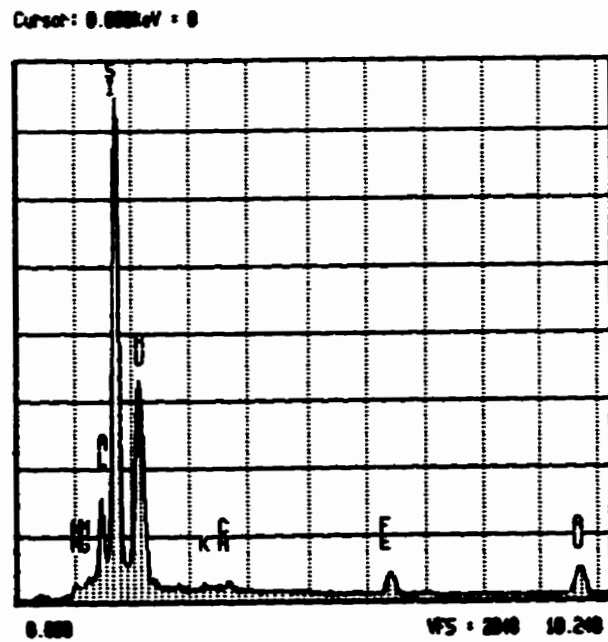


Figure 5-30b: Elemental Analysis of Vein Material Extracted from Frozen Core Samples at the Massey Tunnel Site.

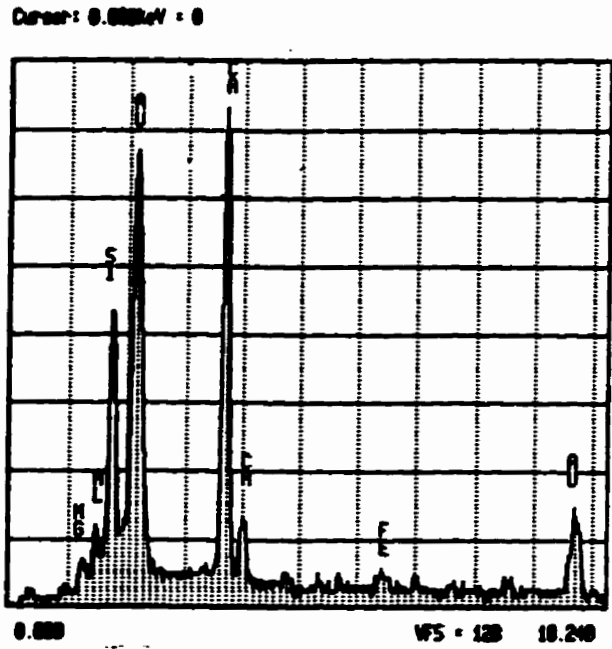


Figure 5-31: Elemental Analysis of KIM Drilling Mud used at the KIDD 2 Site.

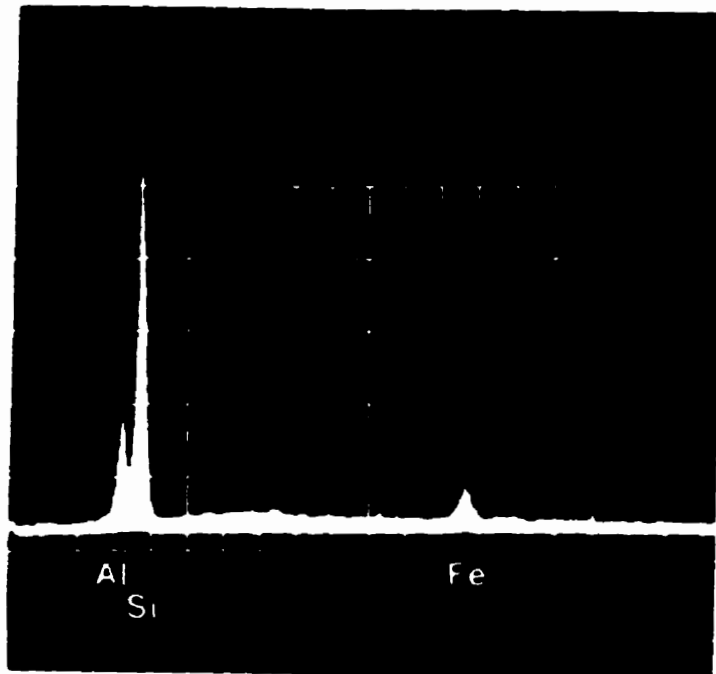


Figure 5-32: Elemental Analysis of the Bentonite Drilling Mud used at the Massey Tunnel Site.

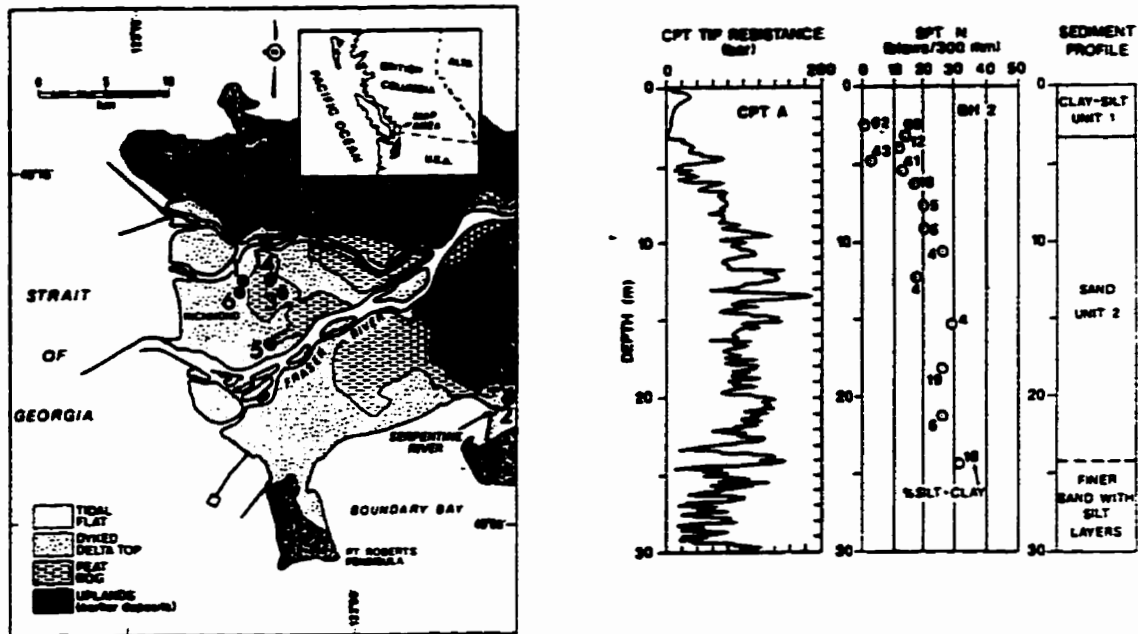


Figure 5-33: Sites in the Fraser River Delta where Sand Dykes were Encountered (after Clague et al., 1992).

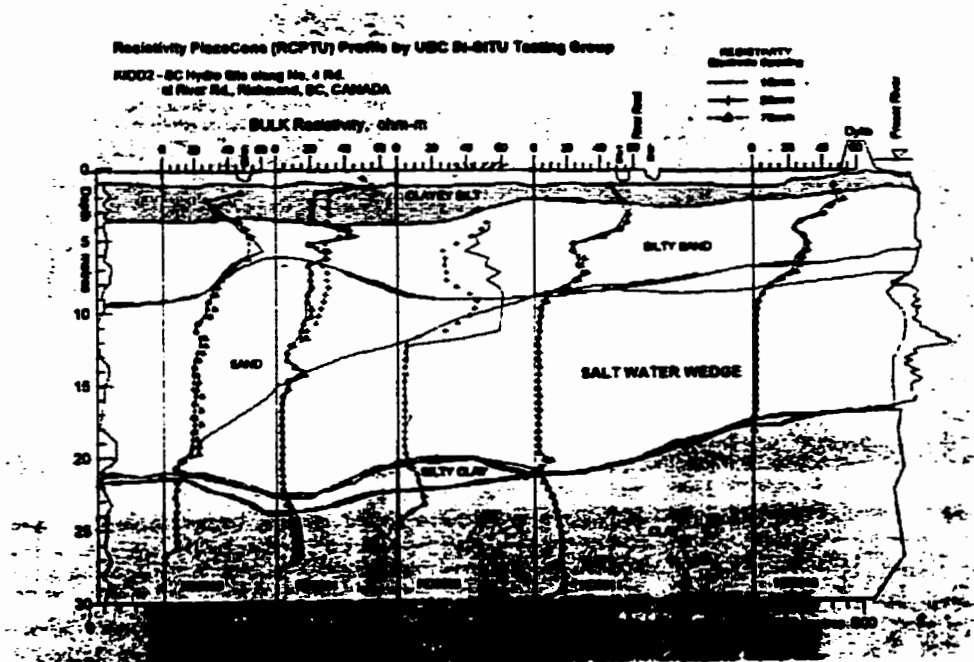


Figure 5-34: Geological Profile of the KIDD 2 Site Based on PiezoCone Resistivity Logs (prepared by the University of British Columbia for CANLEX).

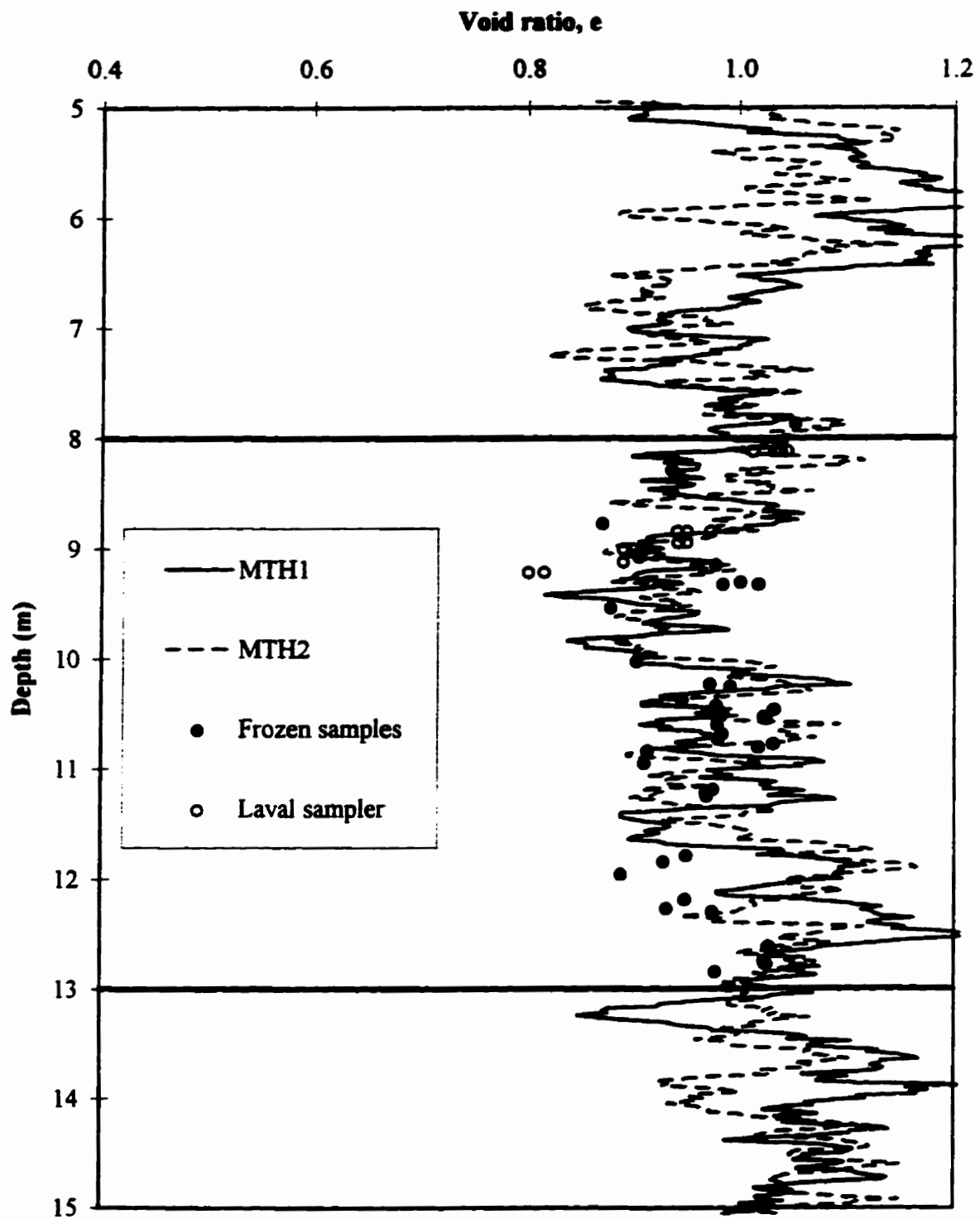


Figure 5-35: Comparison of Void Ratios Determined from In-Situ Frozen Core and Geophysical Logging at the Massey Tunnel Test Site.

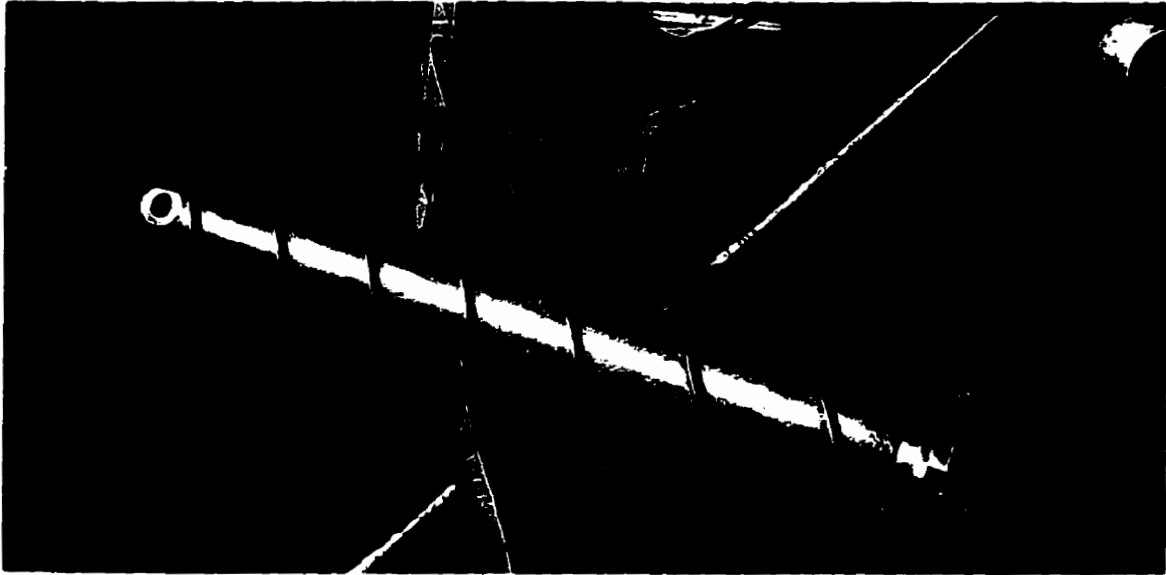


Photo 5-1: 150 mm Diameter CRREL Core Barrel Used to Recover Samples of In-Situ frozen Sand from the Phase II Test Sites.



Photo 5-2: Hydraulic Extruder used to Remove In-Situ Frozen Core from the CRREL Core Barrel.

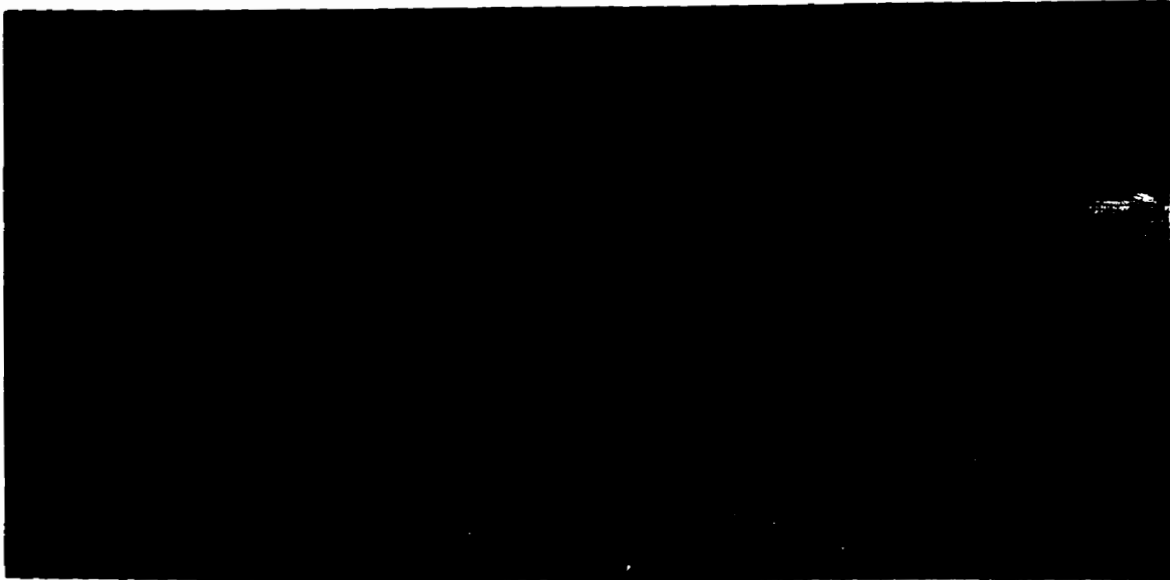


Photo 5-3: In-Situ frozen Core Sample Obtained from the Massey Tunnel Site - shown after Extrusion into an Insulated Box Containing Dry Ice.



Photo 5-4: In-Situ Frozen Core Stored in a Freezer for Transportation from the Site to the University of Alberta.



Photo 5-5: Fine Grain Vein Feature Encountered in In-Situ frozen Core Sample M94F6-C7A Obtained from the Massey Tunnel Site.

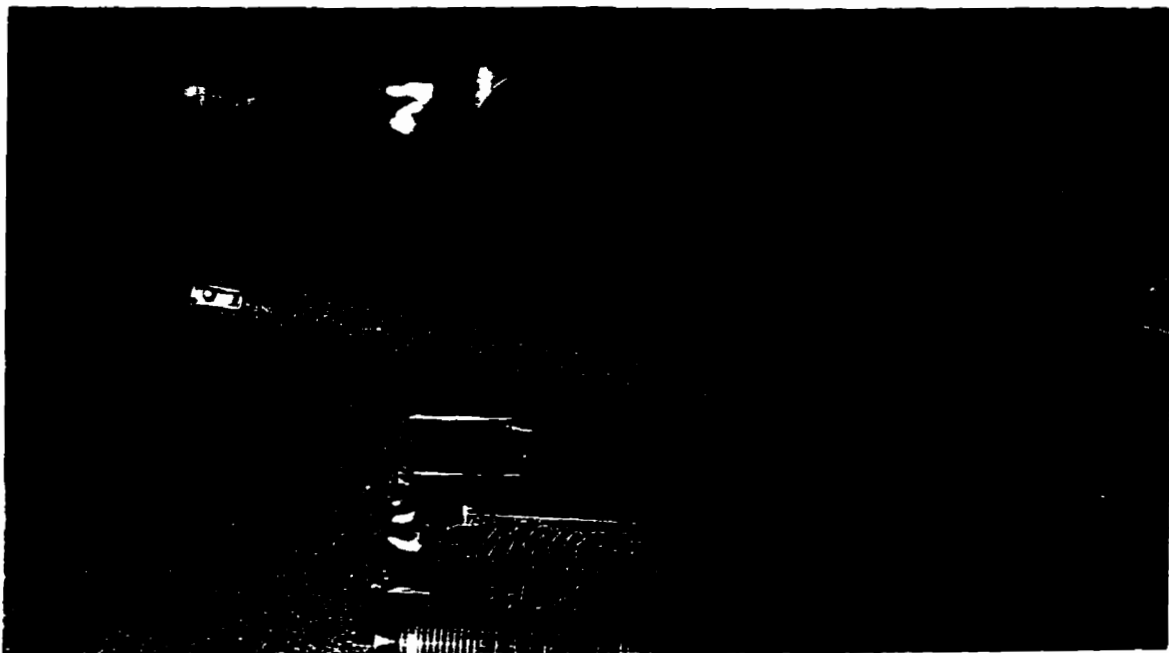


Photo 5-6: Fine Grain Vein Feature Encountered in In-Situ frozen Core Sample M94F5-C2C Obtained from the Massey Tunnel Site.

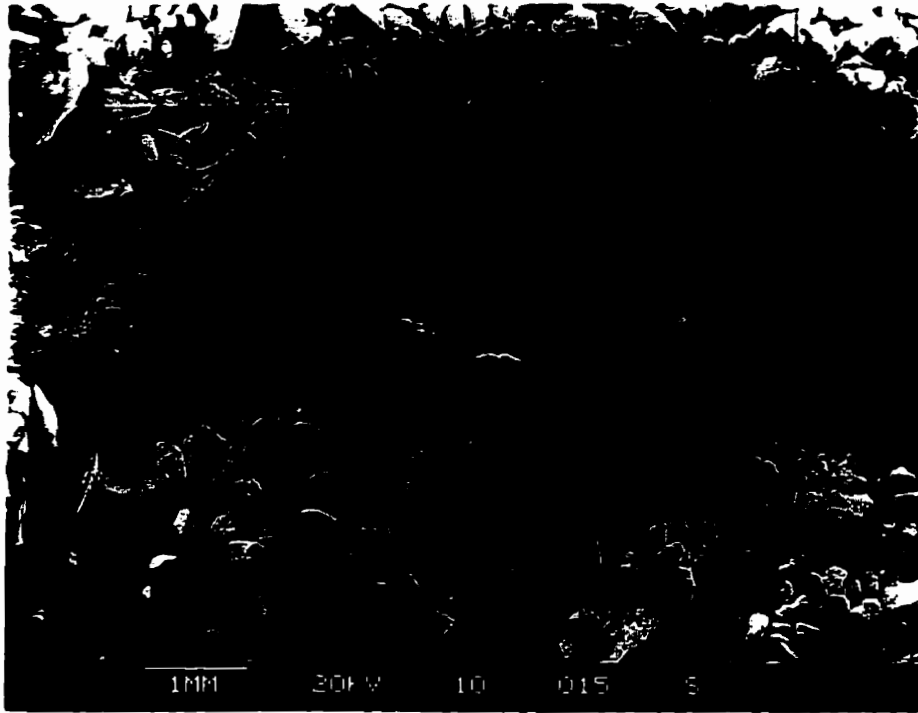


Photo 5-7: SEM Image of Fine Grain Vein Feature Encountered in In-Situ frozen Core Sample from the KIDD 2 Site.

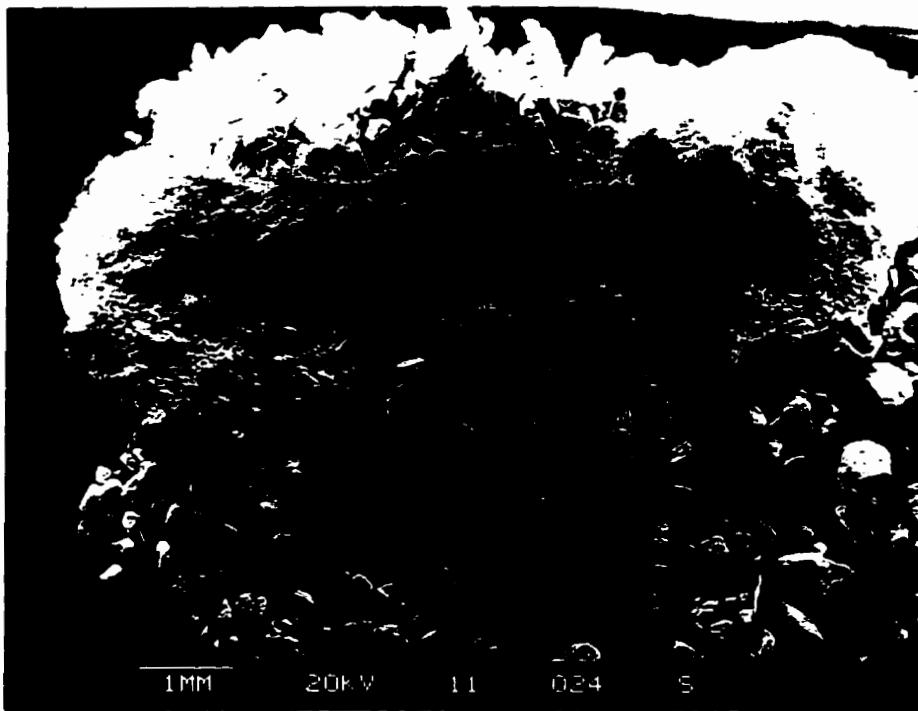


Photo 5-8: SEM Image of Fine Grain Vein Feature Encountered in In-Situ frozen Core Sample from the Massey Tunnel Site.

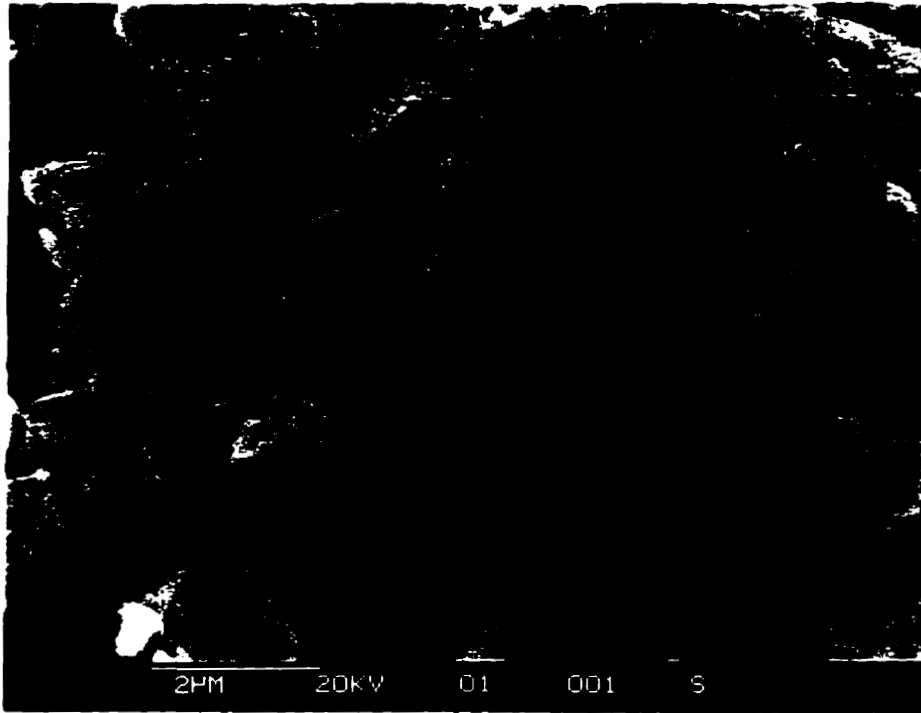


Photo 5-9: SEM Image of Platey Clay Minerals Comprising Fine Grain Vein Feature at the KIDD 2 Site.

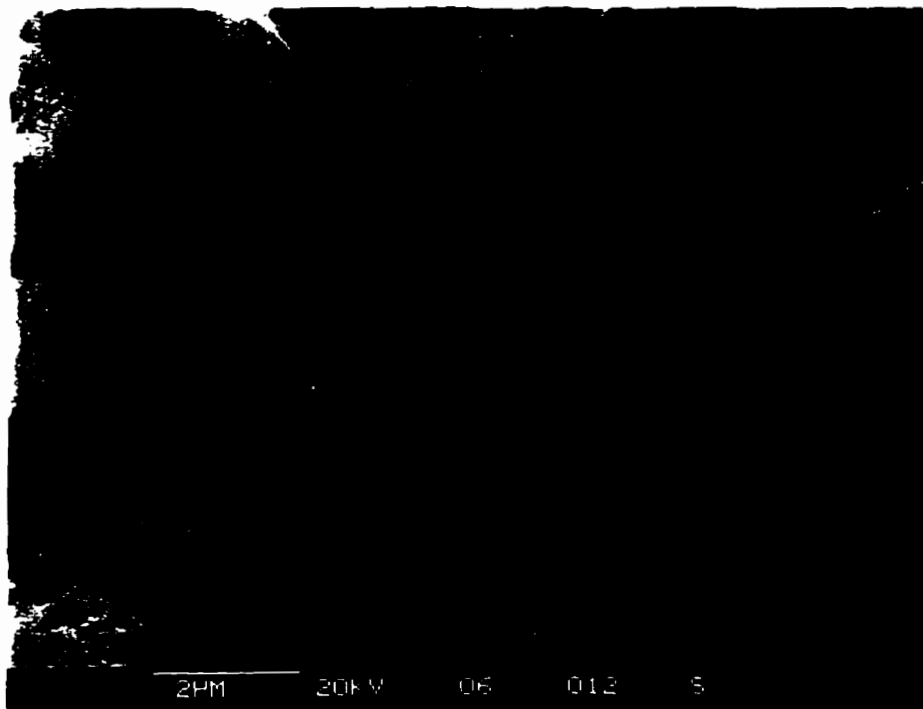


Photo 5-10: SEM Image of Platey Clay Minerals Comprising Fine Grain Vein Feature at the Massey Tunnel Site.

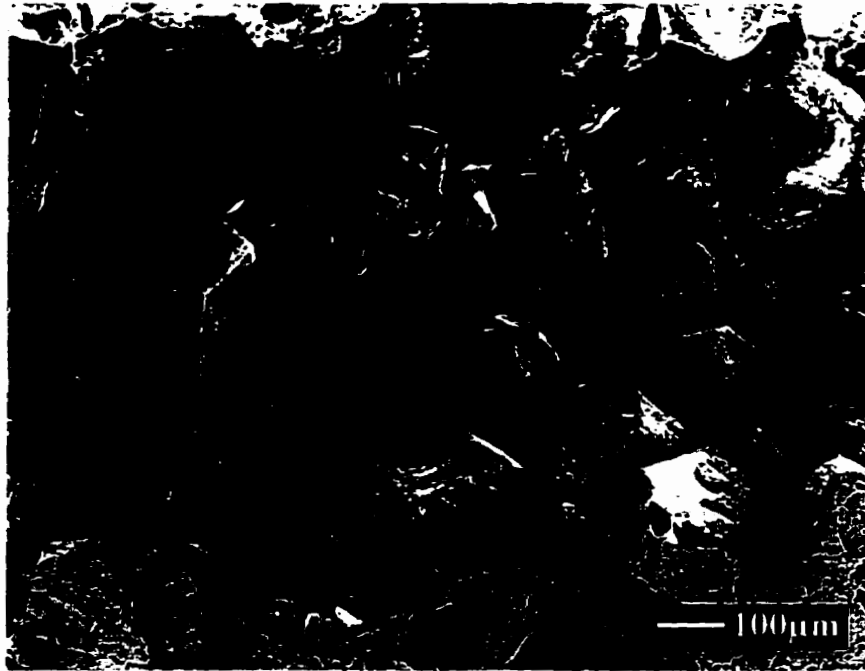


Photo 5-11: SEM Image of Reconstituted Sand Sample Subject to Freezing Cycles showing Alignment of the Thin Clay Mineral Edge Perpendicular to the Freeze Front.

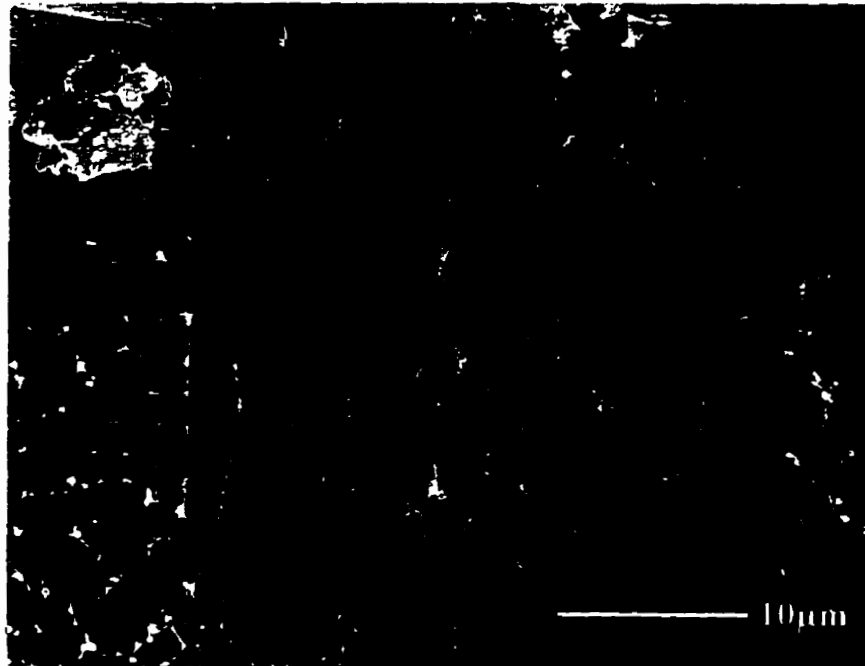


Photo 5-12: SEM Image of Reconstituted Sand Sample Subject to Freezing Cycles showing a Clay Mineral Particle Aligned with an Ice Grain Boundary.

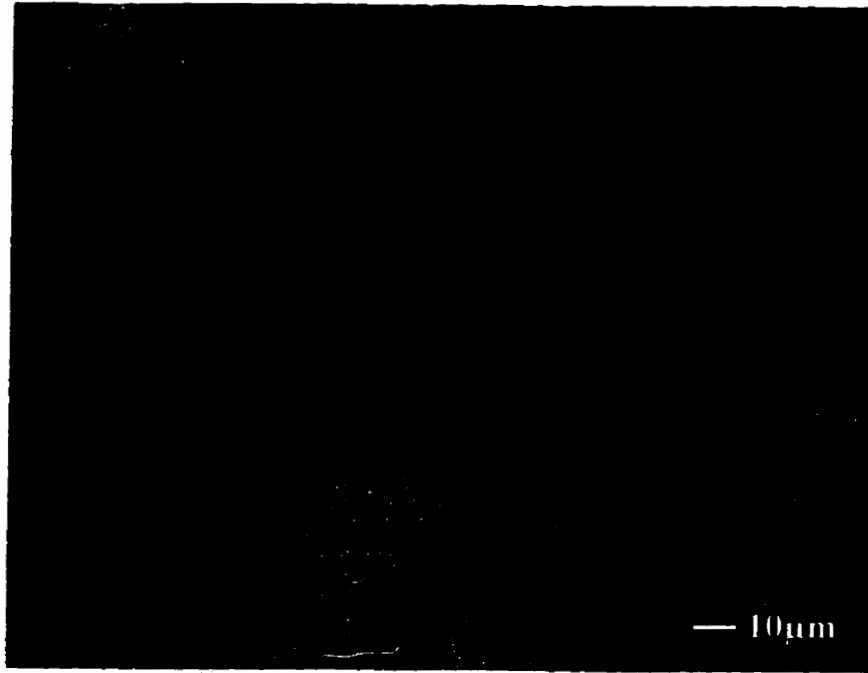


Photo 5-13: SEM Image of Reconstituted Sand Sample Subject to Freezing Cycles showing Clay Mineral Particles Aligned both Perpendicular and Parallel to the Freezing Front.

Chapter 6.0 In-situ Ground Freezing and Sampling at the Phase III Event Site

6.1 Introduction

Phase III of the Canadian Liquefaction Experiment (CANLEX) involved attempting to statically trigger a liquefaction flow slide by rapidly loading a loose, saturated sand deposit. The rapid loading was carried out by pumping tailings into a reservoir bounded by a containment dyke constructed on a 10 m thick loose sand foundation deposit. The foundation sand was placed hydraulically into standing water in an abandoned borrow pit (J-pit), at Syncrude Canada Ltd. (SCL), near Fort McMurray, Alberta. This resulted in approximately 7 m of loose beach below water (BBW) sand, underlying 3 m of slightly more dense beach above water (BAW) sand. The containment dyke was constructed as a clay-sand composite ring dyke overlying the hydraulically placed foundation sand. The test section of the embankment, where instrumentation would be installed to measure the pore pressure and deformational response of the foundation sand, was constructed using clay shale fill to a height of 8 m, with sideslopes varying from 2.5:1 to 2.0:1. A 9 m high hydraulically placed sand berm, with sideslopes of 2.5:1, was then tied into the completed clay embankment to form the back portion of the ring containment dyke. A Plan view of the test site in J-pit is shown in Figure 6-1. Further details regarding the scope of work for Phase III are presented by Byrne et al. (1995).

Prior to rapid loading, the BBW sand was fully characterized by various in-situ testing and sampling techniques, carried out in a manner similar to that undertaken during Phases I and II of the CANLEX project. Detailed characterization was undertaken within an 8 m radius circle located near the south end of the clay embankment footprint. To obtain undisturbed samples and to estimate the void ratio of the loose sand deposit (BBW), in-situ ground freezing and frozen core sampling was undertaken in the centre of

the detailed characterization zone. Liquid nitrogen was utilized to radially freeze a column of loose sand between depths of 3 and 7 m below the ground surface. The frozen sand was then sampled using core barrels developed at the University of Alberta, with a design similar to the Cold Regions Research Engineering Laboratory (CRREL) barrel commonly used for sampling frozen ground. Two core barrels were used, one with an inner diameter of 100 mm and one with an inner diameter of 200 mm.

Chapter 6 describes the in-situ ground freezing and sampling of the frozen sand at the Phase III test site. Further details regarding the instrumentation, construction and site characterization undertaken as part of the Phase III full scale liquefaction test are given by Hofmann et al. (1996a and 1996b).

6.2 Location of Undisturbed Sampling

Once the loose sand had been placed in J-pit, the deposit was characterized by ConeTec Investigations Ltd. (ConeTec) to confirm that there was a potential to trigger flow liquefaction of the loose sand foundation and to identify the best locations for the containment dyke, instrumentation lines and zone for detailed characterization. Under the supervision of the University of Alberta, ConeTec conducted 22 Cone Penetration Tests (CPTs) and 4 Seismic Cone Penetration Tests (SCPT) in an 80 m by 80 m grid across the site.

At the location of the CPT grid, the upper 3 m of the sand foundation was more dense, indicating BAW, while the sand below 3 m was looser, comprising BBW. The CPT screening indicated that the foundation sand was loosest at the southeast corner of the approximate clay embankment footprint. Based on the CPT screening, the zone for detailed characterization was located immediately downstream of the southeast corner of the clay embankment, where the foundation sand was loosest. The target depth for detailed characterization, where in-situ ground freezing and undisturbed sampling would

be carried out, was identified between 3 and 7 m, where the lowest CPT end bearing resistances were encountered. Figure 6-1 shows the location of the 8 m radius circle where detailed characterization was carried out and Figure 6-2 shows the CPT profiles obtained within the 8 m radius circle. The average normalized cone tip resistance, q_{cl} , in the target zone was 2.4 MPa.

6.3 Ground Freezing Feasibility Studies

Prior to undertaking ground freezing and sampling at the Phase III event site, it was necessary to first confirm that the sand deposit could be frozen without causing disturbance due to frost heaving. Feasibility studies were carried out considering both the nature of the sand deposit and the site conditions, with respect to the potential for utilizing in-situ ground freezing to obtain undisturbed samples of loose sand.

6.3.1 Frost Heave Susceptibility

Phase I of the CANLEX project involved undisturbed sampling of sand at the Mildred Lake Settling Basin, Syncrude Canada Ltd. The same type of sand that was used to construct the Mildred Lake Settling Basin was deposited in J-pit for Phase III. Therefore it was assumed that the mineralogy of the fines in J-pit would be the same as that determined during Phase I, as shown in Table 6-1. However, since most of the Phase III foundation sand was known to comprise BBW, the percentage of fines contained within the sand deposited in J-pit was expected to be greater than the fines content at the Phase I test site.

Prior to site characterization, Syncrude indicated that the fines content of the sand placed in J-pit could be as high as 22 percent. Grain size tests carried out on split spoon samples obtained from the Phase III test site during detailed characterization, indicated that the

fines varied between approximately 5 and 20 percent in the target zone. The distribution of the fines content with depth, determined from 17 samples in 3 boreholes advanced within the 8 m radius circle at the site, is shown in Figure 6-3. The average fines content of the SPT samples in the target zone was only 10 %. The grain size curves established for each of the SPT samples are provided in Appendix D.

Based on the grain size information, and the mineralogical evaluation carried out on the fines fraction during Phase I, Davila et als' (1992) criteria was used to evaluate the frost heave potential of Syncrude sand, containing 22 percent fines. As shown in Figure 6-4. according to Davila et al's criteria the risk of frost heave was negligible, even if the fines content was assumed to be higher than the average value determined from the grain size analyses.

As part of the feasibility study conducted prior to undertaking in-situ freezing, frost heave tests were also carried out on reconstituted samples of Syncrude sand with a fines content of 22 percent. The rate of cooling used for the tests was 0.4 °C/cm. This cooling rate is approximately the same as that which typically occurs at the radial distance from the freeze pipe of about 0.5 to 0.6 m, where sampling would be undertaken. Although the specimens took in water during freezing over a period of about 90 to 165 hours, as shown in Figure 6-5, the measured axial heave of two samples with a fines content of 22 percent was only 0.1 and 0.2 mm, under confining stresses of 24 kPa and 55 kPa, respectively. The average effective overburden stress in the target zone was about 58 kPa, ranging from approximately 38 kPa at the top of the target zone, to 77 kPa at the bottom of the target zone. If all of the pore water had frozen in place, causing a 9 % pore water volume expansion, the measured heave would have been about 6 mm. Therefore, heaves of 0.1 to 0.2 mm were likely due to the effect of temperature on the equipment in the cooler. It should be noted that the large volume of pore water taken in by Sample 2, under an overburden stress of 24 kPa, was associated with a leak in the burette and was not the actual volume of pore water taken in by the sample.

Given the negligible heave exhibited by the specimens during frost heave testing and considering that the average fines content of the SPT samples in the target zone was only 10 %, it was decided that in-situ ground freezing remained the best method for obtaining undisturbed samples from the Phase III test site.

6.3.2 Site Conditions

To estimate the permeability of the sand deposit in which in-situ ground freezing would be undertaken, permeability tests were carried out on reconstituted sand samples with fines contents of 22 percent. The permeabilities measured from these tests were 7.6×10^{-4} cm/s. under an overburden stress of 30 kPa, and 6.2×10^{-4} cm/s. under an overburden stress of 100 kPa.

Based on the permeability test results, the maximum rate at which water could be expelled from the freezing front was calculated to be approximately 2.7 cm/hr. The freezing gradient, at a radial distance from the freeze pipe where sampling would be undertaken, was estimated to be approximately 0.4 cm/hr. Therefore, the relatively high permeability of the sand would not inhibit pore water expulsion.

During the CPT screening, ground temperatures measurements were taken. Figure 6-6 shows the groundwater temperature profiles measured in Boreholes CPT 18 to CPT 25 from May 19 to 22, 1995. The profile indicates that the ground temperature increased from 20 °C near the ground surface to 40 °C at a depth of approximately 4 to 5 m and then decreased to 20 °C at a depth of about 12 m. This information was used for prediction of the heat extraction requirements to carry out ground freezing.

6.4 Prediction of Ground Freezing Process

6.4.1 Growth of Frozen Radius

A 1 m radius column of sand was seen as the smallest practical frozen radius that would allow for sufficient volume of frozen sand to carry out sampling. Based on thermal heat flow equations developed by Sanger and Sayles (1979), a prediction was made on the amount of energy that would have to be extracted from the ground and the time required to freeze a 1 m radius column of sand, assuming that the freeze pipe reservoir would be full of liquid nitrogen in the target zone at all times during ground freezing. Preliminary information, regarding the moisture content and dry density of the BBW sand and the groundwater temperatures obtained during detailed characterization, were utilized as input parameters for the predictions; Table 6-2 lists these input parameters and the spread sheet used for thermal calculations is shown in Appendix D.

Figure 6-7 shows the predicted growth of the frozen radius versus time for the Phase III test site. It was estimated that approximately 22 days would be required to freeze a 1 m radius, given an average initial ground temperature of 35 °C.

6.4.2 Consumption of Liquid Nitrogen

The equations developed by Sanger and Sayles (1979) were also used to predict the volume of liquid nitrogen that would be required to freeze a 1 m radius column of sand at the test site, assuming that liquid nitrogen would be contained within the freeze pipe reservoir in the target zone at all times during freezing. The predicted volume of liquid nitrogen required for completing ground freezing was approximately 18,100 m³ (equivalent gaseous volume) per meter length of the frozen column. Therefore, as shown in Figure 6-8, for a 4 m long target zone located between 3 and 7 m below the ground surface, the total volume of liquid nitrogen was estimated to be approximately 72,500 m³ (equivalent gaseous volume).

6.5 Phase III Ground Freezing and Sampling System

6.5.1 Installation of Freeze Pipe

Prior to installing the ground freezing system, Standard Penetration Tests (SPTs) and CPTs conducted at a 8 m radius from the center of the circle, where the freeze pipe would be installed, confirmed that the sand was very loose. The normalized SPT and CPT data indicated that the average $(N_1)_{60}$ was about 3 and the average q_{ct} was about 2.4 MPa. Given the loose subsoil conditions, it was initially intended that the freeze pipe would be jetted into place, without exceeding the overburden stress and causing hydraulic fracturing of the ground. However, due to difficulties with the drilling equipment and jetting system it was not possible to install the freeze pipe in this manner. As an alternative, it was envisioned that the freeze pipe, equipped with a cone tip at the bottom end, could be slowly pushed into place, using the drilling rig, without causing excessive radial disturbance.

A 150 mm diameter PVC casing was first installed through the more dense, upper 2.5 m of sand. A 50 mm diameter, steel freeze pipe was then slowly rotated down through the center of the casing and pushed to a depth of 6.9 m. The resistance to pushing the freeze pipe into place was minimal. Once the freeze pipe was in place, the 25 mm diameter copper inflow and outflow pipes were installed inside the steel freeze pipe, with a rubber seal at a depth of 2.6 m. The reservoir for liquid nitrogen therefore extended through the target freezing zone, from 2.6 m to 6.9 m. A back pressure valve was installed on the copper outflow pipe to allow for better control of the liquid nitrogen level in the freeze pipe reservoir. Installation of the freeze pipe was complete on May 29, 1995. Figure 6-9 shows a schematic of the freeze pipe installation.

6.5.2 Borehole Layout

On May 30, 1995, after the freeze pipe was in place, the casings for five sample boreholes were advanced at a radial distance of 0.56 m from the freeze pipe, to a depth of approximately 2.5 m. A hollow stem auger, with an outer diameter of 280 mm, was first advanced through the more dense sand to a depth of about 2.0 m and then the PVC casing, with an outer diameter of 330 mm, was pushed to approximately 2.5 m. Figure 6-10 shows a plan view of the freeze pipe and sample boreholes.

Two small diameter (64 mm) PVC casings were also installed at center to center radii of 0.56 m and 1.0 m from the freeze pipe for monitoring the temperature distribution within the target zone during freezing. The casings were installed by first drilling down to a depth of 3.5 m with A-rod drill stem and then pushing a 50 mm diameter steel pipe, with a cone tip designed to remain at the bottom of the borehole, to a depth of 8 m. A 25 mm diameter PVC casing was then installed through the center of the steel pipe to 8 m and the steel casing was removed. As shown in Figure 6-10, to avoid causing disturbance in the sampling zone, the boreholes for monitoring temperatures were installed at a radial distance of 0.28 m, or more, away from any of the boreholes where samples would be recovered.

A string of Resistance Temperature Devices (RTDs), spaced at regular intervals, was then lowered down each of the 25 mm diameter PVC casings. Once freezing commenced, ground temperatures were monitored using the RTD readings. Figure 6-10 shows the location of Boreholes RTD 2 and RTD 1 located at a 0.56 m and 1.0 m radius from the freeze pipe, respectively.

6.6 Ground Freezing at the Phase III Event Site

6.6.1 Initiation of Ground Freezing

Prior to commencing ground freezing, the average groundwater temperature measured in Boreholes RTD 1 and RTD 2 on June 1, 1995, was 35 °C. To cool the groundwater in the target zone, ice-chilled water was circulated through the copper lines in the freeze pipe. The cold water was circulated until the liquid nitrogen tank arrived on site, several days later; however, this process reduced the average groundwater temperature by only 1 °C. to an average of 34 °C.

Ground freezing commenced on June 7, 1995. Liquid nitrogen was circulated through the freeze pipe until June 27, 1995, when coring of the frozen sand began. The total freezing time was approximately 480 hours.

6.6.2 Consumption of Liquid Nitrogen

Due to the high groundwater temperature, it was necessary to circulate liquid nitrogen through the freeze pipe at a high flow rate to maintain liquid in the reservoir. The average liquid nitrogen consumption rate was approximately 159 m³/hr (equivalent gaseous volume). The flow of liquid nitrogen was interrupted on three occasions, due to site access problems associated with excessive rain, for approximately 11 hours or more each time. The rate of liquid nitrogen consumption during ground freezing is shown in Figure 6-11, for each of 5 tanks. The ordinate of Figure 6-11, shown as inches of liquid nitrogen, represents the volume of liquid nitrogen remaining in the tank, where the inches of liquid nitrogen are read from a dial gauge on the tank that has been calibrated to an equivalent gaseous volume of liquid nitrogen. The conversion rate for the liquid nitrogen tank used at the Phase III site was, on average, 329 m³/inch (equivalent gaseous volume).

6.6.3 Monitoring of Ground Temperatures During Freezing

Ground temperatures were monitored during the freezing process in Boreholes RTD 1 and RTD 2, at distances of 1.0 m and 0.56 m, respectively, from the freeze pipe, respectively. Figures 6-12 and 6-13 show the ground temperature profiles during freezing at the two borehole locations. The temperature data gathered during ground freezing is provided in Appendix D.

The high heat extraction requirements associated with the warm initial ground temperature, made it difficult to completely fill the freeze pipe reservoir with liquid nitrogen during the early stages of ground freezing. As shown in Figure 6-13 for RTD 2, the high thermal gradient evident on June 13 and 14, between about 4.3 m and 7 m in the target zone, indicated that the level of liquid nitrogen in the freeze pipe was likely at an average depth of about 4.3 m for approximately the first week of ground freezing. This resulted in slower growth of the frozen zone between depths of 2.5 and 4.3 m where only nitrogen gas was contained within the freeze pipe.

On June 27, 1995, near the completion of ground freezing, the ground temperatures in RTD 2 varied from about -3°C , at a depth of 2.4 m, to -25°C at a depth of 6.4 m. Comparison of Figures 6-12 and 6-13 also indicated that a significant temperature gradient of about $2^{\circ}\text{C}/\text{cm}$ existed between the freeze pipe (-196°C) and the unfrozen soil at the 1 m radius (10°C).

6.7 Comparison of Theoretical Predictions with Field Conditions

6.7.1 Growth of Frozen Radius

Based on the temperature measurements taken in Borehole RTD 2, at a distance of 0.56 m from the freeze pipe, the time at which the sand in the target zone became frozen was determined at each RTD depth. Figure 6-14 shows a comparison between the frozen

radius at each RTD depth, with two theoretical predictions for the growth of the frozen radius assuming the freeze pipe contained liquid nitrogen and gaseous nitrogen.

Figure 6-14 shows that the rate of freezing between depths of 3.4 and 6.9 m agrees on average with the theoretical prediction for liquid nitrogen as the coolant in the freeze pipe, while the freezing rate at depths of 2.4 to 2.9 m agrees reasonably well with the theoretical predictions for gaseous nitrogen as the coolant. This illustrates that the upper portion of the freeze pipe reservoir in the target zone likely contained gaseous nitrogen rather than liquid nitrogen during much of the time that ground freezing was carried out. A revised theoretical analysis was conducted assuming that the freeze pipe reservoir contained approximately 1/3 gaseous nitrogen and 2/3 liquid nitrogen, on average, during the freezing process. The revised theoretical prediction, given in Figure 6-15, shows better agreement with the average actual frozen radius.

6.7.2 Consumption of Liquid Nitrogen

In Figure 6-16, the actual consumption rate of liquid nitrogen during ground freezing is plotted against the predicted rate of consumption, assuming that the freeze pipe was completely full of liquid nitrogen in the target zone. The actual usage of liquid nitrogen fell below the predicted usage in the early stages of ground freezing. During this time, the warm initial ground temperatures resulted in phase change of the liquid nitrogen to gas in the freeze pipe during the first approximately 200 hours of ground freezing. After 200 hours of freezing, it was possible to maintain liquid nitrogen within the freeze pipe reservoir and the rate of consumption was increased to the predicted rate, as illustrated by the fact that the actual and predicted curves are nearly parallel. The actual total volume of liquid nitrogen used was about 65,000 m³ (equivalent gaseous volume), compared to the predicted total volume of 72,500 m³ (equivalent gaseous volume).

Figure 6-17 shows the revised theoretical analysis of the rate of liquid nitrogen consumption established based on assuming that the freeze pipe reservoir contained 1/3 gaseous nitrogen and 2/3 liquid nitrogen, on average, during the freezing process. Good agreement is shown between the actual data and revised theoretical prediction for the first 200 hours of freezing when the freeze pipe reservoir likely contained both gaseous and liquid nitrogen. After 200 hours of freezing, the rate of liquid nitrogen consumption increased to that predicted by assuming that the freezing pipe reservoir contained only liquid nitrogen, corresponding to the time period during which it was possible to maintain the freeze pipe reservoir full of liquid nitrogen.

6.8 Coring of In-situ Frozen Sand

After approximately 480 hours (20 days) of freezing, the temperature profile in Borehole RTD 2 indicated that the sand in the target zone was frozen at a radius of 0.56 m. Since the budgeted volume of liquid nitrogen had been consumed, on June 28, 1995, coring of the frozen sand commenced. Coring was complete by June 30, 1995.

A 200 mm diameter CRREL barrel was used to core the frozen sand at Boreholes FS4, FS5 and FS6, where the large diameter casing had been installed (see Figure 6-10). During coring of the frozen sand the CRREL barrel tended to diverge into the weaker (warmer) frozen sand. As a result of the steep temperature gradient within the frozen zone, the core barrel eventually moved out of the frozen sand during each run. Coring was then attempted with the 100 mm diameter CRREL barrel in Boreholes FS2 and FS3, where the large diameter casing had been installed. However, the smaller diameter barrel also eventually diverged out of the frozen zone. Frozen core sampling was also attempted at three locations between the cased sample boreholes and the freeze pipe at a radial distance of about 0.3 m from the freeze pipe. As shown in Figure 6-10, Boreholes FS52 and FS34 were advanced using the 100 mm inner diameter CRREL barrel and Borehole FS26 was advanced using the 200 mm inner diameter CRREL barrel.

Due to the difficulties with CRREL barrel alignment, the majority of the frozen core samples were obtained from depths of between 3 and 4 m. In total, 6.4 m of 200 mm diameter frozen core and 3.9 m of 100 mm diameter frozen core were recovered from the target zone. It should be noted that the 200 mm diameter frozen core yields three to four times as many triaxial specimens as the 100 mm diameter frozen core, since three to four adjacent specimens can be trimmed from the same depth interval.

During coring, the depth and sample condition of all the frozen cores were catalogued on site. The frozen core was extruded directly into plastic bags at the ground surface utilizing a hydraulic ram and placed into freezers containing dry ice. Immediately after coring was complete, the frozen samples, contained within the freezers, were driven back to the University of Alberta (U of A) where they were re-logged in a walk-in freezer and double-wrapped for storage prior to laboratory testing.

6.9 In-situ Frozen Core Quality

To establish detailed core catalogues of the in-situ frozen core samples obtained from the Phase III test site, the core was examined in the walk-in freezer, at a temperature of approximately -20°C , as follows:

- the core samples were checked for signs of frost heave or other disturbance;
- the ends of each segment of core were trimmed for moisture content and void ratio determination;
- several core samples were photographed;
- the depths of all fractures within each core run were recorded and an estimate was made of the number of specimens that could be trimmed for either triaxial or direct simple shear testing.

Void ratio estimates were made from 3 cm by 3 cm by 2 cm frozen cubes of sand trimmed from the ends of the in-situ frozen core. A list of the core samples recovered, with the estimated void ratios, is provided in Appendix D.

No sign of frost heave was noted in all but two of the in-situ frozen core samples examined. Thin ice lenses, of approximately 1 mm in thickness, were encountered in core samples FS26C3-1A and FS4C1-3B. In an attempt to identify the cause and possible extent of the ice lenses, the locations of these features were plotted with respect to the approximate progression of the 0 °C isotherm, as shown in Figure 6-18. Specimen FS26C3-1A was located at a depth of 4.42 m and a radius of 0.30 m from the freeze pipe, while Specimen FS4C1-3B was located at a depth of 3.86 m and a radius of 0.56 m from the freeze pipe. The progression of the frozen column of sand, shown in Figure 6-18, was estimated based on RTD data and the theoretically predicted growth of the frozen radius, assuming gaseous nitrogen at the top of the freeze pipe reservoir and liquid nitrogen at the bottom of the freeze pipe reservoir. The times at which each tank of liquid nitrogen was consumed and then refilled are also shown in the figure.

Two potential causes of the ice lens features were examined. These included: the presence of sand pockets with a very high fines content that may have either caused water to be locally attracted to the freezing front or may have inhibited pore water expulsion, and changes in the rate of freezing, corresponding to changes in the rate of liquid nitrogen supply to the freeze pipe reservoir, that may have affected the direction of pore water flow. As indicated in Figure 6-18, the locations of the two ice lenses detected do not appear to correlate with the periods of time during which liquid nitrogen was not supplied to the freeze pipe due to delivery delays. However, the location of the 0 °C isotherm at the time of the liquid nitrogen supply delays, shown in Figure 6-18, was not known accurately and was estimated based on limited RTD data and theoretical predictions. Therefore, it is possible that delays in the liquid nitrogen supply contributed to slowing of the freezing rate beyond that which normally occurs as the frozen radius becomes larger.

Arvidson (1973) demonstrated through extensive laboratory testing of Devon Silt and Ottawa sand, that there exists an effective overburden stress, P_o , for a given soil which defines the boundary between pore water being attracted to or expelled away from the freezing front during freezing. According to Arvidson's work, at stresses greater than P_o , pore water pressure is positive, resulting in expulsion of pore water in advance of the freeze front; at stresses less than P_o , pore water pressure is negative and pore water is sucked towards the freezing front. As shown in Figure 6-19 established for Devon Silt (after Arvidson, 1973), the P_o intercept, defined by the curve for changes in pore water volume of a freezing soil versus effective stress ($\Delta V - \sigma'$), is also a function of the applied temperature gradient. In the figure, the dashed line was obtained from freezing the silt under a step temperature of -5°C , with a corresponding overall temperature gradient of approximately $0.9^\circ\text{C}/\text{cm}$, and the solid line represents data from silt frozen under a step temperature of -10°C , with a corresponding overall temperature gradient of about $1.6^\circ\text{C}/\text{cm}$.

Figure 6-19 shows that, for a given overburden stress, when the applied freezing step temperature was doubled, the pore water that was being sucked into the sample under a step temperature of -5°C , was expelled in advance of the freezing front under a step temperature of -10°C . At the Phase III test site, the overburden stress at a given depth was constant, however, as the freezing front progresses through the sand, both the rate of freezing and the fines content varied. Therefore, if the rate of freezing in the field was reduced sufficiently either due to a delay in refilling the liquid nitrogen tank or the tendency for the rate of freezing to slow down as the frozen radius grew larger, pore water may have been attracted to the freeze front. This could have resulted in the growth of a thin ice lens.

Figure 6-20 shows the approximate progression of the frozen radius at a depth of 4.5 m below the ground surface, based on the progression of the 0°C isotherm estimated from the RTD data shown in Figure 6-18. Approximating the frozen radius versus time curve

with linear segments, the freezing rates between the time periods when temperatures of 0 °C were measured at the RTD locations, were estimated as follows:

Time increment (hrs)	Approximate Freezing Rate (cm/hr)
0 to 135	0.37
135 to 161	0.14
161 to 233	0.18
233 to 351	0.12

Both the measured growth of the frozen radius and the theoretical relationship between frozen radius and time, shown in Figure 6-18, clearly indicate that the progression of the freezing front slows as the frozen radius increases.

For comparison, the progression of the zero degree isotherm in the laboratory tests conducted by Arvidson on Devon silt, approximated by a linear segment between 75 and 150 minutes of freezing time, was 3.0 cm/hr, for the tests conducted under a step temperature of -10 °C, and 1.85 cm/hr, for tests conducted under a step temperature of -5 °C. In these tests, when the rate of progression of the zero degree isotherm was decreased by about 60 %, the direction of pore water flow was reversed from expulsion to suction. As indicated by the approximate freezing rates followed at the Phase III test site, the rate of freezing between 161 and 233 hrs was about 50 % slower than the initial rate of freezing between 0 and 135 hrs of freezing. It may be that this decrease in freezing rate was enough to alter the direction of pore water flow in the vicinity of the frozen core specimen FS4C1-3B..

Arvidson's work also indicated that the P_0 intercept is a function of grain size distribution and soil permeability, as well as the temperature gradient. Both the slope of the $\Delta V-\sigma'$ curve and the P_0 intercept are significantly affected by the fines content where, for a given overburden stress, if the fines content increases sufficiently, the pore water behaviour changes from expulsion to attraction at the freeze front.

As shown in Figure 6-3, the fines content varied considerably with depth at the Phase III test site, with a range of 6 % to 20 % in the target zone. The fines contents determined for undisturbed Specimens FS4C1-3B and FS26C3-1A, in which ice lenses were encountered, were 7.4 % and 10.6 %, respectively. Although these fines contents were not excessively high, they represent average values for 1120 g samples and it is possible that local concentrations of fines existed near the locations of the ice lenses. The grain size data for Specimens FS4C1-3B and FS26C3-1A is presented in Appendix D.

To determine whether or not an ice lens would grow under a slower freezing rate in Phase III sand, an additional frost heave test was conducted under the freezing rate of approximately 0.15 cm/hr that existed in the field near the radius where the ice lens was encountered in Specimen FS4C1-3B. Considering that the fines content may have been higher near the ice lens encountered, fines obtained from a bulk sample of Phase III sand were added to the sand from frozen core FS26C3-1, resulting in a fines content of 18 %. A frost heave test was then conducted on this sand, under a freezing rate that eventually dropped to about 0.15 cm/hr over a period of 378 hrs. The overburden pressure used for the test was 55 kPa.

Figure 6-21 shows a plot of the water intake and heave that occurred during the frost heave test. After 378 hrs, the thickness of the frozen sand had reached 6.38 cm and, although the sample appeared to have taken in 18.6 cc of water, careful visual inspection of the frozen section of the sample showed that no ice lens had formed. Later examination of the frost heave cell indicated that a tiny leak existed in the frost heave cell sidewall, accounting for at least a portion of the water taken in by the sample. Given the diameter of the frost heave cell, the heave that would have occurred in the absence of pore water expulsion, due to a 9 % pore water volume expansion during freezing of 6.38 cm of sand, would have been at least 3 mm. Since the measured heave was only 0.2 mm, it can be concluded that pore water expulsion actually occurred over a significant period of the frost heave test and therefore that the leak was likely responsible for much of the apparent water intake.

Since an ice lens did not form during the long-term frost heave test under the slower freezing rate, it is not likely that the slower freezing rate which occurred due to the high initial groundwater temperature was responsible for the isolated ice lens feature. Moreover, if the overall rate of freezing in the field became slow enough to encourage ice lens growth, as the frozen radius reached some $R(t)$, ice lens features would have been encountered in most of the frozen core samples that intersected the cylindrical freezing front at that radius. Since the progress of the $0\text{ }^{\circ}\text{C}$ isotherm in the field was estimated based on limited RTD data, detailed information regarding the effect of halting the supply of liquid nitrogen for 11 hours or more during freezing on the growth of the frozen radius was not available. Therefore, it is possible that the freezing rate slowed down over that period of time to a value much smaller than 0.15 cm/hr , which may have resulted in temporary attraction of pore water to the freezing front, thereby causing a small ice lens to form. The possibility that pore water expulsion was inhibited, due to bitumen in the tailings sand or local pockets of sand with very high fines contents that created a damming effect, also cannot be ruled out as a factor contributing to the formation of the ice lenses encountered in Specimens FS26C3-1 and FS4C1-3.

The frozen core samples in which ice lenses were encountered were also viewed under the scanning electron microscope (SEM) to look for evidence of thinner ice lens features that were not visible to the naked eye. Photograph 6-1 shows an SEM image of frozen Specimen FS26C3-1 and Photograph 6-2 shows an SEM image of frozen Specimen FS4C1-3. Although visual inspection of these frozen core specimens indicated a thin ice lens present in each core, the SEM images did not show any additional structural separation of sand grains that would indicate disturbance due to frost heave.

It should be emphasized that in Chapter 5, it was demonstrated that the alignment of clay minerals, shown in SEM images of frozen Syncrude tailing sand, was not an artifact of the freezing process. Moreover, according to the Alberta Department of Energy, Oil Sands and Research Division (1995), the Mature Fine Tailing (MFT) at Syncrude is characterized by a flocculated clay structure that is determined by the water chemistry of

the tailings during deposition. SEM images of untreated MFT (Alberta Department of Energy, Oil Sands and Research Division, 1995), indicate a similar clay mineral structure to that encountered in the frozen core samples obtained from the Phase III test site at Syncrude. Photo 6-3 shows an example SEM image obtained of the MFT structure. Taking into consideration that the fines content in the MFT is considerably higher than the fines within the frozen core samples, comparison of Photos 6-1 and 6-3 indicates similar parallel alignment of clay minerals.

6.10 Comparison of In-situ Frozen Core and Geophysical Logging Void Ratios

The void ratio estimates obtained from the in-situ frozen core specimens, trimmed for triaxial testing, were compared with void ratio estimates based on geophysical logging conducted in two boreholes, advanced within a 5 m radius of the freeze pipe. Figure 6-22 shows that, on average, the void ratios determined independently from the in-situ frozen core and the geophysical logging show good agreement. However, the geophysical logging shows considerably more variation with depth, most likely due to the higher frequency at which void ratio measurements were taken. During geophysical logging, bulk density measurements, from which the void ratios were determined, were taken every 20 mm, whereas the interval of void ratio determination from the frozen core was significantly greater. Based on the agreement between the frozen core void ratio measurements and the void ratios determined by geophysical logging at the same depths, it was concluded that the majority of the in-situ frozen core was of high quality and could be considered as undisturbed.

6.11 Conclusions

The feasibility studies conducted prior to undertaking ground freezing at the Phase III test site, indicated that in-situ ground freezing could be used to recover undisturbed samples.

Both the evaluation of frost heave potential based on mineralogical analysis of the fines contained within the same sand obtained during Phase I and the laboratory frost heave tests conducted on the Syncrude sand with a high fines content, showed that disturbance of the soil due to frost heave or to the excess 9 % pore water volume freezing in place would be negligible.

A freezing system was designed to freeze a 4 m long target zone between depths of 3 m and 7 m below the ground surface. The actual growth of the frozen radius was reasonably well predicted using the theoretical equations for heat extraction provided by Sanger and Sayles (1979) and assuming that liquid nitrogen was contained within the freeze pipe reservoir in the target zone at all times during freezing. Better agreement between field data and the theoretical predictions was achieved by assuming that the freeze pipe reservoir contained approximately 1/3 gaseous nitrogen and 2/3 liquid nitrogen, during the first 200 hours of freezing, and then that the freeze pipe was full of liquid nitrogen thereafter.

Dry coring of the in-situ frozen sand with both a 100 mm and 200 mm inner diameter CRREL core barrel was an effective means of obtaining the undisturbed samples. In total, 6.9 m of 200 mm diameter frozen core and 3.9 m of 100 mm diameter frozen core were recovered from the Phase III test site. Since 3 to 4 triaxial specimens can be trimmed at a given depth from the 200 mm diameter core, the total frozen core recovered was approximately equivalent to 25 m of 100 mm diameter core.

Only two of the in-situ frozen core samples showed evidence of disturbance due to the formation of thin ice lenses. Based on the result of a frost heave test carried out under a freezing rate 0.15 cm/hr, these features do not appear to have been caused by the slower growth of the frozen radius caused by the warm groundwater temperature. However, the effect of halting the supply of liquid nitrogen, for 11 hours or more during freezing, on the growth of the frozen radius was unknown, therefore, it is possible that the freezing rate slowed down over that period of time to a value much smaller than 0.15 cm/hr. This

may have resulted in temporary attraction of pore water to the freezing front, thereby causing a small ice lens to form. The possibility that pore water expulsion was inhibited, due to bitumen in the tailings sand or local pockets of sand with very high fines contents that created a damming effect, also cannot be ruled out as a factor contributing to the formation of the ice lenses encountered in Specimens FS26C3-1 and FS4C1-3.

The void ratios measured from the in-situ frozen core, trimmed for triaxial testing, showed very good agreement with the void ratios measured independently by geophysical logging, conducted in boreholes located at a radial distance of 5 m from the freeze pipe. Therefore, the work undertaken at the Phase III test site showed that in-situ ground freezing could be used to recover undisturbed samples of sand containing up to 22 % fines, with the approximate mineral composition shown in Table 6-1, in the presence of a very high initial average ground temperature of 35 °C.

6.12 References

- Alberta Department of Energy, Oil Sands and Research Division. 1995. Advances in Oil Sands Tailings Research. Fine Tailings Fundamentals Consortium, Volumes 1 to 4, 296 pp.
- Arvidson, W. D., 1973. Water Flow Induced by Soil Freezing. M.Sc. Thesis, University of Alberta, Edmonton, AB, 128 pp.
- Byrne, P. M., Robertson, P. K., Plewes, H. D., List, B. R. and Tan, S. (1995). Liquefaction Event Planning, 49th Canadian Geotechnical Conference, Vancouver, British Columbia.
- Davila, R. S., Segó, D. C., and Robertson, P. K., 1992. Undisturbed Sampling of Sandy Soils by Freezing, 45th Canadian Geotechnical Conference, Toronto, October 26-28, 10 p.

- Hofmann, B. A., Robertson, P. K., Segoo, D. C., Fear, C. E., Lefebvre, M., Natarajan, S.,
Cyre, G., Woeller, D., Hughes, J. and Gräpel, C. K., 1996a. CANLEX Phase III -
Full Scale Liquefaction Test: Site Characterization. 49th Canadian Geotechnical
Conference, St. John's, Newfoundland, pp. 579-586.
- Hofmann, B. A., Robertson, P. K., Gräpel, C. K., Cyre, G., Lefebvre, M., and Natarajan,
S., 1996b. CANLEX Phase III - Full Scale Liquefaction Test: Instrumentation
and Construction. 49th Canadian Geotechnical Conference, St. John's,
Newfoundland, pp. 587-596.
- Sanger, F. J. and Sayles, F. H., 1978. Thermal and Rheological Computations for
Artificially Frozen Ground Construction. International Symposium on Ground
Freezing. March 8-10, Bochum. pp. 311-337 or Engineering Geology, Vol. 13.
pp. 311-337.

Table 6-1: Mineralogy of Fines Fraction Determined for Phase I Test Site.

Sample #	Surface Area Silt Fraction 2-74 μm (m^2/g)	Surface Area Clay Fraction < 2 μm (m^2/g)	Clay Content as a % of fines (%<2 μm)	Silt Content as a % of fines (%< 74 μm)
28.7 m	11	108	10	14.4
31.7 m	17	159	8	12.2
34.8 m	14	138	9	11.4

Sample #	Clay Mineralogy* (<2 μm)	Silt Mineralogy* (2-74 μm)
28.7 m	Kt(60), Mi(26), Qtz(14)	Kt(5), Mi(tr), Fd(5), Qtz(90)
31.7 m	Kt(64), Mi(26), Qtz(10)	Kt(5), Mi(tr), Fd(5), Qtz(90)
34.8 m	Kt(63), Mi(25), Qtz(12)	Kt(5), Mi(tr), Fd(10), Qtz(85)

* Note: estimate of amount based on area of the major x-ray reflection (in percent)
Kt = kaolinite, Mi = mica, Fd = Feldspar, Qtz = quartz

Table 6-2: Input Parameters for Prediction of Freezing Process

Parameter	Value
Initial Ground Temperature	35 °C
Temperature of Liquid Nitrogen	-196 °C
Temperature of Gas Nitrogen	-60 °C
Unfrozen Thermal Conductivity	1.45 W/m ⁰ K
Frozen Thermal Conductivity	2.8 W/m ⁰ K
Unfrozen Heat Capacity	3.25 MJ/m ³ °K
Frozen Heat Capacity	2.16 MJ/m ³ °K

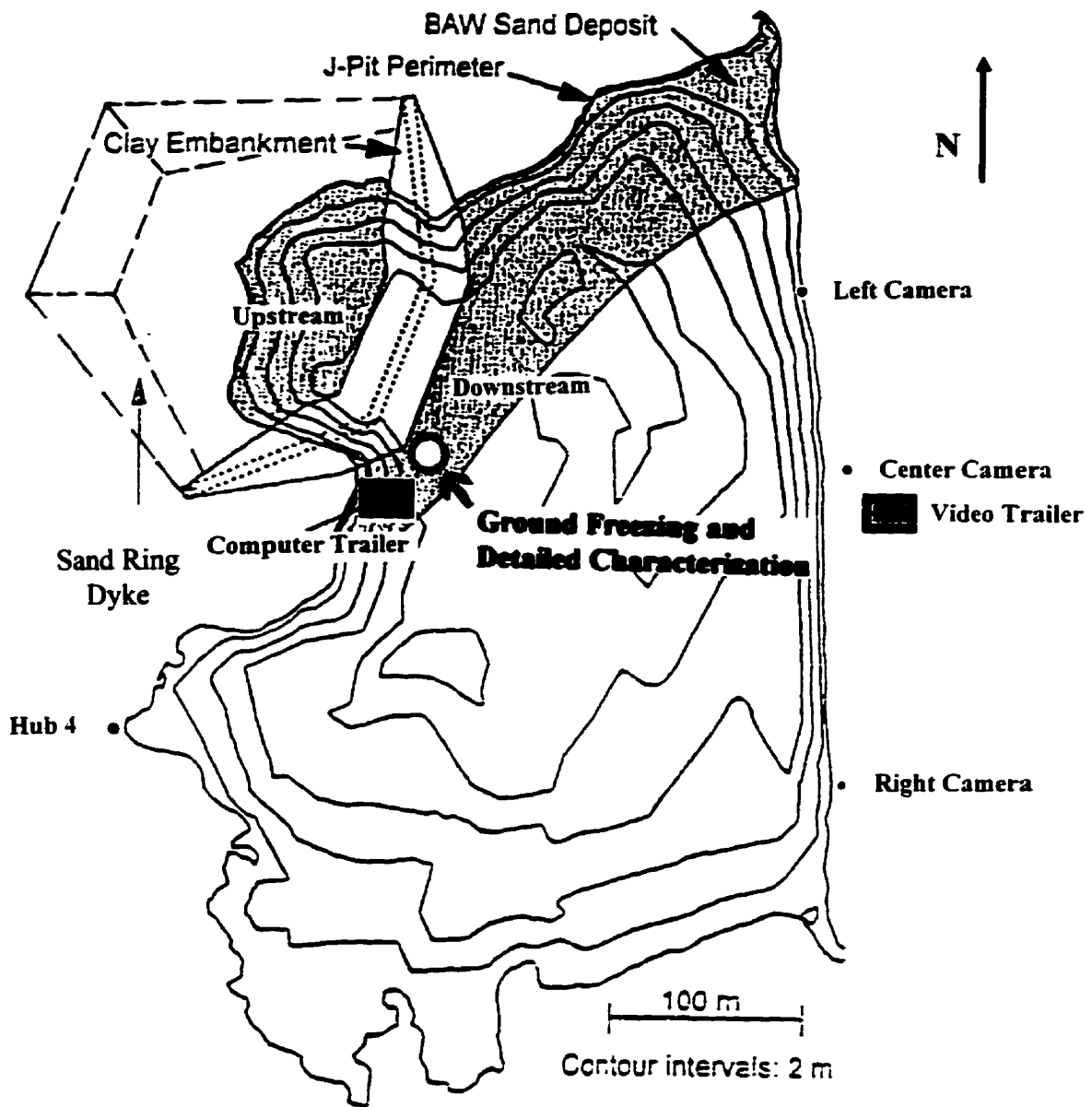


Figure 6-1: Phase III Test Site

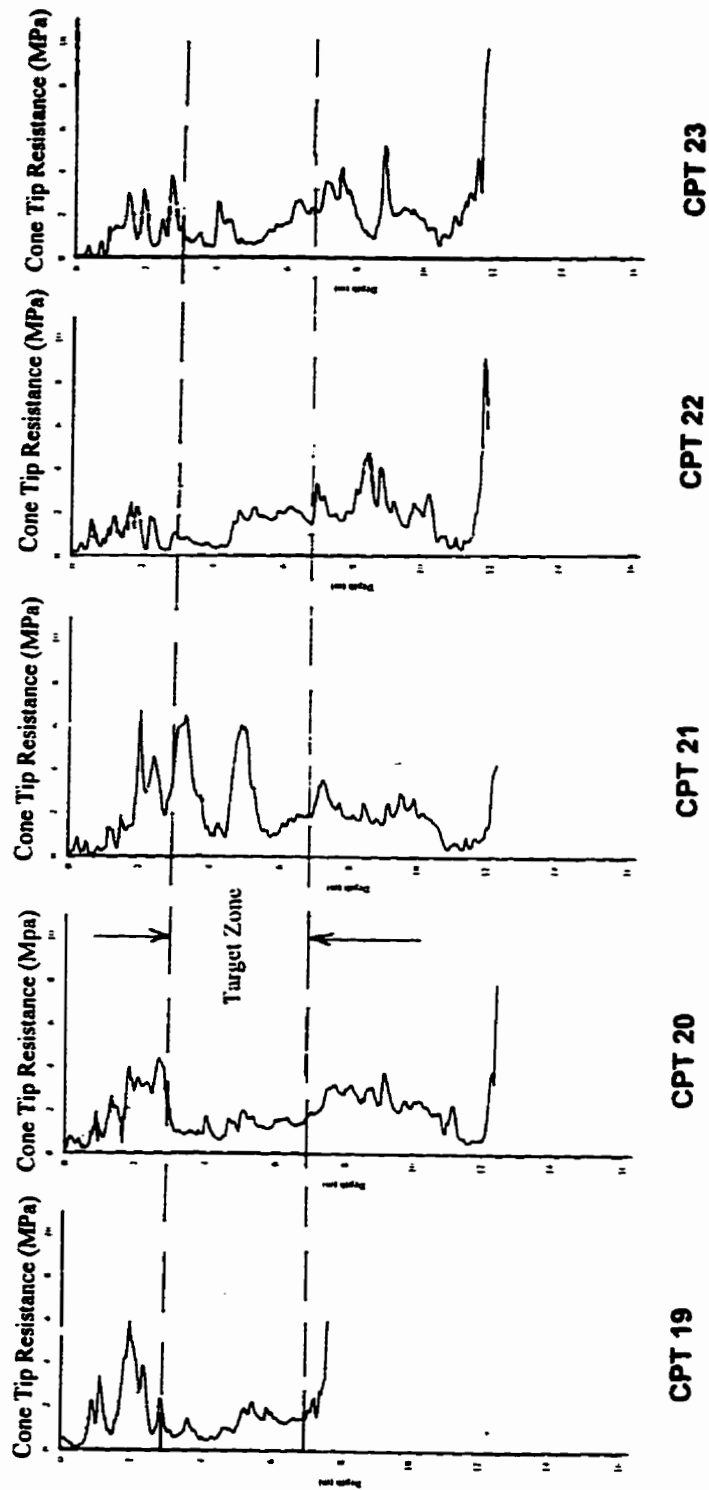


Figure 6-2: Cone Penetration Test Profiles in Detailed Characterization Zone

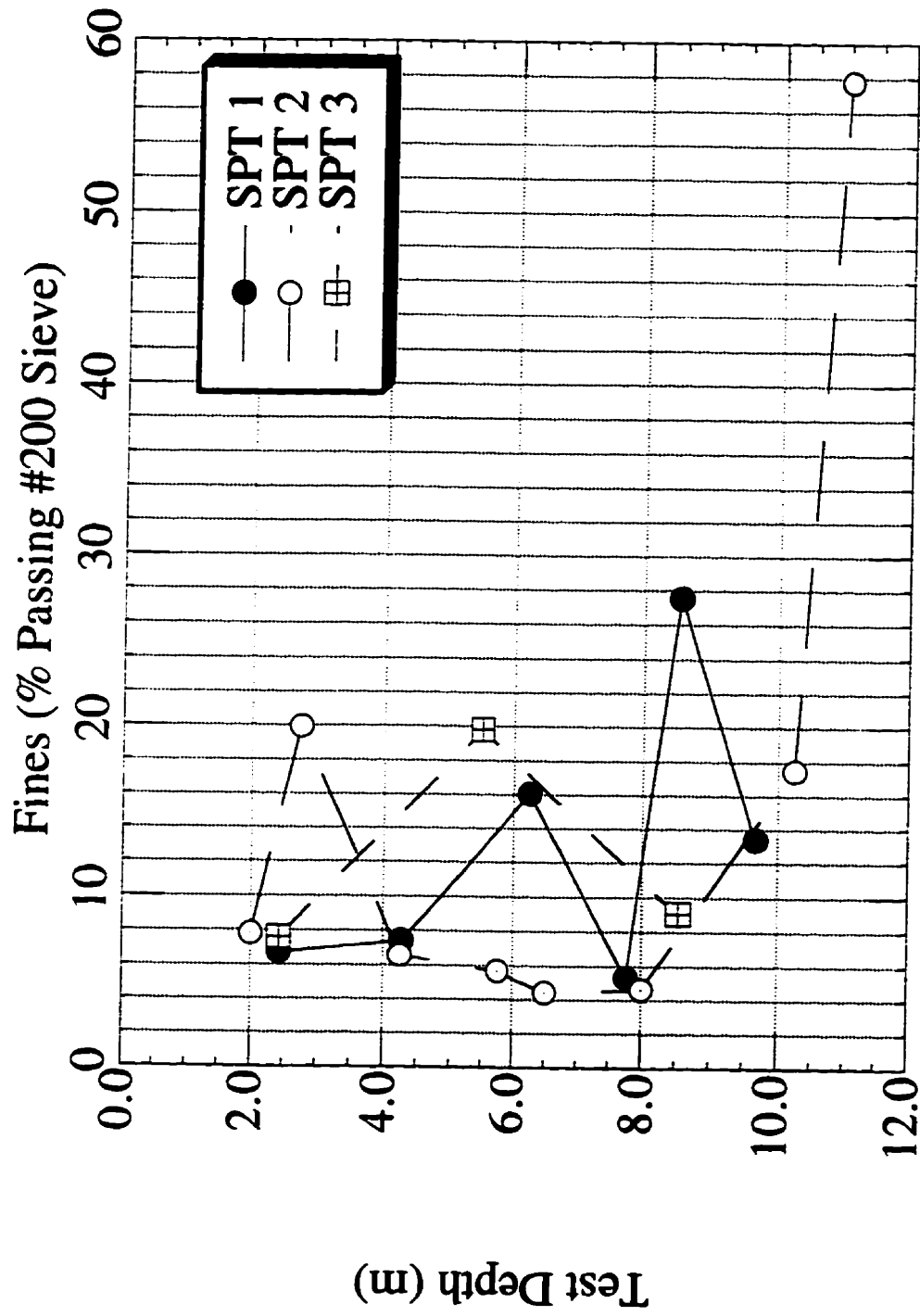


Figure 6-3: Fines Content Determined from SPT Samples in Detailed Characterization Zone

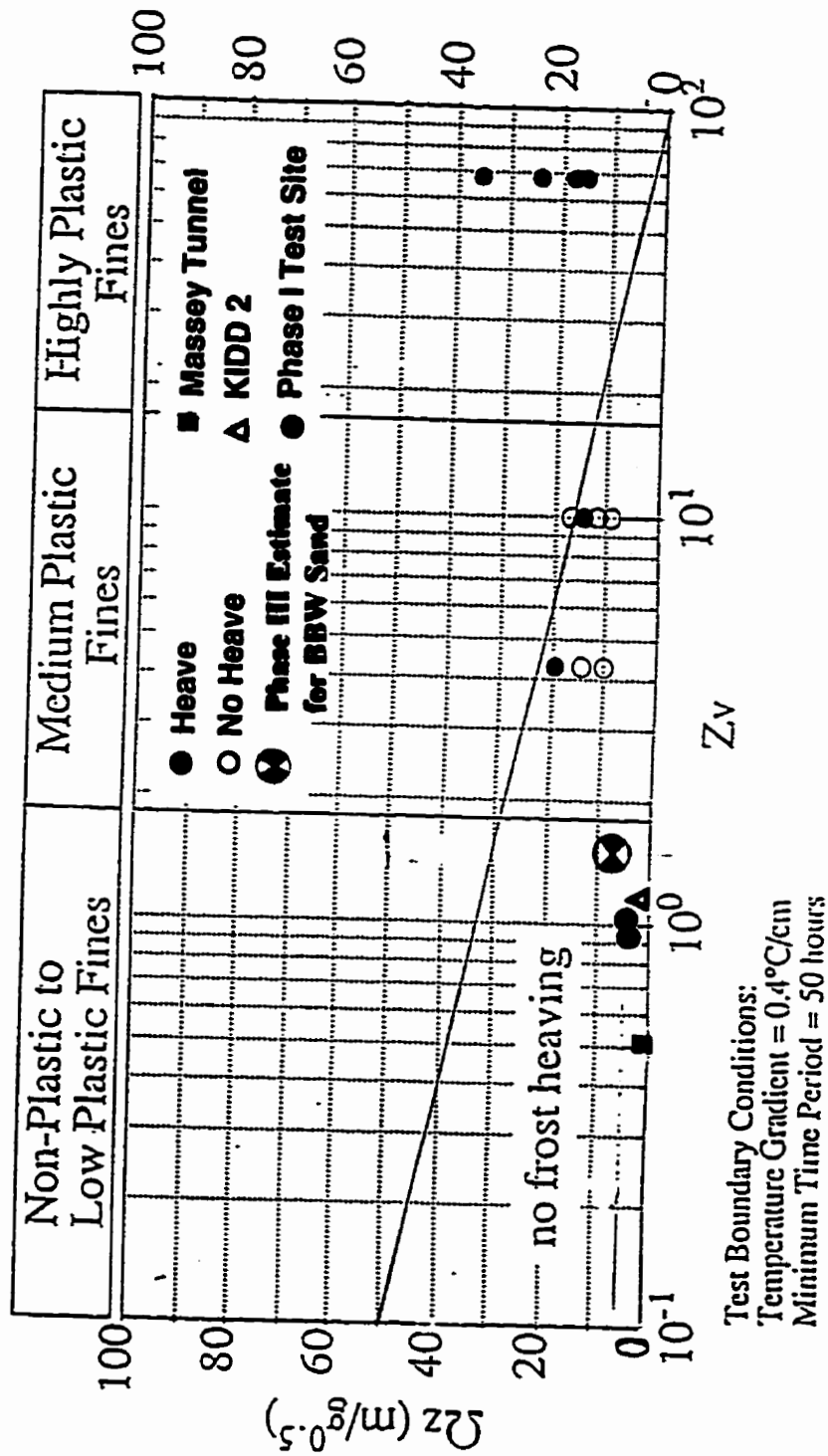


Figure 6-4: Surface Area Criteria Plot for Evaluation of Frost Heave Susceptibility (after Davila et al., 1992)

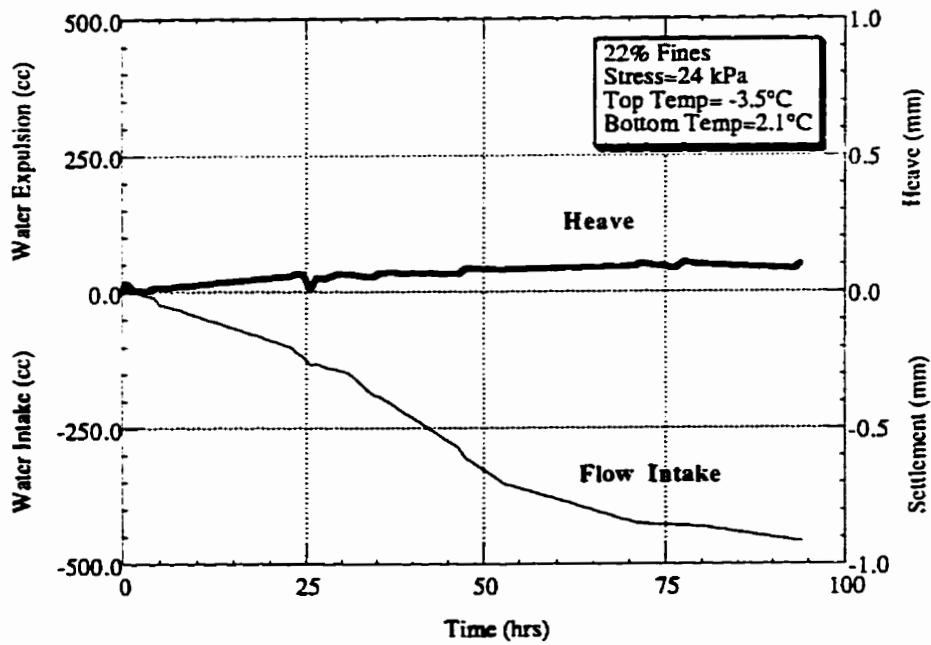
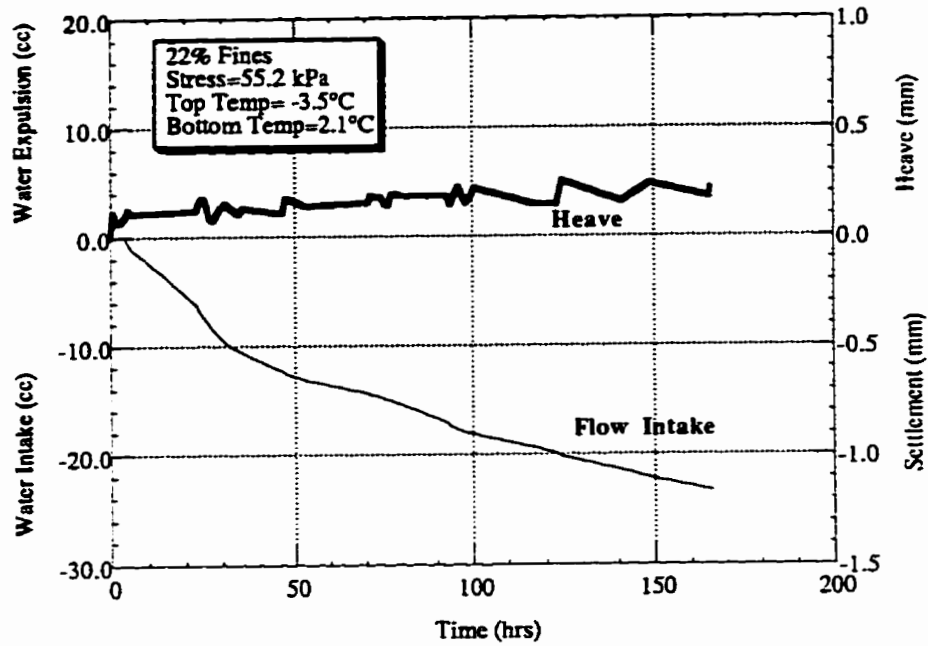


Figure 6-5: Frost Heave Test Results for Phase III Sand with 22 % Fines

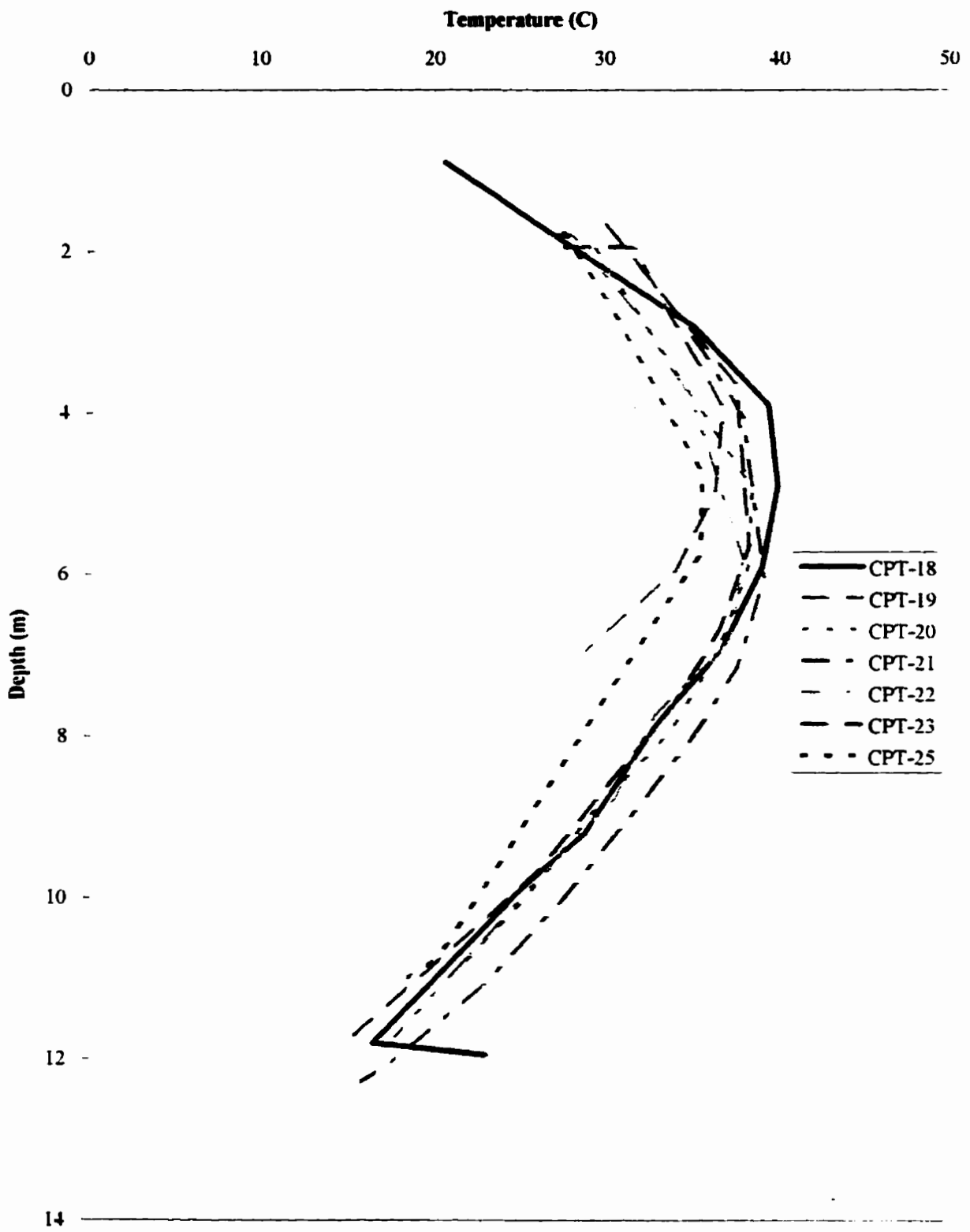


Figure 6-6: Ground Temperature Prior to Conducting *In-Situ* Ground Freezing

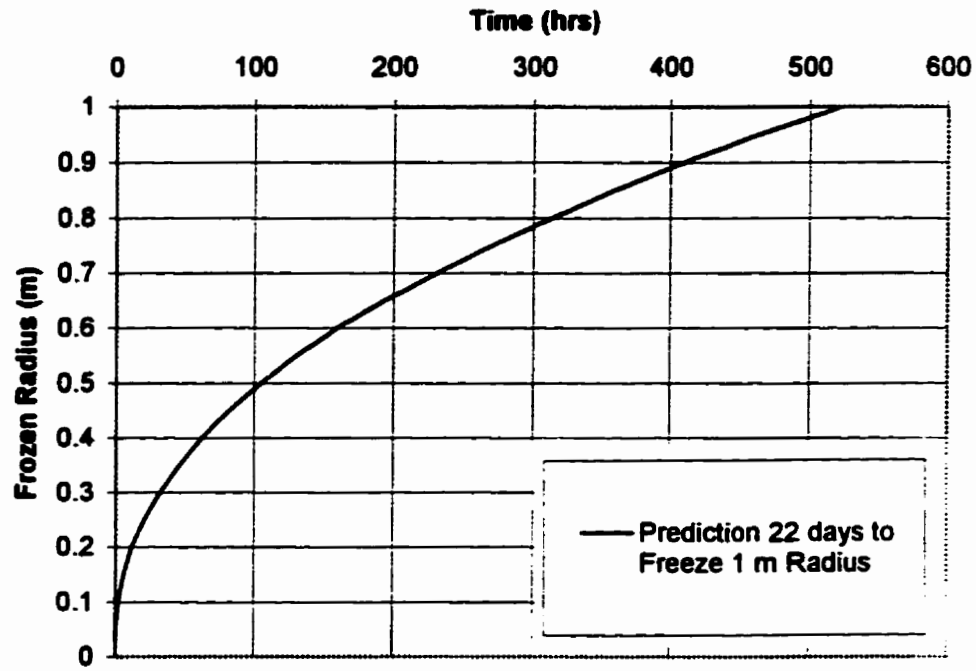


Figure 6-7: Prediction of Growth of Frozen Zone

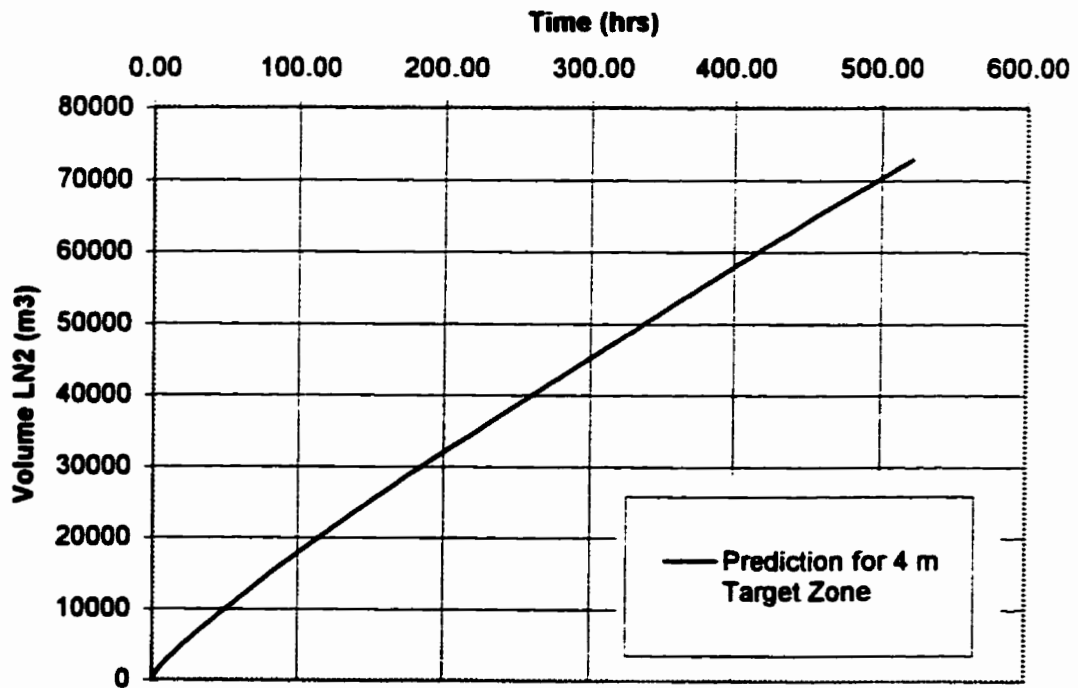


Figure 6-8: Prediction of Volume of Liquid Nitrogen

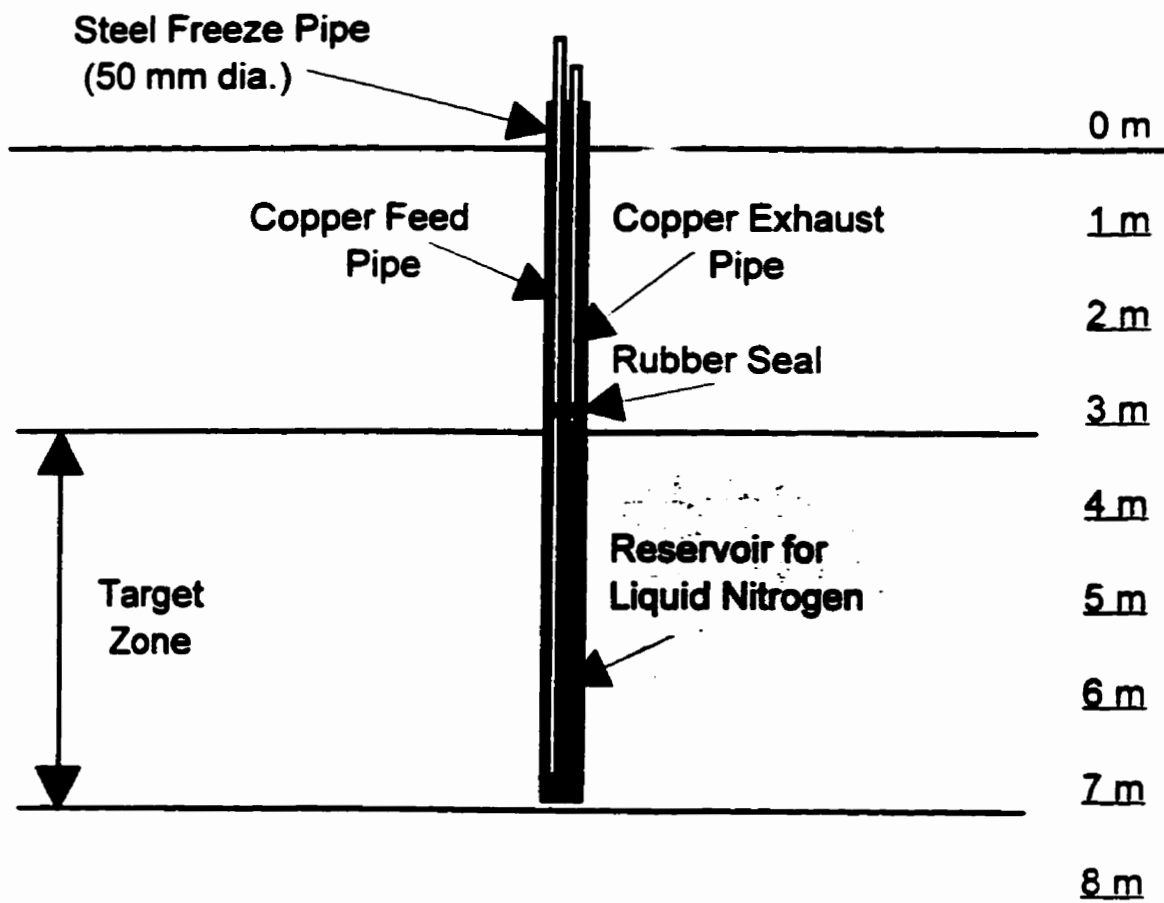


Figure 6-9: Schematic of Freeze Pipe Installation

Scale: 1:15

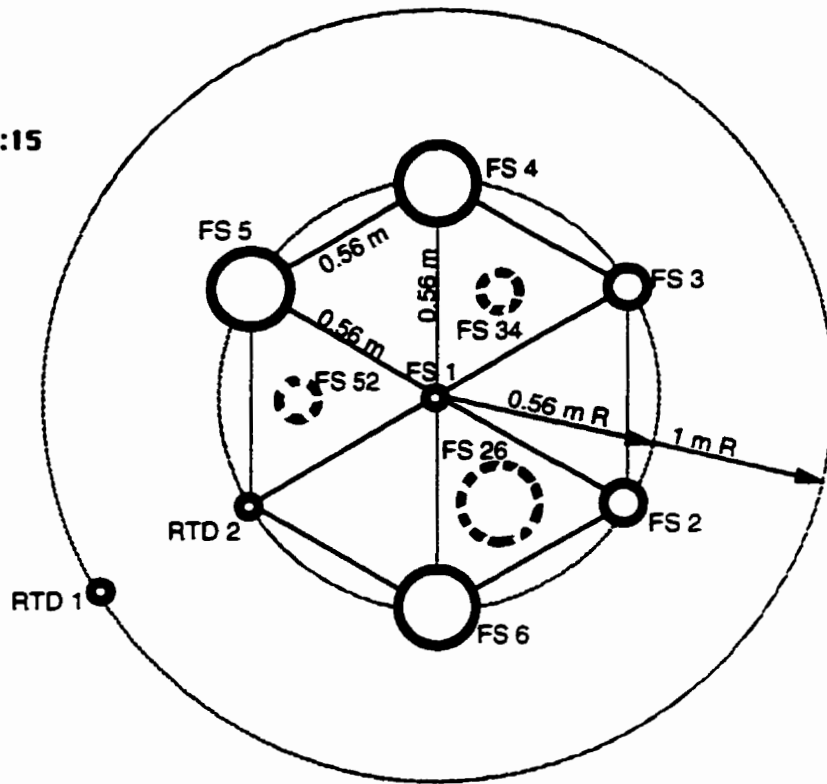


Figure 6-10: Layout of Freeze Pipe and Sample Boreholes.

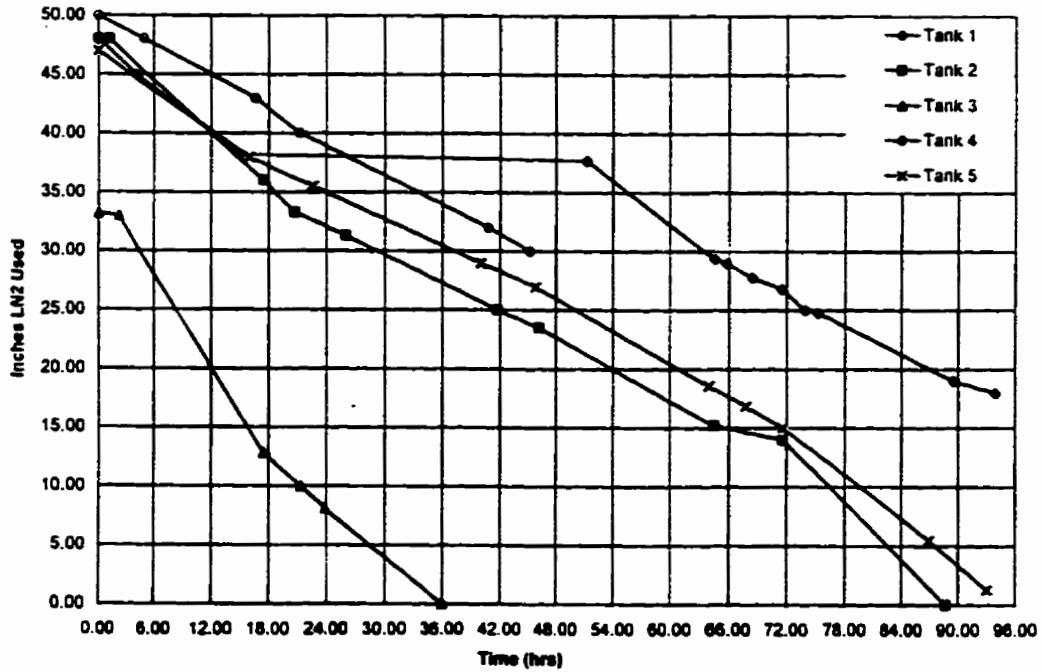


Figure 6-11: Actual Liquid Nitrogen Consumption at Phase III Test Site

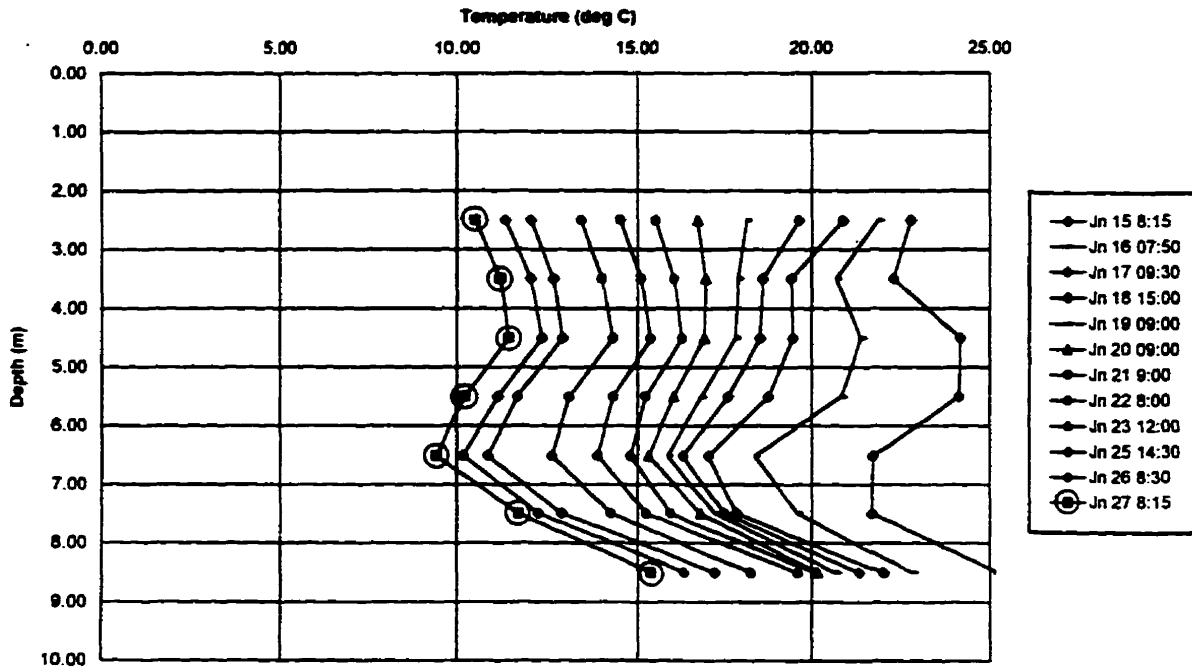


Figure 6-12: RTD 1 Temperature Measurements at 1.0 m during Ground Freezing

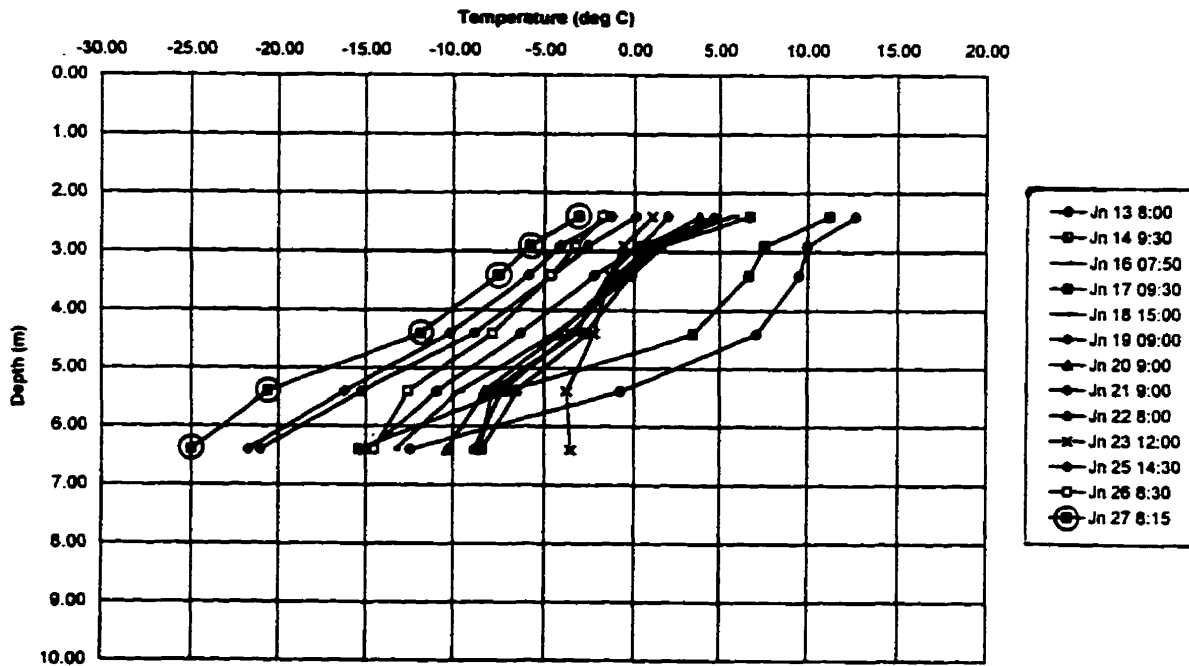


Figure 6-13: RTD 2 Temperature Measurements at 0.56 m during Ground Freezing

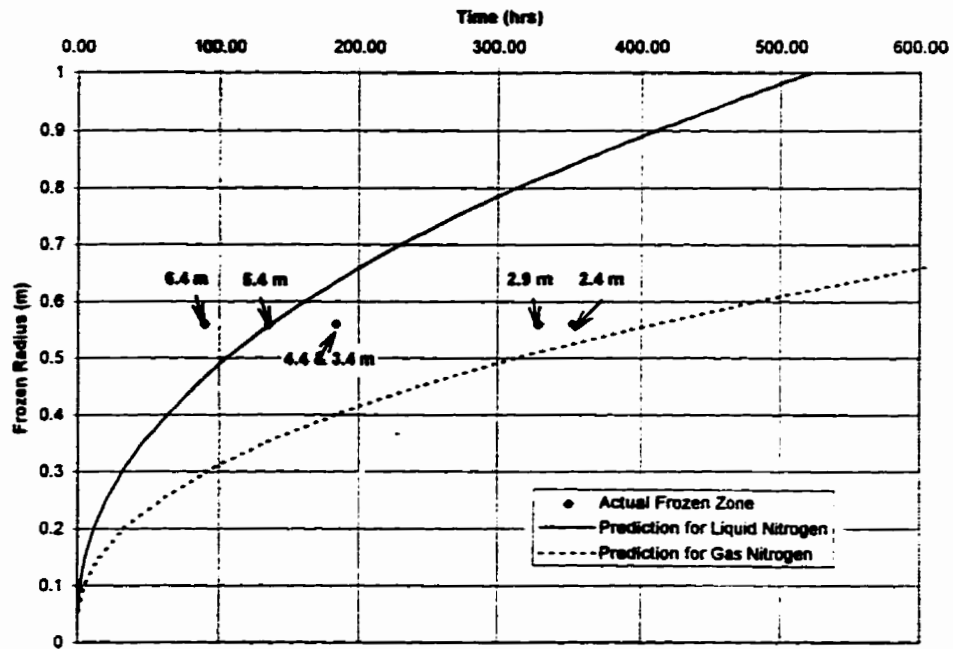


Figure 6-14: Comparison of Actual Growth of the Frozen Radius with Predictions for Gaseous Nitrogen and Liquid Nitrogen in Freeze Pipe Reservoir

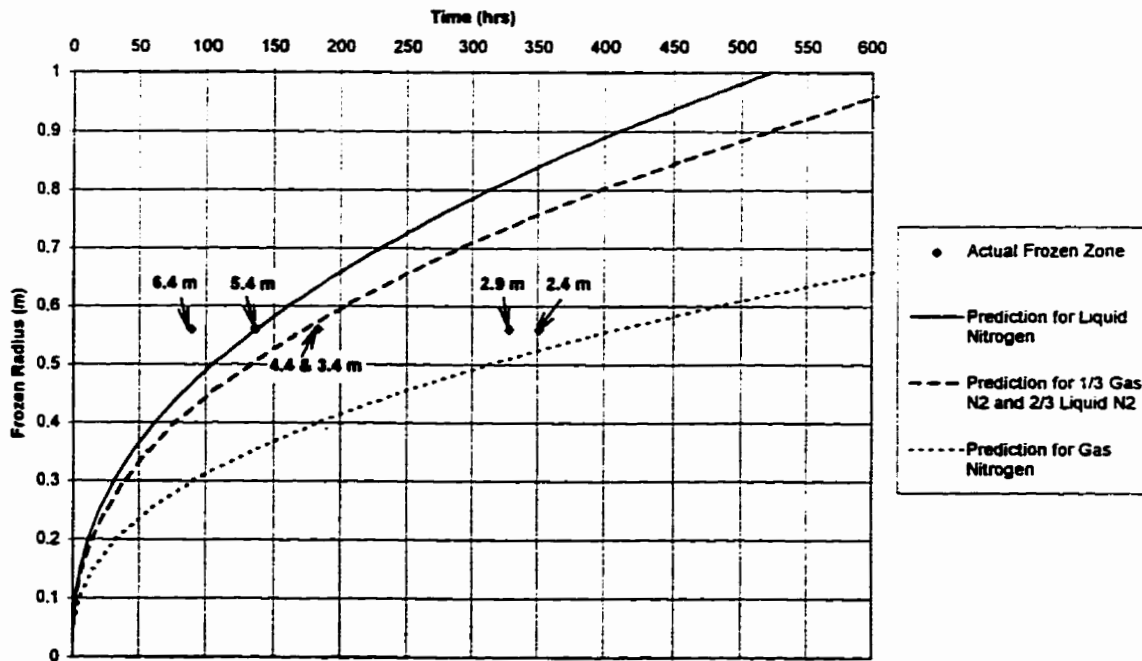


Figure 6-15: Comparison of Actual Growth of the Frozen Radius with Prediction for 1/3 Gaseous Nitrogen and 2/3 Liquid Nitrogen in Freeze Pipe Reservoir

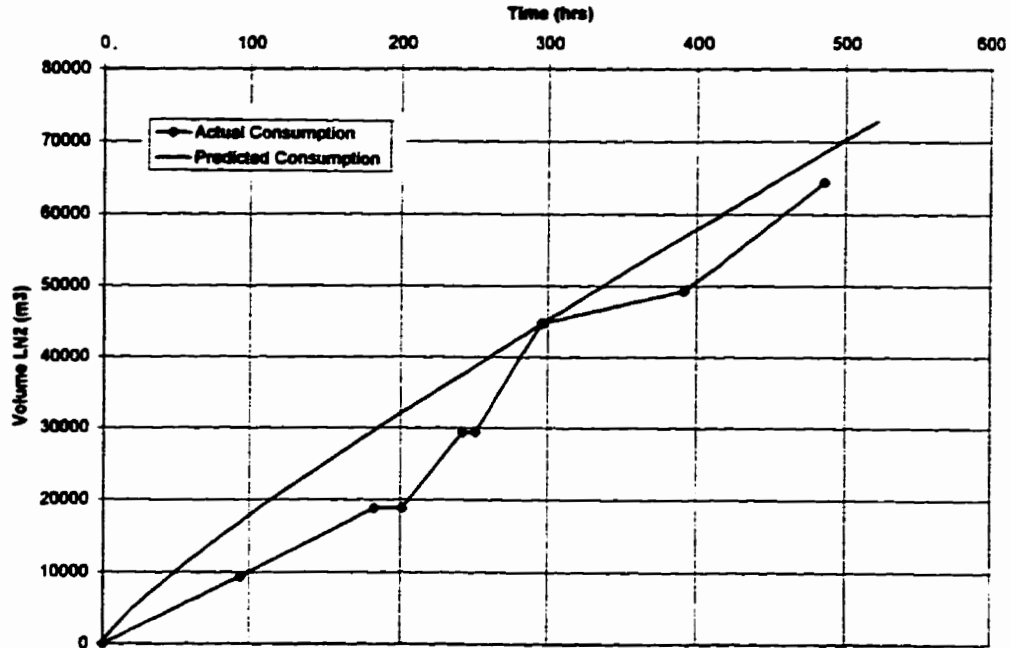


Figure 6-16: Comparison of Actual Liquid Nitrogen Consumption with Predictions for Liquid Nitrogen in Freeze Pipe Reservoir

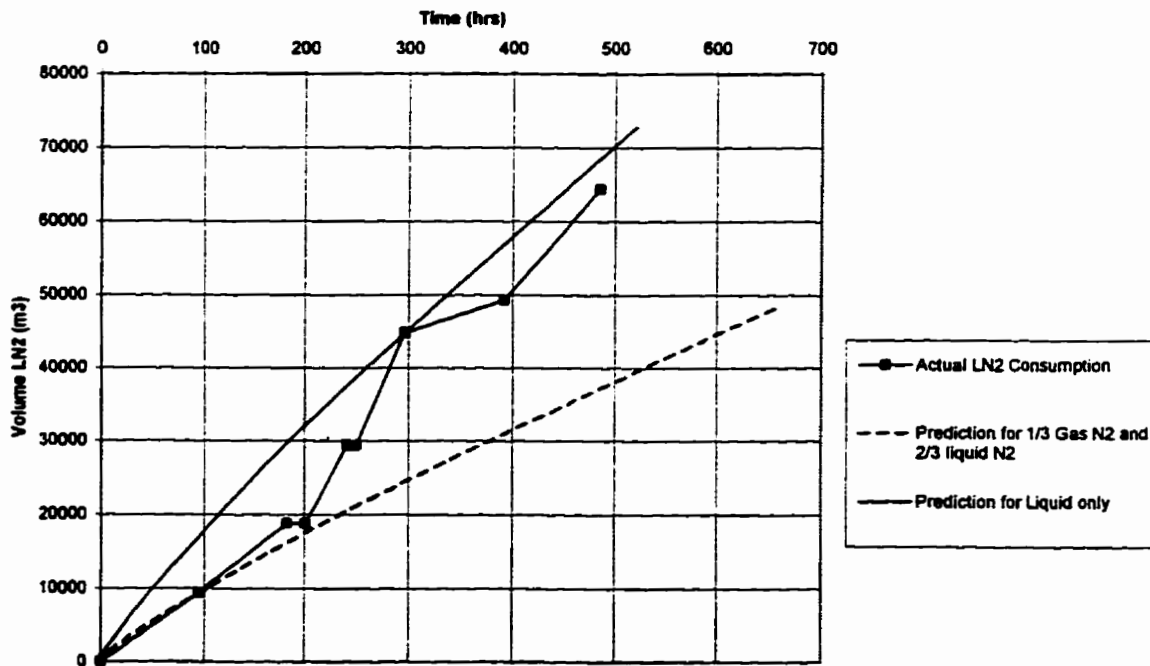


Figure 6-17: Comparison of Actual Liquid Nitrogen Consumption with Prediction for 1/3 Gaseous Nitrogen and 2/3 Liquid Nitrogen in Freeze Pipe Reservoir

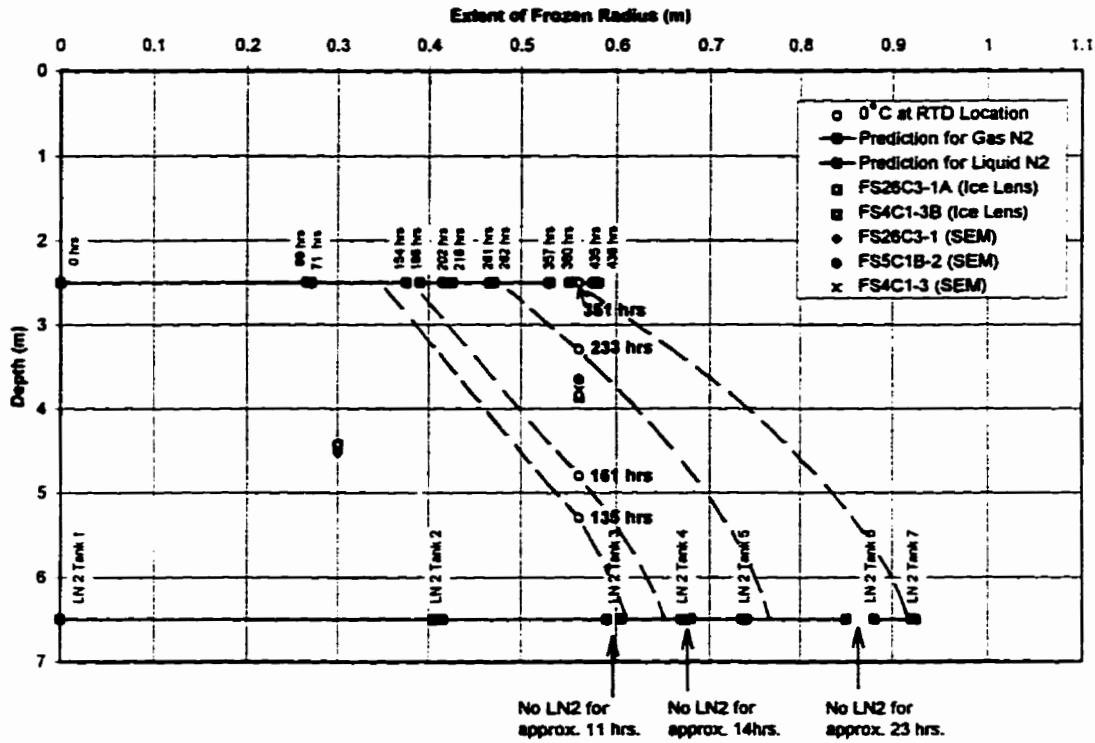


Figure 6-18: Estimated Progression of the Freezing Front at the Phase III Test Site

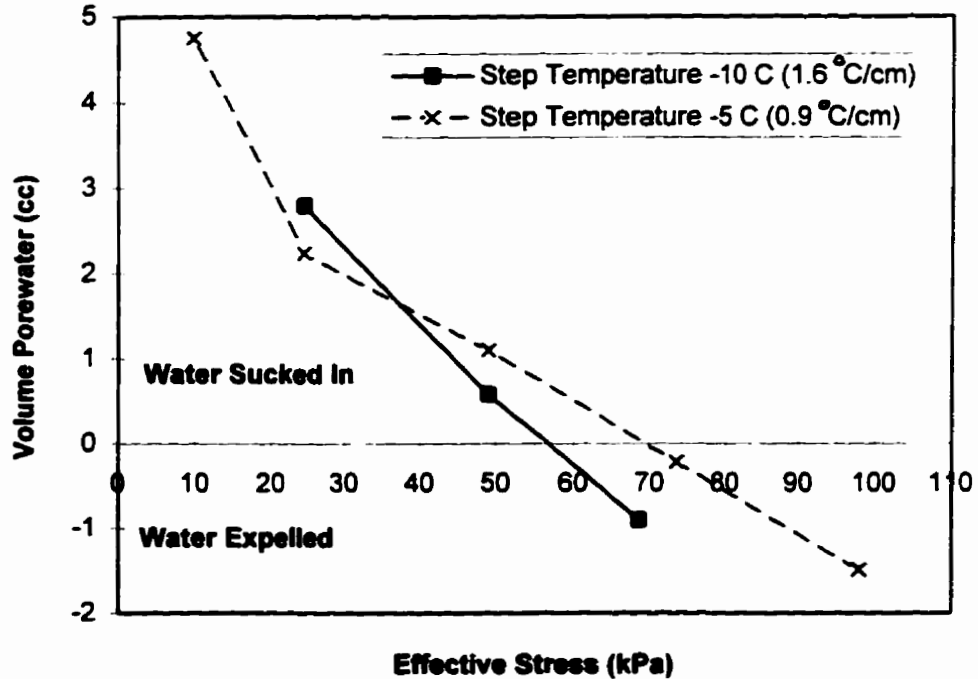


Figure 6-19: Porewater Attraction and Expulsion During Freezing as a Function of Effective Stress and Applied Step Temperature

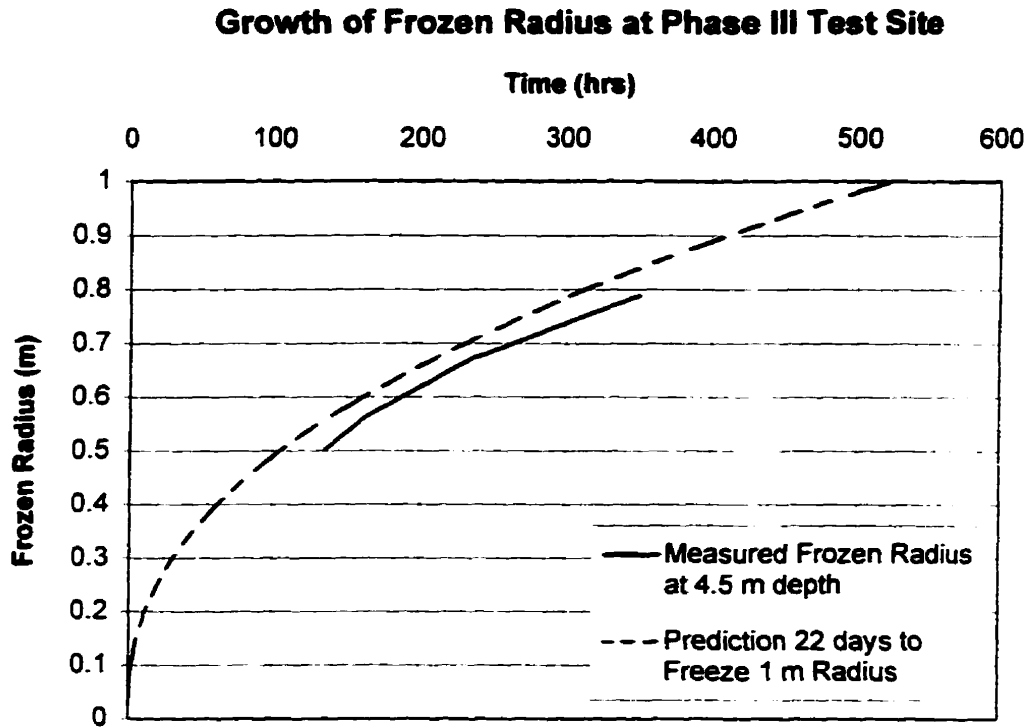


Figure 6-20: Comparison of Estimated Actual Progression of the Freezing Front at the Phase III Test Site with the Theoretical Prediction

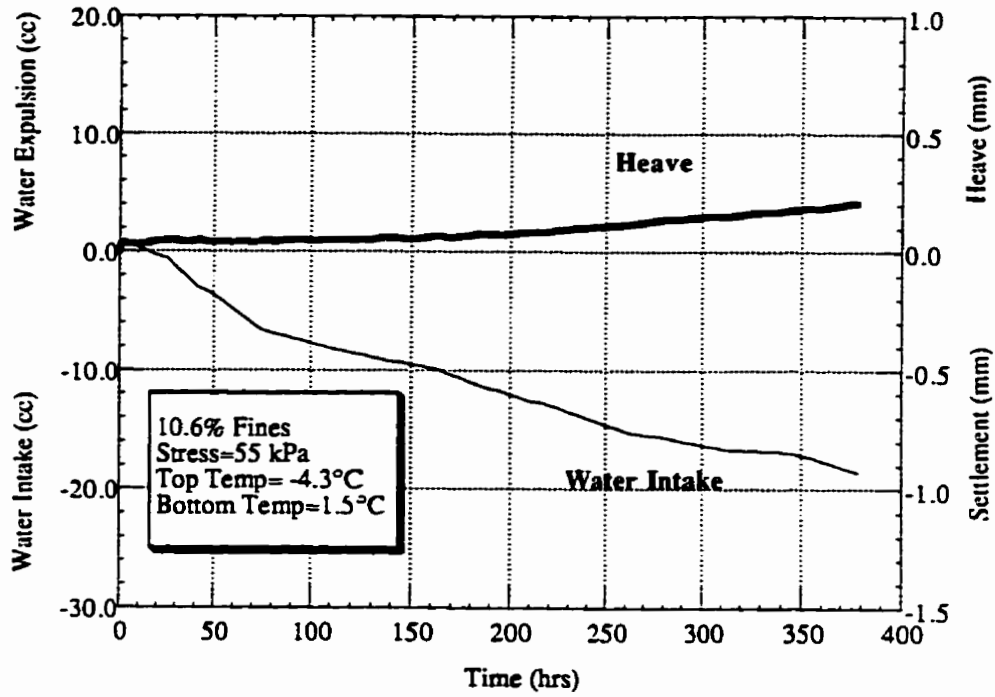


Figure 6-21: Frost Heave Test Results for Sand from Specimen FS26C3-1 with Fines Added.

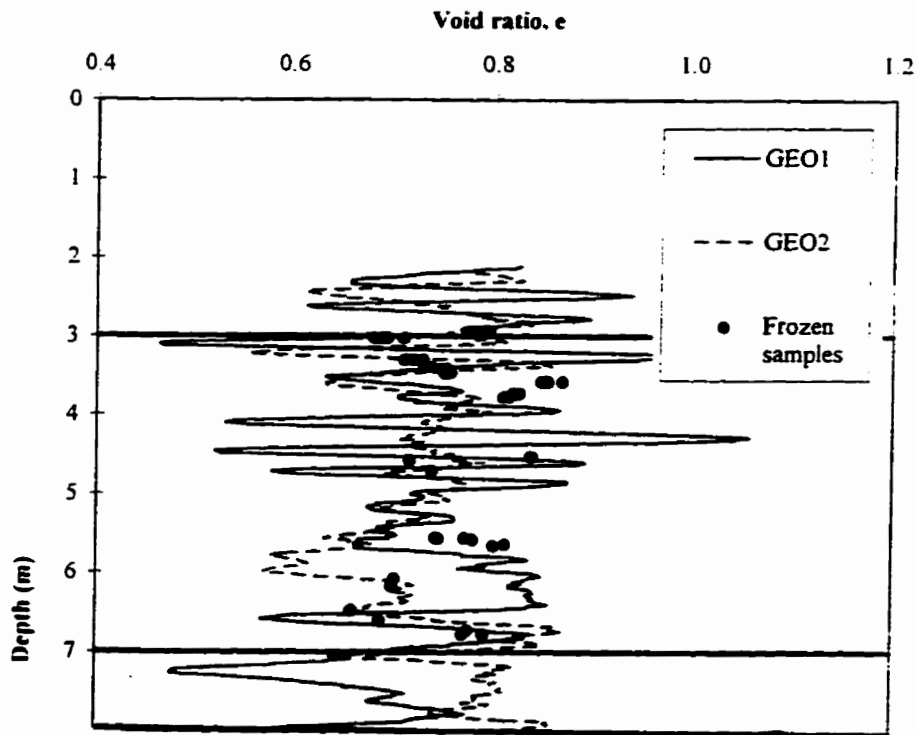
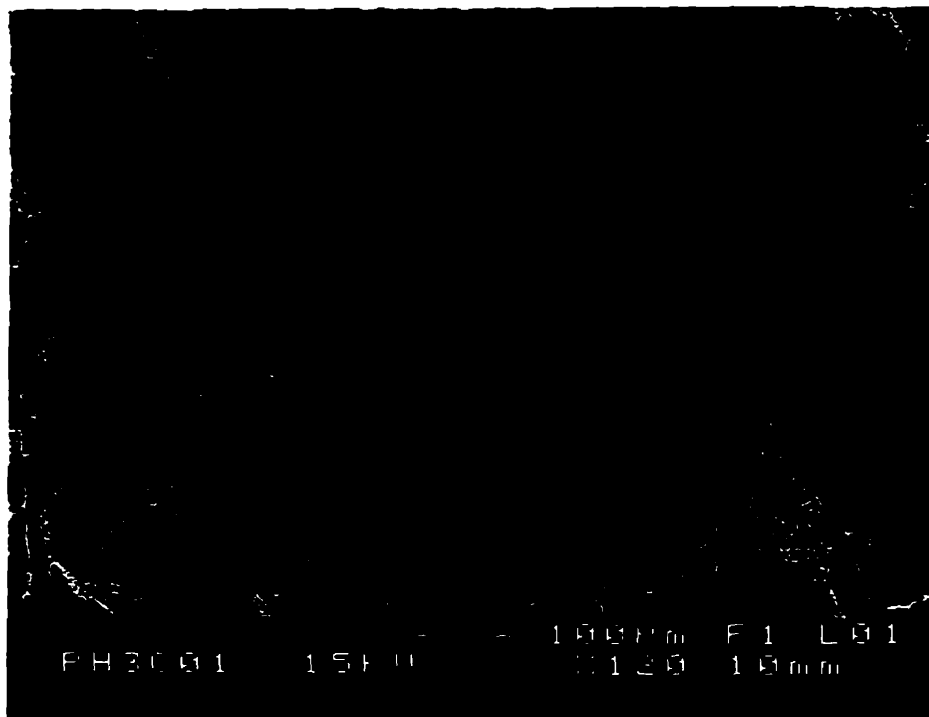
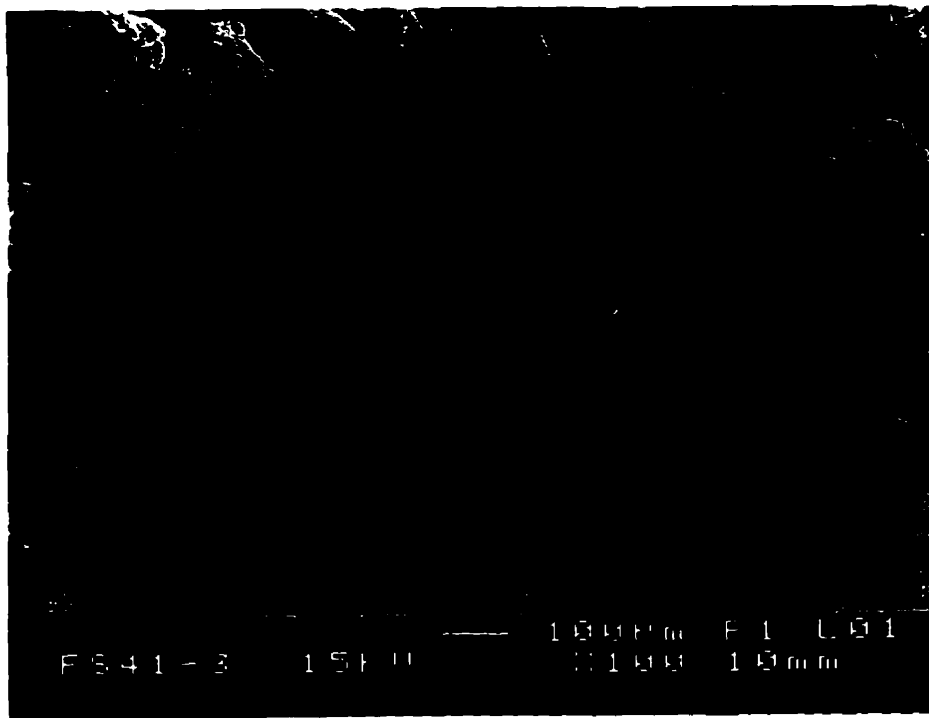


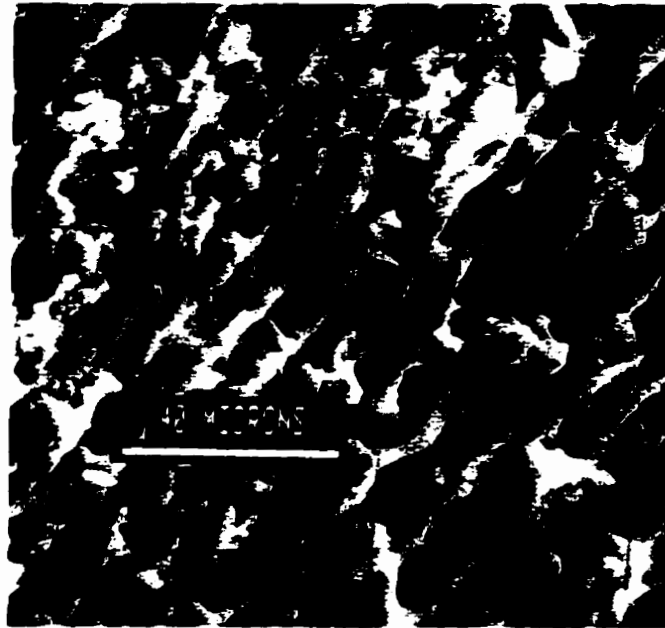
Figure 6-22: Comparison of In-Situ Void Ratios Determined from Frozen Core and Geophysical Logging at the Phase III Test Site



Photograph 6-1: SEM Image of In-Situ Frozen Specimen FS26C3-1



Photograph 6-2: SEM Image of In-Situ Frozen Specimen FS4C1-3



Photograph 6-3: SEM Image of Clay Particle Alignment Found in MFT (after Alberta Department of Energy, Oil Sands and Research Division, 1995)

Chapter 7.0 Thawing Protocol for Undisturbed In-Situ Frozen Specimens

7.1 Introduction

Undisturbed samples of loose, saturated sand have been obtained successfully by Yoshimi et al. (1978), Konrad (1990), Sego et al. (1994), and Hofmann et al.(1995) utilizing in-situ ground freezing. Evaluation of the liquefaction potential of the sand deposit from which undisturbed samples have been recovered may be undertaken by allowing the specimens to thaw under controlled conditions in the laboratory and then conducting shear tests for evaluation of the in-situ response of the sand to various loading conditions. At sites where Fixed Piston or tube samples of sand are recovered, they are usually frozen on site in a controlled manner to avoid disturbance associated with transportation of the samples from the field to the laboratory. Tube samples that have been frozen on site, although often more disturbed than in-situ frozen specimens, must also be thawed carefully in the laboratory to prevent further disturbance.

Yoshimi et al. (1978), Singh et al. (1982), Seed et. al. (1982), and Konrad and St-Laurent (1995) have shown that the undrained static and/or cyclic shear strength of sand was not affected by a freeze-thaw cycle, provided that disturbance did not occur due to impeded drainage during freezing. However, possible disturbance due to thawing was not addressed by these researchers.

To correctly evaluate the liquefaction potential based on undisturbed samples of a sand deposit obtained by in-situ ground freezing, it is extremely important to preserve the undisturbed nature of the specimens while thawing and handling them in the laboratory prior to testing. Ideally, the in-situ conditions that existed in the ground prior to freezing and sampling of a sand deposit should be restored if samples are to be considered truly

undisturbed. This includes preservation of the void ratio, fabric, structure, stress history and degree of saturation, during thawing and handling of specimens. Both the in-situ drainage conditions and degree of saturation should be considered as boundary conditions since these affect the development of pore pressure and/or volume change. Therefore, to evaluate the liquefaction potential at the current state, laboratory tests should be designed to evaluate the behaviour of the sand under expected loading conditions while maintaining boundary conditions that are similar to those that existed in-situ.

At the time that this thawing protocol study was being undertaken, four relatively loose sand deposits had been investigated for the Canadian Liquefaction Experiment (CANLEX). Two man-made sites were located in hydraulically placed loose sand deposits, at Syncrude Canada Ltd. (SCL), and two natural sites were located in the lower mainland of the Fraser River delta. The characteristics and depositional history of these deposits differed significantly as described by Hofmann, et al. (1994a, 1995) and presented in Chapters 4, 5 and 6 of this document.

Once laboratory testing of these specimens commenced, it became evident that many of the specimens were not saturated in-situ and that the procedures required to avoid disturbance during thawing and handling of these specimens was sensitive to the nature of the sand and the in-situ stresses. Therefore, a thaw protocol study was undertaken to examine the most appropriate method of thawing undisturbed frozen sand samples, that would minimize disturbance of the in-situ void ratio and fabric of the specimens. This chapter describes the thaw protocol study undertaken.

The thaw protocol evaluation included a theoretical evaluation of the stress states in specimens thawed unidirectionally under the in-situ stress conditions and those thawed unidirectionally under a small effective stress, of about 20 to 30 kPa, and then consolidated to the in-situ effective stress once thawing was complete. Conditions imposed during thawing by researchers in the past have included either: subjecting frozen

specimens to a small effective stress and allowing them to thaw multidirectionally, with access to water at both ends as the temperature warms to that of the room or, immediately subjecting frozen specimens to the stress conditions that existed in-situ and then thawing them unidirectionally, with access to water at the end where thawing commences, under the same temperature gradient under which they were frozen. Therefore the laboratory thaw protocol study included an evaluation of which of these two thawing techniques resulted in the least disturbance. The results obtained from the laboratory study, conducted on both reconstituted and undisturbed specimens, to evaluate the void ratio changes associated with these two thawing techniques are presented. The response of several undisturbed specimens, obtained from the CANLEX Phase I test site, to undrained triaxial compression and triaxial extension tests are also presented.

7.2 Freezing Process

It is important that the mechanisms invoked during freezing of a soil be understood since they must be reversed under similar boundary conditions during thawing. The conditions required for carrying out in-situ freezing without causing disturbance are described in detail by Hofmann et al. (1994a). The freezing process was also described in detail in Chapter 2, however, some aspects will be reviewed here.

When soils freeze, disturbance of the in-situ void ratio or fabric may result from either pore water freezing in place and undergoing a 9 % volume expansion when freezing is undertaken too rapidly, or due to the formation of ice lenses in frost heave susceptible soils. As the freezing front progresses through soil, the conditions which develop near the freezing front depend upon a number of factors. Water may either be expelled away from or attracted to the freezing front, depending upon the soil type, stress level, and rate of freezing (McRoberts and Morgenstern, 1975; see Chapter 2). In fine grain soils, such as clay or silt, water tends to be attracted to the freezing front while in coarse grain soils, such as sand or gravel, water tends to be expelled in advance of the freezing front.

In sands the mineralogy and chemistry are such that attractive forces between soil particles and water molecules are extremely weak. Less energy is required to expel the excess 9 % pore water volume than to move apart soil grains to accommodate an increase in volume. Therefore, as the freezing front progresses through sandy soil, 9 % of the free pore water volume is expelled away from the freezing front. Provided that drainage around the zone in which in-situ ground freezing is being undertaken is unimpeded by physical constraints, and that the soil is frozen at a rate which is slow enough compared to the permeability of the soil to allow for expulsion of pore water, there is little or no disturbance of the in-situ void ratio or fabric.

The most effective method of undertaking in-situ ground freezing, without causing disturbance of the void ratio or fabric, involves unidirectional freezing from a central freeze pipe through which liquid nitrogen is circulated. A 1 m radius column of sand is frozen and continuous core samples are recovered around the freeze pipe at a radius of about 0.6 m where the freezing gradient is approximately 0.40 °C/hr. This method, which allows for unimpeded drainage of pore water in advance of the freeze front, was used at each of the CANLEX test sites as described in detail by Hofmann et al. (1994a; see Chapters 4, 5 and 6). The quality of the in-situ frozen samples and the methods used to trim specimens for laboratory testing are also presented by Hofmann et al.(1994a, 1994b and 1995).

7.3 Disturbance during Thawing

7.3.1 Thawing Methodology

To avoid disturbance during the thawing process, the sand must be allowed to recover the excess 9 % pore water volume that was expelled during freezing and the in-situ stress condition should be fully restored such that the in-situ void ratio and soil fabric remain unchanged. Laboratory testing conducted by Konrad and St-Laurent (1995) on frozen undisturbed samples indicated that, provided that the water intake during thawing is

identical to the water expelled during freezing, the small strain characteristics, and therefore the soil structure, established by undrained load cycles and shear wave velocity measurements are preserved.

Singh et al. (1982) showed that specimens thawed under the stresses and pore water pressure that existed prior to freezing, exhibited negligible disturbance during thawing, where disturbance was assessed in terms of the effect on the cyclic liquefaction resistance. They showed that the effect of previous strain history on Monterey #0 sand, subject to unidirectionally freezing followed by unidirectional thawing under the effective consolidation stress, was preserved. Base line specimens were prepared and subject to a known seismic history and then cyclically loaded to 100 % pore pressure ratio condition. Similar specimens, consolidated under an effective confining stress of 50 kPa, with a cell pressure of 200 kPa and a back pressure of 150 kPa, and subject to the same seismic history, were then frozen from the base of the sample, allowing drainage at the top of the specimen. The test results showed that the cyclic strength characteristics were not affected by freezing and subsequent unidirectional thawing under the same effective consolidation stresses.

On the other hand, Vaid (1996) contends that thawing specimens multidirectionally, under a small effective stress of about 20 kPa and then consolidating the thawed specimens to the in-situ effective stress condition, avoids shear stress concentrations at the thawing front and thereby results in the least sample disturbance. The laboratory study conducted as part of this thesis included an investigation of these two thawing techniques to evaluate which method results in the least amount of disturbance.

7.3.2 Degree of Saturation

The pore pressures which develop during undrained loading in the field are affected by the in-situ degree of saturation. Soils that are contractant at large strains and are not

saturated, can exhibit lower pore pressures in response to undrained loading than saturated soils. Therefore, unless conservatism is warranted, determination of the liquefaction potential of an existing unsaturated sand deposit, in its current state, requires that specimens be tested in the laboratory at the in-situ degree of saturation. Of course, analysis of long term conditions may require testing of undisturbed specimens that are fully saturated in the laboratory, if it is expected that the deposit will eventually become saturated in-situ.

If undisturbed frozen specimens are thawed in the laboratory under effective stresses that are significantly smaller than those which existed in-situ, gas may be liberated from the pore water, thereby reducing the degree of saturation of the specimens from that which existed in the field. If the degree of saturation prior to freezing and sampling is unknown, the initial conditions cannot be restored by back saturating the specimens. With a degree of saturation in the laboratory of less than that which exists in-situ, specimens would likely behave in a more compressible manner and the permeability would be reduced due to the presence of air in the void spaces (Lowe et al., 1964). Conversely, a higher degree of saturation in the laboratory may result in the development of higher pore pressures than would exist in-situ under similar loading conditions. Therefore, it is desirable to preserve the initial degree of saturation by thawing the specimens under the in-situ effective stresses.

As noted previously, the undisturbed samples obtained from several of the CANLEX test sites indicated that the subaqueous sand deposits were not fully saturated in-situ. Figures 7-1 to 7-3 show the degrees of saturation estimated for triaxial specimens trimmed for laboratory testing from the Phase I, Phase II and Phase III test sites, respectively. The degree of saturation was estimated based on calculation of the dry density, water content and void ratio of frozen cubes trimmed from either end of triaxial specimens, using the following relations:

$$\rho_d = \rho_f / (1 + \omega_{ice}) = (M_f/V_f) / (1 + \omega_{ice})$$

$$e = G_s (\rho_w / \rho_d) - 1$$

$$S_r = (G_s \omega_{ice}) / (e G_{ice}) \quad [7-1]$$

where, ρ_d is the dry density (g/cc), ρ_f is the frozen total density (g/cc), ω_{ice} is the ice content, M_f is the frozen mass of the cube (g), V_f is the frozen volume of the cube (cc), e is the void ratio, G_s is the specific gravity of the soil grains (2.62), ρ_w is the density of water (g/cc), S_r is the degree of saturation and G_{ice} is the specific gravity of ice (0.917). The frozen cubes from which void ratio estimates were made had dimensions of approximately 3 cm by 3 cm by 2 cm. The physical dimensions were measured with electronic calipers, precise to the nearest 0.1 mm.

It is recognized that this method of estimating the degree of saturation involves some errors associated with the small volume of material from which the void ratio was determined and the inaccuracy of physical volume measurements of the frozen cubes. However, the fact that the estimated degrees of saturation are scattered well below 100 %, suggests that even if all measurement errors were eliminated the degree of saturation of many of the specimens would fall below 100 %. Further discussion regarding errors associated with void ratio estimates are presented later in the chapter.

As an independent measurement of degree of saturation, a study was undertaken by CANMET (1996) to examine several in-situ frozen cores from the Phase I test site, obtained from depths of 10 to 15 m below the groundwater table in the Mildred Lake Settling Basin (tailings dyke) at Syncrude. During the study, laser scanning confocal and cryogenic electron microscopy clearly identified isolated gas pockets within the void spaces of five frozen core specimens. The frozen specimens were then thawed in a closed chamber filled with water. Gas released during thawing was captured in a water column calibrated for volume measurement. This procedure indicated that the percentage of void space occupied by gas varied from 1 to 7 %. The gas was then collected in a septum at the top of the burette and characterized by gas chromatography. Evaluation of the gas composition indicated that the gas contained significantly elevated concentrations

of carbon dioxide and methane, likely associated with aneorobic biological activity within the Phase I sand deposit at significant depth.

Since the specimens were thawed under a lower confining stress than existed in-situ during the CANMET study, the volume of gas liberated during thawing would have comprised not only gas bubbles trapped in the frozen core but also gas that came out of solution from the pore water. Therefore, quantitative determination of the in-situ degree of saturation was not possible using this technique. However, the isolated gas pockets encountered with the laser scanning confocal and cryogenic electron microscopy positively confirmed that the sand deposit and the Phase I test site was not saturated.

7.4 In-Situ Stress Conditions during Freezing and Sampling

To determine the most appropriate stress conditions under which the in-situ frozen specimens should be thawed, the stress changes that occur during in-situ ground freezing and sampling were first evaluated to determine the state of stress in the frozen samples. Figure 7-4a shows an element of saturated sand under an arbitrary in-situ stress and pore water pressure. Assuming that the sand can be frozen without causing disturbance. Figure 7-4b shows that the in-situ stresses are locked in by the freezing process. The relationship between the initial pore water pressure and the pore ice pressure can be calculated using an equation derived from capillary theory and the thermodynamics of the ice-water system (Williams, 1967), which is given by:

$$P_i - P_w \cong (1-T/T_0) L/ V_w \quad [7-2]$$

where P_i is the pressure in the ice (kPa); P_w is the pressure in the water; T is the absolute temperature ($^{\circ}\text{K}$); T_0 is the normal freezing point, which is equal to $273.15-0.0074P_i$ (MPa); L is the latent heat of fusion, and V_w is the molar volume of water. Using the appropriate terms, where L/ V_w is equal to 3.2 and P_w is equal to the initial in-situ pore

water pressure, Equation [7-2] indicates that the pore ice pressure is approximately equal to the pore water pressure that existed prior to freezing.

Simulating sampling, Figure 7-4c shows that the stress changes that occur in the frozen sand element as it is removed from the ground. Assuming for a moment that ice behaves like a highly viscous pore fluid, upon sampling, a tensile stress would develop in the pore ice that is similar to the negative pore water pressure (Broms, 1980) that develops in response to sampling of saturated clay. In this case, the stress change that occurs in the pore ice in response to sampling could be approximated using the following equation:

$$\sigma_{icc} = \sigma_{vo} \left\{ \left(\frac{1 + 2k_o}{3} \right) + (A_u - 1/3)(1 - k_o) \right\} \quad [7-3]$$

However, the behaviour of ice differs from that of pore water in that it is able to support a certain portion of shear stress, at least temporarily (Ladanyi, 1981). Therefore, when a frozen soil sample is removed from an in-situ anisotropic stress state, the ice is initially able to maintain at least a portion of the anisotropic stress.

If the frozen soil sample is allowed to undergo primary creep, with a decreasing rate of strain, under unconfined, undrained conditions, such as would exist in a frozen sample protected from sublimation but subject to a temperature that is not significantly below 0 °C, the anisotropic stress within the ice would gradually approach an isotropic condition. In this case, Equation [7-3] could be used to approximate the isotropic pore ice pressure within a frozen sample that has been stored for some time under relatively small subzero temperatures. Assuming that the response is elastic, A_u is equal to 1/3; hence, given a k_o of 0.5, as shown in Figure 7-4c, an isotropic tensile stress of -33 kPa eventually develops in the pore ice within the frozen element of soil due to creep.

If creep is avoided either by storing the specimen at very cold temperatures, or by controlled thawing of the frozen specimen immediately after removal from the ground, upon re-application of the in-situ confining stresses in the triaxial cell prior to thawing, the anisotropic in-situ stress condition should be fully restored to the soil skeleton,

thereby relieving the ice of any anisotropic stress. If, however, a small proportion of the anisotropic stress remains in the ice, shear strains would develop during thawing due to the difference in stress between the isotropic pore water pressure and the anisotropic pore ice pressure.

Either in the former case, where the anisotropic stress condition is restored to the soil skeleton, or in the case where creep has resulted in an isotropic stress of -33 kPa in the pore ice, Figure 7-4d, indicates that the in-situ stress of the pore ice prior to sampling is restored to 50 kPa. Given an initial tension of -33 kPa prior to application of the triaxial stresses, the pressure in the pore ice was derived by assuming that the equation developed by Skempton (1954) regarding undrained pore pressure response to triaxial loading can be used to estimate the change in stress in the pore ice, where:

$$\Delta\sigma_{ice} = B [\Delta\sigma_3 + A (\Delta\sigma_1 - \Delta\sigma_3)] \quad [7-4]$$

Singh et al. (1982) conducted laboratory tests to examine the possible effects of creep during unconfined storage of in-situ frozen samples that had been subject to an isotropic stress condition. After Monterey #0 sand specimens were frozen under an isotropic effective confining stress of 50 kPa, the confining stress was removed and the specimens were kept frozen in this condition for 24 hours, in a triaxial cell packed with dry ice, to simulate unconfined storage of frozen specimens. The specimens were then again subject to the confining stress that existed during freezing and they were thawed unidirectionally, but opposite to the direction of freezing, allowing access to water at the top of the specimen. During thawing, the same effective stress conditions were imposed by applying a back pressure to the drainage lines equal to that which existed during freezing. The thawed specimens were then cyclically loaded to a pore pressure ratio condition of 100 %. The test results showed that no difference existed between the cyclic liquefaction resistance of frozen samples stored for 24 hours and frozen samples tested immediately after freezing, without removal of the confining stress. From these experiments Singh et al. (1982) concluded that the effect of previous strain history had been preserved and the structure of the sand was not altered by a period of unconfined, frozen storage.

However, the effects of longer periods of storage under temperatures that are not significantly below 0 °C and of initially anisotropic in-situ stresses should be investigated, especially in terms of the effect on static liquefaction potential, which is more sensitive to disturbance than cyclic liquefaction. If significant stress concentrations develop as a result of thawing under stresses that are significantly different from the stresses remaining within the frozen specimen, this could cause disturbance of the sand fabric and may change the void ratio. The laboratory study described here has allowed for indirect evaluation of whether or not stress concentrations associated with different thawing techniques are sufficient to result in disturbance during thawing.

7.5 Stress Conditions during Thawing

7.5.1 Stresses Induced in the Triaxial Cell

The stresses induced during thawing of frozen specimens in a triaxial cell can be modeled for different applied stresses, in a manner similar to that used to determine the stresses during freezing and sampling. To avoid difficulties associated with determining the stress condition of the pore ice immediately prior to thawing, it is simplest to consider a case where the in-situ stress conditions are assumed to be isotropic. Figures 7-5a to 7-5c show the stress changes within an element of soil subject to ground freezing and sampling under an isotropic stress condition. In this case, it can be assumed that the tensile stress that develops in the ice upon sampling is equal in magnitude to the isotropic in-situ effective stress of 50 kPa.

In Figure 7-5d, the in-situ stresses are applied immediately after setting up the frozen specimen in the triaxial cell. Prior to commencing thawing, as an approximation, it can be assumed that the pore ice behaves in an undrained manner, in response to the re-applied in-situ total stress that is similar to the pore water pressure response in unfrozen soil. Hence, Equation [7-4] can be used to estimate the change in stress in the pore ice. Assuming full saturation and an elastic response, the change in pore ice pressure in

response to the applied vertical stress and cell pressure is 100 kPa, yielding a final ice pressure of 50 kPa. Hence, the stress condition that existed in the frozen ground prior to sampling has been restored.

As shown in Figure 7-5e, during unidirectional thawing under the in-situ effective stress, provided that a back pressure equal to the pore pressure that existed in-situ is applied to the end of the specimen where thawing commences, the effective stresses in the frozen and unfrozen sand are identical.

Alternatively, the frozen specimen could be thawed under a small isotropic effective stress and then consolidated to the in-situ stress once thawing is complete. Figure 7-5f shows the stresses induced in a frozen sample, subject to an all-round stress of 20 kPa in the triaxial cell. Using Equation [7-4], the change in pore ice pressure in response to the applied stress is 20 kPa, yielding a net tension of -30 kPa in the ice. In this case, although the in-situ effective stress that existed in the frozen ground has been re-established in the specimen prior to commencing thawing, the pore ice retains a stress of -30 kPa. Figure 7-5g shows the stresses that exist in the frozen and unfrozen sand as thawing progresses under a small effective stress. It is evident that the effective stresses in the frozen and unfrozen sand, or the stresses in the pore ice and pore water, are not the same, thereby leading to stress concentrations at the thaw boundaries.

Differences between the two thawing methodologies can also be represented in terms of the stress path followed by an element of soil subject to an anisotropic in-situ stress condition, followed by ground freezing, sampling and then thawing either under the in-situ effective stresses or under a small effective stress. Figures 7-6a shows the stress path followed by an element of soil subject to unidirectional thawing under the in-situ effective stress and Figure 7-6b shows the stress path followed by an element of soil thawed unidirectionally under a small effective stress.

In Figures 7-6a and 7-6b, Points (a) and (a') along the stress paths represent an anisotropic in-situ state of stress, similar to that illustrated in Figure 7-4a, and Points (b) and (b') represent the soil elements after ground freezing. When the frozen soil elements are removed from the ground, the state of stress will initially remain locked in since the anisotropic state of stress is transferred to the pore ice and the state of stress will remain at Point (b) or (b'). However, if creep is allowed to take place, the state of stress will eventually fall to Points (c) and (c'), since creep reduces the pore ice pressure to a value equal in magnitude to the isotropic pore water pressure that would exist in an undisturbed sample of clay subject to the same stress relief. As illustrated in Figures 7-6a and 7-6b, the change in stress from Point (b) or (b') to the isotropic stress at Point (c) or (c'), should result in very little disturbance since the yield surface of the frozen soil is significantly larger than that for the unfrozen soil.

The stress paths followed up to this stage by each of the soil elements are the same. However, depending upon whether the in-situ stress or a small confining stress is applied to the frozen specimen in the triaxial cell, the stress paths induced in the frozen sand beyond this point differ. If creep has taken place, when the in-situ stress state is restored in the triaxial cell, the stress path of the element in Figure 7-6a moves from Point (c) up to Point (d) along the k_0 line, while the stress path of the specimen in Figure 7-6b, subject to a small effective stress, remains on the effective mean principle stress axis at Point (d'). If creep has not been allowed to occur during storage, application of the in-situ total stress to the frozen specimen in the triaxial cell will maintain the state of stress at Point (d), while application of a small total stress to the frozen specimen will likely result in reducing the mean effective principal stress in the frozen specimen.

Finally, the stress path of the specimen subject to thawing under the in-situ effective stress remains on the k_0 line at Point (e), while the stress path of the element thawed under a small effective stress moves down the effective mean principle stress axis from Point (d') to Point (e'). After thawing is complete, the specimen thawed under a small effective stress must be consolidated to the in-situ effective stress, as represented by the

stress path moving towards the k_0 line to Point (f'). This illustration shows that the state of stress in the thawed soil, of the element that was thawed under a small effective stress and then consolidated, was changed significantly from the in-situ stress condition, thereby increasing the risk of disturbance to the in-situ soil fabric and/or void ratio. Furthermore, if Point (e') lies close to the unfrozen soil yield surface, disturbance may be very significant.

7.5.2 Finite Element Analysis of Thawing in the Triaxial Cell

Frozen sand may be described as a two-phase granular material comprising sand grains in a visco-plastic ice matrix. As discussed in Section 7.4, the stresses within the pore ice are a function of time due to its visco-plastic nature. As pointed out by Ladanyi (1981), shear stresses imposed on a frozen sand sample in a triaxial cell are initially shared between the soil skeleton and the ice bonds. With time, relaxation of the ice bonds occurs resulting in the gradual transfer of shear stress from the ice to the soil skeleton. After sufficient creep takes place, under undrained conditions, the stress within the ice becomes isotropic and is similar to that which would exist in the pore fluid of an unfrozen specimen subject to the same stresses.

Thawing of frozen sand to evaluate stress concentrations at the thaw front could be modeled at one instant in time when unidirectional thawing has advanced through a portion of the specimen. This requires that an assumption be made regarding the state of stress in the pore ice at the time under consideration.

After sufficient creep has taken place to alleviate any shear stress within the pore ice, if the pore ice is assumed to act like a highly viscous pore fluid, then an effective stress analysis could be carried out. In this case, the modulus used for the frozen and unfrozen soil should be the same and equal to the effective modulus of the soil skeleton, since the shear modulus of the pore ice, modeled as a fluid, could be assumed to be close to zero.

Therefore, referring to Figure 7-5e, if the in-situ effective stresses were restored in the frozen sand, and thawing is carried out under the in-situ effective stress and pore water pressure conditions, no shear strains at the thaw front should exist, since the stress and modulus in both materials are the same. However, if thawing is carried out under a small effective stress, as shown in Figure 7-5g, shear strains would be expected as a result of the different stress conditions in the frozen and unfrozen sand.

Conversely, if shear stresses exist in the pore ice immediately prior to thawing, then the ice cannot be modeled as a highly viscous pore fluid. In this case it would be necessary to assign a different modulus to the frozen sand skeleton and the ice matrix. Shear strains at the thaw interface could then be determined by applying the triaxial stress boundary conditions to a separate finite element mesh for the soil skeleton and pore ice matrix, but invoking strain compatibility between all nodes of separate finite element meshes.

At the time of undertaking this study, a model was not readily available that would allow for superposition of the sand skeleton and the ice matrix behaviour through strain compatibility. Therefore, an anisotropic stress condition could not be modeled accurately. However, to examine the magnitude of possible shear strains at the thaw front in a triaxial specimen subject to isotropic stresses, simplified finite element analyses were carried out.

The first analysis involved assuming that, at the time of thawing, the pore ice could be approximated as a highly viscous pore fluid. In this case, the same effective stress modulus of 150.6 MPa was used for both the frozen and unfrozen soil. Since the pore water and the pore ice pressures were assumed equal, as stated previously, no shear strain could develop in the specimens thawed under the in-situ stress. However, to examine the shear stresses that may develop in specimens thawed under a small effective stress, an axisymmetric triaxial specimen thawed under an effective stress of 20 kPa was modeled using the finite element program SIGMA/W, written by Geo-Slope International. The

in-situ effective stress was assumed to be 50 kPa, hence, the effective stresses in the frozen and unfrozen soil were similar to those shown in Figure 7-5g.

Figures 7-7a and 7-7b show the maximum shear strain and maximum shear stress developed in the specimen. As indicated in the figures, the maximum shear strain at the thaw front was 1.5×10^{-4} and the maximum shear stress was 14 kPa. The shear strain and shear stress developed at the thaw front in the specimen thawed under a small effective stress would be larger for larger values of in-situ stress, such as would exist in a frozen sample recovered from significant depth. As stated previously, the same specimen thawed under the in-situ effective stress would be subject to zero shear stress and shear strain at the thaw front.

To compare the two thawing techniques in terms of the possible upper bound shear strains that could develop at the thaw front, a second set of finite element analyses were conducted. The maximum shear strains that could develop at the thaw front were estimated by assuming that the modulus of the thawed soil was much smaller than that of the frozen sand. In this case the stiffness of the frozen soil was assumed to be derived from the soil skeleton and the ice matrix acting together. The frozen sand was modeled as elastic with a modulus of 2,000 MPa and the unfrozen sand was assumed to be elastic with a modulus of 150.6 MPa. A Poisson's ratio of 0.13 was used for both materials. These parameters were estimated from data available in the literature on triaxial testing of frozen sand and laboratory triaxial tests conducted on thawed Phase I specimens.

SIGMA/W was used to model both unidirectional thawing under an isotropic in-situ effective stress and pore water pressure and unidirectional thawing under a small effective stress of 20 kPa. For these analyses, since both the pore ice and pore water pressure were constant during thawing, the effective stresses induced in the frozen and unfrozen sand were used under drained conditions. The effective axial stress and cell pressure applied in each case were set equal to the effective stresses shown in

Figures 7-5e and 7-5g. These stresses were modeled as boundary stresses acting along the perimeter of the finite element meshes.

Figure 7-8a shows that the maximum shear strain induced at the thaw front in the specimen thawed unidirectionally under the in-situ stress and pore water pressure condition was approximately 1.4×10^{-4} . The corresponding maximum shear stress was 10 kPa, as shown in Figure 7-8b. To check the computer output, the maximum shear strain at the thaw interface was also calculated based on the maximum shear stress shown in Figure 7-8b, using the expression:

$$\gamma_{\max} = \tau_{\max} 2(1 + \nu)/E_{\text{ufz}} \quad [7-5]$$

where τ_{\max} is the maximum shear stress (kPa); ν is poison's ratio and E_{ufz} is the modulus of the unfrozen soil (kPa). The calculated maximum shear strain was found to be 1.5×10^{-4} , which agrees with the maximum shear strain contours obtained from the SIGMA/W analysis.

The SIGMA/W results indicated that the maximum shear strain induced at the thaw front in the specimen thawed unidirectionally under a small effective stress was about 6.0×10^{-5} and the corresponding maximum shear stress was approximately 12 kPa, as shown in Figures 7-9a and Figure 7-9b. Therefore, the analyses indicated that the specimen thawed under the in-situ effective stresses experienced a slightly higher shear strain at the frozen/unfrozen boundary. However, this was primarily due to the fact that the unfrozen, more compressible portion of the sample, thawed under the in-situ effective stress, was subject to a higher confining stress than the specimen thawed under a small effective stress.

If the in-situ stress level is considered to be higher, as shown in Figures 7-10a and 7-10b, because a much higher confining stress is placed on the unfrozen soil thawed under the in-situ stress, the maximum shear strains at the thaw front in this specimen appear to be higher than those induced in the specimen thawed under a small effective stress. In

Figure 7-10a the maximum shear strain at the thaw front in the specimen thawed under the in-situ stress is approximately 2×10^{-3} , while, as shown in Figure 7-10b, the maximum shear strain at the thaw front in the specimen thawed under a small effective stress is about 2×10^{-4} . However, these results are a function of the present modeling restrictions and the inaccuracies associated with assuming a different frozen and unfrozen modulus.

As pointed out previously, the finite element analyses conducted here do not accurately represent the behaviour of the specimen during thawing due to the inability to invoke strain compatibility between the pore ice matrix and the soil skeleton. However, the results do provide an upper bound and indicate that the maximum shear strains at the thawing front would be in the order of about 10^{-5} to 10^{-4} , for frozen specimens recovered from relatively shallow depths and approximately 10^{-4} to 10^{-3} , for specimens recovered from greater depths. To determine whether or not these small shear strains would significantly alter the in-situ void ratio of undisturbed frozen sand specimens, it was necessary to carry out a laboratory thawing study, as will be discussed in the following sections of this chapter.

7.6 Laboratory Thawing Protocol Study

To examine which of the two thawing methodologies used by researchers to date resulted in the least sample disturbance, a laboratory study was undertaken on reconstituted and undisturbed samples of sand. To compare the two thawing techniques, the void ratio changes exhibited by specimens thawed multidirectionally under a small effective stress and then consolidated to the in-situ effective stress level were compared with those exhibited by the specimens thawed unidirectionally under the in-situ effective stress. To examine the effect of stress level alone, the void ratio changes experienced by specimens thawed unidirectionally, either under the in-situ effective stress or under a small effective stress, were also compared. The primary objective of this study was to develop a thawing protocol that, if followed, would reduce or eliminate disturbance during thawing of

undisturbed samples of loose sand obtained by in-situ ground freezing. Provided that correct thawing protocol is followed, specimens would thus remain at their in-situ state. Utilizing the most effective techniques for undisturbed sampling and handling of loose sand specimens, the effective stress, void ratio and degree of saturation would be as close to the field conditions as possible.

7.6.1 Reconstituted Specimens

For the first part of the study, thawing procedures were evaluated for reconstituted sand specimens prepared from bulk samples obtained in the vicinity of the Phase I test site. The sand from the Phase I test site was fine and relatively uniform, with a D_{50} of approximately 0.20 mm. The fines varied across the site from 8 to 15 %, hence to eliminate specimen variability, the particle sizes less than 75 μm (fines) were removed by washing the sand over the #200 sieve. Grain size analysis of the washed sand indicated that the sand contained 2 % by weight of fines, as shown in the grain size curve in Appendix E. This relatively clean Syncrude sand (CSS) was then used for preparation of reconstituted specimens that were frozen in the laboratory under similar stress conditions as those existing at the Phase I test site.

Two methods of preparing reconstituted samples were used. The first group of reconstituted samples were prepared using a water pluviation technique that was modified slightly to produce a more uniform variation of particle sizes within the specimen, as described in detail below. De-aired water was used to reconstitute saturated specimens and carbonated water was used for unsaturated specimens. These specimens were consolidated under an effective stress of 400 kPa and then frozen unidirectionally by circulating liquid nitrogen through the triaxial cell base plate. This method of sample preparation was similar to that described by Sasitharan et al. (1989) and is described

below:

- Approximately 3000 g of CSS was covered with distilled water and boiled for 2 to 3 hours on a hot plate.
- An acrylic tube, with a diameter of 9.5 cm, a height of 30.5 cm and a removable base, was filled with de-aired water for saturated specimens or with carbonated water for unsaturated specimens to approximately the 1/3 mark.
- The boiled sand was then spooned into the acrylic tube using a large metal spoon to avoid grain size segregation that occurs when sand settles through a column of water.
- Once full, the tube was sealed with a stopper inverted 5 to 10 times to distribute the particle sizes evenly.
- A 15 cm diameter, de-aired porous stone was placed on the base plate of a triaxial cell. The acrylic tube was placed on the porous stone and the bottom lid of the tube was removed from between the sand and the porous stone.
- A 1.6 mm thick neoprene membrane was then fitted over the acrylic tube and o-rings were secured around the membrane, sealing it against the base plate.
- A split mold was set up to support the membrane and the acrylic tube was removed.
- The top cap was then assembled and o-rings were fitted around the top of the membrane, securing it to the top cap.
- A drainage line was attached to the top of the specimen through the top cap and a vacuum of 25 to 30 kPa was established to maintain specimen integrity while the split mold was removed.
- The triaxial cell was assembled and filled with mineral oil.
- A cell pressure of 30 kPa was applied, with specimen drainage valves closed, and the vacuum was released.
- Specimens prepared with carbonated water were not back saturated; they were consolidated immediately after they were assembled in the triaxial cell.
- Specimens prepared with de-aired water were back saturated. Once the triaxial cell had been assembled, the cell pressure was set at approximately 105 kPa with a back

pressure of 100 kPa. The drainage valves were then opened and the specimen was allowed to sit under an effective stress of about 5 kPa until equilibrium conditions were established. In cases where back saturation of CSS specimens was ineffective under these stress levels, the cell and back pressure were increased in steps to 305 kPa and 300 kPa, respectively. It was generally necessary to allow the CSS specimens to sit overnight to reach equilibrium conditions.

- After the specimen stopped taking in water while subject to a back pressure, the drainage valve was closed and the pore pressure coefficient B (Lee et al., 1969) was determined by conducting a B test to confirm whether or not the specimen was fully saturated. B tests were conducted by increasing the cell pressure by increments of 50 kPa, with the drainage valve closed, and measuring the corresponding increase in pore pressure.
- For specimens that had been subject to a cell pressure of 105 kPa with a back pressure of 100 kPa, the cell pressure was increased in increments of 50 kPa up to a pressure of 500 kPa. For the specimens that had been subjected to a cell pressure of 305 kPa and a back pressure of 300 kPa, the cell pressure was increased in increments of 50 kPa up to a pressure of 700 kPa. The pore pressure response was measured for each increment and an incremental B value was determined.
- Consolidation of saturated specimens was undertaken once the B tests were complete. Prior to opening the drainage valve, the cell and back pressures were reduced to those that existed during back saturation ($\sigma_c / \sigma_b = 105/100$ kPa or 305/300 kPa). The drainage valve was then opened and the sample was allowed to sit under these stresses until volume changes ceased. Isotropic consolidation of saturated specimens was achieved by increasing the cell pressure by increments of 50 kPa, up to an effective stress of 400 kPa, allowing the specimen to consolidate under each stress increment.
- Consolidation under each cell pressure increment took place in approximately 5 to 10 minutes. Once an effective stress of 400 kPa had been established, the specimen was allowed to sit for at least 2 hours to allow for creep effects.

- Unsaturated specimens were consolidated immediately after assembly in the triaxial cell. To reduce the amount of water entering the specimen during this stage, prior to opening the drainage valve, the cell pressure was increased to 200 kPa with a back pressure of 100 kPa, and the drainage valve was opened. The cell pressure was then increased by 50 kPa increments to a value of 500 kPa, leaving the back pressure at 100 kPa. The specimen was allowed to come to equilibrium after the application of each cell pressure increment. Approximately 5 minutes was required after each cell pressure increment before volume changes ceased. Consolidation under the final effective stress level of 400 kPa was allowed for at least 2 hours.
- Once consolidation of the unsaturated specimens was complete, B tests were conducted. The drainage valve was closed and the cell pressure was increased by increments of 50 kPa. The pore pressure increase in response to each cell pressure increment was recorded and the B value was calculated. After completion of the B test, the cell pressure was reduced to 500 kPa and the back pressure was set at 100 kPa.
- After consolidation was complete the specimens were frozen by circulating liquid nitrogen through the base plate under a pressure of approximately 50 kPa, allowing full drainage at the top of the specimen. Specimens of approximately 19.5 cm in height were frozen in approximately 6 hours.
- After the completion of freezing, the triaxial cell was disassembled and the test specimen was trimmed as right cylinders with a lathe in a cold room. The average dimensions of the specimens were about 6.3 cm in diameter and 13 cm in height for triaxial testing. Ice contents were determined from the trimmings and the specimen dimensions were measured with an electronic caliper, precise to the nearest 0.1 mm, for estimation of the initial void ratio. Three measurements of the specimen diameter and three measurements of the specimen height were taken and averaged to increase the accuracy of the volume estimates.
- Prior to assembling the frozen specimens, a number of steps were taken to reduce the risk of premature thawing of specimens. The water that would be used to fill the

triaxial cell was maintained in a walk-in cooler at a temperature of approximately 2 °C for several hours prior to testing. At least one hour before each undisturbed specimen was assembled, the triaxial cell was placed in the cooler and ice was mixed with the cell water. Boiled porous stones, membranes and all other equipment used to assemble specimens were also placed in the cooler.

- A water-saturated, cold porous stone was placed on the base of the triaxial cell in the cooler, followed by filter paper. The specimen was then removed from the freezer and placed on the filter paper. After placing a filter paper and cold porous stone on the top of the specimen, two latex membranes were placed over the specimen and sealed against the base plate and top cap with two o-rings at each end. The triaxial cell was then placed over the specimen and the cell was filled with ice water. The loading ram and top seal were then installed. An electronic LVDT was attached to the loading ram to measure vertical displacements of the specimen during setup, thawing and consolidation.
- The sample was then moved quickly to a room where testing would be carried out. The average temperature in the laboratory where testing was carried out was about 20 °C. In the testing room, glycol coolant was immediately circulated through a cooling coil that surrounded the specimen inside the triaxial cell to prevent premature thawing of the specimen in the warm laboratory. The triaxial cell and cooling coil are shown in Figure 7-11. The glycol coolant temperature was maintained at approximately 0 °C by a constant temperature bath. Zero readings were taken on all measurement apparatus, including the initial vertical LVDT reading. These readings were input into the computer data logging system and collection of data commenced.
- Unidirectional thawing was accomplished by circulating warm water through the base plate beneath the sample, while allowing access to water at the bottom of the sample. The water circulated through the base plate was kept at a temperature of approximately 10 °C. To prevent uncontrolled thawing in a radial direction, glycol coolant was circulated through the cooling coil surrounding the sample within the

triaxial cell at a temperature of approximately 0 °C. CSS specimens subject to these conditions thawed in approximately 35 minutes.

- To evaluate the effect of stress level at the time of thawing, some of the reconstituted specimens were thawed under the effective consolidation stress that the sand was subject to prior to and during freezing and some of the specimens were subject to a small effective confining stress of about 20 to 35 kPa.
- Changes in volume and specimen height were monitored throughout the thawing process both manually and with electronic transducers.

Although some of the samples prepared in this manner were of good quality and could be used for the thaw protocol study, a large number of them had to be discarded due to problems associated with back saturation, disturbance during rapid freezing with liquid nitrogen or disturbance due to some uncontrolled thawing during setup. Although the relatively clean sand specimens were frozen under a high effective stress, the freezing rate used in the laboratory (about 3.25 cm/ hr) was about 10 times faster than that used in the field at a radial distance of 0.6 m from the freeze pipe, where sampling was undertaken. The specimens that were of good quality included CSS8, CSS9, CSS11, thawed unidirectionally under the in-situ effective stress, and Specimens CSS14, and CSS15, thawed unidirectionally under a small effective stress. The results of these tests were used in the evaluation of the most appropriate thaw protocol.

As a result of the difficulties encountered with the first set of reconstituted specimens, the methodology used to prepare the specimens was changed. The second set reconstituted specimens were prepared using the slurry deposition technique described by Kuerbis and Vaid (1988) to obtain fully saturated specimens. These specimens were frozen more slowly to avoid disturbance by circulating a glycol bath solution at a temperature of -7 °C, through the triaxial base plate. To evaluate the two main thawing techniques used by researchers in the past, the specimens were then thawed either unidirectionally, with a controlled temperature gradient, under the in-situ effective stress and pore water pressure

that existed when the samples were frozen or, multidirectionally, under a small effective stress where they were allowed to gradually warm up to room temperature.

To reduce the risk of premature uncontrolled thawing, setting up of the frozen specimens in the triaxial apparatus and subsequent thawing were undertaken in a walk-in cooler where the temperature was maintained at about 2 °C. The triaxial cell was then filled with a cold water-glycol solution to prevent the specimen from thawing non-uniformly. Specimens thawed unidirectionally, maintain an approximately horizontal thawing front that progresses from the base of the sample, where thawing commences, to the top of the specimen, provided that the cell fluid temperature is not significantly colder than the specimen. It was recognized that the optimal cell fluid temperature should be evaluated and therefore a study was carried out as part of the thawing protocol to determine the cell fluid temperature that would result in the least settlement during thawing. The study indicated that utilizing a water-glycol solution (1 part water to 2 parts glycol) in the triaxial cell at an initial temperature of about -4 °C resulted in the smallest thaw settlements, without risking premature uncontrolled thawing.

The second method of sample preparation was as follows:

- Approximately 1000 g of CSS was boiled in a flask of distilled water for 2 hours on a hot plate.
- A rubber stopper was fitted into one end of an acrylic tube with an inside diameter of 6 cm and a length of 18 cm. The tube was then submerged in a 5 gallon pail containing de-aired water, with the sealed end at the bottom of the pail.
- The flask containing boiled sand was then inverted beneath the surface of the water in the pail and the sand was poured into the acrylic tube.
- Beneath the water surface, a filter paper and saturated porous stone, followed by an acrylic lid were placed over the sand-filled tube. The tube filled with saturated sand was then removed from the pail and inverted several times to distribute the fines evenly within the sample.

- The tube was then placed on the triaxial base, with the porous stone on the base plate, and a hydrocarbon resistant, Nitrile (0.3 mm thick) membrane was placed around the tube. After sealing the membrane to the triaxial base plate with o-rings, a split mould was fitted around the specimen. The split mould was then connected to a vacuum of about 30 kPa and the acrylic tube was carefully removed from between the sand and the membrane.
- A filter paper, de-aired porous stone and the triaxial cell top cap were placed on the top of the specimen and the membrane was sealed onto the top cap with o-rings.
- A vacuum of about 25 to 20 kPa was applied at the top of the specimen through a drainage line in the top cap to maintain specimen integrity while the split mould was removed.
- After filling the cell with a 1:2 solution of water-glycol at a temperature of about -4°C , a cell pressure of 30 kPa was applied to the specimen with the drainage valve closed and the vacuum was disconnected.
- The triaxial cell was then moved to a walk-in cooler where the temperature was maintained at about 2°C and a B-test was conducted to determine whether or not the sample was fully saturated. The majority of the samples had an initially very high degree of saturation as evidenced by B values of close to 1.0. The specimens that were not fully saturated were exposed to a back pressure of 100 kPa, under an isotropic cell pressure of about 110 kPa, for several hours until a B value of 1.0 was achieved.
- The specimens were then consolidated isotropically by increasing the cell pressure in 50 kPa increments up to 500 kPa, while maintaining a constant back pressure of 100 kPa. The specimens were allowed to come to equilibrium over a period of about 2 to 5 hours under the final isotropic effective consolidation stress of 400 kPa.
- After consolidation was complete, the base plate of the triaxial cell was connected to a cold glycol bath at a temperature of about -7°C . The specimens were then frozen over a 12 hour period by circulation of the cold glycol through the base plate.

A schematic diagram of the triaxial cell base plate through which the cold glycol was circulated to freeze the specimens is included in Appendix E.

- Changes in specimen height and pore water volume were monitored during freezing to check for disturbance. Specimens that were disturbed due to heave during freezing were not used in the thaw protocol study.
- The specimens that were frozen without disturbance were moved to a walk-in freezer, maintained at a temperature of about $-20\text{ }^{\circ}\text{C}$, where the triaxial cell fluid was drained. The specimens were then weighed and measurements of the frozen specimen dimensions were recorded for later estimation of the initial void ratio.
- The frozen specimens were then re-assembled in the triaxial cell and moved back to the walk-in cooler. The cell was filled with a 1:1 mixture of water and glycol at a temperature of about $-4\text{ }^{\circ}\text{C}$ to prevent premature, uncontrolled thawing.
- The triaxial cell was set in the loading frame and saturated pressure lines were connected to the cell pressure, back pressure and pore pressure ports. An electronic LVDT was attached to the loading ram to measure the vertical displacements of the specimen during the application of stresses, thawing and consolidation.
- For those specimens thawed unidirectionally under the in-situ effective stress, a cell pressure of 500 kPa was applied to the frozen specimen under undrained conditions. For those specimens thawed multidirectionally under a small effective stress, a cell pressure of about 20 kPa to 30 kPa was applied to the frozen specimen under undrained conditions. During setup and application of the confining stresses, the cell fluid warmed up gradually but remained at a temperature of below $0\text{ }^{\circ}\text{C}$.
- For specimens thawed unidirectionally under the in-situ stress, the triaxial base plate was connected to a warm glycol bath at a temperature of $7\text{ }^{\circ}\text{C}$ and the drainage line at the base of the specimen was opened to a back pressure of 100 kPa. Thawing was then accomplished by circulation of the warm glycol through the base plate over a period of approximately 5 to 12 hours.
- For specimens thawed multidirectionally under a small stress of about 30 kPa, the drainage lines at the top and bottom of the specimen were opened, but no back

pressure was applied. The specimen was then allowed to warm up gradually to the walk-in cooler of about 2 °C over about 12 to 24 hours.

- Changes in specimen height and the volume of water taken in were recorded during thawing of all specimens. This data was then used to determine the void ratio changes that occurred during thawing, as will be discussed latter in this chapter.

7.6.2 Undisturbed Specimens

Based on the results obtained from the study on reconstituted specimens, five undisturbed specimens obtained from the Phase I test site were thawed under stresses that were close to the in-situ effective stress. Thawing was undertaken unidirectionally, under 90 % of the estimated anisotropic in-situ effective stresses. The specimens were subject to only 90 % of the estimated in-situ effective stress to prevent exposing the specimens to higher stresses than those existing in the field, in case the in-situ state of the sample was close to the yield surface and the estimated in-situ stresses were not accurate. Based on the sample depth and groundwater table location, the in-situ total stresses, pore water pressure and effective stress were determined. The effective stress was then reduced by 90 % and, by adding the in-situ pore water pressure corresponding to the sample depth, the total axial stress and cell pressure were calculated. During thawing, the back pressure was set equal to the in-situ pore pressure, calculated based on sample depth, to restore the in-situ degree of saturation.

The methodology used to thaw the undisturbed specimens was as follows:

- Prior to testing, the undisturbed specimens were weighed and the frozen volumes were determined from repeated measurements of diameter and height with electronic calipers. This allowed for estimation of the initial void ratio, based on the total frozen density of the specimen and the ice content determined from cuttings removed during trimming of the frozen specimen.

- Specimens were then removed from the freezer and placed in a triaxial cell in a large walk-in cooler at a temperature of 2 °C. The specimen was set on the triaxial pedestal, onto which a de-aired porous stone and filter paper had been placed. A filter paper and de-aired porous stone were then placed on the top end of the specimen, followed by the triaxial top cap and load cell.
- A hydrocarbon resistant, Nitrile membrane was placed over the frozen specimen so that the triaxial cell could be filled with a glycol solution. The triaxial cell was then filled with a 1:1 water and glycol solution at a temperature of about -4 °C, to prevent premature uncontrolled thawing of the specimen. The temperature of the water-glycol solution gradually warmed up to about -1 °C to -2 °C as the rest of the setup was complete.
- De-aired cell pressure, back pressure and pore pressure lines were connected to the triaxial cell, with the drainage port closed. An LVDT was connected to the loading ram to measure changes in specimen height during the application of stresses and thawing.
- The anisotropic stress condition, adjusted to reflect 90 % of the in-situ effective stress, was then applied to the frozen specimen through the axial load cell and cell pressure. The average vertical stress applied to the undisturbed specimens was approximately 600 kPa. The back pressure was set equal to the estimated in-situ pore pressure, but with the drainage port to the specimen closed.
- To commence thawing, with the triaxial cell water-glycol solution at a temperature of about -1 °C to -2 °C, a warm glycol solution with a temperature of about 7 °C was circulated through the base plate of the triaxial cell and the drainage line at the bottom of the specimen was opened to the back pressure line which had been set equal to the in-situ pore pressure.
- The changes in specimen height and pore water volume were monitored continuously during thawing.

The void ratio changes that occurred in these specimens were then compared with the void ratio changes determined for undisturbed Phase I Syncrude sand specimens thawed at the University of British Columbia's geotechnical laboratory, where the specimens were thawed multidirectionally under a small effective stress of about 20 kPa. The comparison will be discussed later in this chapter.

After thawing of the undisturbed specimens was complete, undrained triaxial tests were conducted to examine the stress strain behaviour of the Phase I sand. Undrained triaxial compression tests were carried out on four undisturbed specimens and undrained triaxial extension tests were carried out on two specimens. The results from these tests are presented in Section 7.8.

7.7 Calculation of Void Ratio Changes during Thawing

During setup, thawing and consolidation, the changes in height and volume of the specimen were monitored for determination of the void ratio at each step during testing. Changes in height were monitored with an LVDT attached to the loading ram and changes in volume were monitored both by an electronic volume change device and visually with a kerosene filled burette. The various relations utilized for calculation of void ratio changes are discussed in the following sections.

The void ratios at the end of each step during setup, thawing and consolidation can either be determined based on working backwards from the final void ratio or, by starting with the initial void ratio and working forwards. The void ratio changes can be determined by working backwards from final conditions only if the specimen is fully saturated. In this case, the final void ratio may be determined based on the final moisture content of the specimen.

If, however, the specimen was not fully saturated initially, the degree of saturation at the end of the test is unknown and void ratio changes cannot be estimated based on working backwards from the final void ratio. For either saturated or unsaturated specimens, void ratio calculations can be made based on the conditions at the start of the test. The initial void ratio of saturated specimens can be determined based on initial frozen volume measurements, or based on the final dry weight of solids. For unsaturated specimens, the initial void ratio must be estimated based on the initial frozen volume. For consistency between saturated and unsaturated specimens, all void ratio calculations in this study were made based on working forward from the initial void ratio.

The equations utilized for tracking void ratio changes for saturated and unsaturated specimens during setup, thawing and consolidation, and the parameters necessary for performing calculations are discussed below.

7.7.1 Saturated Specimens

For specimens known to be initially fully saturated, it is possible to estimate the initial void ratio from the total frozen weight and the final dry weight of solids. The equation used for calculating the initial void ratio for fully saturated specimens is given by:

$$e_o = \frac{(W - W_s) G_s}{W_s G_{ice}} \quad [7-6]$$

where: W is the total weight of specimen, g; W_s is the dry weight of solids at the end of the test, g; G_s is the specific gravity of solids; and G_{ice} is the specific gravity of ice, equal to 0.917.

The change in void ratio during setup of the specimens was estimated based on the change in height that occurred due to premature thawing, assuming that this was indicative of a thin layer around the perimeter of the specimen that thawed before controlled thawing commenced. Prior to calculating the change in void ratio during

setup, specimen compression, due to elastic deformation under the applied cell pressure and vertical stress, and vertical deformation due to apparatus compliance, were subtracted from the total vertical deformation measured with the LVDT. The remaining change in height due to thawing was assumed to be equal to half the thickness of the thawed surface layer. Based on this assumption, the equation used to calculate the void ratio after setup can be written as:

$$e_s = e_o - \frac{(\Delta h A_o + (A_o - A)(h_o - \Delta h))}{V_s} \quad [7-7]$$

where: Δh is the change in specimen height due to thawing of outermost surface layer. cm; h is the specimen height remaining frozen, cm; A_o is the initial specimen area prior to thawing of the outermost surface layer. cm^2 ; A is the specimen area remaining frozen. cm^2 ; and V_s is the volume of solids, cc.

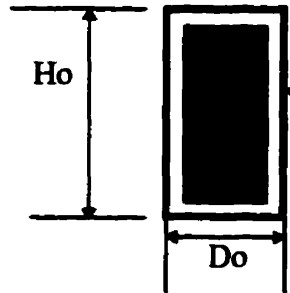
Alternatively, Equation [7-7] can be expressed in the following more general form:

$$e_s = e_o - \frac{\epsilon_{ax} (1 + 2(\epsilon_r / \epsilon_{ax})) V}{V_s} \quad [7-8]$$

where: ϵ_{ax} is the axial thermal strain during thawing, cm/cm; ϵ_r is the radial thermal strain during thawing, cm/cm; and V is the total frozen volume of specimen prior to thawing, cc.

Assuming that the thickness of the thawed surface layer around the specimen is constant. for a specimen with a 2:1 height to diameter ratio, the radial strain is equal to approximately two times the axial strain. Drawing an analogy between an ice cube submerged in a warm constant temperature bath, the perimeter of the ice cube that has melted at any given time will be of a constant thickness. If the ice cube, or soil sample, has dimensions of 2:1, then the radial thermal strain will automatically be equal to 2 times the axial thermal strain, since thermal strain is defined as the melted thickness

divided by the initial dimension, as shown in the schematic diagram below.



Constant Thickness
of Thawed
Zone = $dt/2$

$$\epsilon_{\text{radial}} = dt/(Do)$$

$$\epsilon_{\text{axial}} = dt/Ho$$

For a 2:1 specimen, $Ho = 2 Do$,

$$\text{hence, } \epsilon_{\text{radial}} = dt/(Ho/2) = 2 dt/Ho$$

$$\text{and } \epsilon_{\text{radial}} = 2 \epsilon_{\text{axial}}$$

Therefore, using a ratio of ϵ_r/ϵ_{ax} equal to 2, Equation [7-8] becomes:

$$e_s = e_o - \epsilon_{ax} \frac{5V}{V_s} \quad [7-9]$$

Since during thawing, water is taken into the specimen to recover the 9 % pore water volume expelled during freezing, the change in void ratio cannot be determined based on pore water volume change. Therefore, the change in void ratio during thawing must be estimated based on the change in height of the specimen.

Specimens thawed unidirectionally, maintain an approximately horizontal thawing front that progresses from the base of the sample, where thawing commences, to the top of the specimen, provided that the cell fluid temperature is not significantly colder than the specimen. Hence, the measured change in height can be assumed to directly reflect the void ratio change during unidirectional thawing, where the radial thermal strain is set equal to zero.

In the case where specimens were thawed unidirectionally, the radial strain was therefore set equal to zero and Equation [7-8] becomes:

$$e_t = e_s - \epsilon_{ax} \frac{V}{V_s} = e_s - \frac{\Delta h_u A_s}{V_s} \quad [7-10]$$

where: Δh_u is the change in specimen height during unidirectional thawing, cm; and A_s is the frozen area of specimen after setup, cm^2 .

For 2:1 specimens, thawed multidirectionally, the ratio of radial to axial thaw strain was assumed to be equal to two and an equation of the form of Equation [7-9] was used to calculate the void ratio change after multidirectional thawing;

$$e_t = e_s - \frac{\epsilon_{ax} \cdot 5V}{V_s} = e_s - \frac{5 \Delta h_m A_s}{V_s} \quad [7-11]$$

where: Δh_m is the change in specimen height during multidirectional thawing, cm.

Calculation of the void ratio change during consolidation to the final in-situ stresses was carried out in one of two ways, depending upon the stress level under which the specimen was thawed. For specimens that were thawed under the in-situ stresses, the consolidation phase was taken as the stage where the specimen ceased taking in water and began to expel water. The change in void ratio during consolidation of these specimens was determined based on volume change using the following equation:

$$e_c = e_t - \frac{\Delta V_c}{V_s} \quad [7-12]$$

where: e_t is the void ratio after thawing; ΔV_c is the change in volume during consolidation, cc; and V_s is the volume of solids, cc.

For specimens thawed under a small effective stress, in some cases, water was taken into the specimen when the cell pressure and back pressure were increased to the consolidation stress. In this case, the change in void ratio was determined based on the change in height of the specimen. Assuming that the measured axial strain was equal to the radial strain, due to consolidation, the change in void ratio was estimated based on the following equation:

$$e_c = e_t - \frac{\epsilon_{ax} \cdot 3V}{V_s} = e_t - \frac{3 \Delta h_c A_t}{V_s} \quad [7-13]$$

where: Δh_c is the change in specimen height during consolidation, cm; and A_t is the frozen area of specimen after thawing, cm^2 .

The final void ratio was assumed equal to the void ratio after consolidation since only undrained triaxial tests were carried out. Hence,

$$e_f = e_c \quad [7-14]$$

The spread sheets used for void ratio change calculations are included in Appendix E.

7.7.2 Unsaturated Specimens

For specimens that were not fully saturated, the initial void ratio was calculated based on the initial volume estimated from the frozen dimensions and the ice content determined from cuttings when the specimens were trimmed. The equation utilized for calculation the initial void ratio for unsaturated specimens was:

$$e_o = \frac{(V-V_s)}{V_s} = \frac{G_s \rho_w}{\rho_d} - 1 \quad [7-15]$$

where: V is the total frozen volume of specimen, cc; V_s is the volume of solids, cc; G_s is the specific gravity of solids; ρ_w is the density of water, g/cc; and ρ_d is the dry density of specimen, g/cc.

The changes in void ratio during setup, thawing and consolidation were then calculated based on Equations [7-9] to [7-13] given above, as shown in Appendix E.

7.7.3 Source of Errors Involved in Void Ratio Determination

Errors in void ratio calculations may occur as a result of a number of factors. An accurate measurement of the final dry weight is required to calculate the initial void ratio, e_o , of both saturated and unsaturated specimens. In Equation [7-6], the dry weight of solids at the end of the test, W_s , is used directly to calculate the initial void ratio for saturated specimens. For unsaturated specimens, calculation of the initial void ratio depends on

either the volume of solids or the dry density, both of which can be determined based on the final dry weight of the specimen. However, it is usually not possible to recover all of the grains of the sand from the membranes and triaxial cell base and as a result, the final dry weight tends to be underestimated.

As an example of the potential error involved in calculation of e_0 , assuming a typical total initial frozen weight of 788 g and a measured dry weight of solids at the end of the test of 634 g, the e_0 calculated using Equation [7-6] would be 0.702. If the dry weight of solids had been underestimated by 2 g, the calculated initial void ratio would be 0.713. Underestimation of the final dry weight by only 2 g, which could reasonably occur even if a great deal of care is taken, therefore, results in an overestimation of the initial void ratio by 0.011. In other words, a 0.32 % error in the dry weight of solids, results in a void ratio error of 1.6 %.

Moreover, solution of Equations [7-7] to [7-13] requires the volume of solids, V_s . Hence if the final weight of solids at the end of the test is underestimated, this creates inaccuracies each time void ratio calculations are carried out.

For unsaturated specimens, determination of the initial void ratio using Equation [7-15] requires measurement of the initial frozen volume of the specimen. Volume estimates for this study were undertaken using the average of three diameter and three height measurements taken with electronic calipers, precise to the nearest 0.1 mm. Assuming that the actual average dimensions of a triaxial specimen are 13.00 cm in height and 6.30 cm in diameter, the total volume is 405.24 cc. Assuming that both dimensions are underestimated by 0.1 mm, results in a total volume of 403.65 cc, while overestimating both dimensions by 0.1 mm results in a total volume of 406.84 cc. Using Equation [7-15], these volumes result in calculated void ratios that range from 0.748 to 0.762. This represents a potential error in the void ratio of ± 0.007 .

Calculation of the void ratio at the end of thawing also involves error. Since it is usually not possible to measure the change in specimen radius during thawing, it is necessary to make an assumption regarding the radial thaw strain. As stated previously, for specimens thawed multidirectionally, the radial strain was assumed to be equal to two times the vertical strain in simplifying Equation [7-8]. However, this assumption may not be accurate due to specimen heterogeneities.

At the end of a triaxial test the final void ratio can be estimated based on the final moisture content, if the specimen is fully saturated. This relation is given by:

$$e_f = \frac{w_f G_s}{S_r} \quad [7-16]$$

However, when pressures are relieved in the triaxial apparatus and the sample is disconnected, water may be sucked from the sample into the porous stones or drainage lines (Vaid, 1996). This results in an under-estimation of the final water content and of the final void ratio. Conversely, it is possible for excess cell water that has accumulated on the base plate, top cap or in folds of the membrane, to be included with the specimen at the end of the test, thereby resulting in an overestimation of e_f .

The above discussion indicates that the accuracy of void ratio calculations for in-situ frozen core specimens is approximately - 0.007 to + 0.011.

7.8 Test results

7.8.1 Reconstituted Specimens

The tests results obtained for four reconstituted specimens thawed under the in-situ effective stress and five specimens thawed under a small effective stress of about 26 to 35 kPa and then consolidated to the pre-freezing stress level are shown in Figure 7-12. Specimens SS1, CSS8, CSS9, CSS11, CSS14 and CSS15 were thawed unidirectionally, with the first four of these thawed under the in-situ effective stress and the last two

specimens thawed under a small effective stress. Specimens SS3, SS4 and SS8 were all thawed multidirectionally under a small effective stress. Summary tables showing the height and volume changes that occurred in each sample during setup, thawing and consolidation and spread sheets used for void ratio change calculations are presented in Appendix E.

As shown in Figure 7-12, the data obtained from the two thawing techniques was compared in terms of total calculated void ratio change due to thawing and consolidation. The test results indicate that the total void ratio change due to thawing and consolidation was significantly higher for unsaturated specimens thawed unidirectionally under a small effective stress and then consolidated to the in-situ stress, once thawing was complete, than the total void ratio change exhibited by the unsaturated specimens thawed unidirectionally under the in-situ effective stress. The total void ratio changes that occurred in the fully saturated specimens appeared to be less dependent upon the thawing technique utilized.

The test results for the reconstituted specimens suggest that the total void ratio changes during thawing and consolidation are a function of the initial degree of saturation of the specimen. Figure 7-12, shows that the total void ratio change decreases as the degree of saturation increases. This trend is more pronounced for the specimens thawed under a small effective stress, and it therefore appears that disturbance may be related to discrepancies between the in-situ degree of saturation and the degree of saturation restored in the triaxial cell during thawing. Specimens which are thawed under a small effective stress, with no back pressure, will have a much lower degree of saturation than the in-situ value due gas coming out of solution as the pore ice melts under the lower pressures and, therefore, significantly more compressible and vulnerable to disturbance.

It is recognized that restoring the in-situ degree of saturation is difficult due to differences in gas solubility related not only to the pore water pressure but also to temperature and perhaps, pore water chemistry (Sobkowicz, 1982). Diffusion of gas through the

membrane may also alter the degree of saturation as thawing progresses. However, if specimens are thawed such that the volume water taken in during thawing is close to the theoretical 9 % pore water volume expelled during freezing, the degree of saturation should not be significantly different from the initial field conditions.

Figure 7-13 shows a comparison of the change in void ratio with time during both thawing and consolidation of fully saturated, reconstituted specimens, either thawed under the in-situ effective stress or under a small effective stress. To facilitate the comparison, the initial void ratios of the specimens were assumed to be the same. The figure shows that the specimens thawed under a small effective stress heaved slightly during thawing and then experienced a decrease in void ratio during consolidation, whereas specimens thawed under the in-situ effective stress underwent a gradual decrease in void ratio until simultaneous thawing and consolidation was complete. The total change in void ratio of the specimens thawed under the in-situ effective stress was slightly less than that exhibited by the specimens thawed under a small effective stress.

7.8.2 Undisturbed Specimens

The total changes in void ratio that occurred due to thawing and consolidation of undisturbed Phase I Syncrude sand specimens are plotted against degree of saturation in Figure 7-14. The undisturbed specimens thawed unidirectionally as part of this study, under 90 % of the in-situ effective stress, are shown in comparison to undisturbed specimens thawed multidirectionally at the University of British Columbia (UBC), under the direction of Dr. Y. P. Vaid, under a small effective stress level and then consolidated to the in-situ stress after thawing was complete. Summary tables showing the height and volume changes and spreadsheets showing the calculated void ratio changes that occurred in the specimens tested as part of this study during setup, thawing and consolidation are presented in Appendix E. Summary data available for the tests conducted at UBC is also presented in Appendix E.

As shown in Figure 7-14, the test results indicate that the specimens thawed under 90 % of the in-situ effective stress underwent an average total decrease in the void ratio of approximately 0.019 while those thawed under a small effective stress and then consolidated to the in-situ stress level underwent an average total decrease in the void ratio of 0.083. Therefore, for the undisturbed samples tested from the Phase I test site, thawing under an effective anisotropic stress that is slightly less than that estimated to exist in-situ, under the in-situ pore pressure condition, results in significantly less disturbance of the void ratio than that exhibited by specimens thawed under a small effective stress and then consolidated to the in-situ stress once thawing was complete.

Due to the deep target zone at the Phase I test site, the in-situ effective stresses were high, with an average value of about 400 kPa. Therefore, thawing under a small effective stress of about 20 kPa to 30 kPa, resulted in significant changes to the in-situ stress condition initially locked into the sample by the ground freezing process. At sites where frozen samples are recovered from relatively shallow depths, where the in-situ effective stresses are approximately 50 kPa or less, it would be expected that thawing the specimens under a small effective stress would not result in as much disturbance as that experienced by the undisturbed frozen specimens recovered from the Phase I test site.

To evaluate this hypothesis, a comparison was made of the void ratio changes exhibited by undisturbed specimens obtained from each of the CANLEX test sites, where the in-situ effective stresses varied considerably from site to site. These specimens, tested at UBC, were thawed under a small effective stress and then consolidated to the in-situ effective stress once thawing was complete. As shown in Table 7-1, the total void ratio change during thawing and consolidation of these specimens decreased as the difference between the in-situ effective stress and the effective stress under which the specimens were thawed in the laboratory decreased.

It is interesting to note that all of the undisturbed specimens had saturation levels of less than 100 %. However, the void ratio changes exhibited by the undisturbed specimens do

not appear to be related to the degree of saturation. This may be due to the fact that the initial void ratios of the undisturbed specimens were much more variable than the initial void ratios of the reconstituted specimens (see Appendix E). Therefore, the initial compressibility of the soil skeleton in each of the undisturbed specimens would have been different and this variability likely masked any trend between void ratio change and degree of saturation.

The test results obtained from triaxial tests conducted on the undisturbed specimens after thawing was complete are summarized for each specimen, including the stress strain curve, the pore pressure response and stress path, in Figures 7-15 to 7-20. Three undisturbed specimens were tested in undrained triaxial compression and two undisturbed specimens were tested in undrained triaxial extension. After testing of Specimen FS5C14, the sand from this specimen was used to prepare a reconstituted specimen, FS5C14R, using the slurry deposition technique to create a fully saturated specimen. The undisturbed specimen, FS5C14, had a degree of saturation of approximately 96 %. The initial intention was to compare the behaviour of the undisturbed and reconstituted specimens, with the same void ratio but different degrees of saturation. However, the reconstituted specimen had a void ratio of about 0.702, after consolidation under an isotropic effective stress of only 35 kPa, while the undisturbed specimen, that had been consolidated in-situ under an effective stress of about 300 kPa, had an initial void ratio of 0.746. This void ratio discrepancy made comparison of the effect of saturation difficult.

Figures 7-21a and 7-21b show the stress strain and pore pressure response curves obtained from the undrained triaxial compression tests conducted on undisturbed Specimen FS5C14 and reconstituted Specimen FS5C14R, as well as the test results obtained for undisturbed Specimen FS3C17B. Both Specimens FS5C14R and FS3C17B were fully saturated, while Specimen FS5C14 had a degree of saturation of about 96 %. Although it is difficult to compare the test results due to discrepancies between the void ratios and the initial effective mean normal stress, corresponding to the consolidation pressures, the data shows that the pore pressure response of the two saturated specimens

were similar, while, the unsaturated specimen developed a much smaller negative pore pressure. However, it should be noted that differences in fabric between reconstituted and undisturbed specimens can also affect the volume change or pore pressure behaviour. To determine the effects of degree of saturation on the liquefaction susceptibility, further testing should be carried out on loose sand specimens, with the same initial void ratio, to examine whether or not smaller positive pore pressures develop in loose unsaturated specimens than in loose saturated specimens.

Figure 7-22 shows the stress paths obtained from all of the tests, in terms of effective mean principle stress, p' , plotted against shear stress, q' . None of the specimens tested exhibited contractive or strain softening behaviour. The dilatent behaviour of the Phase I sand can be attributed to the relatively low in-situ void ratios which, as shown in Figure 7-23, fell below the steady state line determined, based on previous CANLEX test data, for Phase I Syncrude sand.

The steady state line serves to illustrate the importance of avoiding disturbance of the in-situ void ratio during thawing of undisturbed specimens. Figure 7-24 shows the void ratio changes that occurred during thawing of undisturbed Phase I specimens under a small effective stress. Although the initial in-situ void ratios of the specimens plotted close to the estimated steady state line, the large void ratio changes that occurred during thawing and consolidation of these specimens moved the initial state to a zone where the specimens would most certainly behave in a dilatent manner. If the specimens had been thawed without disturbance, undrained triaxial tests could have provided better data to confirm the location of the steady state line.

7.9 Conclusions

It is important that undisturbed frozen specimens, obtained by in-situ ground freezing, be stored at very cold temperatures of -20°C or lower, to avoid relaxation of anisotropic

stresses locked into the pore ice by ground freezing. Storage of frozen specimens in this manner will preserve the in-situ stress condition, thereby facilitating restoration of the anisotropic field stresses to the soil skeleton in the triaxial cell prior to thawing. This, in turn, results in less disturbance.

The thawing protocol study conducted to evaluate two different thawing techniques indicated that thawing of both reconstituted and undisturbed specimens under the in-situ effective stress results in less disturbance than thawing specimens under a small effective stress and then consolidating them to the in-situ effective stress once thawing is complete. Theoretical confirmation of the laboratory findings was not obtained from finite element analyses, which indicated slightly higher maximum shear strains at the thaw front in specimens thawed under the in-situ effective stress. However, this discrepancy likely resulted from the fact that the present analyses were not able to accurately model the material behaviour. Future analytical work could be undertaken to modify an existing finite element program to accommodate strain compatibility between the soil skeleton and the pore ice, each with different stiffnesses, but subject to the same boundary stresses.

The in-situ frozen core samples obtained from all four subaqueous sand deposits, investigated as part of the CANLEX project, indicated that the sand deposits were not fully saturated. This could have major implications regarding the pore pressure development during undrained loading. To determine the effects of degree of saturation on the liquefaction susceptibility, further testing should be carried out on loose sand specimens, with the same initial void ratio, to examine whether or not smaller positive pore pressures develop in loose unsaturated specimens than in loose saturated specimens.

Void ratio changes that occurred during thawing of reconstituted Syncrude sand specimens appeared to be a function of degree of saturation, where the total void ratio change decreases as the degree of saturation increases. The average total void ratio change due to thawing and consolidation of unsaturated reconstituted specimens was

significantly smaller for specimens thawed under the in-situ stress than for those thawed under a small effective stress, followed by consolidation to the in-situ effective stress. For fully saturated reconstituted specimens, the void ratio changes due to thawing and consolidation were less sensitive to the thawing method used.

Multidirectional thawing of reconstituted specimens under an effective stress that was much smaller than the effective stress that the specimens were subject to prior to freezing, resulted in heave, followed by a decrease in void ratio during consolidation to the in-situ stresses after thawing was complete. The total void ratio change due to thawing and consolidation that occurred in reconstituted specimens subject to unidirectional thawing under the in-situ effective stress, was smaller than the total decrease in void ratio exhibited by specimens thawed multidirectionally under a small effective stress and then consolidated to the in-situ stress.

Unidirectional thawing of undisturbed Phase I Syncrude sand specimens under 90 % of the effective stress level that existed in-situ prior to freezing and the in-situ pore pressure condition, resulted in significantly smaller void ratio changes than those that occurred in specimens thawed multidirectionally under a small effective stress of 20 kPa to 35 kPa, with no back pressure, and then consolidated to the in-situ effective stress. The specimens thawed under 90 % of the in-situ stresses underwent an average total decrease in void ratio of 0.019, while the specimens thawed under a small effective stress underwent an average total void ratio change of 0.083. The decrease in void ratio, as a percentage of the initial void ratio, due to unidirectional thawing and consolidation of undisturbed specimens ranged from 1.4 % to 3.9 %, with an average of 2.4 %. The average total decrease in void ratio that occurred during multidirectional thawing, as a percentage of the initial void ratio, ranged from 5.6 % to 15.6 %, with an average of 10.9 %.

A trend between the void ratio change and degree of saturation was not evident for the undisturbed specimens tested. However, this was likely due to the large variation of

initial void ratio between specimens, resulting in variable soil skeleton compressibilities that masked the effects of degree of saturation on void ratio changes during thawing.

The results from the thawing protocol study indicate that the most appropriate method of thawing undisturbed, unsaturated sand samples, obtained by in-situ ground freezing, involves thawing the specimens unidirectionally, in a controlled manner, under 90 % of the estimated in-situ effective stress. Specimens should be maintained in a frozen state prior to commencing thawing by filling the triaxial cell with a glycol solution at a temperature of about -4°C . The temperature of the glycol solution warms slightly to about -1°C to -2°C as set up is complete. The specimen should be allowed access to chilled water at the end of the specimen at which thawing will commence. Warm glycol, at about 7°C , should then be circulated through the base plate of the triaxial cell to thaw the specimen unidirectionally.

All of the undisturbed specimens exhibited dilatent behaviour during undrained triaxial compression and triaxial extension testing, indicating that the specimens were dense of the steady state line for Syncrude sand. The steady state line serves to illustrate the importance of avoiding disturbance during thawing of in-situ frozen specimens, since even small changes in the void ratio of specimens with an in-situ void ratio that falls slightly above the steady state line will change the behaviour from contractant to dilatent. Therefore, accurate evaluation of the liquefaction potential of a sand deposit from undisturbed in-situ frozen specimens, requires that careful handling and thawing procedures be followed in the laboratory to avoid disturbance of the in-situ void ratio and fabric.

7.10 References

Broms, B. B., 1980. Soil Sampling in Europe: State-of-the-Art. Journal of Geotechnical Division, ASCE GT1, paper 15149, pp. 65-98.

- CANMET, 1996. Gas Entrained in Tailings Deposits. Canada Centre for Mineralogical Technology, Western Research Centre, Division Report WRC 96-37 (CF), 8 pp.
- Hofmann, B. A., Segó, D. C., and Robertson, P. K., 1994a. Undisturbed Sampling of a Deep Loose Sand Deposit Using Ground Freezing. 47th Canadian Geotechnical Conference, September 21-23, 1994, Halifax, Nova Scotia, pp. 287-296.
- Hofmann, B. A., Segó, D. C., and Robertson, P. K., 1994b. CANLEX Activity 4D - Sample Collection and Handling Procedures Report - Phase I Test Site. CANLEX Report, University of Alberta, Edmonton, 14p.
- Hofmann, B. A., Segó, D. C., and Robertson, P. K., 1995. In-Situ Ground Freezing for Undisturbed Samples of Loose Sand - Phase II. 48th Canadian Geotechnical Conference, September 21-23, 1994, Vancouver, British Columbia, pp. 197-204.
- Konrad, J.-M. 1990. Sampling of Saturated and Unsaturated Sands by Freezing. Geotechnical Testing Journal, ASCE Vol. 13(2), pp. 88-96.
- Konrad, J.-M., 1995. Controlled Freezing and Thawing as a way to Test Intact Sand: A Laboratory Investigation. 48th Canadian Geotechnical Conference, September 21-23, 1994, Vancouver, British Columbia, pp. 213-222.
- Konrad, J.-M. and St-Laurent, S., 1995, Controlled Freezing and Thawing as a way to Test Intact Sand: A Laboratory Investigation., 48th Canadian Geotechnical Conference Proceedings, Vancouver, September, 1995, pp. 213-222.
- Küpper, A., Lawrence, M. and Howie, J., 1995. The Use of Geophysical Logging Techniques at the CANLEX Project. 48th Canadian Geotechnical Conference, September 21-23, 1994, Vancouver, British Columbia, pp. 81-88.
- Kuerbis, R. and Vaid, Y. P., 1988. Sand Sample Preparation - The Slurry Deposition Method. Soils and Foundations, Vol. 28, No. 4, December, pp. 107-118.
- Ladanyi, B. ,1981. Mechanical Behaviour of Frozen Soils. Proceedings of International Symposium on the Mechanical Behaviour of Structured Media., Ottawa, pp.205-245.
- Lee, K. L., Morrison, R. A., and Haley, S. C., 1969. A Note on the Pore Pressure Parameter B. Proceedings of the 7th International Conference on Soil Mechanics and Foundation Engineering, Mexico, pp. 231-238.

- Lowe, J., Zaacheo, P. F. and Feldman, X., 1964. Consolidation Testing With Back Pressure. ASCE, Vol. 90, SM5, Proc. Paper 4058, 69-86.
- McRoberts, E. C. and Morgenstern, N. R., 1975. Pore Water Expulsion during Freezing. Canadian Geotechnical Journal, Vol. 12, No. 1, pp. 130-141.
- Seed, H. B., Singh, M., Chan, C. K., and Vilela, T. F., 1982. Considerations in Undisturbed Sampling of Sands. ASCE GT2 Vol. 108, pp. 265-283
- Sego, D. C., Robertson, P. K., Sasitharan, S., Kilpatrick, B. L. and Pillai, V. S., 1994. Ground Freezing and Sampling of Foundation Soils at Duncan Dam, Canadian. Geotechnical Journal, Vol. 31, No. 6, pp. 939-950.
- Sasitharan, S., 1989. Stress Path Dependency of Dilatancy and Stress-Strain Response of Sand. M.A.Sc. Thesis, University of British Columbia, Vancouver, BC.
- Singh, S., Seed, H. B. and Chan, C. K., 1982. Undisturbed Sampling of Saturated Sands by Freezing. ASCE GT2 Vol. 108, pp. 247-263.
- Skempton, A. W., 1954. The Pore-Pressure Coefficients A and B. Géotechnique. Vol. 4. No. 4, pp. 143-147.
- Sobkowicz, J. C., 1982. The Mechanics of Gassy Sediments. Ph.D. Thesis, University of Alberta, Edmonton, AB, 531 pp.
- Vaid, Y. P., 1996. CANLEX - Scientific Committee and Management Committee Meetings, May 28-29, 1996, Kamloops, B.C. 400 pp.
- Williams P. J., 1967. The Nature of Freezing Soil and its Field Behaviour. Norwegian Geotechnical Institute, Publication No. 72., pp. 91-119.
- Yoshimi, Y., Hatanaka, M., and Oh-Oka, H., 1978. Undisturbed Sampling of Saturated Sands by Freezing. Soils and Foundations, Vol. 18, No. 3, September, pp. 59-73.

Table 7-1: Summary of Void Ratio Changes During Thawing of Undisturbed Specimens.
 Recovered from the CANLEX Test Sites, under an Effective Stress of 20 kPa.

Test Site	p' (in-situ) kPa	P' (lab) kPa	Δe (thaw/Consol.)
Phase I	350	20	0.077
Phase II	86	20	0.043
Phase III	29	20	0.021

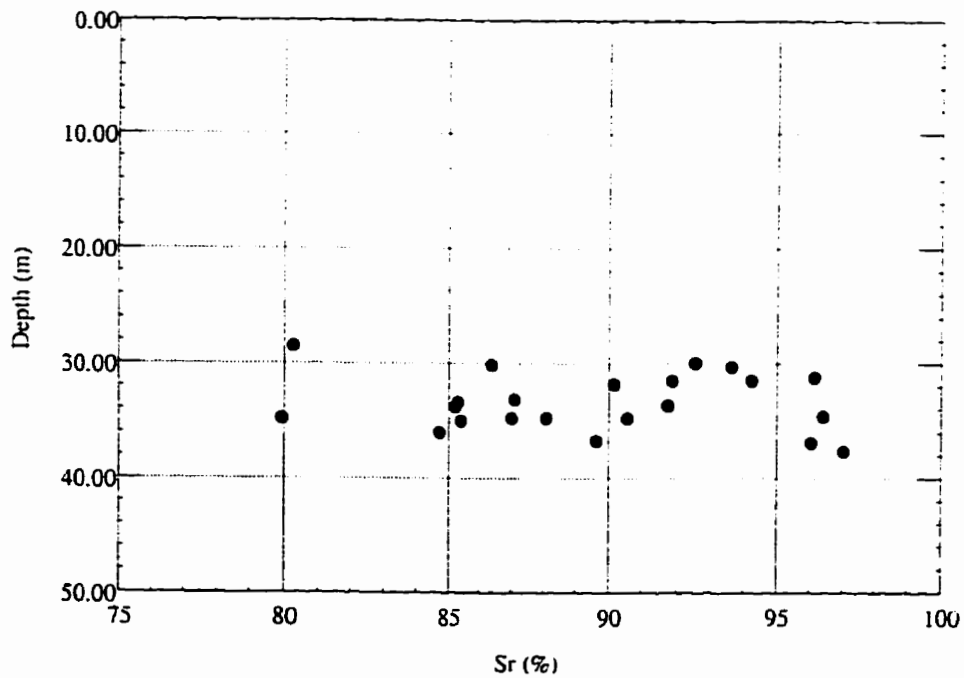


Figure 7-1: Estimated In-Situ Degree of Saturation for Phase I Undisturbed Specimens

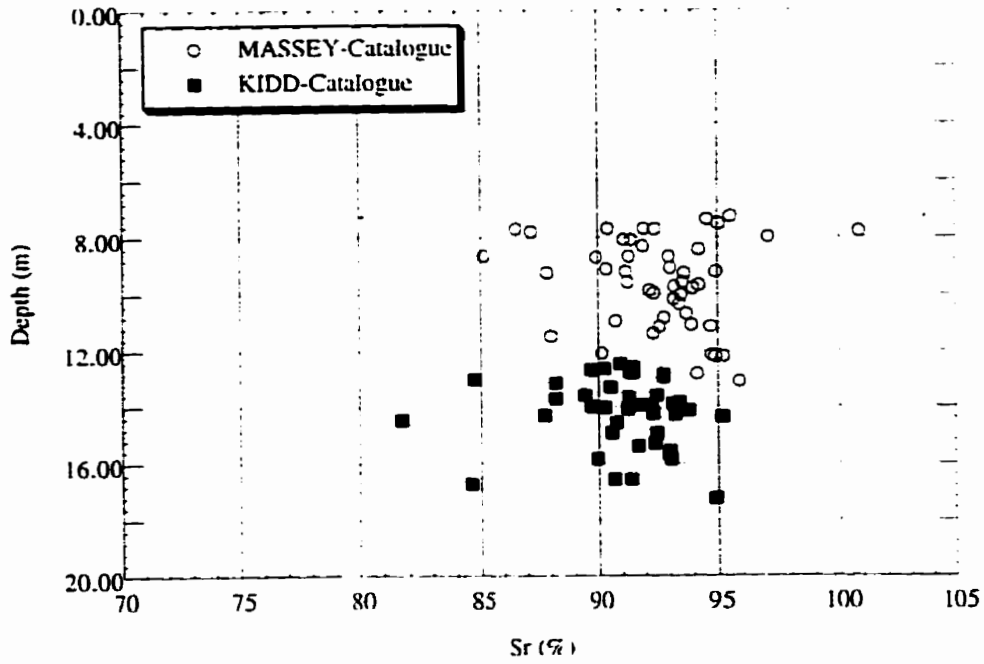


Figure 7-2: Estimated In-Situ Degree of Saturation for Phase II Undisturbed Specimens

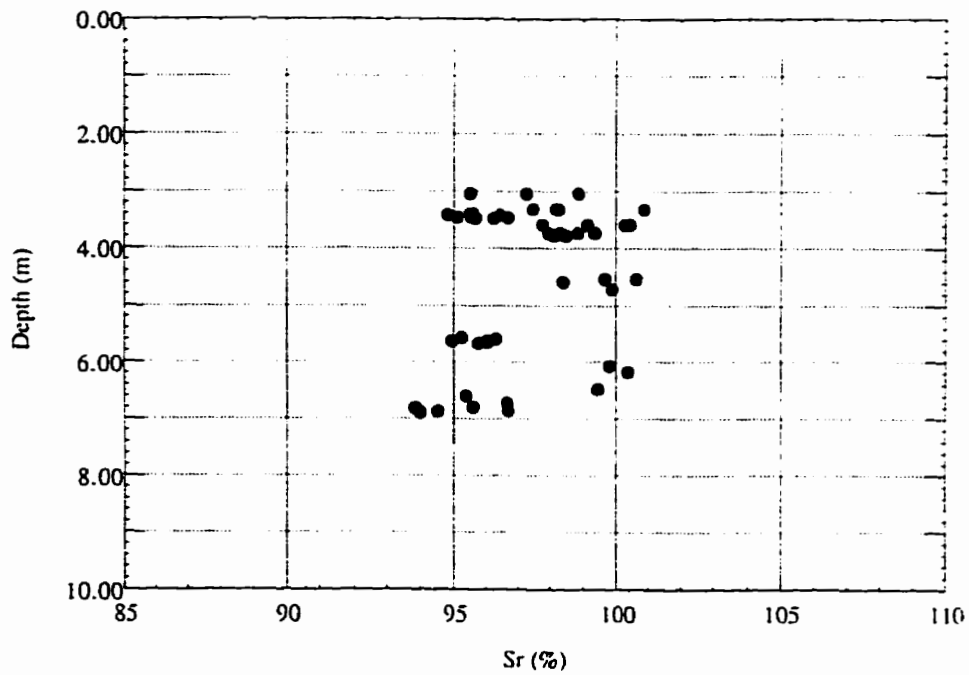


Figure 7-3: Estimated In-Situ Degree of Saturation for Phase III Undisturbed Specimens

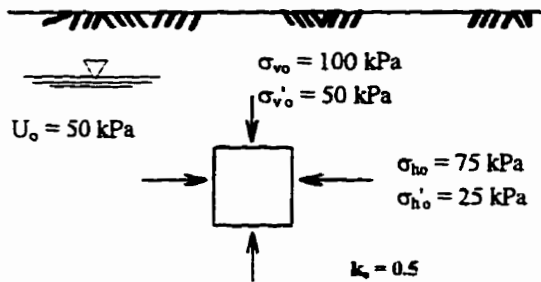


Figure 7-4a: Unfrozen Soil Element in Ground Under Anisotropic Stress Condition

- Assume expulsion of excess 9% porewater volume and soil is frozen without disturbance where, $U_o = \sigma_{ice}$

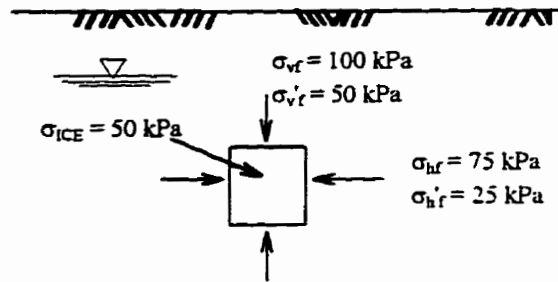


Figure 7-4b: Soil Element after In-Situ Ground Freezing

- Tensile stress develops in the ice, similar to the negative pore pressure response to sampling clay
- $$\sigma_{ICE} = \sigma_{v'o} \left\{ \left(\frac{1+2k_o}{3} \right) + (A_u - 1/3)(1-k_o) \right\}$$
- Assuming $A_u = 1/3$ for an elastic response,
- $$\sigma_{ICE} = 2/3 \sigma_{v'o} = -33 \text{ kPa}$$

- Note: Ice resembles a highly viscous pore fluid which responds to loading in an undrained manner.
- $$\Delta\sigma_{ICE} = B[\Delta\sigma_3 + A(\Delta\sigma_1 - \Delta\sigma_3)]$$
- For fully saturated, elastic soil:
- $$\Delta\sigma_{ICE} = 1.0[75 + 1/3(100 - 75)] = 83 \text{ kPa}$$
- $$\sigma_{ICE} = -33 + 83 = 50 \text{ kPa}$$

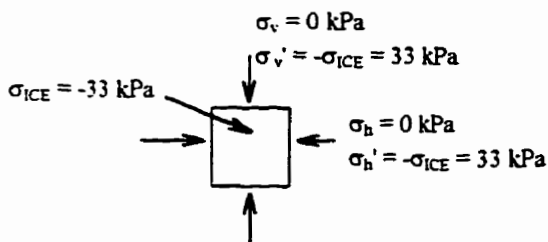


Figure 7-4c: Frozen Soil Element Removed from the Ground

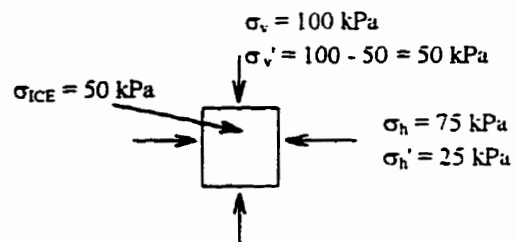


Figure 7-4d: Apply In-Situ Stresses to Frozen Soil in Triaxial Cell

- Assume expulsion of excess 9% porewater volume and soil is frozen without disturbance where, $U_o = \sigma_{ice}$

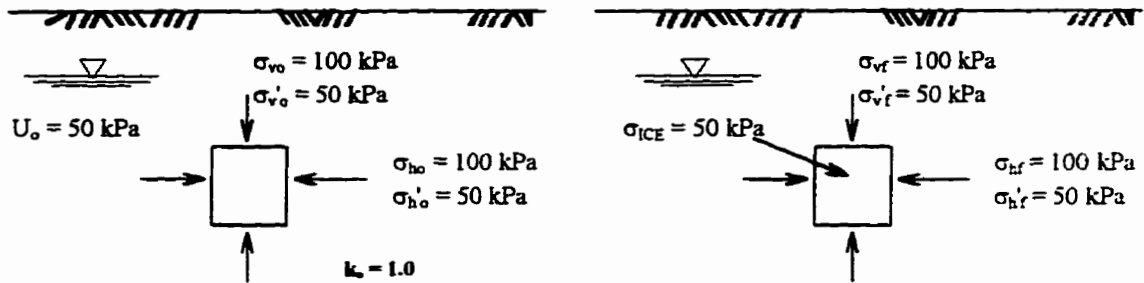


Figure 7-5a: Unfrozen Soil Element in Ground Under Isotropic In-Situ Stress Condition

Figure 7-5b: Soil Element after In-Situ Ground Freezing

- Tensile stress develops in the ice, similar to the negative pore pressure response to sampling clay
 $\sigma_{ICE} = \sigma_{vo}' = \sigma_{ho}' = 50 \text{ kPa}$

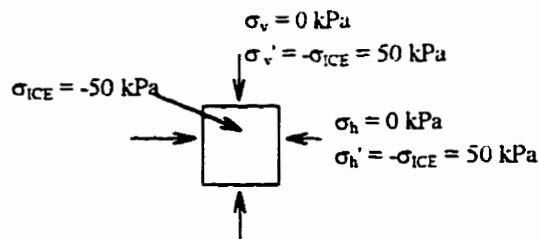


Figure 7-5c: Frozen Soil Element Removed from the Ground

- Note: Ice resembles a highly viscous pore fluid which responds to loading in an undrained manner.

$$\Delta\sigma_{ICE} = B[\Delta\sigma_3 + A(\Delta\sigma_1 - \Delta\sigma_3)] = 100 \text{ kPa}$$

$$\sigma_{ICE} = -50 + 100 = 50 \text{ kPa}$$

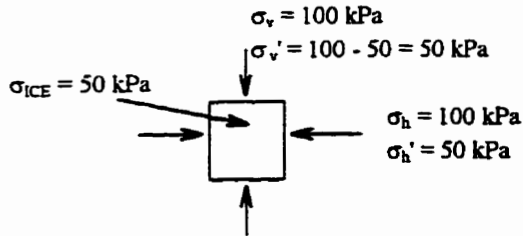


Figure 7-5d: Apply In-Situ Stresses to Frozen Soil in Triaxial Cell

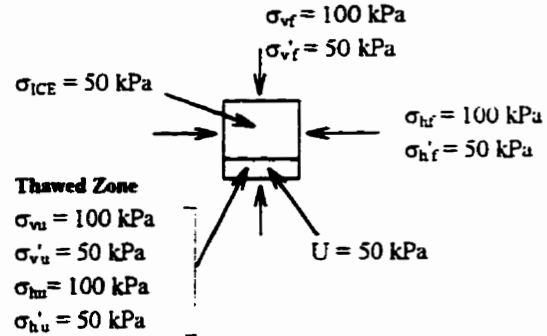


Figure 7-5e: Commence Thawing at Bottom of Specimen where Soil has Access to Pore Water at 50 kPa.

$$\Delta\sigma_{ICE} = B[\Delta\sigma_3 + A(\Delta\sigma_1 - \Delta\sigma_3)] = 20$$

$$\sigma_{ICE} = -50 + 20 = -30 \text{ kPa}$$

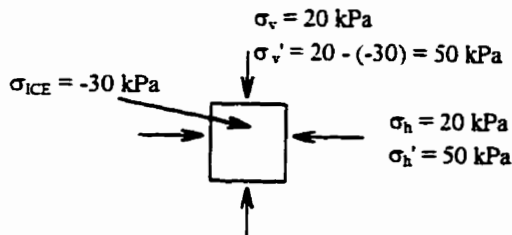


Figure 7-5f: Apply Isotropic Stresses of 20 kPa to Frozen Soil in Triaxial Cell

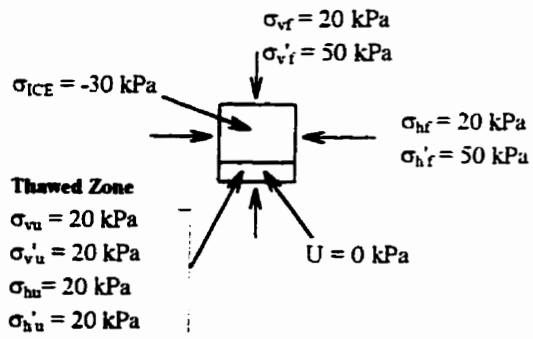


Figure 7-5g: Commence Thawing at Bottom of Specimen where Soil has Access to Pore Water at 0 kPa.

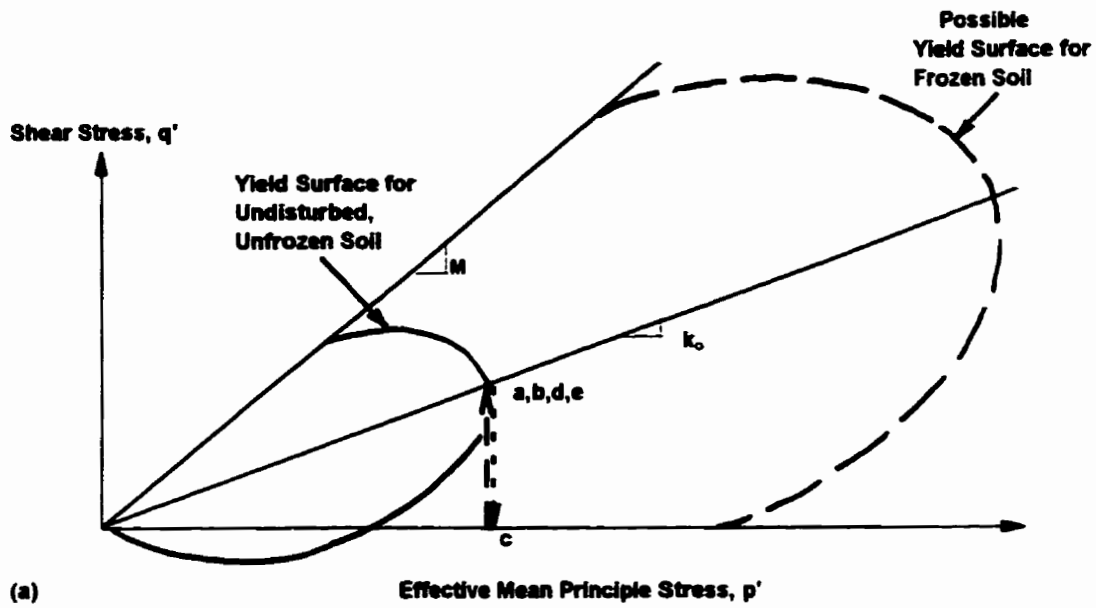


Figure 7-6a: Stress Path Taken by Specimen Thawed under the In-Situ Effective Stress

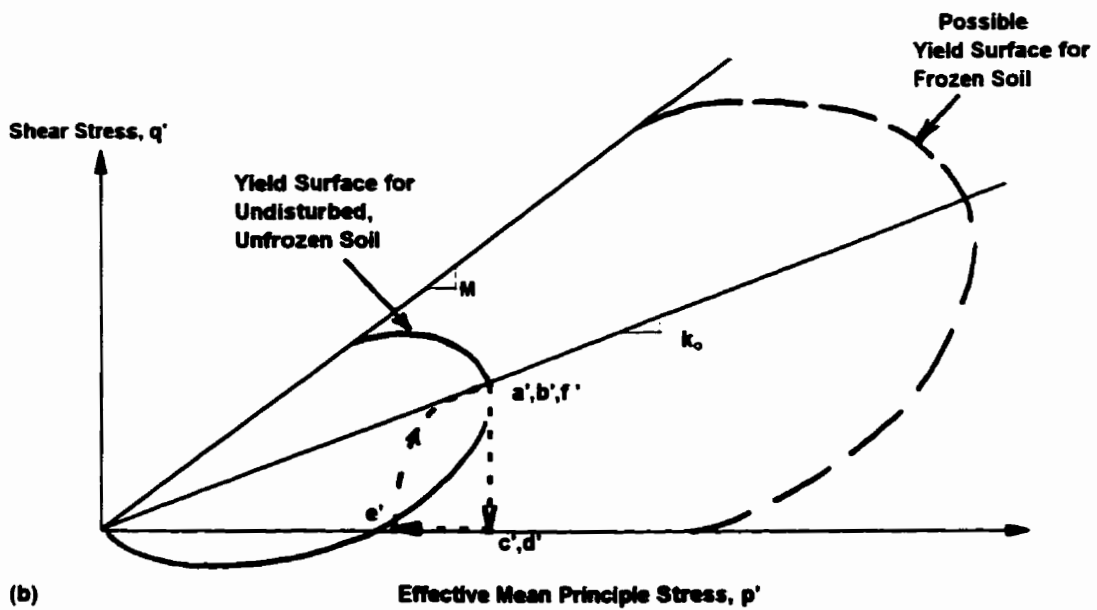


Figure 7-6b: Stress Path Taken by Specimen Thawed under a Small Effective Stress

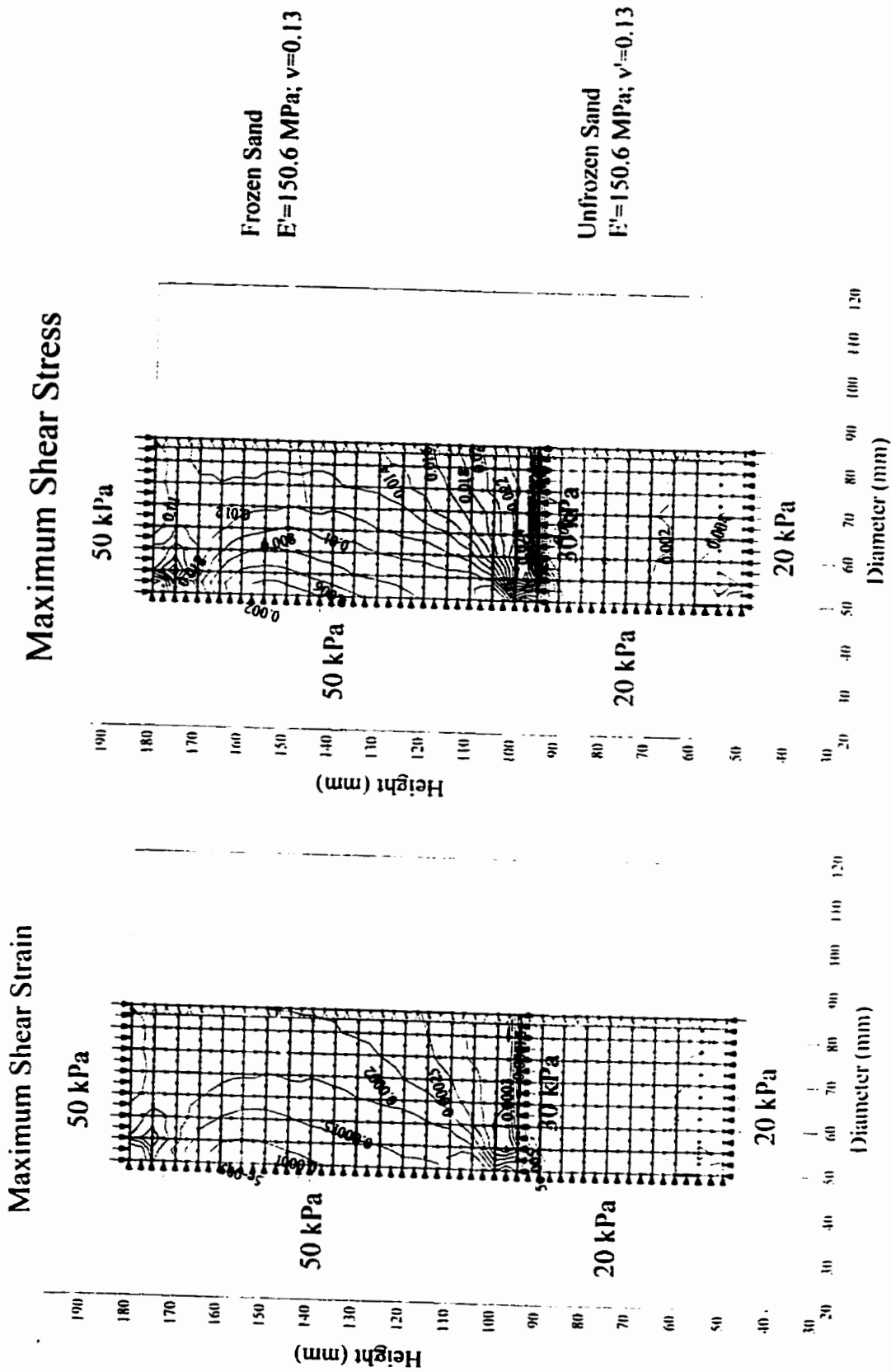


Figure 7-7: SIGMA/W Results, assuming Ice Acts Like a Viscous Pore Fluid, for Specimen Thawed Under a Small Effective Stress

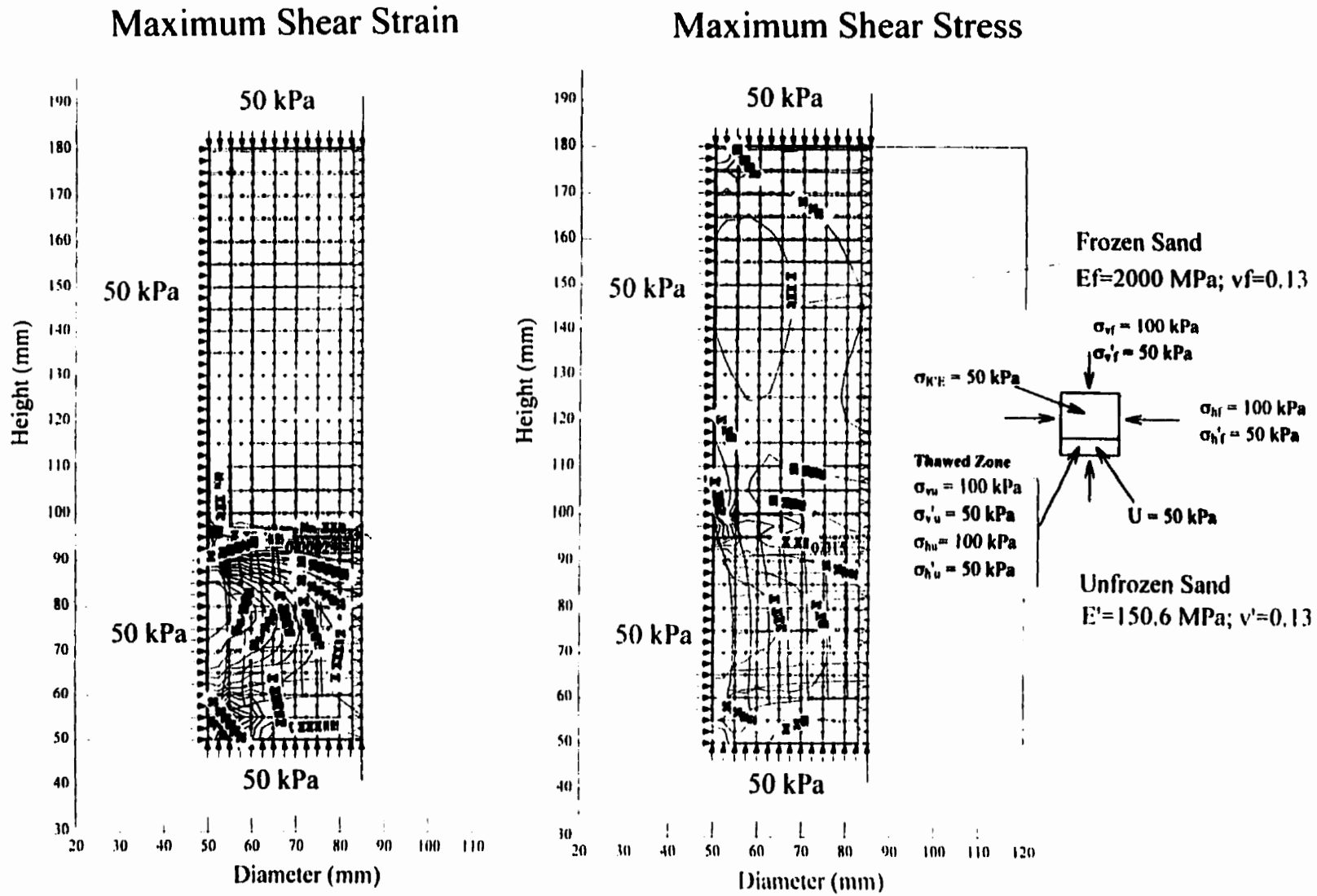
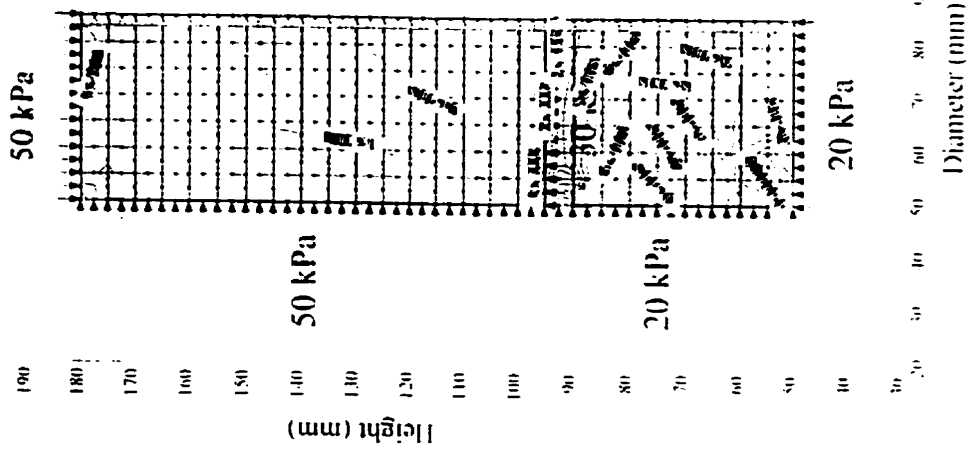


Figure 7-8: SIGMA/W Results, assuming Modulus of Frozen and Unfrozen Sand are Different, for Specimen Thawed Under the In-Situ Effective Stress

Maximum Shear Strain



Maximum Shear Stress (N/mm²)

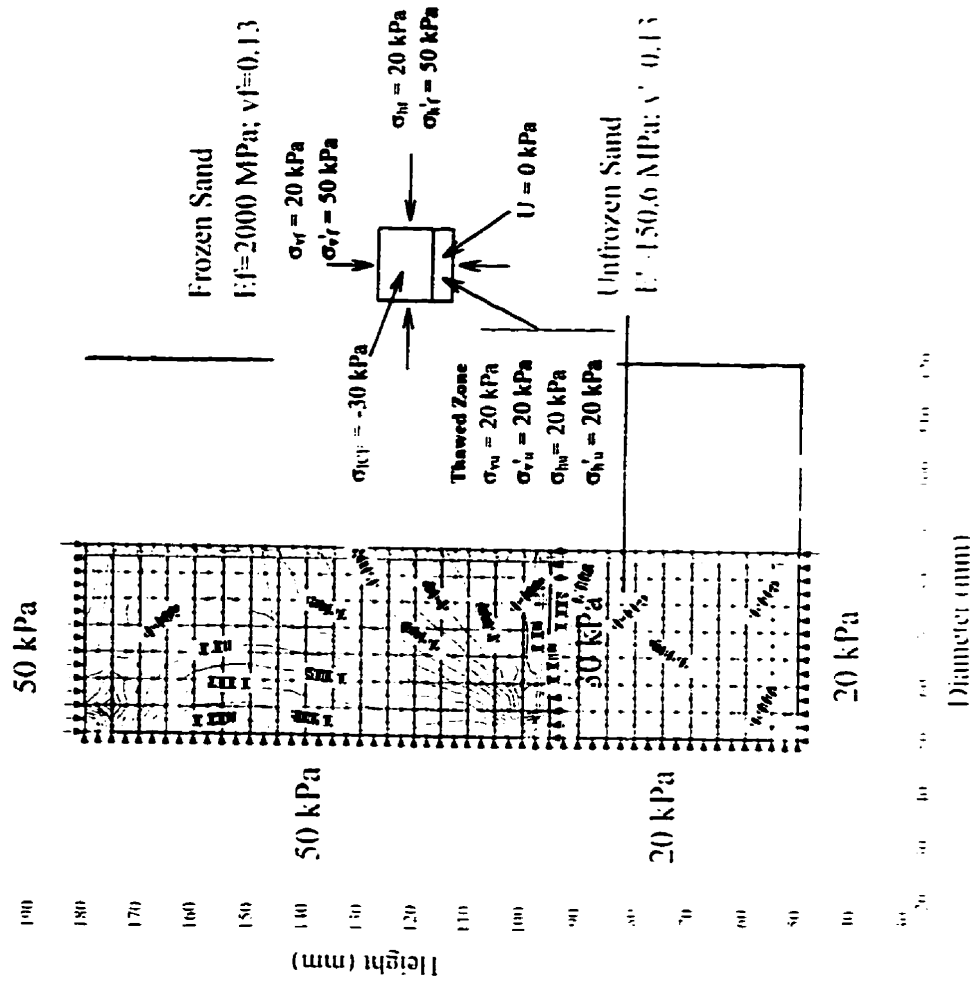
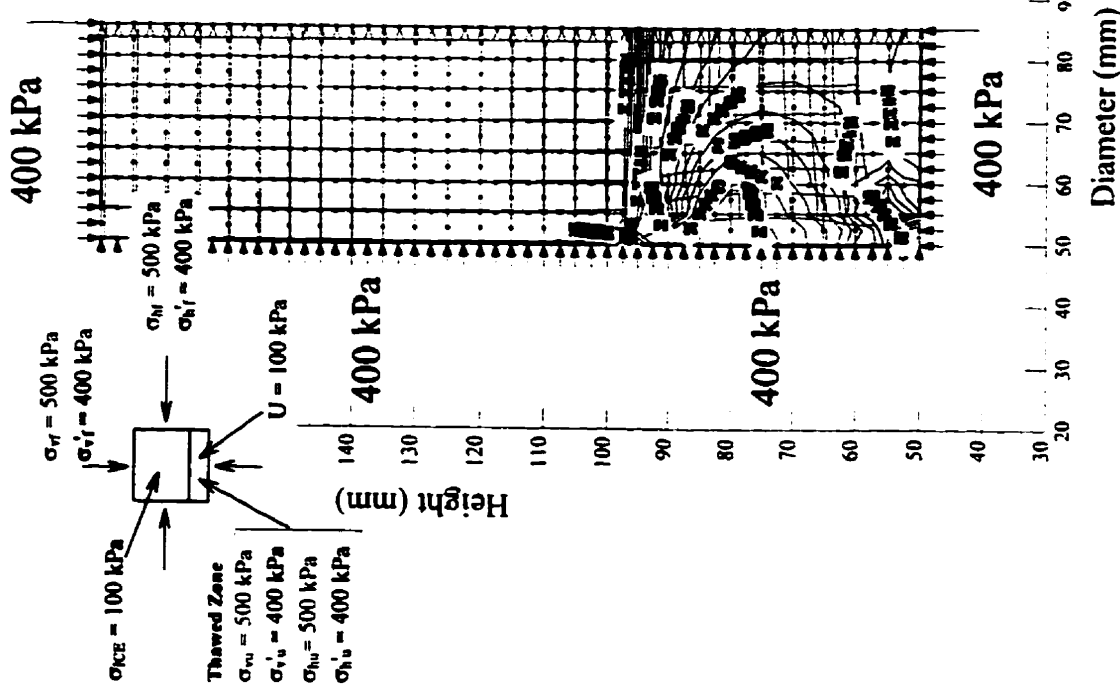


Figure 7-9: SIGMA/W Results, assuming Modulus of Frozen and Unfrozen Sand are Different, for Specimen Thawed Under a Small Effective Stress

Maximum Shear Strain



Maximum Shear Strain

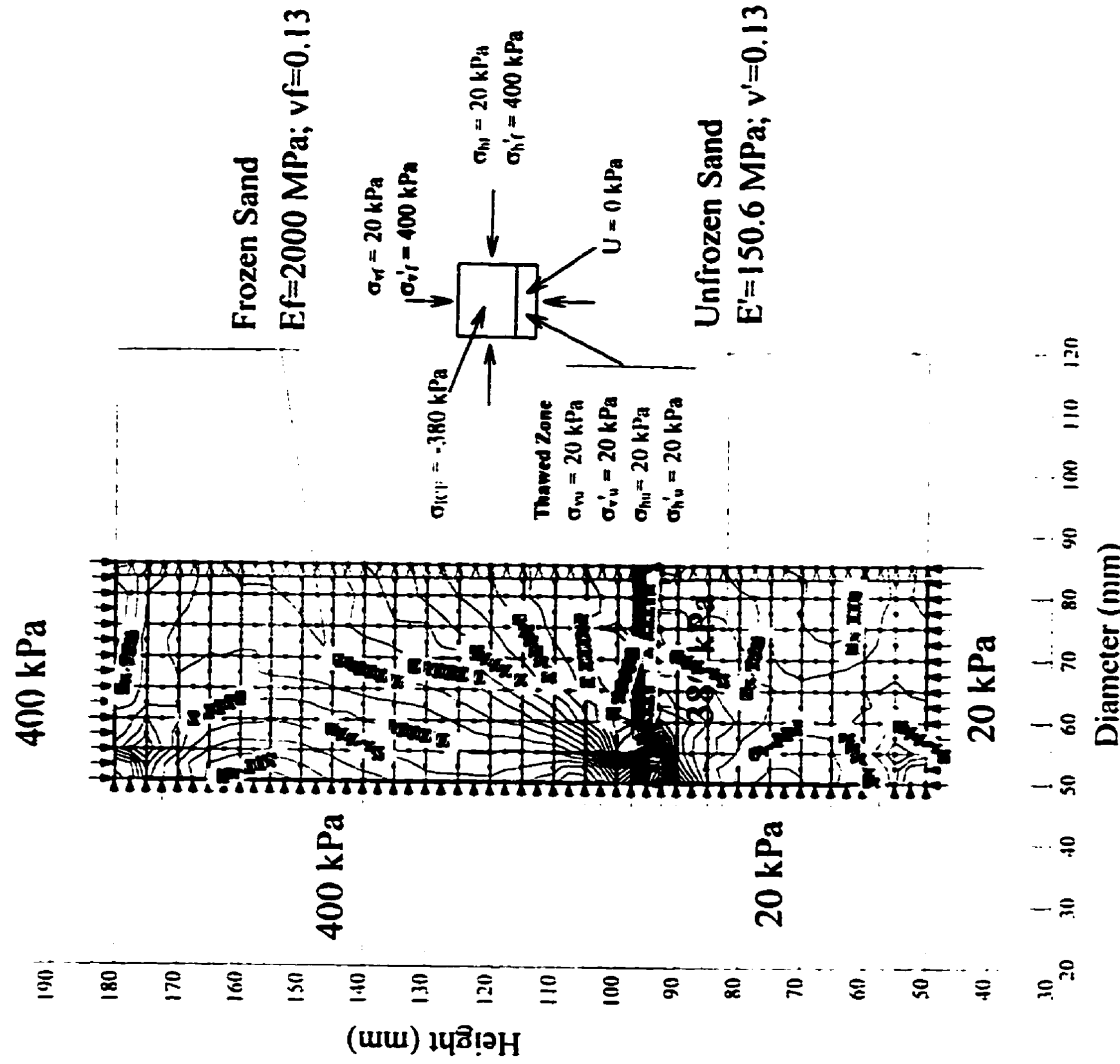


Figure 7-10: SIGMA/W Results, Comparing Maximum Shear Strains for Specimens with High In-Situ Stresses, Thawed Under a Small Effective Stress or Under the In-Situ Effective Stress.

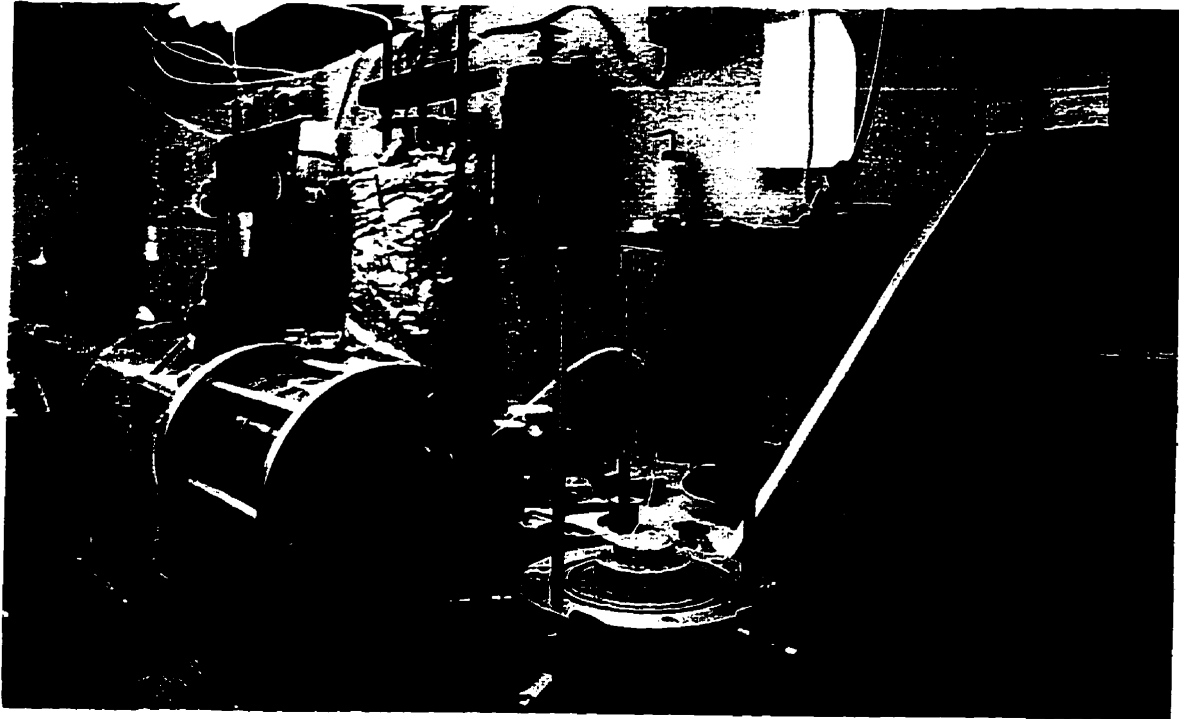


Figure 7-11: Triaxial Cell Cooling Coil used to Prevent Premature Uncontrolled Thawing of Reconstituted Specimens

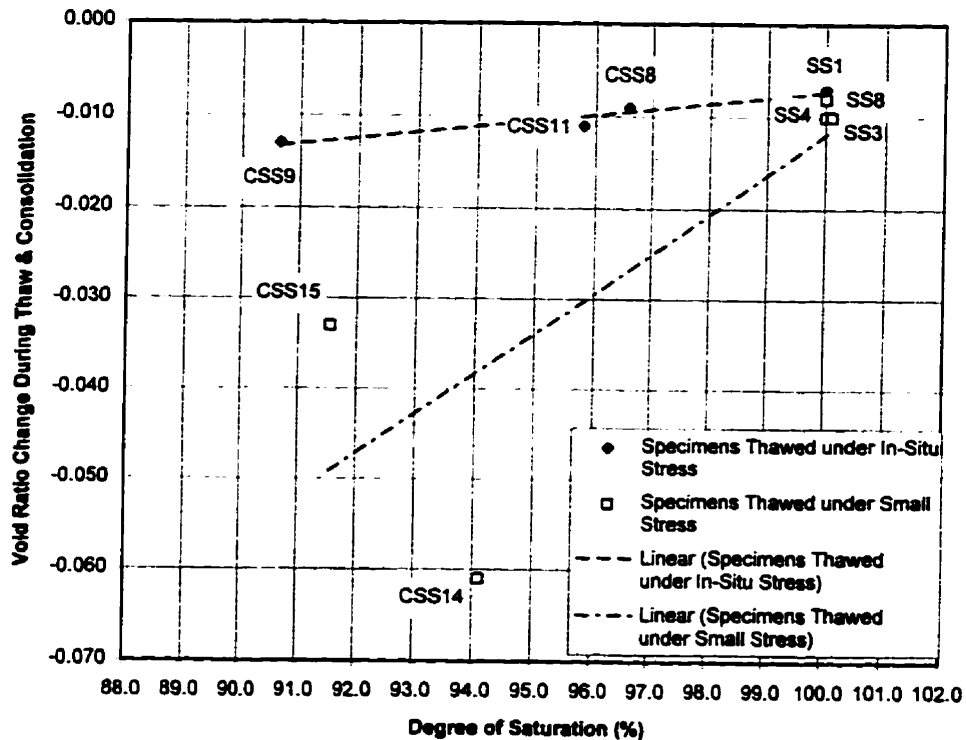


Figure 7-12: Comparison of Void Ratio Changes for Different Thawing Methodologies used on Reconstituted Syncrude Sand Specimens and the Effect of Degree of Saturation.

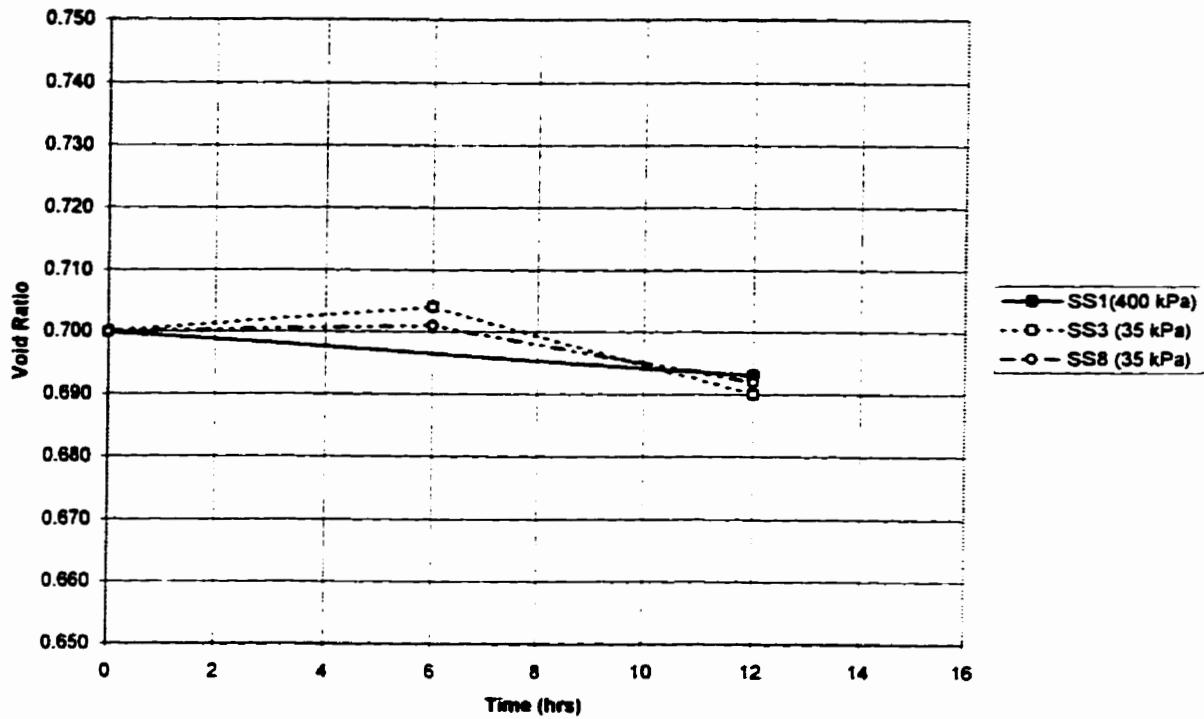


Figure 7-13: Comparison of Void Ratio Changes during Thawing and Consolidation of Reconstituted Syncrude Sand Specimens Thawed under the In-Situ Effective Stress or under a Small Effective Stress.

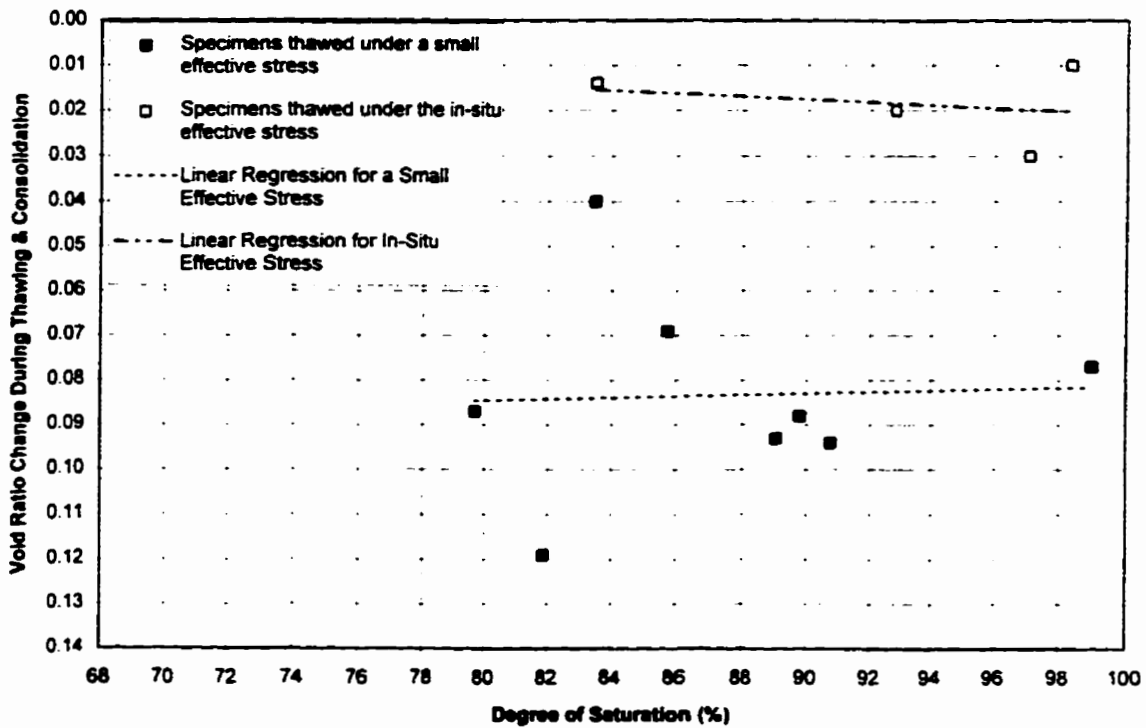
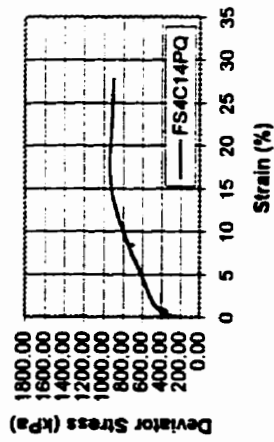
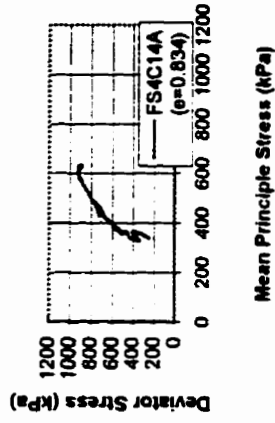


Figure 7-14: Comparison of Change in Void Ratio During Thawing and Consolidation of Undisturbed Phase I Specimens subject to the In-Situ Effective Stress or a Small Effective Stress during Thawing.

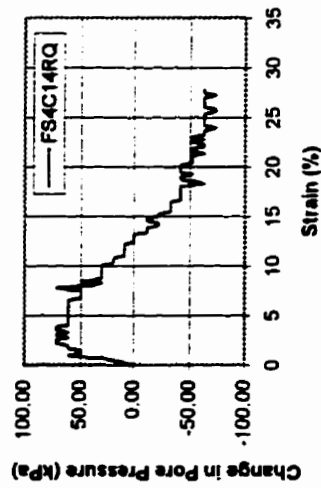
Stress Strain Curve



P'-Q Diagram for Phase I Undisturbed Syncrude Sand Specimens



Pore Pressure Response



Triaxial Compression Test on Undisturbed Phase I Syncrude Sand Specimen FS4C14

Initial Frozen Void Ratio: $Sr = 86\%$
 $B_{bar} = 1$

Thawing Conditions: Unidirectional thawing from base of specimen under in-situ stresses

Stresses During Thawing and Consolidation:

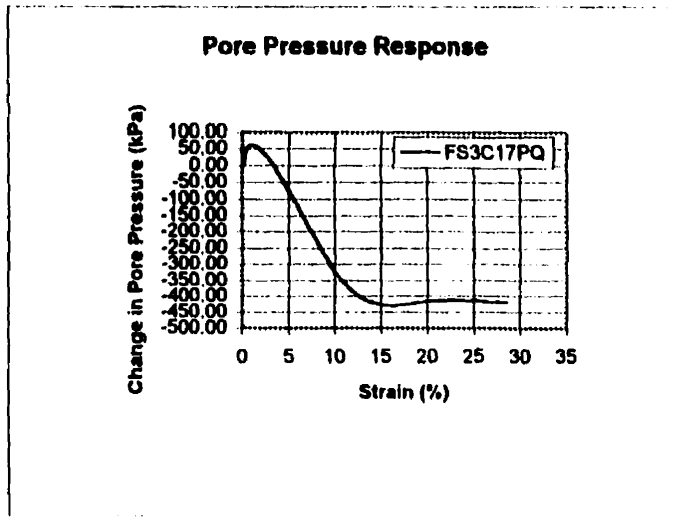
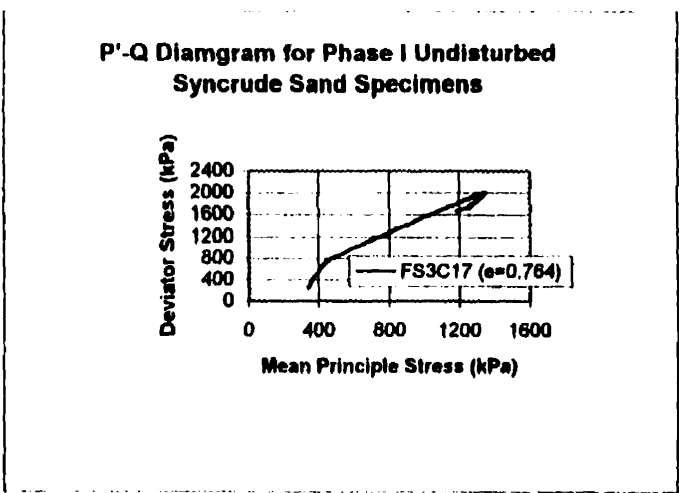
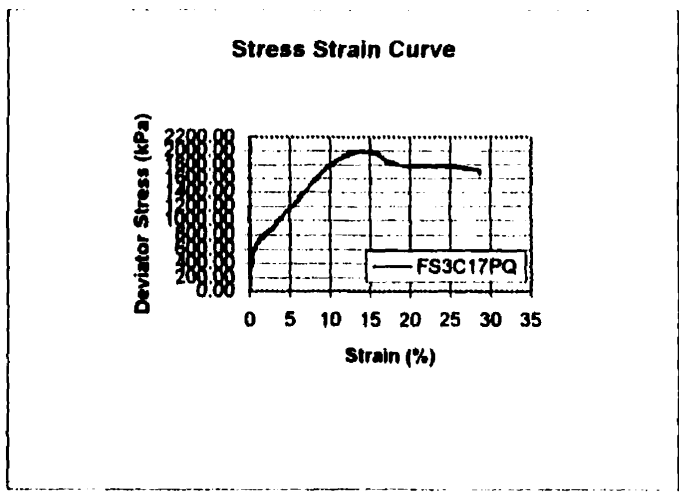
$\sigma_{total} = 627$ kPa	$q_u = 240$ kPa
$\sigma_{cell} = 387$ kPa	$p'_u = 320$ kPa
$U = 147$ kPa	
$k_c = 0.5$	

Void Ratio after Thawing and Consolidation: 0.834

Steady State Condition Reached :

$q_u = 934$ kPa
$p'_u = 634$ kPa

Figure 7-15: Undrained Triaxial Compression Test Results for Undisturbed Specimen FS4C14A



Triaxial Compression Test on Undisturbed Phase I Syncrude Sand Specimen FS3C17

Initial Frozen Void Ratio: 0.764 Sr = 100% (back saturated)

B bar = 1

Thawing Conditions: Unidirectional thawing from base of specimen under in-situ stresses

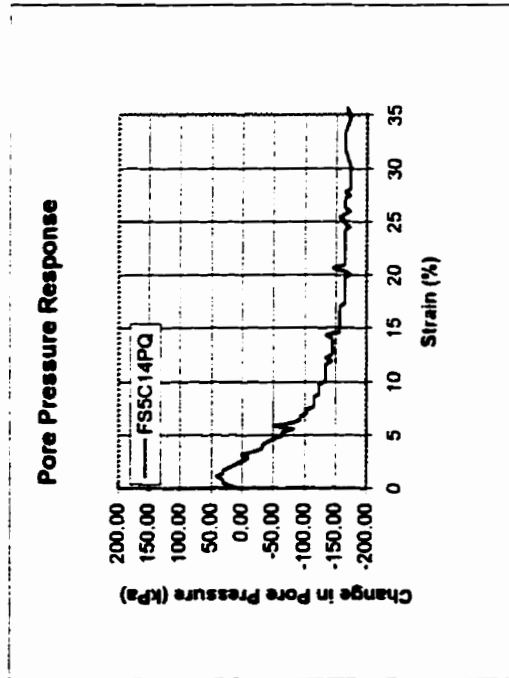
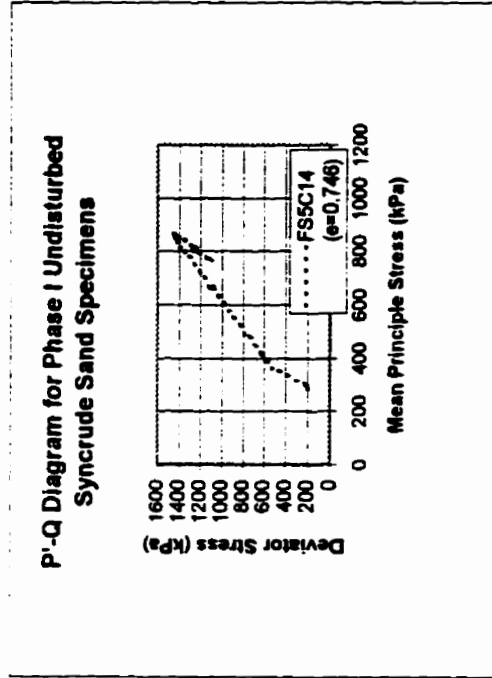
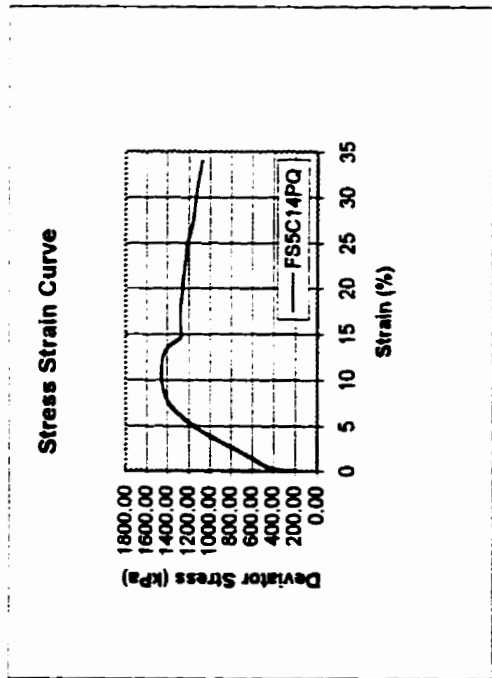
Stresses During Thawing and Consolidation:

σ_{axial} = 658 kPa	q_u = 247 kPa	
σ_{cell} = 411 kPa	p'_u = 330 kPa	
U = 163 kPa		
k_a = 0.6		

Void Ratio after Thawing and Consolidation: 0.734

Steady State Condition Reached : q_{ss} = 2007 kPa
 p'_{ss} = 1355 kPa

Figure 7-16: Undrained Triaxial Compression Test Results for Undisturbed Specimen FS3C17B



Triaxial Compression Test on Undisturbed Phase I Syncrude Sand Specimen FS5C14

Initial Frozen Void Ratio: $Sr = 96\%$
 $B_{bar} = 0.372$

Thawing Conditions: Unidirectional thawing from base of specimen under in-situ stresses

Stresses During Thawing and Consolidation:

$\sigma_{solid} = 602$ kPa	$q_u = 234$ kPa
$\sigma_{cell} = 368$ kPa	$p'_{cs} = 312$ kPa
$U = 133$ kPa	
$k_c = 0.5$	

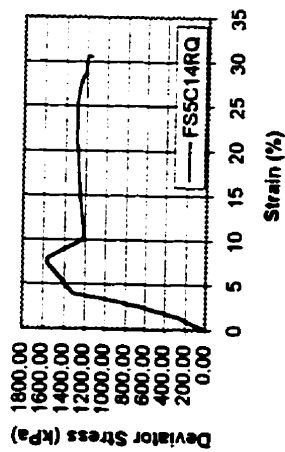
Void Ratio after Thawing and Consolidation: 0.737

Steady State Condition Reached :

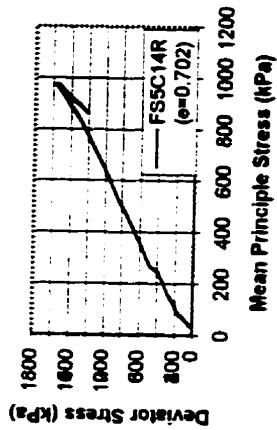
$q_{ss} = 1458$ kPa
$p'_{ss} = 869$ kPa

Figure 7-17: Undrained Triaxial Compression Test Results for Undisturbed Specimen FS5C14

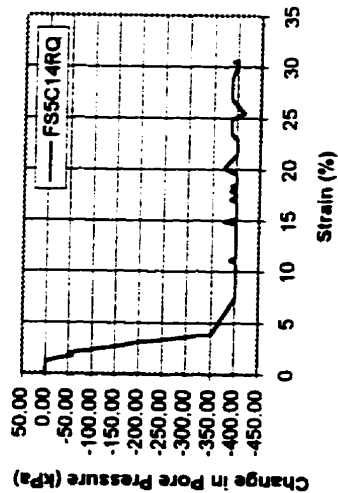
Stress Strain Curve



P'-Q Diagram for Phase I Reconstituted Undisturbed Syncrude Sand Specimens



Pore Pressure Response



Triaxial Compression Test on Undisturbed Phase I Syncrude Sand Specimen FS5C14R

Initial Frozen Void Ratio: 0.702 $S_r = 100\%$
 $B \text{ bar} = 1$

Thawing Conditions: Unidirectional thawing from base of specimen under in-situ stresses

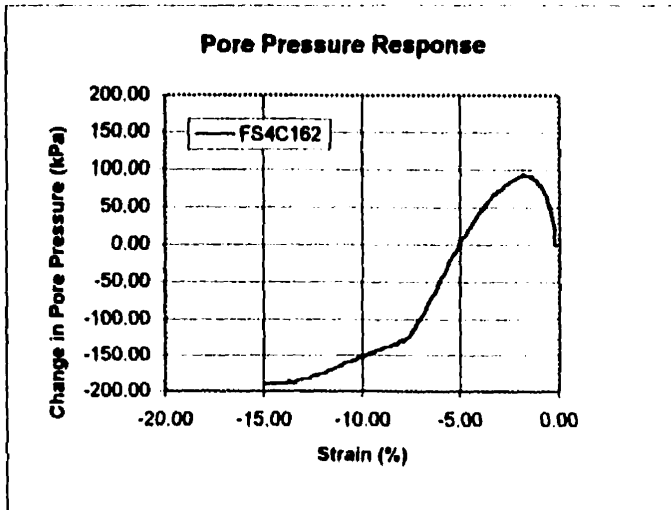
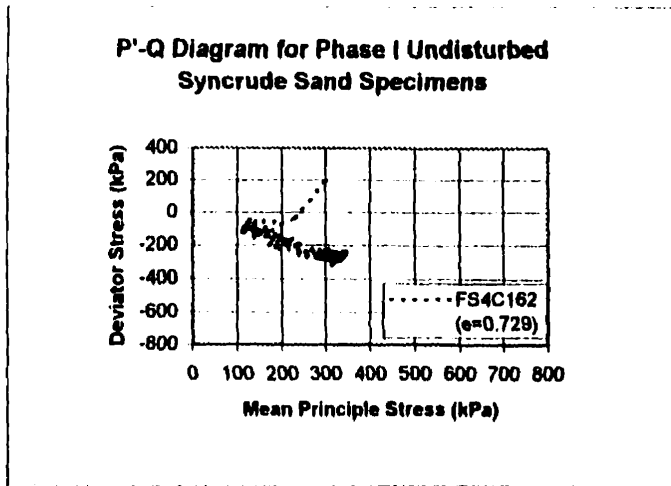
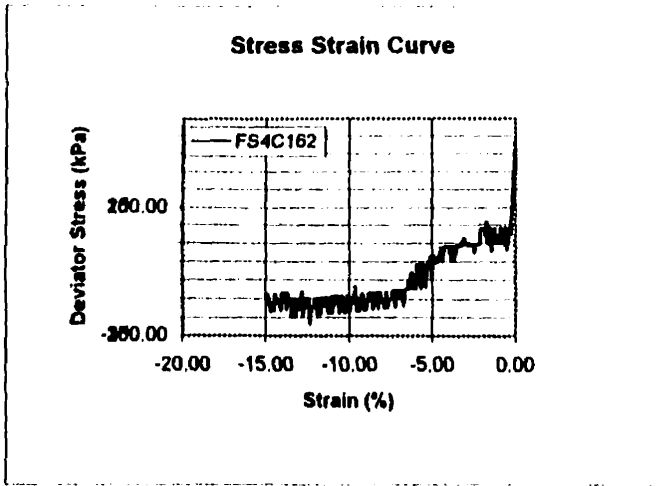
Stresses During Thawing and Consolidation:

$\sigma_{\text{total}} = 315 \text{ kPa}$	$q_p = 0 \text{ kPa}$
$\sigma_{\text{cell}} = 315 \text{ kPa}$	$p'_s = 36 \text{ kPa}$
$U = 280 \text{ kPa}$	
$k_s = 0.5$	

Void Ratio after Thawing and Consolidation: 0.700

Steady State Condition Reached: $q_{ss} = 1584 \text{ kPa}$
 $p'_{ss} = 997 \text{ kPa}$

Figure 7-18: Undrained Triaxial Compression Test Results for Reconstituted Specimen FS5C14R



Triaxial Extension Test on Undisturbed Phase I Syncrude Sand Specimen FS4C16-2

Initial Frozen Void Ratio: 0.729 $S_r = 97.46\%$
 $B_{bar} = 0.55$
 Thawing Conditions: Unidirectional thawing from base of specimen under in-situ stresses

Stresses During Thawing and Consolidation:

$\sigma_{axial} = 655$ kPa $q_o = 248$ kPa
 $\sigma_{cell} = 408$ kPa $p'_{o1} = 329$ kPa
 $U = 181$ kPa
 $k_o = 0.5$

Void Ratio after Thawing and Consolidation: 0.612

Steady State Condition Reached : $q_{ss} = -281$ kPa
 $p'_{ss} = 282$ kPa

Figure 7-20: Undrained Triaxial Compression Test Results for Undisturbed Specimen FS4C16-2

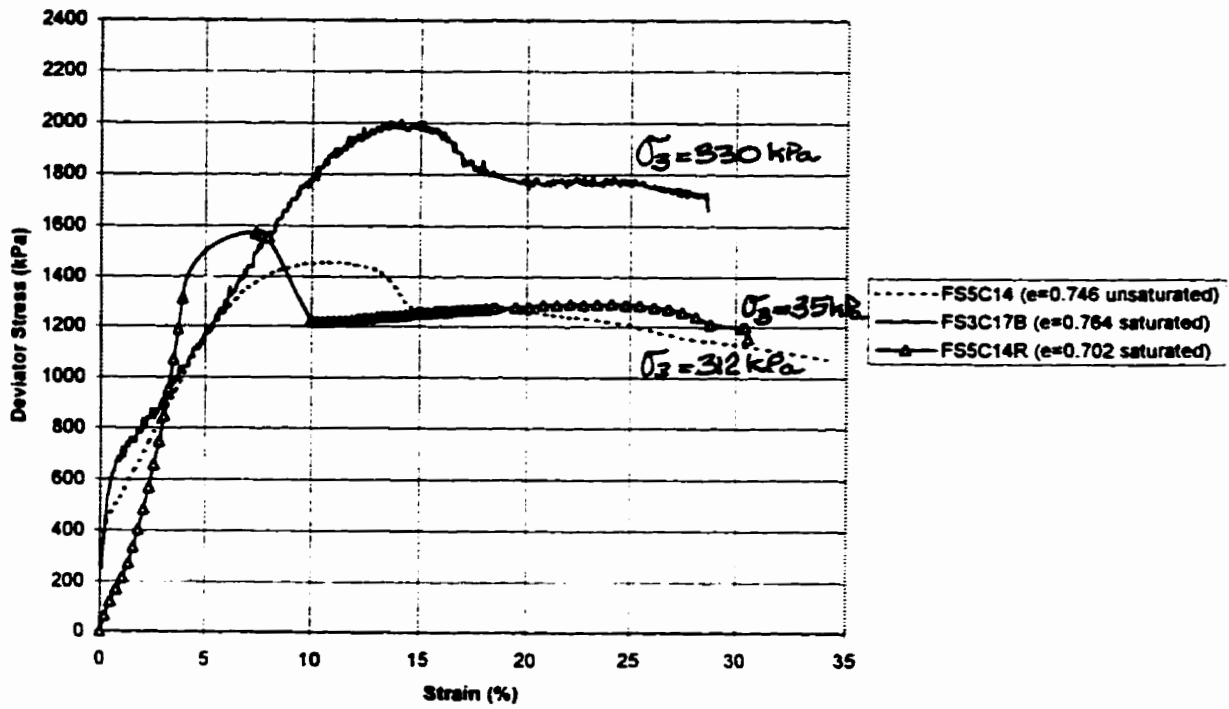


Figure 7-21a: Stress Strain Curves Obtained for Specimens FS5C14, FS5C14R and FS3C17B, Illustrating Effect of Degree of Saturation.

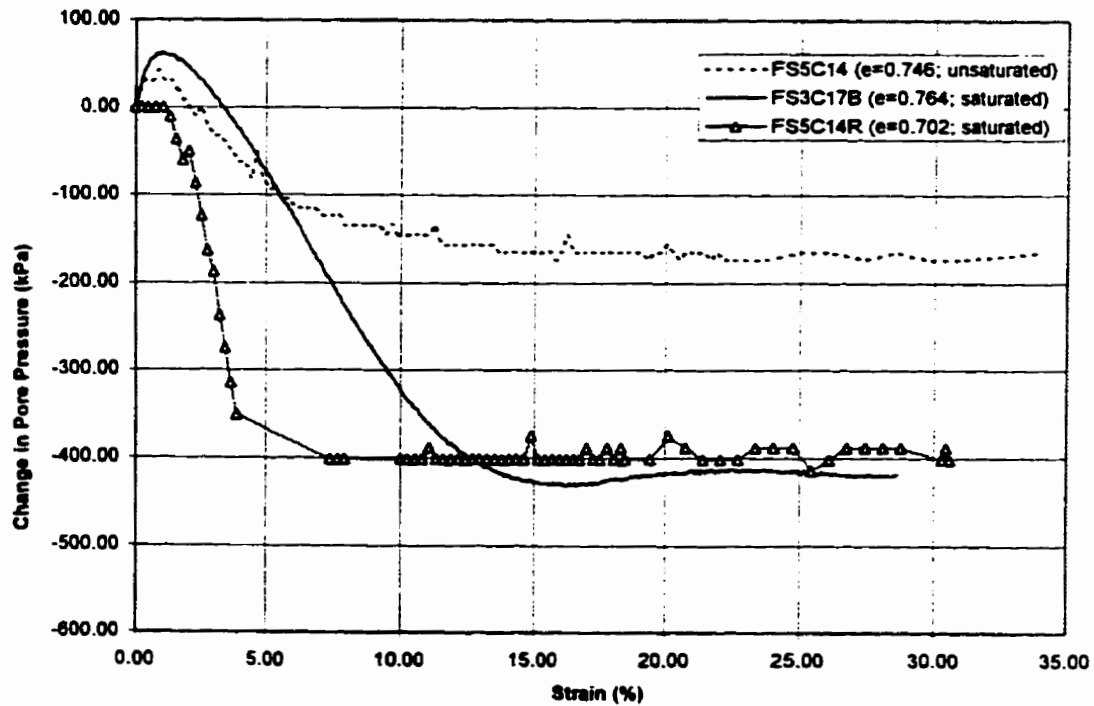


Figure 7-21b: Pore Pressure Response Curves Obtained for Specimens FS5C14, FS5C14R and FS3C17B, Illustrating Effect of Degree of Saturation.

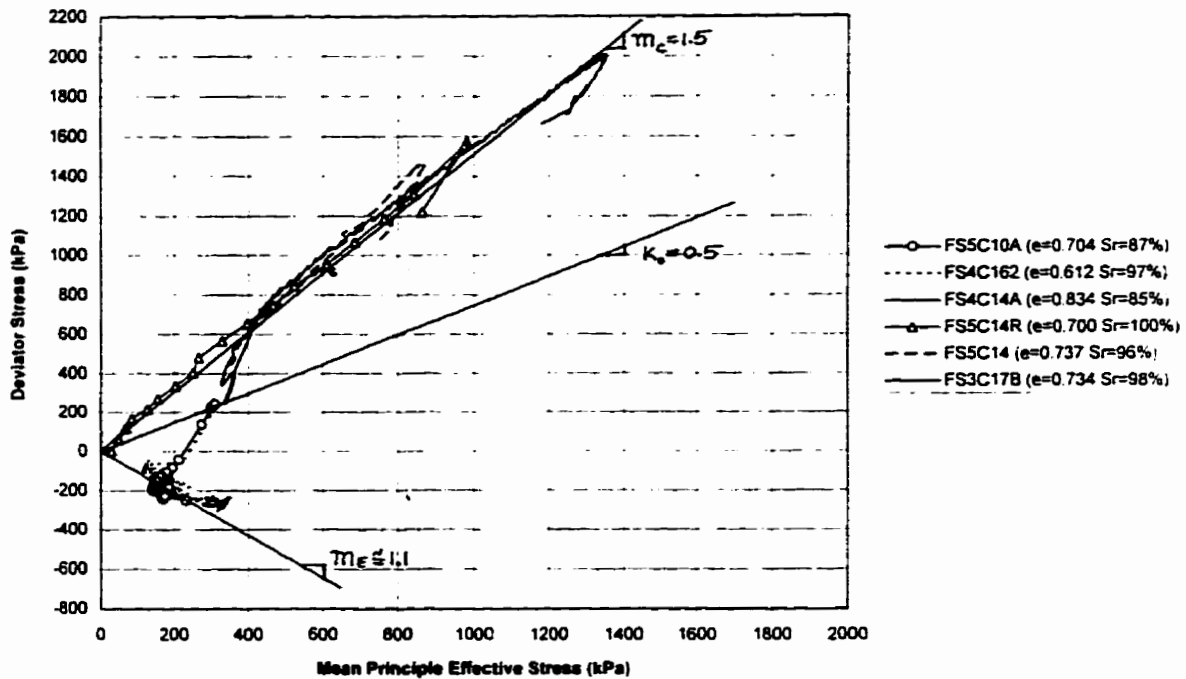


Figure 7-22: Summary of Stress Paths followed by Undisturbed Phase I Specimens during Undrained Triaxial Compression and Triaxial Extension Tests

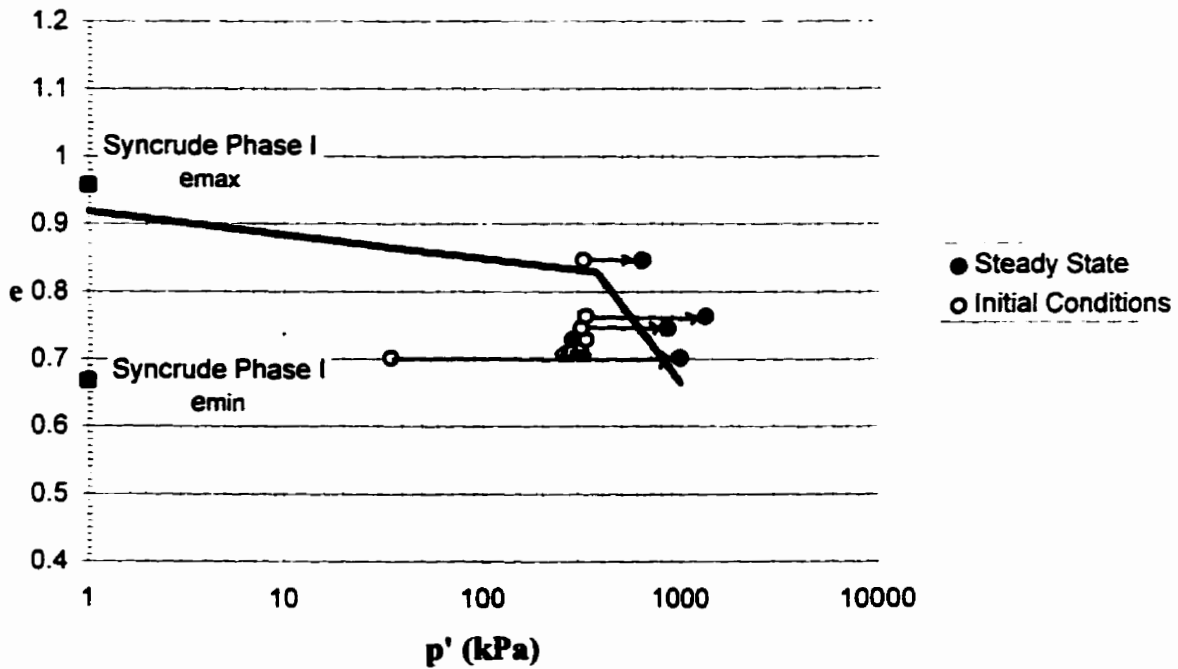


Figure 7-23: Steady State Diagram for Undisturbed Phase I Specimens

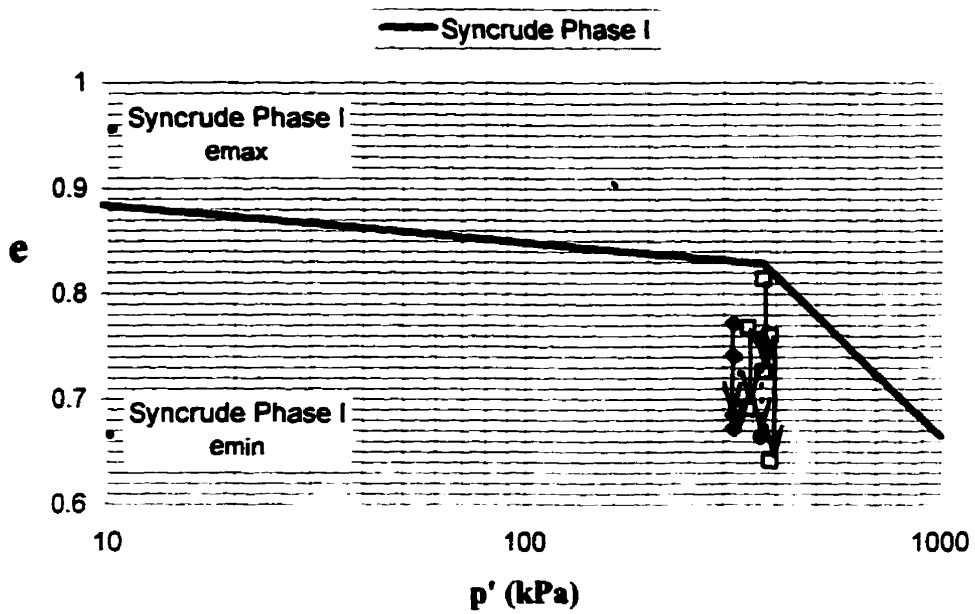


Figure 7-24: Effective of Void Ratio Disturbance Caused by Thawing Undisturbed Phase I Specimens under a Small Effective Stress with Respect to the Steady State Line.

CHAPTER 8: Conclusions and Recommendations

8.1 Conclusions

Evaluating whether or not a sand deposit has the potential to undergo a liquefaction failure in the event of adverse loading conditions, is an important engineering task that requires detailed characterization of the in-situ state of the deposit. Liquefaction assessment requires that the in-situ values of void ratio, shear stress, and mean normal effective stress be determined and compared with the ultimate or steady state conditions that develop after significant deformation. To completely characterize a sand deposit, it is necessary to obtain undisturbed samples from the ground for carrying out laboratory assessment of the in-situ strength and deformation properties. Ultimately, the laboratory response of undisturbed specimens can then be linked with the results of field tests, such as Cone Penetration Testing and Standard Penetration testing, that can be carried out over a much greater area across a given site or within many sites containing sands with similar characteristics and geological history.

The factors which affect the actual flow liquefaction susceptibility of a soil deposit include material properties which govern the relative positions of the steady state line, the loosest isotropic consolidation line and the densest isotropic consolidation line and hence, the range of in-situ states where flow liquefaction could be triggered. These properties include grain size distribution, particle shape, particle hardness, fines content and fines plasticity. Similarly, the cyclic liquefaction characteristics of a sand deposit is a function of both material properties and site conditions, including the void ratio, structural arrangement of sand grains (fabric, mineralogy, and degree of cementation), seismic history, the in-situ lateral stress condition and the age of the deposit. Directly assessing

the net effect of these factors on the response of sand to certain loading conditions requires appropriate laboratory testing of undisturbed samples.

If conventional sampling techniques are utilized, it is difficult to obtain high quality undisturbed samples of loose sand below the groundwater table. Disturbance associated with conventional sampling may result in misleading laboratory test results. Ideally, if samples are to be considered as truly undisturbed, the void ratio, fabric, structure, stress history and degree of saturation should be preserved during the sampling and handling process. To meet this requirement, in the last approximately fifteen years, the technique of utilizing in-situ ground freezing for obtaining undisturbed samples of loose, saturated sand has been demonstrated to be effective by both Japanese and North American researchers.

This thesis was undertaken to evaluate the extent to which characteristics such as void ratio, fabric, structure and degree of saturation can be preserved during in-situ ground freezing for a variety of subsoil and site conditions. Feasibility studies were carried out to confirm that ground freezing could be used at four different test sites to obtain undisturbed samples, where the in-situ void ratio and fabric would be preserved. Ground freezing and coring of the frozen sand was then successfully carried out at each of the test sites. A thawing protocol study was then undertaken to determine the most appropriate method of thawing the frozen undisturbed specimens, without causing disturbance of the in-situ conditions.

The research conducted showed that in-situ ground freezing is an excellent technique for obtaining high quality undisturbed samples of sand from a wide range of granular deposits. The main conclusions that were drawn from this research are summarized below:

- The frost heave susceptibility of a soil depends on the soil grain size distribution, including the percentage of fines and their mineralogy, the unfrozen water content,

the drainage boundary conditions, the overburden stress and rate of cooling compared to the permeability of the deposit. Disturbance by frost heave is caused by either ice lenses forming in frost heave susceptible soils or when the excess 9 % of pore water volume freezes in place.

- The chart presented by Davila et al. (1992), which takes into account the effect of the fines mineralogy on frost heave potential, can be utilized, in conjunction with bulk samples obtained from a specific site, as a preliminary estimate of the frost heave susceptibility of the deposit.
- Prior to conducting in-situ ground freezing, it is prudent to carry out frost heave tests in the laboratory, under the overburden stress and rate of cooling that would exist during ground freezing, to confirm that this method is appropriate for obtaining undisturbed samples.
- The risk of disturbance due to frost heave can be reduced by conducting radial ground freezing, such that pore water expulsion can take place in advance of the freezing front. Use of liquid nitrogen as the coolant in the freeze pipe is an efficient means of conducting in-situ ground freezing.
- To predict the heat extraction requirements when liquid nitrogen is used as the coolant, the equation given by Sanger and Sayles (1979) for the total energy extracted from the ground to freeze a cylinder of soil can be utilized by dividing the expression for the energy extracted by the latent heat of phase change of liquid nitrogen. The time required to freeze a given radius of soil can then be calculated based on setting the rate of heat flow through the wall of the freeze pipe, equal to the rate of heat extraction required to sustain the growth of the freezing soil column.
- Large scale ground freezing experiments indicated that the theoretical equations presented by Sanger and Sayles (1979) can be used to predict the time required to freeze a specified average radius reasonably well. However, if the level of liquid nitrogen in the freeze pipe falls below the top of the target zone during much of the freezing process, the predicted volume of liquid nitrogen will likely be significantly higher than the actual requirement, since freezing in the upper region of the target

zone occurs by conduction of heat to the cold gaseous nitrogen. Unfortunately, this scenario results in an irregularly shaped frozen column which is more difficult to sample.

- To better predict the growth of the frozen radius, although it may be possible to determine the relative proportions of gas and liquid nitrogen by installing temperature measurement devices that can withstand the temperatures and turbulence in the freeze pipe, it is preferable to freeze the soil in the form of a right cylinder by maintaining only liquid nitrogen in the freeze pipe. Freezing a uniform column of soil will both reduce the risk of disturbance of the soils, due to sub-vertical freezing fronts, and facilitate coring of the frozen sand upon completion of in-situ ground freezing. To avoid difficulties associated with coring of the frozen sand and inaccurate prediction of the liquid nitrogen requirements, utilizing higher liquid nitrogen flow rates and installation of a valve on the exhaust pipe, to apply a slight back pressure, should aid in keeping the freeze pipe reservoir consistently full of liquid nitrogen.
- If the freeze pipe reservoir is maintained full of liquid nitrogen at all times during freezing, the theoretical equation given by Sanger and Sayles (1979) to predict growth of the frozen radius with time is slightly conservative. This conservatism likely results from two factors. Firstly, the theory assumes that steady state conditions have been attained, whereas during the initial stages of freezing, the growth of the frozen radius appears to progress more quickly than steady state growth, as a result of the high heat extraction capacity of liquid nitrogen. Secondly, the frozen thermal conductivity used for the theoretical prediction was determined based on Johansen's method (Farouki, 1986), which neglects the temperature dependence of this parameter. However, at temperatures of close to that at which liquid nitrogen undergoes phase change (-196°C), the frozen thermal conductivity is likely much higher than that used for the theoretical prediction, resulting in more rapid growth of the frozen radius.
- Groundwater flow can have a detrimental effect on the ground freezing process and must be considered when estimating the energy and length of time required to carry

out ground freezing. However, the negative effects of groundwater flow are somewhat overcome if liquid nitrogen is used as the coolant in the freeze pipe due to its high heat extraction capability. In Chapter 2 it was shown that the critical groundwater flow velocity under which the groundwater cannot be frozen in place before it is transported away from the freezing zone, is approximately 5 times higher when liquid nitrogen is used as the coolant in the freeze pipe than when brine is used as the coolant.

- In-situ ground freezing was carried out successfully at two man-made, hydraulically placed test sites, located at Syncrude Canada Ltd., and two natural sites, located in the Fraser River Delta. After the completion of ground freezing, dry coring of the in-situ frozen sand with a CRREL core barrel was an effective means of obtaining the undisturbed samples. At all four test sites, the void ratios measured from the in-situ frozen core showed very good agreement with the void ratios measured independently by geophysical logging, conducted in boreholes located at a radial distance of 5 m from the freeze pipe.
- The errors associated with measuring void ratios from frozen core specimens was determined to be -0.007 to +0.011. Errors of this magnitude are slightly less than the precision associated with geophysical measurements of the in-situ bulk density, which results in errors of ± 0.03 in determining the in-situ void ratios.
- Utilizing a 150 mm outer diameter (100 mm inner diameter) CRREL core barrel, a total of 20 m of undisturbed frozen core samples were recovered from the Phase I test site and 20 m of undisturbed core was recovered from each of the two Phase II test sites. At the Phase III test site, CRREL core barrels with two different diameters were used. A total of 6.4 m of 200 mm inner diameter frozen core and 3.9 m of 100 mm inner diameter frozen core were recovered from the target zone. The 200 mm diameter core barrel yielded 3 to 4 times as many triaxial samples as the 100 mm diameter core barrel since three to four adjacent specimens could be trimmed from the same depth interval.

- At the Phase II test site, it was determined that self-jetting techniques for installation of the freeze pipe should be avoided unless it can be demonstrated that hydraulic fracturing of the ground will not occur. At sites where undisturbed samples are required from relatively shallow depths, it is preferable to install the freeze pipe in a predrilled, small diameter borehole, as was carried out successfully at the Phase I test site.
- The study conducted with a scanning electron microscope on reconstituted sand specimens subject to a freeze-thaw-freeze cycle, indicated that clay minerals were not moved *en masse* to form discrete, fine grain veins within the sand matrix. Although it appeared that freezing resulted in alignment of many clay mineral particles with the thin edge perpendicular to the freezing front, this structure is believed to be an artifact of the sedimentation process. The fact that some clay minerals remained oriented parallel to the freezing front, indicated that movement during freezing was not sufficient to overcome the original clay mineral alignment.
- It is important that undisturbed frozen specimens, obtained by in-situ ground freezing, be stored at very cold temperatures of -20°C or lower, to avoid relaxation of anisotropic stresses locked into the pore ice by ground freezing. Storage of frozen specimens in this manner will preserve the in-situ stress condition, thereby facilitating restoration of the anisotropic field stresses to the soil skeleton in the triaxial cell prior to thawing. This, in turn, results in less disturbance.
- The in-situ frozen core samples obtained from all four subaqueous sand deposits, investigated as part of the CANLEX project, indicated that the sand deposits were not fully saturated. This could have major implications regarding the pore pressure development during undrained loading. To determine the effects of degree of saturation on the liquefaction susceptibility, further testing should be carried out on loose sand specimens, with the same initial void ratio, to examine whether or not smaller positive pore pressures develop in loose unsaturated specimens than in loose saturated specimens.

- The thawing protocol study was conducted to evaluate two different thawing techniques. The results indicated that thawing of both reconstituted and undisturbed specimens under the in-situ effective stress resulted in less disturbance than thawing specimens under a small effective stress and then consolidating them to the in-situ effective stress once thawing was complete. Theoretical confirmation of the laboratory findings was not obtained from finite element analyses that indicated slightly higher maximum shear strains at the thaw front in specimens thawed under the in-situ effective stress. However, this discrepancy likely resulted from the fact that the present analyses were not able to accurately model the material behaviour.
- Void ratio changes that occurred during thawing of reconstituted Syncrude sand specimens appeared to be a function of degree of saturation, where the total void ratio change decreases as the degree of saturation increases. The average total void ratio change due to thawing and consolidation of unsaturated reconstituted specimens was significantly smaller for specimens thawed under the in-situ stress than for those thawed under a small effective stress, followed by consolidation to the in-situ effective stress. For fully saturated reconstituted specimens, the void ratio changes due to thawing and consolidation were less sensitive to the thawing method used.
- Multidirectional thawing of reconstituted specimens under an effective stress that was much smaller than the effective stress that the specimens were subject to prior to freezing, resulted in heave, followed by a decrease in void ratio during consolidation to the in-situ stresses after thawing was complete. The total void ratio change due to thawing and consolidation that occurred in reconstituted specimens subject to unidirectional thawing under the in-situ effective stress, was smaller than the total decrease in void ratio exhibited by specimens thawed multidirectionally under a small effective stress and then consolidated to the in-situ stress.
- Unidirectional thawing of undisturbed Phase I Syncrude sand specimens under 90 % of the effective stress level that existed in-situ prior to freezing and the in-situ pore pressure condition, resulted in significantly smaller void ratio changes than those that occurred in specimens thawed multidirectionally under a small effective stress of

20 kPa to 35 kPa, with no back pressure, and then consolidated to the in-situ effective stress. The specimens thawed under 90 % of the in-situ stresses underwent an average total decrease in void ratio of 0.019, while the specimens thawed under a small effective stress underwent an average total void ratio change of 0.083. The decrease in void ratio, as a percentage of the initial void ratio, due to thawing of undisturbed specimens under the in-situ effective stress ranged from 1.4 % to 3.9 %, with an average of 2.4 %. The average total decrease in void ratio that occurred during thawing under a small effective stress, followed by consolidation to the in-situ stress after thawing was complete, as a percentage of the initial void ratio, ranged from 5.6 % to 15.6 %, with an average of 10.9 %. However, the degree of disturbance due to thawing frozen specimens under a small effective stress of about 20 kPa decreases as the difference between the in-situ effective stress and the effective stress imposed during thawing in the laboratory decreases.

- A trend between the void ratio change and degree of saturation was not evident for the undisturbed specimens tested. However, this was likely due to the large variation of initial void ratio between specimens, resulting in variable soil skeleton compressibilities that masked the effects of degree of saturation on void ratio changes during thawing.
- The results from the thawing protocol study indicate that the most appropriate method of thawing undisturbed, unsaturated sand samples, obtained by in-situ ground freezing, involves thawing the specimens unidirectionally, in a controlled manner, under 90 % of the estimated in-situ effective stress. Specimens should be maintained in a frozen state prior to commencing thawing by filling the triaxial cell with a glycol solution at a temperature of about $-4\text{ }^{\circ}\text{C}$. The temperature of this solution then gradually warms to -1 to $-2\text{ }^{\circ}\text{C}$, as the remainder of the specimen setup is completed. The specimen should be allowed access to chilled water at the end of the specimen where thawing will commence. Once the triaxial cell fluid has reached about $-1\text{ }^{\circ}\text{C}$, warm glycol, at about $7\text{ }^{\circ}\text{C}$, should be circulated through the base plate of the triaxial cell to thaw the specimen unidirectionally.

- All of the undisturbed specimens exhibited dilatent behaviour during undrained triaxial compression and triaxial extension testing, indicating that the specimens were dense of the steady state line for Syncrude sand. The steady state line serves to illustrate the importance of avoiding disturbance during thawing of in-situ frozen specimens, since even small changes in the void ratio of specimens with an in-situ void ratio that falls slightly above the steady state line will change the behaviour from contractant to dilatent. Therefore, accurate evaluation of the liquefaction potential of a sand deposit from undisturbed in-situ frozen specimens, requires that careful handling and thawing procedures be followed in the laboratory to avoid disturbance of the in-situ void ratio and fabric.
- In summary, high quality undisturbed samples of sand are an instrumental part of carrying out a liquefaction assessment. This research demonstrated that in-situ ground freezing is an excellent technique for obtaining undisturbed samples of loose sand from below the groundwater table. The technique of undisturbed sampling can be used to assess the stability of many existing structures, such as dams, embankments, tailings impoundments, etc., that have been constructed on or with sand and may be at risk of liquefaction. The liquefaction potential of natural, often highly structured, sand deposits existing along many coastal regions near major cities, can also be more accurately assessed, utilizing high quality undisturbed samples obtained by in-situ ground freezing.

8.2 Recommendations for Further Research

In preparing this thesis, several areas of potential future research were identified that would either aid in refining the predictive capabilities, carried out as part of ground freezing feasibility studies, or would contribute to a better understanding of how to avoid disturbance of undisturbed frozen specimens during thawing in the laboratory. The requirements for future research in these areas are discussed in more detail below.

In Chapter 2 it was noted that groundwater flow conditions can have a significant effect on the ground freezing process and must be considered when estimating the energy and length of time required to carry out ground freezing. In general, groundwater flow across a site where in-situ ground freezing is being undertaken causes elongation of the frozen column in the downstream direction and foreshortening in the upstream direction. Since an exact solution does not exist that simultaneously solves the groundwater flow velocity and the temperature distribution in two dimension, evaluation of the effect of groundwater flow on the shape of the frozen zone requires numerical analysis. At the time of undertaking the research for this thesis, a numerical model was not available at the University of Alberta (U of A) that incorporated transient heat and groundwater flow conditions. Therefore, in Chapter 4, data presented by Hashemi and Sliepcevich (1973) that was based on finite difference analyses, were used to estimate the effects of seepage at the Phase I test site. However, it would be more accurate to develop a numerical analysis technique at the U of A that could be used to predict the deformed shape of the frozen radius under different groundwater flow velocities.

Additional frost heave tests could be carried out on various sands, with relatively high fines contents, to evaluate the freezing temperature gradients required to cause the direction of pore water flow to change from expulsion to attraction during freezing. These tests results could be used to modify the Segregation Potential concepts developed by Konrad and Morgenstern (1983), to allow for prediction of the direction of pore water flow during freezing.

As stated in Chapter 7, to better model thawing of frozen specimens in the triaxial cell under different stress conditions, future analytical work could be undertaken to modify an existing finite element program to accommodate strain compatibility between the soil skeleton and the pore ice, each with different stiffnesses, but subject to the same boundary stresses. This would allow for modeling of anisotropic stresses in the pore ice that exist after sampling frozen ground, in the absence of creep associated with long-term

storage under relatively warm subzero temperatures, and would contribute to a better understanding of how to avoid disturbance of undisturbed frozen specimens during thawing in the laboratory.

It is also recommended that the creep rates associated with unloading of confining stresses during sampling of frozen sand be investigated. This study should include an evaluation of the effect of storage time and temperature on stress relaxation within the frozen specimens.

As stated in the previous section, the in-situ frozen core samples obtained from all four subaqueous sand deposits, investigated as part of the CANLEX project, indicated that the sand deposits were not fully saturated. Since this could have major implications regarding the pore pressure development during undrained loading, it is recommended that the effects of degree of saturation on the liquefaction susceptibility of sand be determined. Further testing should be carried out on loose, contractive sand specimens, with the same initial void ratio, to examine whether or not smaller positive pore pressures develop in loose unsaturated specimens than in loose saturated specimens.

8.3 References

- Davila, R. S., Segó, D. C. and Robertson, P. K., 1992. Undisturbed Sampling of Sandy Soil by freezing, Canadian Geotechnical Conference Proceedings, Toronto, pp. 13A-1 to 13A-10.
- Farouki, O. T., 1986. Thermal Properties of Soils. Trans Tech Publications, Series on Rock and Soil Mechanics, Vol. 11, D-3392 Clausthal-Zellerfeld, Germany, 135 p.
- Hashemi, H. T. and Sliepcevich, C. M., 1973, Effect of Seepage Stream on Artificial Soil Freezing, Proceedings, Ground Freezing Conference, Developments in Geotechnical Engineering, V 28,189-201.

Konrad, J.-M. and Morgenstern, N. R., 1983, Frost Susceptibility of Soils in Terms of their Segregation Potential, 4th International Conference on Permafrost, Fairbanks National Academy of Science, Washington, D. C., pp. 660-665.

Sanger, F. J. and Sayles, F. H., 1978. Thermal and rheological computations for artificially frozen ground construction. International Symposium on Ground Freezing. 8-10 March, Bochum. pp. 311-337 or Engineering Geology, Vol. 13. pp. 311-337.

Appendix A: Data Obtained from Freezing Experiments

A.1. Introduction

Appendix A contains data gathered during large scale freezing experiments conducted at the University of Alberta farm, where a 10 m deep freezing chamber was used to freeze columns of water and sand. Resistance temperature devices were installed at regular intervals along the length of the freeze pipe and with increasing radial distance to monitor the growth of the frozen columns with time. The following appendix contains data regarding the measured frozen radii and the rates of liquid nitrogen consumption obtained during these experiments. The grain size curves of the sand used in the freezing experiments are presented. The spread sheets used for predicting the liquid nitrogen volumes and the temperature data collected during freezing are also included.

Table A1: Ice Bulb Radii Measured During Field Experiments.

EXPERIMENT NO.	LENGTH TARGET ZONE (m)	ELAPSED TIME (hrs)	TARGET ZONE DIMENSIONS			PREDICTED RADIUS (m)
			MAX RADIUS FROZEN (m)	MIN RADIUS FROZEN (m)	AVE RADIUS FROZEN (m)	
1 water	1 m	11.83	0.22	0.18	0.20	0.21
2 water	2 x 1m	8.00	0.23	0.19	0.21	
2 water	2 x 1 m	18.77	0.32	0.28	0.30	0.26
3 water	2 x 1 m	18.00	0.32	0.27	0.30	0.26
4 water	8 m	18.58	0.28	0.18	0.23	0.26
5 sand	4.4 m	22.50	0.46	0.31	0.39	0.40
6 sand	4.4 m	10.00	0.38	0.24	0.31	0.25

Table A2: Liquid Nitrogen Consumption During Field Experiments

Note: For Exp. #1, #2, and #3 the Conversion Rate is Approximately 134.8 m3 per inch of LN2

Experiment #1: July 26 and 27, 1993					Experiment #6: August 4 and 5, 1993				
Time	Elapsed Time	Inches Remaining	Inches Used	Cumulative Volume LN2 Used (m3)	Time	Elapsed Time	Inches Remaining	Inches Used	Cumulative Volume LN2 Used (m3)
1462.917	0	35.5	0	0	1462.511	0	22.9	0	0
1462.972	1.33	34.75	0.75	101.1	1462.566	1.32	21.95	0.95	124.26
1462.319	16.42	31.75	3.75	505.5	1462.601	2.15	21.3	1.6	209.28
1462.451	19.58	30.6	4.9	660.52	1462.625	2.73	21	1.9	248.52
Note: The inches of LN2 remaining at 23:20 (34.75) hrs was estimated based on the consumption of LN2 during cooling of the water prior to freezing.					1462.649	3.32	20.8	2.1	274.68
Experiment #2: July 27 and 28, 1993					1462.691	4.32	19.8	3.1	405.48
Time	Elapsed Time	Inches Remaining	Inches Used	Cumulative Volume LN2 Used (m3)	1462.729	5.23	19	3.9	510.12
1462.497	0	29	0	0	1462.816	7.32	17	5.9	771.72
1462.583	2.49	27.3	1.7	229.16	1462.858	8.32	16.4	6.5	850.2
1462.653	4.16	26.4	2.6	350.48	1462.941	10.32	14.2	8.7	1137.96
1462.708	5.49	24.8	4.2	566.16	1462.007	11.9	12.1	10.8	1412.64
1462.833	8.49	23.6	5.4	727.92	1462.083	13.73	10	12.9	1687.32
1462.917	10.49	22.6	6.4	862.72	1462.125	14.73	9.5	13.4	1752.72
1462.229	15.99	16.9	12.1	1631.08	1462.313	19.23	3.2	19.7	2576.76
1462.302	18.24	16	13	1752.4	1462.344	19.98	2.2	20.7	2707.56
1462.333	20.49	15.7	13.3	1792.84	1462.362	20.41	1.6	21.3	2786.04
Experiment #3: July 29 and 30, 1993					1462.472	23.06	0.9	22	2877.6
Time	Elapsed Time	Inches Remaining	Inches Used	Cumulative Volume LN2 Used (m3)	Experiment #6: September 20 and 21, 1993				
1462.708	0	14.2	0	0	Note: For Exp. #6 the Conversion Rate is Approximately 122 m3 per inch of LN2				
1462.854	3.5	11.3	2.9	390.92	1462.184	0	43	0	0
1462.958	6.5	10	4.2	566.16	1462.205	0.5	41.9	1.1	134.2
1462.11	9.65	7.8	6.4	862.72	1462.226	1	40.9	2.1	256.2
1462.271	13.5	3.9	10.3	1388.44	1462.247	1.5	39.9	3.1	378.2
1462.34	15.17	1.8	12.4	1671.52	1462.288	2.5	39	4	488
Note: During Experiment #3, at 8:10 the flow of LN2 was turned down to preserve the frozen bulb until a crane could reach the site to pull it out.					1462.309	3	38.5	4.5	549
Experiment #4: August 3 and 4, 1993					1462.33	3.5	37.9	5.1	622.2
Time	Elapsed Time	Inches Remaining	Inches Used	Cumulative Volume LN2 Used (m3)	1462.351	4	37.4	5.6	683.2
1462.517	0	40	0	0	1462.392	5	36.9	6.1	744.2
1462.547	0	40	0	0	1462.442	6.18	35.2	7.8	951.6
1462.601	1.28	38.8	1.2	156.96	1462.455	6.5	34.9	8.1	988.2
1462.631	2	38	2	261.6	1462.476	7	34.4	8.6	1049.2
1462.66	2.7	37.2	2.8	366.24	1462.497	7.5	34	9	1098
1462.712	3.95	36.25	3.75	490.5	1462.517	8	33.6	9.4	1146.8
1462.819	6.53	35	5	654	1462.538	8.5	33.1	9.9	1207.8
1462.854	7.37	33.5	6.5	850.2	1462.559	9	32.8	10.2	1244.4
1462.883	8.07	32.8	7.2	941.76	1462.583	9.58	32.2	10.8	1317.6
1462.931	9.2	31.6	8.4	1098.72	1462.601	10	31.9	11.1	1354.2
1462.993	10.7	30.1	9.9	1294.92					
1462.028	11.53	29.5	10.5	1373.4					
1462.118	13.7	27.2	12.8	1674.24					
1462.285	17.7	24.1	15.9	2079.72					
1462.337	19.28	23.5	16.5	2158.2					

Table A3: Spread Sheet used for Freezing Predictions during Experiment #1.

FREEZING TEST AT U OF A FARM: Experiment #1															
LIQUID NITROGEN TEMPERATURE = 196 C															
WATER TEMPERATURE =3.3 C															
100Sr m.c	1.00		p dry=	1.00	Mg/m3										
Vs(LN2)=	196.00	K	Vo=	3.30	K	Vs(GN2)=	120.00								
Cu=C2=	4.19	MJ/m3 K	Cf=C1=	1.88	MJ/m3 K										
L=	334.00	MJ/m3	Li=	384.31	MJ/m3										
K1=Kf=	2.20	W/m K	Ku=	0.61	W/m K										
ro=	0.03	m	ar=	3.00											
Li=	1.00	m	STE=	2.46											
0.00			S+S	S+S											
			method	method	C+J										
			LN2	GN2	method										
R (m)	R/ro	LN (R/ro)	t (hr)	t (hr)	t (hr)	Q(MJ/m)	Qt (W/m)	N2 l requirement using Q			LN2 (m3)	* non-stea	R*/ro	ln R*/ro	C+J
0.03	0.98	0.00	0.00	0.00	0.00	0.00	0.00	P (W/m)	N2 l (Mg)	N2 l (l)	x Ltarget	state	on-steady		non steady
0.05	1.97	0.68	0.20	0.24	0.30	5.15	7046.17							-0.02	0.00
0.10	3.94	1.37	1.67	2.35	3.50	16.30	2108.80	4000.32	0.03	32.04	46.93	0.04	1.65	0.50	0.13
0.15	5.91	1.78	4.89	7.14	11.26	34.50	1571.21	1976.99	0.08	101.28	148.37	0.08	3.31	1.20	2.03
0.20	7.87	2.06	10.12	15.02	24.39	59.51	1329.40	1525.61	0.17	214.39	314.09	0.13	4.96	1.60	6.90
0.25	9.84	2.29	17.53	26.29	43.45	91.28	1189.76	1312.92	0.30	369.85	541.83	0.17	6.61	1.89	15.33
0.30	11.81	2.47	27.28	41.17	68.88	129.76	1096.84	1184.81	0.46	567.26	831.03	0.21	8.27	2.11	27.89
0.35	13.78	2.62	39.45	59.88	101.04	174.93	1029.50	1097.32	0.65	806.40	1181.37	0.25	9.92	2.28	44.31
0.40	15.75	2.76	54.19	82.50	140.22	226.77	977.87	1032.83	0.88	1087.11	1592.62	0.29	11.57	2.45	65.43
0.45	17.72	2.87	71.84	109.23	186.89	285.26	936.66	982.80	1.14	1409.27	2064.59	0.34	13.22	2.58	91.27
0.50	19.69	2.98	91.58	140.18	240.67	350.39	902.78	942.53	1.43	1772.78	2597.13	0.38	14.88	2.70	122.00
0.55	21.65	3.08	114.38	175.45	302.37	422.16	874.28	909.21	1.76	2177.56	3190.13	0.42	16.53	2.81	157.80
0.60	23.62	3.16	140.00	215.13	371.98	500.54	849.85	881.03	2.12	2623.53	3843.47	0.46	18.18	2.90	198.80
0.65	25.59	3.24	168.49	259.32	449.65	585.53	828.61	856.79	2.52	3110.63	4557.08	0.50	19.84	2.99	245.13
0.70	27.56	3.32	199.90	308.09	535.56	677.12	809.91	835.63	2.94	3638.81	5330.85	0.55	21.49	3.07	296.92
0.75	29.53	3.39	234.28	361.52	629.84	775.30	793.27	816.96	3.40	4208.01	6164.73	0.59	23.14	3.14	354.27
0.80	31.50	3.45	271.67	419.68	732.63	880.07	778.33	800.31	3.90	4818.19	7058.84	0.63	24.80	3.21	417.29
0.85	33.46	3.51	312.12	482.64	844.05	991.43	764.83	785.34	4.42	5469.30	8012.53	0.67	26.45	3.28	486.07
0.90	35.43	3.57	355.65	550.45	964.22	1109.36	752.53	771.78	4.98	6161.32	9026.33	0.71	28.10	3.34	560.69
0.95	37.40	3.62	402.30	623.17	1093.25	1233.86	741.27	759.41	5.57	6894.20	10100.01	0.76	29.75	3.39	641.25
1.00	39.37	3.67	452.11	700.87	1231.24	1364.92	730.90	748.07	6.20	7667.92	11233.50	0.80	31.41	3.45	727.82
								737.63	6.86	8482.44	12426.78	0.84	33.06	3.50	820.46

Table A4: Actual Freezing Data gathered during Experiment #1.

Actual Experiment #1 Results				Predicted LN2 Consumption		
Duration of Freezing (hrs)	Target Zone Dimensions			Predicted Rf@t=18.83 hrs	0.21	m
	R(max) (m)	R(min) (m)	R(ave) (m)			
11.83	0.22	0.18	0.2			
Elapsed Time (hrs)	LN2 Used (m3)	Actual Norm LN2 (m3/m3)		Predicted Norm LN2 (m3/m3)		
0	0	0		0		
1.33	101.1	804.9363		338.9228		
16.42	505.5	4024.682		1071.492		
19.58	660.52	5258.917		2268.202		

Table A5: Spread Sheet used for Revised Freezing Predictions during Experiment #1, assuming 2/3 Liquid and 1/3 gas nitrogen.

FREEZING TEST AT U OF A FARM: Experiment #1																
WEIGHTED AVERAGE OF LIQUID AND GAS NITROGEN TEMPERATURES = ((2/3)100+(1/3)120)/2 = 170 C																
WATER TEMPERATURE = 3.3 C																
100Sr m.c.	1.00	p dry=	1.00 Mg/m3	Q (MJ/m)	OR (W/m)	P (W/m)	Gas N2 (m3)	Contribution to Cooling by Gas LN2 (m3)	LN2 requirement using LN2 (l)	LN2 (m3) x L target	Contribution to Cooling by liquid N2 (m3)	Weighted average Total N2 (m3)	R' non-steady state	R' on-steady	In R' no	C+J non-steady state l (hr)
Vs (ave)=	170.00 K	Vo=	3.30 K													
Cu=C2=	4.16 MJ/m3 K	Cf=C1=	1.86 MJ/m3 K													
L=	334.00 MJ/m3	Li=	384.31 MJ/m3													
K1=Kf=	2.20 W/m K	Ku=	0.61 W/m K													
fo=	0.03 m	ar=	3.00													
Li=	1 m	STE=	2.13													
		S+S method	C+J method													
R (m)	R/no	l (hr)	l (hr)													
0.03	0.96	0.00	0.00	0.00	6394.75	3489.66	0.00	0.00	0.00	0.00	0.00	0.00	0.03	0.96	-0.02	0.00
0.05	1.97	0.21	0.34	4.67	1858.38	1714.74	0.03	0.01	0.02	30.27	44.35	29.67	0.04	1.70	0.53	0.17
0.10	3.94	1.84	4.04	15.74	1373.91	1323.23	0.08	0.03	0.08	97.80	143.27	96.62	0.09	3.40	1.22	2.55
0.15	5.91	5.43	12.99	33.53	1199.86	1138.76	0.18	0.06	0.17	206.35	306.23	203.49	0.13	5.09	1.63	8.60
0.20	7.87	11.30	26.12	58.02	1036.88	1027.64	0.31	0.10	0.29	360.60	528.28	382.19	0.17	6.79	1.82	19.00
0.25	9.84	19.65	50.10	89.18	955.25	951.75	0.48	0.16	0.45	554.22	811.93	541.29	0.22	8.49	2.14	34.25
0.30	11.81	30.63	79.42	126.96	896.20	895.82	0.68	0.22	0.64	789.01	1185.89	779.60	0.26	10.19	2.32	54.72
0.35	13.78	44.39	116.49	171.34	850.97	852.43	0.91	0.30	0.86	1064.83	1689.87	1038.66	0.30	11.89	2.48	80.72
0.40	15.75	61.03	161.67	223.31	814.90	817.50	1.19	0.39	1.12	1381.58	2024.01	1348.34	0.35	13.59	2.61	112.49
0.45	17.72	80.64	215.24	279.85	785.26	788.60	1.49	0.49	1.41	1739.17	2547.88	1896.98	0.39	15.28	2.73	150.28
0.50	19.69	103.32	277.48	343.95	760.34	764.16	1.83	0.61	1.73	2137.53	3131.48	2387.65	0.43	16.96	2.83	194.26
0.55	21.65	129.13	348.82	414.60	739.00	743.13	2.21	0.73	2.06	2576.59	3774.71	2887.20	0.47	18.68	2.93	244.63
0.60	23.62	160.14	428.87	491.78	720.44	724.78	2.62	0.87	2.47	3056.31	4477.49	3493.17	0.52	20.38	3.01	301.53
0.65	25.59	190.42	518.42	575.52	704.11	708.59	3.07	1.01	2.89	3576.63	5339.76	4093.17	0.56	22.08	3.09	365.11
0.70	27.56	226.03	617.47	665.77	689.58	694.15	3.55	1.17	3.35	4137.50	6401.44	4942.13	0.60	23.78	3.17	435.51
0.75	29.53	265.01	726.17	762.54	676.55	681.16	4.07	1.34	3.83	4738.90	7642.49	5828.33	0.65	25.47	3.24	512.84
0.80	31.50	307.42	844.68	865.83	664.78	669.40	4.62	1.52	4.35	5390.78	9042.85	6923.76	0.69	27.17	3.30	597.24
0.85	33.46	353.30	973.14	975.62	654.03	658.67	5.20	1.72	4.90	6083.12	10482.48	8023.36	0.73	28.87	3.36	688.79
0.90	35.43	402.59	1111.69	1091.92	644.21	648.84	5.82	1.92	5.49	6785.87	11941.30	9129.45	0.78	30.57	3.42	787.60
0.95	37.40	455.84	1260.45	1214.72	635.17	639.78	6.46	2.14	6.10	7548.02	13372.87	10275.01	0.82	32.27	3.47	893.77
1.00	39.37	512.18	1419.55	1344.02			7.17	2.37	6.75	8352.53	12238.48	11160.00	0.86	33.98	3.53	1007.39

Table A6: Spread Sheet used for Freezing Predictions during Experiment #2.

FREEZING TEST AT U OF A FARM: Experiment #2																
LIQUID NITROGEN TEMPERATURE = 196 C																
WATER TEMPERATURE =0.6 C																
100Sr m.c	1.00		p dry=	1.00	Mg/m3											
Vs=	196.00	K	Vo=	0.60	K											
Cu=C2=	4.19	MJ/m3 K	Cf=C1=	1.88	MJ/m3 K											
L=	334.00	MJ/m3	Li=	343.15	MJ/m3											
K1=Kf=	2.20	W/m K	Ku=	0.61	W/m K											
ro=	0.03	m	ar=	3.00												
Lt=	2.00	m	STE=	2.46												
0																
R (m)	R/ro	LN (R/ro)	S+S method t (hr)	C+J method t (hr)	Q(MJ/m)	Q/t (W/m)	P (W/m)	N2 l requirement usin N2 l (Mg)	N2 l (l)	LN2 (m3) x Ltarget	R* non-stead state	R*/ro non-steady	ln R*/ro	C+J non stead state t (hr)		
0.03	0.98	0.00	0.00	0.00	0.00			0.00	0.00	0.00	0.03	0.98	-0.02	0.00		
0.05	1.97	0.68	0.20	0.30	4.83	6800.93	4000.32	0.02	30.03	87.98	0.04	1.65	0.50	0.13		
0.10	3.94	1.37	1.56	3.50	15.00	2080.51	1976.99	0.08	93.24	273.20	0.08	3.31	1.20	2.03		
0.15	5.91	1.78	4.51	11.26	31.59	1560.26	1525.61	0.16	196.31	575.20	0.13	4.96	1.60	6.90		
0.20	7.87	2.06	9.29	24.39	54.34	1322.65	1312.92	0.27	337.71	989.48	0.17	6.61	1.89	15.33		
0.25	9.84	2.29	16.05	43.45	83.20	1184.84	1184.81	0.42	517.03	1514.91	0.21	8.27	2.11	27.69		
0.30	11.81	2.47	24.93	68.88	118.12	1092.93	1097.32	0.59	734.07	2150.84	0.25	9.92	2.29	44.31		
0.35	13.78	2.62	36.02	101.04	159.09	1026.24	1032.83	0.80	988.67	2896.80	0.29	11.57	2.45	65.43		
0.40	15.75	2.76	49.40	140.22	206.08	975.05	982.80	1.04	1280.69	3752.44	0.34	13.22	2.58	91.27		
0.45	17.72	2.87	65.16	186.69	259.08	934.17	942.53	1.30	1610.05	4717.45	0.38	14.88	2.70	122.00		
0.50	19.69	2.98	83.36	240.67	318.07	900.53	909.21	1.60	1976.66	5791.61	0.42	16.53	2.81	157.80		
0.55	21.65	3.08	104.05	302.37	383.04	872.22	881.03	1.92	2380.44	6974.69	0.46	18.18	2.90	198.80		
0.60	23.62	3.16	127.29	371.98	453.98	847.96	856.79	2.28	2821.33	8286.50	0.50	19.84	2.99	245.13		
0.65	25.59	3.24	153.13	449.65	530.89	826.85	835.63	2.67	3299.28	9666.90	0.55	21.49	3.07	296.92		
0.70	27.56	3.32	181.61	535.56	613.75	808.25	816.96	3.08	3814.24	11175.72	0.59	23.14	3.14	354.27		
0.75	29.53	3.39	212.77	629.84	702.56	791.71	800.31	3.53	4366.16	12792.83	0.63	24.80	3.21	417.29		
0.80	31.50	3.45	246.65	732.63	797.31	776.86	785.34	4.01	4954.99	14518.13	0.67	26.45	3.28	486.07		
0.85	33.46	3.51	283.28	844.05	898.00	763.42	771.78	4.51	5580.71	16351.49	0.71	28.10	3.34	560.69		
0.90	35.43	3.57	322.71	964.22	1004.61	751.19	759.41	5.05	6243.28	18292.81	0.76	29.75	3.39	641.25		
0.95	37.40	3.62	364.95	1093.25	1117.15	739.98	748.07	5.61	6942.66	20342.00	0.80	31.41	3.45	727.82		
1.00	39.37	3.67	410.05	1231.24	1235.61	729.66	737.63	6.21	7678.83	22498.98	0.84	33.06	3.50	820.46		

Table A7: Actual Freezing Data gathered during Experiment #2.

Actual Experiment #2 Results				Predicted LN2 Consumption	
Duration of Freezing (hrs)	Target Zone Dimensions			Predicted Rf@t=18.778 hrs	0.255 m
	R(max) (m)	R(min) (m)	R(ave) (m)		
18.77	0.35	0.28	0.315		
Elapsed Time (hrs)	LN2 Used (m3)	Actual Norm LN2 (m3/m3)	Predicted Norm LN2 (m3/m3)		
0	0	0	0		
2.49	229.16	367.7546	215.4428		
4.16	350.48	562.4481	669.0266		
5.49	566.16	908.5701	1408.562		
8.49	727.92	1168.162	2423.068		
10.49	862.72	1384.488	3709.764		
15.99	1631.08	2617.547	5267.05		
18.24	1752.4	2812.241	7093.791		
20.49	1792.84	2877.139	9189.107		

Table A8: Spread Sheet used for Freezing Predictions during Experiment #3.

FREEZING TEST AT U OF A FARM: Experiment #3														
LIQUID NITROGEN TEMPERATURE = 196 C														
WATER TEMPERATURE =0.7 C														
100Sr m.c	1.00		p dry=	1.00	Mg/m3									
Vs=	196.00	K	Vo=	0.90	K									
Cu=C2=	4.19	MJ/m3 K	Cf=C1=	1.88	MJ/m3 K									
L=	334.00	MJ/m3	Li=	347.72	MJ/m3									
K1=Kf=	2.20	W/m K	Ku=	0.61	W/m K									
ro=	0.03	m	ar=	3.00										
Li=	2.00	m	STE=	2.46										
0														
R (m)	R/ro	LN (R/ro)	S+S method t (hr)	C+J method t (hr)	Q(MJ/m)	Q/t (W/m)	P (W/m)	N2 l requirement N2 l (Mg)	N2 l (l)	LN2 (m3) x Ltarget	R* non-stead state	R*/ro non-steady	ln R*/ro	
0.03	0.98	0.00	0.00	0.00	0.00			0.00	0.00	0.00	0.03	0.98	-0.02	
0.05	1.97	0.68	0.20	0.30	4.87	6828.89	4000.32	0.02	30.25	88.63	0.04	1.65	0.50	
0.10	3.94	1.37	1.57	3.50	15.15	2083.87	1976.99	0.08	94.14	275.82	0.08	3.31	1.20	
0.15	5.91	1.78	4.55	11.26	31.91	1561.57	1525.61	0.16	198.32	581.08	0.13	4.96	1.60	
0.20	7.87	2.06	9.38	24.39	54.92	1323.46	1312.92	0.28	341.28	999.94	0.17	6.61	1.89	
0.25	9.84	2.29	16.22	43.45	84.09	1185.44	1184.81	0.42	522.61	1531.26	0.21	8.27	2.11	
0.30	11.81	2.47	25.19	68.88	119.41	1093.41	1097.32	0.60	742.11	2174.38	0.25	9.92	2.29	
0.35	13.78	2.62	36.40	101.04	160.85	1026.63	1032.83	0.81	999.61	2928.85	0.29	11.57	2.45	
0.40	15.75	2.76	49.94	140.22	208.38	975.39	982.80	1.05	1294.98	3794.30	0.34	13.22	2.58	
0.45	17.72	2.87	65.87	186.69	261.99	934.47	942.53	1.32	1628.13	4770.43	0.38	14.88	2.70	
0.50	19.69	2.98	84.27	240.67	321.66	900.81	909.21	1.62	1998.98	5857.01	0.42	16.53	2.81	
0.55	21.65	3.08	105.20	302.37	387.39	872.47	881.03	1.95	2407.45	7053.83	0.46	18.18	2.90	
0.60	23.62	3.16	128.70	371.98	459.16	848.19	856.79	2.31	2853.48	8360.69	0.50	19.84	2.99	
0.65	25.59	3.24	154.83	449.65	536.96	827.06	835.63	2.70	3337.01	9777.43	0.55	21.49	3.07	
0.70	27.56	3.32	183.64	535.56	620.79	808.45	816.96	3.12	3857.99	11303.91	0.59	23.14	3.14	
0.75	29.53	3.39	215.16	629.84	710.65	791.90	800.31	3.57	4416.38	12940.00	0.63	24.80	3.21	
0.80	31.50	3.45	249.43	732.63	806.51	777.04	785.34	4.05	5012.14	14685.56	0.67	26.45	3.28	
0.85	33.46	3.51	286.48	844.05	908.38	763.59	771.78	4.56	5645.22	16540.51	0.71	28.10	3.34	
0.90	35.43	3.57	326.37	964.22	1016.25	751.35	759.41	5.11	6315.60	18504.72	0.76	29.75	3.39	
0.95	37.40	3.62	369.10	1093.25	1130.12	740.14	748.07	5.68	7023.25	20578.11	0.80	31.41	3.45	
1.00	39.37	3.67	414.72	1231.24	1249.98	729.81	737.63	6.28	7768.12	22760.60	0.84	33.06	3.50	

Table A9: Actual Freezing Data gathered during Experiment #3.

Actual Experiment #3 Results				Predicted LN2 Consumption		
Duration of Freezing (hrs)	Target Zone Dimensions			Predicted Rf@t=18.00 hrs	0.26	m
	R(max) (m)	R(min) (m)	R(ave) (m)			
18	0.32	0.27	0.295			
Elapsed Time (hrs)	LN2 Used (m3)	Actual Norm LN2 (m3/m3)	Predicted Norm LN2 (m3/m3)			
0.00	0.00	0.00	0.00			
3.50	390.92	715.29	208.78			
6.50	566.16	1035.94	649.70			
9.65	862.72	1578.58	1368.77			
13.50	1388.44	2540.52	2355.42			
15.17	1671.52	3058.50	3606.97			

Table A10: Spread Sheet used for Freezing Predictions during Experiment #4.

FREEZING TEST AT U OF A FARM: Experiment #4														
LIQUID NITROGEN TEMPERATURE = 196 C														
WATER TEMPERATURE = 1.9 C														
100% Sr	1.00		p dry=	1.00	Mg/m3									
Vs=	196.00	K	Vo=	1.90	K									
Cu=C2=	4.19	MJ/m3 K	Cf=C1=	1.88	MJ/m3 K									
L=	334.00	MJ/m3	Li=	362.96	MJ/m3									
K1=Kf=	2.20	W/m K	Ku=	0.61	W/m K									
ro=	0.03	m	ar=	3.00										
Lt=	8.00	m	STE=	2.46										
0														
R (m)	R/ro	LN (R/ro)	S+S method t (hr)	C+J method t (hr)	Q(MJ/m)	Q/t (W/m)	P (W/m)	N2 l requirement usin N2 l (Mg)	N2 l (l)	LN2 (m3) x Lt target	R* non-stead state	R*/ro non-steady	ln R*/ro	C+J non stead state t (hr)
0.03	0.98	0.00	0.00	0.00	0.00			0.00	0.00	0.00	0.03	0.98	-0.02	0.00
0.05	1.97	0.68	0.20	0.30	4.99	6920.80	4000.32	0.03	30.99	363.25	0.04	1.65	0.50	0.13
0.10	3.94	1.37	1.61	3.50	15.63	2094.68	1976.99	0.08	97.11	1138.15	0.08	3.31	1.20	2.03
0.15	5.91	1.78	4.69	11.26	32.99	1565.77	1525.61	0.17	205.02	2402.82	0.13	4.96	1.60	6.90
0.20	7.87	2.06	9.69	24.39	56.83	1326.05	1312.92	0.29	353.18	4139.30	0.17	6.61	1.89	15.33
0.25	9.84	2.29	16.76	43.45	87.09	1187.32	1184.81	0.44	541.22	6343.05	0.21	8.27	2.11	27.69
0.30	11.81	2.47	26.06	68.88	123.72	1094.91	1097.32	0.62	768.90	9011.47	0.25	9.92	2.29	44.31
0.35	13.78	2.62	37.68	101.04	166.71	1027.89	1032.83	0.84	1036.07	12142.70	0.29	11.57	2.46	65.43
0.40	15.75	2.76	51.71	140.22	216.04	976.47	982.80	1.09	1342.60	15735.30	0.34	13.22	2.58	91.27
0.45	17.72	2.87	68.23	186.69	271.68	935.43	942.53	1.37	1688.40	19788.10	0.38	14.88	2.70	122.00
0.50	19.69	2.98	87.32	240.67	333.63	901.67	909.21	1.68	2073.39	24300.12	0.42	16.53	2.81	157.80
0.55	21.65	3.08	109.02	302.37	401.87	873.26	881.03	2.02	2497.48	29270.50	0.46	18.18	2.90	198.80
0.60	23.62	3.16	133.41	371.98	476.40	848.92	856.79	2.39	2960.62	34698.52	0.50	19.84	2.99	245.13
0.65	25.59	3.24	160.52	449.65	557.20	827.74	835.63	2.80	3462.76	40583.51	0.55	21.49	3.07	296.92
0.70	27.56	3.32	190.41	535.56	644.26	809.09	816.96	3.24	4003.83	46924.89	0.59	23.14	3.14	354.27
0.75	29.53	3.39	223.13	629.84	737.59	792.50	800.31	3.71	4583.80	53722.13	0.63	24.80	3.21	417.29
0.80	31.50	3.45	258.70	732.63	837.16	777.60	785.34	4.21	5202.62	60974.75	0.67	26.45	3.28	486.07
0.85	33.46	3.51	297.16	844.05	942.98	764.13	771.78	4.74	5860.26	68682.30	0.71	28.10	3.34	560.69
0.90	35.43	3.57	338.57	964.22	1055.05	751.87	759.41	5.30	6556.69	76844.38	0.76	29.75	3.39	641.25
0.95	37.40	3.62	382.93	1093.25	1173.34	740.63	748.07	5.90	7291.86	85460.61	0.80	31.41	3.45	727.82
1.00	39.37	3.67	430.30	1231.24	1297.87	730.29	737.63	6.52	8065.75	94530.65	0.84	33.06	3.50	820.46

Table A11: Actual Freezing Data gathered during Experiment #4.

Actual Experiment # 4 Results		Target Zone Dimensions		Predicted LN2 Consumption	
Duration of Freezing (hrs)	R(max) (m)	R(min) (m)	R(ave) (m)	Predicted Rf@t=18.58 hrs	0.26 m
18.58	0.28	0.18	0.23		
Elapsed Time (hrs)	LN2 Used (m3)	Norm LN2 (m3/m3)		Norm LN2 (m3/m3)	
0.00	0.00	0.00		0.00	
1.28	156.96	118.12		213.91	
2.00	261.60	196.86		670.25	
2.70	366.24	275.61		1414.99	
3.95	490.50	369.12		2437.59	
6.53	654.00	492.16		3735.36	
7.37	850.20	639.80		5306.76	
8.07	941.76	708.70		7150.71	
9.20	1098.72	826.82		9266.35	
10.70	1294.92	974.47		11653.00	
11.53	1373.40	1033.53		14310.08	
13.70	1674.24	1259.92		17237.09	
17.70	2079.72	1565.05		20433.59	
19.28	2158.20	1624.11		23899.19	

Table A12: Spread Sheet used for Revised Freezing Predictions during Experiment #4, assuming 1/3 Liquid and 2/3 gas nitrogen.

FREEZING TEST AT U OF A FARM: Experiment #4																	
WEIGHTED AVERAGE OF LIQUID AND GAS NITROGEN TEMPERATURES = ((1/3)196+(2/3)120)/2 = 145 C																	
WATER TEMPERATURE = 1.9 C																	
100Sr m.c	1.00	p dry=	1.00	Mp/m3													
Va (ave)=	145.00	Vo=	1.90	K													
Cu=C2=	4.19	MJ/m3 K	1.88	MJ/m3 K													
L=	334.00	MJ/m3	362.96	MJ/m3													
K1=K1=	2.20	W/m K	0.61	W/m K													
ro=	0.03	m	3.00														
Lt=	8.00	m	1.82														
R (m)	R/ro	LN (R/ro)	S+S method	C+S method	Q(MJ/m)	Qr (W/m)	P (W/m)	Gas N2 (m3)	2/3 Contribution to Cooling by Gas N2 (m3)	LN2 requirement ush LN2 (l)	LN2 (m3) x L Target	1/3 Contribution to Cooling by liquid N2 (m3)	Weighted average for 6 m N2 (m3)	R* non-steady state	R'/ro non-steady	In R'/ro	C+J non-steady state I (hr)
0.03	0.96	0.00	0.00	0.01	0.00	0.00	0.00	0.00	0.00	0.00	0.00	0.00	0.00	0.03	0.96	-0.02	0.00
0.05	1.97	0.66	0.22	0.40	4.43	5836.21	2959.42	0.09	0.06	27.54	40.34	13.48	104.09	0.04	1.74	0.55	0.22
0.10	3.94	1.37	1.97	4.73	14.53	1602.04	1462.57	0.31	0.21	60.28	132.26	44.09	364.36	0.09	3.48	1.25	0.23
0.15	5.91	1.78	5.87	15.23	31.06	1178.19	1128.64	0.66	0.44	193.16	282.96	94.33	759.16	0.13	5.22	1.65	10.81
0.20	7.87	2.06	12.26	32.97	53.91	993.13	971.30	1.15	0.77	335.04	490.83	163.61	1315.02	0.18	6.95	1.94	23.80
0.25	9.84	2.29	21.36	56.74	82.97	897.17	876.51	1.77	1.18	515.63	755.40	251.60	2023.88	0.22	8.70	2.16	42.61
0.30	11.81	2.47	33.35	83.11	118.23	816.96	811.79	2.52	1.68	734.78	1076.45	358.82	2893.99	0.27	10.44	2.35	66.30
0.35	13.78	2.62	48.37	136.58	159.68	766.23	764.09	3.41	2.27	992.36	1483.60	494.60	3694.98	0.31	12.18	2.50	100.64
0.40	15.75	2.76	66.56	189.54	207.30	727.39	727.07	4.42	2.98	1288.29	1887.33	629.11	6096.46	0.35	13.92	2.63	140.16
0.45	17.72	2.87	88.00	252.35	281.07	696.45	697.28	5.57	3.71	1622.47	2376.92	792.31	8368.16	0.40	15.67	2.75	187.13
0.50	19.69	2.96	112.81	325.32	321.00	671.03	672.63	6.86	4.57	1984.66	2922.49	874.16	7878.78	0.44	17.41	2.86	241.78
0.55	21.65	3.08	141.06	408.72	307.06	649.66	651.78	8.26	5.50	2405.41	3523.93	974.16	9441.19	0.49	19.15	2.95	304.34
0.60	23.62	3.16	172.82	502.81	459.25	631.37	633.85	9.60	6.53	2854.07	4181.21	1393.74	11202.18	0.53	20.89	3.04	378.01
0.65	25.59	3.24	206.17	607.81	537.57	615.47	618.20	11.47	7.68	3340.79	4894.26	1631.42	13112.81	0.57	22.63	3.12	453.95
0.70	27.56	3.32	247.16	723.93	622.01	601.48	604.36	13.27	8.95	3965.54	5663.01	1887.67	15172.16	0.62	24.37	3.19	541.34
0.75	29.53	3.39	289.66	851.37	712.56	589.03	592.07	15.20	10.13	4428.28	6487.43	2182.46	17380.89	0.66	26.11	3.26	637.33
0.80	31.50	3.45	336.33	990.31	809.22	577.87	580.99	17.26	11.51	5028.99	7367.47	2485.82	19739.89	0.71	27.65	3.33	742.05
0.85	33.46	3.51	386.60	1140.92	911.99	567.77	570.96	19.46	12.97	5667.63	8303.08	2787.89	22345.31	0.75	29.59	3.39	856.64
0.90	35.43	3.57	440.74	1303.35	1020.65	558.59	561.81	21.78	14.52	6344.19	9294.23	3096.08	24900.77	0.80	31.33	3.44	978.23
0.95	37.40	3.62	498.78	1477.77	1135.81	550.18	553.42	24.23	16.15	7059.63	10340.89	3446.96	27764.63	0.84	33.07	3.50	1109.93
1.00	39.37	3.67	560.78	1664.30	1256.87	542.44	545.69	26.81	17.88	7810.93	11443.01	3874.34	30857.71	0.88	34.81	3.55	1250.86

Table A13: Spread Sheet used for Freezing Predictions during Experiment #5.

FREEZING TEST AT U OF A FARM: Experiment #5															
LIQUID NITROGEN TEMPERATURE = 196 C															
WATER TEMPERATURE =3.5 C															
100% Sr	4.30			2.30											
Vs=	0.26		p dry=	1.60	Mg/m3										
Cu=C2=	196.00	K	Vo=	3.50	K										
L=	2.74	MJ/m3 K	Cf=C1=	1.94	MJ/m3 K										
K1=Kf=	137.34	MJ/m3	Li=	172.32	MJ/m3										
ro=	4.30	W/m K	Ku=	2.30	W/m K										
Li=	0.03	m	ar=	3.00											
	4.40	m	STE=	3.92											
0															
R (m)	R/ro	LN (R/ro)	S+S mentod t (hr)	C+J method t (hr)	Q(MJ/m)	Q/t (W/m)	P (W/m)	N2 I requirement usin N2 I (Mg)	N2 I (l)	LN2 (m3) x Ltarget	R* non-stead state	R*/ro non-steady	ln R*/ro	C+J non stead state t (hr)	
0.03	0.98	0.00	0.00	0.00	0.00			0.00	0.00	0.00	0.03	0.98	-0.02	0.00	
0.05	1.97	0.68	0.09	0.03	3.56	10874.94	7818.80	0.02	22.09	142.42	0.04	1.43	0.36	0.01	
0.10	3.94	1.37	0.56	0.38	9.77	3676.53	3864.12	0.05	60.69	391.23	0.07	2.87	1.05	0.14	
0.15	5.91	1.78	1.52	1.23	19.74	2887.88	2981.87	0.10	122.66	790.69	0.11	4.30	1.46	0.50	
0.20	7.87	2.06	3.03	2.66	33.22	2482.15	2566.17	0.17	206.43	1330.64	0.15	5.73	1.75	1.13	
0.25	9.84	2.29	5.13	4.74	50.14	2239.25	2315.76	0.25	311.59	2008.50	0.18	7.17	1.97	2.07	
0.30	11.81	2.47	7.85	7.51	70.47	2074.58	2144.75	0.35	437.91	2822.79	0.22	8.60	2.15	3.35	
0.35	13.78	2.62	11.22	11.02	94.17	1953.83	2018.72	0.47	585.24	3772.46	0.25	10.03	2.31	4.97	
0.40	15.75	2.76	15.26	15.29	121.24	1860.47	1920.93	0.61	753.44	4856.69	0.29	11.46	2.44	6.97	
0.45	17.72	2.87	19.99	20.36	151.65	1785.52	1842.22	0.76	942.42	6074.83	0.33	12.90	2.56	9.36	
0.50	19.69	2.98	25.43	26.25	185.38	1723.59	1777.09	0.93	1152.08	7426.30	0.36	14.33	2.66	12.14	
0.55	21.65	3.08	31.59	32.98	222.44	1671.28	1722.01	1.12	1382.35	8910.64	0.40	15.76	2.76	15.33	
0.60	23.62	3.16	38.48	40.57	262.80	1626.32	1674.63	1.32	1633.17	10527.42	0.44	17.20	2.84	18.94	
0.65	25.59	3.24	46.12	49.04	306.45	1587.11	1633.28	1.54	1904.48	12276.28	0.47	18.63	2.92	22.99	
0.70	27.56	3.32	54.52	58.41	353.40	1552.51	1596.79	1.78	2196.23	14156.87	0.51	20.06	3.00	27.47	
0.75	29.53	3.39	63.69	68.69	403.62	1521.66	1564.24	2.03	2508.36	16168.91	0.55	21.50	3.07	32.41	
0.80	31.50	3.45	73.64	79.90	457.12	1493.93	1534.98	2.30	2840.85	18312.11	0.58	22.93	3.13	37.80	
0.85	33.46	3.51	84.37	92.05	513.89	1468.80	1508.47	2.58	3193.64	20586.23	0.62	24.36	3.19	43.65	
0.90	35.43	3.57	95.91	105.15	573.92	1445.89	1484.30	2.88	3566.71	22991.04	0.66	25.80	3.25	49.97	
0.95	37.40	3.62	108.24	119.23	637.21	1424.89	1462.14	3.20	3960.02	25526.31	0.69	27.23	3.30	56.77	
1.00	39.37	3.67	121.39	134.28	703.75	1405.53	1441.73	3.54	4373.54	28191.86	0.73	28.66	3.36	64.05	

Table A14: Actual Freezing Data gathered during Experiment #5.

Actual Experiment # 5 Results				Predicted LN2 Consumption	
Duration of Freezing (hrs)	Target Zone Dimensions			Predicted Rf@t=18.58 hrs	0.26 m
	R(max) (m)	R(min) (m)	R(ave) (m)		
20.4	0.46	0.31	0.385		
Elapsed Time (hrs)	LN2 Used (m3)	Norm LN2 (m3/m3)		Norm LN2 (m3/m3)	
0.00	0.00	0.00		0.00	
1.32	124.26	60.68		152.49	
2.15	209.28	102.19		418.89	
2.73	248.52	121.35		846.60	
3.32	274.68	134.13		1424.73	
4.32	405.48	198.00		2150.52	
5.23	510.12	249.10		3022.38	
7.32	771.72	376.84		4039.20	
8.32	850.20	415.16		5200.10	
10.32	1137.96	555.68		6504.36	
11.90	1412.64	689.81		7951.40	
13.73	1687.32	823.94		9540.69	
14.73	1752.72	855.87		11271.79	
19.23	2576.76	1258.26		13144.31	
19.98	2707.56	1322.13		15157.88	
20.41	2786.04	1360.45		17312.18	
23.06	2877.60	1405.16		19606.92	

Table A15: Spread Sheet used for Freezing Predictions during Experiment #6.

FREEZING TEST AT U OF A FARM: Experiment #6														
LIQUID NITROGEN TEMPERATURE = 196 C														
WATER TEMPERATURE = 9.9 C														
100% Sr	0.26		p dry=	1.60	Mg/m3									
Vs=	196.00	K	Vo=	9.90	K									
Cu=C2=	2.74	MJ/m3 K	Cf=C1=	1.94	MJ/m3 K									
L=	137.34	MJ/m3	Li=	236.27	MJ/m3									
K1=Kf=	4.30	W/m K	Ku=	2.30	W/m K									
ro=	0.03	m	ar=	3.00										
Lt=	4.40	m	STE=	3.92										
0														
R (m)	R/ro	LN (R/ro)	S+S method t (hr)	C+J method t (hr)	Q(MJ/m)	Q/t (W/m)	P (W/m)	N2 l requirement usin N2 l (Mg)	N2 l (l)	LN2 (m3) x Ltarget	R* non-stead state	R*/ro non-steady	ln R*/ro	C+J non steady state t (hr)
0.03	0.98	0.00	0.00	0.00	0.00			0.00	0.00	0.00	0.03	0.98	-0.02	0.00
0.05	1.97	0.68	0.10	0.03	4.06	11804.23	7818.80	0.02	25.22	162.54	0.04	1.43	0.36	0.01
0.10	3.94	1.37	0.65	0.38	11.78	3853.55	3864.12	0.06	73.18	471.72	0.07	2.87	1.05	0.14
0.15	5.91	1.78	1.82	1.23	24.26	2963.77	2981.87	0.12	150.76	971.79	0.11	4.30	1.46	0.50
0.20	7.87	2.06	3.69	2.66	41.25	2531.24	2566.17	0.21	256.37	1652.59	0.15	5.73	1.75	1.13
0.25	9.84	2.29	6.30	4.74	62.70	2276.07	2315.76	0.32	389.63	2511.54	0.18	7.17	1.97	2.07
0.30	11.81	2.47	9.72	7.51	88.55	2104.38	2144.75	0.44	550.29	3547.17	0.22	8.60	2.15	3.35
0.35	13.78	2.62	13.96	11.02	118.78	1979.10	2018.72	0.60	738.20	4758.42	0.25	10.03	2.31	4.97
0.40	15.75	2.76	19.07	15.29	153.38	1882.57	1920.93	0.77	953.22	6144.48	0.29	11.46	2.44	6.97
0.45	17.72	2.87	25.06	20.36	192.33	1805.25	1842.22	0.97	1195.27	7704.68	0.33	12.90	2.56	9.36
0.50	19.69	2.98	31.96	26.25	235.61	1741.50	1777.09	1.18	1464.24	9438.47	0.36	14.33	2.66	12.14
0.55	21.65	3.08	39.80	32.98	283.21	1687.75	1722.01	1.42	1760.06	11345.36	0.40	15.76	2.76	15.33
0.60	23.62	3.16	48.58	40.57	335.13	1641.60	1674.63	1.68	2082.68	13424.95	0.44	17.20	2.84	18.94
0.65	25.59	3.24	58.33	49.04	391.34	1601.40	1633.28	1.97	2432.03	15676.84	0.47	18.63	2.92	22.99
0.70	27.56	3.32	69.06	58.41	451.85	1565.96	1596.79	2.27	2808.06	18100.73	0.51	20.06	3.00	27.47
0.75	29.53	3.39	80.79	68.69	516.64	1534.39	1564.24	2.60	3210.72	20696.29	0.55	21.50	3.07	32.41
0.80	31.50	3.45	93.53	79.90	585.71	1506.03	1534.98	2.94	3639.97	23463.27	0.58	22.93	3.13	37.80
0.85	33.46	3.51	107.30	92.05	659.06	1480.35	1508.47	3.31	4095.78	26401.40	0.62	24.36	3.19	43.65
0.90	35.43	3.57	122.09	105.15	736.67	1456.96	1484.30	3.70	4578.11	29510.47	0.66	25.80	3.25	49.97
0.95	37.40	3.62	137.94	119.23	818.54	1435.52	1462.14	4.11	5086.91	32790.24	0.69	27.23	3.30	56.77
1.00	39.37	3.67	154.84	134.28	904.67	1415.77	1441.73	4.55	5622.18	36240.54	0.73	28.66	3.36	64.05

Table A16: Actual Freezing Data gathered during Experiment #6.

Actual Experiment # 6 Results				Predicted LN2 Consumption	
Duration of Freezing (hrs)	Target Zone Dimensions			Predicted Rf@t=18.58 hrs	0.26 m
	R(max) (m)	R(min) (m)	R(ave) (m)		
10	0.24	0.38	0.31		
Elapsed Time (hrs)	LN2 Used (m3)	Norm LN2 (m3/m3)		Norm LN2 (m3/m3)	
0.00	0.00	0.00		0.00	
0.50	134.20	101.08		174.04	
1.00	256.20	192.96		505.07	
1.50	378.20	284.85		1040.50	
2.50	488.00	367.55		1769.44	
3.00	549.00	413.49		2689.13	
3.50	622.20	468.62		3797.98	
4.00	683.20	514.57		5094.88	
5.00	744.20	560.51		6578.94	
6.18	951.60	716.72		8249.46	
6.50	988.20	744.28		10105.84	
7.00	1049.20	790.23		12147.57	
7.50	1098.00	826.98		14374.20	
8.00	1146.80	863.74		16785.32	
8.50	1207.80	909.68		19380.59	
9.00	1244.40	937.25		22159.68	
9.58	1317.60	992.38		25122.30	
10.00	1354.20	1019.95		28268.19	

Table A17: Spread Sheet used for Revised Freezing Predictions during Experiment #6,
 assuming (2/4.4)m Liquid and (2.4/4.4)m gas nitrogen.

FREEZING TEST AT U OF A FARM: Experiment #6																		
WEIGHTED AVERAGE OF LIQUID AND GAS NITROGEN TEMPERATURES = ((2/4.4)106+(2.4/4.4)120)/2 = 155 C																		
POREWATER TEMPERATURE = 5.9 C																		
100Sr m.c.	0.26		p dry=	1.60	Mg/m3													
Vs (ave)=	155.00	K	Vo=	9.90	K													
Cu=C2=	2.74	MJ/m3 K	Cf=C1=	1.94	MJ/m3 K													
L=	137.34	MJ/m3	Lj=	236.27	MJ/m3													
K1=Kf=	4.30	W/m K	Ku=	2.30	W/m K													
ro=	0.03	m	sr=	3.00														
Li=	4.40	m	STE=	3.92														
	0																	
			S+S	C+J					(2.4/4.4)	(2.4/4.4)								
			method	method				Gas N2	Contribution	Contribution	Weighted	R*						
R (m)	R/ro	LN (R/ro)	t (hr)	t (hr)	Q(MJ/m)	Qn (W/m)	P (W/m)	(m3)	to Cooling	to Cooling	average	non-stead	R*/ro	ln R*/ro	non-stead	C+J		
									by Gas	LN2 requirement usin	LN2 (m3)	by Liquid	for 4.4 m	state	non-steady	state t (hr)		
									N2 (m3)	LN2 (Mg)	LN2 (l)	N2 (m3)	N2 (m3)					
									x Ltarget									
0.03	0.98	0.00	0.00	0.00	0.00			0.00	0.00	0.00	0.00	0.00	0.00	0.03	0.98	-0.02	0.00	
0.05	1.97	0.68	0.10	0.04	3.60	9966.84	6183.23	0.05	0.03	0.02	22.35	32.76	14.89	66.62	0.04	1.43	0.36	0.01
0.10	3.94	1.37	0.74	0.48	10.86	3147.53	3055.81	0.16	0.09	0.05	67.52	98.92	44.96	196.22	0.07	2.87	1.05	0.17
0.15	5.91	1.78	2.12	1.55	22.68	2384.69	2358.11	0.33	0.18	0.11	140.93	206.47	93.88	413.73	0.11	4.30	1.48	0.63
0.20	7.87	2.06	4.33	3.36	38.83	2027.60	2029.37	0.57	0.31	0.20	241.34	353.87	160.71	708.60	0.15	5.73	1.75	1.43
0.25	9.84	2.29	7.45	5.99	59.29	1819.08	1831.34	0.87	0.47	0.30	368.43	539.76	248.34	1081.60	0.18	7.17	1.97	2.62
0.30	11.81	2.47	11.54	9.50	84.00	1679.52	1696.11	1.23	0.67	0.42	522.02	764.76	347.62	1632.48	0.22	8.60	2.15	4.23
0.35	13.78	2.62	16.64	13.93	112.98	1578.01	1596.44	1.66	0.90	0.57	701.98	1028.41	487.46	2060.79	0.25	10.03	2.31	6.29
0.40	15.75	2.78	22.78	19.34	146.14	1499.99	1519.11	2.14	1.17	0.73	908.22	1330.64	604.79	2666.21	0.29	11.46	2.44	8.82
0.45	17.72	2.87	30.01	25.75	183.54	1437.60	1456.88	2.69	1.47	0.92	1140.64	1671.03	799.58	3348.62	0.33	12.90	2.56	11.63
0.50	19.69	2.98	38.35	33.19	225.14	1386.24	1405.35	3.30	1.80	1.13	1399.18	2049.79	931.72	4167.61	0.36	14.33	2.66	15.35
0.55	21.65	3.08	47.82	41.70	270.94	1342.97	1361.79	3.97	2.17	1.36	1683.78	2466.74	1121.24	4943.01	0.40	15.76	2.76	19.38
0.60	23.62	3.16	58.45	51.30	320.92	1305.86	1324.32	4.71	2.57	1.61	1994.39	2921.79	1328.09	5854.87	0.44	17.20	2.84	23.95
0.65	25.59	3.24	70.26	62.01	375.08	1273.56	1291.63	5.50	3.00	1.88	2330.97	3414.88	1582.22	6842.96	0.47	18.63	2.92	29.07
0.70	27.56	3.32	83.28	73.86	433.41	1245.10	1262.76	6.36	3.47	2.18	2693.48	3945.94	1793.61	7907.14	0.51	20.06	3.00	34.74
0.75	29.53	3.39	97.51	86.86	495.91	1219.76	1237.03	7.27	3.97	2.49	3081.87	4514.94	2062.24	9047.33	0.55	21.50	3.07	40.98
0.80	31.50	3.45	112.96	101.03	562.56	1197.01	1213.89	8.26	4.50	2.83	3496.11	5121.80	2328.09	10293.41	0.58	22.93	3.13	47.79
0.85	33.46	3.51	129.70	116.40	633.38	1176.42	1192.92	9.29	5.07	3.18	3936.18	5768.60	2621.14	11555.30	0.62	24.36	3.19	55.19
0.90	35.43	3.57	147.69	132.97	708.34	1157.67	1173.81	10.39	5.67	3.56	4402.04	6448.99	2931.36	12922.92	0.66	25.80	3.25	63.19
0.95	37.40	3.62	166.95	150.76	787.45	1140.49	1156.29	11.55	6.30	3.96	4893.67	7189.23	3258.74	14386.18	0.69	27.23	3.30	71.79
1.00	39.37	3.67	187.51	169.79	870.70	1124.67	1140.14	12.77	6.97	4.38	5411.05	7927.18	3603.27	15885.02	0.73	28.66	3.36	80.99

Table A18 continued: Temperature Data gathered during Experiment #1.

EXPERIMENT No. 1 4 of 6 DATE: JULY 27th 1993 TIME: 04:30 t=5.5 hrs		TEMP.	ROW 1	TEMP.	ROW 2	TEMP.	ROW 3	TEMP.	ROW 4	TEMP.	ROW 5
EXPERIMENT No. 1 5 of 6 DATE: JULY 27th 1993 TIME: 07:40 t=8.67 hrs											
EXPERIMENT No. 1 4 of 6 DATE: JULY 27th 1993 TIME: 04:30 t=5.5 hrs											
EXPERIMENT No. 1 5 of 6 DATE: JULY 27th 1993 TIME: 07:40 t=8.67 hrs											

Table A 18 continued: Temperature Data gathered during Experiment #1.

EXPERIMENT No. 1		0.06m		0.26m		0.16m		0.36m		TEMP.	
ROW	TEMP.	ROW 3	TEMP.	ROW 2	TEMP.	ROW 4	TEMP.	ROW 4	TEMP.	ROW 4	TEMP.
601	-6.91	607	0.88	816	0.88	823	0.91	823	0.91	823	0.91
602	-4.65	608	0.86	816	0.86	824	0.91	824	0.91	824	0.91
603	-19.17	609	1.22	817	1.22	825	1.00	825	1.00	825	0.91
604	-19.51	610	1.17	818	1.17	826	1.30	826	1.30	826	1.12
605	-19.92	611	1.27	819	1.27	827	1.46	827	1.46	827	0.91
606	-41.59	612	1.51	820	1.51	828	1.66	828	1.66	828	1.30
1201	-5.22	613	3.59	821	3.59	829	3.77	829	3.77	829	1.29
1202	3.67	614	3.67	822	3.67	830	4.13	830	4.13	830	3.90
1203	3.90	1209	4.00	1215	4.00	831	4.00	831	4.00	831	4.00
1204	3.92	1210	4.06	1216	4.06	1221	2.88	1221	2.88	1221	4.10
1205	4.05	1211	4.16	1217	4.16	1222	4.05	1222	4.05	1222	3.92
1206	3.92	1212	4.13	1218	4.13	1223	4.03	1223	4.03	1223	4.10
1207	4.08	1213	4.10	1219	4.10	1224	4.13	1224	4.13	1224	3.92
1208	3.97	1214	4.10	1220	4.10	1225	3.92	1225	3.92	1225	4.13
						1226	1227	1226	1227	1226	4.23
											3.97

Table A19: Temperature Data gathered during Experiment #2.

CAMLEX ACTIVITY #8 GROUND FREEZING FIELD TEST EXPERIMENTS AUGUST TO SEPTEMBER, 1963									
Experiment No. 2 - Target Zone of 4 to 6 m and 7 to 8 m									
DATE: 28th JULY 1963									
TIME: 12:10 140 hrs									
ROW 1		ROW 2		ROW 3		ROW 4		ROW 5	
Depth (m)	TEMP.	Depth (m)	TEMP.	Depth (m)	TEMP.	Depth (m)	TEMP.	Depth (m)	TEMP.
2.75	0.65	0.49	0.15	0.49	0.15	0.49	0.15	0.49	0.15
3.30	0.42	0.44	0.16	0.44	0.16	0.44	0.16	0.44	0.16
3.75	0.57	0.73	0.17	0.73	0.17	0.73	0.17	0.73	0.17
4.33	0.44	0.62	0.18	0.62	0.18	0.62	0.18	0.62	0.18
4.83	0.31	0.60	0.19	0.60	0.19	0.60	0.19	0.60	0.19
5.30	0.47	0.65	0.20	0.65	0.20	0.65	0.20	0.65	0.20
5.70	0.47	0.49	0.21	0.49	0.21	0.49	0.21	0.49	0.21
6.00	0.49	0.52	0.22	0.52	0.22	0.52	0.22	0.52	0.22
6.78	0.42	0.55	0.25	0.55	0.25	0.55	0.25	0.55	0.25
7.30	0.44	0.65	0.28	0.65	0.28	0.65	0.28	0.65	0.28
7.79	0.60	0.68	0.27	0.68	0.27	0.68	0.27	0.68	0.27
8.29	0.47	0.69	0.28	0.69	0.28	0.69	0.28	0.69	0.28
8.78	0.60	0.69	0.29	0.69	0.29	0.69	0.29	0.69	0.29
9.31	0.65	0.67	0.31	0.67	0.31	0.67	0.31	0.67	0.31
9.31	0.65	0.67	0.31	0.67	0.31	0.67	0.31	0.67	0.31
DEPTH OF RTD'S BELOW GROUND SURFACE									
ROW1(0.06m)		ROW2(0.16m)		ROW3(0.26m)		ROW4(0.36m)		ROW 5	
Depth (m)	TEMP.	Depth (m)	TEMP.	Depth (m)	TEMP.	Depth (m)	TEMP.	Depth (m)	TEMP.
2.75	0.65	2.75	0.25	2.75	0.25	2.75	0.25	2.75	0.25
3.30	0.42	3.30	0.27	3.30	0.27	3.30	0.27	3.30	0.27
3.75	0.57	3.75	0.29	3.75	0.29	3.75	0.29	3.75	0.29
4.33	0.44	4.33	0.31	4.33	0.31	4.33	0.31	4.33	0.31
4.83	0.31	4.83	0.32	4.83	0.32	4.83	0.32	4.83	0.32
5.30	0.47	5.30	0.34	5.30	0.34	5.30	0.34	5.30	0.34
5.70	0.47	5.70	0.35	5.70	0.35	5.70	0.35	5.70	0.35
6.00	0.49	6.00	0.36	6.00	0.36	6.00	0.36	6.00	0.36
6.78	0.42	6.78	0.37	6.78	0.37	6.78	0.37	6.78	0.37
7.30	0.44	7.30	0.38	7.30	0.38	7.30	0.38	7.30	0.38
7.79	0.60	7.79	0.39	7.79	0.39	7.79	0.39	7.79	0.39
8.29	0.47	8.29	0.40	8.29	0.40	8.29	0.40	8.29	0.40
8.78	0.60	8.78	0.41	8.78	0.41	8.78	0.41	8.78	0.41
9.31	0.65	9.31	0.42	9.31	0.42	9.31	0.42	9.31	0.42
9.31	0.65	9.31	0.42	9.31	0.42	9.31	0.42	9.31	0.42
Time versus Temperature Changes									
RTD		Depth (m)		Time (hrs)		Temp (C)		Row 4	
RTD	Depth (m)	Time (hrs)	Temp (C)	Row 4	Temp (C)	Row 3	Temp (C)	Row 2	Temp (C)
806	5.3	0.00	0.47	0.65	0.65	0.65	0.65	0.65	0.65
		2.33	-42.65	0.66	0.66	0.66	0.66	0.66	0.66
		4.42	-67.02	0.63	0.63	0.63	0.63	0.63	0.63
		6.77	-58.32	0.75	0.75	0.75	0.75	0.75	0.75
		10.27	-52.34	-2.85	-2.85	-2.85	-2.85	-2.85	-2.85
		17.02	-52.70	-16.49	-16.49	-16.49	-16.49	-16.49	-16.49
		18.77	-85.35	-18.69	-18.69	-18.69	-18.69	-18.69	-18.69
		0.00	0.60	0.62	0.62	0.62	0.62	0.62	0.62
		2.33	-32.16	1.01	1.01	1.01	1.01	1.01	1.01
		4.42	-67.92	1.04	1.04	1.04	1.04	1.04	1.04
		6.77	-77.92	1.01	1.01	1.01	1.01	1.01	1.01
		10.27	-68.03	-4.94	-4.94	-4.94	-4.94	-4.94	-4.94
		17.02	-98.55	-20.91	-20.91	-20.91	-20.91	-20.91	-20.91
		18.77	-95.79	-24.62	-24.62	-24.62	-24.62	-24.62	-24.62

Table A19 continued: Temperature Data gathered during Experiment #2.

Experiment #3 2 of 7 DATE: July 26, 1993 TIME: 1:20 (±2.33 hrs)		Experiment #2 3 of 7 DATE: July 26, 1993 TIME: 1:35 (±4.42 hrs)					
ROW 1	ROW 2	ROW 3	ROW 4	ROW 1	ROW 2	ROW 3	ROW 4
①0.06m	①0.16m	①0.28m	①0.36m	①0.06m	①0.16m	①0.28m	①0.36m
Depth (m)	Depth (m)	Depth (m)	Depth (m)	Depth (m)	Depth (m)	Depth (m)	Depth (m)
TEMP.	TEMP.	TEMP.	TEMP.	TEMP.	TEMP.	TEMP.	TEMP.
601 99.87	815 101.14	807 101.13	823 101.10	601 83.43	815 101.11	807 101.13	823 101.10
602 97.65	816 101.14	808 101.10	824 101.16	602 87.65	816 101.11	808 101.09	824 101.16
603 99.06	817 101.36	809 101.24	825 101.10	603 99.06	817 101.64	809 101.22	825 101.07
604 88.12	818 101.28	810 101.20	826 101.13	604 88.12	818 101.32	811 101.15	826 101.13
605 92.18	819 101.28	811 101.22	827 101.14	605 92.18	819 101.21	812 101.17	827 101.09
606 74.73	820 101.25	812 101.20	828 101.24	606 74.73	820 101.23	813 101.21	828 101.19
1201 98.04	821 101.24	813 101.19	829 101.21	1201 98.04	821 101.23	814 101.21	829 101.18
1202 101.58	822 101.27	814 101.20	830 101.23	1202 101.58	822 101.29	815 101.23	830 101.25
1203 101.56	823 101.28	815 101.65	831 101.28	1203 101.56	823 101.28	816 101.66	831 101.28
1204 101.42	824 101.28	816 101.65	832 101.28	1204 101.42	824 101.28	817 101.66	832 101.28
1205 76.11	825 101.28	817 101.65	833 101.28	1205 76.11	825 101.28	818 101.66	833 101.28
1206 60.19	826 101.28	818 101.65	834 101.28	1206 60.19	826 101.28	819 101.66	834 101.28
1207 100.93	827 101.28	819 101.65	835 101.28	1207 100.93	827 101.28	820 101.66	835 101.28
1208 101.69	828 101.28	820 101.65	836 101.28	1208 101.69	828 101.28	821 101.66	836 101.28
	829 101.28	821 101.65	837 101.28		829 101.28	822 101.66	837 101.28
	830 101.28	822 101.65	838 101.28		830 101.28	823 101.66	838 101.28
	831 101.28	823 101.65	839 101.28		831 101.28	824 101.66	839 101.28
	832 101.28	824 101.65	840 101.28		832 101.28	825 101.66	840 101.28
	833 101.28	825 101.65	841 101.28		833 101.28	826 101.66	841 101.28
	834 101.28	826 101.65	842 101.28		834 101.28	827 101.66	842 101.28
	835 101.28	827 101.65	843 101.28		835 101.28	828 101.66	843 101.28
	836 101.28	828 101.65	844 101.28		836 101.28	829 101.66	844 101.28
	837 101.28	829 101.65	845 101.28		837 101.28	830 101.66	845 101.28
	838 101.28	830 101.65	846 101.28		838 101.28	831 101.66	846 101.28
	839 101.28	831 101.65	847 101.28		839 101.28	832 101.66	847 101.28
	840 101.28	832 101.65	848 101.28		840 101.28	833 101.66	848 101.28
	841 101.28	833 101.65	849 101.28		841 101.28	834 101.66	849 101.28
	842 101.28	834 101.65	850 101.28		842 101.28	835 101.66	850 101.28
	843 101.28	835 101.65	851 101.28		843 101.28	836 101.66	851 101.28
	844 101.28	836 101.65	852 101.28		844 101.28	837 101.66	852 101.28
	845 101.28	837 101.65	853 101.28		845 101.28	838 101.66	853 101.28
	846 101.28	838 101.65	854 101.28		846 101.28	839 101.66	854 101.28
	847 101.28	839 101.65	855 101.28		847 101.28	840 101.66	855 101.28
	848 101.28	840 101.65	856 101.28		848 101.28	841 101.66	856 101.28
	849 101.28	841 101.65	857 101.28		849 101.28	842 101.66	857 101.28
	850 101.28	842 101.65	858 101.28		850 101.28	843 101.66	858 101.28
	851 101.28	843 101.65	859 101.28		851 101.28	844 101.66	859 101.28
	852 101.28	844 101.65	860 101.28		852 101.28	845 101.66	860 101.28
	853 101.28	845 101.65	861 101.28		853 101.28	846 101.66	861 101.28
	854 101.28	846 101.65	862 101.28		854 101.28	847 101.66	862 101.28
	855 101.28	847 101.65	863 101.28		855 101.28	848 101.66	863 101.28
	856 101.28	848 101.65	864 101.28		856 101.28	849 101.66	864 101.28
	857 101.28	849 101.65	865 101.28		857 101.28	850 101.66	865 101.28
	858 101.28	850 101.65	866 101.28		858 101.28	851 101.66	866 101.28
	859 101.28	851 101.65	867 101.28		859 101.28	852 101.66	867 101.28
	860 101.28	852 101.65	868 101.28		860 101.28	853 101.66	868 101.28
	861 101.28	853 101.65	869 101.28		861 101.28	854 101.66	869 101.28
	862 101.28	854 101.65	870 101.28		862 101.28	855 101.66	870 101.28
	863 101.28	855 101.65	871 101.28		863 101.28	856 101.66	871 101.28
	864 101.28	856 101.65	872 101.28		864 101.28	857 101.66	872 101.28
	865 101.28	857 101.65	873 101.28		865 101.28	858 101.66	873 101.28
	866 101.28	858 101.65	874 101.28		866 101.28	859 101.66	874 101.28
	867 101.28	859 101.65	875 101.28		867 101.28	860 101.66	875 101.28
	868 101.28	860 101.65	876 101.28		868 101.28	861 101.66	876 101.28
	869 101.28	861 101.65	877 101.28		869 101.28	862 101.66	877 101.28
	870 101.28	862 101.65	878 101.28		870 101.28	863 101.66	878 101.28
	871 101.28	863 101.65	879 101.28		871 101.28	864 101.66	879 101.28
	872 101.28	864 101.65	880 101.28		872 101.28	865 101.66	880 101.28
	873 101.28	865 101.65	881 101.28		873 101.28	866 101.66	881 101.28
	874 101.28	866 101.65	882 101.28		874 101.28	867 101.66	882 101.28
	875 101.28	867 101.65	883 101.28		875 101.28	868 101.66	883 101.28
	876 101.28	868 101.65	884 101.28		876 101.28	869 101.66	884 101.28
	877 101.28	869 101.65	885 101.28		877 101.28	870 101.66	885 101.28
	878 101.28	870 101.65	886 101.28		878 101.28	871 101.66	886 101.28
	879 101.28	871 101.65	887 101.28		879 101.28	872 101.66	887 101.28
	880 101.28	872 101.65	888 101.28		880 101.28	873 101.66	888 101.28
	881 101.28	873 101.65	889 101.28		881 101.28	874 101.66	889 101.28
	882 101.28	874 101.65	890 101.28		882 101.28	875 101.66	890 101.28
	883 101.28	875 101.65	891 101.28		883 101.28	876 101.66	891 101.28
	884 101.28	876 101.65	892 101.28		884 101.28	877 101.66	892 101.28
	885 101.28	877 101.65	893 101.28		885 101.28	878 101.66	893 101.28
	886 101.28	878 101.65	894 101.28		886 101.28	879 101.66	894 101.28
	887 101.28	879 101.65	895 101.28		887 101.28	880 101.66	895 101.28
	888 101.28	880 101.65	896 101.28		888 101.28	881 101.66	896 101.28
	889 101.28	881 101.65	897 101.28		889 101.28	882 101.66	897 101.28
	890 101.28	882 101.65	898 101.28		890 101.28	883 101.66	898 101.28
	891 101.28	883 101.65	899 101.28		891 101.28	884 101.66	899 101.28
	892 101.28	884 101.65	900 101.28		892 101.28	885 101.66	900 101.28
	893 101.28	885 101.65	901 101.28		893 101.28	886 101.66	901 101.28
	894 101.28	886 101.65	902 101.28		894 101.28	887 101.66	902 101.28
	895 101.28	887 101.65	903 101.28		895 101.28	888 101.66	903 101.28
	896 101.28	888 101.65	904 101.28		896 101.28	889 101.66	904 101.28
	897 101.28	889 101.65	905 101.28		897 101.28	890 101.66	905 101.28
	898 101.28	890 101.65	906 101.28		898 101.28	891 101.66	906 101.28
	899 101.28	891 101.65	907 101.28		899 101.28	892 101.66	907 101.28
	900 101.28	892 101.65	908 101.28		900 101.28	893 101.66	908 101.28
	901 101.28	893 101.65	909 101.28		901 101.28	894 101.66	909 101.28
	902 101.28	894 101.65	910 101.28		902 101.28	895 101.66	910 101.28
	903 101.28	895 101.65	911 101.28		903 101.28	896 101.66	911 101.28
	904 101.28	896 101.65	912 101.28		904 101.28	897 101.66	912 101.28
	905 101.28	897 101.65	913 101.28		905 101.28	898 101.66	913 101.28
	906 101.28	898 101.65	914 101.28		906 101.28	899 101.66	914 101.28
	907 101.28	899 101.65	915 101.28		907 101.28	900 101.66	915 101.28
	908 101.28	900 101.65	916 101.28		908 101.28	901 101.66	916 101.28
	909 101.28	901 101.65	917 101.28		909 101.28	902 101.66	917 101.28
	910 101.28	902 101.65	918 101.28		910 101.28	903 101.66	918 101.28
	911 101.28	903 101.65	919 101.28		911 101.28	904 101.66	919 101.28
	912 101.28	904 101.65	920 101.28		912 101.28	905 101.66	920 101.28
	913 101.28	905 101.65	921 101.28		913 101.28	906 101.66	921 101.28
	914 101.28	906 101.65	922 101.28		914 101.28	907 101.66	922 101.28
	915 101.28	907 101.65	923 101.28		915 101.28	908 101.66	923 101.28
	916 101.28	908 101.65	924 101.28		916 101.28	909 101.66	924 101.28
	917 101.28						

Table A20: Temperature Data gathered during Experiment #3.

CARLEE ACTIVITY 48 CONCORD PRESERVE FIELD TRIAL EXPERIMENTS AUGUST TO SEPTEMBER, 1983										
Experiment #3 - Target Zone at 4 to 6 m, and 7 to 9 m										
DATE: 29th JULY 1983										
TIME: 17:00 (±0 hrs)										
ROW 1	ROW 2	ROW 3	ROW 4	ROW 5	ROW 6	ROW 7	ROW 8	ROW 9	ROW 10	ROW 11
TEMP	TEMP	TEMP	TEMP	TEMP	TEMP	TEMP	TEMP	TEMP	TEMP	TEMP
0.06m	0.15m	0.25m	0.35m	0.45m	0.55m	0.65m	0.75m	0.85m	0.95m	1.05m
801 101.14	815 101.24	807 101.24	823 101.24	816 101.17	822 101.17	819 101.17	825 101.17	817 101.14	823 101.14	819 101.14
802 101.19	816 101.19	808 101.26	824 101.26	816 101.26	822 101.26	819 101.26	825 101.26	817 101.23	823 101.23	819 101.23
803 101.24	817 101.24	809 101.31	825 101.31	817 101.31	823 101.31	820 101.31	826 101.31	818 101.28	824 101.28	820 101.28
804 101.29	818 101.29	810 101.34	826 101.34	818 101.34	824 101.34	821 101.34	827 101.34	819 101.31	825 101.31	821 101.31
805 101.34	819 101.34	811 101.39	827 101.39	819 101.39	825 101.39	822 101.39	828 101.39	820 101.36	826 101.36	822 101.36
806 101.39	820 101.39	812 101.44	828 101.44	820 101.44	826 101.44	823 101.44	829 101.44	821 101.41	827 101.41	823 101.41
807 101.44	821 101.44	813 101.49	829 101.49	821 101.49	827 101.49	824 101.49	830 101.49	822 101.46	828 101.46	824 101.46
808 101.49	822 101.49	814 101.54	830 101.54	822 101.54	828 101.54	825 101.54	831 101.54	823 101.51	829 101.51	825 101.51
809 101.54	823 101.54	815 101.59	831 101.59	823 101.59	829 101.59	826 101.59	832 101.59	824 101.56	830 101.56	826 101.56
810 101.59	824 101.59	816 101.64	832 101.64	824 101.64	830 101.64	827 101.64	833 101.64	825 101.61	831 101.61	827 101.61
811 101.64	825 101.64	817 101.69	833 101.69	825 101.69	831 101.69	828 101.69	834 101.69	826 101.66	832 101.66	828 101.66
812 101.69	826 101.69	818 101.74	834 101.74	826 101.74	832 101.74	829 101.74	835 101.74	827 101.71	833 101.71	829 101.71
813 101.74	827 101.74	819 101.79	835 101.79	827 101.79	833 101.79	830 101.79	836 101.79	828 101.76	834 101.76	830 101.76
814 101.79	828 101.79	820 101.84	836 101.84	828 101.84	834 101.84	831 101.84	837 101.84	829 101.81	835 101.81	831 101.81
815 101.84	829 101.84	821 101.89	837 101.89	829 101.89	835 101.89	832 101.89	838 101.89	830 101.86	836 101.86	832 101.86
816 101.89	830 101.89	822 101.94	838 101.94	830 101.94	836 101.94	833 101.94	839 101.94	831 101.91	837 101.91	833 101.91
817 101.94	831 101.94	823 101.99	839 101.99	831 101.99	837 101.99	834 101.99	840 101.99	832 101.96	838 101.96	834 101.96
818 101.99	832 101.99	824 102.04	840 102.04	832 102.04	838 102.04	835 102.04	841 102.04	833 102.01	839 102.01	835 102.01
819 102.04	833 102.04	825 102.09	841 102.09	833 102.09	839 102.09	836 102.09	842 102.09	834 102.06	840 102.06	836 102.06
820 102.09	834 102.09	826 102.14	842 102.14	834 102.14	840 102.14	837 102.14	843 102.14	835 102.11	841 102.11	837 102.11
821 102.14	835 102.14	827 102.19	843 102.19	835 102.19	841 102.19	838 102.19	844 102.19	836 102.16	842 102.16	838 102.16
822 102.19	836 102.19	828 102.24	844 102.24	836 102.24	842 102.24	839 102.24	845 102.24	837 102.21	843 102.21	839 102.21
823 102.24	837 102.24	829 102.29	845 102.29	837 102.29	843 102.29	840 102.29	846 102.29	838 102.26	844 102.26	840 102.26
824 102.29	838 102.29	830 102.34	846 102.34	838 102.34	844 102.34	841 102.34	847 102.34	839 102.31	845 102.31	841 102.31
825 102.34	839 102.34	831 102.39	847 102.39	839 102.39	845 102.39	842 102.39	848 102.39	840 102.36	846 102.36	842 102.36
826 102.39	840 102.39	832 102.44	848 102.44	840 102.44	846 102.44	843 102.44	849 102.44	841 102.41	847 102.41	843 102.41
827 102.44	841 102.44	833 102.49	849 102.49	841 102.49	847 102.49	844 102.49	850 102.49	842 102.46	848 102.46	844 102.46
828 102.49	842 102.49	834 102.54	850 102.54	842 102.54	848 102.54	845 102.54	851 102.54	843 102.51	849 102.51	845 102.51
829 102.54	843 102.54	835 102.59	851 102.59	843 102.59	849 102.59	846 102.59	852 102.59	844 102.56	850 102.56	846 102.56
830 102.59	844 102.59	836 102.64	852 102.64	844 102.64	850 102.64	847 102.64	853 102.64	845 102.61	851 102.61	847 102.61
831 102.64	845 102.64	837 102.69	853 102.69	845 102.69	851 102.69	848 102.69	854 102.69	846 102.66	852 102.66	848 102.66
832 102.69	846 102.69	838 102.74	854 102.74	846 102.74	852 102.74	849 102.74	855 102.74	847 102.71	853 102.71	849 102.71
833 102.74	847 102.74	839 102.79	855 102.79	847 102.79	853 102.79	850 102.79	856 102.79	848 102.76	854 102.76	850 102.76
834 102.79	848 102.79	840 102.84	856 102.84	848 102.84	854 102.84	851 102.84	857 102.84	849 102.81	855 102.81	851 102.81
835 102.84	849 102.84	841 102.89	857 102.89	849 102.89	855 102.89	852 102.89	858 102.89	850 102.86	856 102.86	852 102.86
836 102.89	850 102.89	842 102.94	858 102.94	850 102.94	856 102.94	853 102.94	859 102.94	851 102.91	857 102.91	853 102.91
837 102.94	851 102.94	843 102.99	859 102.99	851 102.99	857 102.99	854 102.99	860 102.99	852 102.96	858 102.96	854 102.96
838 102.99	852 102.99	844 103.04	860 103.04	852 103.04	858 103.04	855 103.04	861 103.04	853 103.01	859 103.01	855 103.01
839 103.04	853 103.04	845 103.09	861 103.09	853 103.09	859 103.09	856 103.09	862 103.09	854 103.06	860 103.06	856 103.06
840 103.09	854 103.09	846 103.14	862 103.14	854 103.14	860 103.14	857 103.14	863 103.14	855 103.11	861 103.11	857 103.11
841 103.14	855 103.14	847 103.19	863 103.19	855 103.19	861 103.19	858 103.19	864 103.19	856 103.16	862 103.16	858 103.16
842 103.19	856 103.19	848 103.24	864 103.24	856 103.24	862 103.24	859 103.24	865 103.24	857 103.21	863 103.21	859 103.21
843 103.24	857 103.24	849 103.29	865 103.29	857 103.29	863 103.29	860 103.29	866 103.29	858 103.26	864 103.26	860 103.26
844 103.29	858 103.29	850 103.34	866 103.34	858 103.34	864 103.34	861 103.34	867 103.34	859 103.31	865 103.31	861 103.31
845 103.34	859 103.34	851 103.39	867 103.39	859 103.39	865 103.39	862 103.39	868 103.39	860 103.36	866 103.36	862 103.36
846 103.39	860 103.39	852 103.44	868 103.44	860 103.44	866 103.44	863 103.44	869 103.44	861 103.41	867 103.41	863 103.41
847 103.44	861 103.44	853 103.49	869 103.49	861 103.49	867 103.49	864 103.49	870 103.49	862 103.46	868 103.46	864 103.46
848 103.49	862 103.49	854 103.54	870 103.54	862 103.54	868 103.54	865 103.54	871 103.54	863 103.51	869 103.51	865 103.51
849 103.54	863 103.54	855 103.59	871 103.59	863 103.59	869 103.59	866 103.59	872 103.59	864 103.56	870 103.56	866 103.56
850 103.59	864 103.59	856 103.64	872 103.64	864 103.64	870 103.64	867 103.64	873 103.64	865 103.61	871 103.61	867 103.61
851 103.64	865 103.64	857 103.69	873 103.69	865 103.69	871 103.69	868 103.69	874 103.69	866 103.66	872 103.66	868 103.66
852 103.69	866 103.69	858 103.74	874 103.74	866 103.74	872 103.74	869 103.74	875 103.74	867 103.71	873 103.71	869 103.71
853 103.74	867 103.74	859 103.79	875 103.79	867 103.79	873 103.79	870 103.79	876 103.79	868 103.76	874 103.76	870 103.76
854 103.79	868 103.79	860 103.84	876 103.84	868 103.84	874 103.84	871 103.84	877 103.84	869 103.81	875 103.81	871 103.81
855 103.84	869 103.84	861 103.89	877 103.89	869 103.89	875 103.89	872 103.89	878 103.89	870 103.86	876 103.86	872 103.86
856 103.89	870 103.89	862 103.94	878 103.94	870 103.94	876 103.94	873 103.94	879 103.94	871 103.91	877 103.91	873 103.91
857 103.94	871 103.94	863 103.99	879 103.99	871 103.99	877 103.99	874 103.99	880 103.99	872 103.96	878 103.96	874 103.96
858 103.99	872 103.99	864 104.04	880 104.04	872 104.04	878 104.04	875 104.04	881 104.04	873 104.01	879 104.01	875 104.01
859 104.04	873 104.04	865 104.09	881 104.09	873 104.09	879 104.09	876 104.09	882 104.09	874 104.06	880 104.06	876 104.06
860 104.09	874 104.09	866 104.14	882 104.14	874 104.14	880 104.14	877 104.14	883 104.14	875 104.11	881 104.11	877 104.11
861 104.14	875 104.14	867 104.19	883 104.19	875 104.19	881 104.19	878 104.19	884 104.19	876 104.16	882 104.16	878 104.16
862 104.19	876 104.19	868 104.24	884 104.24	876 104.24	882 104.24	879 104.24	885 104.24	877 104.21	883 104.21	879 104.21
863 104.24	877 104.24	869 104.29	885 104.29	877 104.29	883 104.29	880 104.29	886 104.29	878 104.26	884 104.26	880 104.26
864 104.29	878 104.29	870 104.34	886 104.34	878 104.34	884 104.34	881 104.34	887 104.34	879 104.31	885 104.31	881 104.31
865 104.34	879 104.34	871 104.39	887 104.39	879 104.39	885 104.39	882 104				

Table A20 continued: Temperature Data gathered during Experiment #3.

EXPERIMENT No. 3												
2 of 7												
DATE: July 29, 1963												
TIME: 20:00 1-5 hrs												
ROW 1	●0.06m	●0.26m	ROW 3	●0.26m	TEMP.	ROW 2	●0.16m	●0.16m	TEMP.	ROW 4	●0.36m	TEMP.
801	100.98	807	101.22	0.92	0.78	815	101.23	823	0.93	101.27	0.93	0.89
802	101.22	808	101.16	0.91	0.70	816	101.21	824	0.92	101.24	0.92	0.89
803	101.22	809	101.33	0.92	1.08	817	109.92	825	23.38	101.24	0.91	0.70
804	101.19	810	101.24	0.9	0.88	818	101.32	826	1.04	101.24	0.91	0.68
805	97.12	811	101.24	0.91	0.68	819	101.25	827	0.91	101.17	0.91	0.69
806	87.47	812	101.20	0.9	0.78	820	101.23	828	0.93	101.25	0.93	0.93
1201	101.57	813	101.21	0.89	0.93	821	101.25	829	0.91	101.22	0.91	0.91
1202	101.91	814	101.19	0.9	0.75	822	101.27	830	0.99	101.20	0.91	0.79
1203	101.59	1209	101.61	1.28	0.91	1215	101.65	831	0.98	101.25	0.90	0.91
1204	101.76	1210	101.61	1.26	0.91	1216	101.72	1221	1.12	101.62	1.28	0.88
1205	72.58	1211	101.61	1.24	0.98	1217	101.62	1222	0.88	101.61	1.28	0.88
1206	86.57	1212	101.62	1.26	0.84	1218	101.60	1223	0.93	101.63	1.28	0.81
1207	101.63	1213	101.62	1.24	1.06	1219	101.59	1224	0.99	101.59	1.27	0.99
1208	101.61	1214	101.67	1.22	0.91	1220	101.59	1225	0.93	101.64	1.28	1.01
								1226		101.64	1.28	1.01
								1227		101.64	1.28	0.88

EXPERIMENT No. 3												
3 of 7												
DATE: July 29, 1963												
TIME: 22:00 1-5 hrs												
ROW 1	●0.06m	●0.26m	ROW 3	●0.26m	TEMP.	ROW 2	●0.16m	●0.16m	TEMP.	ROW 4	●0.36m	TEMP.
801	88.95	807	101.21	0.88	0.60	815	101.20	823	0.89	101.26	0.92	0.88
802	101.18	808	101.19	0.90	0.75	816	101.19	824	0.90	101.24	0.90	0.89
803	101.19	809	101.3	0.81	1.01	817	109.80	825	23.12	101.27	0.89	0.86
804	101.1	810	101.23	0.89	0.88	818	101.28	826	0.93	101.21	0.88	0.83
805	91.02	811	101.23	0.89	0.85	819	101.26	827	0.98	101.17	0.90	0.76
806	72.29	812	101.2	0.88	0.83	820	101.22	828	0.98	101.25	0.90	0.91
1201	100.68	813	101.19	0.88	0.81	821	101.22	829	0.89	101.22	0.93	0.75
1202	101.54	814	101.21	0.89	0.83	822	101.25	830	0.94	101.21	0.90	0.81
1203	101.5	1208	101.57	1.24	0.86	1215	101.61	831	0.91	101.23	0.89	0.89
1204	101.4	1209	101.6	1.24	0.94	1216	101.67	1221	1.04	101.64	1.28	0.94
1205	65.78	1210	101.61	1.23	0.99	1217	100.19	1222	-2.78	101.56	1.27	0.78
1206	81.73	1211	101.61	1.23	1.06	1218	99.72	1223	-4.00	101.64	1.26	0.96
1207	101.58	1212	101.64	1.23	1.06	1219	101.69	1224	1.12	101.60	1.26	0.88
1208	101.61	1213	101.64	1.21	1.12	1220	101.65	1225	1.01	101.61	1.24	0.96
								1226		101.67	1.24	1.12
								1227		101.65	1.24	1.06

Table A20 continued: Temperature Data gathered during Experiment #3.

Experiment No. 3									
6 of 7									
DATE: July 30, 1993									
TIME: 09:00 h-18 hrs									
ROW 1	ROW 2	ROW 3	ROW 4	ROW 5	ROW 6	ROW 7	ROW 8	ROW 9	ROW 10
TEMP.	TEMP.	TEMP.	TEMP.	TEMP.	TEMP.	TEMP.	TEMP.	TEMP.	TEMP.
801	807	813	819	825	831	837	843	849	855
802	808	814	820	826	832	838	844	850	856
803	809	815	821	827	833	839	845	851	857
804	810	816	822	828	834	840	846	852	858
805	811	817	823	829	835	841	847	853	859
806	812	818	824	830	836	842	848	854	860
807	813	819	825	831	837	843	849	855	861
808	814	820	826	832	838	844	850	856	862
809	815	821	827	833	839	845	851	857	863
810	816	822	828	834	840	846	852	858	864
811	817	823	829	835	841	847	853	859	865
812	818	824	830	836	842	848	854	860	866
813	819	825	831	837	843	849	855	861	867
814	820	826	832	838	844	850	856	862	868
815	821	827	833	839	845	851	857	863	869
816	822	828	834	840	846	852	858	864	870
817	823	829	835	841	847	853	859	865	871
818	824	830	836	842	848	854	860	866	872
819	825	831	837	843	849	855	861	867	873
820	826	832	838	844	850	856	862	868	874
821	827	833	839	845	851	857	863	869	875
822	828	834	840	846	852	858	864	870	876
823	829	835	841	847	853	859	865	871	877
824	830	836	842	848	854	860	866	872	878
825	831	837	843	849	855	861	867	873	879
826	832	838	844	850	856	862	868	874	880
827	833	839	845	851	857	863	869	875	881
828	834	840	846	852	858	864	870	876	882
829	835	841	847	853	859	865	871	877	883
830	836	842	848	854	860	866	872	878	884
831	837	843	849	855	861	867	873	879	885
832	838	844	850	856	862	868	874	880	886
833	839	845	851	857	863	869	875	881	887
834	840	846	852	858	864	870	876	882	888
835	841	847	853	859	865	871	877	883	889
836	842	848	854	860	866	872	878	884	890
837	843	849	855	861	867	873	879	885	891
838	844	850	856	862	868	874	880	886	892
839	845	851	857	863	869	875	881	887	893
840	846	852	858	864	870	876	882	888	894
841	847	853	859	865	871	877	883	889	895
842	848	854	860	866	872	878	884	890	896
843	849	855	861	867	873	879	885	891	897
844	850	856	862	868	874	880	886	892	898
845	851	857	863	869	875	881	887	893	899
846	852	858	864	870	876	882	888	894	900
847	853	859	865	871	877	883	889	895	901
848	854	860	866	872	878	884	890	896	902
849	855	861	867	873	879	885	891	897	903
850	856	862	868	874	880	886	892	898	904
851	857	863	869	875	881	887	893	899	905
852	858	864	870	876	882	888	894	900	906
853	859	865	871	877	883	889	895	901	907
854	860	866	872	878	884	890	896	902	908
855	861	867	873	879	885	891	897	903	909
856	862	868	874	880	886	892	898	904	910
857	863	869	875	881	887	893	899	905	911
858	864	870	876	882	888	894	900	906	912
859	865	871	877	883	889	895	901	907	913
860	866	872	878	884	890	896	902	908	914
861	867	873	879	885	891	897	903	909	915
862	868	874	880	886	892	898	904	910	916
863	869	875	881	887	893	899	905	911	917
864	870	876	882	888	894	900	906	912	918
865	871	877	883	889	895	901	907	913	919
866	872	878	884	890	896	902	908	914	920
867	873	879	885	891	897	903	909	915	921
868	874	880	886	892	898	904	910	916	922
869	875	881	887	893	899	905	911	917	923
870	876	882	888	894	900	906	912	918	924
871	877	883	889	895	901	907	913	919	925
872	878	884	890	896	902	908	914	920	926
873	879	885	891	897	903	909	915	921	927
874	880	886	892	898	904	910	916	922	928
875	881	887	893	899	905	911	917	923	929
876	882	888	894	900	906	912	918	924	930
877	883	889	895	901	907	913	919	925	931
878	884	890	896	902	908	914	920	926	932
879	885	891	897	903	909	915	921	927	933
880	886	892	898	904	910	916	922	928	934
881	887	893	899	905	911	917	923	929	935
882	888	894	900	906	912	918	924	930	936
883	889	895	901	907	913	919	925	931	937
884	890	896	902	908	914	920	926	932	938
885	891	897	903	909	915	921	927	933	939
886	892	898	904	910	916	922	928	934	940
887	893	899	905	911	917	923	929	935	941
888	894	900	906	912	918	924	930	936	942
889	895	901	907	913	919	925	931	937	943
890	896	902	908	914	920	926	932	938	944
891	897	903	909	915	921	927	933	939	945
892	898	904	910	916	922	928	934	940	946
893	899	905	911	917	923	929	935	941	947
894	900	906	912	918	924	930	936	942	948
895	901	907	913	919	925	931	937	943	949
896	902	908	914	920	926	932	938	944	950
897	903	909	915	921	927	933	939	945	951
898	904	910	916	922	928	934	940	946	952
899	905	911	917	923	929	935	941	947	953
900	906	912	918	924	930	936	942	948	954

Table A21 continued: Temperature Data gathered during Experiment #4.

Experiment No. 4		8 of 7		DATE: August 4, 1993		TIME: 02:00 (±13.58 hrs)					
ROW 1	86.00	1.37	101.62	816	101.60	0.76	1.51	823	70.80	1.53	79.82
	91.11	1.51	101.78	819	101.63	0.69	1.52	824	70.23	1.49	-81.19
	86.80	1.50	101.99	817	101.63	0.68	1.52	825	69.92	1.47	-81.95
	88.54	1.48	101.87	819	101.93	0.68	1.53	826	69.92	1.47	-83.12
	86.80	1.49	101.85	819	101.89	0.68	1.51	827	69.41	1.45	-83.25
	85.59	1.47	101.67	820	101.84	0.64	1.51	828	68.66	1.45	-85.17
	85.94	1.85	101.67	821	101.81	0.64	1.51	829	68.37	1.44	-85.90
	86.05	1.81	101.85	822	101.85	0.68	1.52	830	68.19	1.43	-84.16
	86.00	1.51	101.96	822	101.85	0.68	1.52	831	61.39	1.40	-103.02
	86.00	1.78	102.32	1215	102.39	1.17	1.90	832	61.39	1.40	-103.02
	87.11	1.79	102.34	1216	102.39	1.17	1.90	833	32.81	1.78	-179.14
	86.00	1.79	102.44	1217	102.39	1.17	1.90	834	31.89	1.72	-181.40
	86.81	1.75	102.44	1218	102.37	1.16	1.89	835	33.38	1.71	-177.48
	87.07	1.70	102.45	1219	102.49	1.16	1.89	836	32.44	1.69	-179.32
			102.43	1220	97.38	1.56	1.88	837	34.93	1.64	-179.27
								838	31.65	1.59	-182.18
								839	32.27	1.59	-179.97
Experiment No. 4											
7 of 7											
DATE: August 4, 1993											
TIME: 07:00 (±16.58 hrs)											
ROW 1	801	85.82	103.00	807	103.00	2.63	3.04	830	823	71.89	-79.71
	802	80.28	102.98	808	102.98	2.78	3.10	831	824	71.54	-81.04
	803	86.55	103.10	809	103.10	2.76	3.07	832	825	71.21	-81.65
	804	88.00	103.04	810	103.04	2.76	3.07	833	826	70.90	-82.73
	805	85.68	103.01	811	103.01	2.76	3.07	834	827	70.61	-83.22
	806	85.11	103.03	812	103.03	2.75	3.07	835	828	70.35	-84.65
	8201	83.54	102.98	813	102.98	2.76	3.07	836	829	69.81	-85.43
	8202	80.98	103.00	814	103.00	2.77	3.07	837	830	68.98	-82.55
			103.47	1210	103.43	3.10	3.00	838	821	62.59	-104.81
			103.47	1211	103.35	3.10	2.99	839	822	57.49	-118.10
			103.55	1212	103.35	3.11	2.98	840	823	34.69	-177.30
			103.56	1213	103.56	3.10	2.98	841	824	32.67	-182.42
			103.53	1214	103.41	3.07	2.97	842	825	34.18	-176.39
				1220	92.88	3.07	2.97	843	826	31.62	-184.68
								844	31.64	2.80	-184.75
								845	32.27	2.77	-179.97

Table A22 continued: Temperature Data gathered during Experiment #5.

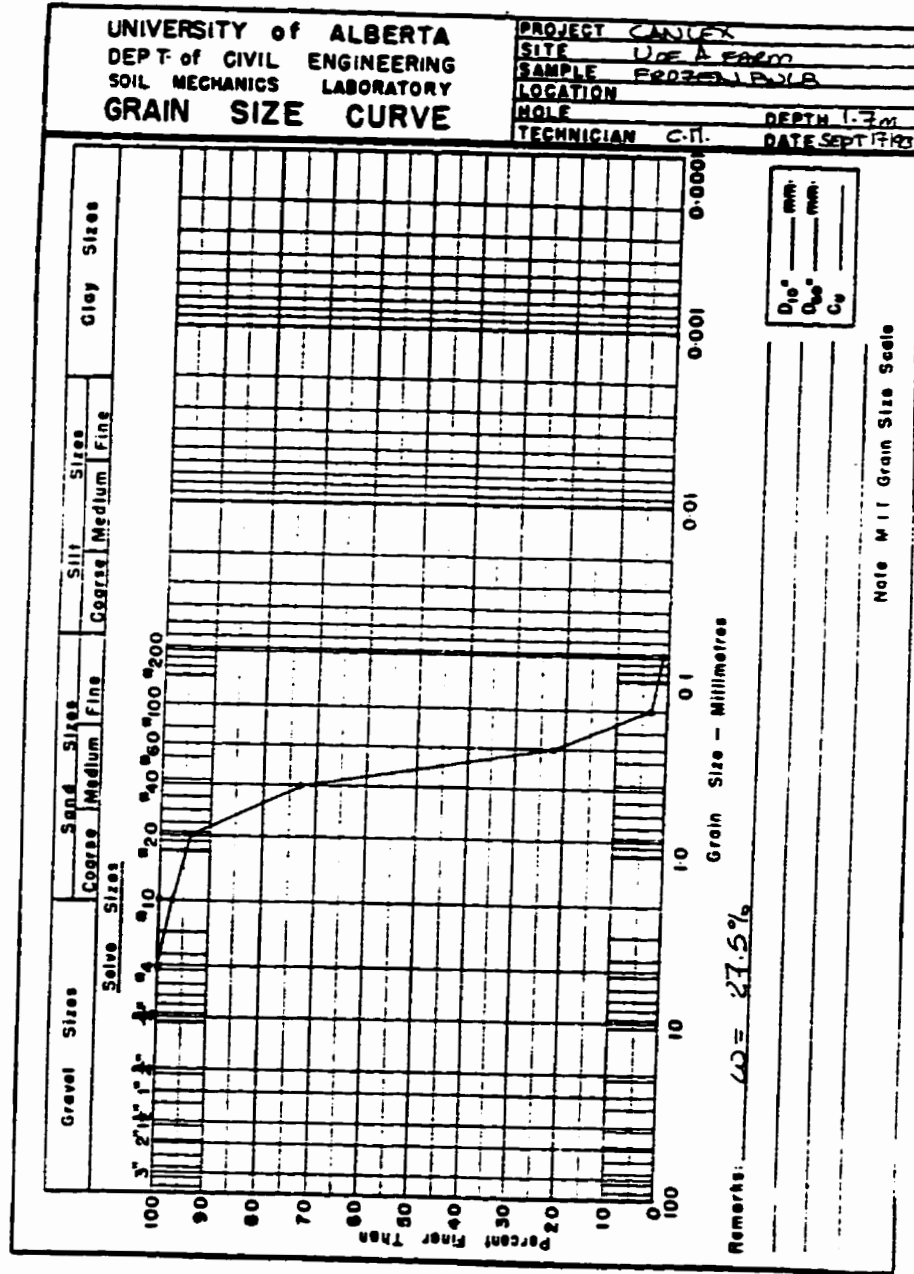
Experiment No. 5 4 of 7 DATE: August 4, 1993 TIME: 20:00 ±0.5 Hz												
ROW 1	0.00m	0.02m	ROW 3	0.02m	TEMP	ROW 3	0.16m	TEMP	ROW 0	Freeze Pts	TEMP	
881	168.82	168.71	007	168.71	1.85	17.83	019	168.75	2.70	15.71	023	17.87
882	168.89	168.07	008	168.07	1.87	19.44	019	168.75	2.71	17.25	024	18.39
883	169.02	168.13	009	168.13	1.87	19.00	017	168.35			024	18.39
884	167.40	167.82	010	167.82	1.82	15.58	018	168.35			028	18.39
885	168.30	168.13	011	168.13	1.87	10.81	018	168.35	2.72	14.23	028	18.39
886	167.85	168.07	012	168.07	1.82	10.26	020	167.81	2.71	12.47	027	17.38
1201	85.73	84.28	013	84.28	1.88	8.63	020	168.09	2.71	6.70	028	18.39
1202	84.39	83.06	014	83.06	1.87	2.08	022	88.60	2.71	2.65	028	18.39
1203	88.60	83.06	1208	83.06	2.28	2.03	022	88.60	2.71	-10.94	028	18.39
1204	88.60	83.06	1210	83.06	2.33	1.64	022	88.60	2.71	-9.95	028	18.39
1205	88.20	80.52	1211	80.52	2.31	1.61	022	88.60	3.08	-9.95	028	18.39
1206	85.70	86.45	1212	86.45	2.32	-1.14	022	88.60	3.08	-12.18	028	18.39
1207	82.09	85.92	1213	85.92	2.30	-7.51	022	88.60	3.07	-20.26	028	18.39
1208		108.05	1214	85.92	2.29	-16.55	022	88.60	3.05	-43.17	028	18.39
							1220	83.34		-61.19	028	18.39
											1225	177.89
											1226	-183.87
											1227	-180.89

Experiment No. 5 5 of 7 DATE: August 5, 1993 TIME: 02:15 ±15.75 Hz												
ROW 1	0.00m	0.02m	ROW 3	0.02m	TEMP	ROW 3	0.16m	TEMP	ROW 0	Freeze Pts	TEMP	
891	187.81	187.72	007	187.72	2.72	12.88	018	187.73	2.71	13.04	033	13.82
892	187.88	188.05	008	188.05	2.72	13.86	018	187.73	2.72	13.86	034	13.82
893	187.88	188.04	009	188.04	2.72	10.89	017	188.09	2.72	13.86	034	13.82
894	188.88	187.33	010	187.33	2.71	12.00	018	188.09	2.72	13.86	034	13.82
895	185.88	189.42	011	189.42	2.73	9.58	018	188.09	2.72	13.86	034	13.82
896	183.38	189.42	012	189.42	2.71	9.12	020	188.09	2.72	13.86	034	13.82
1201	83.74	189.42	013	189.42	2.71	3.58	021	188.09	2.72	13.86	034	13.82
1202	81.23	189.42	014	189.42	2.71	-24.31	022	95.25	2.72	-0.33	038	13.82
1203	78.85	101.73	014	101.73	2.72	-2.57	022	95.25	2.71	-16.38	038	13.82
1204	76.74	101.73	1209	101.73	3.07	-2.13	022	95.25	2.71	-16.38	038	13.82
1205	51.12	88.92	1210	88.92	3.07	-3.48	1215	96.18	3.08	-17.92	031	49.31
1206	68.77	88.92	1211	88.92	3.08	-10.75	1218	94.35	3.08	-23.65	031	49.31
1207	68.52	94.65	1212	94.65	3.07	-21.97	1217	86.93	3.07	-41.92	036	85.53
1208	68.52	93.04	1213	93.04	3.04	-25.97	1218	86.93	3.07	-41.92	036	85.53
1209	59.59	90.82	1214	90.82	3.03	-31.71	1219	80.81	3.08	-57.79	033	178.12
							1220	79.08	3.05	-82.26	033	178.12
											1225	-178.58
											1226	-160.82
											1227	-164.73
											1227	-162.10

Table A23: Temperature Data gathered during Experiment #6.

CAMLEX ACTIVITY 4B GROUND FREEZING FIELD TRIAL EXPERIMENTS AUGUST TO SEPTEMBER, 1993												
EXPERIMENT #6B - Freezing 4.4 m of Sand 1 of 6												
Date: September 20, 1993 (±0 hrs)												
Time: 15:00 - Temperatures assumed to be same for September 21 @ 04:25												
NOTE: Freezing Started at 04:25 on September 21, 1993												
ROW 0	TEMP.	ROW 1	TEMP.	ROW 2	TEMP.	ROW 3	TEMP.	ROW 4	TEMP.	ROW 5	TEMP.	ROW 6
① Freeze Pipe	① 0.00 m	① 0.06 m	① 0.16 m	① 0.26 m	① 0.36 m	① 0.46 m	① 0.56 m	① 0.66 m	① 0.76 m	① 0.86 m	① 0.96 m	① 1.06 m
828	104.29	8.73	820	106.60	0.84	812	14.66	804	0.91	104.25	13.87	
829	104.40	9.01	821	104.16	0.94	813	8.42	805	0.92	104.10	8.28	
830	104.35	8.63	822	105.36	1.30	814	10.65	806	0.93	104.99	10.55	
831	105.04	10.65	1215	105.62	1.33	1208	11.14	1209	1.30	105.58	11.12	
1221	105.67	11.27	1216	105.63	1.34	1210	11.14	1211	1.30	105.54	11.01	
1222	105.69	11.34	1217	105.37	1.33	1211	10.49	1212	1.28	105.30	10.44	
1223	105.50	10.76	1218	105.04	1.33	1212	9.64	1213	1.32	104.99	9.53	
1224	105.36	10.52	1219	104.76	1.34	1213	8.88	1214	1.27	104.65	8.78	
1225	105.00	9.61	1220	104.26	1.28	1214	7.88			104.22	7.64	
1226	104.72	8.91	1221									
1227	104.30	7.79	1222									
EXPERIMENT #6B - Freezing 4.4 m of Sand 2 of 6												
Date: September 21, 1993												
Time: 08:25 (±2.0 hrs)												
Started Freezing @ 04:25 on Sept. 21/93												
ROW 0	TEMP.	ROW 1	TEMP.	ROW 2	TEMP.	ROW 3	TEMP.	ROW 4	TEMP.	ROW 5	TEMP.	ROW 6
① Freeze Pipe	① 0.06 m	① 0.16 m	① 0.26 m	① 0.36 m	① 0.46 m	① 0.56 m	① 0.66 m	① 0.76 m	① 0.86 m	① 0.96 m	① 1.06 m	① 1.16 m
826	105.10	0.87	820	101.70	0.87	812	2.16	804	0.88	101.89	2.88	
829	89.20	0.87	821	103.52	0.86	813	6.91	805	0.86	104.09	6.39	
830	69.44	0.87	822	103.96	0.86	814	8.05	806	0.86	104.77	10.16	
831	81.52	0.85	1215	104.65	1.22	1209	8.94	1208	1.21	105.40	10.88	
1221	83.56	1.21	1216	105.00	1.24	1210	9.77	1211	1.21	105.39	10.88	
1222	83.30	1.20	1217	104.32	1.25	1211	7.97	1212	1.20	105.13	10.88	
1223	81.38	1.19	1218	104.14	1.23	1212	7.56	1213	1.22	104.82	10.21	
1224	79.99	1.17	1219	103.85	1.23	1213	6.81	1214	1.23	104.49	9.35	
1225	77.99	1.16	1220	103.49	1.24	1214	5.84			104.07	8.47	
1226	76.82	1.16	1221								7.48	
1227	33.52	1.12	1222									

Figure A1: Grain Size Curve for Sand Used in Experiments 5 at 1.7 m.



Appendix B: Phase I Test Site Ground Freezing Data

B.1. Introduction

Appendix B contains data associated with the in-situ ground freezing activities conducted at the Phase I test site. Information available from the test site is presented, including Cone Penetration Test data, used to select the target zone for in-situ freezing and sampling, and grain size curves established from Split Spoon samples recovered in the vicinity of the test site. Detailed calculations, carried out as part of the feasibility study to confirm that disturbance would not occur as a result of the initially unfrozen water freezing in place at very cold temperatures, are included at the back of the appendix.

The temperatures measured during ground freezing are included in summary tables. Plots of the alignment determined for each of the boreholes for sampling of the frozen core once freezing was complete are provided. Schematic diagrams, showing the locations of the frozen cores recovered from each sample boreholes are shown and the core catalogue established for the frozen core samples recovered from the site is given.

Table B1: Summary of Normalized In-Situ Testing Data.

	Minimum	Average	Maximum
CPT, q_{c1} , (MPa)	6.0	8.0	14.0
Equivalent, SPT, N_1	12	16	28
Shear Wave Velocity, V_{s1} , (m/s)	140	150	174

Table B2: Summary of Sample Borehole Deflections.

Borehole No.	Direction	Deflection (mm)	Deflection (in)	Direction	Deflection (mm)	Deflection (in)
FS1 casing	North	90	3.5	East	40	1.6
FS1 bh	East	35	1.4	South	12	0.5
FS2	North	70	2.8	East	235	9.3
FS3	North	40	1.6	East	375	14.8
FS4	South	30	1.2	East	310	12.2
FS5	North	150	5.9	East	280	11.0
Frze. Pipe	South	20	0.8	East	155	6.1
RTD 1	South	62	2.4	West	50	2.0
RTD 2	North	430	16.9	East	320	12.6
RTD3	North	0	0.0	East	80	3.1

Table B3: Temperature Data Recorded at 27 m in Each Sample Borehole.

TEMPERATURE VERSUS TIME PLOTS								
Start Freezing At 6:00 pm, November 11, 1993								
Date	Time	Elapsed	1) FS3	2) FS1	3) FS4	4) FS6	5) FS2	6)FP SFC
(1993)		Time (hrs)	Temperature (deg C)	Temperature (deg C)	Temperature (deg C)	Temperature (deg C)	Temperature (deg C)	Temperature (deg C)
11-Nov	6:00 PM	0.00	14.49	15.97	14.31	15.54	0.00	0.00
11-Nov	8:30 PM	2.50	14.59	15.97	14.46	15.67	9.41	-76.33
12-Nov	7:30 AM	13.50	14.59	16.05	13.82	15.41	3.82	-90.15
12-Nov	10:15 AM	15.25	14.33	16.05	13.13	14.92	4.05	
12-Nov	2:30 PM	19.50	13.85	15.97	11.92	14.05	2.51	-2.23
12-Nov	8:00 PM	25.00	12.90	15.74	10.13	12.67	2.05	-4.20
13-Nov	2:30 AM	31.50	11.72	15.44	8.15	11.00	1.74	-3.57
13-Nov	7:45 AM	36.75	10.72	15.00	6.64	9.74	1.54	-2.75
13-Nov	2:00 PM	43.00	9.62	14.49	5.13	8.38	1.33	-2.47
13-Nov	7:30 PM	48.50	8.59	13.97	3.54	7.21	0.44	-4.87
13-Nov	2:30 AM	55.50	7.26	13.36	1.77	5.38	-0.26	-10.48
14-Nov	8:00 AM	61.00	6.15	12.85	1.03	3.90	-1.13	-6.85
14-Nov	2:00 PM	67.00	5.05	12.23	0.44	2.95	-4.28	1.35
14-Nov	4:30 PM	68.00	4.64	11.97	0.23	2.59	-0.28	2.60
14-Nov	7:30 PM	71.00	4.21	11.69	0.10	2.33	-2.59	3.22
15-Nov	2:30 AM	78.00	3.36	11.10	-0.31	1.64	-4.38	3.05
15-Nov	8:00 AM	83.50	2.54	10.59	-0.59	1.18	-3.92	-2.15
15-Nov	2:00 PM	89.50	2.05	10.15	-0.85	0.87	-4.28	-1.77
15-Nov	7:30 PM	95.00	1.68	9.74	-1.23	0.56	-4.41	-5.23
16-Nov	7:45 AM	107.25	0.59	8.87	-2.54	-0.10	-5.05	-8.65
16-Nov	2:00 PM	113.50	0.82	8.49	-3.23	-0.56	-5.18	-5.15
16-Nov	7:00 PM	118.50	0.69	8.15	-3.72	-1.10	-5.13	-9.15
17-Nov	2:00 AM	125.50						
17-Nov	7:00 AM	125.50	0.38	7.41	-3.69	-1.82	-2.90	-12.50
17-Nov	9:30 AM	128.00	0.36	7.26	-3.38	-1.85	-0.49	-8.80
17-Nov	1:15 PM	131.75	0.38	7.10	-3.62	-1.87	-5.87	-129.30
17-Nov	7:00 PM	137.50	0.23	6.85	-4.36	-2.44	-6.10	
18-Nov	1:45 AM	144.25	0.10	6.54	-4.52	-2.79	-6.38	
18-Nov	7:20 AM	149.83	0.00	6.36	-5.00	-3.18	-6.74	
18-Nov	12:30 PM	155.00	-0.13	6.18	-5.15	-3.51	-6.77	
18-Nov	6:45 PM	161.25	-0.21	5.92	-5.64	-3.97	-7.64	
18-Nov	11:45 PM	166.25	-0.33	5.87	-6.62	-4.74	-8.46	
19-Nov	8:00 AM	174.50	-0.90	5.38	-8.54	-6.90	-8.13	
19-Nov	1:45 PM	180.25	-1.13	5.15	-8.54	-7.21	-7.56	
19-Nov	4:00 PM	182.50	-1.23	5.00	-8.67	-7.23	-7.44	
19-Nov	8:00 PM	186.50	-1.31	4.74	-8.31	-7.08	-2.90	
19-Nov	9:00 PM	187.50	-1.28	4.72	-7.92	-6.87	-0.82	
20-Nov	8:15 AM	198.75	-1.41	4.26	-8.03	-6.69	-7.92	
20-Nov	2:00 PM	215.75	-1.44	4.15	-8.08	-6.64	-8.72	
20-Nov	5:50 PM	219.58	-1.59	3.95	-8.75	-7.13	-8.56	
21-Nov	8:30 AM	234.25	-2.18	3.56	-9.79	-8.21	-9.05	
21-Nov	2:10 PM	239.92	-2.44	3.36	-10.36	-8.64	-9.23	
21-Nov	8:30 PM	246.25	-2.82	3.21	-11.23	-9.33	-9.51	
22-Nov	8:30 AM	258.25	-3.00	2.85	-10.90	-9.18	-7.33	
22-Nov	11:40 AM	261.42	-2.87	2.77	-9.85	-8.62	-0.67	
22-Nov	2:00 PM	263.75	-2.54	2.69	-8.41	-7.59	0.05	
22-Nov	3:10 PM	264.92	-2.33	2.67	-7.69	-7.03	0.13	
22-Nov	4:40 PM	266.42	-2.15	2.64	-6.87	-6.36	-0.69	
22-Nov	8:20 PM	270.09	-1.97	2.62	-7.67	-6.18	-8.72	
23-Nov	8:30 AM	282.25	-2.69	2.54	-9.26	-7.79	-8.54	
23-Nov	9:15 AM	283.00	-2.72	2.54	-9.21	-7.74	-8.56	
24-Nov	7:30 AM	293.25		2.44	-10.77	-8.18	-9.51	
25-Nov	7:30 AM	317.25		2.15	-13.00		-8.03	
25-Nov	9:00 PM	330.75		1.92	-6.31		0.08	
26-Nov	7:30 AM	341.25		1.97	-12.74		-11.18	

Table B4: Temperature Data Recorded in RTD Boreholes.

7) RTD 1	Temperatures (degrees Celsius)						10) RTD 3	Date	Time
3-30	3-32	3-34	3-36	3-38	3-40	40-13	(1993)		
27 m	29 m	31 m	33 m	35 m	37 m				
16.41	16.28	15.82	15.36	15.36	14.44	16.59	11-Nov	6:00 PM	
16.41	16.31	15.79	15.33	15.28	14.46	16.54	11-Nov	8:30 PM	
16.44	16.28	15.82	15.31	15.36	14.38	16.54	12-Nov	7:30 AM	
16.46	16.31	15.82	15.33	15.26	14.38	16.51	12-Nov	10:15 AM	
16.49	16.15	15.85	15.26	15.34	14.36	16.33	12-Nov	2:30 PM	
16.28	16.15	15.77	15.23	15.21	14.31	16.33	12-Nov	8:00 PM	
16.05	15.90	15.62	15.08	15.10	14.31	16.05	13-Nov	2:30 AM	
15.77	15.69	15.38	14.92	14.95	14.05	15.67	13-Nov	7:45 AM	
15.44	15.33	15.08	14.67	14.74	13.74	15.23	13-Nov	2:00 PM	
15.10	14.92	14.77	14.33	14.51	13.44	14.79	13-Nov	7:30 PM	
14.62	14.44	14.26	13.87	14.08	12.87	14.26	13-Nov	2:30 AM	
14.21	13.95	13.74	13.46	13.69	12.18	13.72	14-Nov	8:00 AM	
13.74	13.38	13.15	12.90	13.13	11.23	13.18	14-Nov	2:00 PM	
13.51	13.15	12.85	12.67	12.85	10.79	12.97	14-Nov	4:30 PM	
13.28	12.85	12.54	12.36	12.51	10.33	12.64	14-Nov	7:30 PM	
12.74	12.21	11.82	11.72	11.79	9.03	12.05	15-Nov	2:30 AM	
12.33	11.69	11.26	11.15	11.15	8.15	11.54	15-Nov	8:00 AM	
11.90	11.15	10.64	10.56	10.54	7.23	11.10	15-Nov	2:00 PM	
11.51	10.69	10.18	10.05	10.00	6.59	10.64	15-Nov	7:30 PM	
10.74	9.77	9.10	9.00	8.90	5.00	9.77	16-Nov	7:45 AM	
10.36	9.28	8.54	8.44	8.28	4.00	9.31	16-Nov	2:00 PM	
10.08	8.92	8.05	8.00	7.67	3.15	8.97	16-Nov	7:00 PM	
							17-Nov	2:00 AM	
9.33	7.95	6.82	6.77	5.90	1.03		17-Nov	7:00 AM	
9.18	7.74	6.62	6.56	5.64	0.69	8.10	17-Nov	9:30 AM	
8.97	7.56	6.38	6.28	5.28	0.15	7.74	17-Nov	1:15 PM	
8.72	7.23	6.00	5.82	4.67	-0.10	7.44	17-Nov	7:00 PM	
8.36	6.85	5.56	5.38	3.69	-0.44	7.05	18-Nov	1:45 AM	
8.15	6.54	5.26	5.05	3.08	-0.69	6.77	18-Nov	7:20 AM	
7.95	6.33	5.00	4.74	2.87	-1.13	6.62	18-Nov	12:30 PM	
7.87	6.00	4.67	4.41	2.62	-1.72	6.33	18-Nov	6:45 PM	
7.51	5.87	4.46	4.18	2.49	-2.03	6.18	18-Nov	11:45 PM	
7.10	5.33	3.85	3.41	1.97	-3.62	5.72	19-Nov	8:00 AM	
6.82	4.97	3.46	2.85	1.56	-4.77	5.41	19-Nov	1:45 PM	
6.67	4.79	3.23	2.49	1.31	-5.33	5.26	19-Nov	4:00 PM	
6.49	4.49	2.79	2.13	0.74	-6.23	5.03	19-Nov	8:00 PM	
6.21	4.38	2.72	2.00	0.44	-6.41	5.00	19-Nov	9:00 PM	
5.90	3.51	2.10	0.87	-0.08	-6.79	4.51	20-Nov	8:15 AM	
5.67	3.15	1.54	0.51	-0.31	-6.87	4.28	20-Nov	2:00 PM	
5.54	3.03	1.38	0.41	-0.51	-6.95	4.15	20-Nov	5:50 PM	
4.95	2.44	0.62	0.36	-2.46	-9.23	3.67	21-Nov	8:30 AM	
4.72	2.28	0.33	0.23	-3.33	-10.26	3.44	21-Nov	2:10 PM	
4.44	1.87	-0.15	0.05	-4.44	-11.38	3.23	21-Nov	8:30 PM	
3.85	-0.15	-0.41	-0.67	-6.00	-13.28	2.77	22-Nov	8:30 AM	
3.62	-0.31	-0.49	-1.23	-6.13	-13.69	2.67	22-Nov	11:40 AM	
3.64	1.13	-0.64	-1.72	-6.15	-13.72	2.59	22-Nov	2:00 PM	
3.56	1.13	-0.69	-1.97	-6.10	-13.56		22-Nov	3:10 PM	
3.59	1.08	-0.74	-2.18	-6.03	-13.31	2.51	22-Nov	4:40 PM	
3.49	1.05	-0.79	-2.31	-5.72	-12.46	2.41	22-Nov	8:20 PM	
3.33	1.00	-1.15	-2.62	-5.74	-11.44	2.23	23-Nov	8:30 AM	
3.33	0.95	-1.18	-2.69	-5.77	-11.26	2.18	23-Nov	9:15 AM	
3.15	0.97	-1.56	-2.62	-4.87	-8.74	1.95	24-Nov	7:30 AM	
2.79	0.64	-2.54	-4.05	-6.33	-9.54	0.31	25-Nov	7:30 AM	
2.46	0.44	-2.85	-4.38	-6.87	-9.64	0.00	25-Nov	9:00 PM	
2.46	0.38	-2.85	-4.08	-6.95	-8.54	0.08	26-Nov	7:30 AM	

Table B5: Liquid Nitrogen Consumption during Ground Freezing.

Elapsed Time (hrs)	LN2 Used (m3)
	0.00
2.50	512.50
13.50	3387.50
15.25	4306.25
19.50	5537.50
25.00	7025.00
31.50	9037.50
36.75	10893.75
43.00	13075.00
48.50	15162.50
55.50	18337.50
61.00	20525.00
67.00	23140.00
68.00	23265.00
71.00	24286.00
78.00	27420.00
83.50	29036.50
89.50	30879.50
95.00	32816.00
107.25	37542.25
113.50	40316.50
118.50	42214.50
125.50	44596.00
125.50	44596.00
128.00	44759.00
131.75	45827.00
137.50	46808.00
144.25	48031.00
149.83	49195.00
155.00	50216.00
161.25	52107.00
166.25	53150.00
174.50	56947.00
180.25	58371.80
182.50	59307.60

185.00	59676.00
186.50	59676.00
187.50	59676.00
198.75	62547.50
215.75	63887.00
219.58	64793.00
234.25	68416.00
239.92	69689.00
246.25	71767.00
258.25	74298.00
261.42	74368.00
263.75	74368.00
264.92	74368.00
266.42	74511.00
270.09	76742.00
282.25	78234.00
283.00	78523.00
296.00	83381.00
308.00	89448.00
308.00	89448.00
318.50	96788.60
318.50	98220.00
331.50	99549.00

Table B6: Phase I Test Site - Frozen Core Catalogue.

CATALOGUE OF FROZEN CORE SAMPLES										
Legend:										
I	Excellent Core - insignificant zone of melting around perimeter during extrusion									
II	Good Core - minor zone of melting around perimeter of core during extrusion which can be trimmed from laboratory samples									
III	Fair Core - questionable whether the core contains some refrozen slough and/or significant melting at time of extrusion									
IV	Poor Core - Due to excessive melting, disturbance or fracturing									
Note: No evidence of ice lens formation was found in any of the frozen core samples										
Barrel Number	Core Number	Depth Interval (m)	Length of Core (cm)	Comments Regarding Core Quality	Rating of Core Quality	W (corrected) (%)	Pd (g/cc)	P1 (g/cc)	Void Ratio (v)	No. of Measurements for True D. S. Shear
F81	C1	26.98 - 27.33	35	outside 1 cm previously melted around perimeter, occasional coarse dry pockets and bitumen inclusions	II					2
F81	C7D	28.57 - 28.62	5	good core but upper 30 mm of CRREL barrel was full of unfrozen slough	III					0
F81	C3A	29.65 - 29.70	5	good core, homogeneous	II					0
F81	C3B	29.73 - 30.05	9 + 23	good core, crack noted at 29.87 m	II	24.74	1.500	1.87	0.753	1
F81	C4	30.56 - 30.72	16	outside 1 cm previously melted around perimeter	II					1
F81	C5	30.81 - 30.99	18	core contains a 7.5 cm diameter core inside previously melted perimeter - small cracks and dry veins at bottom of core	III					0
F81	C6A	31.24 - 31.30	6	good core	II					0
F81	C6C	31.42 - 31.66	24	excellent core	I	27.65	1.483	1.87	0.788	2
F81	C6D	31.68 - 31.77	6 + 5	excellent core but cracked at 31.72 m	I					1
F81	C6E	31.77 - 31.83	16	sand is bitumen rich from 31.82 to 31.86	I					3
F81	C7	32.43 - 32.63	20	good core	II					1
F81	C8A	32.83 - 33.03	10	noted a 1 cm diameter patch of ice in the middle of the core at 32.99 cm (?)	II					2
F81	C8B	33.05 - 33.32	27	good core	II					3
F81	C9A	33.73								0
F81	C9B	33.76 - 33.9	14	core contains a 7.5 cm diameter core inside previously melted perimeter	III	24.71	1.448	1.81	0.816	2
F81	C9C	33.93 - 34.25	32	outside 1 cm previously melted around perimeter	II					0
F81	C10A	34.30 - 34.44	14	occasional bitumen inclusions at bottom core, otherwise excellent core	I					1
F81	C10B	34.46 - 34.64	18	occasional bitumen inclusions at top of	I					1

Table B6 continued: Phase I Test Site - Frozen Core Catalogue.

Core ID	Depth (m)	Core Description	Notes	Core Type	Length (m)	Weight (kg)	Volume (m³)	Area (m²)	Other
C10 C	34.65 - 34.89	23	core, otherwise excellent core	I					
F81	35.05 - 35.25	20	sample retrieved from previous core run, debris core centre with 8 cm diameter	IV					
C11 B	35.35 - 35.36	3	outside 0.5 cm previously melted around perimeter	I					
C11 D	35.44 35.47 - 35.54	7	outside 0.5 cm previously melted around perimeter	I	29.68	1.90	0.692		
C11 F	35.57 35.73 - 35.85	12	outside 1 cm previously melted around perimeter	II	25.10	1.66	0.767		
C1 A	35.70 27.87 - 28.15	28	white blotch at bottom of core indicates that this core may be refrozen slough	IV	23.32	1.528	0.723		
C1 B	28.20 - 28.24	4	large voids, bentonite and bitumen inclusions	IV					
C1 C	28.27 - 28.38 28.40	10.5	fair core, homogeneous sand	III	22.80	1.517	0.734		
F83	28.57 - 28.79	23	core contains many dry voids at ends and along the sides of the core	IV					
C2 B	28.81 - 28.96	17	core cracked in two places	II					
C3 B	29.10 - 29.19	8.5	voids at end of core, core cracked in half	II					
C3 C	29.22 - 29.33	11	core cracked through middle	II					
C3 G	29.35 - 29.45	10	core cracked through middle	II					
C3 H	29.46 - 29.64	17	core is cracked throughout at 3 to 4 cm intervals	III					
F83	29.64 - 29.87 29.87	23	sand is more coarse and contains bitumen inclusions	III	21.66	1.578	0.667		
F83	29.89 - 30.08	18.5	excellent core	I					
C5 B	30.07 - 30.36	31	excellent core, thin dry vein at bottom of	I					
F83	30.47 - 30.69	22	outside perimeter of core is disturbed probably due to melting during extrusion	III					
F83	30.80 - 31.08	28	good core	II					
C7 B	31.11 - 31.25	14	good core	II					
F83	31.71 - 31.89	8+10	bitumen layering at 31.79 m, otherwise excellent core	I					
F83	32.33 - 32.57	13 + 11	thin bitumen vein at 32.46, otherwise excellent core	I					
F83	32.79 - 33.02	23	generally good core but use caution when trimming since top of core indicated some	II					

Table B6 continued: Phase I Test Site - Frozen Core Catalogue.

Core ID	Core Range	Count	Description	Notes	Mass (g)	Length (cm)	Volume (cm³)	Notes	Count	Notes
P84	C8A	22	contains core retrieved from previous run	H						
	C8B	10	core is cracked but may get one DSS as good quality core	H						
	C8C	16		H						
P84	C7B	22	fair core but some dry veins at bottom of core retrieved from previous run	H						
P84	C8A	31	fair core retrieved from previous run	H						
	C8B	7	bottom of core was dry with large voids. core may also be cracked	H						
	C8C	6	at top of core 0.8 cm perimeter shows pz at bottom of core 0.7 cm perimeter shows previous melting	H						
	C8D	10	outside 2.5 cm previously melted around perimeter at top of core and 1.0 cm previously melted around perimeter at bottom of core	H						
P84	C9	12	smaller 6 cm diameter ring inside core at top but only 1 cm outside perimeter previously melted at bottom of core	H						
P84	G11A	34	outside 1 cm previously melted around perimeter	H						
	G11B	18	excellent core	H						
P84	G12A	7	excellent core	I						
	G12B	19	excellent core, bitumen at bottom of core	I						
P84	G13A	40	outside 1 cm previously melted around perimeter	H						
	G13B	19	excellent core	I						
P84	G14A	25	1 to 2 cm of uneven melting around pen due to torch during extrusion	H						
	G14B	23	1 to 2 cm of uneven melting around pen due to torch during extrusion	H						
P84	G15A	21	excellent core	I						
	G15B	28	excellent core	I						
P84	G16	49	excellent core	I						
P85	G2	27	outside 0.5 cm previously melted around perimeter, signs of shearing at bottom of core	H						

Figure B1: CPT Profiles obtained at Phase I Test Site.

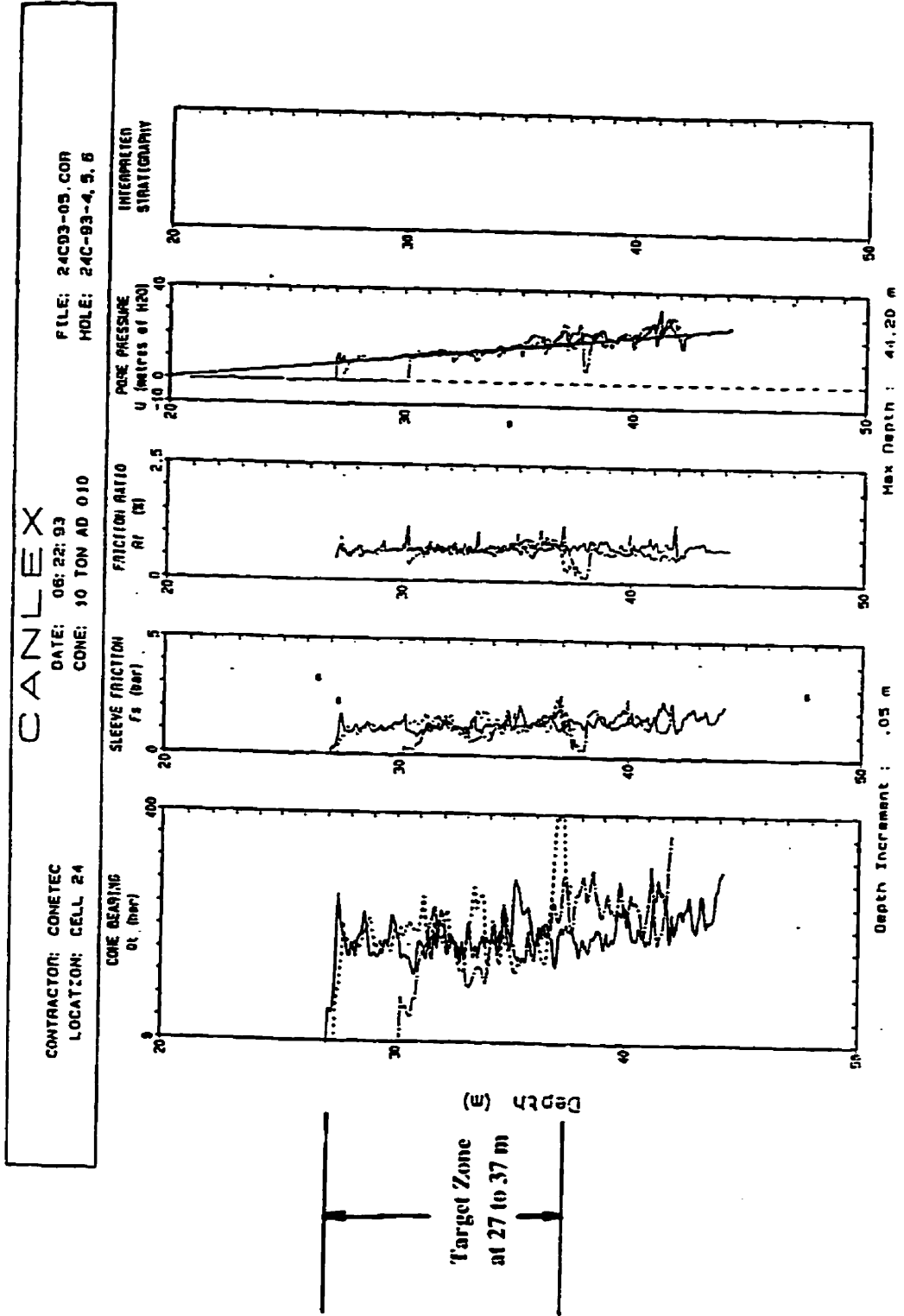


Figure B2: Grain Size Curve obtained for Sample recovered at 18.29 m.

PROJECT : CANLEX

FILE No. : *SLA 24593-07*

TESTHOLE No. : CELL 24

DEPTH (m.) : 18.29

SAMPLE No. : 1494

TESTED BY : K.W.

DATE : 93-07-30

ATTENTION :

NATURAL MOISTURE CONTENT :

REMARKS :

% GRAVEL = .5
 % SAND = 90.5
 % FINES = 9
 Cu = 2.1
 Cc = .86

SIEVE No.	% PASSING
3 in	100
2.5 in	100
2 in	100
1.5 in	100
1 in	100
.75 in	100
.385 in	100
No. 4	99.5
No. 10	98.8
No. 20	98.4
No. 40	97.1
No. 60	92.6
No. 100	54.6
No. 200	9

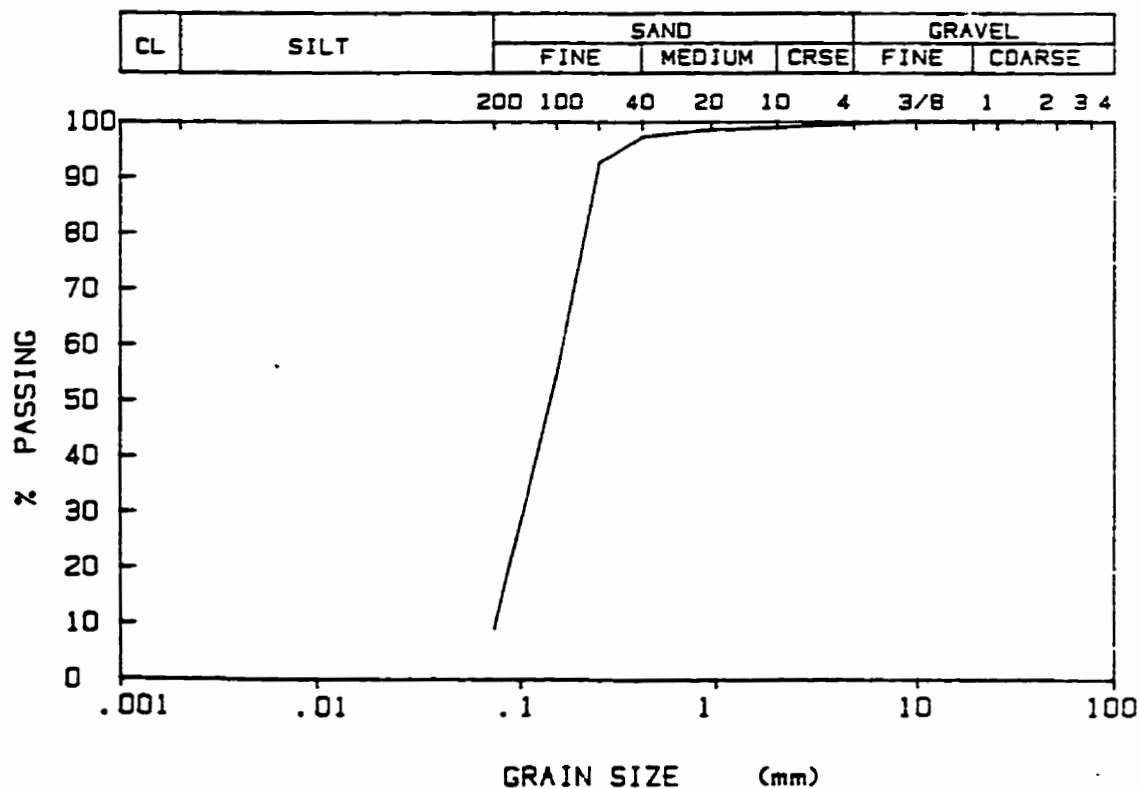


Figure B3: Grain Size Curve obtained for Sample recovered at 19.81 m.

PROJECT : CANLEX

FILE No. : SPA 24593-07

TESTHOLE No. : CELL 24

DEPTH (m.) : 19.81

SAMPLE No. : 1495

TESTED BY : K.W.

DATE : 93-07-30

ATTENTION :

NATURAL MOISTURE CONTENT :

REMARKS :

% GRAVEL = 0
 % SAND = 64.8
 % FINES = 35.2

SIEVE No.	% PASSING
3 in	100
2.5 in	100
2 in	100
1.5 in	100
1 in	100
.75 in	100
.385 in	100
No. 4	100
No. 10	100
No. 20	99
No. 40	97.9
No. 60	95.5
No. 100	69.7
No. 200	35.2

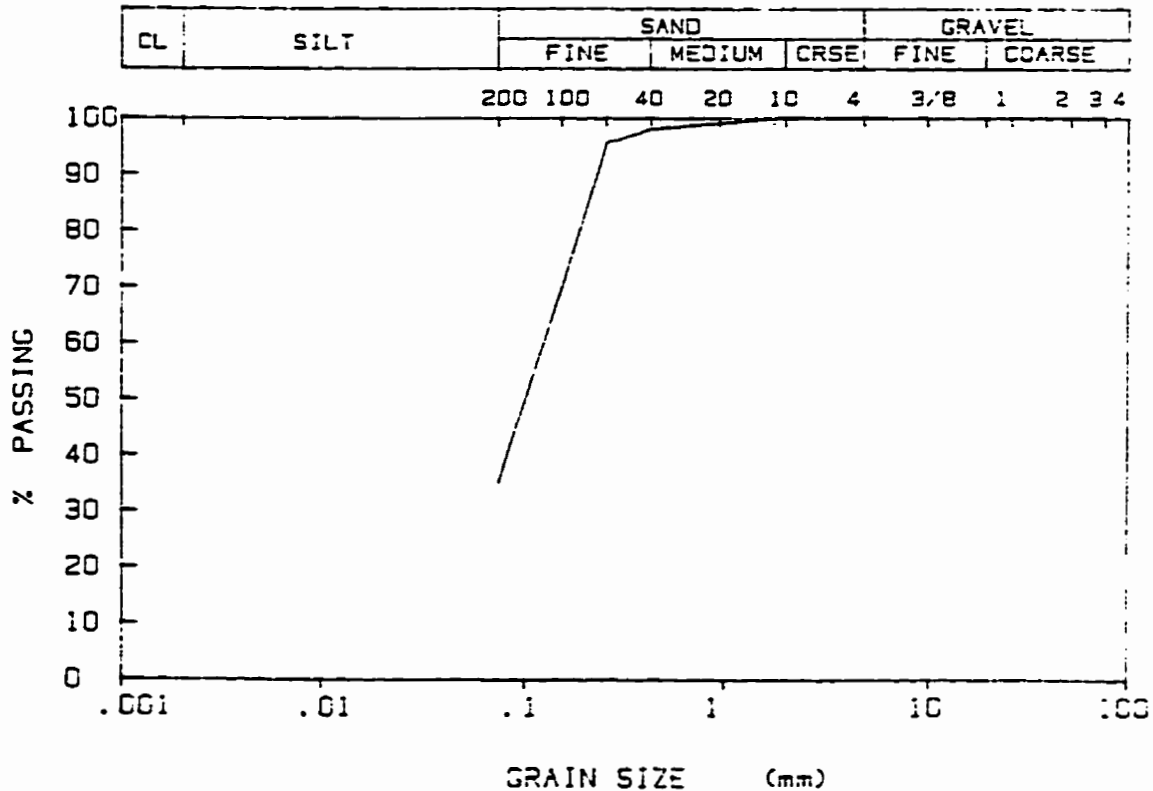


Figure B4: Grain Size Curve obtained for Sample recovered at 21.34 m.

PROJECT : CANLEX

FILE No. :
 TESTHOLE No. : CELL 24
 DEPTH (m.) : 21.34
 SAMPLE No. : 1496
 TESTED BY : K.W.
 DATE : 93-07-30
 ATTENTION :
 NATURAL MOISTURE CONTENT :
 REMARKS :

% GRAVEL = 0
 % SAND = 86.4
 % FINES = 13.6

SIEVE No.	% PASSING
3 in	100
2.5 in	100
2 in	100
1.5 in	100
1 in	100
.75 in	100
.385 in	100
No. 4	100
No. 10	99.9
No. 20	99.6
No. 40	98
No. 60	90.6
No. 100	45.4
No. 200	13.6

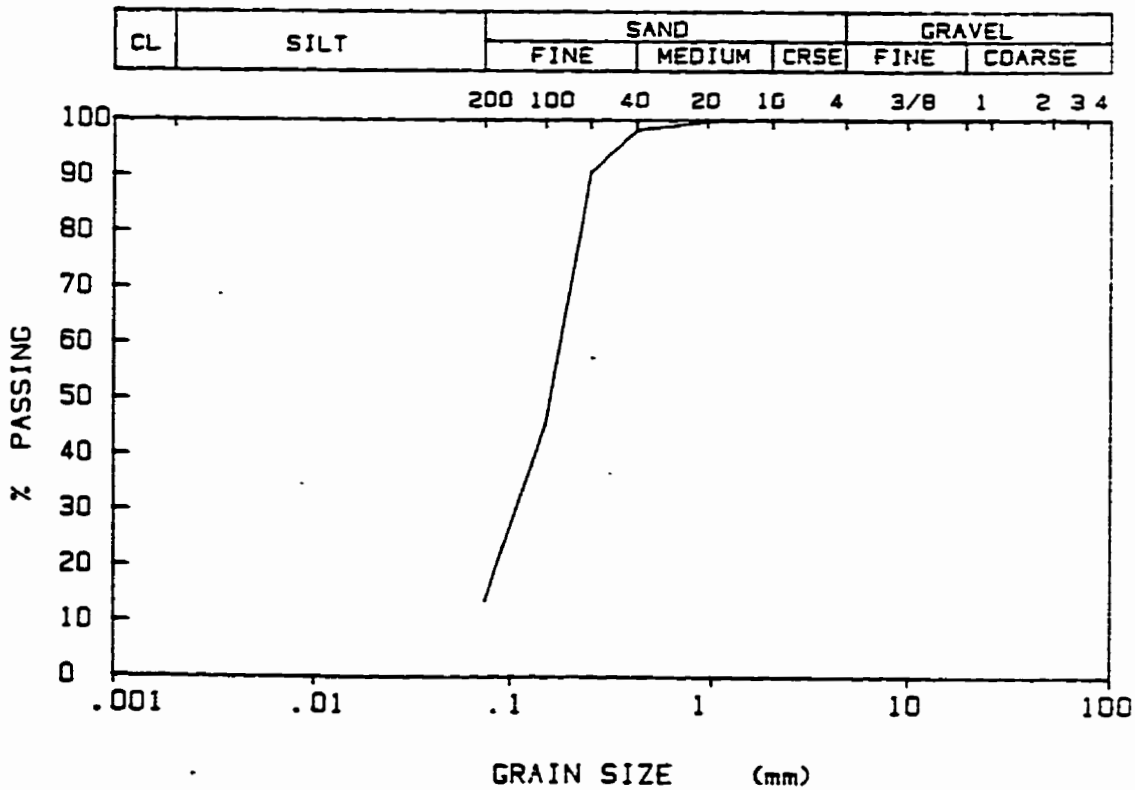


Figure B5: Grain Size Curve obtained for Sample recovered at 22.86 m.

PROJECT : CANLEX

FILE No. :
 TESTHOLE No. : CELL 24
 DEPTH (m.) : 22.86
 SAMPLE No. : 1497
 TESTED BY : K.W.
 DATE : 93-07-30
 ATTENTION :
 NATURAL MOISTURE CONTENT :
 REMARKS :

% GRAVEL = 0
 % SAND = 86.1
 % FINES = 13.9

SIEVE No.	% PASSING
3 in	100
2.5 in	100
2 in	100
1.5 in	100
1 in	100
.75 in	100
.385 in	100
No. 4	100
No. 10	99.9
No. 20	99.2
No. 40	95.5
No. 60	86
No. 100	42.9
No. 200	13.9

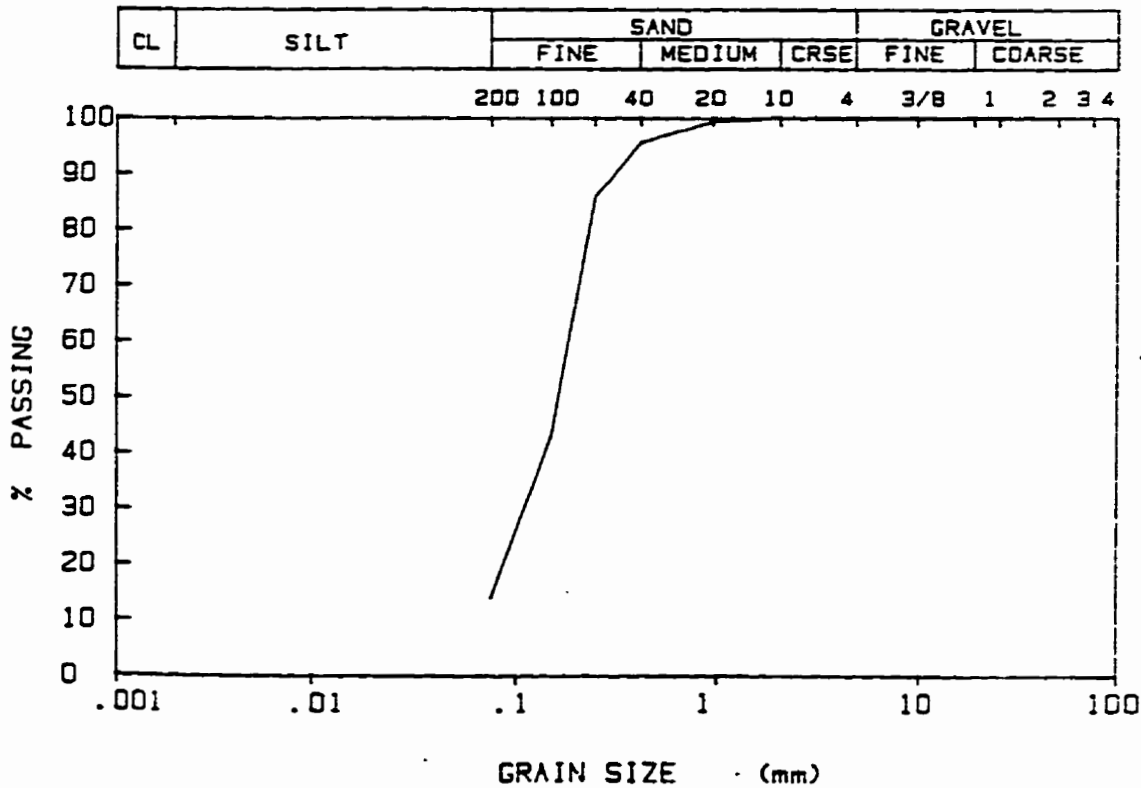


Figure B6: Grain Size Curve obtained for Sample recovered at 25.91 m.

PROJECT : CANLEX

FILE No. :
 TESTHOLE No. : CELL 24
 DEPTH (m.) : 25.91
 SAMPLE No. : 1498
 TESTED BY : K.W.
 DATE : 93-07-30
 ATTENTION :
 NATURAL MOISTURE CONTENT :
 REMARKS :

% GRAVEL = 1.6
 % SAND = 86.4
 % FINES = 12

SIEVE No.	% PASSING
3 in	100
2.5 in	100
2 in	100
1.5 in	100
1 in	100
.75 in	100
.385 in	100
No. 4	98.4
No. 10	95
No. 20	87.9
No. 40	81.2
No. 60	73
No. 100	36
No. 200	12

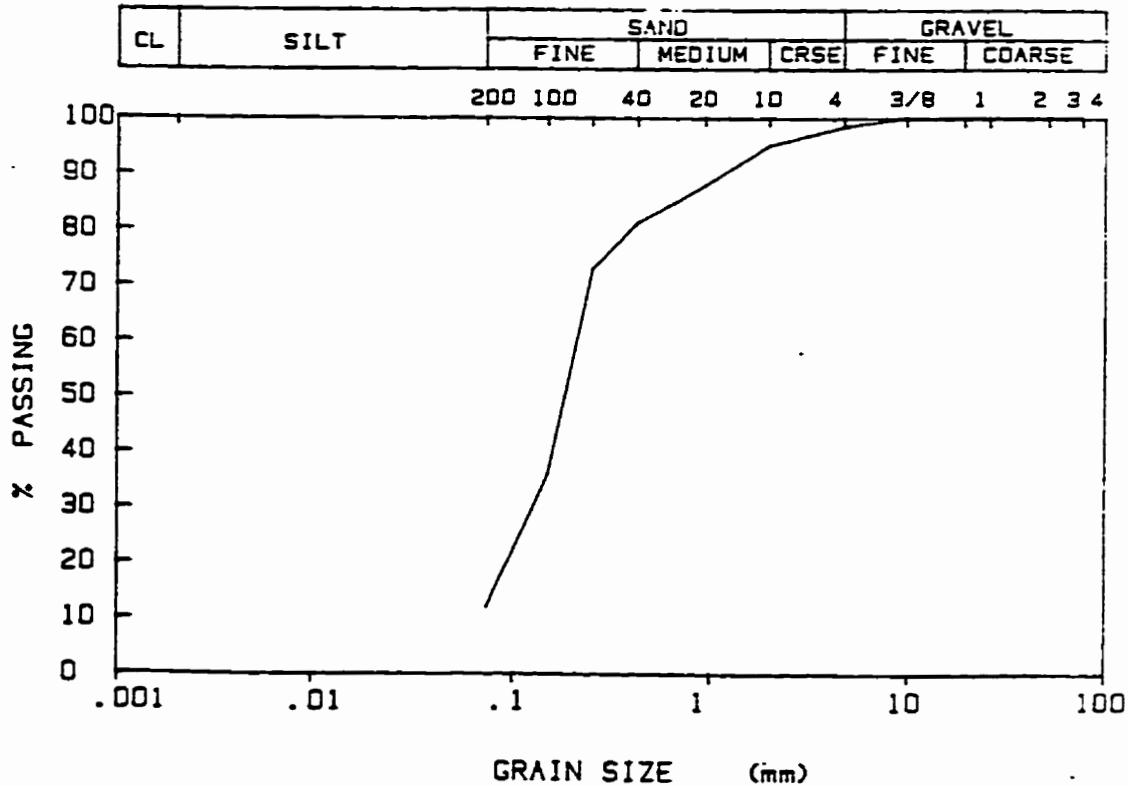


Figure B7: Grain Size Curve obtained for Sample recovered at 27.43 m.

PROJECT : CANLEX

FILE No. :

TESTHOLE No. : CELL 24

DEPTH (m.) : 27.43

SAMPLE No. : 1499

TESTED BY : K.W.

DATE : 93-07-30

ATTENTION :

NATURAL MOISTURE CONTENT :

REMARKS :

% GRAVEL = 0
 % SAND = 90.5
 % FINES = 9.5
 $C_u = 3.1$
 $C_c = 1.25$

SIEVE No.	% PASSING
3 in	100
2.5 in	100
2 in	100
1.5 in	100
1 in	100
.75 in	100
.385 in	100
No. 4	100
No. 10	99.1
No. 20	89.3
No. 40	76.9
No. 60	64.3
No. 100	30.2
No. 200	9.5

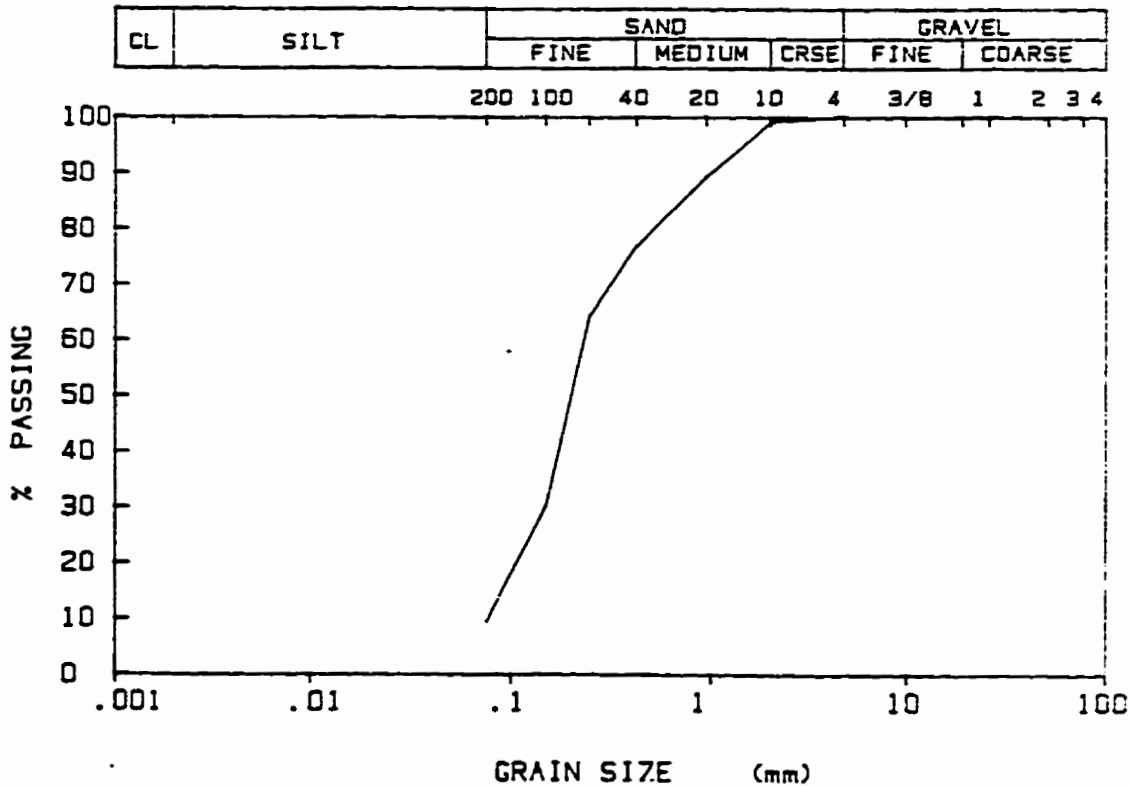


Figure B8: Grain Size Curve obtained for Sample recovered at 30.48 m.

PROJECT : CANLEX

FILE No. :
 TESTHOLE No. : CELL 24
 DEPTH (m.) : 30.48
 SAMPLE No. : 1500
 TESTED BY : K.W.
 DATE : 93-07-30
 ATTENTION :
 NATURAL MOISTURE CONTENT :
 REMARKS :

% GRAVEL = 0
 % SAND = 92.1
 % FINES = 7.9
 $C_u = 2.4$
 $C_c = 1.21$

SIEVE No.	% PASSING
3 in	100
2.5 in	100
2 in	100
1.5 in	100
1 in	100
.75 in	100
.385 in	100
No. 4	100
No. 10	99.9
No. 20	99.1
No. 40	97.9
No. 60	90.3
No. 100	34
No. 200	7.9

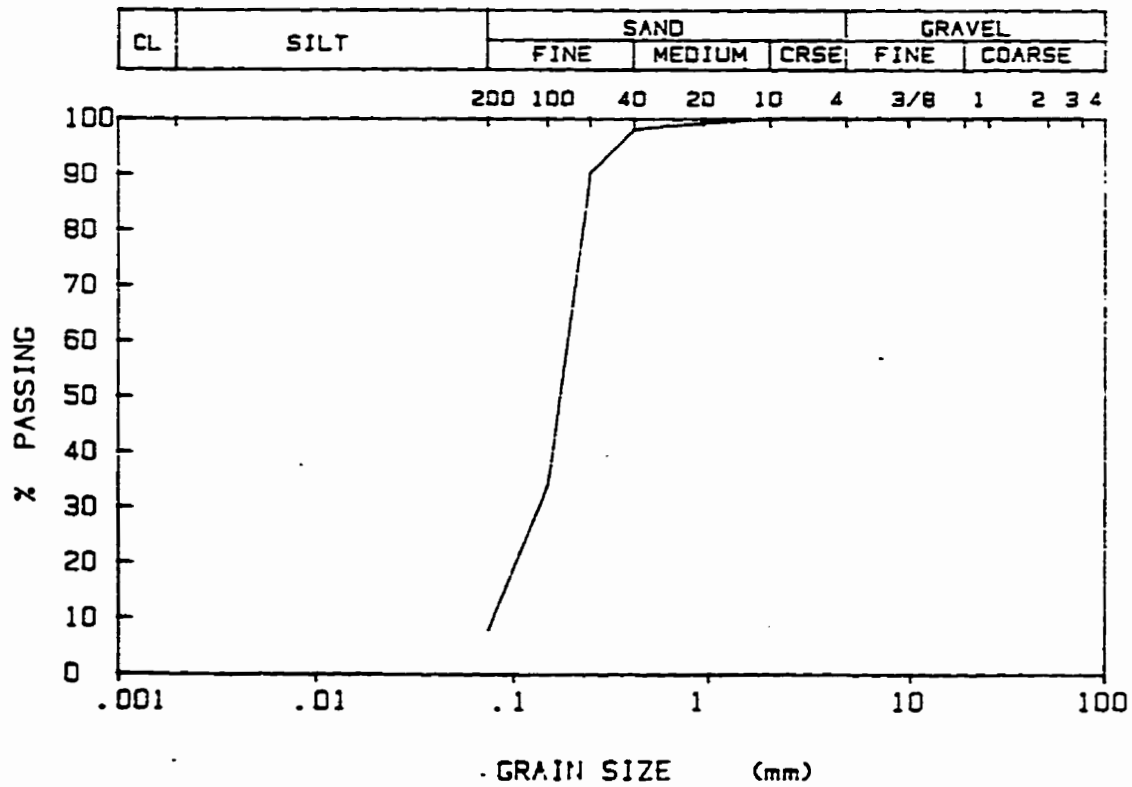


Figure B9: Grain Size Curve obtained for Sample recovered at 36.58 m.

PROJECT : CANLEX SITE SCREENING

FILE No. :
 TESTHOLE No. : BHA-24C-93-06
 DEPTH (m.) : 36.58
 SAMPLE No. : 2
 TESTED BY : H. JARA
 DATE : 93-07-06
 ATTENTION : CANLEX GROUP
 NATURAL MOISTURE CONTENT :
 REMARKS : SOIL TYPE = TAILINGS

SIEVE No.	% PASSING
3 in	100
2.5 in	100
2 in	100
1.5 in	100
1 in	100
.75 in	100
.365 in	100
No. 4	99.3
No. 10	99
No. 20	95.7
No. 40	94.6
No. 60	91.2
No. 100	57.6
No. 200	14.7

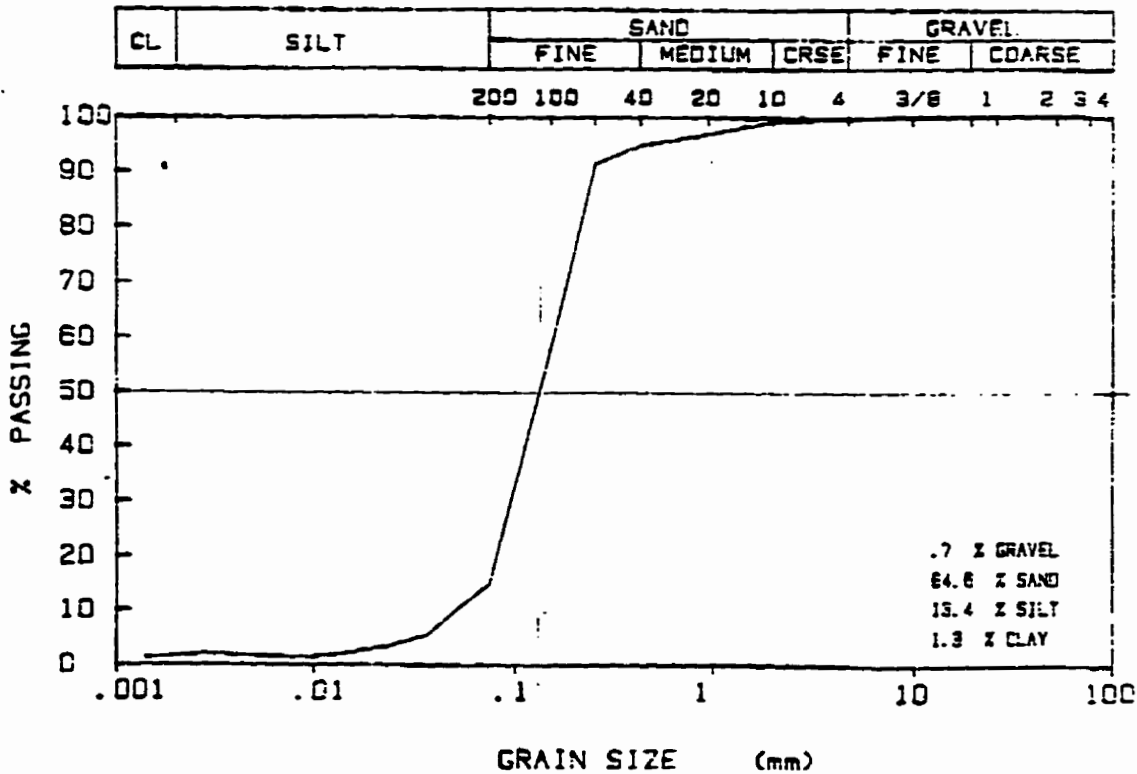


Figure B10: Grain Size Curve obtained for Sample recovered at 24.38 m.

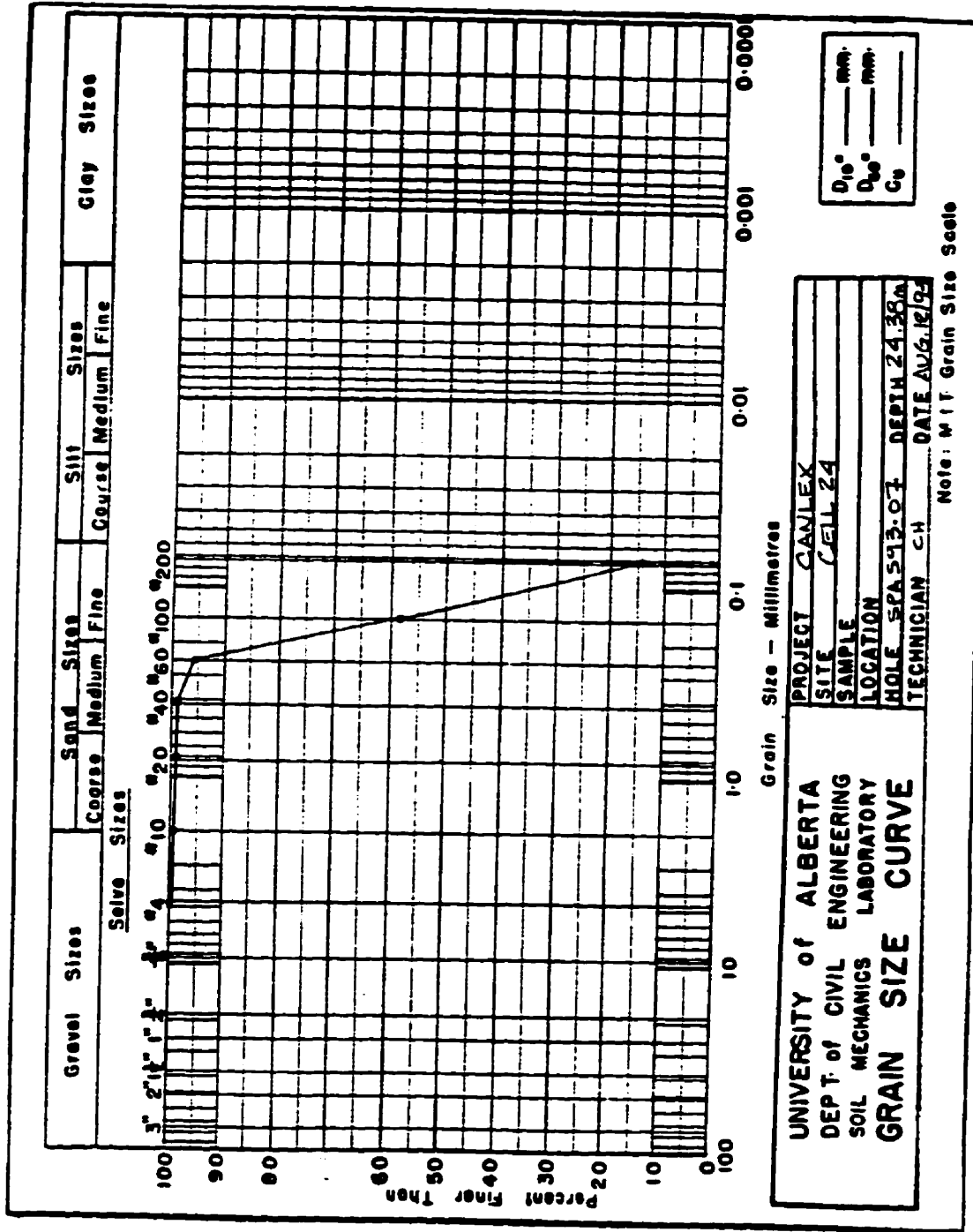


Figure B11: Grain Size Curve obtained for Sample recovered at 28.96 m.

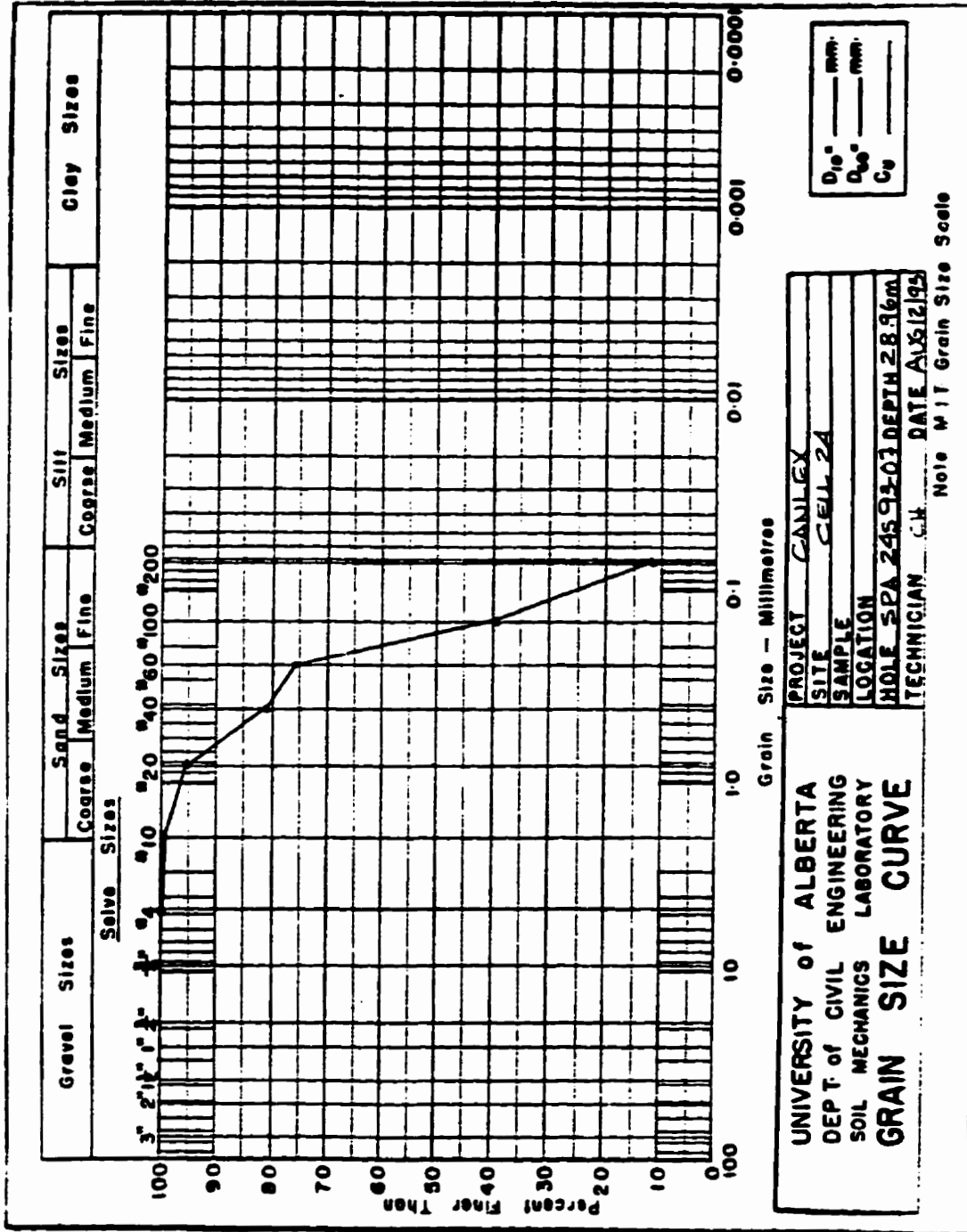
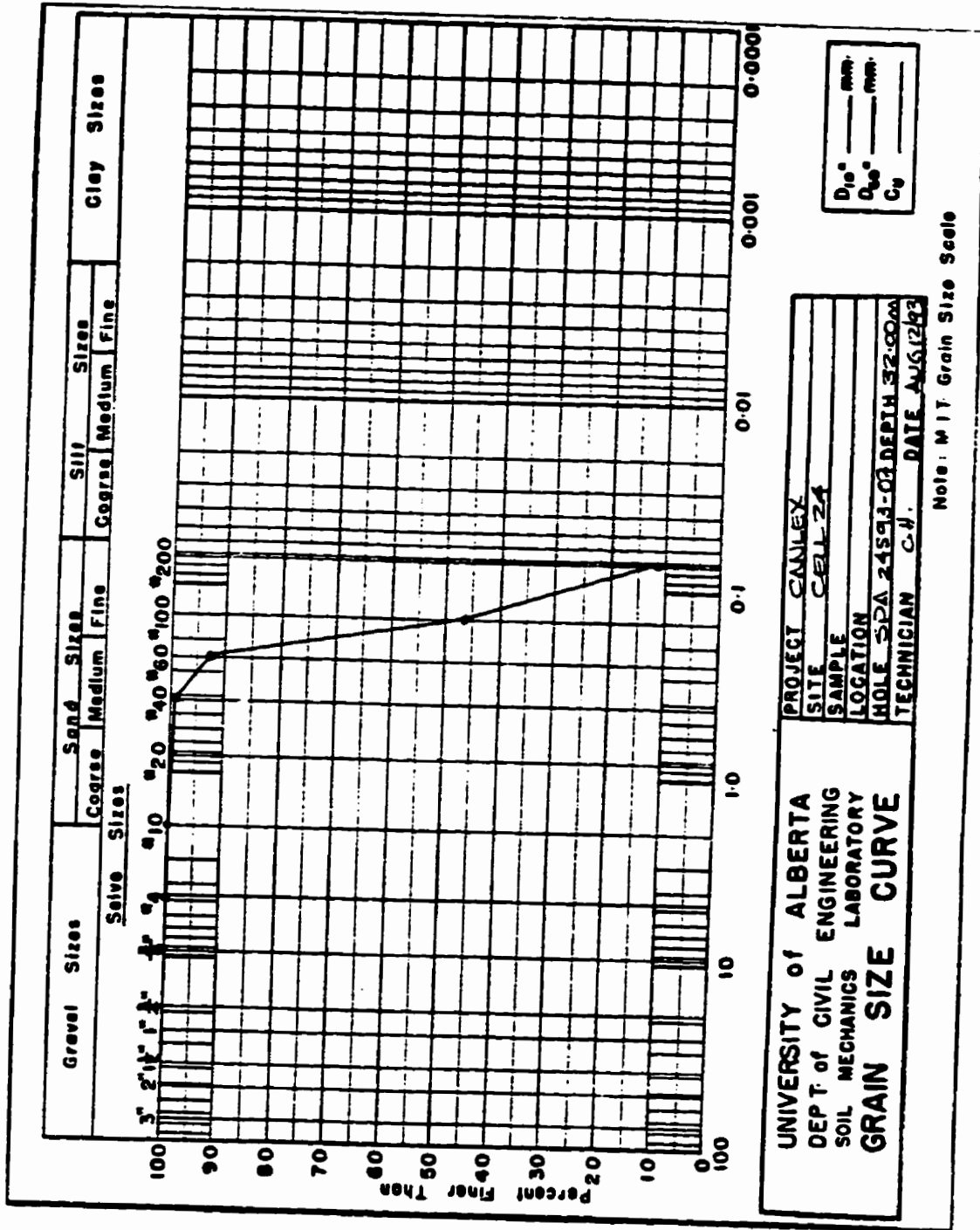


Figure B12: Grain Size Curve obtained for Sample recovered at 32.00 m.



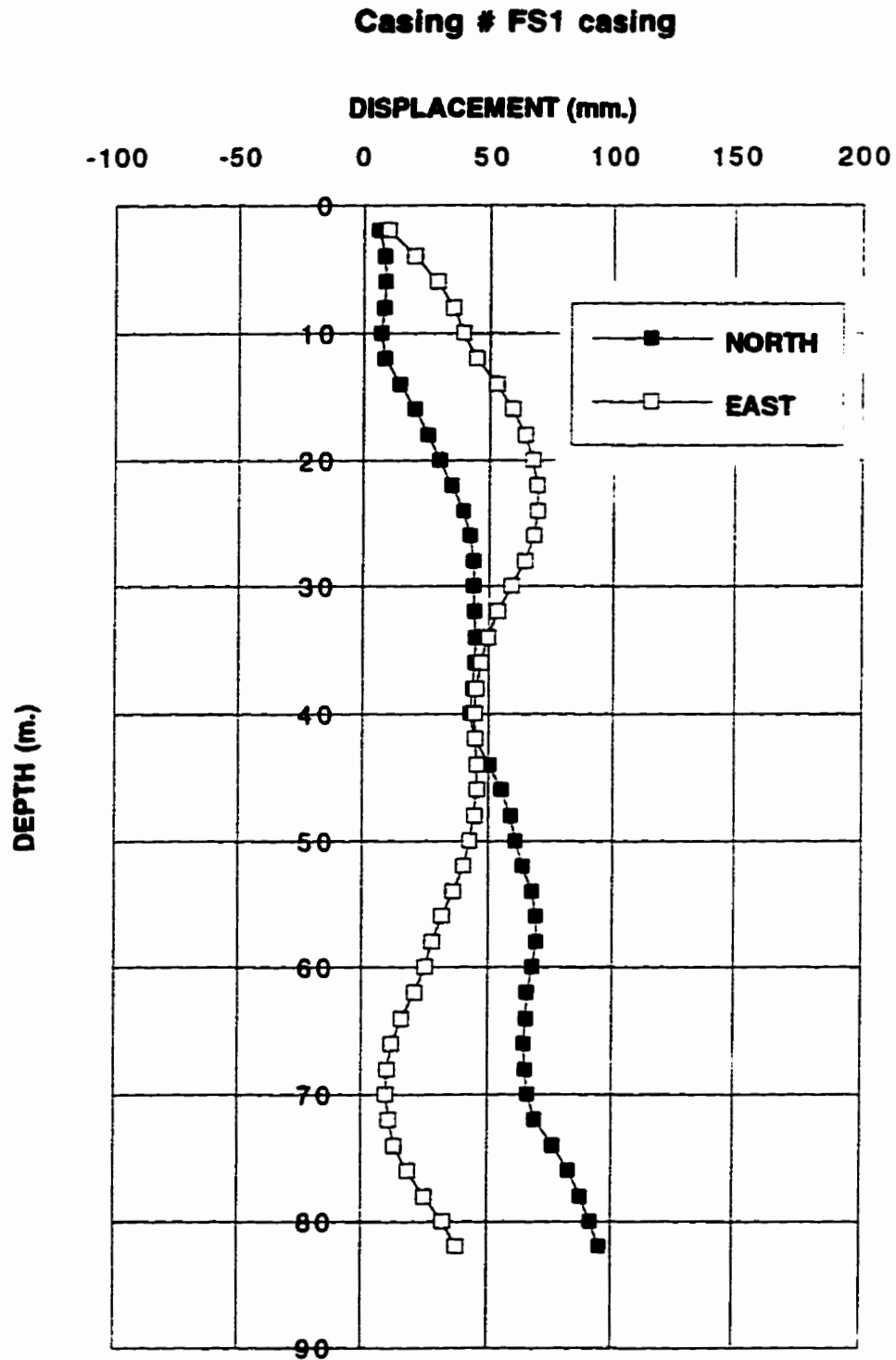


Figure B13: Deflection Profile of Sample Borehole FS1.

Casing # FS 2

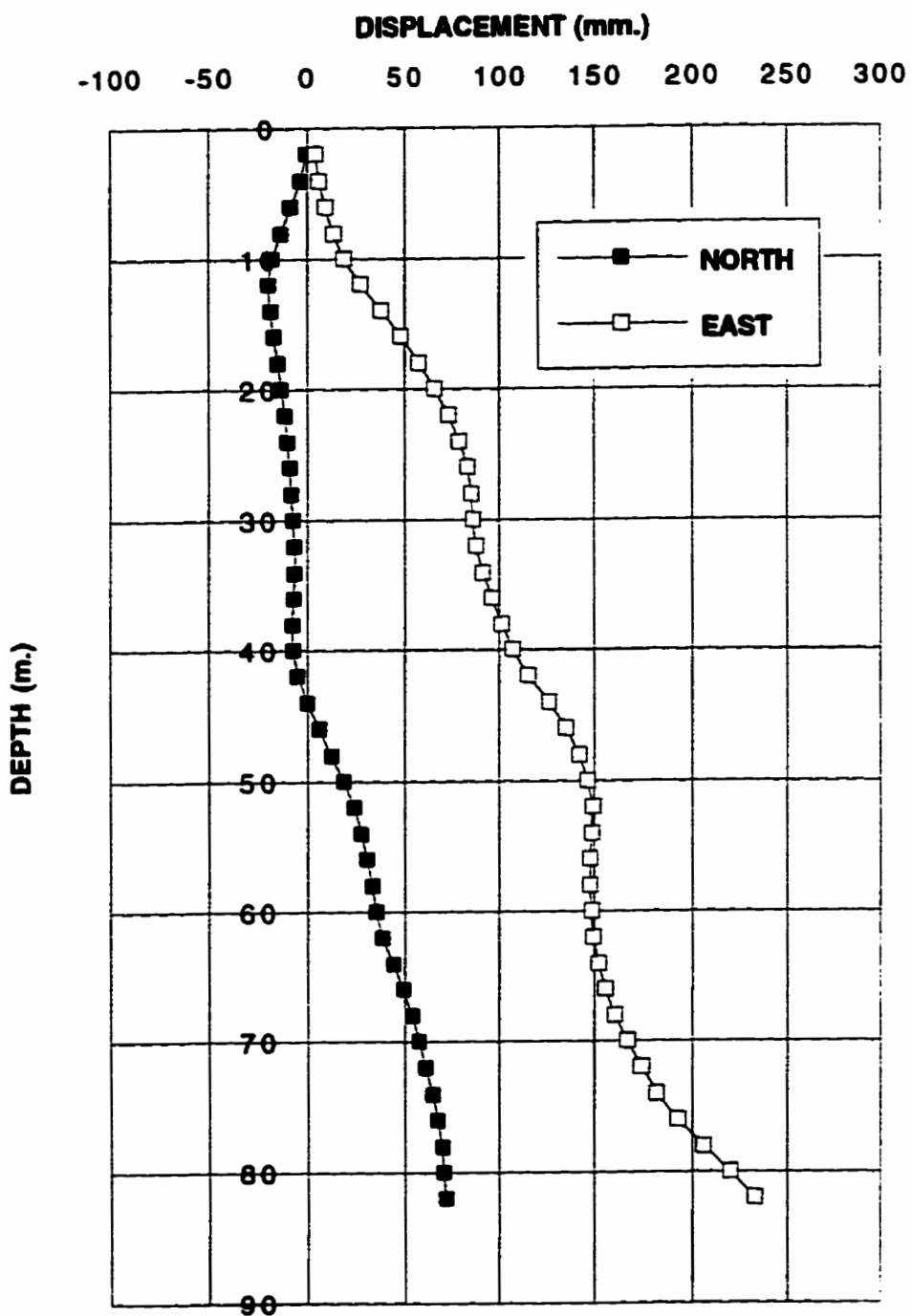


Figure B14: Deflection Profile of Sample Borehole FS2.

Casing # FS3

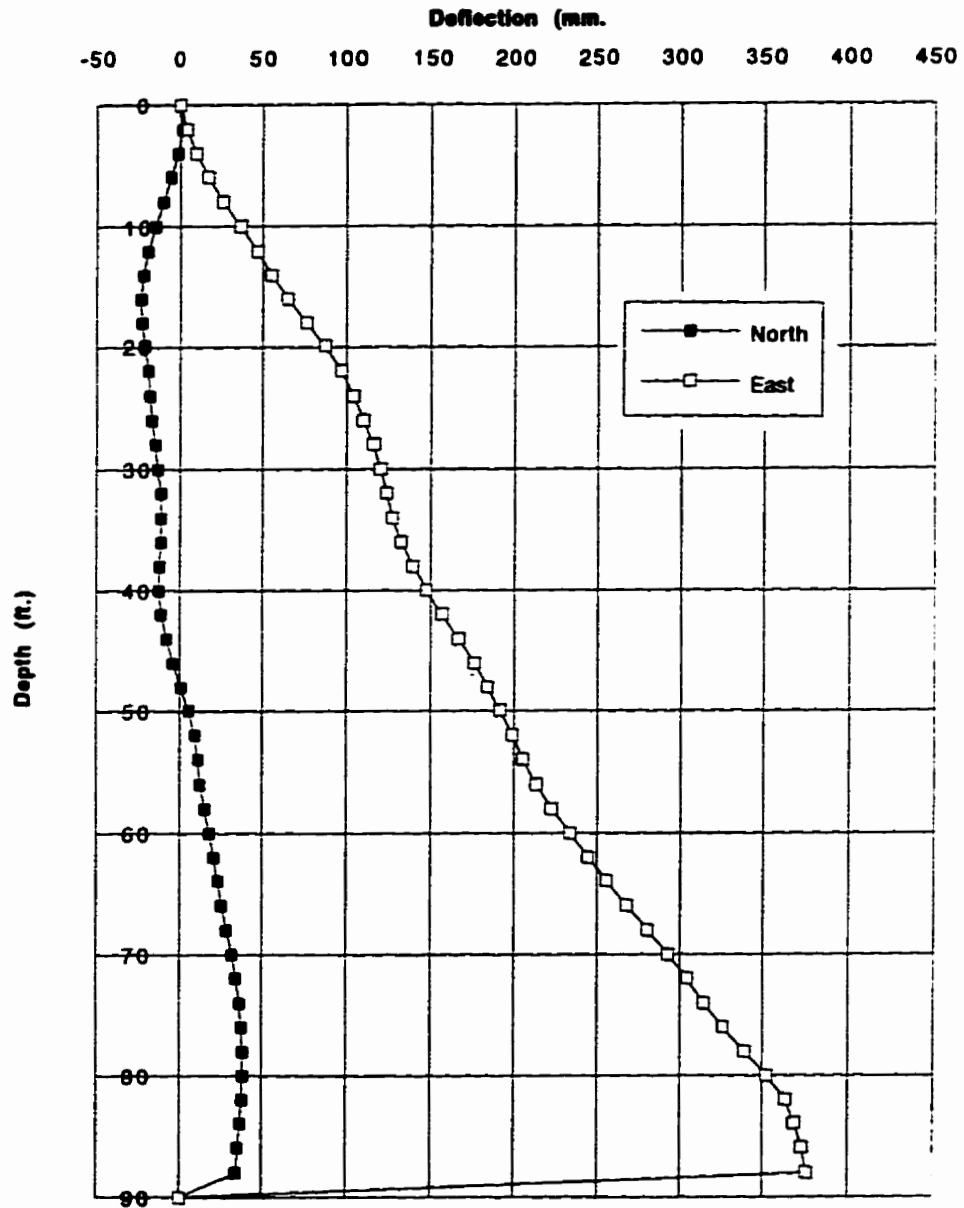


Figure B15: Deflection Profile of Sample Borehole FS3.

Casing # FS4 - 93

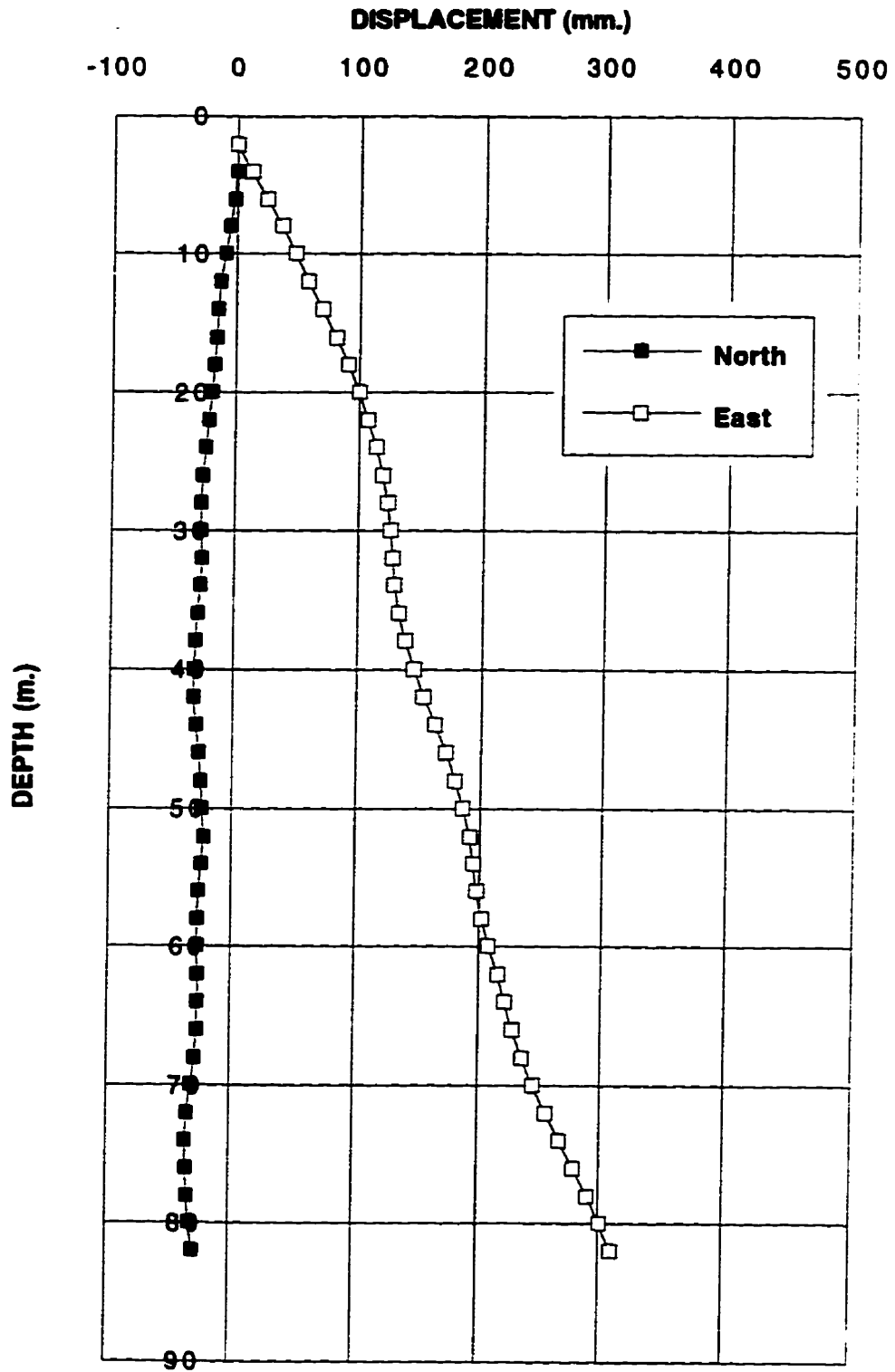


Figure B16: Deflection Profile of Sample Borehole FS4.

Casing # FS5 - 93

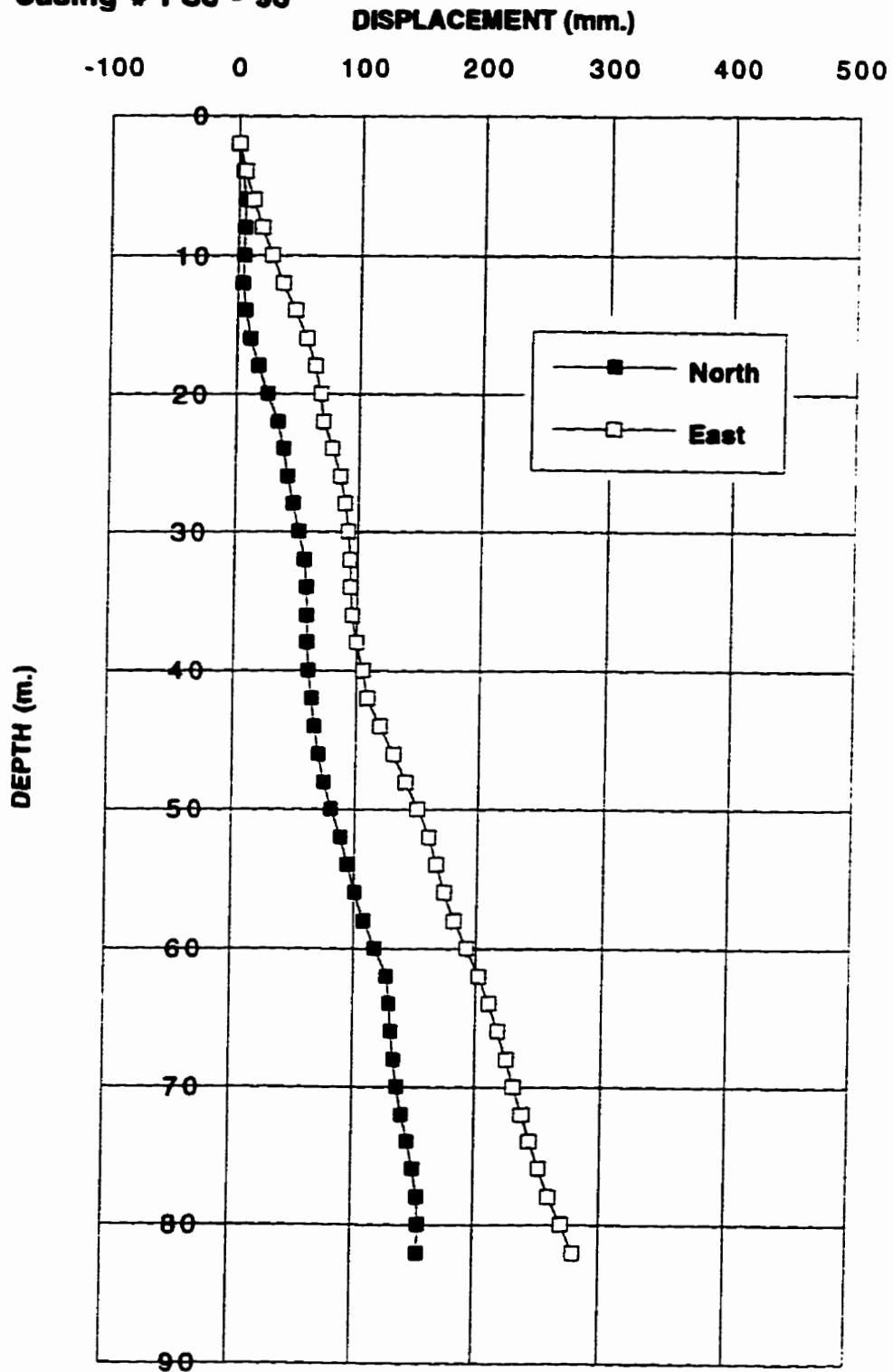


Figure B17: Deflection Profile of Sample Borehole FS5.

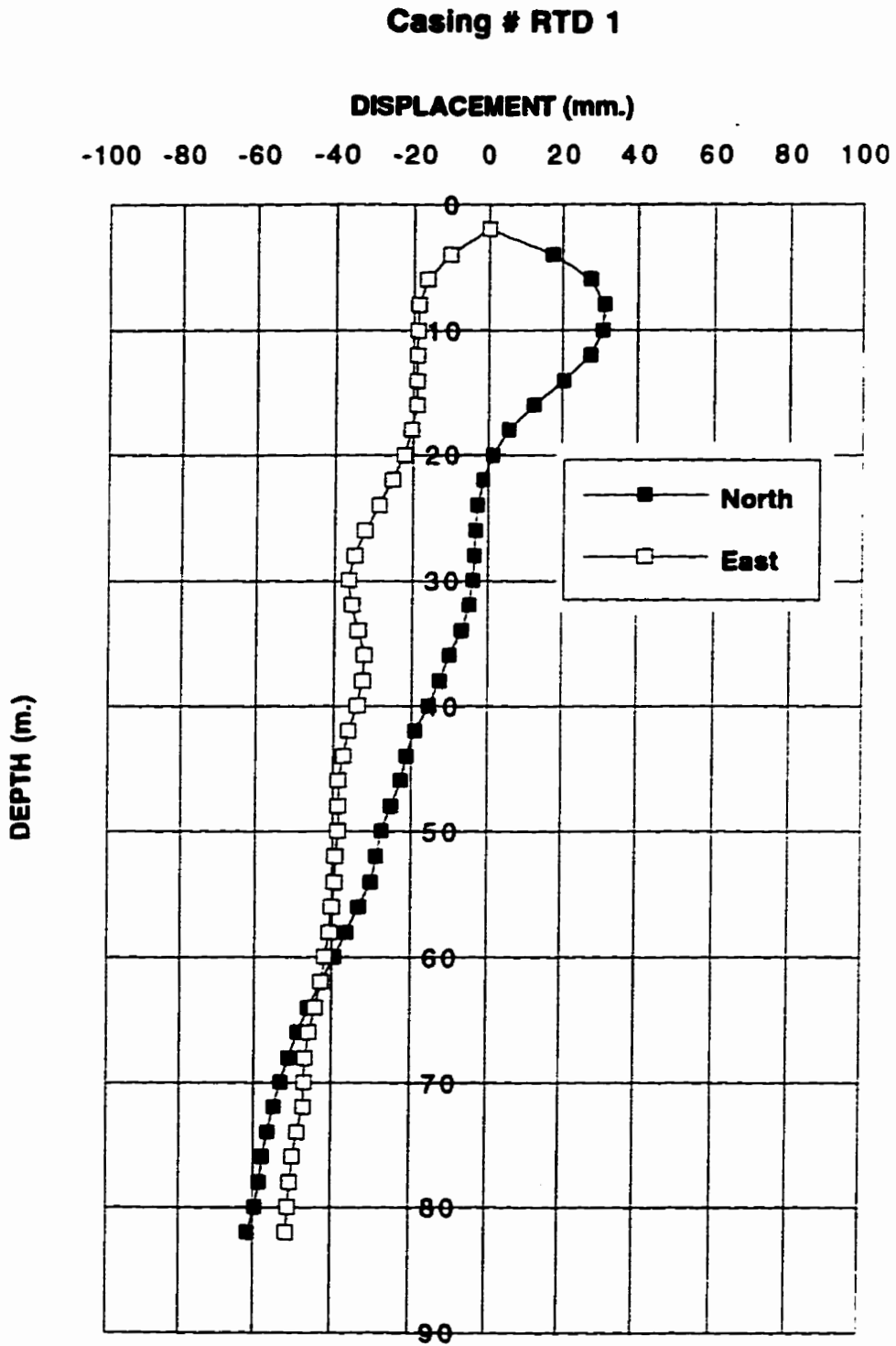


Figure B18: Deflection Profile of Sample Borehole RTD1.

RTD #2

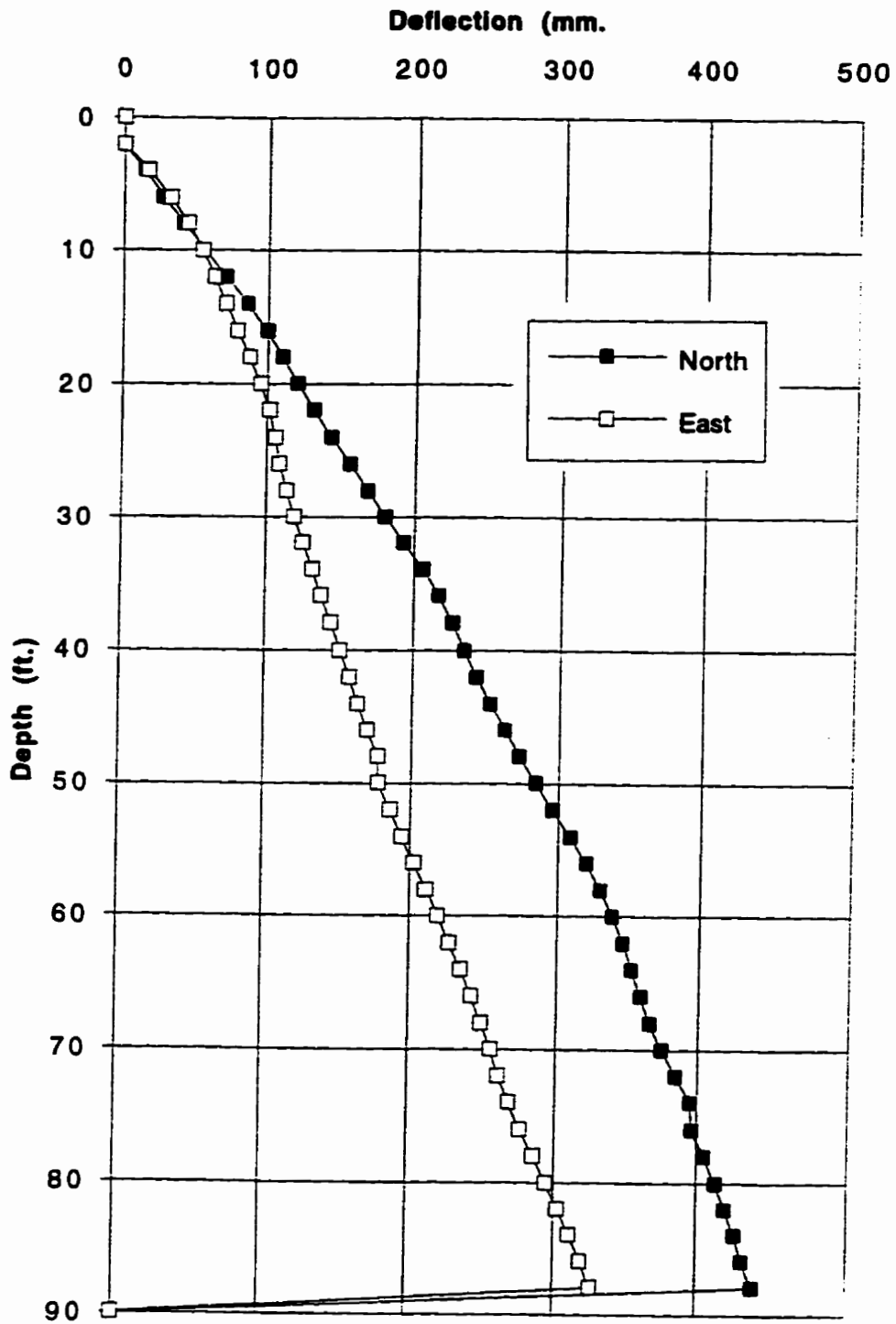


Figure B19: Deflection Profile of Sample Borehole RTD2.

RTD #3

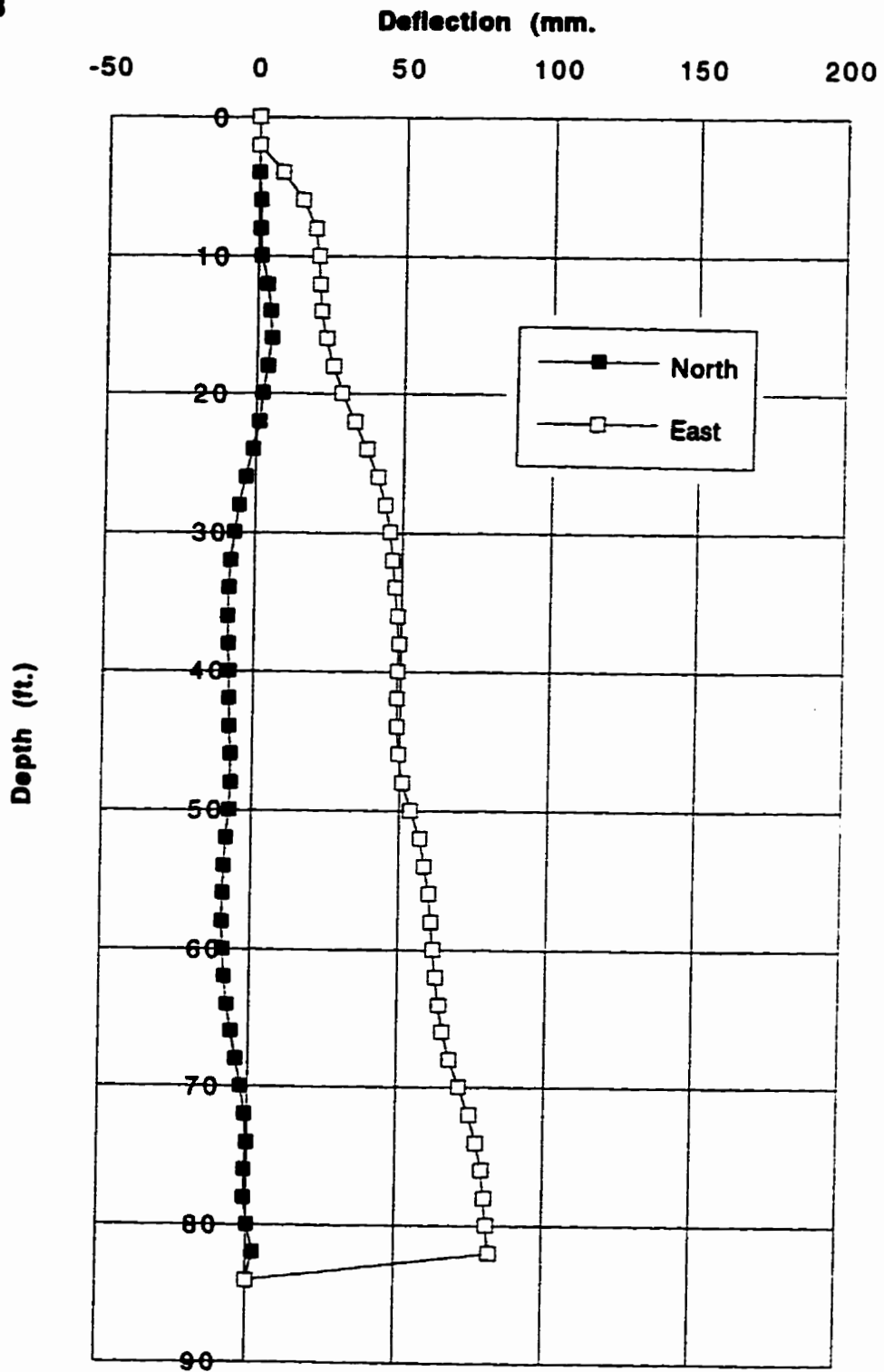


Figure B20: Deflection Profile of Sample Borehole RTD3.

LEGEND	
	EXCELLENT CORE
	GOOD CORE
	FAIR CORE
	POOR CORE

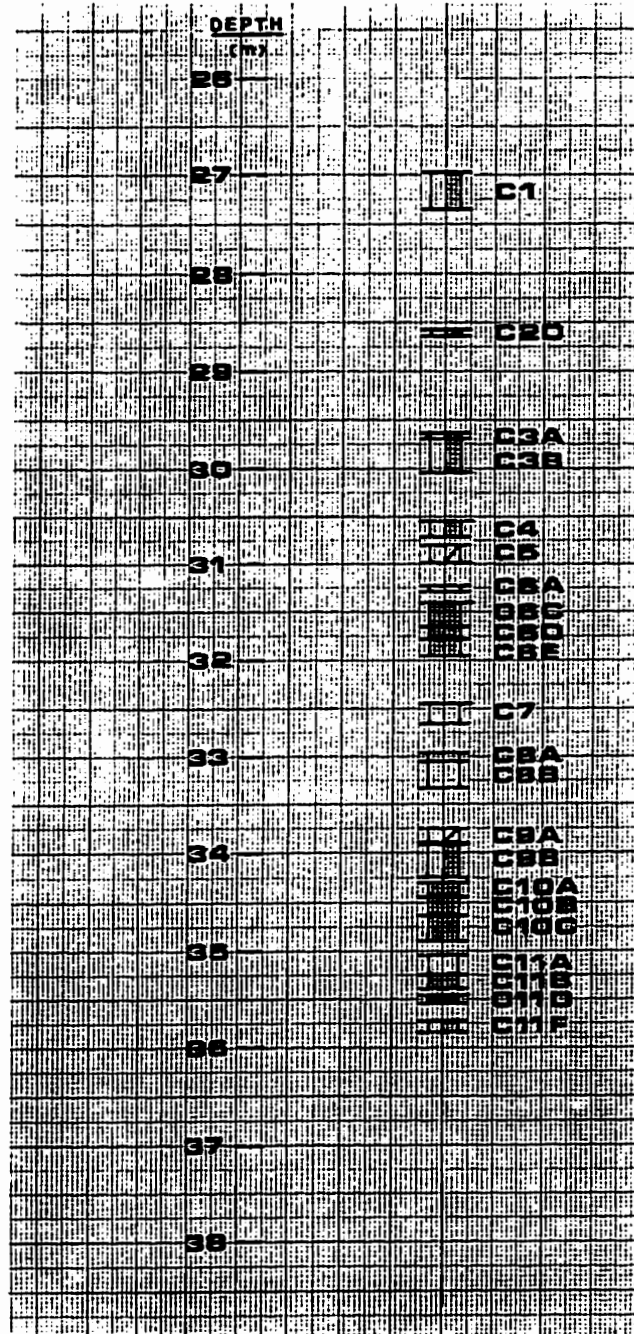
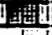





Figure B21: Frozen Cores Recovered from Sample Borehole FS1.

LEGEND	
	EXCELLENT CORE
	GOOD CORE
	FAIR CORE
	POOR CORE

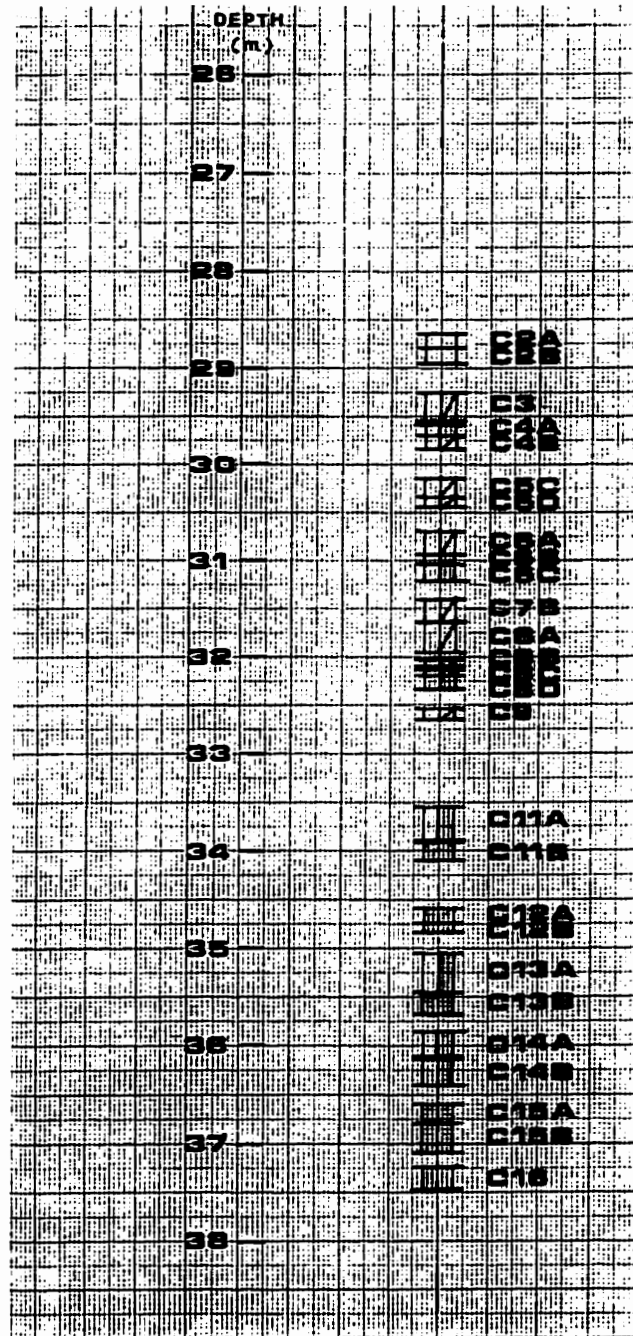






Figure B23: Frozen Cores Recovered from Sample Borehole FS4.

LEGEND	
	EXCELLENT CORE
	GOOD CORE
	FAIR CORE
	POOR CORE

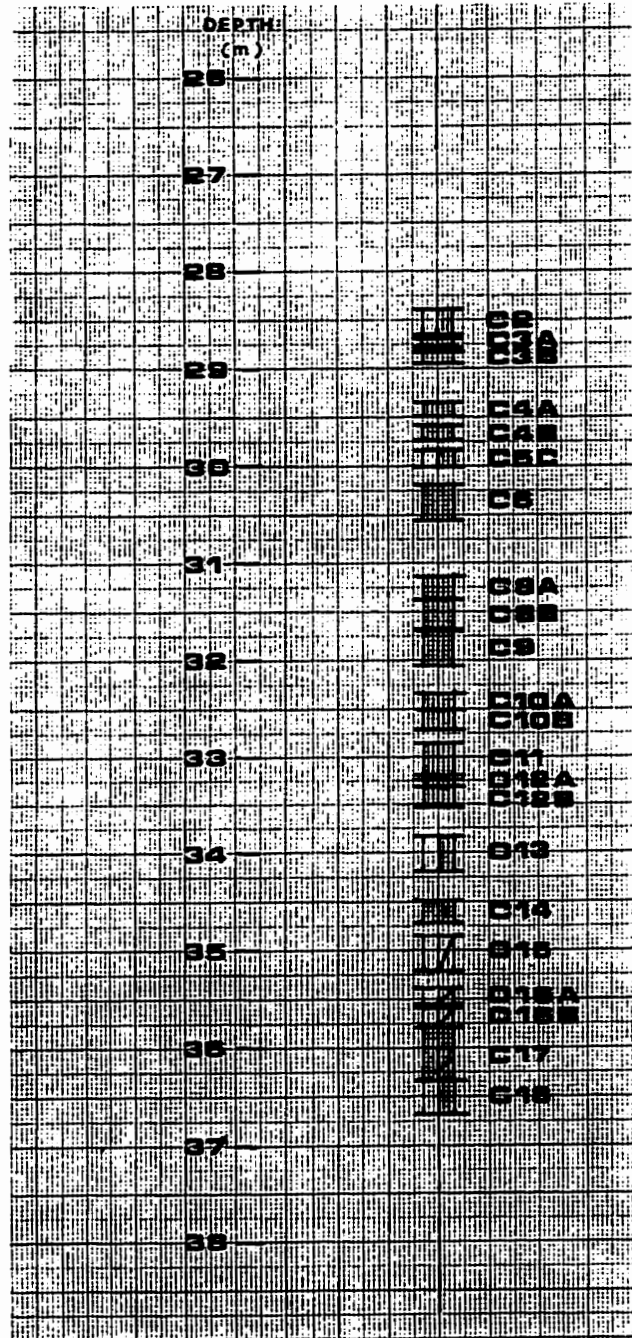


Figure B24: Frozen Cores Recovered from Sample Borehole FS5.

Sample Calculation of Void Ratio Changes due to Unfrozen Water Freezing in Place at colder Temperatures.

SAMPLE:	ASSUME: Syncrude Sand with 12 % fines	
DATE:	8-Feb-96	G_s = 2.65
Sand Type:	Syncrude	G_{ice} = 0.917
Cell Pressure:	500 kPa	
Axial Stress:	500 kPa	K_o = 1.0
Back Pressure:	100 kPa	
Calculated Saturation:	99.20 %	B = 1 (before freezing)
Diameter	63.50 mm	Total Frozen Vol. = 411.70 cc
Height	130.00 mm	Sample Area = 31.67 cm²
Frozen Total Weight	780.00 g	
Ice Content	30.00 %	V_s = M_s / ρ_s = M_s / ρ_w G_s = 218.87 cc
Dry Weight of Sample	580 g	V_v = V_t - V_s = 192.83 cc

Unfrozen Water Content Calculations:

Syncrude sand has:

- 0.28 % Mica Minerals with SA = 5 m²/g (% by dry weight of sand sample)
- 0.70 % Kaoline Minerals with SA = 5 m²/g (% by dry weight of sand sample)

Kaolinite at -1°C: Wu = 0.30 g water / g dry soil (clay)

Volume of Unfrozen Water = Wu

$$0.30 \text{ g water/g clay} \times 580 \text{ g soil} \times ((0.28+0.70)/100) \text{ g clay/g soil} = 1.7052 \text{ g water}$$

Expansion due to Unfrozen Water Freezing in Place = 9 %

$$\Delta V = 0.09 \times 1.7052 \text{ cc} = 0.1535 \text{ cc water}$$

Change in Volume during Freezing = 0.1535 cc (mi)

Void Ratio Calculations:

$$e_o = (V - V_s) / V_s = G_{spw} / \rho_d - 1 = 0.881$$

$$e_o = (W - W_s) / W_s \cdot (G_s / G_{ice}) = 0.997 \text{ (for saturated specimens)}$$

$$S_r i = (w_i G_s) / (e G_i) = 98.40 \quad S_{r o} = S_r i / 0.9919 = 99.20$$

$$\Delta e = \Delta V_{tz} / V_s = 0.00070$$

$$e_{tz} = e_o + \Delta V_{tz} / V_s = 0.882$$

$$\Delta h_{tz} = (e_{tz} - e_o) (V_s h) / (3 V) = 0.016 \text{ mm}$$

Appendix C: Phase II Test Sites Ground Freezing Data

C.1. Introduction

Appendix C contains data associated with the in-situ ground freezing activities conducted at the Phase II test sites. The temperature data gathered during freezing at the KIDD 2 and Massey Tunnel sites are included in summary tables. Plans showing the sample borehole locations are provided along with plots of the sample borehole deflections. Catalogues of the frozen core samples obtained from these sites are also given.

Table C1: RTD Ground Temperature Data at the KIDD 2 Site.

KIDD2 TEMPERATURE DATA									
DATE & TIME	TIME (HRS)	ELAPSED TIME (HRS)	RTD 1 (0.67m) 6-15	6-16	6-17	6-18	6-19	6-20	6-21
12/7/94	18:00	0							
13/7/94	11:40	19.67							
13/7/94	14:00	22							
14/7/94	9:45	41.75	8.78	6.57	4.8	3.8	1.8	-1.83	0.33
15/7/94	16:30	66.50	5.75	2	0.12	-0.55	-11.35	-19.78	-12.82
16/7/94	11:00	91.00		0.32	-3.95	-7.95	-18.33	-26.43	-18.2
17/7/94	8:00	114.33	1.37	-3.25	-7.58	-10.98	-21.23	-28.42	-19.8
18/7/94	8:20	137.83	0.45	-6.68	-11.55	-16.12	-30.25	-36.53	-25.63
19/7/94	8:00	162.17	-0.17	-8.7	-13.58	-18.85	-31.85	-39.35	-29
19/7/94	16:45	170.92	-0.12	-8.77	-13.55	-18.4	-29.73	-37.18	-28.15
21/7/94	9:10	213.33	-1.6	-11.88	-17.33	-23.07	-35.83	-43.5	-32.6
21/7/94	17:10	220.33	-1.85	-12	-16.57	-21.65	-31.75	-38.53	-30

RTD 2 (1.05m) 5-15	FREEZE PIPE RTD'S													
	5-16	5-17	5-18	5-19	5-20	5-21	UPPER							
11.2	11.07	10.25	10.18	9.75	9.4	8.17	-175.19							
10.43	9.63	8.33	8.1	6.88	5.45	3.15	-174.98							
10	8.55	7.1		5.13	2.55	0.32	-159.16							
9.35	7.43	5.65	5.12	2.45	0.03	-3.15	-175.81							
8.75	6.32	4.1	3.37	0.93	-4.67	-7.98	-175.63							
8.2	5.23	2.58	0.55	-0.3	-8.98	-11.68	-175.44							
7.98	4.85	2.08	0.08	-1.1	-10.15	-12.6	-174.65							
7.15	2.82	-0.15	-0.52	-7.3	-14.23	-16.58	-175.44							
1.73	2.67	-0.63	-1.22	-8.13	-15.16	-16.6	-64.7							

Table C2: RTD Ground Temperature Data at the Massey Tunnel Site.

DATE & TIME		ELAPSED TIME (HRS)	RTD 1 (0.6m)	3-12	3-13	3-14	3-15	3-16	3-17
TIME (HRS)		TIME (HRS)	3-11						
9/7/94	10:30	0.00							
10/7/94	16:30	30.00	11.57	11.53	12.80	11.58	11.27	11.15	10.90
11/7/94	9:15	46.75	10.17	7.47	13.42	5.55	5.33	2.97	2.60
12/7/94	10:10	71.67	7.80	1.18	12.73	-0.55	0.08	-6.08	-4.10
12/7/94	15:45	77.25	7.35	1.88	1.93	-2.68	-4.45	-9.58	-6.15
13/07/94	10:30	96.00	3.28	-1.45	-3.40	-11.53	-13.00	-17.88	-11.47
14/7/94	9:00	118.50	1.78	-8.63	-10.32	-18.6	-20.2	-24.65	-16.28
15/7/94	9:00	142.50	0.75	-12.78	-14.7	-22.55	-24.85	-29.05	-19.33
16/7/94	9:30	167.00	0.3	-16.1	-18.7	-27.5	-29.95	-33.73	-22.63
17/7/94	8:50	190.33	0.23	-16.4	-19.07	-26.05	-27.63	-31.25	-20.5
18/7/94	8:20	213.63	-0.32	-19.13	-21.8	-27.83	-29.03	-32.32	-21.53

RTD 2 (1.0m)		FREEZE PIPE RTD'S									
4-11		4-12	4-13	4-14	4-15	4-16	4-17	UPPER		LOWER	
11.42	11.20	11.35	11.22	11.22	11.22	11.40	10.98	-175.49	-172.56		
11.30	11.05	10.83	10.58	10.85	10.65	10.65	9.73	-158.12	-172.07		
10.87	9.77	8.75	8.48	7.60	8.08	8.08	7.43	-172.88	-173.95		
10.63	9.45	8.68	7.98	7.25	8.05	8.05	6.68	-171.26	-173.51		
10.03	8.03	6.97	5.83	4.70	9.68	9.68	4.73	-166.07	-173.84		
9.18	6.37	4.87	3.25	1.57	5.5	5.5	2.32	-177.09	-174.86		
8.28	4.5	2.6	0.72	-1.33	58.5	58.5	0.17	-175.19	-173.09		
7.35	3.1	0.57	-1.88	-6.8	44.65	44.65	-2.8	-159.16	-173.72		
6.57	2.15	-1	-5.2	-8.75			-4.23		-174.14		
4.25	1.25	-5.05	-7.52	-10.65			-5.52		-174.49		

Table C3 continued: KIDD 2 Site core catalogue.

K94F2	C1A	40.08	41.58	12.22	12.67	1.60	7.5	9.5	Coarse grey & black sand, esp. coarse @ 13.0 m ; some melting around perimeter of core; homog.	B
	C1B	41.75	43.06	12.73	13.13	1.33	9.0	10.0		
K94F2	C2A	43.29	43.93	13.20	13.36	6.5"	7.0	9.0	Med. to Coarse, Dark grey , homogeneous sand	B
	C2B	44.08	44.92	13.44	13.69	10"	9.0	10.0		
K94F2	C3A	45.17	45.71	13.77	13.93	6.5"	8.0	9.0	Med. coarse grey sand, homogeneous	I
	C3B	46.92	46.83	14.00	14.27	11"	10.0	10.0		
	C3C	46.92	47.13	14.30	14.36	2.5"	Cut up for e measurements			
	C3D	47.25	47.83	14.40	14.58	8"	10.0	10.0		
K94F2	C4A	48.25	49.00	14.71	14.94	9"	8.0	9.0	Med. coarse grey sand, homogeneous	B
	C4B	49.17	49.75	14.99	15.16	7"	9.5	10.0		
	C4C	50.00	50.92	15.24	15.52	11"	10.0	10.0		
	C4D	50.92	51.25	15.52	15.62	4"	10.0	9.0		
K94F2	C5A	54.59	55.38	16.84	16.88	9.5"	8.0	9.0	Med. coarse grey sand, homogeneous	B
	C5B	55.50	56.50	16.92	17.22	12"+	10.0	10.0		
	C5C	56.75	57.50	17.30	17.53	9"	10.0	10.0		
K94F3	C1A	39.50	40.58	12.04	12.37	13"	Core had hairline cracks - forced open with knife & found brown infilling - sand sample for		B	
	C1B	40.79	41.33	12.43	12.80	11"	10.0	10.0		
K94F3	C2	42.17	43.50	12.85	13.26	16"	8.0	10.0	Coarse, dark grey, homogeneous sand; organics were trimmed from bottom end of core	I
K94F3	C3A	43.92	44.42	13.39	13.54	6"	8.0	7.0	Coarse, dark grey, homogeneous sand; some exterior melting	B
	C3B	44.92	45.42	13.69	13.84	6"	8.0	9.5		
K94F3	C4A	47.63	47.92	14.52	14.61	4.5"			Coarse, black, homogeneous sand	I
	C4B	48.08	49.00	14.66	14.94	11"				
	C4C	49.25	50.38	15.01	15.35	13.5"				

Table C3 continued: KIDD 2 Site core catalogue.

K04F3	C8A	51.08	51.67	15.57	15.75	7'	9.5	9.5	Med. to Coarse, grey & black, homogeneous sand	I
	C8B	51.75	52.33	15.77	15.95	7'+	9.5	9.5	Med. to Coarse, grey & black, homogeneous sand	I
	C8C	52.33	52.67	15.95	16.05	4'	9.5	9.5	Med. to Coarse, grey & black, homogeneous sand core left untrimmed since just long enough for DSS	II
K04F5	C1	39.92	40.00	11.66	12.19	0'	Core turned out to be slough			IV
K04F5	C2A	40.08	41.25	12.22	12.57	1.17	7.0	10.0	Coarse grey & black sand; homogeneous	II
	C2B	41.33	42.00	12.60	12.80	0.67	10.0	10.0	Coarse grey & black sand; homogeneous	I
	C2C	42.21	42.58	12.87	12.98	0.38	10.0	10.0	Coarse grey & black sand; homogeneous	I
K04F5	C3	No Core Recovered								
K04F6	C1A	45.58	46.02	13.69	14.30	6.5'	Core was cut up for void ratio profile with depth (since couldn't find distinction of where in-situ frozen core at top of target zone started)			
	C1B									
K04F6	C2A	47.00	47.17	14.33	14.38	2'	Core cut up for void ratio profile			
	C2B	47.25	47.58	14.40	14.50	4.5'	10.0	10.0	Med. to Coarse grey & black, homogeneous sand	I
	C2C	47.75	48.33	14.55	14.73	7'	10.0	10.0	Med. to Coarse grey & black, homogeneous sand	I
K04F6	C3	Core recovered at ground surface was not frozen								
K04F7	C1	39.90	39.92	12.04	12.17	5'	Cut up for e measurements		Med. to Coarse grey & black, homogeneous sand	II
K04F7	C2A	41.08	41.83	12.52	12.75	9'	9.0	9.0	Med. to Coarse grey & black, homogeneous sand	II
	C2B	41.92	42.08	12.78	12.83	2'	Cut up for e measurements		Mostly Slough with pebbles & refrozen sand	V
	C2C	42.50	43.68	12.95	13.37	16.5'	7.0	10.0	Med. to Coarse grey & black, homogeneous sand organic inclusions at bottom end of core	II
K04F7	C3A	44.58	45.25	13.59	13.79	5'	10.0	10.0	Med. to coarse, black & grey, homogeneous sand	I
	C3B	45.58	46.67	13.69	14.22	13'	10.0	10.0	Med. to coarse, black & grey, homogeneous sand small circular crack @ top end of core (void)	II
	C3C	46.67	46.83	14.22	14.27	2'	10.0	10.0	Med. to coarse, black & grey, homogeneous sand	I
K04F7	C4A	47.08	47.75	14.35	14.55	8'	9.0	9.0	Med. grey, homogeneous sand; some exterior	I

Table C3 continued: KIDD 2 Site core catalogue.

	C6B	47.92	48.92	14.61	14.91	12°	9.0	9.0	melting Med. grey, homogeneous sand; some exterior melting	I
K84F7	C6A	49.08	50.08	14.98	15.27	12°	10.0	10.0	Med. grey, homogeneous sand	I
	C6B	50.33	51.68	15.34	15.61	18.5°	10.0	10.0	Med. grey, homogeneous sand	I
K84F7	C6A	52.08	53.08	15.88	16.18	12°	8.0	9.0	Med. grey, homogeneous sand; some exterior melting	B
	C6B	53.33	54.17	16.26	16.51	10°	8.0	9.0	Med. grey, homogeneous sand; some exterior melting	B
K84F7	C7	54.42	55.21	16.59	16.83	9.5°	8.5	9.0	Med. grey, homogeneous sand; some exterior melting	B

Table C4: KIDD 2 Site Trimmed Frozen Core Samples.

CANLEX PHASE II - Quality I - Trimmed Frozen Specimens RCD 03-072 Mass 03-030

Core Comment	Sample #	Depth (m)	Height(m)	Diameter(m)	Fr. Weight(kg)	Ice Content	Volume	Frozen Density	Dry Density	Void Ratio
USC-Feb 1995	RMF1 C4C	14.00-14.00	12.000	0.000	602.00	32.40	305.5200	1.5100	1.2600	0.3055
USC-Feb 1995	RMF1 C1B	12.20-12.20	12.700	0.070	602.00	28.54	307.5115	1.5500	1.4400	0.3030
USC-Mar 1995	RMF1 C3-1	12.00-12.71	2.102	0.070	152.15	27.30	82.4791	1.5447	1.4404	0.3770
USC-Mar 1995	RMF1 C3-2	12.72-12.74	2.100	0.070	151.20	27.30	82.4150	1.5340	1.4405	0.3682
USC-Mar 1995	RMF1 C3-3	12.75-12.81	12.475	0.010	607.57	30.31	354.8011	1.5500	1.4210	0.3120
USC-Mar 1995	RMF1 C7D	10.40-10.50	12.310	0.040	657.01	29.01	353.0070	1.5587	1.4310	0.3090
USC-June 1995	RMF4 C3A	0.20-0.24	2.000	0.000	141.57	33.30	70.9737	1.7700	1.3275	1.0180
USC-June 1995	RMF4 C4-1	10.10-10.32	12.700	0.040	650.50	33.51	304.7474	1.7000	1.3440	0.3020
USC-June 1995	RMF4 C4-2	10.30-10.40	12.400	0.030	630.42	32.00	305.3050	1.7000	1.3540	0.3700
USC-June 1995	RMF4 C4-3	10.54-10.57	12.700	0.037	657.00	33.10	304.5311	1.6021	1.3533	0.3003
USC-June 1995	RMF4 C5-1	0.20-0.22	2.007	0.000	140.00	31.00	70.8401	1.7010	1.3300	1.0025
USC-June 1995	RMF4 C5-2	0.22-0.24	2.070	0.000	140.70	31.00	70.2064	1.7700	1.3400	0.3055
USC-June 1995	RMF4 C4-2	10.31-10.44	12.740	0.053	600.21	32.01	306.8953	1.6100	1.3700	0.3473
USC-June 1995	RMF2 C7B-1	10.02-10.75	12.500	0.005	654.47	33.03	302.2420	1.6007	1.3500	0.3052
USC-June 1995	RMF2 C7B-2	10.77-10.79	2.200	0.070	148.17	33.03	83.0410	1.7052	1.3100	1.0310
USC-June 1995	RMF2 C7B-3	10.00-10.02	2.172	0.070	147.50	33.03	83.0000	1.7700	1.3275	1.0180
USC-June 1995	RMF4 C7A	11.70-11.81	12.200	0.003	641.00	30.41	304.0000	1.6110	1.3007	0.3200
USC-June 1995	RMF2 C3B-1	0.24-0.27	12.400	0.053	652.52	29.00	300.3010	1.6211	1.4010	0.3120
USC-June 1995	RMF2 C3B-2	0.28-0.31	2.100	0.070	152.40	29.00	82.2240	1.6542	1.4204	0.3700
USC-June 1995	RMF2 C3B-3	10.02-10.04	2.170	0.070	152.07	29.00	83.1151	1.6200	1.4075	0.3041
USC-July 1995	RMF4 C3C-1	10.40-10.40	2.000	0.070	137.17	32.02	70.2307	1.7012	1.3104	1.0327
USC-July 1995	RMF4 C3C-2	10.40-10.51	2.122	0.070	140.00	32.02	81.0001	1.7000	1.3400	0.3054
USC-July 1995	RMF2 C11B-1	12.74-12.76	1.007	0.000	182.74	33.00	74.8717	1.7700	1.3235	1.0250
USC-July 1995	RMF2 C11B-2	12.77-12.79	2.000	0.070	141.01	33.00	70.0044	1.7714	1.3220	1.0207
USC-July 1995	RMF4 C4B-1	10.52-10.54	2.070	0.070	140.50	34.02	70.2223	1.7745	1.3241	1.0241
USC-July 1995	RMF4 C4B-2	10.54-10.56	2.110	0.070	142.00	34.02	80.0233	1.7731	1.3230	1.0257
USC-July 1995	RMF4 C5-1	11.10-11.20	2.010	0.000	137.00	31.00	77.1000	1.7004	1.3050	0.3700
USC-July 1995	RMF4 C5-2	11.21-11.23	2.007	0.000	143.00	31.00	80.2200	1.7040	1.3000	0.3007
USC-July 1995	RMF4 C5-3	11.24-11.26	2.077	0.000	142.50	31.00	70.4000	1.7000	1.3001	0.3700
USC-July 1995	RMF4 C5B	0.20-0.22	12.550	0.037	641.00	31.00	300.2302	1.7057	1.3043	0.3700
USC-Mar-99	RMF3 C3A	13.30-13.52	12.570	0.077	650.70	30.00	304.5401	1.7002	1.3120	1.0722
USC-Mar-99	RMF4 C3C-1	14.50-14.57	2.100	0.070	141.00	30.01	81.4017	1.7410	1.3020	1.1207
USC-Mar-99	RMF4 C3C-2	14.50-14.72	12.300	0.037	620.00	30.01	303.5000	1.7001	1.3020	1.0810
USC-Mar-99	RMF4 C3B-1	12.00-12.72	12.300	0.045	601.01	32.50	304.0202	1.6304	1.3053	0.3034
USC-Mar-99	RMF4 C3B-2	12.74-12.76	2.003	0.077	140.50	32.50	80.0247	1.7000	1.3247	1.0534
USC-Mar-99	RMF4 C3B-3	14.00-14.50	12.000	0.040	641.00	32.00	302.1102	1.7710	1.3340	1.0370
Lev-Feb 2795	RMF4 C3B	0.00-0.10	17.000	0.070	220.00	31.10	120.0010	1.6420	1.4057	0.3005
Lev-Feb 2795	RMF4 C3A	0.00-0.00	17.000	0.045	230.00	29.22	124.0700	1.6512	1.4320	0.3700
Lev-May 095	Messy Lar.Ds	Level next sample to U OF A to be installed for them	0.000	0.000	0.000	0.000	0.000	0.000	0.000	0.000
Lev-May 095	Messy Lar.Ds		0.000	0.000	0.000	0.000	0.000	0.000	0.000	0.000
Lev-May 095	Messy Lar.Ds		0.000	0.000	0.000	0.000	0.000	0.000	0.000	0.000
Lev-May 095	Messy Lar.Ds		0.000	0.000	0.000	0.000	0.000	0.000	0.000	0.000
Lev-May 2995	RMF4 C4	33°S-33°S	0.012	0.010	120.00	32.07	607.1040	1.6000	1.3501	0.3733
Lev-June1495	RMF2 C1B	12.57-12.57	10.000	0.000	304.30	34.04	100.7120	1.7020	1.3212	1.0205
Lev-June1495	RMF2 C7B-1	10.70-10.80	10.000	0.000	371.44	34.47	107.2310	1.6020	1.3000	0.3140
Lev-June1495	RMF2 C7B-2	10.80-11.00	0.070	0.000	305.30	34.00	107.3207	1.7007	1.3301	1.0140
Lev-June1495	RMF4 C4-4	10.00-10.70	10.040	0.000	300.00	32.10	100.4417	1.7077	1.3030	0.3000
Lev-June2995	RMF4 C1B	7.02-7.02	10.007	0.000	300.00	31.00	200.4300	1.7204	1.3000	1.0512
Lev-June2995	RMF2 C3A-1	0.13-0.20	0.070	0.002	301.07	30.40	100.1737	1.6004	1.3030	0.3070
Lev-June2995	RMF2 C3A-2	0.24-0.24	10.007	0.002	300.70	30.40	107.7000	1.6004	1.3030	0.3070
Lev-June2995	RMF2 C1B-1	12.14-12.24	0.042	0.000	307.70	33.30	100.2042	1.6000	1.3741	0.3004
Lev-June2995	RMF2 C1B-2	12.25-12.34	0.700	0.000	307.00	30.00	101.4400	1.6120	1.3000	0.3700
Lev-June2995	RMF4 C4-1	10.40-10.30	0.077	0.000	307.10	32.70	100.0302	1.7040	1.3014	0.3001
Lev-Aug1795	Sample Tube 02 1-1	0.00-0.10	0.000	0.000	343.00	34.22	100.0000	1.7000	1.3102	1.0300
Lev-Aug1795	Sample Tube 02 1-2	0.00-0.10	10.002	0.007	347.30	34.23	100.7000	1.7000	1.3103	1.0370
Lev-Aug1795	Sample Tube 02 1-3	0.00-0.10	10.007	0.002	340.07	34.17	100.3700	1.7000	1.3115	1.0435
Lev-Aug1795	Sample Tube 02 1-4	0.00-0.10	10.000	0.000	340.00	32.00	107.1204	1.7004	1.3300	1.0141
Lev-Sept 2095	Tube 02 A-1	0.70-0.91	0.000	0.010	300.14	32.00	107.4300	1.6100	1.3700	0.3015
Lev-Sept 2095	Tube 02 A-2	0.70-0.91	10.010	0.000	300.00	30.04	100.2204	1.6000	1.3700	0.3420
Lev-Sept 2095	Tube 02 A-4	0.70-0.91	10.000	0.002	300.00	32.37	100.0540	1.7000	1.3570	0.3740
Lev-Sept 2095	Tube 02 B-1	0.00-0.00	0.000	0.000	307.00	31.32	100.3104	1.6000	1.3700	0.3013
Lev-Sept 2095	Tube 02 B-2	0.00-0.00	0.000	0.000	340.00	30.74	100.0102	1.6020	1.3700	0.3430
Lev-Sept 2095	Tube 02 B-3	0.00-0.04	10.010	0.000	303.01	29.02	100.0110	1.6200	1.4000	0.3017
Lev-Sept 2095	Tube 02 B-4	0.00-0.04	10.000	0.007	303.01	29.30	100.4400	1.6300	1.4172	0.3010
Lev-Sept 2095	Tube 02 MC Sub	0.04-0.07								
Lev-Sept 2095	Tube 02 C-1	0.07-0.10	10.000	10.000	1400.00	29.72	700.3700	1.6300	1.4173	0.3000
Lev-Sept 2095	Tube 02 D-1	0.10-0.20	10.000	0.010	370.00	29.50	100.3004	1.6001	1.4077	0.3010
Lev-Sept 2095	Tube 02 D-2	0.10-0.20	0.000	0.010	370.00	27.00	107.4300	1.6770	1.4700	0.3102
Lev-June 2095	RMF4 C3-1	10.00-10.70	10.107	0.047						

Table C5: Massey Tunnel Site core catalogue.

CANLEX - PHASE I: MASSEY TUNNEL												19-Nov-84
CATALOGUE OF FROZEN CORE SAMPLES												
Legend:												
I Excellent Core - Insignificant zone of melting around perimeter during extrusion												
II Good Core - Minor zone of melting around perimeter of core during extrusion which can be trimmed from laboratory samples												
III Fair Core - Questionable whether the core contains some retrozen slough and/or significant melting at time of extrusion												
IV Poor Core - Due to excessive melting, disturbance or fracturing												
Note: No evidence of ice lens formation was found in any of the frozen core samples												
Borehole Number	Core Number	Start Depth Interval (ft)	End Depth Interval (ft)	Start Depth Interval (m)	End Depth Interval (m)	Length of Core (m)	a(top) (cm)	a(bottom) (cm)	Comments Regarding Core Quality	Quality Rating		
M94F2	C1	24.08	24.58	7.34	7.49	6'	7.0	10.0	Coarse, grey sand, homogeneous; top end of core comprised drilling mud; top of core still has one corner that is drilling mud.	II		
M94F2	C2A	24.78	25.17	7.58	7.87	4.5'	10.0	10.0	Coarse, grey & black sand, homogeneous	I		
	C2B	25.42	25.71	7.75	7.84	3.5'	10.0	10.0	Coarse, grey & black sand, homogeneous			
	C2C	25.87	25.88	7.82	7.89	2.5'	10.0	10.0	Coarse, grey & black sand, homogeneous			
	C2C	25.42	26.58	8.05	8.10	2'	10.0	10.0	Coarse, grey & black sand, homogeneous			
M94F2	C3A	26.87	27.54	8.13	8.39	10.5'	10.0	10.0	Med. to coarse, grey sand, homogeneous	I		
	C3B	27.67	28.50	8.43	8.89	10'	10.0	10.0	Med. to coarse, grey sand, some small grey cracks visible at each end, infilled with lighter material; thin dark lines may indicate crack at bottom end is ice rich	II		
M94F2	C4A	28.83	29.25	8.79	8.92	5'	10.0	10.0	Med. to coarse, grey sand, homogeneous, organic at bottom end	I		
	C4B	29.33	30.17	8.94	9.19	10'	10.0	10.0	Med. to coarse, grey sand, homogeneous, organic at bottom end	I		
M94F2	C5A	30.92	32.00	9.42	9.75	13.5'	10.0	10.0	Med. to coarse grey sand, homogeneous; some some organics at top end of core	I		
	C5B(U)	32.21	32.67	9.82	9.96	5.5'						
M94F2	C6A	33.00	33.33	10.06	10.16	4'	10.0	10.0	Med. to coarse grey sand, homogeneous	I		
	C6B	33.42	33.75	10.19	10.29	4'	10.0	10.0	Med. to coarse grey sand, homogeneous	I		
M94F2	C7A	33.92	34.67	10.34	10.57	9'	10.0	10.0	Coarse, grey & black sand, homogeneous	I		

Table C5 continued: Massey Tunnel Site core catalogue.

	C7B	34.75	38.00	10.59	10.97	15'	10.0	10.0	10.0	10.0	10.0	Coarse, grey & black sand, homogeneous	I
M84F2	C8A	36.25	37.08	11.05	11.30	10'	10.0	10.0	10.0	10.0	10.0	Coarse, grey & black sand, homogeneous	I
	C8B(1)	37.33	37.79	11.38	11.62	6.5'	10.0	10.0	10.0	10.0	10.0	Med. to coarse grey sand, homogeneous	I
M84F2	C9A(2)	38.08	38.58	11.81	11.76	6'	10.0	10.0	10.0	10.0	10.0	Medium to Coarse, grey & black, homogeneous sa	I
	C9B	38.87	38.92	11.79	11.88	3.5'	10.0	10.0	10.0	10.0	10.0	Medium, grey & black, homogeneous sand	I
	C9C	39.00	39.50	11.89	12.04	6.5'	10.0	10.0	10.0	10.0	10.0	Medium, grey & black, homogeneous sand	I
M84F2	C10	39.83	40.58	12.14	12.37	9'	10.0	10.0	10.0	10.0	10.0	Medium, grey & black, homogeneous sand; small shear crack at bottom end of core where it was broken off down the borehole	I
M84F2	C11A	40.71	41.13	12.41	12.53	5'	10	10	10	10	10	Med. to coarse grey & black sand, homogeneous	I
	C11B	41.25	42.00	12.57	12.80	9'	10	10	10	10	9.5	Med. to coarse grey & black sand, homogeneous	I
	C11C	42.17	42.50	12.85	12.95	4'	10	10	10	10	10	Noted large crack through middle of core length	
	C11D	42.75	42.88	13.03	13.09	2.5'	10	10	10	10	10	Med. to coarse grey & black sand, homogeneous	I
M84F4	C1A	24.54	25.17	7.48	7.67	7.5'	10.0	10.0	10.0	10.0	10.0	Coarse, grey & black sand, homogeneous	I
	C1B	25.33	27.17	7.72	8.28	22'	10.0	10.0	10.0	10.0	10.0	Coarse, grey & black sand, homogeneous; firm; bottom end of core that had 3' of fine, grey slough.	I
M84F4	C2A												
	C2B	29.50	30.33	9.02	9.25	10'	10.0	10.0	10.0	10.0	10.0	Med., grey sand, homogeneous	I
M84F4	C3A	30.50	31.67	9.30	9.65	14'	10.0	10.0	10.0	10.0	10.0	Med. to coarse, grey sand, homogeneous	I
	C3B	32.92	33.33	10.03	10.18	5'	10.0	10.0	10.0	10.0	10.0	Med. to coarse, grey sand, homogeneous	I
M84F4	C4	33.42	36.25	10.19	11.05	34'	10.0	10.0	10.0	10.0	10.0	Med. to coarse grey sand, homogeneous	I
M84F4	C5A	36.33	36.67	11.07	11.18	4'						core cut up for void ratio determination	
	C5B	37.50	37.92	11.43	11.56	5'	10.0	10.0	10.0	10.0	9.0	Med. to coarse grey sand, homogeneous	I
M84F4	C6	39.08	42.00	11.91	12.60	35'	10.0	10.0	10.0	10.0	10.0	Med. to coarse grey sand, homogeneous	I

Table C.5 continued: Massey Tunnel Site core catalogue.

M04FS	C1A	25.97	26.46	7.62	6.09	9.5'	10.0	10.0	Med. to coarse grey sand, noted random vertical cracking throughout core C1A to C1D, but more pronounced near top of core; removed piece of core along cracks & cracks were dry with no signs of ice lenses - see pore ice only.	IV
	C1B	26.71	27.08	6.14	6.26	4.5'	10.0	10.0		III
	C1C	27.42	27.71	6.36	6.45	3.5'	10.0	10.0		III
	C1D	27.92	28.07	6.51	6.74	9'	10.0	10.0		III
M04FS	C2A(T)	28.67	29.78	6.74	9.07	13'	10.0	10.0	Med. grey sand, noted fine sand filled cracks at top and bottom ends of core	
	C2B	29.63	30.75	9.09	9.37	11' but sliced core to measure a change w/ depth				
	C2C	30.63	31.67	9.40	9.65	10'	10.0	10.0	Med. grey sand	III
M04FS	C3A	31.92	33.08	9.73	10.08	14'	10.0	10.0	Med. grey sand, noted fine sand & silt filled cracks (filling comprises white fine sand with some black spaces)	III
	C3B	33.25	33.67	10.13	10.26	5'	10.0	10.0		III
	C3C	33.63	34.92	10.31	10.64	13'	10.0	10.0		III
M04FS	C4A	35.00	36.92	10.67	11.25	23'	10.0	10.0	Med. grey sand, fine sand & silt filled cracks at bottom end	III
	C4B	37.00	37.98	11.28	11.46	7'	10.0	10.0	cut core lengths to examine fine sand cross-bedding & sent for SEM	III
M04FS	C5A(T)	38.08	39.08	11.61	11.91	12'	10.0	10.0	Med. to coarse grey & black sand, homogeneous	I
	C5B	39.25	39.62	11.96	12.17	7.5'	10.0	10.0	Med. to coarse grey & black sand, homogeneous	I
M04FS	C6	40.25	42.67	12.27	13.00	29'	10.0	10.0	Med. to coarse grey & black sand, homogeneous	I
M04FS	C1A	25.56	26.92	7.80	6.20	16'	7.6	10.0	Med. to coarse grey sand, homogeneous, silt filled cracks at bottom end of core	III
	C1B	27.00	27.59	6.23	6.41	7.5'	10.0	19.0	Med. to coarse grey sand, homogeneous	I
	C1C	27.89	28.42	6.46	6.66	7'	10.0	10.0	Med. to coarse grey sand, homogeneous	I
M04FS	C2A	28.50	29.63	6.69	9.03	14.5'	10.0	10.5	Med. to coarse, grey & black sand, homogeneous	I
	C2B(T)	29.63	30.29	9.09	9.23	5.5'	10.0	10.0	Med. to coarse, grey & black sand, homogeneous; noted rust streak at 307' & 307.2'	I
M04FS	C3A	30.42	31.75	9.27	9.66	16'	10.0	10.0	Med. to coarse, grey & black sand, noted silt and fine sand filled cracks	III
	C3B	31.93	32.08	9.70	9.79	3'	10.0	10.0	Med. to coarse, grey & black sand, noted silt and fine sand filled cracks	III
	C3C	32.08	32.50	9.76	9.91	5'	10.0	10.0		IV

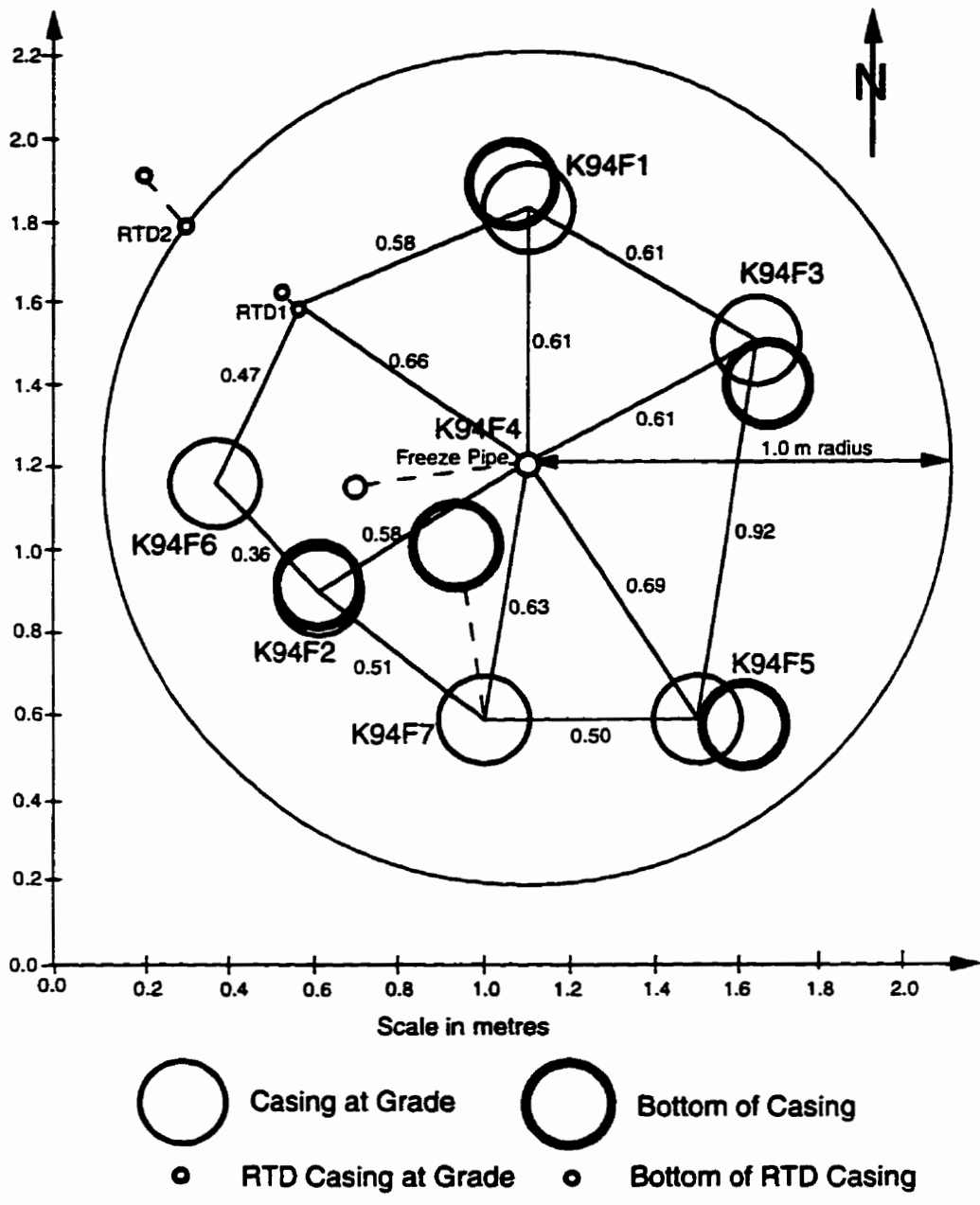


Figure C1: Alignment of Frozen Sample Boreholes at KIDD 2 Site.

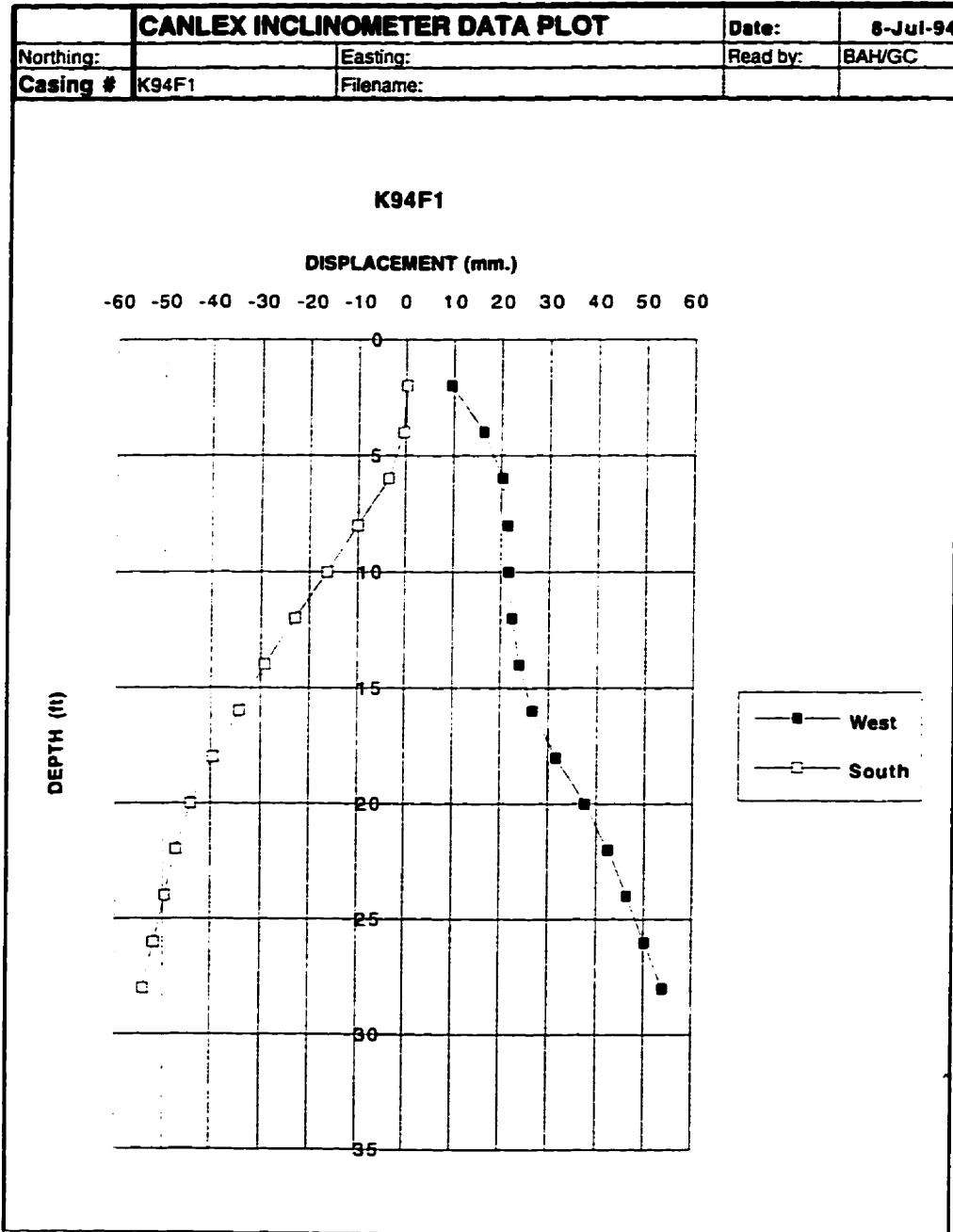


Figure C2: Deflection of Sample Borehole K94F1.

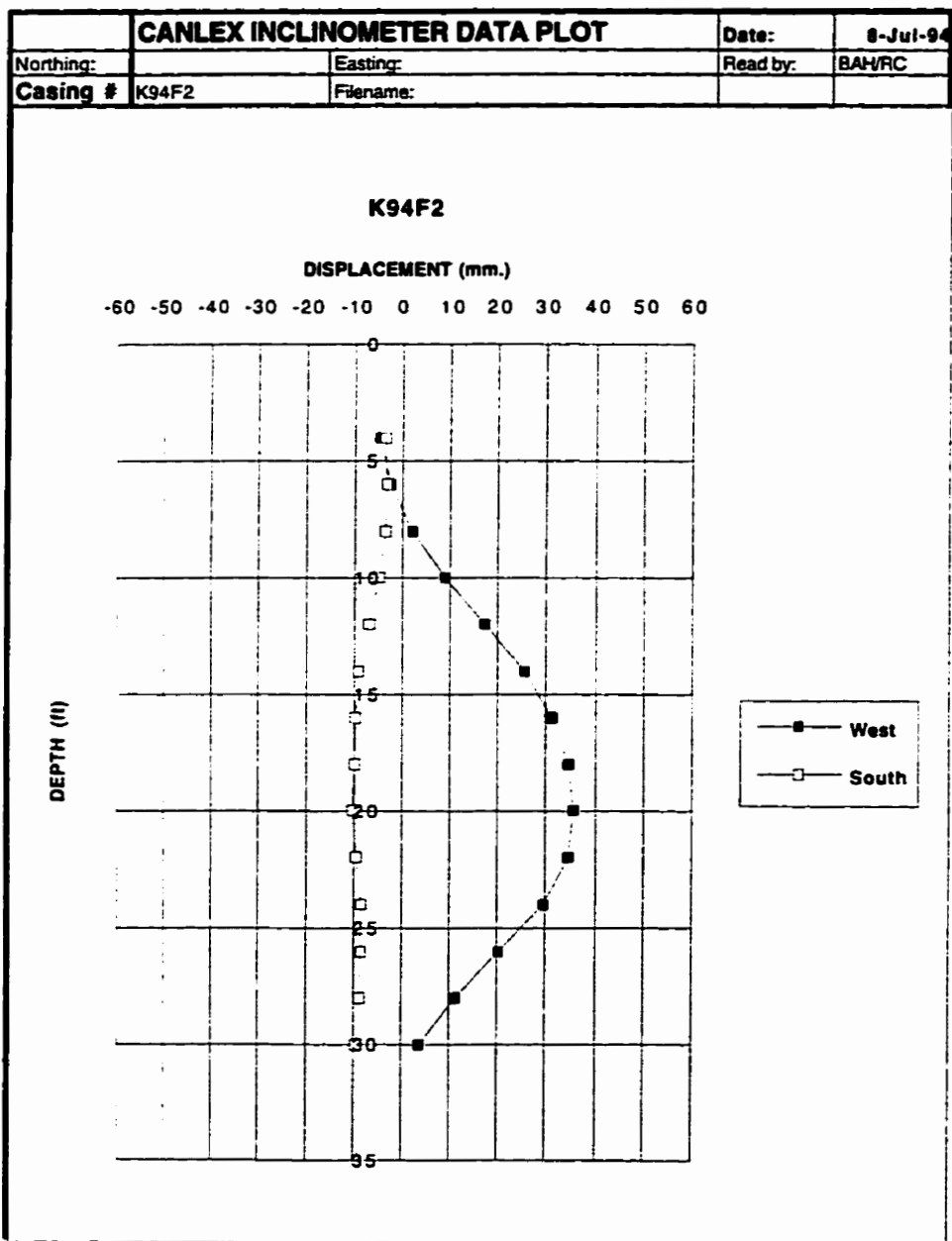


Figure C3: Deflection of Sample Borehole K94F2.

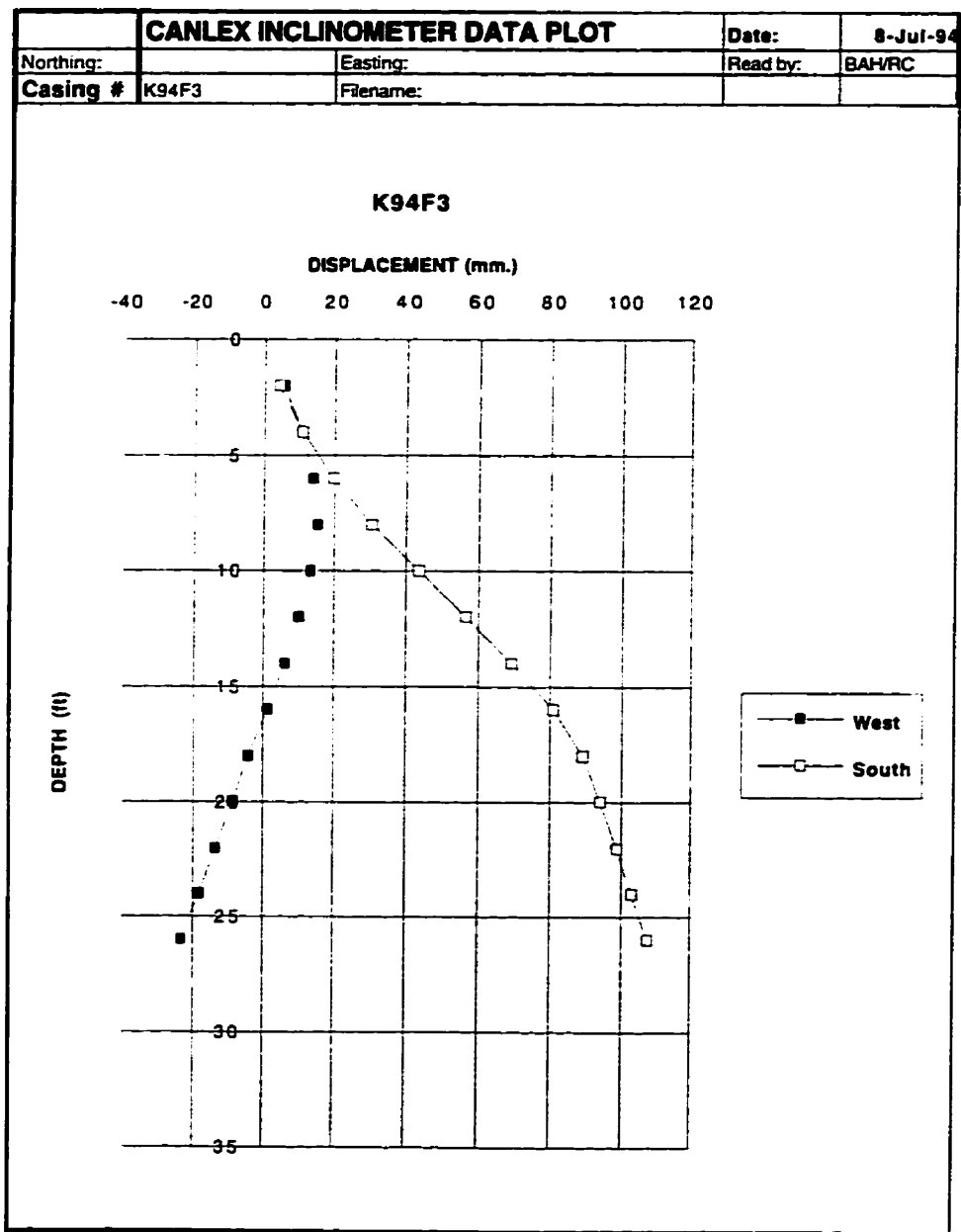


Figure C4: Deflection of Sample Borehole K94F3.

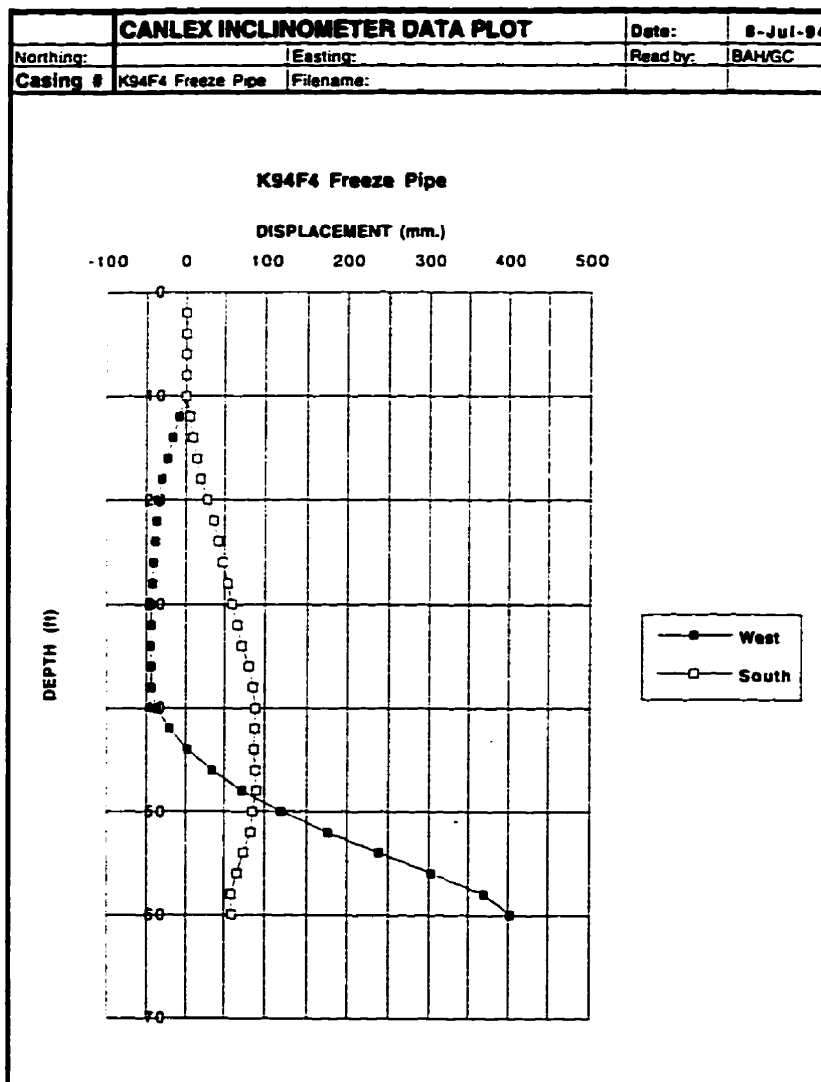


Figure C5: Deflection of Sample Borehole K94F4.

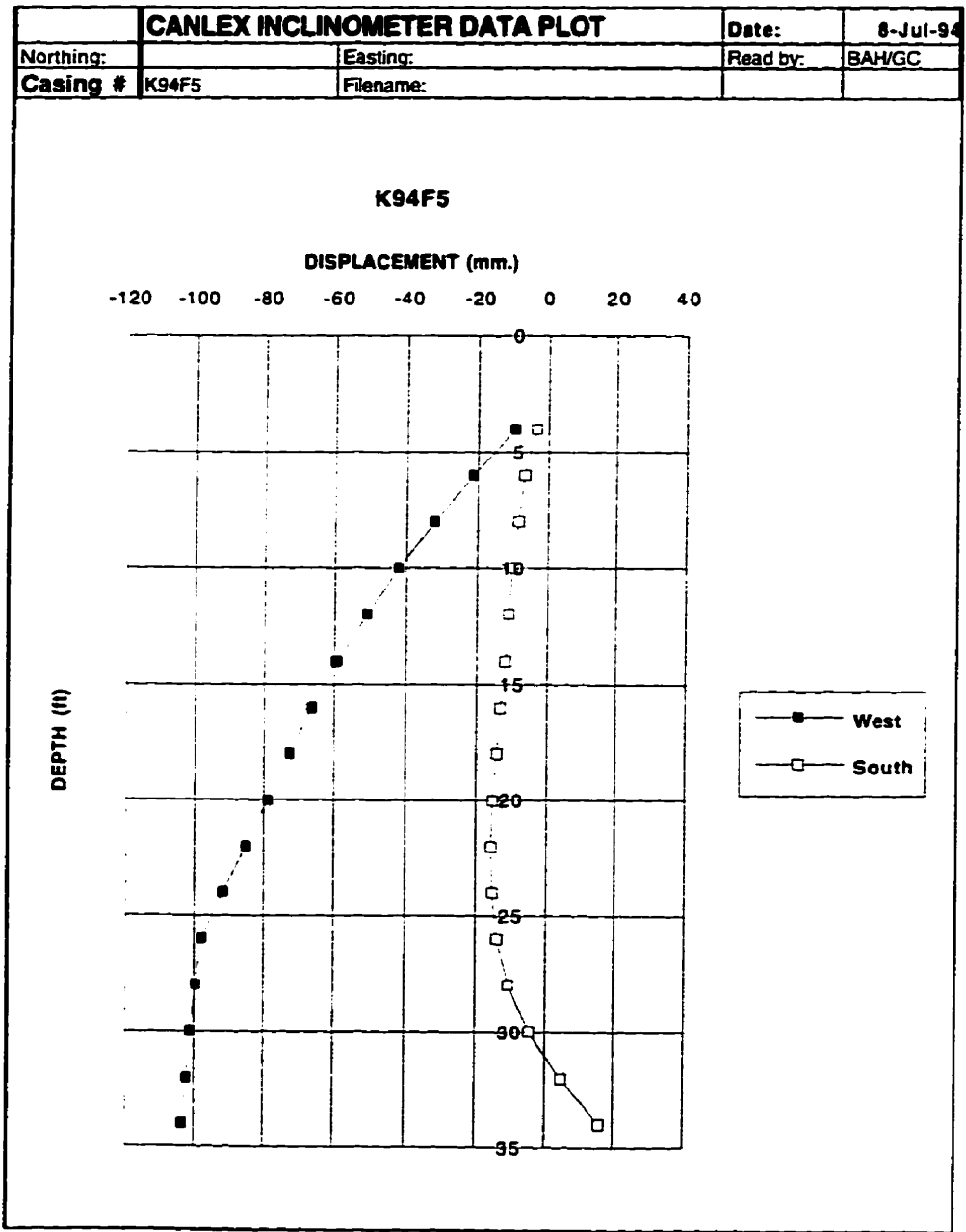


Figure C6: Deflection of Sample Borehole K94F5.

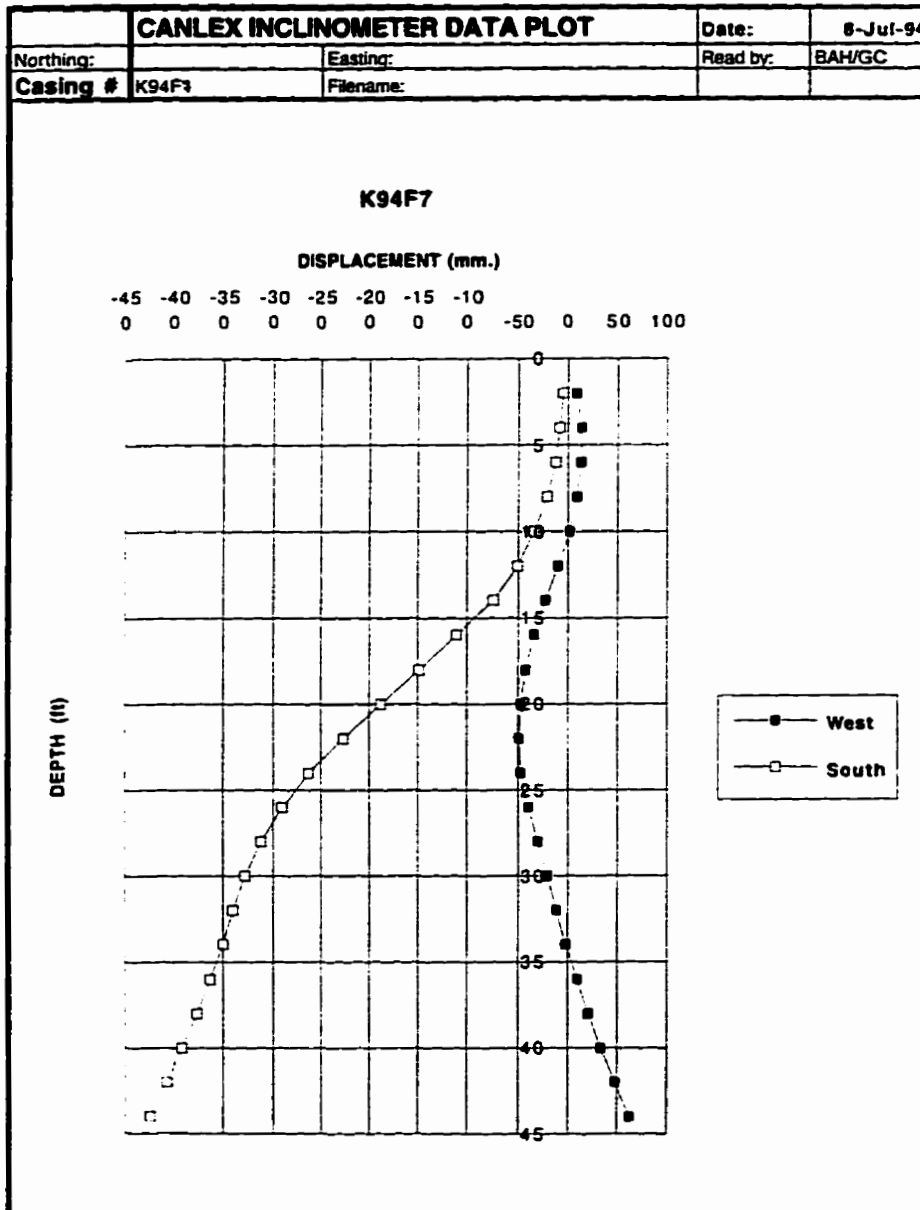


Figure C7: Deflection of Sample Borehole K94F7.

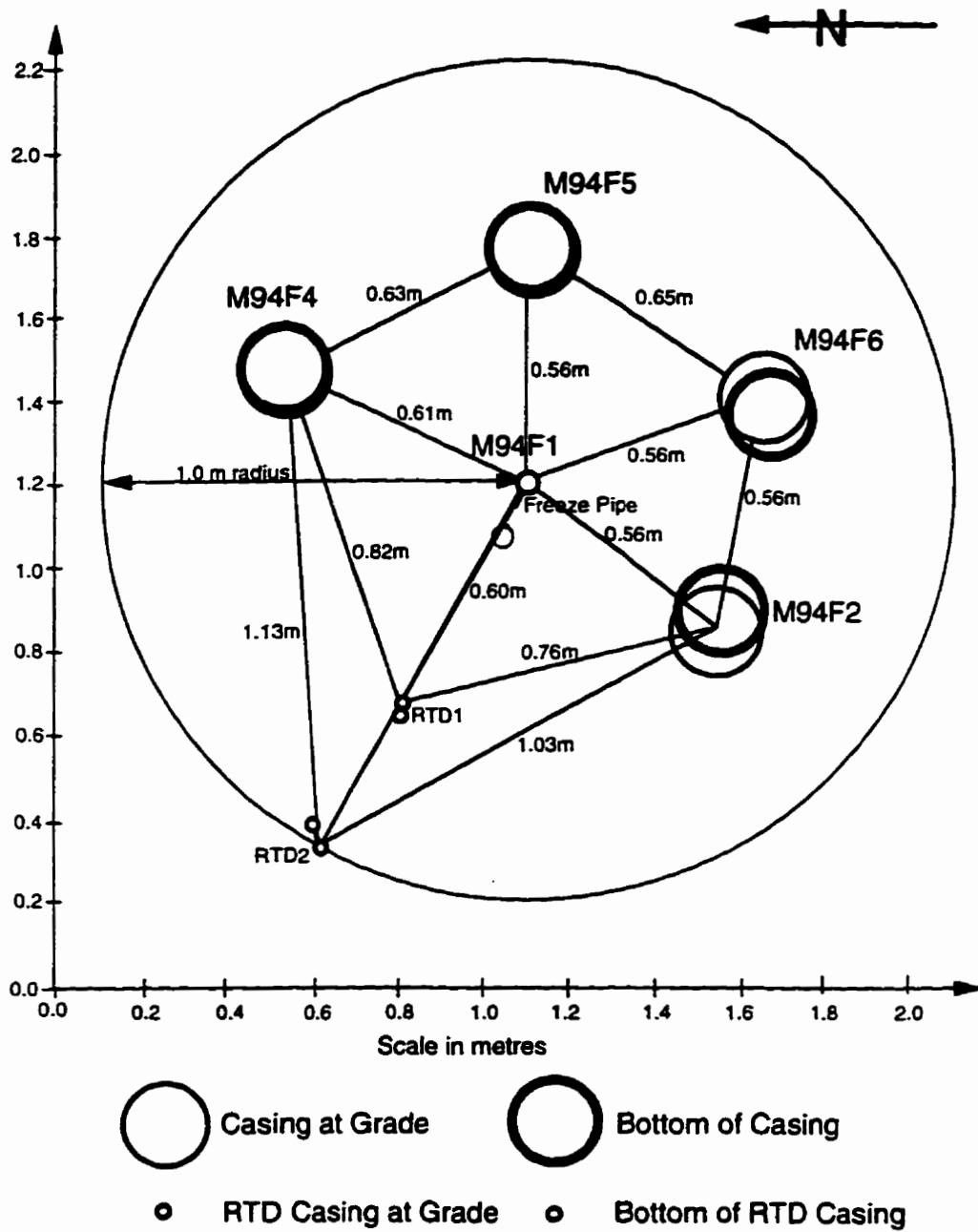


Figure C8: Alignment of Frozen Sample Boreholes at Massey Tunnel Site.

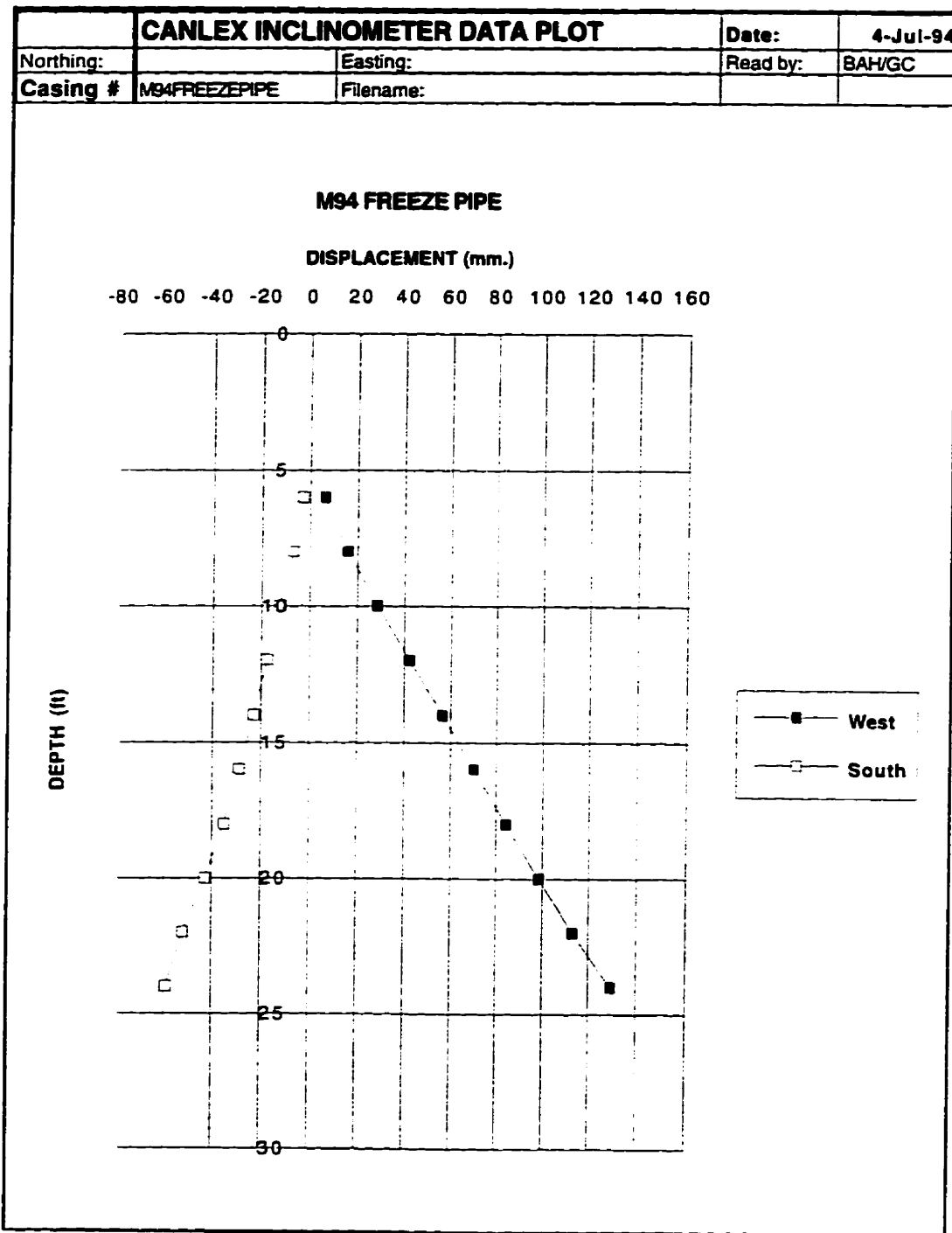


Figure C9: Deflection of Freeze Pipe Borehole at Massey Tunnel Site.

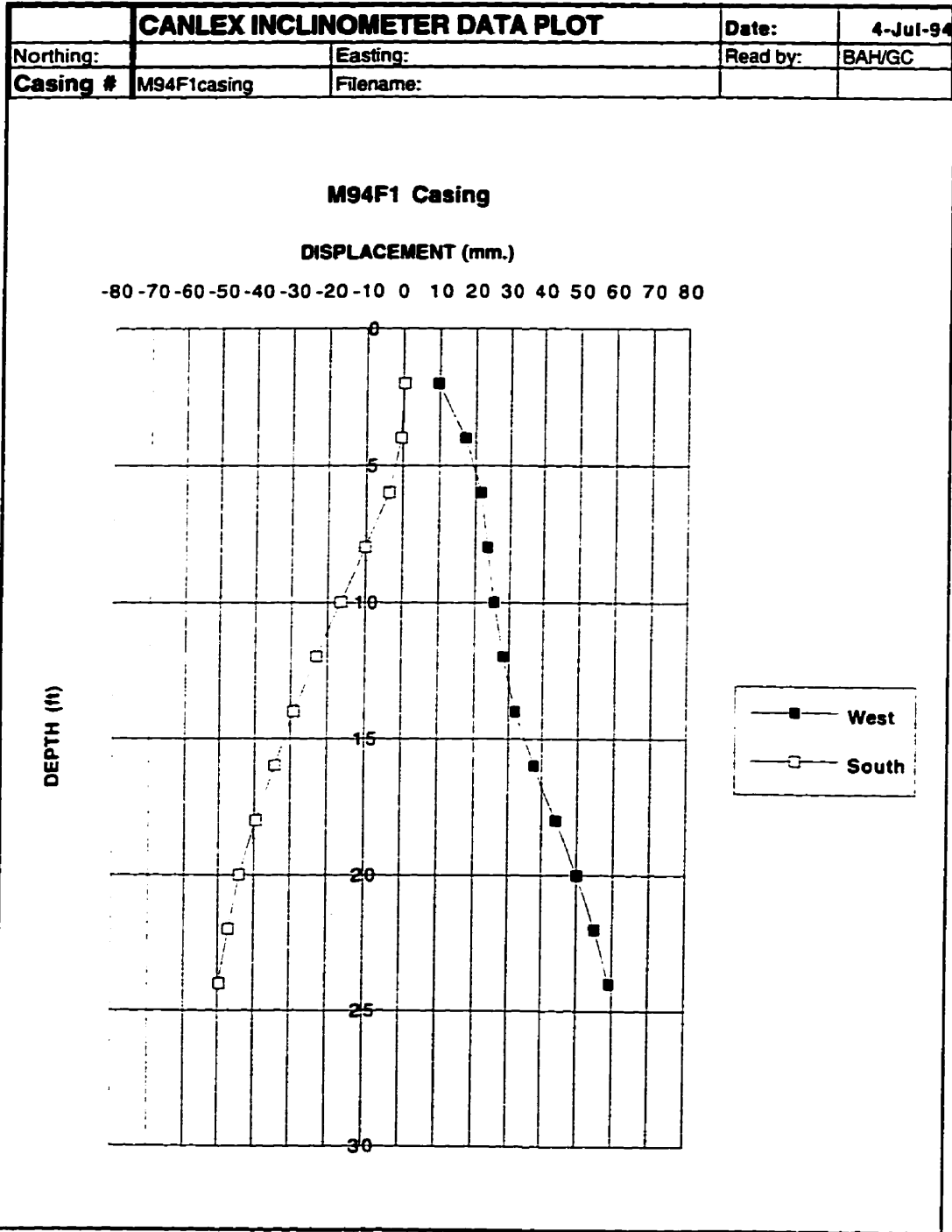


Figure C10: Deflection of Sample Borehole M94F1.

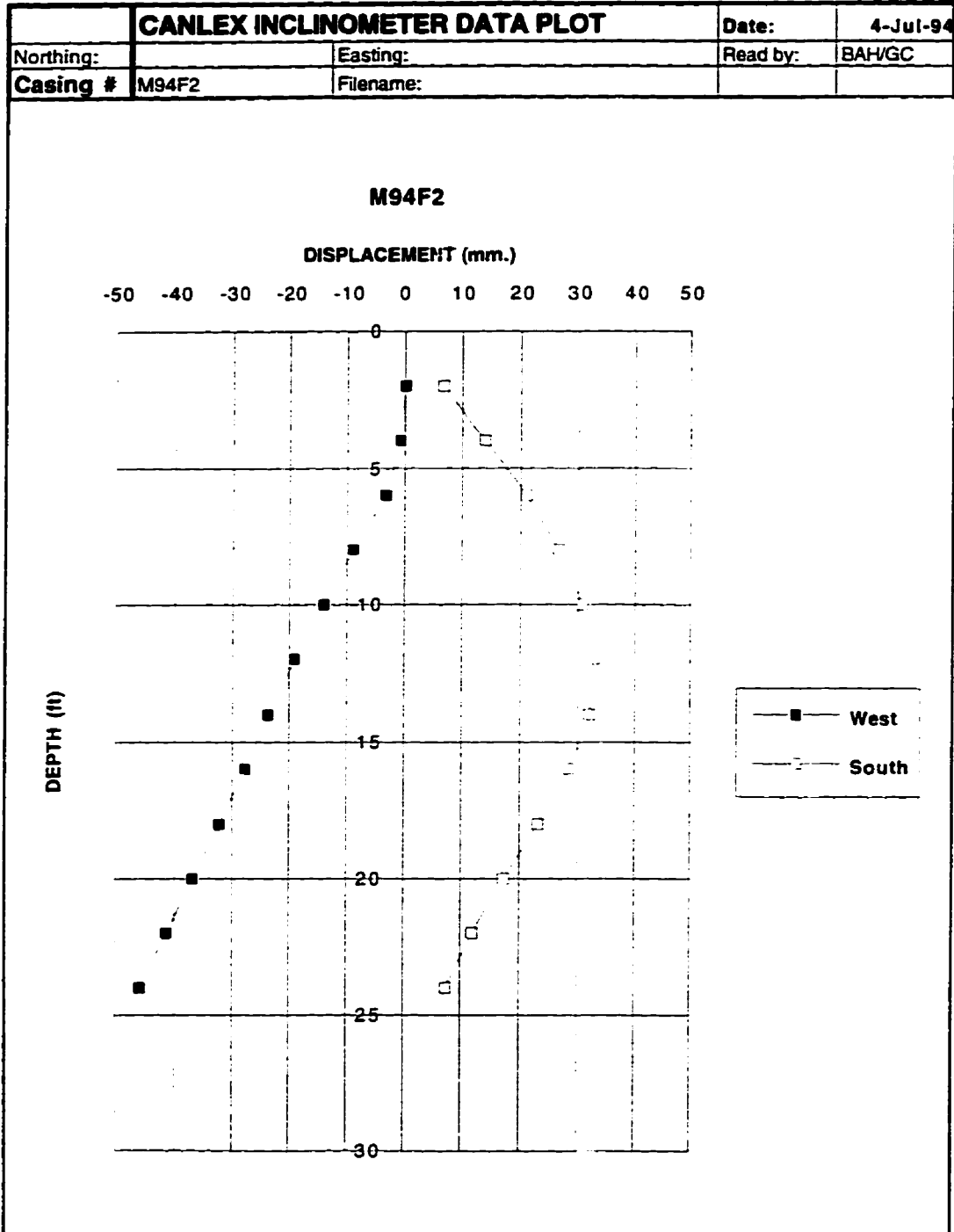


Figure C11: Deflection of Sample Borehole M94F2.

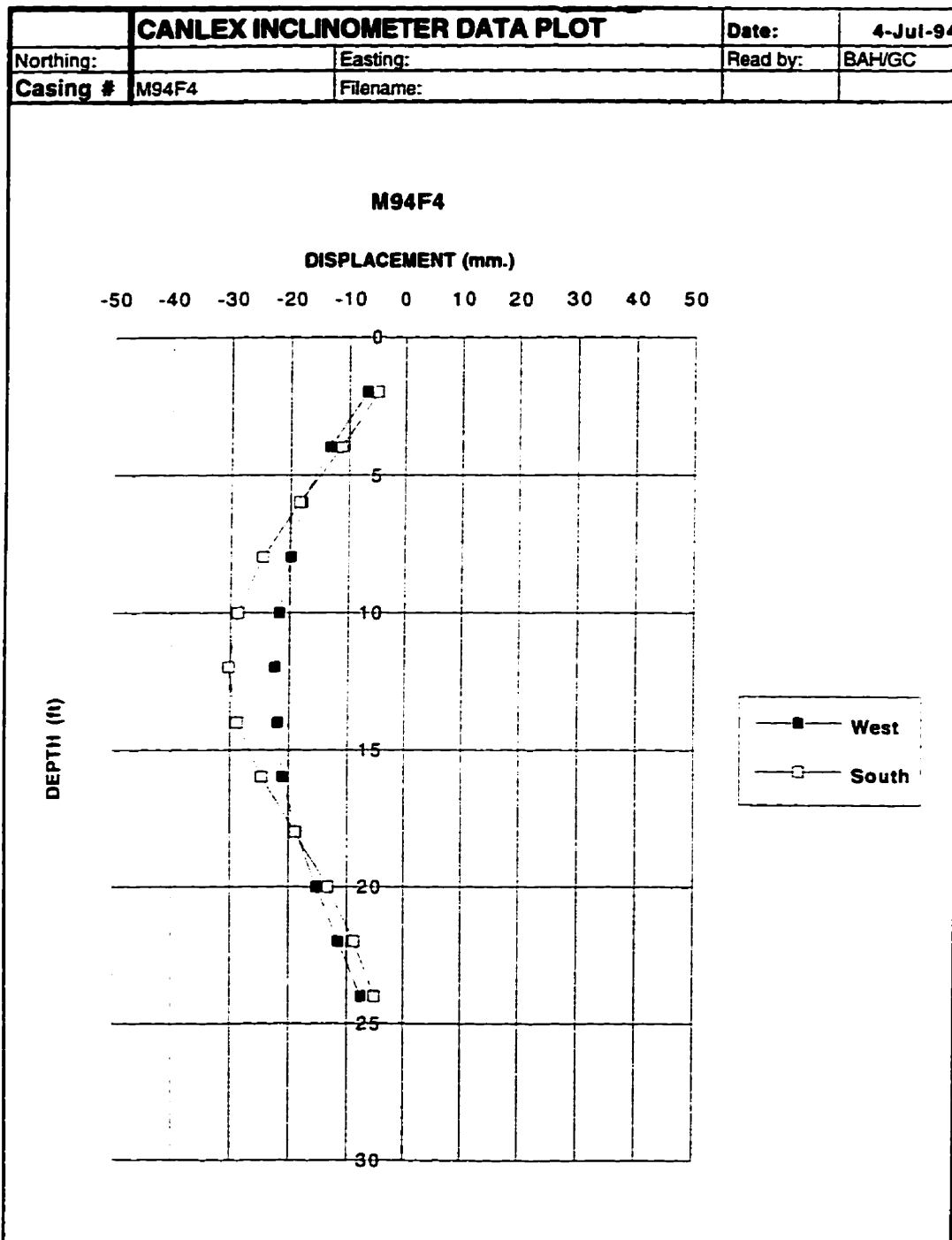


Figure C12: Deflection of Sample Borehole M94F4.

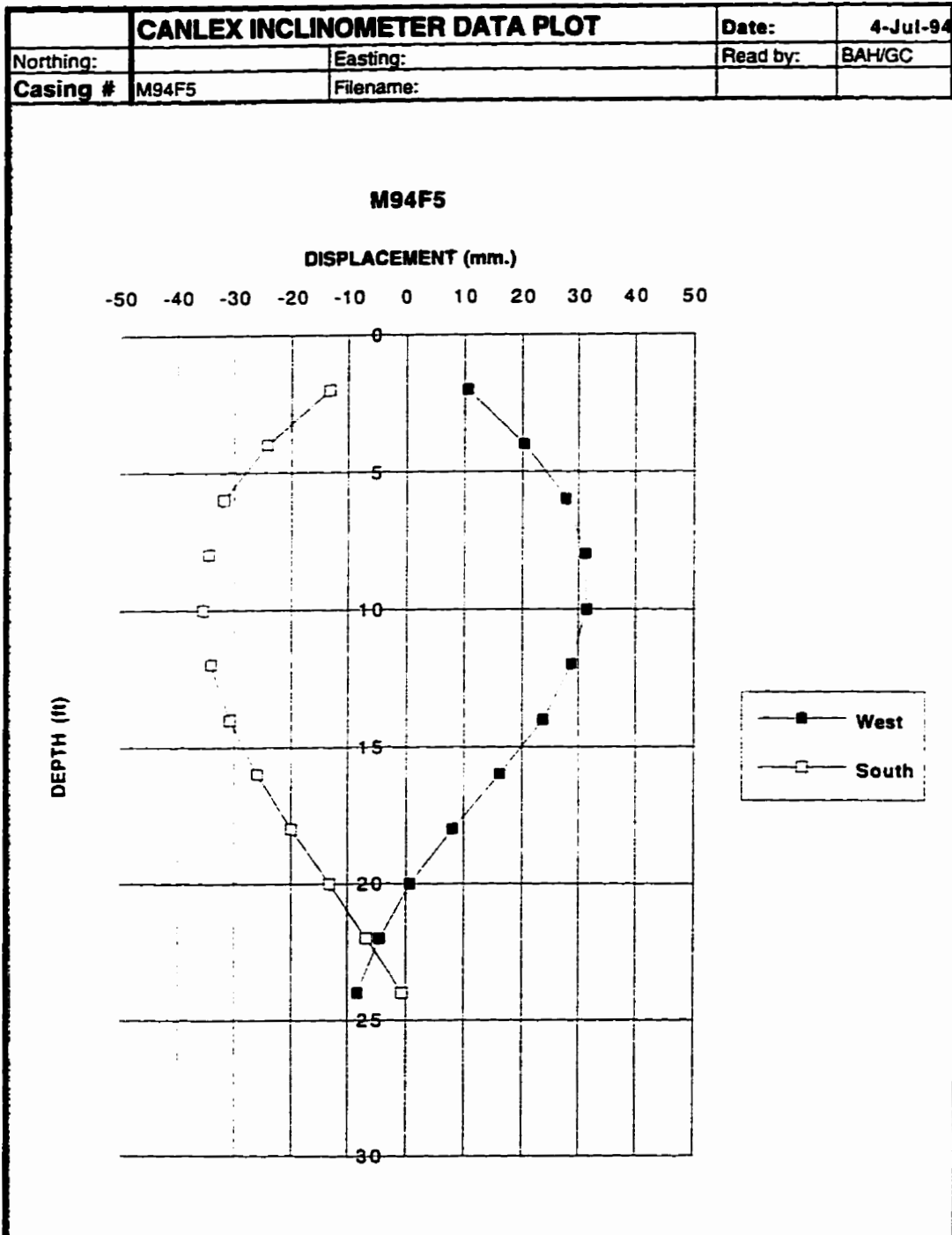


Figure C13: Deflection of Sample Borehole M94F5.

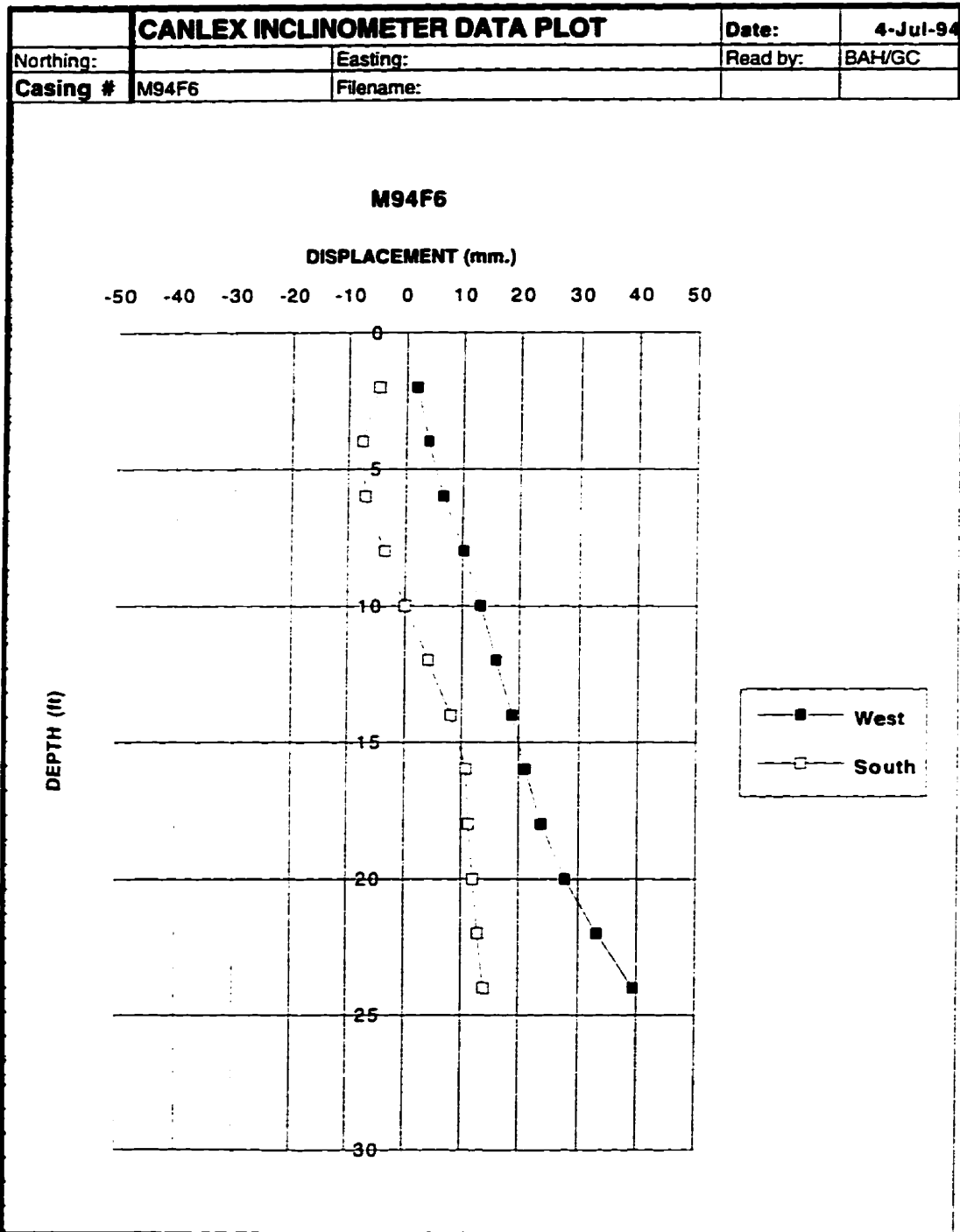


Figure C14: Deflection of Sample Borehole M94F6.

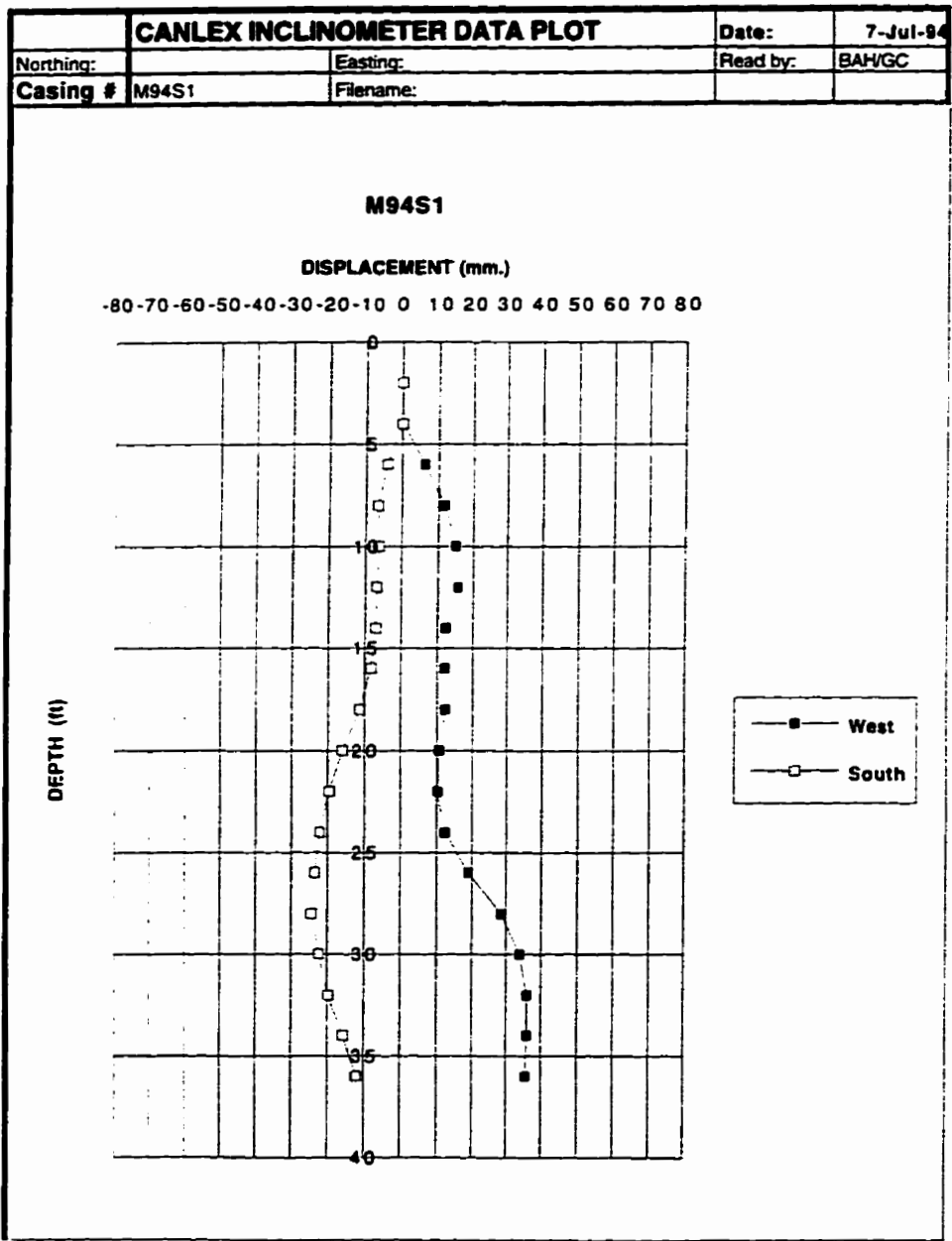


Figure C15: Deflection of Sample Borehole M94S1.

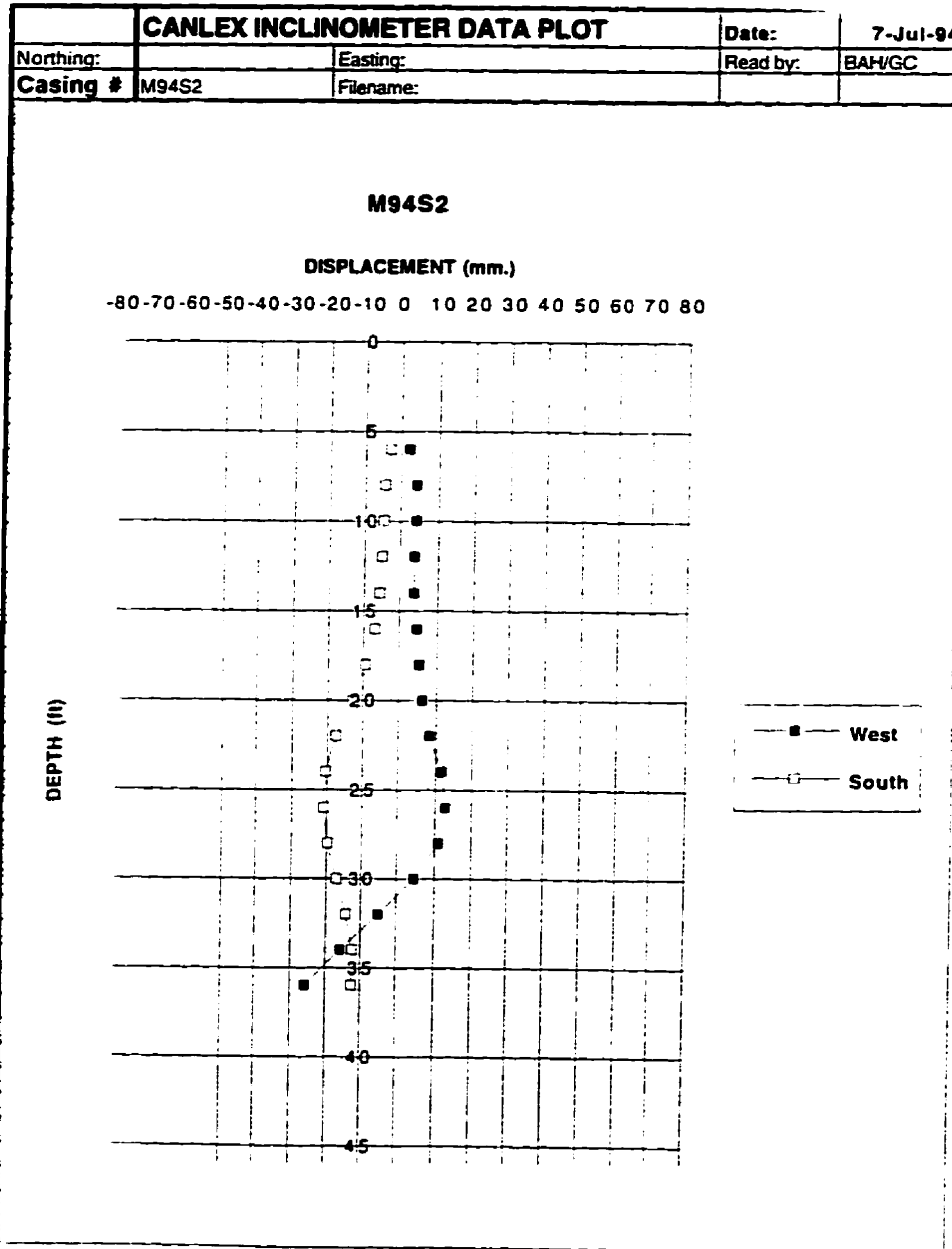


Figure C16: Deflection of Sample Borehole M94S2.

Appendix D: Phase III Test Site Ground Freezing Data

D.1. Introduction

Appendix D contains data associated with the in-situ ground freezing activities conducted at the Phase III test site. The spread sheet used for predicting the growth of the frozen zone is included in Table D1. The grain size curves determined from Split Spoon samples obtained from the detailed characterization zone are given and the grain size curves established for the two frozen core samples where thin, isolated ice lenses were encountered are also provided. The temperature data gathered during freezing at the Phase III test site is included in a summary table. Catalogues of the frozen core samples obtained using the 100 mm inner diameter and 200 mm inner diameter CRREL core barrel are also given.

Table D1: Spread Sheet used for Ground Freezing Predictions at the Phase III Test Site.

CANLEX - PHASE III LOOSE SAND CONDITIONS: EVENT SITE
 LIQUID NITROGEN
 GROUND TEMPERATURE 35°C

Sr m.c. = 0.33 p dry = 1.50 Mg/m³
 Va = 196 K Vo = 35.00 K
 Cu = C2 = 3.25 MJ/m³ K Cf = C1 = 2.16 MJ/m³ K
 L = 165.3 MJ/m³ Li = 579.49 MJ/m³
 K1 = Kf = 2.8 W/m K Ku = 1.45 W/m K
 ro = 0.025 m ar = 3.00
 STE = 3.85

R (m)	R/ro	LN (R/ro)	S+S meth		+J method		P (W/m)	N2 l requirement usin x l m lengt			Total Vol. LN2 (4m)	R* non-ste state	R*/ro non-steady	ln R*/ non steady state	non steady state t (hr)	Temperature distribution for R = 1m	
			t (hr)	t (hr)	Q(MJ/m)	Q/t (W/m)		N2 l (Mg)	N2 l (l)	N2 (m3/m)						r (m)	T (°C)
0.025	1	0.00	0.00	0.00	0.00	0.00	0.00	0	0	0	0	0.025	1.000	0.000	0	0.03	-196
0.05	2	0.69	0.20	0.06	6.95	9428.9	4974.7	0.03	43	63.27	253.0955	0.037	1.466	0.383	0.01	0.10	-122
0.1	4	1.39	1.84	0.74	23.00	2734.3	2487.4	0.12	143	209.42	837.685	0.073	2.933	1.076	0.28	0.15	-101
0.15	6	1.79	5.47	2.37	49.31	2012.0	1924.5	0.25	306	448.96	1795.842	0.110	4.399	1.481	0.98	0.20	-86
0.2	8	2.08	11.41	5.13	85.61	1697.4	1658.2	0.43	532	779.45	3117.811	0.147	5.866	1.769	2.23	0.25	-74
0.25	10	2.30	19.87	9.13	131.83	1517.2	1497.5	0.66	819	1200.26	4801.038	0.183	7.332	1.992	4.08	0.30	-64
0.3	12	2.48	31.02	14.46	187.93	1397.6	1387.7	0.94	1168	1711.01	6844.041	0.220	8.799	2.175	6.57	0.35	-56
0.35	14	2.64	44.99	21.20	253.88	1311.2	1306.6	1.28	1578	2311.44	9245.764	0.257	10.265	2.329	9.76	0.40	-49
0.4	16	2.77	61.90	29.40	329.66	1245.1	1243.7	1.66	2049	3001.35	12005.38	0.293	11.732	2.462	13.66	0.45	-42
0.45	18	2.89	81.84	39.14	415.25	1192.3	1193.0	2.09	2581	3780.56	15122.24	0.330	13.198	2.580	18.32	0.50	-37
0.5	20	3.00	104.90	50.44	510.63	1149.0	1151.0	2.57	3173	4648.94	18595.76	0.367	14.665	2.685	23.76	0.60	-27
0.55	22	3.09	131.15	63.35	615.79	1112.5	1115.5	3.09	3827	5606.36	22425.46	0.403	16.131	2.781	30.00	0.70	-19
0.6	24	3.18	160.68	77.92	730.72	1081.3	1085.0	3.67	4541	6652.73	26610.93	0.440	17.598	2.868	37.03	0.80	-12
0.65	26	3.26	193.53	94.18	855.41	1054.2	1058.4	4.30	5316	7787.95	31151.78	0.477	19.064	2.948	44.95	0.90	-6
0.7	28	3.33	229.78	112.15	989.84	1030.3	1034.8	4.97	6151	9011.92	36047.69	0.513	20.531	3.022	53.71	1.00	0
0.75	30	3.40	269.46	131.88	1134.02	1009.1	1013.8	5.70	7047	10324.59	41298.35	0.550	21.997	3.091	63.34	1.05	1.55
0.8	32	3.47	312.65	153.38	1287.94	990.0	994.9	6.47	8004	11725.87	46903.48	0.587	23.464	3.155	73.85	1.10	3.04
0.85	34	3.53	359.37	176.69	1451.58	972.8	977.8	7.29	9021	13215.71	52862.83	0.623	24.930	3.216	85.27	1.20	5.81
0.9	36	3.58	409.69	201.83	1624.94	957.1	962.2	8.17	10098	14794.04	59176.18	0.660	26.397	3.273	97.61	1.30	8.36
0.95	38	3.64	463.63	228.82	1808.01	942.8	947.9	9.09	11236	16460.82	65843.3	0.697	27.863	3.327	110.87	1.40	10.72
1	40	3.68888	521.24	257.68	2000.79	929.5	934.8	10.05	12434	18216.00	72863.98	0.733	29.330	3.379	125.07	1.50	12.92

Table D2: RTD Ground Temperature Data obtained at the Phase III Test Site.

CANLEX PHASE III - Ground Freezing RTD Readings														
RTD 1 Number	Depth (m)	Jun-07 BR	8:40 BW	Jun-07 BR	16:20 BW	Jun-08 BR	9:30 BW	Jun-08 BR	15:45 BW	Jun-09 BR	10:00 BW	Jun-09 BR		
25-12	2.50	115.92	1.34	116.27	1.69	111.30	1.05	111.63	1.38	111.28	1.17	111.40		
22-8	3.50	115.27	1.40	115.57	1.70	113.25	1.13	113.52	1.49	113.11	1.29	113.13		
7-12	4.50	115.93	1.36	116.27	1.65	115.35	1.58	115.66	1.89	115.20	1.68	115.13		
8-12	5.50	114.74	1.41	115.03	1.72	116.02	1.53	116.30	1.88	115.87	1.70	115.98		
2-12	6.50	115.40	1.41	115.70	1.72	116.03	1.54	116.32	1.84	115.90	1.68	115.89		
12-1	7.50	111.20	0.87	111.51	1.19	115.51	1.56	115.77	1.87	115.22	1.69	115.66		
6-12	8.50	113.16	0.96	113.43	1.23	114.79	1.59	115.08	1.91	114.90	1.78	115.12		
RTD 1 Number	Depth (m)	Jun-07 8:40 Temp.	Jun-07 16:20 Temp.	Jun-08 9:30 Temp.	Jun-08 15:45 Temp.	Jun-09 10:00 Temp.	Jun-09 15:40 Temp.	Jun-10 9:40 Temp.	Jun-10 16:40 Temp.	Jun-11 8:50 Temp.	Jun-11 17:20 Temp.	Jun-12 9:00 Temp.		
		25-12	37.36	37.38	28.28	28.28	25.92	25.77	25.49	25.21	24.92	24.64	24.49	
		22-8	35.56	35.56	31.08	30.85	30.31	29.97	29.08	28.69	27.77	27.28	26.49	
		7-12	37.36	37.48	35.31	35.31	34.67	34.44	33.44	33.05	31.95	31.28	29.90	
		8-12	34.18	34.13	37.15	38.97	36.33	36.05	35.03	34.69	34.74	33.36	33.10	30.97
		2-12	35.87	35.85	37.15	37.13	36.46	36.05	34.69	34.13	34.13	32.85	31.82	29.51
		12-1	28.49	28.46	35.77	35.64	34.69	35.26	32.87	32.44	32.44	31.36	30.36	28.56
		6-12	31.28	31.28	33.85	33.77	33.64	33.87	33.05	33.05	32.84	31.87	31.21	30.15

Table D2 continued: RTD Ground Temperature Data obtained at the Phase III Test Site.

15:40 BW	1.25	108.91	1.19	109.65	1.30	108.47	1.05	108.10	1.44	107.50	1.66	106.01	1.05	8:00 BW
1.28	110.13	1.22	110.34	1.33	108.25	1.06	107.64	1.46	106.81	1.66	104.96	1.06	9:00 BW	
1.28	110.34	1.17	110.30	1.28	108.27	1.06	107.53	1.44	106.67	1.63	104.74	1.03	9:00 BW	
1.61	110.63	1.53	110.31	1.67	108.42	1.40	107.57	1.81	106.25	1.98	104.15	1.38	9:00 BW	
1.66	109.44	1.56	109.06	1.68	105.71	1.42	103.95	1.81	103.06	2.03	101.23	1.53	9:00 BW	
1.65	106.70	1.58	106.26	1.68	101.02	1.41	100.15	1.81	98.72	2.00	98.56	1.41	9:00 BW	
Jun-13 8:00 Temp.	12.72	11.26	10.90	9.21	8.49	5.79	5.85	6.74	6.69	5.59	4.67	5.15	3.67	Jun-20 9:00 Temp.
10.00	7.54	7.23	1.26	0.64	0.08	0.79	0.79	1.56	1.59	1.18	0.97	0.92	0.79	Jun-19 16:00 Temp.
9.51	6.67	6.38	-0.03	-1.08	-1.44	-1.03	-1.03	-0.23	-0.10	-0.15	-0.69	-0.79	-0.92	Jun-19 9:00 Temp.
7.10	3.49	3.15	-6	-8.41	-3.31	-2.33	-2.33	-2.72	-2.23	-4.41	-3.54	-3.51	-4.18	Jun-18 15:00 Temp.
-0.77	-7.03	-3.51	-17.97	-18.87	-7.92	-5.31	-5.31	-6.56	-5.62	-9.69	-7.38	-7.15	-8.33	Jun-17 14:00 Temp.
-12.44	-15.38	-7.13	-21.03	-22.33	-8.56	-5.51	-5.51	-8.49	-6.90	-13.31	-8.90	-8.62	-10.36	Jun-17 9:30 Temp.
														Jun-16 13:00 Temp.
														Jun-16 7:50 Temp.
														Jun-16 13:00 Temp.
														Jun-17 14:00 Temp.
														Jun-17 9:30 Temp.
														Jun-18 15:00 Temp.
														Jun-19 9:00 Temp.
														Jun-19 16:00 Temp.
														Jun-20 9:00 Temp.

Table D2 continued: RTD Ground Temperature Data obtained at the Phase III Test Site.

Jun-14	9:30	Jun-14	17:00	Jun-16	8:15	Jun-15	13:00	Jun-16	7:50	Jun-16	13:00	Jun-17
BR	BW	BR	BW	BR	BW	BR	BW	BR	BW	BR	BW	BR
105.27	0.88	105.15	0.90	104.44	0.85	104.24	0.93	103.11	0.85	103.19	0.91	103.49
103.82	0.88	103.72	0.90	101.36	0.87	101.16	0.91	100.90	0.87	101.22	0.91	101.48
103.48	0.88	103.36	0.87	100.84	0.85	100.43	0.85	100.28	0.84	100.50	0.90	100.75
102.56	1.20	102.45	1.22	14.44	1.18	97.93	1.21	98.89	1.18	100.33	1.24	100.14
98.48	1.22	99.86	1.23	94.18	1.19	93.85	1.21	98.11	1.20	99.16	1.25	98.65
95.22	1.22	98.47	1.25	92.98	1.18	92.49	1.20	97.86	1.20	99.09	1.24	97.89

Table D2 continued: RTD Ground Temperature Data obtained at the Phase III Test Site.

9:30 BW	Jun-17 BR	14:00 BW	Jun-18 BR	15:00 BW	Jun-19 BR	9:00 BW	Jun-19 BR	15:00 BW	Jun-20 BR	9:00 BW
0.86	103.48	0.87	103.02	0.84	102.64	0.82	102.83	0.82	102.33	0.82
0.87	101.52	0.90	101.31	0.85	101.22	0.84	101.19	0.83	101.14	0.83
0.84	100.81	0.85	100.77	0.83	100.54	0.81	100.50	0.81	100.45	0.81
1.20	100.34	1.21	99.47	1.19	99.78	1.16	99.78	1.15	99.51	1.14
1.21	99.03	1.22	97.41	1.19	98.29	1.17	98.37	1.16	97.91	1.16
1.20	98.52	1.21	95.99	1.18	97.70	1.17	97.80	1.16	97.12	1.16

Table D3: Catalogue of 100 mm diameter Frozen Core.

SYNCRUDE PHASE III - 4" Diameter

Sample #	Depth (ft.)	Dry Weight	Ice Content	Dry Weight	Proton Weight	Volume (cm ³)	P(Lab)		WAVI		Comments	Lab Testing	Proton/Gross
							Proton density	Dry density	Proton density	Dry density			
F50 C1	10'11"-11'0"	26.29	241.01	304.37	187.84	1.4351	1.4351	1.4351	1.4351				90.87
F50 C2	10'-10'7"	5.88											
F50 C3	21'0"	6.65											
F50 C4	21'7"-22'7"	6.87											
F502 C1-Top	7'0"	18.06	204.30	243.24	120.22	1.8894	1.8894	1.8894	1.8894				100.82
F502 C1-1	7'10"-8'4"	2.28											
F502 C1-2	8'4"-8'10"	2.48											
F502 C1-3	8'10"-9'4"	2.77											
F502 C1-Bot.	9'0"	2.80											
F502 C2-Top	9'8"-9'10"	2.85											
F502 C2-1	10'0"-10'6"	3.12											
F502 C2-Mid.	10'7"	3.23											
F502 C2-2	10'8"-11'2"	3.33											
F502 C2-3	11'2"-11'8"	3.48											
F502 C2-Bot.	12'0"	3.88											
F502 C3-Top	12'3"	3.73											
F502 C3-1	12'9"-12'11"	3.86											
F502 C3-2	12'11"-13'5"	4.01											
F502 C3-Mid.	13'6"	4.11											
F502 C3-3	13'6"-14'0"	4.16											
F502 C3-4	14'0"-14'6"	4.34											
F502 C3-Bot.	14'10"	4.82											
F502 C4A	14'10"-15'10"	4.85											
F502 C4C	15'10"-16'2"	4.88											
F502 C4B	16'3"-16'9"	5.03											
F502 C4E	17'4"	5.26											
F502 C4F	16'11"-16'7"	5.69											
F502 C4D	16'7"-16'10"	6.70											
F502 C4H	18'10"-20'1"	5.78											
F502 C4A	20'1"-21'1"	6.17											
F502 C4B	21'1"-22'6"	6.61											
F502 C7	20'1"-20'4"	6.16											
		28.35	307.88	388.33	217.54	1.8311	1.8311	1.8311	1.8311				88.81

Table D4: Catalogue of 200 mm diameter Frozen Core.

SYNCRUDE PHASE III - 8" Diameter

Sample #	Depth (ft.)	Ice Content	Dry Weight	Frozen Weight	Volume (cu ft)	Frozen density	Dry density	Yield ratio	Dry density	Comments	Lab Testing	Specific Gravity
FS20 C1-1	10'0"-10'2"	23.00	328.50	400.35	208.89	1.9168	1.5582	0.6815	1.5582	Few specks of bitumen.		99.43
FS20 C1-2	10'2"-10'8"	22.23	287.27	351.13	189.12	1.8987	1.5190	0.7248	1.5190	Several bitumen specks.		97.63
FS20 C1-3	10'8"-10'9"	24.08	390.00	483.65	259.27	1.8802	1.5043	0.7417	1.5042	Several bitumen specks.		92.66
FS20 C1-4B	10'9"-11'0"	24.16	729.83	906.29	483.75	1.8735	1.5089	0.7383	1.5089	Little bitumen, cracking.		93.74
FS20 C2-A	10'9"	24.65	211.84	264.24	143.26	1.8445	1.4787	0.7708	1.4787	Few specks of bitumen.		91.39
FS20 C2-B	10'9"	24.44	192.32	239.33	127.59	1.8762	1.5077	0.7377	1.5077	Few specks of bitumen.	UBC	94.86
FS20 C2-1	10'7"-11'1"	3.30								N/A	UBC	
FS20 C2-2	11'1"-11'7"	3.45								N/A	UBC	
FS20 C2-2A	11'7.5"	25.84	236.65	299.83	160.49	1.8882	1.4870	0.7820	1.4870	Few specks of bitumen.		96.14
FS20 C2-2B	11'7.5"	25.36	260.72	326.84	174.40	1.8741	1.4950	0.7526	1.4950	Few specks of bitumen.		96.26
FS20 C2-3	11'9"-12'3"	3.66								N/A		
FS20 C2-4	12'3"-12'9"	3.81								N/A		
FS20 C2-5	12'9"-13'3"	3.86								N/A		
FS20 C2-6	13'3"-13'9"	4.11								N/A		
FS20 C3-5A	13'9"	26.94	243.76	308.45	164.42	1.8760	1.4825	0.7873	1.4825	Several bitumen specks.		96.83
FS20 C3-6B	13'9"	26.11	243.97	312.55	170.05	1.8280	1.4347	0.8282	1.4347	Loaded bitumen.		97.21
FS20 C3-A	14'9"	26.30	237.85	305.16	167.30	1.8240	1.4217	0.8429	1.4217	Little bitumen, cracking.		95.89
FS20 C3-B	14'9"	26.74	255.07	330.93	182.28	1.8155	1.3993	0.8723	1.3993	Few specks of bitumen.		97.41
FS20 C3-1	14'7"-15'1"	4.82								Cracks, lots of bitumen.	UBC	
FS20 C3-2	15'2"-15'8"	4.70								Cracks, fines, bitumen.		
FS20 C3-3	15'8"-16'2"	4.85								Cracks, fine pebbles.		
FS20 C3-4	16'3"-16'9"	5.03								Cracks only.		
FS20 C3-5	16'9"-17'3"	5.16								Cracks, fine pebbles.		
FS20 C3-6	17'3"	5.26								Few specks of bitumen.		96.17
FS20 C4	17'9"	5.33	172.03	220.74	120.89	1.8260	1.4231	0.8411	1.4230	Few specks of bitumen.		93.21
FS20 C4-1	17'9"-18'3"	5.49	244.06	302.77	161.44	1.8764	1.5149	0.7289	1.5149	Few specks of bitumen.		
FS20 C4-2	18'3"-18'9"	5.64								Top: Cracks visible.	UBC	
FS20 C4-3	18'9"-19'3"	5.79								Top: OK, Bot: Fines.		
FS20 C4-3A	19'3.5"	5.88	332.11	419.01	223.36	1.8759	1.4868	0.7821	1.4869	Top: Fines, bitumen.		96.11
FS20 C4-3B	19'3.5"	5.88	332.86	416.99	223.79	1.8722	1.4973	0.7816	1.4974	Few specks of bitumen.		97.10
FS20 C4-4	19'6"-20'0"	6.02								Few specks of bitumen.		
FS20 C4-4A	20'1.5"	6.13	249.80	308.25	164.63	1.8735	1.5122	0.7325	1.5122	Top Bot: Cracks, fines.		93.16
FS20 C4-4B	20'1.5"	6.13	248.55	310.38	163.38	1.8999	1.5278	0.7191	1.5278	Little bitumen, fines pebb.		97.38
FS20 C5-A	20'9"	23.96	226.84	279.84	150.10	1.8650	1.5045	0.7414	1.5046	Several bitumen specks.		92.33
FS20 C5-B	20'9"	23.85	230.89	289.82	151.84	1.8611	1.5177	0.7283	1.5178	Several bitumen specks.		94.21
FS20 C5-1	20'7"-21'1"	6.35								Top: Lots of bitumen.		
FS20 C5-2	21'2"-21'8"	6.53								N/A		
FS20 C5-3	21'8"-22'2"	6.68								N/A		
FS20 C5-4	22'2"-22'8"	6.83								Top: Lots of bitumen.	UBC	

Table D4 continued: Catalogue of 200 mm diameter Frozen Core.

SYNCRUDE PHASE III - 8" Diameter

Sample #	Depth (ft)	Depth (ft)	Ice Content	Dry Weight	Frozen Weight	Volume (cu ft)	Frozen density	PM100		WAVI		Comments	Lab Testing	Percent Oil
								Dry density	Void ratio	Dry density	Void ratio			
F54 C1	11'1"	3.28	24.76	184.08	182.20	101.72	1.8886	1.6145	0.7289	1.6146		No bitumen. Top tapered; bottom OK Blumen specks.		88.82
F54 C1-1	11'3"-11'7"	3.48												
F54 C1-2	11'7"-12'2"	3.62												
F54 C1-3	12'2"-12'8"	3.78												
F54 C1-3A	12'8"	3.88	30.18	225.76	283.89	165.18	1.7781	1.3688	0.9171	1.3687		Bot.: open, and cracks Little bitumen, cracking LEC		84.02
F54 C1-3B	12'8"	3.88	30.17	223.62	281.09	162.78	1.7881	1.3737	0.9073	1.3737		Little bitumen, cracking LEC		85.01
F55 CIA-1Top	10'8"	3.20	26.54	126.48	166.78	95.78	1.8508	1.4743	0.7772	1.4743		Very little bitumen.		93.80
F55 CIA-1Bot	10'8"	3.20	26.03	107.60	135.94	73.82	1.8495	1.4851	0.7882	1.4851		Very little bitumen Too short for analysis.		84.35
F55 CIA	10'8"-10'11"	3.26												
F55 CIB-1Top	11'0"	3.35	26.78	82.34	104.40	56.42	1.8504	1.4584	0.7852	1.4584		No bitumen.		96.25
F55 CIB-1Bot	11'0"	3.35	26.16	58.22	73.45	39.71	1.8497	1.4681	0.7870	1.4681		Cracks on bottom		84.97
F55 CIB-1	11'0"-11'6"	3.43												
F55 CIB-2	11'6"-12'0"	3.58												
F55 CIB-2A	12'0"	3.66	26.89	100.03	128.93	72.16	1.7887	1.3882	0.8900	1.3882		Cracks on top.		82.74
F55 CIB-2B	12'0"	3.66	26.71	83.45	107.41	59.37	1.8092	1.4058	0.8660	1.4058		Very little bitumen. Very little bitumen.		84.85
F55 CIB-3	12'0"-12'8"	3.73												
F55 CIB-4	12'8"-13'0"	3.89												
F55 CIB-4Bot	13'3"	4.04	25.83	144.15	181.58	97.18	1.8593	1.4834	0.7415	1.4834		N/A N/A Very little bitumen.		88.88
F56 CIA-A	8'8"	1.96	24.63	186.33	207.13	119.24	1.7371	1.3949	0.7008	1.3949		Several bitumen specks.		100.00
F56 CIA-B	9'5"	1.96	24.93	188.63	199.42	113.67	1.7559	1.4055	0.7122	1.4058		Very little bitumen. Bot.: Leth 2" from side Top: Leth 2" from side.		100.01
F56 CIA-1	8'8"-7'0"	2.08												
F56 CIA-2	7'0"-7'8"	2.21												
F56 CIA-3	7'8"-8'0"	2.38												
F56 CIB-A	8'7"-8'8"	2.84	23.40	150.10	185.22	87.85	1.8810	1.5324	0.7088	1.5324		Bottom: Cracking		84.20
F56 CIB-B	8'7"-8'8"	2.84	22.18	316.48	386.71	201.03	1.9239	1.5743	0.6842	1.5743		Little bitumen, cracking.		85.48
F56 CIB	8'0"	2.74	24.88	529.03	689.65	353.77	1.8646	1.4854	0.7820	1.4854		Loaded bitumen, cracking Several bitumen specks.		83.80
F56 CIB-A	9'0"	2.74	26.18	328.71	415.85	220.89	1.8822	1.4818	0.7881	1.4820		Few specks of bitumen		88.88
F56 CIB-B	9'0"	2.74	25.88	321.30	404.39	214.68	1.8838	1.4888	0.7804	1.4888		Little bitumen, cracking		88.48
F56 CIB-1	8'1"-8'7"	2.84												
F56 CIB-B	9'7"	2.82	24.78	272.48	334.78	177.28	1.8887	1.5158	0.7307	1.5158		Top: cracks, bitumen Several bitumen specks.		88.82
F56 CIB-A	9'7"	2.82	23.82	272.28	337.18	178.60	1.8878	1.5248	0.7188	1.5248		Few specks of bitumen Blumen specks		84.73
F56 CIB-2	8'8"-10'3"	3.04												

Figure D1: Grain Size Curves Obtained from Split Spoon Samples recovered from Borehole SPT1.

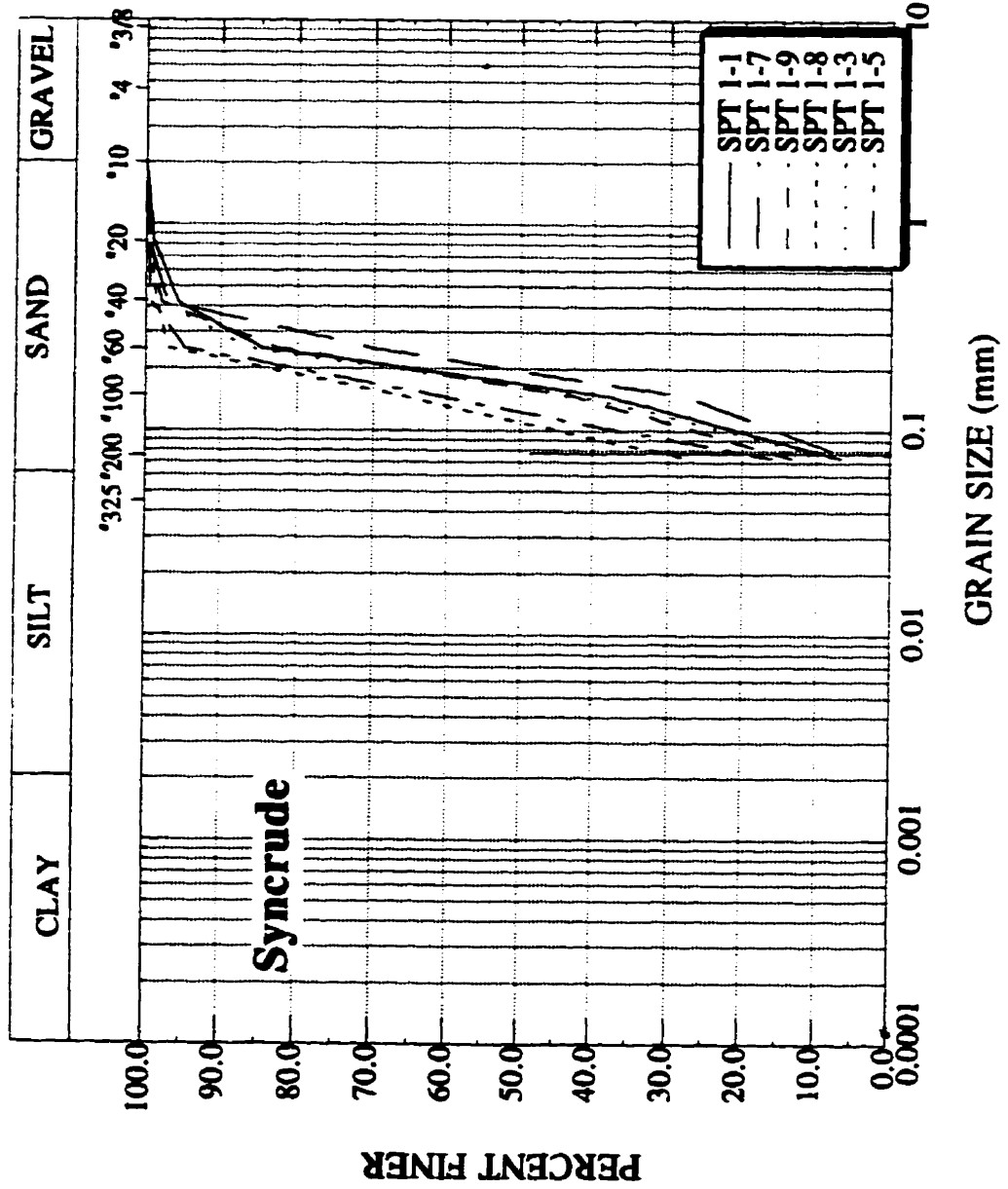


Figure D2: Grain Size Curves Obtained from Split Spoon Samples recovered from Borehole SPT2.

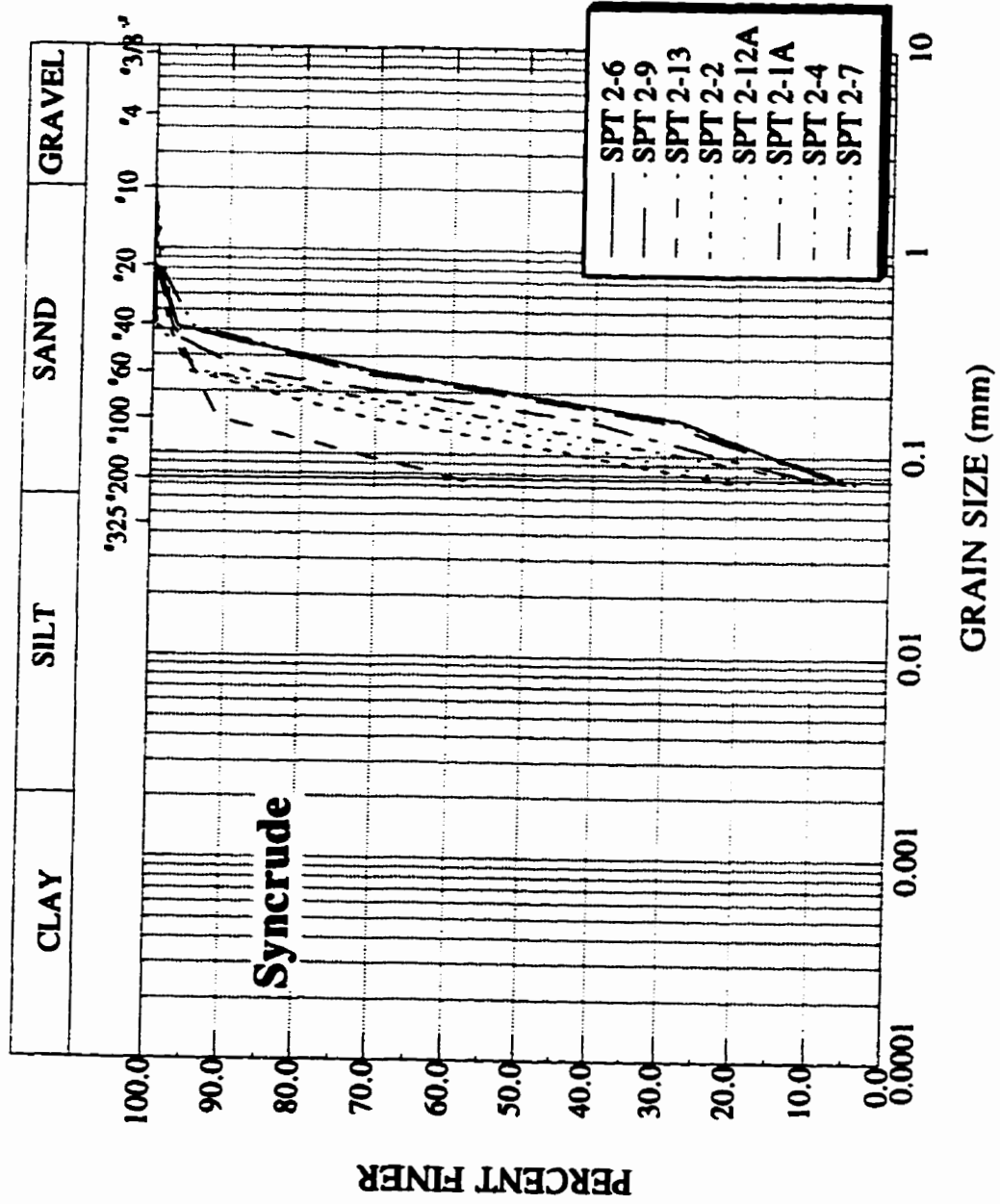
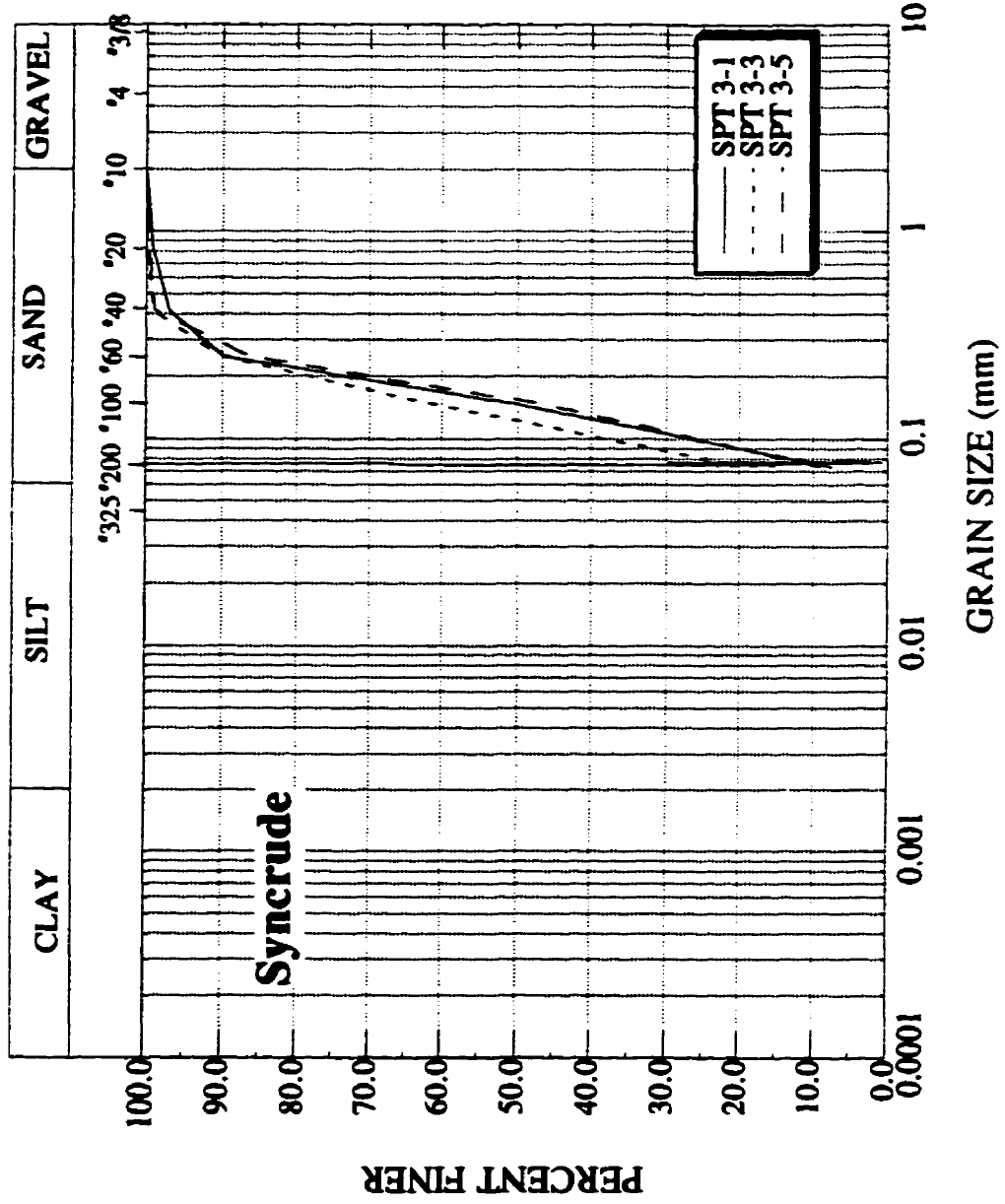


Figure D3: Grain Size Curves Obtained from Split Spoon Samples recovered from Borehole SPT3.



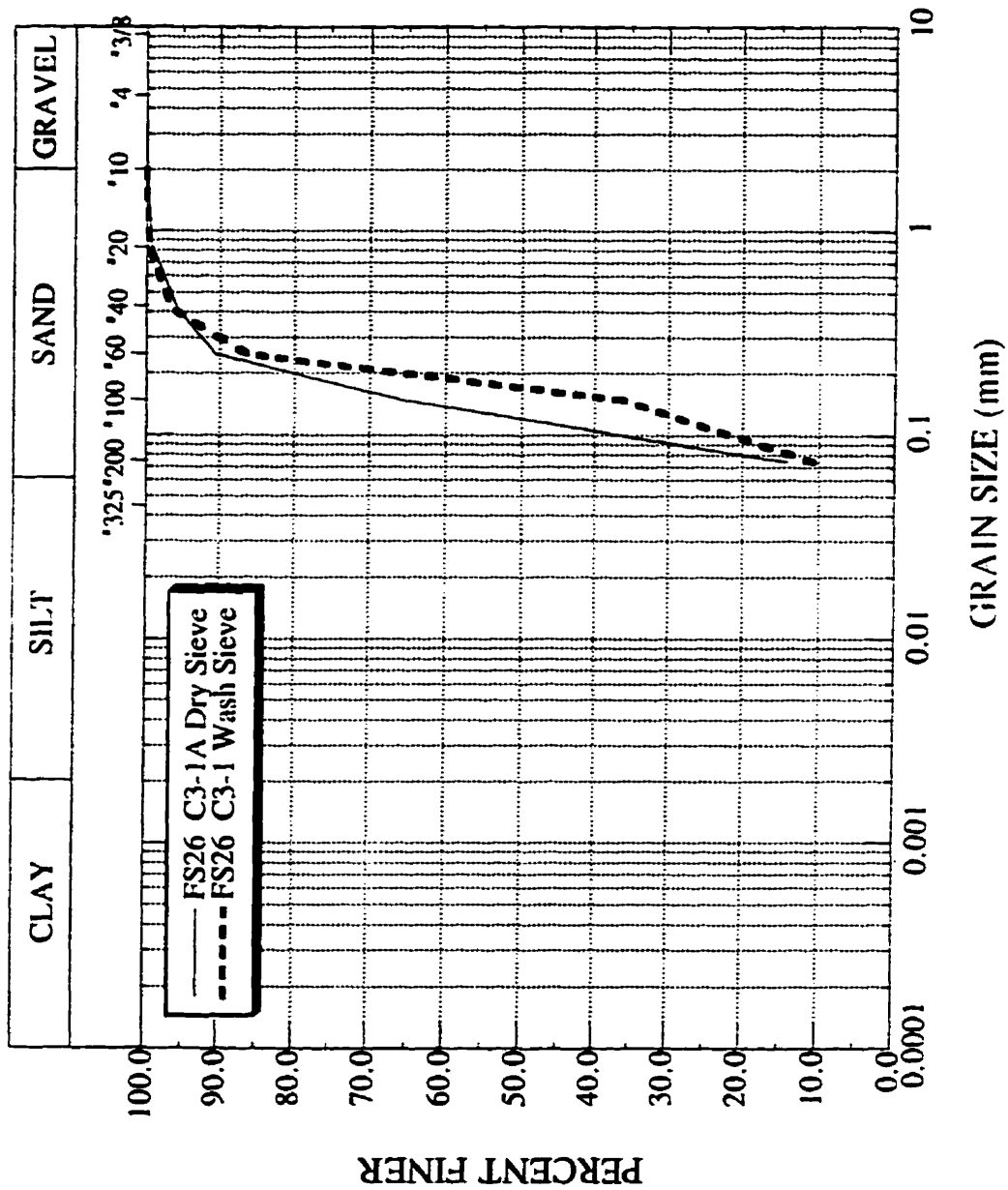


Figure D4: Grain Size Curves Obtained from FS26 C3-1.

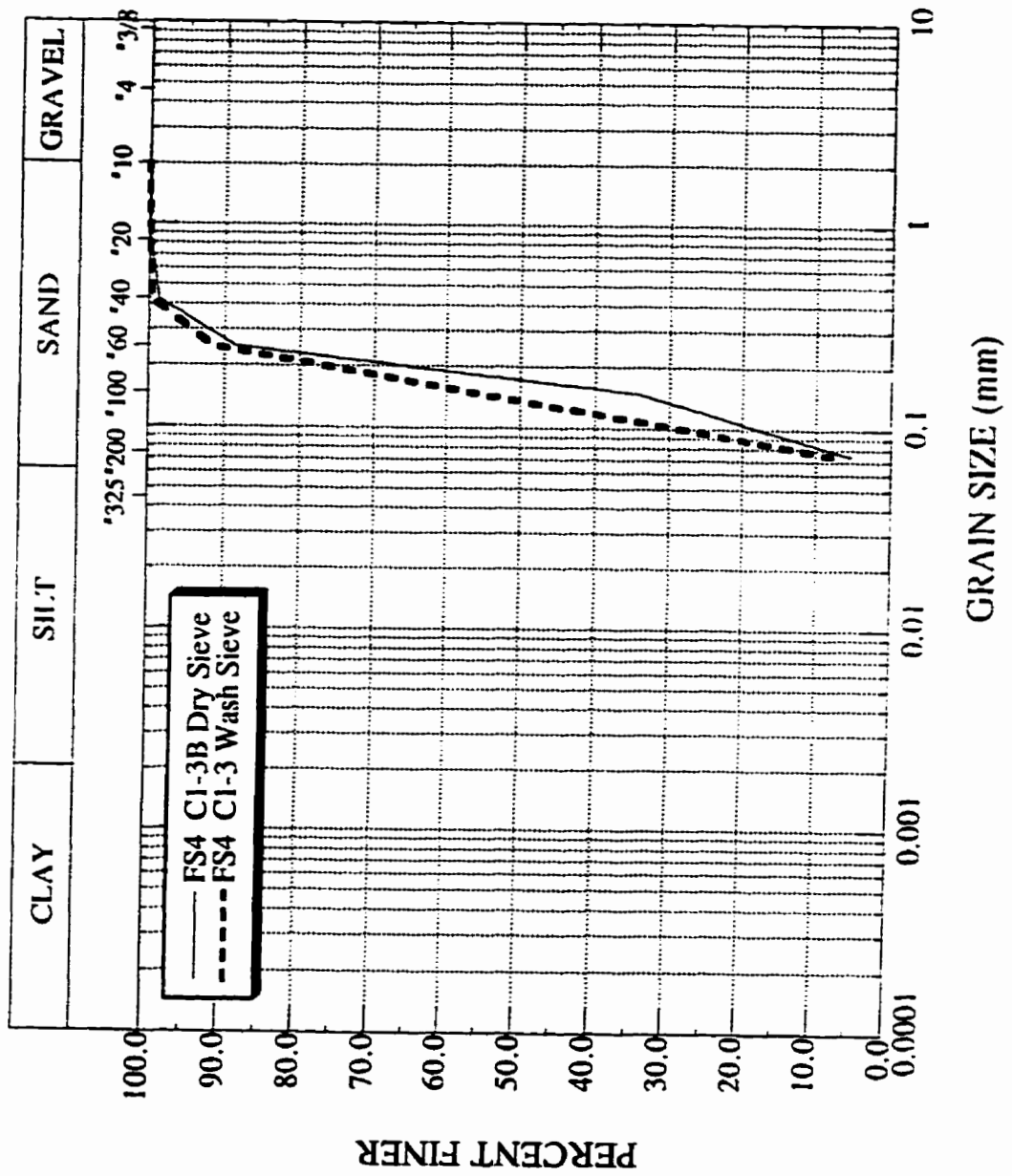


Figure D5: Grain Size Curves Obtained from FS4 CI-3.

Appendix E: Thaw Protocol and Laboratory Testing Data

E.1. Introduction

Appendix E contains data gathered during the thawing protocol study conducted on both reconstituted and undisturbed frozen core specimens. A schematic diagram of the triaxial cell thawing base used in the study is shown in Figure E2. The changes in specimen height and volume recorded during thawing and consolidation are given in summary tables followed by tables which present the void ratio changes that were calculated based on the height and volumetric change data. Plots of these void ratio changes during setup, thawing and consolidation are also given. Information available from the University of British Columbia regarding undisturbed Phase I specimens thawed multidirectionally under a small effective stress is also given. At the back of the appendix, data sheets are provided which show the void ratio change calculations made for each of the reconstituted and undisturbed specimens.

Table E1: Reconstituted CSS Specimen Summary Sheet.

Specimen Number	LVDT Height Change (mm)	Buret Volume Change (cc)	Electronic Height Change (mm)	Electronic Volume Change (cc)
CSS8				
setup	1.06	-1.80	-	-
thawing	0.29	10.00	1.35	-
consolid.	<u>0.07</u>	<u>-1.20</u>	<u>0.06</u>	-
	1.42	7.00	1.41	
CSS9				
setup	0.47	-2.20	-	-1.60
thawing	0.56	6.60	0.93	6.70
consolid.	<u>0.07</u>	<u>0.00</u>	<u>-0.04</u>	<u>-1.35</u>
	1.10	4.40	0.89	3.75
CSS11				
setup	0.32	-1.70	-	-1.00
thawing	0.36	9.50	1.5	7.10
consolid.	<u>0.05</u>	<u>-1.40</u>	<u>-0.05</u>	<u>-1.30</u>
	0.73	6.40	1.45	4.80
CSS14				
setup	-0.28	-1.90	-0.35	-0.70
thawing	1.63	4.65	1.73	4.70
consolid.	<u>0.94</u>	<u>2.30</u>	<u>0.92</u>	<u>2.00</u>
	2.29	5.05	2.30	6.00
CSS15				
setup	0.46	-0.40	0.16	-0.20
thawing	0.24	7.00	0.24	6.70
consolid.	<u>0.03</u>	<u>0.70</u>	<u>0.75</u>	<u>0.35</u>
	0.73	7.30	1.15	6.85
CSS17				
setup	-	-	-	-
thawing	0.6	5.60	1.21	7.92
consolid.	-	<u>-8.30</u>	<u>0.89</u>	<u>-5.45</u>
		-2.70	2.10	2.47
CSS18				
setup	-	-	0.47	-0.02
thawing	2.2	4.70	2.33	10.70
consolid.	<u>0.74</u>	<u>0.10</u>	<u>0.79</u>	<u>-0.20</u>
	2.94	4.80	3.59	10.48

Table E2: Reconstituted SS Specimen Summary Sheet.

Specimen Number	Effective Stress during Thawing	LVDT Height Change (mm)	Buret Volume Change (cc)	Electronic Height Change (mm)	Electronic Volume Change (cc)
SS1 freezing thawing consolid.	400 kpa	0.05	10.00	0.23	10.09
		0.50	15.00	0.70	18.40
		0.00	0.00	0.00	0.00
SS2 freezing thawing consolid.	400 kPa	0.42	10.50	0.61	12.00
		0.86	9.30	0.85	10.45
		0.00	0.00	0.00	0.00
SS3 freezing thawing consolid.	35 kPa	-	9.10	0.04	12.95
		0.058	-	0.071	13.16
		*0.25	*2.17	-	-
SS4 freezing thawing consolid.	35 kPa	0.03	11.26	0.04	11.24
		0.062	14.99	0.13	15.02
		*0.25	*2.17	-	-
SS7 freezing thawing consolid.	35 kPa	0.35	7.90	0.36	8.64
		0.03	12.10	0.03	12.94
		0.21	1.30	0.26	2.32
SS8 freezing thawing consolid.	35 kPa	0.33	3.40	0.03	4.01
		0.05	-	0.02	12.93
		0.39	1.30	0.24	2.02

*Note: due to a similarity of boundary conditions and specimens dimensions, the average height and volume changes that occurred in Specimens SS7 & SS8 were used to estimate the these changes in Specimens SS3 and SS4, since this data was lost.

Table E3: Summary of Reconstituted Specimen Void Ratio Changes.

SYNCRUDE SAND THAW PROTOCOL - SUMMARY

Sample Number	Cell Sro (%)	Cell Press. (kPa)	Δh Thaw & Consol.	Δe Setup	Δe Thaw	Δe Consol.	Δe Th & Con	Δe Total	Direction Thawing	Cell Press. (kPa)	Percent Theor. Intake (cc/cc)	Thaw V_{theor} 0.09VvSro Gs = 2.65 (cc)	Actual Thaw Intake (cc)
CSS8	96.6	501	0.36	-0.059	-0.004	-0.005	-0.009	-0.068	Uni	501	66.15	15.12	10.00
CSS11	95.8	503	0.41	-0.009	-0.005	-0.006	-0.011	-0.020	Uni	503	63.00	15.08	9.50
CSS9	90.7	503	0.63	-0.019	-0.007	-0.006	-0.013	-0.032	Uni	503	47.78	14.02	6.70
SS1	100.0	500	0.50	0.000	-0.007	0.000	-0.007	-0.007	Uni	500	106.16	14.13	15.00
CSS14	94.1	28	2.65	-0.023	-0.023	-0.038	-0.061	-0.084	Uni	28	31.20	14.90	4.65
CSS15	91.5	26	0.99	-0.010	-0.003	-0.030	-0.033	-0.043	Uni	26	49.40	14.17	7.00
SS3	100.0	35	0.192	0.000	0.004	-0.014	-0.010	-0.010	Multi	35	93.14	14.13	13.16
SS4	100.1	35	0.188	0.000	0.004	-0.014	-0.010	-0.010	Multi	35	106.12	14.13	14.99
SS8	100.0	35	0.22	0.000	0.001	-0.009	-0.008	-0.008	Multi	35	105.97	12.20	12.93
CSS17	92.0	48	0.769	0.000	-0.077	-0.034	-0.111	-0.111	Multi	48	57.49	13.78	7.92
CSS18	90.1	61	3.120	-0.029	-0.155	-0.032	-0.187	-0.216	Multi	61	32.75	14.35	4.70

Had air in top drainage line during Multidirectional thawing

Table E4: Comparison of Void Ratio Changes for Reconstituted Specimens Thawed Under the In-Situ Stress or a Small Effective Stress.

Specimen Number	Stress During Thaw	Change in Void Ratio	Void Ratio	Normalized Void Ratio	Time (hrs)	
SS1*	400 kPa	eo	0.711	0.700	0	
		Δe_{th}	-0.007	0.704	0.693	12
		Δe_c	0.000	0.704	0.693	12
SS3	35 kPa	eo	0.669	0.700	0	
		Δe_{th}	0.004	0.673	0.704	6
		Δe_c	-0.014	0.659	0.69	12
SS4	35 kPa	eo	0.681	0.700	0	
		Δe_{th}	0.004	0.685	0.704	6
		Δe_c	-0.014	0.671	0.69	12
SS8	35 kPa	eo	0.643	0.700	0	
		Δe_{th}	0.001	0.644	0.701	6
		Δe_c	-0.009	0.635	0.692	12

*Note: for Specimen SS1
thawing and consolidation
occurred together

Table E5: Undisturbed Phase I Specimen Summary Sheet.

VOID RATIO CHANGES EXHIBITED BY UNDISTURBED SYNCRUDE SAND SPECIMENS THAWED AT UBC

Specimen No.	Degree Saturation	Δe UA Thawing	Δe UBC Thawing	Δe Consol.	Δe UA Total	Δe UBC Total
FS3C7A	98.99	0.063	0.056	0.014	0.077	0.070
FS5C181	81.87	0.093	0.054	0.026	0.119	0.080
FS5C182	83.47	0.021	0.056	0.019	0.040	0.075
FS4C13A	89.79	0.070	0.072	0.018	0.088	0.090
FS1C9B1	89.06	0.075	0.057	0.018	0.093	0.075
FS1C9B2	90.77	0.071	0.047	0.023	0.094	0.070
FS5C131	79.70	0.065	0.063	0.022	0.087	0.085
FS5C132	85.74	0.051	0.056	0.018	0.069	0.074

VOID RATIO CHANGES EXHIBITED BY UNDISTURBED SYNCRUDE SAND SPECIMENS THAWED AT U of A

Specimen No.	Degree Saturation	Δe UA Thawing	Δe Consol.	Δe UA Total
FS3C17B	97.06	0.0300	0.00	0.030
FS5C14	98.36	0.0100	0.00	0.010
FS4C14A	83.48	0.0140	0.00	0.014
FS1C6C1	92.81	0.0200	0.00	0.020

Table E6: Specimen Summary Data Sheet from UBC.

<u>Void Ratio Changes Exhibited by UBC Specimens</u>						
Specimen	Mean Stress p'	Initial e	Final e			
<i>Undrained Tests</i>						
FS3C7A	343	0.769	0.692			
FS5C181	387	0.761	0.642			
FS4C13A	373	0.815	0.727			
<i>Drained Tests</i>						
FS1C9B1	367	0.758	0.665			
FS5C131	317	0.772	0.685			
FS5C132	317	0.741	0.672			
FS1C9B2	367	0.760	0.666			
FS5C182	387	0.754	0.714			
<u>Undisturbed Phase I Syncrude Sand Specimens Tested at U of A.</u>						
	e	po'	qo	e	ps'	qs'
FS4C162	0.729	329	247	0.729	282	-261
FS4C14A	0.847	320	240	0.847	634	934
FS5C14R	0.702	35	0	0.702	997	1584
FS5C14	0.746	312	234	0.746	859	1458
FS3C17B	0.764	330	247	0.764	1355	2007
FS5C10A	0.728	300	225	0.728	230	-250

Table E7: Void Ratio Changes from Initial to Steady State Conditions.

UBC UNDISTURBED SYNCRUDE SAND SPECIMENS - VOID RATIO CHANGES DURING THAWING & CONSOLIDATION																		
Specimen Number	Frozen Diameter	Frozen Height	Frozen Weight	Ice Content	Frozen Volume	Frozen Density pf=WI/V	Dry Density p/(1+wi)	Initial Void Ratio 2.66 Gs/pd - 1	Initial Degree Saturation wiGs/eG	Δh Thaw	Δh Consol.	Δh Thaw & Consol.	Dry Weight Specimen	Volume Solids	ΔV Consol.	Total Void Ratio Change UA	Total Void Ratio Change UBC	Final Void Ratio 2.66 UA
Undrained Tests																		
FS3C7A	6.010	12.500	670.33	25.69	354.608	1.890	1.504	0.769	96.95	0.90	0.918	1.82	538.14	202.308	2.83	0.077	0.07	0.692
FS5C181	6.037	12.550	663.28	22.24	359.193	1.847	1.511	0.761	84.79	1.31	2.123	3.43	534.42	200.910	5.22	0.119	0.06	0.642
FS5C182	6.040	12.405	657.77	22.05	355.435	1.851	1.516	0.754	84.80	0.30	1.634	1.93	535.29	201.237	3.82	0.04	0.075	0.714
FS4C13A	6.012	12.590	654.74	25.00	357.360	1.832	1.466	0.815	89.00	0.97	1.042	2.01	525.92	197.714	3.56	0.068	0.09	0.727
Drained Tests																		
FS1C981	6.030	12.493	665.65	23.3	356.723	1.866	1.513	0.758	89.21	1.06	1.285	2.35	539.49	202.816	3.65	0.093	0.075	0.665
FS1C982	6.026	12.340	658.03	23.9	351.975	1.872	1.511	0.760	91.20	1.00	2.491	3.49	530.77	199.538	4.59	0.094	0.07	0.666
FS5C131	6.013	12.607	657.75	22.39	358.031	1.837	1.501	0.772	84.12	0.90	1.495	2.40	524.69	197.252	4.34	0.087	0.065	0.685
FS5C132	6.000	12.757	672.88	22.13	360.686	1.866	1.528	0.741	86.59	0.75	1.596	2.35	548.66	206.263	3.71	0.069	0.074	0.672

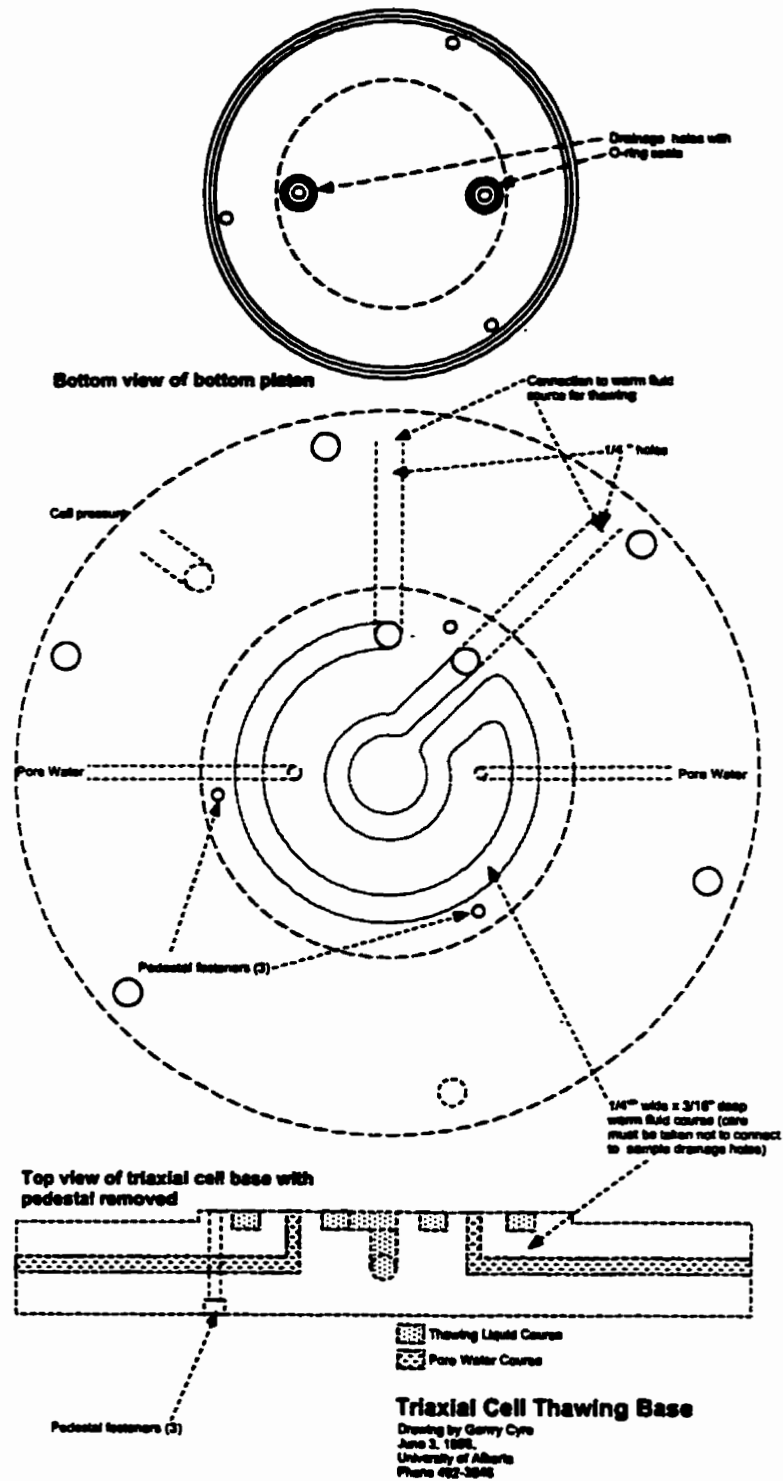


Figure E2: Triaxial Cell Thawing Base.

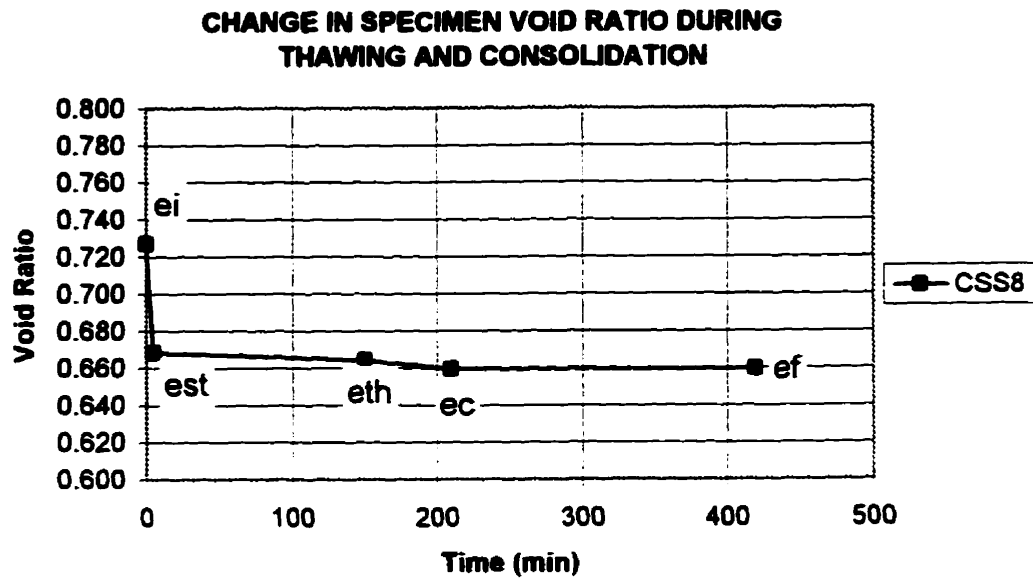


Figure E3: CSS8 Specimen Void Ratio Change Plot.

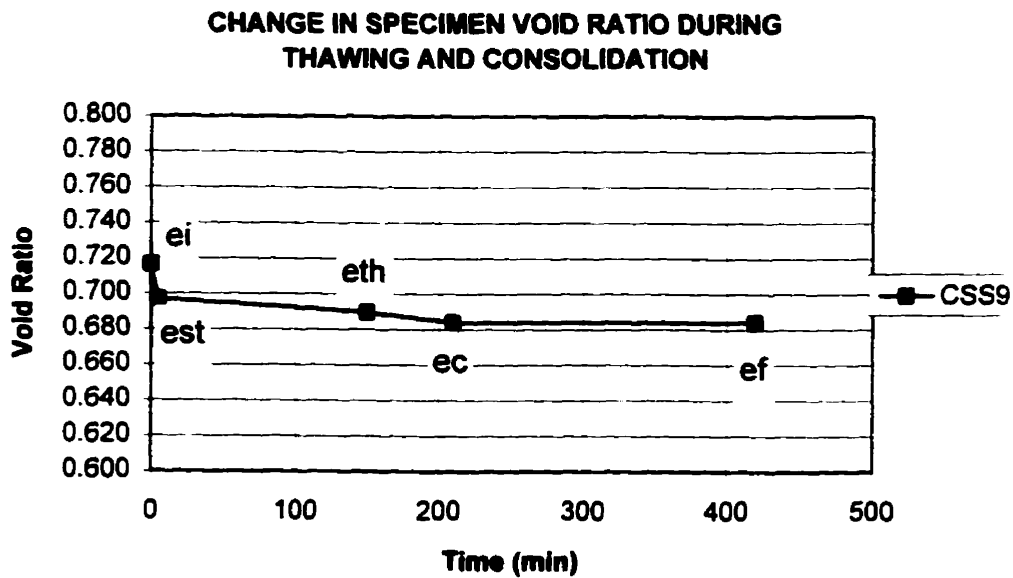


Figure E4: CSS9 Specimen Void Ratio Change Plot.

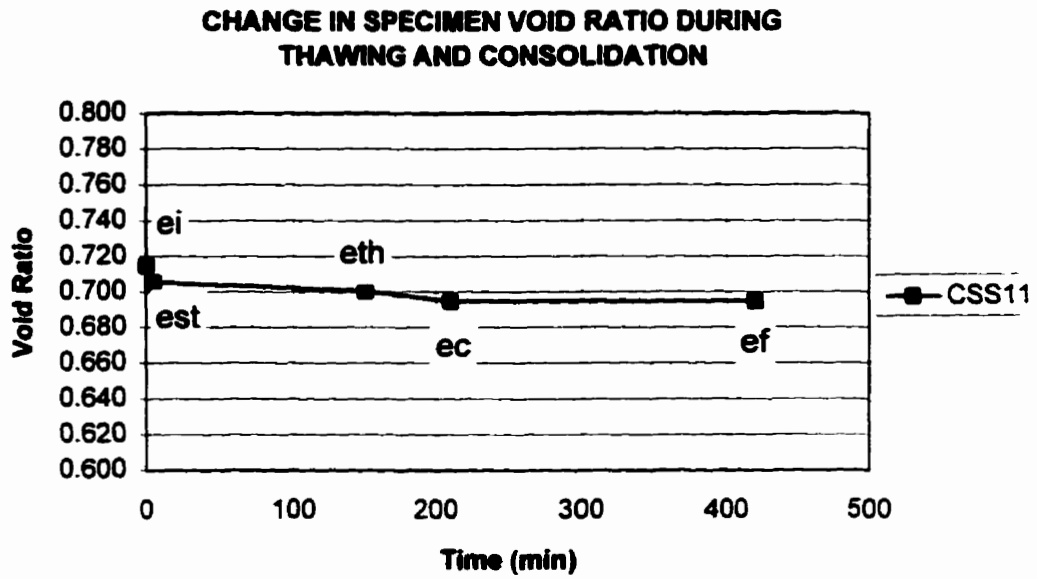


Figure E5: CSS11 Specimen Void Ratio Change Plot.

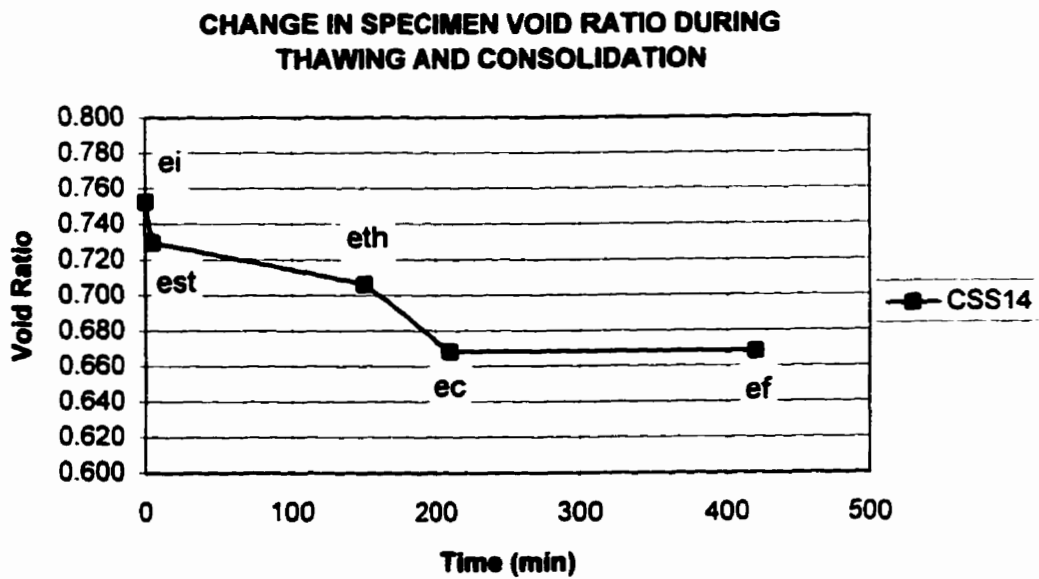


Figure E6: CSS14 Specimen Void Ratio Change Plot.

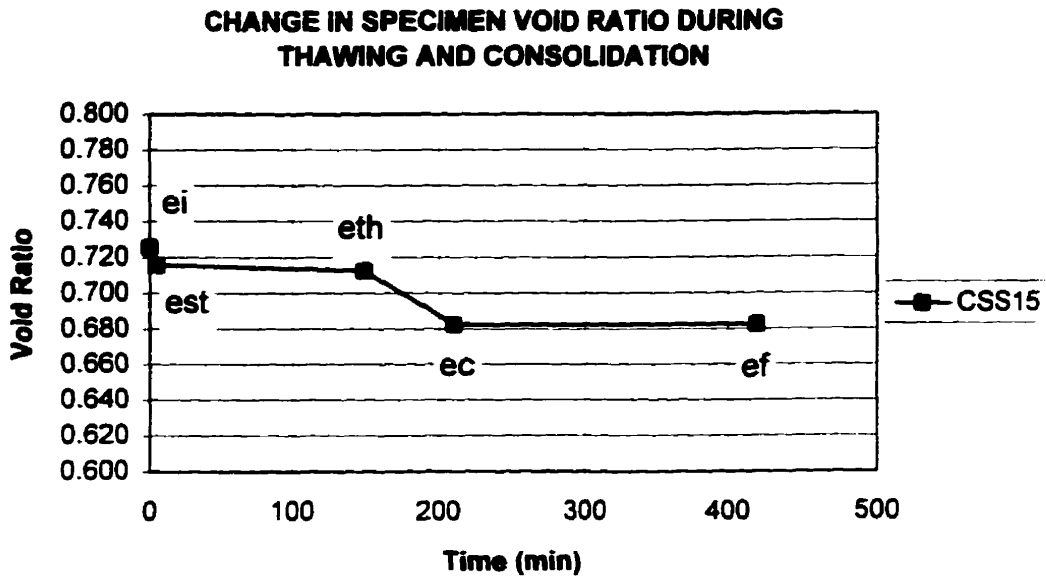


Figure E7: CSS15 Specimen Void Ratio Change Plot.

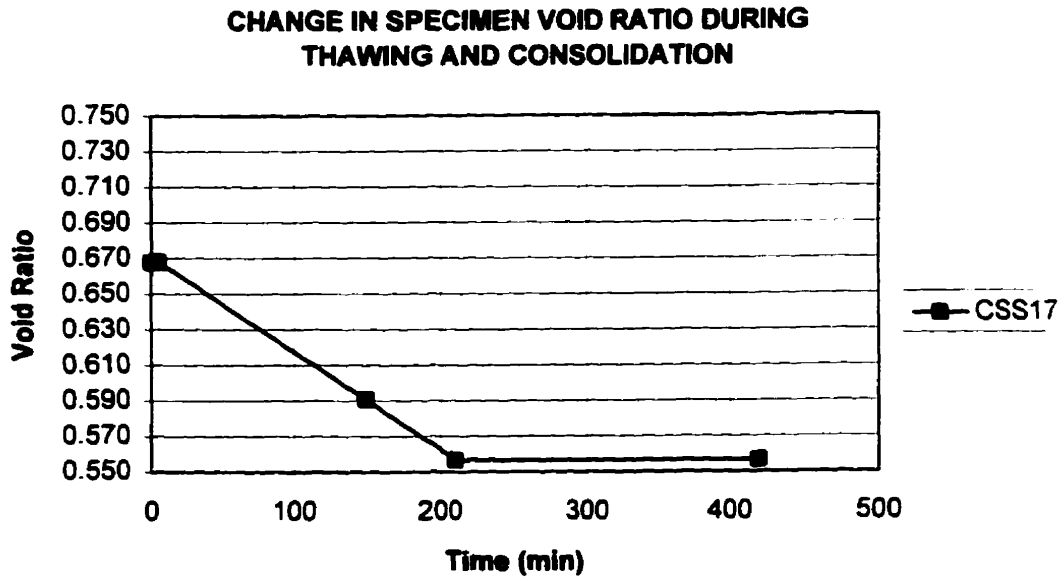


Figure E8: CSS17 Specimen Void Ratio Change Plot.

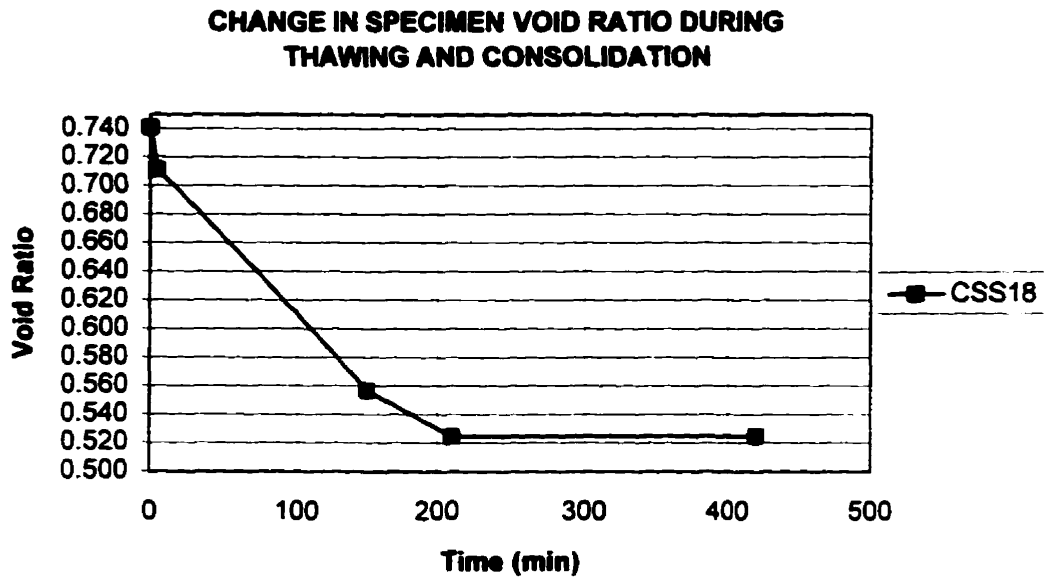


Figure E9: CSS18 Specimen Void Ratio Change Plot.

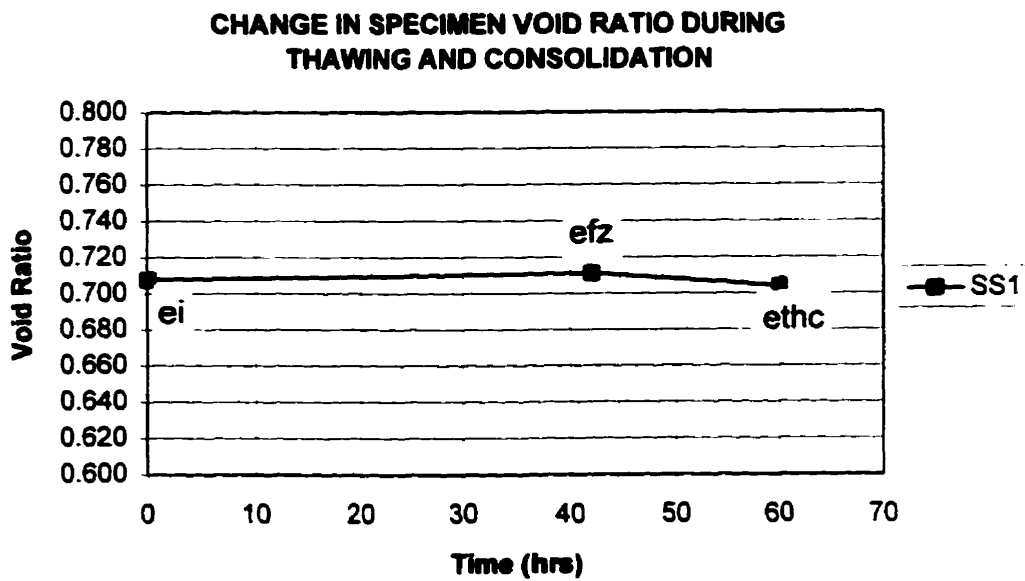


Figure E10: SS1 Specimen Void Ratio Change Plot.

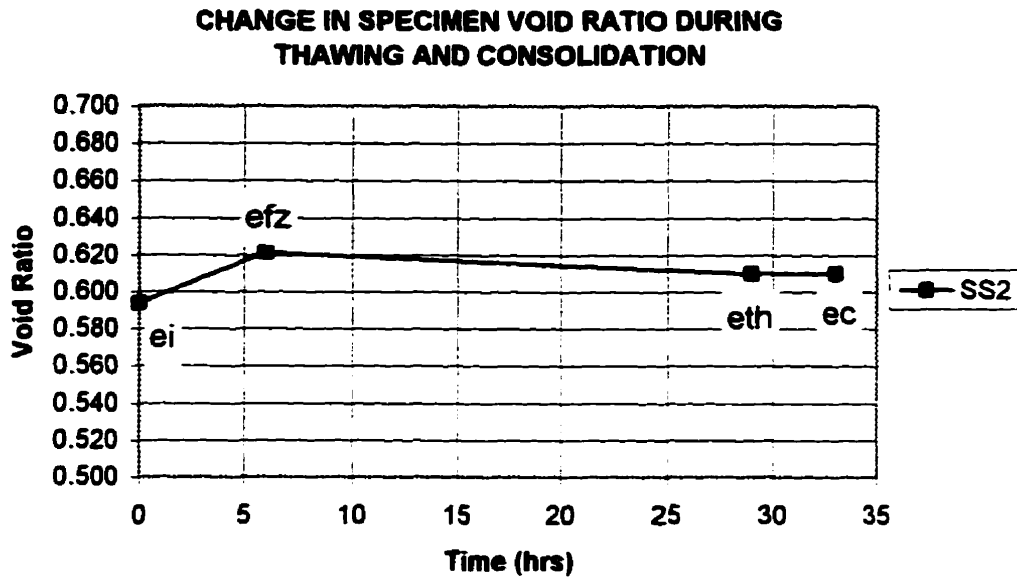


Figure E11: SS2 Specimen Void Ratio Change Plot.

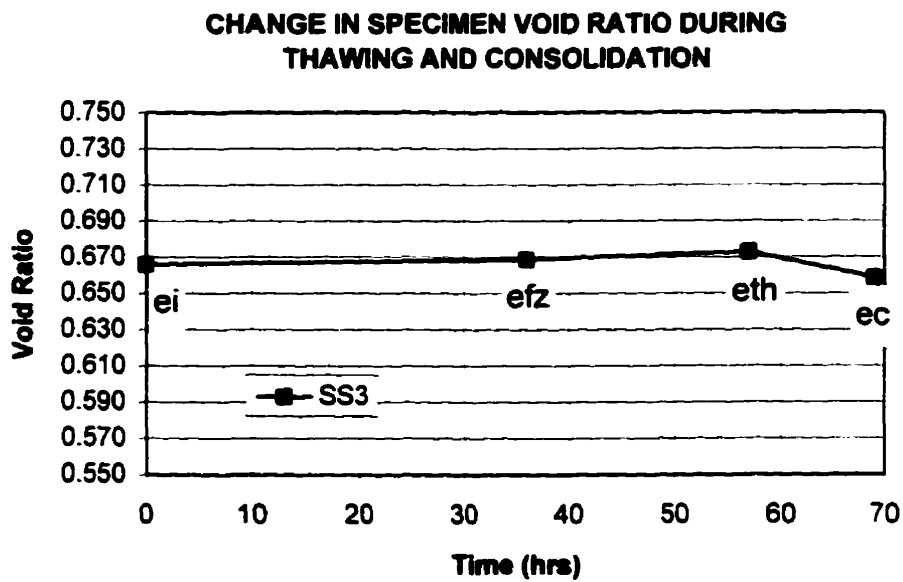


Figure E12: SS3 Specimen Void Ratio Change Plot.

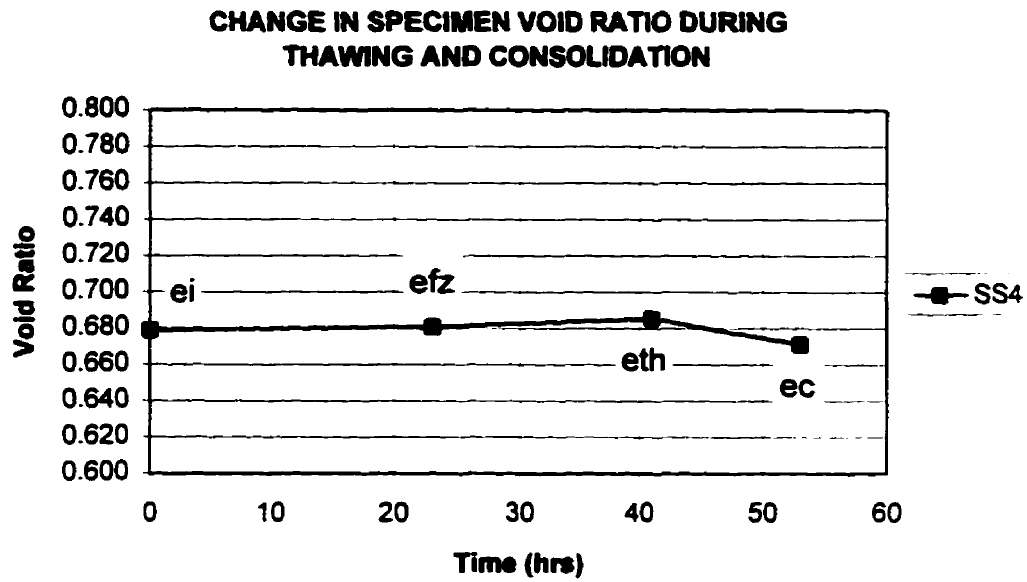


Figure E13: SS4 Specimen Void Ratio Change Plot.

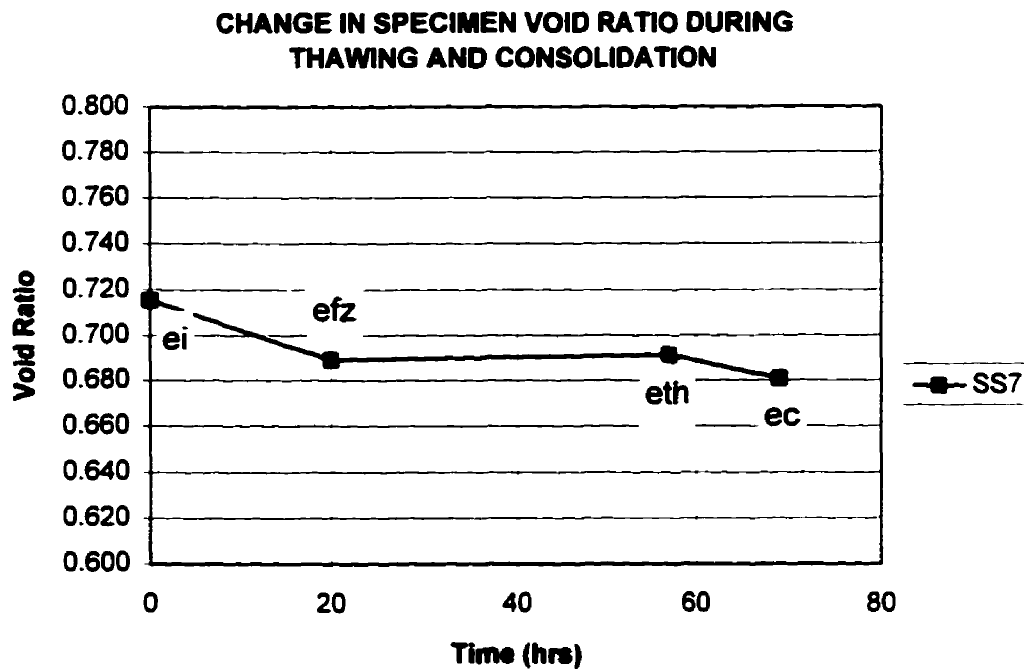


Figure E14: SS7 Specimen Void Ratio Change Plot.

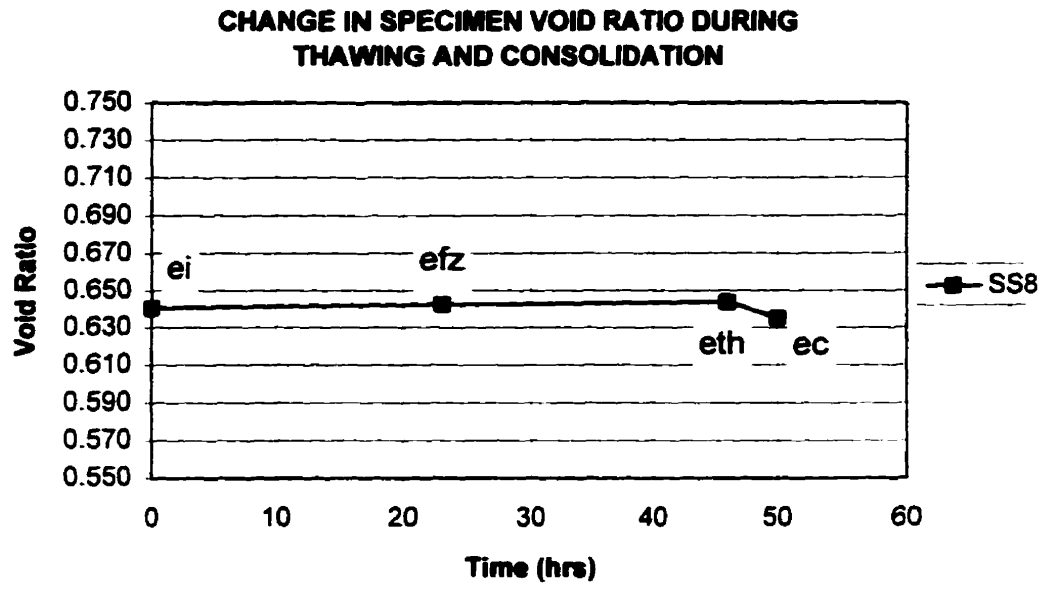


Figure E15: SS8 Specimen Void Ratio Change Plot.

CSS8 Specimen Data Sheet with Void Ratio Calculations.

SAMPLE: CSS8a Clean Syncrude Sand
DATE: 2-Nov-95 $G_s = 2.65$
Sand Type: Syncrude $G_{ice} = 0.917$
Cell Pressure: 501 kPa
Axial Stress: 501 kPa $K_o = 1.0$
Back Pressure: 101 kPa
Calculated Saturation: 96.59 % $B = 0.917$ (before freezing)

Diameter: 63.60 mm **Total Frozen Vol. =** 413.09 cc
Height: 130.03 mm **Sample Area =** 31.77 cm²
Frozen Total Weight: 787.64 g
Ice Content: 24.10 % $V_s = M_s / \rho_s = M_s / \rho_w G_s =$ 239.21 cc
Dry Weight of Sample: 633.9 g $V_v = V_t - V_s =$ 173.89 cc
Final Water Content: 27.53 %

Change in Height during Setup: 1.06 mm
Subtract Cell Compliance & Elastic Deformation: 0.176 mm 500 kPa Sigma V
Net Change in Height during Set up: 0.88 mm
Change in Volume during Setup: 1.80 cc

Change in Height during thawing: 0.29 mm
Change in Volume during Thawing: 10.00 cc

Change in height during Consolidation: 0.07
Change in Volume during Consolidation: 1.20 cc

Void Ratio Calculations:

$$e_i = ((V - V_s)/V_s) = G_s \rho_w / \rho_d - 1 = 0.727$$

$$e_i = ((W - W_s)/W_s) * (G_s/G_{ice}) = 0.701 \quad (\text{for saturated specimens})$$

$$S_r i = (w_i G_s)/(e_i G_i) = 95.81 \quad S_{r0} = S_r i / 0.9919 = 96.59$$

$$e(\text{setup}) = e_i - \Delta V_v / V_s = e_i - (\Delta h A_o + (A_o - A)(h_o - \Delta h)) / V_s = 0.668$$

$$\text{Assume } r = \epsilon_r / \epsilon_{ax} = 2.0$$

$$e(\text{setup}) = e_i - \epsilon_{ax} V/V_s (1 + 2\epsilon_r / \epsilon_{ax}) = e_i - \epsilon_{ax} V/V_s (5) = 0.668$$

$$e_{th} = e_s - \epsilon_{ax}(1 + 2r) V/V_s = e_s - \epsilon_{ax}(1) V/V_s = 0.664$$

$$\text{or, } e_{th} = e_s - \Delta V_v / V_s = e_s - (\Delta h_u A_s) / V_s = 0.664$$

$$e_c = e_{th} - \Delta V_c / V_s = 0.659$$

$$e_c = e_{th} - \epsilon_{ax} V/V_s (3) = 0.662$$

$$\text{for an undrained test, } e_c = e_f = 0.659$$

Final Void Ratio Check

$$S_r t = (V_v S_r i (1 - 0.09) + V_{\text{intake}}) / V_v = 0.929$$

$$e_{ff} = w_f G_s / S_r t = 0.785$$

	Void Ratio e	Time (min)
e_i	0.727	0
e_s	0.668	5
e_{th}	0.664	150
e_c	0.659	210
e_f	0.659	420
Δe_s	-0.059	Settlement
Δe_{th}	-0.004	Settlement
Δe_c	-0.005	Settlement
e_{ff}	0.785	420

CSS9 Specimen Data Sheet with Void Ratio Calculations.

SAMPLE: CSS9a Clean Syncrude Sand
DATE: 8-Nov-95 $G_s = 2.65$
Sand Type: Syncrude $G_{ice} = 0.917$
Cell Pressure: 503 kPa
Axial Stress: 503 kPa $K_o = 1.0$
Back Pressure: 103 kPa
Calculated Saturation: 90.66 % $B = 0.971$ (before freezing)

Diameter 63.40 mm **Total Frozen Vol. =** 411.67 cc
Height 130.40 mm **Sample Area =** 31.57 cm²
Frozen Total Weight 781.50 g
Ice Content 22.30 % $V_s = M_s / \rho_s = M_s / \rho_w G_s =$ 239.81 cc
Dry Weight of Sample 635.5 g $V_v = V_t - V_s =$ 171.86 cc
Final Water Content 24.90 %

Change in Height during Setup 0.47 mm
Subtract Cell Compliance & Elastic Compression 0.176 mm 500 kPa Sigma V
Net Change in Height during Set up 0.29 mm
Change in Volume during Setup 2.20 cc

Change in Height during thawing 0.56 mm
Change in Volume during Thawing 6.70 cc

Change in height during Consolidation 0.07
Change in Volume during Consolidation 1.35 cc

Void Ratio Calculations:

$e_i = ((V - V_s)/V_s) = G_s \rho_w / \rho_d - 1 =$ **0.717**
 $e_i = ((W - W_s)/W_s) * (G_s/G_{ice}) =$ **0.664** (for saturated specimens)
 $S_r i = (w_i G_s)/(e_i G_i) =$ **89.93** $S_{r0} = S_r i / 0.9919 =$ **90.66**

$e(\text{setup}) = e_i - \Delta V_v/V_s = e_i - (\Delta h A_o + (A_o - A)(h_o - \Delta h))/V_s =$ **0.697**
 Assume $r = \epsilon_r/\epsilon_a = 2.0$
 $e(\text{setup}) = e_i - \epsilon_{ax} V/V_s (1 + 2\epsilon_r/\epsilon_{ax}) = e_i - \epsilon_{ax} V/V_s (5) =$ **0.697**

$e_{th} = e_s - \epsilon_{ax}(1 + 2r) V/V_s = e_s - \epsilon_{ax}(1) V/V_s =$ **0.690**
 or, $e_{th} = e_s - \Delta V_v/V_s = e_s - (\Delta h_u A_s)/V_s =$ **0.690**

$e_c = e_{th} - \Delta V_c/V_s =$ **0.684**
 $e_c = e_{th} - \epsilon_{ax} V/V_s (3) =$ **0.687**

for an undrained test, $e_c = e_f =$ **0.684**

Final Void Ratio Check

$S_{rt} = (V_v S_{ri} (1 - 0.09) + V_{intake})/V_v =$ **0.857**
 $e_{ff} = w_f G_s / S_{rt} =$ **0.770**

	Void Ratio e	Time (min)
e_i	0.717	0
e_s	0.697	5
e_{th}	0.690	150
e_c	0.684	210
e_f	0.684	420
Δe_s	-0.019	Settlement
Δe_{th}	-0.007	Settlement
Δe_c	-0.006	Settlement
e_{ff}	0.770	420

CSS11 Specimen Data Sheet with Void Ratio Calculations.

SAMPLE: CSS11a Clean Syncrude Sand
DATE: 14-Nov-95 **Gs = 2.65**
Sand Type: Syncrude **Gice = 0.917**
Cell Pressure: 503 kPa
Axial Stress: 503 kPa **Ko = 1.0**
Back Pressure: 103 kPa
Calculated Saturation: 95.79 % **B = 0.957 (before freezing)**

Diameter 63.90 mm **Total Frozen Vol. = 419.63 cc**
Height 130.85 mm **Sample Area = 32.07 cm²**
Frozen Total Weight 803.03 g
Ice Content 23.50 % **Vs = Ms / ρs = Ms / ρw Gs = 244.72 cc**
Dry Weight of Sample 648.5 g **Vv = Vt - Vs = 174.91 cc**
Final Water Content 24.72 %

Change in Height during Setup 0.32 mm
 Subtract Cell Compliance & Elastic Deformation 0.176 mm 500 kPa Sigma V
Net Change in Height during Set up 0.14 mm
Change in Volume during Setup 1.70 cc

Change in Height during thawing 0.36 mm
Change in Volume during Thawing 9.50 cc

Change in height during Consolidation 0.05
Change in Volume during Consolidation 1.40 cc

Void Ratio Calculations:

$e_i = ((V - V_s)/V_s) = G_s \rho_w / \rho_d - 1 = 0.715$
 $e_i = ((W - W_s)/W_s) * (G_s/G_{ice}) = 0.689$ (for saturated specimens)
 $S_r i = (w_i G_s)/(e_i G_i) = 95.01$ $S_{r0} = S_r i / 0.9919 = 95.79$

 $e(\text{setup}) = e_i - \Delta V_v/V_s = e_i - (\Delta h A_o + (A_o - A)(h_o - \Delta h))/V_s = 0.705$
 Assume $r = \epsilon_r/\epsilon_{ax} = 2.0$
 $e(\text{setup}) = e_i - \epsilon_{ax} V/V_s (1 + 2\epsilon_r/\epsilon_{ax}) = e_i - \epsilon_{ax} V/V_s (5) = 0.705$

 $e_{th} = e_s - \epsilon_{ax}(1 + 2r) V/V_s = e_s - \epsilon_{ax} V/V_s (1) = 0.701$
 or, $e_{th} = e_s - \Delta V_v/V_s = e_s - (\Delta h_u A_s)/V_s = 0.701$

 $e_c = e_{th} - \Delta V_c/V_s = 0.695$
 $e_c = e_{th} - \epsilon_{ax} V/V_s (3) = 0.699$
 for an undrained test, $e_c = e_f = 0.695$

Final Void Ratio Check

$S_{rt} = (V_v S_{ri} (1 - 0.09) + V_{intake})/V_v = 0.919$
 $e_{ff} = w_f G_s / S_{rt} = 0.713$

	Void Ratio e	Time (min)
ei	0.715	0
es	0.705	5
eth	0.701	150
ec	0.695	210
ef	0.695	420
Δes	-0.009	Settlement
Δeth	-0.005	Settlement
Δec	-0.006	Settlement
eff	0.713	420

CSS14 Specimen Data Sheet with Void Ratio Calculations.

SAMPLE: CSS14a Clean Syncrude Sand
DATE: 24-Nov-95 $G_s = 2.65$
Sand Type: Syncrude $G_{ice} = 0.917$
Cell Pressure: 28 kPa
Axial Stress: 28 kPa $K_o = 1.0$
Back Pressure: 8 kPa
Calculated Saturation: 94.09 % $B = 0.337$ (before freezing)

Diameter 63.40 mm **Total Frozen Vol. =** 409.87 cc
Height 129.83 mm **Sample Area =** 31.57 cm²
Frozen Total Weight 770.50 g
Ice Content 24.30 % $V_s = M_s / \rho_s = M_s / \rho_w G_s =$ 233.89 cc
Dry Weight of Sample 619.8 g $V_v = V_t - V_s =$ 175.98 cc
Final Water Content 26.80 %

Change in Height during Setup 0.35 mm
 Subtract Cell Compliance & Elastic Compression 0.0148 mm 40 kPa Sigma V
Net Change in Height during Set up 0.34 mm
Change in Volume during Setup 1.90 cc

Change in Height during thawing 1.73 mm
Change in Volume during Thawing 4.65 cc

Change in height during Consolidation 0.92
Change in Volume during Consolidation -2.30 cc

Void Ratio Calculations:

$e_i = ((V - V_s)/V_s) = G_s \rho_w / \rho_d - 1 =$ **0.752**
 $e_i = ((W - W_s)/W_s) * (G_s/G_{ice}) =$ **0.703** (for saturated specimens)

$S_r i = (w_i G_s)/(e G_i) =$ **93.33** $S_{r o} = S_r i / 0.9919 =$ **94.09**

$e(\text{setup}) = e_i - \Delta V_v/V_s = e_i - (\Delta h A_o + (A_o - A)(h_o - \Delta h))/V_s =$ **0.729**

Assume $r = \epsilon_r/\epsilon_{ax} = 2.0$

$e(\text{setup}) = e_i - \epsilon_{ax} V/V_s (1+2\epsilon_r/\epsilon_{ax}) = e_i - \epsilon_{ax} V/V_s (5) =$ **0.730**

$e_{th} = e_s - \epsilon_{ax}(1+2r) V/V_s = e_s - \epsilon_{ax} V/V_s (1) =$ **0.706**

or, $e_{th} = e_s - \Delta V_v/V_s = e_s - (\Delta h u A_s)/V_s =$ **0.707**

$e_c = e_{th} - \Delta V_c / V_s =$ **0.716**

$e_c = e_{th} - \epsilon_{ax} V/V_s (3) =$ **0.669**

for an undrained test, $e_c = e_f =$ **0.669**

Final Void Ratio Check

$S_{r t} = (V_v S_{r i} (1-0.09) + V_{intake})/V_v =$ **0.889**

$e_{ff} = w_f G_s / S_{r t} =$ **0.799**

	Void Ratio e	Time (min)
e_i	0.752	0
e_s	0.730	5
e_{th}	0.706	150
e_c	0.669	210
e_f	0.669	420
Δe_s	-0.023	Settlement
Δe_{th}	-0.023	Settlement
Δe_c	-0.038	Settlement
e_{ff}	0.799	420

CSS15 Specimen Data Sheet with Void Ratio Calculations.

SAMPLE: CSS15a Clean Syncrude Sand
DATE: 27-Nov-95 $G_s = 2.65$
Sand Type: Syncrude $G_{ice} = 0.917$
Cell Pressure: 26 kPa
Axial Stress: 26 kPa $K_o = 1.0$
Back Pressure: 6 kPa
Calculated Saturation: 91.54 % $B = 0.957$ (before freezing)

Diameter 63.50 mm **Total Frozen Vol. =** 409.01 cc
Height 129.15 mm **Sample Area =** 31.67 cm²
Frozen Total Weight 781.69 g
Ice Content 22.80 % $V_s = M_s / \rho_s = M_s / \rho_w G_s =$ 237.02 cc
Dry Weight of Sample 628.1 g $V_v = V_t - V_s =$ 171.99 cc
Final Water Content 24.74 %

Change in Height during Setup 0.16 mm Settlement
 Subtract Cell Compliance & Elastic Compression 0.0148 mm 26 kPa Sigma V
Net Change in Height during Set up 0.15 mm
Change in Volume during Setup 0.40 cc Expulsion

Change in Height during thawing 0.24 mm Settlement
Change in Volume during Thawing 7.00 cc Intake

Change in height during Consolidation 0.75 Settlement
Change in Volume during Consolidation -0.70 cc Intake

Void Ratio Calculations:

$e_i = ((V - V_s)/V_s) = G_s \rho_w / \rho_d - 1 = 0.726$
 $e_i = ((W - W_s)/W_s) * (G_s/G_{ice}) = 0.707$ (for saturated specimens)

$S_r i = (w_i G_s)/(e_i G_i) = 90.80$ $S_r o = S_r i / 0.9919 = 91.54$

$e(\text{setup}) = e_i - \Delta V_v/V_s = e_i - (\Delta h A_o + (A_o - A)(h_o - \Delta h))/V_s = 0.716$

Assume $r = \epsilon_r/\epsilon_a = 1.0$

$e(\text{setup}) = e_i - \epsilon_{ax} V/V_s (1 + 2\epsilon_r/\epsilon_{ax}) = e_i - \epsilon_{ax} V/V_s (5) = 0.716$

$e_{th} = e_s - \epsilon_{ax}(1 + 2r) V/V_s = e_s - \epsilon_{ax} V/V_s (1) = 0.713$

or, $e_{th} = e_s - \Delta V_v/V_s = e_s - (\Delta h u A_s)/V_s = 0.713$

$e_c = e_{th} - \Delta V_c/V_s = 0.716$

$e_c = e_{th} - \epsilon_{ax} V/V_s (3) = 0.683$

for an undrained test, $e_c = e_f = 0.683$

Final Void Ratio Check

$S_r t = (V_v S_r i (1 - 0.09) + V_{\text{intake}})/V_v = 0.871$

$e_{ff} = w_f G_s / S_r t = 0.753$

	Void Ratio e	Time (min)
e_i	0.726	0
e_s	0.716	5
e_{th}	0.713	150
e_c	0.683	210
e_f	0.683	420
Δe_s	-0.010	Settlement
Δe_{th}	-0.003	Settlement
Δe_c	-0.030	Settlement
e_{ff}	0.753	420

CSS17 Specimen Data Sheet with Void Ratio Calculations.

SAMPLE: CSS17a Clean Syncrude Sand
DATE: 1-Dec-95 $G_s = 2.65$
Sand Type: Syncrude $G_{ice} = 0.917$
Cell Pressure: 48 kPa
Axial Stress: 48 kPa $K_o = 1.0$
Back Pressure: 28 kPa
Calculated Saturation: 92.01 % $B = 0.802$ (before freezing)

Diameter 63.60 mm **Total Frozen Vol. =** 415.44 cc
Height 130.77 mm **Sample Area =** 31.77 cm²
Frozen Total Weight 805.48 g
Ice Content 21.09 % $V_s = M_s / \rho_s = M_s / \rho_w G_s =$ 249.09 cc
Dry Weight of Sample 660.1 g $V_v = V_t - V_s =$ 166.35 cc
Final Water Content 24.07 %

Change in Height during Setup 0.01 mm
Subtract Cell Compliance & Elastic Compression 0.0148 mm 40 kPa Sigma V
Net Change in Height during Set up 0.00 mm
Change in Volume during Setup 0.00 cc

Change in Height during thawing 1.21 mm
Change in Volume during Thawing 7.92 cc

Change in height during Consolidation 0.89
Change in Volume during Consolidation 5.45 cc

Void Ratio Calculations:

$$e_i = ((V - V_s)/V_s) = G_s \rho_w / \rho_d - 1 = \mathbf{0.668}$$

$$e_i = ((W - W_s)/W_s) * (G_s/G_{ice}) = \mathbf{0.636} \quad (\text{for saturated specimens})$$

$$S_r i = (w_i G_s)/(e_i G_i) = \mathbf{91.26} \quad S_{r o} = S_r i / 0.9919 = \mathbf{92.01}$$

$$e(\text{setup}) = e_i - \Delta V_v / V_s = e_i - (\Delta h A_o + (A_o - A)(h_o - \Delta h)) / V_s = \mathbf{0.668}$$

$$\text{Assume } r = \epsilon_r / \epsilon_{ax} = 2.0$$

$$e(\text{setup}) = e_i - \epsilon_{ax} V / V_s (1 + 2\epsilon_r / \epsilon_{ax}) = e_i - \epsilon_{ax} V / V_s (5) = \mathbf{0.668}$$

$$e_{th} = e_s - \epsilon_{ax}(1 + 2r) V / V_s = e_s - \epsilon_{ax} V / V_s (5) = \mathbf{0.591}$$

$$e_c = e_{th} - \Delta V_c / V_s = \mathbf{0.569}$$

$$e_c = e_{th} - \epsilon_{ax} V / V_s (3) = \mathbf{0.557}$$

$$\text{for an undrained test, } e_c = e_f = \mathbf{0.557}$$

Final Void Ratio Check

$$S_{r t} = (V_v S_{r i} (1 - 0.09) + V_{\text{intake}}) / V_v = \mathbf{0.878}$$

$$e_{ff} = w_f G_s / S_{r t} = \mathbf{0.726}$$

	Void Ratio e	Time (min)
e_i	0.668	0
e_s	0.668	5
e_{th}	0.591	150
e_c	0.557	210
e_f	0.557	420
Δe_s	0.000	Settlement
Δe_{th}	-0.077	Settlement
Δe_c	-0.034	Settlement
e_{ff}	0.726	420

SS1 Specimen Data Sheet with Void Ratio Calculations.

THAWING PROTOCOL FOR LABORATORY TESTING OF FROZEN SPECIMENS VOID RATIO CHANGES DURING FREEZING AND THAWING

SAMPLE:	SS1	Clean Syncrude Sand	Thawing: Unidirectional
DATE:	12-Mar-96	Gs = 2.65	
Sand Type:	Syncrude	Gice = 0.917	
Cell Pressure:	500 kPa		
Axial Stress:	500 kPa	Ko = 1.0	
Back Pressure:	100 kPa		
Calculated Saturation:	100.46 %	B = 1.00	(before freezing)
Diameter	63.88 mm	Total Frozen Vol. =	378.82 cc
Height	118.20 mm	Sample Area =	32.05 cm ²
Frozen Total Weight	732.00 g		
Ice Content	24.40 %	Vs = Ms / ρs = Ms / ρw Gs =	221.84 cc
Dry Weight of Sample	587.87 g	Vv = Vt - Vs =	156.99 cc
Final Water Content	25.29 %		

Change in Height during Freezing (heave)	0.05 mm	Heave
Change in Volume during Freezing	10.00 cc	Expulsion
Change in height during Thawing (settlement)	0.50	Settlement
Change in Volume during Thawing	15.00 cc	Intake
Change in height during Consolidation	0.00	Settlement
Change in Volume during Consolidation	0.00 cc	Expulsion

Void Ratio Calculations:

$$e_i = ((V - V_s)/V_s) = G_s \rho_w / \rho_d - 1 = \mathbf{0.708}$$

$$e_i = ((W - W_s)/W_s) * (G_s/G_{ice}) = \mathbf{0.709} \quad (\text{for saturated specimens})$$

$$S_{ri} = (w_i G_s) / (e_i G_i) = \mathbf{99.64} \quad S_{ro} = S_{ri} / 0.9919 = \mathbf{100.46}$$

$$e_{fz} = e_i + \epsilon_{ax}(1+2r) V/V_s = e_i + \epsilon_{ax}(5) V/V_s = \mathbf{0.711}$$

$$e_{th_m} = e_{fz} - \epsilon_{ax} V/V_s (5) = \mathbf{0.675}$$

$$e_{th_u} = e_{fz} - \Delta h A_s / V_s = \mathbf{0.704}$$

$$e_c = e_{th} - \Delta V_c / V_s = \mathbf{0.704}$$

Final Void Ratio Check

$$S_{rt} = (V_v S_{ri} (1-0.09) + V_{intake}) / V_v = \mathbf{1.002}$$

$$e_{ff} = w_f G_s / S_{rt} = \mathbf{0.669}$$

	Void Ratio e	Time (hr)
e _i	0.708	0
e _{fz}	0.711	42
e _{th}	0.704	60
e _c	0.704	60
Δe _{fz}	0.004	Heave
Δe _{th}	-0.007	Settlement
Δe _c	0.000	Settlement
e _{ff}	0.669	60

SS2 Specimen Data Sheet with Void Ratio Calculations.

SAMPLE: SS2 **Clean Syncrude Sand** **Thawing:** Unidirectional
DATE: 15-Mar-96 **Gs = 2.65**
Sand Type: Syncrude **Gice = 0.917**
Cell Pressure: 500 kPa
Axial Stress: 500 kPa **Ko = 1.0**
Back Pressure: 100 kPa
Calculated Saturation: 100.57 % **B = 0.962 (before freezing)**

Diameter 63.93 mm **Total Frozen Vol. =** 392.11 cc
Height 122.14 mm **Sample Area =** 32.10 cm²
Frozen Total Weight 783.80 g
Ice Content 20.50 % **Vs = Ms / ρs = Ms / ρw Gs =** 246.01 cc
Dry Weight of Sample 651.92 g **Vv = Vt - Vs =** 146.10 cc
Final Water Content 24.00 %

Theoretical Volume of Porewater Expulsion During Freezing

$\Delta V = 0.09 Sr Vv = 13.22 \text{ cc}$

Change in Height during Freezing (heave) 0.42 mm **Heave**
Change in Volume during Freezing 10.50 cc **Expulsion**

Change in height during Thawing (settlement) 0.86 mm **Settlement**
Change in Volume during Thawing 9.30 cc **Intake**

Change in height during Consolidation 0.00 **Settlement**
Change in Volume during Consolidation 0.00 cc **Expulsion**

Void Ratio Calculations:

$e_i = ((V - V_s)/V_s) = G_{spw}/\rho_d - 1 = 0.594$
 $e_i = ((W - W_s)/W_s) * (G_s/G_{ice}) = 0.585 \text{ (for saturated specimens)}$

$Sr_i = (w_i G_s)/(e G_i) = 99.76$ $Sr_o = Sr_i / 0.9919 = 100.57$

$efz = e_i + \epsilon_{ax}(1+2r) V/V_s = e_i + \epsilon_{ax}(5) V/V_s = 0.621$

$eth_m = efz - \epsilon_{ax} V/V_s (5) = 0.565$
 $eth_v = efz - \Delta h_{As}/V_s = 0.610$
 $ec = eth - \Delta V_c/V_s = 0.610$

Final Void Ratio Check

$Srt = (V_v Sr_i (1-0.09) + V_{intake})/V_v = 0.971$
 $eff = w_f G_s / Srt = 0.655$

	Void Ratio e	Time (hr)
ei	0.594	0
efz	0.621	6
eth	0.610	29
ec	0.610	33
Δefz	0.027	Heave
Δeth	-0.011	Settlement
Δec	0.000	Settlement
eff	0.655	29

SS3 Specimen Data Sheet with Void Ratio Calculations.

SAMPLE: SS3c Clean Syncrude Sand Thawing: Multidirectional
DATE: 9-Apr-96 $G_s = 2.65$
Sand Type: Syncrude $G_{ice} = 0.917$
Cell Pressure: 35 kPa
Axial Stress: 35 kPa $K_0 = 1.0$
Back Pressure: 15 kPa
Calculated Saturation: 50.31 % $B = 0.96$ (before freezing)

Diameter 63.95 mm **Total Frozen Vol. =** 380.63 cc
Height 118.50 mm **Sample Area =** 32.12 cm²
Frozen Total Weight 748.50 g
Ice Content 11.50 % $V_s = M_s / \rho_s = M_s / \rho_w G_s =$ 228.47 cc
Dry Weight of Sample 605.4 g $V_v = V_t - V_s =$ 152.16 cc
Final Water Content 19.92 %

Change in Height during Freezing 0.04 mm Heave
Change in Volume during Freezing 12.95 cc Expulsion

Change in height during Thawing -0.058 Heave
Change in Volume during Thawing 13.16 cc Intake

Change in height during Consolidation 0.25 Settlement (ave of SS7 & SS8)
Change in Volume during Consolidation 2.17 cc Expulsion (ave of SS7 & SS8)

Void Ratio Calculations:

$$e_i = (V - V_s) / V_s = G_{spw} / \rho_d - 1 = 0.666$$

$$e_i = ((W - W_s) / W_s) * (G_s / G_{ice}) = 0.673 \quad (\text{for saturated specimens})$$

$$S_r i = (w_i G_s) / (e_i G_i) = 49.90 \quad S_{r0} = S_r i / 0.9919 = 50.31$$

$$e_{fz} = e_i + \epsilon_{ax}(1+2r) V / V_s = e_i + \epsilon_{ax}(5) V / V_s = 0.669$$

$$e_{th_m} = e_{fz} - \epsilon_{ax} V / V_s (5) = 0.673$$

$$e_{th_u} = e_{fz} - \Delta h A_s / V_s = 0.670$$

$$e_c = e_{th} - \Delta V_c / V_s = 0.659$$

Final Void Ratio Check

$$S_{rt} = (V_v S_{ri} (1-0.09) + V_{intake}) / V_v = 0.541$$

$$e_{ff} = w_f G_s / S_{rt} = 0.977$$

	Void Ratio e	Time (min)
e_i	0.666	0
e_{fz}	0.669	36
e_{th}	0.673	57
ec	0.659	69
Δe_{fz}	0.003	Heave
Δe_{th}	0.004	Heave
Δe_c	-0.014	Settlement
eff	0.977	57

SS4 Specimen Data Sheet with Void Ratio Calculations.

SAMPLE: SS4 Clean Syncrude Sand Thawing: Multidirectional
DATE: 9-Apr-96 $G_s = 2.65$
Sand Type: Syncrude $G_{ice} = 0.917$
Cell Pressure: 35 kPa
Axial Stress: 35 kPa $K_o = 1.0$
Back Pressure: 15 kPa
Calculated Saturation: 101.29 % $B = 0.96$ (before freezing)

Diameter (SS7) 64.00 mm **Total Frozen Vol. =** 379.60 cc
Height (similar to SS7) 118.00 mm **Sample Area =** 32.17 cm²
Frozen Total Weight 738.00 g
Ice Content 23.60 % $V_s = M_s / \rho_s = M_s / \rho_w G_s =$ 226.11 cc
Dry Weight of Sample 599.2 g (similar to SS7) $V_v = V_t - V_s =$ 153.49 cc
Final Water Content 25.43 %

Change in Height during Freezing (heave) 0.03 mm
Change in Volume during Freezing 11.26 cc

Change in height during Thawing (swelling) -0.062
Change in Volume during Thawing 14.99 cc

Change in height during Consolidation (settlement) 0.25 (ave of SS7 & SS8)
Change in Volume during Consolidation 2.17 cc (ave of SS7 & SS8)

Void Ratio Calculations:

$e_i = ((V - V_s)/V_s) = G_s \rho_w / \rho_d - 1 =$ 0.679
 $e_i = ((W - W_s)/W_s) * (G_s/G_{ice}) =$ 0.669 (for saturated specimens)

$Sr_i = (w_i G_s)/(e G_i) =$ 100.47 $Sr_o = Sr_i / 0.9919 =$ 101.29

$ef_z = e_i + \epsilon_{ax}(1+2r) V/V_s = e_i + \epsilon_{ax}(5) V/V_s =$ 0.681

$eth_m = ef_z - \epsilon_{ax} V/V_s (5) =$ 0.685

$eth_u = ef_z - \Delta h_{As}/V_s =$ 0.682

$ec = eth - \Delta V_c/V_s =$ 0.671

Final Void Ratio Check

$Sr_t = (V_v Sr_i (1-0.09) + V_{intake})/V_v =$ 1.012
 $eff = w_f G_s / Sr_t =$ 0.666

	Void Ratio e	Time (min)
e_i	0.679	0
ef_z	0.681	23
eth	0.685	41
ec	0.671	53
Δef_z	0.002	Heave
Δeth	0.004	Heave
Δec	-0.014	Settlement
eff	0.666	41

SS7 Specimen Data Sheet with Void Ratio Calculations.

SAMPLE: SS7 Clean Syncrude Sand Thawing: Multidirectional
DATE: 23-Apr-96 $G_s = 2.65$
Sand Type: Syncrude $G_{ice} = 0.917$
Cell Pressure: 35 kPa
Axial Stress: 35 kPa $K_o = 1.0$
Back Pressure: 15 kPa
Calculated Saturation: 99.75 % $B = 0.996$ (before freezing)

Diameter 64.14 mm **Total Frozen Vol. =** 378.04 cc
Height 117.00 mm **Sample Area =** 32.31 cm²
Frozen Total Weight 728.00 g
Ice Content 24.50 % $V_s = M_s / \rho_s = M_s / \rho_w G_s =$ 220.36 cc
Dry Weight of Sample 583.95 g $V_v = V_t - V_s =$ 157.68 cc
Final Water Content 25.30 %

Change in Height during Freezing (heave) -0.36 mm Settlement
Change in Volume during Freezing 8.64 cc Expulsion

Change in height during Thawing -0.03 Heave
Change in Volume during Thawing 12.94 cc Intake

Change in height during Consolidation 0.26 Settlement
Change in Volume during Consolidation 2.32 cc Expulsion

Void Ratio Calculations:

$e_i = ((V - V_s)/V_s) = G_s \rho_w / \rho_d - 1 = 0.716$
 $e_i = ((W_f - W_s)/W_s) * (G_s/G_{ice}) = 0.713$ (for saturated specimens)
 $S_r i = (w_i G_s)/(e G_i) = 98.95$ $S_r o = S_r i / 0.9919 = 99.75$

$efz = e_i + \epsilon_{ax}(1+2r) V/V_s = e_i + \epsilon_{ax}(5) V/V_s = 0.689$

$eth_m = efz - \epsilon_{ax} V/V_s (5) = 0.691$

$eth_u = efz - \Delta h A_s / V_s = 0.690$

$ec = eth - \Delta V_c / V_s = 0.681$

Final Void Ratio Check

$S_r t = (V_v S_r i (1-0.09) + V_{intake})/V_v = 0.982$
 $eff = w_f G_s / S_r t = 0.682$

	Void Ratio e	Time (hrs)
e_i	0.716	0
efz	0.689	20
eth	0.691	57
ec	0.681	69
Δefz	-0.026	Settlement
Δeth	0.002	Heave
Δec	-0.011	Settlement
eff	0.682	57

SS8 Specimen Data Sheet with Void Ratio Calculations.

SAMPLE: SS8 Clean Syncrude Sand Thawing: Multidirectional
DATE: 26-Apr-96 $G_s = 2.65$
Sand Type: Syncrude $G_{ice} = 0.917$
Cell Pressure: 35 kPa
Axial Stress: 35 kPa $K_o = 1.0$
Back Pressure: 15 kPa
Calculated Saturation: 100.07 % $B = 0.996$ (before freezing)

Diameter 63.29 mm **Total Frozen Vol. =** 380.67 cc
Height 121.00 mm **Sample Area =** 31.46 cm²
Frozen Total Weight 751.00 g
Ice Content 22.00 % $V_s = M_s / \rho_s = M_s / \rho_w G_s =$ 232.05 cc
Dry Weight of Sample 614.92 g $V_v = V_t - V_s =$ 148.62 cc
Final Water Content 25.04 %

Change in Height during Freezing (heave) 0.03 mm Heave
Change in Volume during Freezing 4.01 cc Expulsion

Change in height during Thawing (swelling) -0.02
Change in Volume during Thawing 12.93 cc Intake

Change in height during Consolidation (settlement) 0.24
Change in Volume during Consolidation 2.02 cc Expulsion

Void Ratio Calculations:

$e_i = ((V - V_s)/V_s) = G_s \rho_w / \rho_d - 1 = 0.640$
 $e_i = ((W_f - W_s)/W_s) * (G_s/G_{ice}) = 0.640$ (for saturated specimens)
 $Sr_i = (w_i G_s)/(e G_i) = 99.26$ $Sr_o = Sr_i / 0.9919 = 100.07$

$ef_z = e_i + \epsilon_{ax}(1+2r) V/V_s = e_i + \epsilon_{ax}(5) V/V_s = 0.643$

$eth_m = ef_z - \epsilon_{ax} V/V_s (5) = 0.644$

$eth_v = ef_z - \Delta h A_s / V_s = 0.643$

$ec = eth - \Delta V_c / V_s = 0.635$

Final Void Ratio Check

$Sr_t = (V_v Sr_i (1-0.09) + V_{intake}) / V_v = 0.990$
 $eff = w_f G_s / Sr_t = 0.670$

	Void Ratio e	Time (hr)
e_i	0.640	0
ef_z	0.643	23
eth	0.644	46
ec	0.635	50
Δef_z	0.002	Heave
Δeth	0.001	Heave
Δec	-0.009	Settlement
eff	0.670	46

Undisturbed Specimen FS4C14A Data Sheet with Void Ratio Calculations.

SAMPLE: FS4C14A Undisturbed Syncrude Sand Thawing: Unidirectional
DATE: 3-May-96 $G_s = 2.66$
Sand Type: Syncrude $G_{ice} = 0.917$
Cell Pressure: 387.15 kPa
Axial Stress: 627.33 kPa $K_o = 0.6$
Back Pressure: 146.96 kPa
Calculated Saturation: 85.41 % $B = 0.962$ (before freezing)

Diameter 63.70 mm **Total Frozen Vol. =** 407.13 cc
Height 127.75 mm **Sample Area =** 31.87 cm²
Frozen Total Weight 731.29 g
Ice Content 24.75 % $V_s = M_s / \rho_s = M_s / \rho_w G_s =$ 218.88 cc
Dry Weight of Sample 582.23 g $V_v = V_t - V_s =$ 188.24 cc
Final Water Content 26.15 %

Theoretical Volume of Porewater Expulsion During Freezing

$$\Delta V = 0.09 S_r V_v = 14.47 \text{ cc}$$

Change in Height during Setup 0.00 mm
Change in Volume during Setup 0.00 cc

Change in height during Thawing (settlement) 0.93 mm
Change in Volume during Thawing 16.56 cc

Void Ratio Calculations:

Before B $e_i = G_{spw}/\rho_d - 1 = 0.847$
 After B $e_i = ((V - V_s)/V_s) = 0.860$ (Note "V" in this eqn should be corrected for Δv during B test)
 $e_i = ((W - W_s)/W_s) * (G_s/G_{ice}) = 0.743$ (for saturated specimens)

Before B $S_r i = (w_i G_s)/(e G_i) = 84.72$
 After B $S_r i = (w_i G_s)/(e G_i) = 83.48$ $S_{r0} = S_r i / 0.9919 = 85.41$

$$e_s = e_i - \epsilon_{ax}(1+2r) V/V_s = e_i - \epsilon_{ax}(5) V/V_s = 0.847$$

$$e_{th_m} = e_{fz} - \epsilon_{ax} V/V_s (5) = 0.780$$

$$e_{th_u} = e_{fz} - \Delta h_{As}/V_s = 0.834$$

$$e_f = e_{th} = 0.834 \text{ (for undrained test)}$$

Final Void Ratio Check

$$S_r t = (V_v S_r i (1-0.09) + V_{intake})/V_v = 0.848$$

$$e_{ff} = w_f G_s / S_r t = 0.821$$

	Void Ratio e	Time (min)
e_i	0.847	0
e_{fz}	0.847	20
e_{th}	0.834	720
e_f	0.834	960
Δe_s	0.000	Settlement
Δe_{th}	-0.014	Settlement
e_{ff}	0.821	960

Undisturbed Specimen FS5C14 Data Sheet with Void Ratio Calculations.

SAMPLE: FS5C14 Undisturbed Syncrude Sand Thawing: Unidirectional
DATE: 2-May-96 $G_s = 2.66$
Sand Type: Syncrude $G_{ice} = 0.917$
Cell Pressure: 367.52 kPa
Axial Stress: 601.67 kPa $K_o = 0.6$
Back Pressure: 133.38 kPa
Calculated Saturation: 97.21 % $B = 0.372$ (before freezing)

Diameter 63.70 mm **Total Frozen Vol. =** 403.68 cc
Height 126.67 mm **Sample Area =** 31.87 cm²
Frozen Total Weight 767.42 g
Ice Content 24.81 % $V_s = M_s / \rho_s = M_s / \rho_w G_s =$ 233.12 cc
Dry Weight of Sample 620.1 g $V_v = V_t - V_s =$ 170.56 cc
Final Water Content 26.26 %

Theoretical Volume of Porewater Expulsion During Freezing

$\Delta V = 0.09 S_r V_v =$ 14.92 cc

Change in Height during Setup 0.00 mm
Change in Volume during Setup 0.00 cc

Change in height during Thawing (settlement) 0.7 mm
Change in Volume during Thawing 11.64 cc

Void Ratio Calculations:

Before B $e_i = G_{spw}/\rho_d - 1 =$ 0.746
 After B $e_i = ((V - V_s)/V_s) =$ 0.732 (Note "V" in this eqn should be corrected for ΔV during B test)
 $e_i = ((W - W_s)/W_s) * (G_s/G_{ice}) =$ 0.689 (for saturated specimens)

Before B $S_r i = (w_i G_s)/(e G_i) =$ 96.42
 After B $S_r i = (w_i G_s)/(e G_i) =$ 98.36 $S_{r0} = S_r i / 0.9919 =$ 97.21

$e_s = e_i - \epsilon_{ax}(1+2r) V/V_s = e_i - \epsilon_{ax}(5) V/V_s =$ 0.746

$e_{th_m} = e_f z - \epsilon_{ax} V/V_s (5) =$ 0.699
 $e_{th_v} = e_f z - \Delta h_{As}/V_s =$ 0.737

$e_f = e_{th} =$ 0.737 (for undrained test)

Final Void Ratio Check

$S_{rt} = (V_v S_{ri} (1-0.09) + V_{intake})/V_v =$ 0.963
 $e_{ff} = w_f G_s / S_{rt} =$ 0.725

	Void Ratio e	Time (min)
e_i	0.746	0
e_s	0.746	20
e_{th}	0.737	95
e_f	0.737	335
Δe_s	0.000	Settlement
Δe_{th}	-0.010	Settlement
e_{ff}	0.725	335

Reconstituted Specimen FS5C14R Data Sheet with Void Ratio Calculations.

SAMPLE: FS5C14r Reconstituted Undisturbed Syncrude Sand Specimen
DATE: 6-May-96 **Gs = 2.64**
Sand Type: Syncrude **Gice = 0.917**
Cell Pressure: 315 kPa 62.26
Axial Stress: 315 kPa **Ko = 1.0** 142.47
Back Pressure: 280 kPa
Calculated Saturation: % **B = 1.00** (before freezing)

Diameter 64.27 mm **Total Frozen Vol. =** 357.20 cc
Height 110.12 mm **Sample Area =** 32.44 cm²
Frozen Total Weight g
Ice Content % **Vs = Ms / ρs = Ms / ρw Gs =** 209.89 cc
Dry Weight of Sample 554.1 g **Vv = Vt - Vs =** 147.31 cc
Final Water Content %

Change in Height during Setup 0.00 mm
Change in Volume during Setup 0.00 cc

Change in height during Back Saturation 0.02
Change in Volume during Back Saturation 1.66 cc

Void Ratio Calculations:

$e_i = ((V - V_s)/V_s) = G_{spw}/\rho_d - 1 =$ **0.702** (0.732)
 $e_i = ((W - W_s)/W_s) * (G_s/G_{ice}) =$ -2.879 (for saturated specimens)

$Sr_i = (w_i G_s)/(e G_i) =$ **0.00** $Sr_o = Sr_i / 0.9919 =$ **0.00**

$e_s = e_i + \epsilon_{ax}(1+2r) V/V_s = e_i + \epsilon_{ax}(5) V/V_s =$ **0.702**

$e_b = e_fz - \epsilon_{ax} V/V_s (5) =$ **0.700**

Final Void Ratio Check

$Sr_t = (V_v Sr_i (1-0.09) + V_{intake})/V_v =$ **0.011**
 $eff = w_f G_s / Sr_t =$ **0.000**

	Void Ratio e	Time (min)
e_i	0.702	0
e_s	0.702	150
e_{th}	0.700	210
Δe_s	0.000	Settlement
Δe_b	-0.002	Settlement
eff	0.000	210

Undisturbed Specimen FS5C10A Data Sheet with Void Ratio Calculations.

SAMPLE:	FS5C10A Undisturbed Syncrude Sand	Thawing: Unidirectional
DATE:	18-Jun-96	Gs = 2.66
Sand Type:	Syncrude	Gice = 0.917
Cell Pressure:	336.85 kPa	
Axial Stress:	561.55 kPa	Ko = 0.5
Back Pressure:	112.14 kPa	
Calculated Saturation:	88.02 %	B = 0.10 (before freezing)
Diameter	63.65 mm	Total Frozen Vol. = 404.17 cc
Height	127.02 mm	Sample Area = 31.82 cm²
Frozen Total Weight	758.58 g	
Ice Content	21.90 %	Vs = Ms / ρs = Ms / ρw Gs = 236.05 cc
Dry Weight of Sample	627.89 g	Vv = Vt - Vs = 168.12 cc
Final Water Content	23.61 %	

Theoretical Volume of Porewater Expulsion During Freezing

$$\Delta V = 0.09 Sr Vv = 13.32 \text{ cc}$$

Change in Height during Freezing (heave) 0.00 mm
Change in Volume during Freezing 0.00 cc

Change in height during Thawing (settlement) 1.77 mm
Change in Volume during Thawing 13.98 cc

Void Ratio Calculations:

Before B $e_i = G_s \rho_w / \rho_d - 1 = 0.728$
 After B $e_i = ((V - V_s) / V_s) = 0.712$ (Note "V" in this equation should be corrected for ΔV during B test)
 $e_i = ((W - W_s) / W_s) * (G_s / G_{ice}) = 0.604$ (for saturated specimens)

Before B $Sr_i = (w_i G_s) / (e G_i) = 87.31$
 After B $Sr_i = (w_i G_s) / (e G_i) = 89.20$ $Sr_o = Sr_i / 0.9919 = 88.02$

$$efz = e_i + \alpha \times (1 + 2r) V / V_s = e_i + \alpha \times (5) V / V_s = 0.728$$

$$eth_m = efz - \alpha \times V / V_s (5) = 0.608$$

$$eth_u = efz - \Delta h \Delta s / V_s = 0.704$$

Final Void Ratio Check

$$Srt = (Vv Sri (1 - 0.09) + Vintake) / Vv = 0.895$$

$$eff = wf Gs / Srt = 0.702$$

	Void Ratio e	Time (min)
ei	0.728	0
efz	0.728	150
eth	0.704	210
Δefz	0.000	Heave
Δeth	-0.024	Settlement
eff	0.702	210

Undisturbed Specimen FS4C16-2 Data Sheet with Void Ratio Calculations.

SAMPLE:	FS4C16-2 Undisturbed Syncrude Sand	Thawing: Unidirectional
DATE:	2-Jun-96	$G_s = 2.66$
Sand Type:	Syncrude	$G_{ice} = 0.917$
Cell Pressure:	408.12 kPa	
Axial Stress:	654.76 kPa	$K_0 = 0.6$
Back Pressure:	161.47 kPa	
Calculated Saturation:	98.26 %	$B = 0.550$ (before freezing)
Diameter	63.80 mm	Total Frozen Vol. = 401.40 cc
Height	126.35 mm	Sample Area = 31.77 cm ²
Frozen Total Weight	768.89 g	
Ice Content	24.48 %	$V_s = M_s / \rho_s = M_s / \rho_w G_s =$ 236.34 cc
Dry Weight of Sample	628.67 g	$V_v = V_t - V_s =$ 165.06 cc
Final Water Content	23.59 %	

Theoretical Volume of Porewater Expulsion During Freezing

$$\Delta V = 0.09 S_r V_v = 14.60 \text{ cc}$$

Change in Height during Freezing (heave) 0.00 mm
 Change in Volume during Freezing 0.00 cc

Change in height during Thawing (settlement) 8.65 mm
 Change in Volume during Thawing 12.31 cc

Void Ratio Calculations:

Before B $e_i = G_{spw}/\rho_d - 1 = 0.729$
 After B $e_i = ((V - V_s)/V_s) = 0.698$ (Note "V" in this equation should be corrected for any volume change during B test)
 $e_i = ((W - W_s)/W_s) * (G_s/G_{ice}) = 0.647$ (for saturated specimens)

Before B $S_r i = (w_i G_s)/(e_i G_i) = 97.46$
 After B $S_r i = (w_i G_s)/(e_i G_i) = 101.68$ $S_{r0} = S_r i / 0.9919 = 98.26$

$$e_{fz} = e_i + c_{ax}(1+2r) V/V_s = e_i + c_{ax}(5) V/V_s = 0.729$$

$$e_{th_{15}} = e_{fz} - c_{ax} V/V_s (5) = 0.147$$

$$e_{th_{210}} = e_{fz} - \Delta h_{As}/V_s = 0.612$$

Final Void Ratio Check

$$S_r t = (V_v S_r i (1-0.09) + V_{intake})/V_v = 1.000$$

$$e_{ff} = w_f G_s / S_r t = 0.628$$

	Void Ratio e	Time (min)
e_i	0.729	0
e_{fz}	0.729	150
e_{th}	0.612	210
Δe_{fz}	0.000	Heave
Δe_{th}	-0.116	Settlement
e_{ff}	0.628	210

Appendix F: Costs Associated with In-Situ Ground Freezing at Each Test Site.

F.1. Introduction

Appendix F contains summary tables of the costs associated with conducting in-situ ground freezing at each of the CANLEX test sites. The costs of field work include not only the liquid nitrogen and drilling fees but also the costs associated with engineering supervision, labour, equipment, accommodation, meals and transportation. The costs related to frozen sample collection (including coring equipment), handling, storage and trimming specimens for triaxial testing are also provided.

Comparison of the costs given for each test site indicates that the expenditures were significantly reduced as experience with carrying out in-situ ground freezing and sampling was gained. The total costs associated with ground freezing and sampling at the Phase I test site was \$ 125,700, while the total cost for conducting the same work at the two Phase II test sites was \$ 118,200, or \$ 59,100 per site. The total cost for conducting in-situ ground freezing and sampling at the Phase III test site was \$ 66,000, which was slightly higher than that for Phase II, due to the high initial groundwater temperature.

Table F1: Costs Associated with Carrying out In-Situ Ground Freezing at the Phase I Test Site.

Category	Expenditures
I. Developmental Freezing Experiments	\$ 13,800
II. Engineering and Technician Supervision	\$ 13,000
III. Drilling and Installation of Freezing System	\$ 54,000
IV. Liquid Nitrogen	\$ 15,700
V. Supplies and Equipment	\$ 11,500
VI. Travel and Accommodations	\$ 2,700
Total	\$ 110,700

Table F2: Costs Associated with Sample Collection and Handling at the Phase I Test Site.

Category	Expenditures
I. Equipment Mobilization/Demobilization	\$ 3,000
II. Sample Handling and Transportation	\$ 3,500
III. Sample Storage	\$ 2,250
IV. Labour for Trimming Frozen Specimens	\$ 6,250
Total	\$ 15,000

Table F3: Costs Associated with Carrying out In-Situ Ground Freezing at the Phase II KIDD 2 and Massey Tunnel Test Sites.

Category	Expenditures
I. Engineering and Technician Supervision	\$ 9,000
II. Drilling and Installation of Freezing System	\$ 41,100
III. Liquid Nitrogen	\$ 40,000
IV. Supplies and Equipment	\$ 5,000
V. Travel and Accomodations	\$ 9,000
Total	\$ 104,100

Table F4: Costs Associated with Sample Collection and Handling at the Phase II KIDD 2 and Massey Tunnel Test Sites.

Category	Expenditures
I. Equipment Mobilization/Demobilization	\$ 1,700
II. Sample Handling and Transportation	\$ 4,100
III. Sample Storage	\$ 1,300
IV. Labour for Trimming Frozen Specimens	\$ 7,000
Total	\$ 14,100

Table F5: Costs Associated with Carrying out In-Situ Ground Freezing at the Phase III Test Site.

Category	Expenditures
I. Engineering and Technician Supervision	\$ 22,000
II. Drilling and Installation of Freezing System	\$ 9,000
III. Liquid Nitrogen	\$ 12,000
IV. Supplies and Equipment	\$ 5,000
V. Travel and Accommodations	\$ 4,400
Total	\$ 52,400

Table F6: Costs Associated with Sample Collection and Handling at the Phase III Test Site.

Category	Expenditures
I. Equipment Mobilization/Demobilization	\$ 3,000
II. Sample Handling and Transportation	\$ 3,500
III. Sample Storage	\$ 2,100
IV. Labour for Trimming Frozen Specimens	\$ 5,000
Total	\$ 13,600